

Field-Cycling NMR as a Tool of Molecular Rheology

Von der Universität Bayreuth
zur Erlangung des Grades eines
Doktors der Naturwissenschaften (Dr. rer. nat.)
genehmigte Abhandlung

von

Marius Johannes Hofmann
geboren am 13.01.1986 in Marktredwitz

Tag der Einreichung: 16.06.2016

Tag des Kolloquiums: 28.09.2016

1. Gutachter: Prof. Dr. Ernst Rößler
2. Gutachter: Prof. Dr. Claudia Schmidt
3. Gutachter: Prof. Dr. Hans Wolfgang Spiess

Table of Contents

Abstract	6
Kurzdarstellung.....	9
Extended Abstract	13
1. Introduction.....	13
1.1 Dynamics in Liquids – Quantities of Interest.....	14
1.2 “Glassy Dynamics” and the Glass Transition.....	18
1.3 Polymer Chains: Structural Modelling.....	20
1.4 Unconstrained Polymer Dynamics: the Rouse Model.....	21
1.5 Entangled Polymer Dynamics: the Tube-Reptation Model.....	24
1.6 Generalized Rouse Models.....	28
1.7 Intra- and Inter-Molecular Relaxation in ^1H	29
1.8 Relaxation in ^2H	35
2. Experiments on Polymer Dynamics Beyond FC NMR – State-of-the-Art	36
3. Principles of Field-Cycling NMR Relaxometry	45
3.1 Overview.....	45
3.2 Technical Principles	46
3.3 Multi-Exponential Spin-Lattice Relaxation	49
4. FC NMR: Previous Work	54
4.1 Susceptibility Representation and Master Curves	54
4.2 FC ^1H NMR in the Time Domain and Comparison to DQ ^1H NMR	56
4.3 Isotope Dilution Experiments.....	58
5. Results - FC NMR as a Tool of Molecular Rheology.....	60
5.1 FC ^1H Relaxometry vs. Atomistic MD Simulations	60
5.2 Reorientation and Finite Length Effects in Polymer Melts	62
5.3 Mean Squared Displacements of Segments in Polymer Melts	68
5.4 NMR Relaxation in Poly(ethylene propylene)	71
5.5 From NMR Relaxometry to “Molecular Rheology”	81
5.6 Molecular Dynamics in Dendrimers	89
6. Publications	94
6.1 List of Included Publications as Referred to in this Thesis	94
6.2 Individual Contributions to Joint Publications	95
6.3 Further Publications	96
6.4 Oral and Poster Presentations.....	98
6.5 PUB1	100

6.6	PUB2	108
6.7	PUB3	122
6.8	PUB4	132
6.9	PUB5	145
6.10	PUB6	160
Acknowledgement.....		174
References.....		175
Versicherung an Eides statt.....		188

Abstract

The frequency dependent relaxation behavior of nuclear magnetization is studied by field-cycling (FC) NMR relaxometry. It yields information on the molecular dynamics in complex fluids, such as linear polymer melts. For describing polymer dynamics, the renormalized Rouse (RR) and especially the tube-reptation (TR) model are popular. For entangled polymers those models predict a hierarchy of four characteristic power-law regimes (I-IV) for the segmental mean square displacement (MSD) $\langle r^2(t) \rangle$ and the 2nd rank re-orientational correlation function $C_2(t)$, respectively. Moreover, such models provide relations between these quantities, like the return-to-origin (RTO) hypothesis of the TR model. Employing the FC technique, it is demonstrated that ^1H NMR relaxometry is able to probe both, segmental translation in terms of $\langle r^2(t) \rangle$, as well as re-orientation in terms of $C_2(t)$. This enables testing relevant forecasts. The scientific field of FC NMR relaxometry on polymer melts was pioneered by R. Kimmich et al. and was later on revisited by the research of A. Herrmann et al. (*Bayreuth*). This PhD work continues the subject and the preceding Extended Abstract summarizes achievements.

Fluctuating local fields caused by molecular motion lead to relaxation within nuclear spin systems. By means of FC NMR relaxometry, the frequency-spectrum of these fluctuations is probed. It is reflected in the measurand of FC NMR, the dispersion of the spin-lattice relaxation rate $R_1(\omega)$, which is essentially proportional to the spectral density $J(\omega)$. Using electromagnets the magnetic field B and thus the Larmor frequency $\omega \propto B$ becomes a variable. In close collaboration between groups in *Bayreuth* and in *Darmstadt* (F. Fajarsa), a commercial FC relaxometer and a home-built apparatus are employed. Endowed with unique low-field equipment the latter provides an extraordinary broad frequency range of $100 \text{ Hz} \leq \nu = \omega/2\pi \leq 30 \text{ MHz}$ concerning protons (^1H). The relaxation data is converted into the susceptibility representation $\chi''(\omega) = \omega R_1(\omega)$. Here, assuming frequency-temperature superposition, the frequency window is effectively extended to about ten decades by constructing master curves $\chi''(\omega\tau_\alpha)$. Thereby, the temperature dependence of the time constant $\tau_\alpha(T)$, associated with the structural relaxation (α -process) is gained for temperatures well above the glass transition temperature T_g , and the frequency axis of the master curve is scaled according to τ_α .

The broad (effective) frequency window obtained enables a Fourier transform of susceptibility data into the time domain. A time auto-correlation function is gained, which is analyzed for various polymers of different molar masses. The α -process leads to an initial correlation loss in form of a stretched exponential decay. In polymers the subsequent decay is retarded by chain modes. The mode distribution features different regimes, which evolve with increasing chain length and lead to power-law behavior, ascribed to Rouse and entanglement dynamics. It is demonstrated that the specific form of the probed correlation function depends on the nature of the interaction, *i.e.* on the studied nucleus. Relaxation in ^1H is caused by fluctuations of the long-ranged dipole-dipole interaction. As a consequence, ^1H relaxation dispersion is additively composed by an intra- and an inter-molecular contribution along $R_1(\omega) = R_1^{\text{intra}}(\omega) + R_1^{\text{inter}}(\omega)$. Fourier transformation of the total relaxation $R_1(\omega)$ yields the dipolar correlation function $C_{DD}(t)$.

A separation is achieved by isotope dilution experiments; *i.e.* protonated chains are diluted in a deuterated matrix. In this way inter-molecular relaxation is suppressed, leaving the intra-molecular relaxation. The inter-part $R_1^{\text{inter}}(\omega)$, which is obtained by subtracting the intra-part from the total

relaxation, is transformed to $C_{inter}(t)$, an inter-molecular pair correlation function. The latter is mainly sensitive to translational dynamics. Applying a theoretical framework provided by N. Fatkullin, the segmental mean square displacement $\langle r^2(t) \rangle$ for the polymers poly(butadiene) (PB), poly(dimethyl siloxane) (PDMS) and poly(ethylene propylene) (PEP) is calculated from $C_{inter}(t)$ data over a wide time range and for different M . In all three polymers, sub-diffusive power-law regimes are found, which conform to Rouse (I) and constrained Rouse dynamics (II) predicted by the TR model. In the case of PB and PDMS, FC NMR relaxometry carried out previously by A. Herrmann et al. is complemented toward even longer times by field-gradient (FG) NMR diffusometry carried out by B. Kresse (PhD thesis, *Darmstadt*). In addition to the hydrodynamic regime (IV) where $\langle r^2(t) \rangle = 6Dt$ holds, a further sub-diffusive regime is found. It is assigned to the reptation regime (III) of the TR model. Combining FC and FG ^1H NMR, all four power-law regimes of the TR model are retrieved for high- M PB and PDMS. Furthermore, in the case of PEP, $\langle r^2(t) \rangle$ obtained by FC ^1H NMR is compared to data of neutron scattering; good agreement is found. In conclusion, FC ^1H relaxometry confirms the TR model with respect to segmental translation essentially.

The intra-molecular relaxation contribution $R_1^{intra}(\omega)$ obtained from isotope dilution transforms to the re-orientational correlation function $C_2(t)$. In isotropic polymer models like the (renormalized) Rouse model, $C_2(t)$ is equivalent to the (squared) bond vector correlation function in a coarsened picture. As was previously discovered by Herrmann et al. in PB, the exponent ε_{II}^{intra} of $C_2(t)$ in the entanglement related power-law regime II decreases with M and saturates at a value of about 0.45 for very long chains. This finding was validated by FC ^2H relaxometry. In contrast to ^1H , relaxation in deuterons (^2H) is purely of intra-molecular nature as the localized quadrupolar interaction dominates, yielding $C_2(t)$ exclusively. The investigation of PB chains deuterated at their ends by FC ^1H relaxometry in the course of this work, reveals the “protracted transition” of the exponent in regime II as a finite length effect. It immediately disappears when merely inner chain segments are probed. However, the TR model predicts a significantly lower value of 0.25 in the constrained Rouse regime than 0.45 observed experimentally. Regarding re-orientation, the TR model is contrary to the FC NMR results. Especially, the RTO hypothesis is challenged, which postulates an inverse proportionality $\langle r^2(t) \rangle \propto (C_2(t))^{-1}$. Unlike, double quantum (DQ) NMR data of PB as well as generic computer simulations actually confirm the TR model, *i.e.* for large M the correct exponent value of 0.25 is reproduced in $C_2(t)$.

A refined analysis of the FC relaxation data in the frequency domain cannot remedy the discrepancies between FC and DQ NMR regarding $C_2(t)$ of PB. Verifying the previous FC NMR results on PB along the further polymer PEP is thus of great importance for this thesis; besides ^1H and ^2H relaxometry on neat protonated/deuterated PEP of different M , an isotope dilution experiment is carried out. The comprehensive investigation of PEP fully confirms the previous findings on PB and the discrepancy with respect to DQ NMR and the TR model is even corroborated. PEP, which was provided by the group of D. Richter (*Forschungszentrum Jülich*), is actually best suited for scrutinizing models as it represents the simplest implementation of a linear chain, expect for poly(ethylene). The latter tends to crystallize easily.

Shear relaxation measurements on the PEP samples used for the FC NMR relaxometry are performed, in cooperation with the group of N. Aksel (*Bayreuth*) in an extraordinarily broad temperature range, reaching down to T_g . The constructed master curves encompass thirteen

decades in reduced frequency and are directly confronted to NMR susceptibility data. Such a comparison between the macroscopic and the microscopic rheology is presented for the first time. While consistent results are found for the α -process, in the Rouse and in the terminal regime, deviations are observed in the entanglement regime due to the different nature of the probed correlation functions. Here, the shear relaxation modulus $G(t)$ is determined by the correlation function of the end-to-end vector, the multi-exponential decay of which is governed by the terminal mode. This causes the rubber-plateau, a characteristic of entangled polymers. Otherwise, spin-lattice relaxation is more sensitive to the whole mode spectrum, therefore the correlation functions $C_{DD}(t)$, $C_2(t)$ and $C_{inter}(t)$ feature distinct power-law regimes. In contrast to shear rheology, this allows the straightforward determination of important regime crossover times like the entanglement time τ_e and, in favorable cases, also the Rouse time τ_R .

The weighting of relaxation modes in the different correlation functions probed by various experimental techniques like shear rheology, FC NMR and also dielectric spectroscopy is reflected in the cumulative mode ratio $F(M)$. The quantity is a measure of the increase of the mean relaxation time of the probed mode spectrum, with respect to that of a low- M reference system. As demonstrated for several polymers, $F(M)$ evolves differently for different methods or correlation functions, respectively. Given the data of FC NMR, shear rheology and supplementary techniques, a comprehensive “relaxation map” of PEP is drawn, including all time constants of all the collective as well as of several local processes.

Finally, another kind of molecular topology is addressed in this work, namely dendrimers, which are studied via FC NMR relaxometry for the first time. Besides the α -process, two regimes of collective dendrimer dynamics are identified. Again, good agreement with accompanying shear measurements is observed. The findings suggest that dendrimers resemble un-entangled polymers.

In conclusion, it is demonstrated that the broad frequency/time range gained by utilizing low-field equipment as well as by assuming FTS, the possibility of generating contrast via isotope labelling and the high information content of the fully probed correlation functions render FC NMR relaxometry as a promising tool of “molecular rheology”.

Kurzdarstellung

Das frequenzabhängige Relaxationsverhalten der Kernmagnetisierung wird mit Hilfe der Field-Cycling- (FC)-NMR studiert. Es liefert Informationen über die Moleküldynamik in komplexen Fluiden, wie beispielsweise Schmelzen linearer Polymere. Zur Beschreibung von Polymerdynamik haben sich hierfür das (renormierte) Rouse- und insbesondere das Reptationsmodell etabliert. Diese Modelle sagen für verschlaufte Polymere (solche mit „Entanglements“) vier hierarchische Regime von Potenzgesetzen (I-IV) für das mittlere Verschiebungsquadrat $\langle r^2(t) \rangle$ sowie die Reorientierungskorrelationsfunktion $C_2(t)$ der Kettensegmente voraus. Darüber hinaus liefern solche Theorien auch Zusammenhänge zwischen diesen Größen, wie beispielsweise die „return-to-origin“ (RTO)-Hypothese des Reptationsmodells. Durch Anwendung der FC-Technik kann mittels NMR-Relaxometrie sowohl segmentale Translation als auch Reorientierung gemessen werden, was eine kritische Überprüfung solcher Modellvorhersagen gestattet. Nachdem R. Kimmich und Mitarbeiter Pionierarbeit geleistet hatten, wurde die Forschung auf diesem Gebiet von A. Herrmann (*Bayreuth*) aufgegriffen. Diese Doktorarbeit stellt wiederum eine Fortsetzung dar. Das vorliegende „Extended Abstract“ fasst die wichtigsten wissenschaftlichen Erkenntnisse zusammen.

Fluktuationen in den lokalen Wechselwirkungen, verursacht durch molekulare Bewegung, führen zur Relaxation in Kernspin-Systemen. Mittels FC-Relaxometrie kann das Frequenzspektrum dieser Fluktuationen sondiert werden. Es ist verknüpft mit der Spin-Gitter Relaxationsrate $R_1(\omega)$, deren Frequenzabhängigkeit (Dispersion) die eigentliche Messgröße in der FC-NMR darstellt. Letztere ist im Wesentlichen proportional zur Spektraldichte $J(\omega)$ der Fluktuationen. Zu diesem Zweck kommen Elektromagnete zum Einsatz, deren Feld B , sowie die resultierende Larmorfrequenz der Kernspins $\omega \propto B$, variiert werden können. In enger Zusammenarbeit zwischen Arbeitsgruppen aus *Bayreuth* und *Darmstadt* (F. Fajara) kommen ein kommerzielles Relaxometer sowie ein Eigenbau zur Anwendung. Letzterer ist mit einzigartiger Niederfeld-Technik ausgestattet. Diese ermöglicht einen besonders breiten Frequenzbereich von $100 \text{ Hz} \leq \nu = \omega/2\pi \leq 30 \text{ MHz}$, bezogen auf Protonen (^1H). Die Relaxationsdaten werden in die Suszeptibilitätsdarstellung $\chi''(\omega) = \omega R_1(\omega)$ überführt. Unter der Annahme von Frequenz-Temperatur-Superposition (FTS) kann hier das effektiv zur Verfügung stehende Frequenzfenster auf zehn Dekaden erweitert werden, indem Masterkurven $\chi''(\omega\tau_\alpha)$ konstruiert werden. Auf diesem Wege erhält man für Temperaturen oberhalb des Glaspunktes die Temperaturabhängigkeit der Zeitkonstanten $\tau_\alpha(T)$. Diese beschreibt die strukturelle Relaxation (den α -Prozess), bezüglich welcher die Frequenzachse einer Masterkurve skaliert wird.

Das so gewonnene Frequenzintervall ist effektiv breit genug, um per Fourier-Transformation in die Zeitdomäne überführt zu werden. Man erhält eine Zeit-Autokorrelationsfunktion, welche für verschiedene Polymere in Abhängigkeit des Molekulargewichts analysiert wird. Rein qualitativ führt der α -Prozess zunächst zu einem anfänglichen Korrelationsverlust in Form eines (gestreckt) exponentiellen Abfalls. Der Korrelationszerfall bei längeren Zeiten ist in Polymeren durch das Auftreten von Kettenmoden verzögert. Deren Modenspektrum weist verschiedene Regime auf. Diese entwickeln sich mit zunehmender Kettenlänge und führen zu den erwähnten Potenzgesetzen, welche Rouse- und „Entanglement“-Dynamik zugeschrieben werden. Wie gezeigt wird, hängt die genaue Form der sondierten Korrelationsfunktion von der Art der lokalen Wechselwirkung und somit vom untersuchten Kern ab. Relaxation in Protonen wird verursacht durch Fluktuationen der

langreichweitigen Dipol-Dipol-Wechselwirkung. Aus diesem Grund ist die Relaxationsdispersion von ^1H additiv aus einem intra- und einem inter-molekularen Beitrag zusammengesetzt, gemäß $R_1(\omega) = R_1^{\text{intra}}(\omega) + R_1^{\text{inter}}(\omega)$. Die Fouriertransformierte der Gesamtrelexation $R_1(\omega)$ ist die dipolare Korrelationsfunktion $C_{DD}(t)$.

Eine Trennung gelingt mittels Isotopenverdünnungsexperimenten, bei denen protonierte Polymerketten in einer deuterierten Matrix verdünnt werden. Dadurch wird die inter-molekulare Relaxation unterdrückt und lediglich der intra-molekulare Beitrag $R_1^{\text{intra}}(\omega)$ bleibt erhalten. Der inter-molekulare Beitrag $R_1^{\text{inter}}(\omega)$ wird durch Subtraktion des intra-molekulare Beitrags von der Gesamtrelexation $R_1(\omega)$ gewonnen. Er führt auf eine Paar-Korrelationsfunktion $C_{\text{inter}}(t)$, welche empfindlich gegenüber (relativer) Translationsdynamik ist. Nach N. Fatkullin steht diese translative Korrelationsfunktion mit dem mittleren Verschiebungsquadrat $\langle r^2(t) \rangle$ von Polymersegmenten im Zusammenhang. Für die Polymere Poly(butadien) (PB), Poly(dimethylsiloxan) (PDMS) und Poly(ethylenpropylen) (PEP) wird jeweils für verschiedene Molekulargewichte der inter-molekulare Beitrag aus der totalen ^1H Relaxationsdispersion extrahiert. Anschließend wird aus $C_{\text{inter}}(t)$ das mittlere segmentale Verschiebungsquadrat $\langle r^2(t) \rangle$ berechnet. In allen diesen drei Polymeren werden sub-diffusive Potenzgesetz-Regime gefunden, welche mit den vom Reptationsmodell vorhergesagten Regimen „Rouse“ (I) bzw. „constrained Rouse“ (II) übereinstimmen. Im Fall von PB und PDMS werden die Daten der FC-Relaxometrie, welche zuvor von A. Herrmann et al. durchgeführt wurde, durch Diffusionsdaten bei noch längeren Zeiten ergänzt, die mittels Feldgradienten (FG) NMR gewonnen werden (vgl. Dissertation von B. Kresse, *Darmstadt*). Zusätzlich zum hydrodynamischen Bereich (IV), in welchem $\langle r^2(t) \rangle = 6Dt$ gilt, wird ein weiteres sub-diffusives Regime entdeckt, welches dem Reptationsregime (III) des Reptationsmodells zugeordnet wird. Durch die Kombination von FC und FG ^1H NMR werden somit im Fall von hochmolekularem PB bzw. PDMS, sämtliche vier Potenzgesetz-Regime des Reptationsmodells gefunden. Im Fall von PEP wird das per FC ^1H Relaxometrie gewonnene $\langle r^2(t) \rangle$ mit Daten aus der Neutronen-Spin-Echo-Spektroskopie verglichen, wobei gute Übereinstimmung gefunden wird. Insgesamt bestätigen die gefundenen Ergebnisse der FC- ^1H -Relaxometrie das Reptationsmodell bezüglich Translation weitgehend.

Der rein intra-molekulare Relaxationsbeitrag $R_1^{\text{intra}}(\omega)$, der ebenfalls aus Isotopenverdünnungsexperimenten gewonnen wird, liefert die erwähnte Reorientierungskorrelationsfunktion $C_2(t)$. In isotropen Modellen der Polymerdynamik, wie dem (renormierten) Rouse Modell, repräsentiert $C_2(t)$ näherungsweise das Quadrat der Korrelationsfunktion des Segment-Segment Verbindungsvektors. Wie zuvor von Herrmann et al. in PB entdeckt, nimmt der Exponent $\epsilon_{II}^{\text{intra}}$ des mit Entanglement-Dynamik in Verbindung gebrachten Potenzgesetz-Regimes (II), mit zunehmendem Molekulargewicht M stetig ab und sättigt bei einem Wert von ungefähr 0.45, jedoch erst im Fall sehr lange Ketten. Der Sättigungsprozess ist somit stark verzögert. Dieses Ergebnis wurde durch Deuteronen- (^2H)-FC-Relaxometrie bestätigt. Im Gegensatz zu ^1H ist Spin-Gitter-Relaxation in Deuteronen (^2H) rein intra-molekularer Natur, da hier die lokalisierte, quadrupolare Wechselwirkung dominiert. Demzufolge wird in FC- ^2H -Relaxometrie $C_2(t)$ direkt gemessen und so eine Überprüfung der ^1H -Isotopenverdünnungsexperimente ermöglicht. Die im Zuge dieser Arbeit durchgeführte Untersuchung von PB Ketten, deren Enden deuteriert wurden, mittels FC ^1H NMR, entlarvt den „stark verzögerten Übergang“ als Folge von Effekten, aufgrund der endlichen Kettenlänge. Er verschwindet, sogleich ausschließlich die innersten Segmente einer Kette sondiert werden, d.h. der Plateauwert $\epsilon_{II}^{\text{intra}}$ ist bereits bei wesentlich kürzeren Ketten erreicht. Dennoch sagt das Reptationsmodell für das

„constrained Rouse“-Regime (II) einen deutlich niedrigeren Exponenten von 0.25 voraus, als der experimentelle Befund 0.45. Die gefundenen Ergebnisse bzgl. $C_2(t)$ widersprechen somit dem Reptationsmodell. Insbesondere wird die RTO-Hypothese in Frage gestellt, welche eine inverse Proportionalität $\langle r^2(t) \rangle \propto (C_2(t))^{-1}$ im Entanglement-Bereich postuliert. Im Gegensatz dazu bestätigen Messungen aus der Doppelquanten-(DQ-) NMR sowie generische Computersimulationen das Reptationsmodell, d.h. für lange Ketten wird der vorhergesagte Exponent von $\varepsilon_{II}^{intra}=0.25$ tatsächlich näherungsweise erreicht.

Ohne Erfolg wird zunächst versucht, diese Diskrepanzen zwischen FC- und DQ-NMR bezüglich $C_2(t)$ von PB im Rahmen einer verfeinerten Analyse der FC-NMR Daten zu beseitigen. Die Überprüfung vorheriger Ergebnisse der FC-NMR an PB anhand des weiteren Polymers PEP ist daher von großer Bedeutung für diese Arbeit; neben ^1H und ^2H Relaxometrie an protonierten/deuterten Reinsystemen verschiedener Molekulargewichte wurde auch ein weiteres isotoopenverdünnungsexperiment an PEP durchgeführt. Die umfassende Untersuchung von PEP bestätigt die vorherigen Ergebnisse in Bezug auf PB vollumfänglich, wodurch die Diskrepanz zu den Ergebnissen der DQ-NMR zusätzlich untermauert wird. PEP wurde von der Arbeitsgruppe von D. Richter (*Forschungszentrum Jülich*) zur Verfügung gestellt. Zur Überprüfung von Modellvorhersagen ist dieses Polymer bestens geeignet, denn es weist, nach Polyethylen, die einfachst mögliche Kettenstruktur auf. Letzteres neigt jedoch zur Kristallisation.

Die gleiche Charge des Polymers PEP, an welcher FC-NMR Untersuchungen durchgeführt werden, wird per Scher-Rheologie vermessen. Diese Messungen wurden in der Gruppe von N. Aksel (*Bayreuth*) über einen besonders breiten Temperaturbereich bis hin zum Glaspunkt durchgeführt. Die generierten Masterkurven umfassen effektiv 13 Dekaden in der Frequenzachse und werden den entsprechenden FC-NMR-Daten in der Suszeptibilitätsdarstellung gegenübergestellt. Auf diese Weise wird zum ersten Mal ein direkter Vergleich zwischen der mikroskopischen und der makroskopischen Rheologie präsentiert. Während konsistente Ergebnisse bezüglich des α -Prozesses, des Rouse Regimes und der terminalen Relaxation gefunden werden, führt die unterschiedliche physikalische Natur der sondierten Korrelationsfunktionen zu Unterschieden im Entanglement-Bereich. Der Schermodul $G(t)$ ist hier bestimmt durch die Korrelationsfunktion des End-zu-End Vektors, deren multi-exponentieller Zerfall von der terminalen Mode dominiert wird. Dieser Umstand führt zum für Polymerschmelzen charakteristischen Gummiplateau. Spin-Gitter-Relaxation hingegen ist sensitiver gegenüber dem gesamten Modenspektrum, weshalb die Korrelationsfunktionen $C_{DD}(t)$, $C_2(t)$ und $C_{inter}(t)$ das erwähnte, deutlich ausgeprägte Potenzgesetzverhalten aufweisen. Anders als in der Rheologie können so kritische Zeitskalen wie die Entanglement-Zeit τ_e oder, unter günstigen Umständen, auch die Relaxationszeit der längsten Rouse-Mode τ_R auf einfachem Wege bestimmt werden.

Die Gewichtung von Relaxationsmoden in den verschiedenen experimentell gemessenen Korrelationsfunktionen ist auch im sog. „kumulativen Modenverhältnis“ $F(M)$ abgebildet. Die Größe ist ein Maß für das Anwachsen der mittleren Relaxationszeit des Modenspektrums mit M , in Bezug zu einem niedermolekularen Referenzsystem. Wie für mehrere Polymere gezeigt wird, entwickelt sich $F(M)$ in unterschiedlicher Weise für verschiedene experimentelle Techniken (Korrelationsfunktionen). Mit den Daten aus FC NMR, der Scher-Rheologie und ergänzenden Techniken, wie der dielektrischen Spektroskopie, wird eine Art „Karte der Relaxationsprozesse“ in PEP erstellt. Diese beinhaltet die

Temperaturabhängigkeiten sämtlicher kollektiver als auch mehrerer lokaler Relaxationsprozesse über einen gigantischen Zeitbereich.

Schließlich werden per FC NMR zum ersten Mal Dendrimere untersucht und damit polymere Moleküle mit einer komplexeren Topologie. Neben dem α -Prozess werden zwei Regime kollektiver Dendrimer-Dynamik identifiziert. Das gefundene Verhalten ähnelt dem nicht verschlaurter (kurzer) Polymere. Auch hier werden viele Gemeinsamkeiten *bzgl.* FC-NMR und Schermessungen aufgedeckt.

Das extrem breite Frequenzfenster, welches man durch Verwendung von Niederfeld-Technik sowie durch Frequenz-Temperatur-Superposition erhält, die Möglichkeit, Kontrast durch gezielte Isotopenmarkierung zu erzeugen und der Informationsgehalt der gemessenen, mikroskopischen Korrelationsfunktionen, etablieren FC-NMR-Relaxometrie als vielversprechende Methode der molekularen Rheologie.

Extended Abstract

1. Introduction

The term “molecular rheology” appearing in the title of this thesis denotes the approach of relating macroscopic, rheological properties of liquids to microscopic, molecular details¹ and was introduced by Williams² and Doi³ in the context of polymers. In this thesis, it will be shown that Field-Cycling (FC) NMR relaxometry is a very powerful method for investigating the molecular dynamics, in particular in polymer melts.

In FC NMR the dependence of the spin-lattice relaxation rate R_1 on the Larmor frequency $\omega = |\gamma B|$ is probed by varying the external magnetic field B . This quantity $R_1(\omega)$ is denoted as relaxation dispersion. For that purpose, electromagnets are employed with fields sometimes reaching well below the earth's. Thus, FC NMR is essentially a “low-field” NMR technique. By quickly cycling between different fields in a well-defined way using transistor controlled currents, relaxation and signal detection are decoupled. Doing so, the issue of tiny NMR signals going along with low fields is evaded. The idea of the FC technique has already dated back to the origins of NMR and was pioneered by F. Noack⁴ and R. Kimmich^{5,6} in its modern form. It gained momentum over time with the technical progress, so that nowadays a commercial relaxometer has become available, namely the STELAR FFC2000. It provides a frequency range of $10 \text{ kHz} \leq \omega/2\pi \leq 20 \text{ MHz}$ concerning protons (^1H). One such device is operated in *Bayreuth* since 2004. Advanced, scientific relaxometer may even reach lower fields. Such an advanced, home-built machine equipped with unique low-field technology is located at the *Technische Universität Darmstadt* in the group of F. Fajarsa, with which the *Bayreuth* group maintains a fruitful collaboration. It allows for dispersion measurements in a range of $100 \text{ Hz} \leq \omega/2\pi \leq 30 \text{ MHz}$, i.e. fields well below the earth's ($\approx 2.5 \text{ kHz}$) are achieved. That device is used to extend the range of $R_1(\omega)$ measurements toward frequencies, where the slow, collective dynamics in entangled polymer melts shows up.

Usually, the abundant nucleus ^1H is studied, the relaxation of which is mainly caused by fluctuations of the long-ranged magnetic dipole-dipole interaction due to molecular motion. The relaxation dispersion $R_1(\omega)$ is a measure of the spectral density $J(\omega)$. The latter quantifies molecular motion in terms of its frequency components. After transformation of $R_1(\omega)$ (or $J(\omega)$, to be precise) into the time domain, the dipolar (auto-)correlation function $C_{DD}(t)$ is gained, which is a pair correlation function between spins. Due to the many-particle character of the dipolar interaction relaxation in ^1H is attributed to an intra- as well as an inter-molecular contribution in the sense that $R_1(\omega)$ is additively composed along $R_1(\omega) = R_1^{\text{intra}}(\omega) + R_1^{\text{inter}}(\omega)$. When the intra-part $R_1^{\text{intra}}(\omega)$ is converted into the time domain, the rank $l=2$ re-orientational correlation function $C_2(t)$ is obtained. In polymers, $C_2(t)$ is approximately equal to the squared bond vector correlation function. Otherwise, $R_1^{\text{inter}}(\omega)$ transforms to an inter-molecular correlation function $C_{\text{inter}}(t)$, which is sensitive to relative translations. It directly reflects the mean square displacement (MSD) $\langle r^2(t) \rangle$ of molecules in the liquid, or segments in a polymer melt, respectively. Exploiting the isotope-selectivity of NMR, however, both relaxation contributions can be distinguished. As a consequence of intra- as well as intermolecular couplings, FC ^1H NMR offers the unique opportunity of probing both, re-orientations as well as translational motion over a huge time/frequency window, as will be demonstrated.

In the same manner as it is often done in rheology or dielectric spectroscopy (DS), for instance, the frequency range is significantly extended by measuring the relaxation dispersion in a broad temperature range and constructing master curves. The resulting (effective) frequency range is so broad that the manifold relaxation behavior of polymer melts can be studied.

The tube-reptation (TR) model is the most accepted theory with regard to the dynamics in entangled polymer melts. Based on a molecular scenario, the TR model predicts a family of hierarchical dynamic regimes for $\langle r^2(t) \rangle$ and also for $C_2(t)$, depending on chain length. As both these quantities can be measured by FC NMR over a wide range of times/frequencies, the technique allows for a critical test of relevant polymer theories, a major issue of this work. The FC NMR results on polymers are also compared to such of other “molecular methods” like atomistic computer simulations, quasi-elastic neutron scattering (NS) or different NMR methods; to mention are double quantum (DQ) NMR and field-gradient (FG) NMR. FC NMR data addressing the microscopic relaxation behavior is also compared to shear measurements, the latter rather probing macroscopic relaxation properties. Thus, micro- and macroscopic rheology are directly confronted. Moreover, results on dendrimers are reported. With respect to linear chains, they feature a more complex macromolecular topology. In the course of this work such systems were studied via FC NMR for the first time.

In the upcoming sections I will briefly summarize my PhD work, which is a continuation of my diploma work, the research on low-molecular liquids of R. Meier and in particular of A. Herrmann together with B. Kresse, on polymer melts. The latter contributed to the latest successful efforts of pushing the FC NMR technique toward record-breaking low fields. The results are published in the articles referred to as PUB1-6 enclosed to this thesis (*cf.* section 6.1). Those articles are also reprinted in section 6. Three further publications dedicated to the results on the polymer poly(ethylene propylene) (PEP), and in particular to the comparison between FC NMR relaxometry and the shear measurements, are currently in preparation or have just been submitted (*cf.* section 6.3).

1.1 Dynamics in Liquids – Quantities of Interest

Polymer melts are viscous liquids. On a microscopic level the dynamics in the liquid must be described by quantities of statistical physics due to the stochastic nature of molecular motion. The physical quantities relevant for this work are introduced in this section.

The liquid is a state of condensed matter resulting from weak and transient attractive inter-molecular forces. Inter-molecular distances are comparable to molecular sizes. In contrast to the crystal, the structure merely features short-range order which may extend over several nm , and is reflected in only a few peaks in the pair-distribution function.⁷⁻¹⁰ Furthermore, liquids differ from solids by the absence of transversal phonons (for ω smaller than the Frenkel frequency¹¹ ω_F) and are consequently characterized by a vanishing shear response (relaxation modulus) at long times as well as a finite viscosity; liquids flow after all. A general connection between macroscopically observable transport coefficients and microscopic, statistical quantities is established via Green-Kubo relations.^{12,13} Those relate transport coefficients to integrals over time auto-correlation functions. For instance, the diffusion coefficient D (transport of mass) is the integral over the velocity auto-correlation function. In molecular systems one has to distinguish between rotational (re-

orientational) and translational motion. The extent of **translational motion** is generally expressed in terms of the mean square displacement (MSD)

$$\langle r^2(t) \rangle = \lim_{N \rightarrow \infty} N^{-1} \sum_{i=1}^N [\bar{R}_i(t) - \bar{R}_i(0)]^2 \quad (1)$$

e.g., of a molecule's center of mass or a polymer segment. The MSD is a key-concept in soft matter physics since the pioneering theoretical works of Einstein and Smoluchowski in the description of Brownian motion.^{14,15} At shortest times, the dynamics in all dense liquids is first ballistic and the MSD $\propto t^2$, until the displacement is "caged" by inter-molecular packaging effects (*cf.* Fig. 1 in section 1.5). At long times, in the so-called hydrodynamic limit, the dynamics in a liquid becomes diffusive and the MSD linear in time, $\langle r^2(t) \rangle = 6Dt$, where D denotes the (self-) diffusion coefficient. In complex fluids such as polymers, motion is sub-diffusive at intermediate times, *i.e.* $\langle r^2(t < \tau_t) \rangle \propto t^{\alpha < 1}$, with τ_t denoting the terminal, *i.e.* the longest relaxation time.

The MSD in liquids is accessible from the intermediate scattering function obtained from incoherent inelastic scattering (*cf.* section 2). The dynamic fluctuation in the intensity of quasi-elastically scattered waves is reflected in the dynamic structure factor $S(\vec{q}, \omega)$ or its temporal Fourier transform, the intermediate scattering function $S(\vec{q}, t)$, respectively. Compared to elastic scattering, the detected signal $S(\vec{q}, \omega)$ is broadened. $S(\vec{q}, t)$ is the spatial Fourier transform of the Van-Hove function

$$G(\vec{r}, t) = N^{-1} \left\langle \sum_{m,n} \delta(\vec{r} + (\vec{r}_m(t) - \vec{r}_n(0))) \right\rangle = \underbrace{N^{-1} \left\langle \sum_m \delta(\vec{r} + (\vec{r}_m(t) - \vec{r}_m(0))) \right\rangle}_{G_{\text{coh}}} + \underbrace{N^{-1} \left\langle \sum_{m \neq n} \delta(\vec{r} + (\vec{r}_m(t) - \vec{r}_n(0))) \right\rangle}_{G_{\text{inc}}} \quad (2)$$

which correlates density fluctuations. As distinguished in eq. 2 $G(\vec{r}, t)$ (and consequently $S(\vec{q}, t)$ and $S(\vec{q}, \omega)$) consists of a coherent and an incoherent contribution. Those can be distinguished by isotopic contrast, exploiting differences in scattering lengths.¹⁶ For $t = 0$ the static particle-particle auto-correlation function $G(\vec{r}, 0) = \delta(\vec{r}) + \rho g(\vec{r})$ is obtained, with ρ denoting the density and $g(\vec{r}) = g(r)$ the pair distribution of a liquid.^{16,17} Assuming a Gaussian propagator (eq. 54, section 1.7), the incoherent intermediate scattering function can be related to the MSD:⁶

$$S_{\text{inc}}(t) \propto \exp\left[-1/6q^2 \langle r^2(t) \rangle\right] \quad (3)$$

Field-gradient (FG) NMR has been established as a standard method for measuring D , *i.e.* in the hydrodynamic limit (*cf.* section 2). As will be demonstrated, $\langle r^2(t) \rangle$ is also related to the inter-molecular spin-lattice relaxation among protons, detectable by FC ^1H NMR (*cf.* section 1.7). More precisely, it is received from the (normalized) inter-molecular correlation function

$$C_{\text{inter}}(t) = \left\langle \frac{P_2[\cos(\vartheta(t))]}{r^3(t)} \cdot \frac{P_2[\cos(\vartheta(0))]}{r^3(0)} \right\rangle \bigg/ \left\langle \left| \frac{P_2[\cos(\vartheta(0))]}{r^3(0)} \right|^2 \right\rangle \quad (4)$$

of the 2nd order Legendre polynomial $P_{l=2}$ of the fluctuating angle $\vartheta(t)$ monitoring the molecular (in polymers segmental) orientation. The distance between particles (spins) is denoted as $r(t)$.

The **rotational motion** of molecules in liquids is typically described by means of the re-orientational auto-correlation functions:

$$C_l(t) = \frac{2l+1}{2} \langle P_l[\cos(\mathcal{Q}(0))] P_l[\cos(\mathcal{Q}(t))] \rangle \quad (5)$$

The rank l depends on the probe and thus on the experimental technique (cf. section 2). It is anticipated that $C_2(t)$ is related to the intra-molecular relaxation $R_1^{intra}(\omega)$ in NMR (cf. section 1.7). After transformation to the frequency domain, the spectral density is gained, according to the Wiener-Khinchin theorem:¹⁸

$$J_l(\omega) = \text{Re} \int_0^\infty C_l(t) e^{-i\omega t} dt \quad (6)$$

Both, correlation functions as well as spectral densities, respectively, are normalized:

$$\int_0^\infty C_l(t) dt = J_l(0) = \langle \tau_l \rangle \quad \text{and} \quad \int_0^\infty J_l(\omega) d\omega = \pi/2 \quad (7)$$

Here, $\langle \tau_l \rangle$ denotes the mean correlation time of the underlying correlation time distribution. In the model case of rotational diffusion with a single correlation time one gets

$$C_l(t) = \exp[-l(l+1)D_r t] \quad J_l = \frac{\tau_l}{1 + (\omega \tau_l)^2} \quad (8)$$

with the rotational time constant $\tau_l = l(l+1)D_r$. The rotational diffusion coefficient is denoted as D_r and is related to the mean square jump angle $\langle \Omega^2(t) \rangle = 4 D_r t$.^{19,20} The corresponding spectral density is a Lorentzian. In practice, however, already in simple liquids re-orientational correlation functions are more elaborate (see section 1.2). Of course, a spectral density is also obtained for $C_{inter}(t)$, defined in eq. 4.

In experiments like dielectric spectroscopy or rheology, however, macroscopic time domain response functions or frequency dependent susceptibilities are probed, instead of correlation functions or spectral densities, respectively, which are defined on a molecular level. A link is necessary, which is accomplished by means of the fluctuation-dissipation theorem (FDT, see below).^{12,13,21,22} A temporal response function $\chi(t-t')$ generally relates the macroscopic response $x(t)$ of a system to an applied perturbation $h(t)$. Under linear conditions this relation reads:^{6,23}

$$x(t) = \int_{-\infty}^t \chi(t-t') h(t') dt' + O(h^2) \dots \quad (9)$$

The linear response formula is applicable if the perturbation $h(t)$ on the system is small. Then the response function $\chi(t-t')$ is time invariant and independent of the perturbation itself. Otherwise, higher orders have to be taken into account. Fourier transformation yields the (linear) frequency domain response

$$\tilde{x}(\omega) = \chi^*(\omega) \tilde{h}(\omega) \quad \text{with} \quad \chi^*(\omega) = \chi'(\omega) + i\chi''(\omega) \quad (10)$$

where $\chi^*(\omega)$ denotes the complex susceptibility. Its imaginary part $\chi''(\omega)$ is the absorptive or dissipative contribution of the response. The real part $\chi'(\omega)$ is the reactive contribution. $\chi'(\omega)$ and $\chi''(\omega)$ are related via the Kramers-Kronig relations. An example important for this work is the linear response relation between shear stress $\sigma(t)$ and an applied step-like shear strain $\gamma(t)$

$$\sigma(t) = \int_{-\infty}^t G(t-t') \frac{\partial \gamma(t')}{\partial t'} dt' \quad (11)$$

where the linear (step)response function $G(t)$ is called relaxation modulus.²⁴ Experimentally, $G(t)$ is measured in a shear step-response experiment. Yet, shear measurements are more often realized in the frequency domain (see below and section 2). The complex shear modulus, *i.e.* the complex “shear susceptibility” reads:²⁴

$$G^*(\omega) = i\omega \int_0^\infty G(t) e^{-i\omega t} dt = G'(\omega) + iG''(\omega) \quad (12)$$

The real part is called storage modulus $G'(\omega)$ and the imaginary part $G''(\omega)$ loss modulus. Oscillatory shear rheology enables measuring both quantities as in- and out-of-phase components with respect to the applied oscillatory strain (*cf.* section 2). Another example is the complex dielectric susceptibility $\epsilon^*(\omega)$ probed in dielectric spectroscopy.

An important feature of susceptibilities in liquids above the glass transition temperature T_g is that frequency-temperature superposition (FTS) applies, meaning that the form a susceptibility curve $\chi^*(\omega)$ doesn't change with temperature (*cf.* section 1.2). This implies that by applying temperature dependent frequency shift factors a_T a master curve $\chi^*(\omega a_T)$ can be constructed from susceptibility curves measured at different temperatures, as for example:

$$\chi'(\omega) \equiv \chi'(\omega a_T) \quad (13)$$

Exploiting FTS the dynamic range of experimental techniques can be strongly extended in many systems (*cf.* sections 4.1 and 5). According to the FDT, the imaginary part of the susceptibility $\chi''(\omega)$ is connected to thermal equilibrium fluctuations, the spectrum of which is quantified by the spectral density $J(\omega)$.^{12,13,21,22}

$$\text{Im}[\chi^*(\omega)] = \chi''(\omega) = \chi_0 \frac{\omega}{k_B T} J(\omega) \quad (14)$$

The static contribution is denoted as $\chi_0(\omega)$. In the time domain the FDT reads:^{6,12,13}

$$\chi(t) = -\frac{\chi_0}{k_B T} \frac{d}{dt} C(t) \quad (15)$$

Within the linear response theory, it can be shown that the time derivative of the correlation function $d/dt C(t)$ corresponding to the fluctuation spectrum $J(\omega)$, is identical to the step-response function, such as $G(t)$ for example.^{6,12} Under linear conditions the FDT provides the mentioned connection between the macroscopic relaxation of a system with respect to a (small) perturbation and the thermal fluctuations on microscopic scale in equilibrium.^{12,21,22} The macroscopic step response function $G(t)$, for instance, is the auto-correlation function of the (off-diagonal) components of the stress-tensor $\sigma_{\alpha\beta}$ in the shear plane.^{6,12,25}

$$G(t) = \frac{V}{k_B T} \langle \sigma_{\alpha\beta}(0) \sigma_{\alpha\beta}(t) \rangle \quad (16)$$

Here, α, β denote Cartesian components defining the shear plane. The stress tensor can be related to molecular quantities via the virial theorem.²⁶ It contains a kinetic and a potential energy contribution in terms of forces acting between particles. The dynamic viscosity formally assumes the role of the spectral density. It is defined as

$$\eta'(\omega) = G''(\omega)/\omega \quad (17)$$

and quantifies transport of momentum.^{12,13} However, in contrast to a spectral density, the dynamic viscosity is not normalized, as can be immediately seen from its zero-frequency limit, which is denoted as the zero-shear viscosity:

$$\eta_0 = \lim_{\omega \rightarrow 0} G''(\omega)/\omega = \int_0^{\infty} G(t)dt = G_0 \int_0^{\infty} C(t)dt = G_0 \langle \tau \rangle \quad (18)$$

Such a time integral over a correlation function given in eq. 18 is an example for a Green-Kubo relation.^{12,13} In analogy to eq. 7 the zero-shear viscosity is interpreted as a measure for the mean correlation time if the static contribution G_0 is divided out.

In section 1.7 it will be discussed that the spin-lattice relaxation rate dispersion $R_1(\omega)$ as the measurand in FC NMR, also reflects a spectral density $J(\omega)$. Via the FDT (eq. 14) an NMR susceptibility $\chi''_{NMR}(\omega)$ is formally defined as:

$$\chi''_{NMR}(\omega) := \omega R_1(\omega) \quad (19)$$

Later in this work it will be just denoted as $\chi''(\omega)$, for brevity. Also the NMR susceptibility representation is used to construct master curves $\chi''(\omega a_T)$ (cf. section 4.1) in the same way as in rheology, for instance.

1.2 “Glassy Dynamics” and the Glass Transition

When a liquid is cooled below its melting point T_m it is called “supercooled”. At even lower temperatures, *i.e.* below the glass temperature $T < T_g < T_m$ a supercooled liquid becomes a glass. Crystallization is avoided if the cooling rate is fast enough, while T_g itself depends on the cooling rate. The glass transition is not a typical phase transition, as even higher order derivatives of the thermodynamic potentials remain continuous. For temperatures below the melting point all correlation functions in supercooled liquids show some universal features. Those features, which also occur in polymers, are often summarized under the term “glassy dynamics”.^{27,28}

(i) Close to T_g time-correlation functions actually decay in two steps.^{29,30} On the time scale of *picoseconds* there is an initial decay caused by fast secondary relaxations, for instance vibrational modes, side-group dynamics (CH_3 group rotations) and the so-called “fast process”. At longer times and above T_g , the structural relaxation called α -process takes place, which is usually associated with the glass transition phenomenon. The α -process is isotropic and mainly involves inter-molecular re-arrangement effects in simple, low-molecular liquids. In high- M polymers intra-molecular energy barriers, like torsional potentials, play an additional role.²⁸

(ii) The correlation decay caused by the α -process is stretched-exponential,²⁷⁻³⁰ reflecting *i.a.* a distribution of correlation times due to the disorder in the liquid. Different distribution functions were proposed like the Cole-Davidson (CD), the Havriliak-Negami (HN) or the less popular “Kahlau” distribution.³¹⁻³³

(iii) The associated correlation time constant $\tau_\alpha(T)$ displays a super-Arrhenius temperature dependence. The α -process drives the glass transition phenomenon, meaning that transport coefficients like the viscosity $\eta_0(T)$ or the diffusion coefficient $D(T)$, are usually proportional to $\tau_\alpha(T)$ or to its inverse, respectively.³⁴ Around the glass transition temperature T_g solid-like values like $\tau_\alpha(T_g) \approx 100\text{s}$, $\eta_0(T_g) \approx 10^{12}\text{Pas}$ or $D(T_g) \approx 10^{-25}\text{m}^2\text{s}^{-1}$, are assumed.^{27-30,35,36} Thus, upon cooling, glass formers undergo a swift slow-down of the molecular dynamics within some 10K, during which the microscopic, amorphous structure of a liquid without long-range order is preserved. Other properties, like the thermal conductivity, the density or the refractive index, merely show subtle

discontinuity in their temperature dependence around T_g . The small, yet characteristic change in the heat capacity resulting from ergodicity breaking enables determining (the calorimetric) T_g^{cal} via thermal analysis like differential scanning calorimetry (DSC).³⁷ Phenomenologically, the super-Arrhenius temperature dependences of $\tau_\alpha(T)$ and $\eta_0(T)$ are often described by the Vogel-Fulcher-Tammann²⁷ (VFT) or the Williams-Landel-Ferry³⁸ (WLF) equation. These functions fail, however, when data on a broad temperature range has to be interpolated. Recently, Schmidtke et al. proposed another function also having three parameters, which satisfyingly describes $\tau_\alpha(T)$ “from the boiling point to the glass transition”.^{39,40}

(iv) Furthermore, in the regime of the α -process and for longer times the correlation functions $C_i(t)$ obey time-temperature superposition (TTS), the time-domain analogue of FTS. Hence, the shape of the correlation functions doesn't change with temperature: $C_i(t) = C_i(t/a_T)$.²⁷⁻³⁰

The probably most successful but not fully accepted theory dedicated to “glassy dynamics” is the mode coupling theory⁴¹⁻⁴³ (MCT), which is an attempt to describe the glass transition in terms of the time auto-correlation function of the particle density. Specifically, it is assumed that the density correlation function obeys a generalized Langevin equation with a memory term, the latter leading to mode-coupling as well as to a damping. The MCT reproduces all generic features of the glassy dynamics (i-iv) mentioned above, but fails below a critical temperature $T_c \approx 1.2T_g$, where the dynamics is predicted to become fully arrested. In order to avoid singularities occurring in the original MCT at temperatures below T_c the theory was extended, *e.g.* by the process of phonon-assisted hopping.⁴³⁻⁴⁵ Otherwise, simplifications concerning the mode coupling term of the original MCT were also proposed, the so-called “schematic” MCT's.⁴⁶⁻⁴⁹ Alternative approaches to the MCT are the “entropy theory of the glass formation”⁵⁰⁻⁵² or the “random first order transition theory”.⁵³ However, the physics of the glass transition is not completely understood yet, rendering it as “...the deepest and most interesting unsolved problem in solid state theory...”.⁵⁴

In polymers τ_α and T_g increase with growing chain length until a saturation is reached.⁵⁵⁻⁵⁹ As the slow, collective dynamics in polymers usually occurs well above T_g ($t \gg \tau_\alpha$), the systems investigated in the course of this work are glass formers with a relatively low T_g , typically well below 300 K. This leaves enough margins for shifting the slow polymer dynamics, showing up for $\omega\tau_\alpha \ll 1$, into the methodical frequency range. The glass transition also drives the polymer dynamics. In so-called rheologically simple systems time constants referring to cooperative (polymer) dynamics are proportional to $\tau_\alpha(T)$. If this is not the case the system is called rheologically complex.

In order to compare different methods with completely different frequency windows, like FC NMR and shear rheology, a common reference point, *e.g.* in the susceptibility spectra or in the correlation functions is required. The α -process, as the dominant relaxation mechanism being immanent in all liquids, poses the most suitable common reference. If it is covered by the measurements, the spectra can be scaled according to $\chi''_{NMR}(\omega\tau_\alpha)$ or $G^*(\omega\tau_\alpha)$, for instance. To cover the α -process, the condition $\omega\tau_\alpha(T) \approx 1$ must be fulfilled. In the studied low- T_g glass formers, τ_α is on the order of 10 ps at room temperature. Thus, FC NMR and in particular rheology, will not cover the α -process, unless the liquid is sufficiently cooled down. Due to the low frequencies accompanied by shear rheology, one has indeed to go down as low as T_g .

1.3 Polymer Chains: Structural Modelling

As linear polymers are important subjects of this work, some aspects of molecular modelling shall be summarized. Linear polymer chains are sequences of monomers of mass m_0 , the stereochemistry of which depends on the chemical composition. Above a certain length scale larger than that of the monomer, the dynamic properties are assumed to be generic. “Ideal” chain models are the simplest and most often encountered ones as they don’t take long-range interactions (like excluded-volume effects) into account. One such an ideal model is the “freely jointed chain”. The coarse-grained conformation of a chain constituted by N so-called Kuhn segments, each of length b (the Kuhn length), is idealized as a three dimensional random-walk. Consequently, the end-to-end distance $|\vec{r}_{ee}|$ follows a Gaussian distribution^{6,24,60-62}

$$W(|\vec{r}_{ee}|) = \left[\frac{3}{2\pi N b^2} \right]^{3/2} \cdot e^{-\frac{3}{2} \frac{r_{ee}^2}{N b^2}} \quad (20)$$

with the moments $\langle \vec{r}_{ee} \rangle = 0$ and $\langle r_{ee}^2 \rangle = N b^2 = L b$, where L denotes the chain contour length. The radius of gyration for an ideal chain is $R_G = \sqrt{\langle r_{ee}^2 \rangle / 6}$. Elastic Scattering techniques are suited to determine structural properties of molecules: by measuring the (time-averaged) scattering intensity $S(q)$ at different scattering wave vectors $|\vec{q}| = q$, properties like R_g (size), M_w (mass), the form factor (shape) and, if present, the static structure factor (spatial order) can be determined.⁶³⁻⁶⁷ A Kuhn segment usually incorporates several monomers (depending on flexibility), just to allow for the presumed Gaussian statistics (eq. 20). The associated molar mass is denoted as the Kuhn mass M_0 ($\geq m_0$). The parameter b (Kuhn-length) is related to the bond-length l via the characteristic ratio $C^\infty = \langle r_{ee}^2 \rangle / n l^2 = N b^2 / n l^2$ (n is the number of bonds). The quantity reflects the steric properties or, in other words, the “stiffness” of the chain.^{6,24,60-62} Other ideal chain models like the “freely rotating chain”, the “worm-like chain” or the “hindered rotation model” provide predictions for C^∞ .⁶² By introducing the Kuhn segment a coarse-graining is performed. All ideal models can be mapped to that of the “freely jointed chain”, provided that the chains are sufficiently long. Hence, the chemical structure and the chain stiffness are eluded. However, the question “when does a molecule become a polymer” (ref. 55) is experimentally difficult to answer, as Gaussian statistics develop asymptotically and may be observed only above $M \sim 50-100 m_0$.⁵⁵ Concerning real polymers in solution, excluded-volume interactions are relevant, which can be modeled by a self-avoiding-random walk, for which eq. 20 doesn’t hold of course. Yet, in polymer melts, in highly concentrated solutions or under Θ -conditions, respectively, attractive and repulsive forces exactly compensate, yielding zero net excluded-volume interactions and consequently ideal chain statistics.⁶⁸ This is the case for all polymer systems studied in the course of this work.

1.4 Unconstrained Polymer Dynamics: the Rouse Model

Due to its simplicity, analytical solvability and its success in describing experimental findings, the Rouse model^{6,24,5,69} is popular to explain the chain dynamics in un-entangled melts, *i.e.* when M is below the crossover molar mass M_c marking the beginning of entanglement effects in experiments (*cf.* sections 1.5 and 2). The N Kuhn segments forming a single chain are modeled as mass bearing “beads” connected by harmonic, entropic springs, each with a temperature dependent elastic constant $\kappa = 3k_b T b^{-2}$, reflecting intra-molecular interactions. Inter-molecular forces, such as those exerted by surrounding chains, are merely incorporated by the monomeric friction coefficient ζ and stochastic forces $\vec{f}_n^s(t)$ acting on the beads. Neglecting inertial terms, a coupled system of N coupled Langevin equations containing the bead positions $\vec{r}_n(t)$ and momenta $\partial/\partial t \vec{r}_n(t)$, is obtained. Often, a continuum approach^a is chosen:^{5,6,24,69}

$$\kappa \frac{\partial^2}{\partial n^2} \vec{r}_n(t) - \zeta \frac{\partial}{\partial t} \vec{r}_n(t) + \vec{f}_n^s(t) = 0 \quad (21)$$

The system (21) is solved by introducing normal coordinates $\vec{X}_p(t)$, with $p \in \{1, 2, \dots, N-1\}$:²⁴

$$\vec{X}_p(t) := N^{-1} \int_0^N \cos\left(n \frac{p\pi}{N}\right) \vec{r}_n(t) dn \quad \vec{r}_n(t) = \vec{X}_0(t) + 2 \sum_{p=1}^{N-1} \vec{X}_p(t) \cdot \cos\left(n \frac{p\pi}{N}\right) \quad (22)$$

The correlation functions of the orthogonal normal modes have the following property

$$\langle \vec{X}_p(t) \cdot \vec{X}_q(0) \rangle = \delta_{p,q} \frac{Nb^2}{2\pi^2 p^2} \cdot e^{-t/\tau_p} \quad (23)$$

and represent the probability that the p -th normal coordinate with relaxation time τ_p has not yet relaxed after time t .⁶ The associated correlation times read $\tau_p = \tau_s N^2/p^2$. The shortest and the longest correlation times occurring in the mode distribution are

$$\tau_s = \frac{\zeta b^2}{3\pi^2 k_b T} \quad \text{and} \quad \tau_R = \tau_{p=1} = \tau_s N^2, \quad (24)$$

respectively. The segmental relaxation time τ_s is usually identified with the time constant of the α -process, controlled by the glassy dynamics, *i.e.* $\tau_s \approx \tau_\alpha$. However, as is discussed in the context of PUB4 and PUB5, the ratio τ_α/τ_s actually may be smaller than unity. The Kuhn segment, relevant for the Gaussian statistics of the whole chain, is usually larger than the smallest unit relevant for local re-orientations. The longest (terminal) time τ_R is called Rouse time. The zeroth mode $\vec{X}_0(t)$ reflects the MSD of the center-of mass (cm) $\vec{r}_{\text{cm}} = N^{-1} \sum_{n=1}^N \vec{r}_n$, the MSD of which follows from eq. 22:

$$\langle (\vec{r}_{\text{cm}}(t) - \vec{r}_{\text{cm}}(0))^2 \rangle = \langle [\vec{X}_0(t) - \vec{X}_0(0)]^2 \rangle = \frac{6k_b T}{\xi} \frac{t}{N} := 6D_R t \quad (25)$$

Thus, the Rouse cm diffusion coefficient scales with the inverse molar mass, *i.e.* $D_R \propto M^{-1}$.

^a The continuum approach often faced in the literature causes mathematical artifacts for very short chains.^{70,71}

The auto-correlation function of the end-to-end vector $\vec{r}_{ee}(t) = \vec{r}_N(t) - \vec{r}_0(t)$ is detected by dielectric spectroscopy (DS) (cf. section 2) in the case of type-A polymers.⁷² The Rouse model predicts

$$\langle \vec{r}_{ee}(t) \cdot \vec{r}_{ee}(0) \rangle = 16 \sum_{p=1,3,5,\dots}^{N-1} \langle \vec{X}_p(t) \cdot \vec{X}_p(0) \rangle = Nb^2 \frac{8}{\pi^2} \sum_{p=1,3,5,\dots}^{N-1} \frac{1}{p^2} e^{-p^2 \frac{t}{\tau_R}} \quad (26)$$

yielding a multi-exponential decay. Due to the weighting with p^{-2} the sum is, however, dominated by the $p = 1$ term reflecting the time scale τ_R , the longest Rouse time. Expression 26 describes what is frequently called “normal mode relaxation”. The MSD of the n -th segment is also readily calculated from eq. 22:²⁴

$$\langle (\vec{r}_n(t) - \vec{r}_n(0))^2 \rangle = 6D_R t + \frac{4Nb^2}{\pi^2} \sum_{p=1}^{N-1} \frac{1}{p^2} \cos^2 \left(p \frac{\pi n}{N} \right) \left[1 - e^{-p^2 \frac{t}{\tau_R}} \right] \quad (27)$$

It can be split into the cm diffusion and the segmental diffusion relative to the cm, the latter depending on the Kuhn segment index n , *i.e.* on the position along the chain. In experiments, it is hardly possible to trace the MSD of single segments. Instead, eq. 27 is averaged over the whole chain; the result features two regimes:²⁴

$$\langle r^2(t) \rangle = N^{-1} \sum_{n=1}^N \langle (\vec{r}_n(t) - \vec{r}_n(0))^2 \rangle = \begin{cases} b^2 (t/\tau_s)^{1/2} & \tau_\alpha < t < \tau_R \\ 6D_R t & t > \tau_R \end{cases} \quad (28)$$

The segmental MSD is first sub-diffusive in the Rouse regime, *i.e.* for $t < \tau_R$. At long times, the center of mass diffusion takes over and the MSD becomes linear. As will be shown in section 1.7, the segmental MSD controls the inter-molecular correlation function $C_{inter}(t)$, and thus the inter-molecular relaxation dispersion $R_1^{inter}(\omega)$. The auto-correlation function of the bond vector $\vec{b}_i = \vec{r}_i - \vec{r}_{i-1} \cong \partial \vec{r} / \partial n$ connecting adjacent Kuhn segments is sensitive to segmental re-orientation. After averaging over the whole chain, the following expression again featuring two limiting cases is obtained:

$$\langle \vec{b}(t) \cdot \vec{b}(0) \rangle \approx \frac{b^2}{N} \sum_{p=1}^{N-1} e^{-p^2 \frac{t}{\tau_R}} \propto \begin{cases} b^2 (t/\tau_s)^{-1/2} & \tau_\alpha < t < \tau_R \\ N^{-1} b^2 e^{-t/\tau_R} & t > \tau_R \end{cases} \quad (29)$$

The terminal relaxation of the bond vector correlation function is exponential, while a power-law results at short times (Rouse regime). $\langle \vec{b}(t) \cdot \vec{b}(0) \rangle$ is proportional to the 1st rank re-orientational correlation function $C_1(t)$.³ The 2nd rank re-orientational correlation function in the Rouse model describing the re-orientation of Kuhn segments reads:^{19,20}

$$C_2(t) = 3b^{-4} \langle \vec{b}(t) \cdot \vec{b}(0) \rangle^2 \propto \langle r^2(t) \rangle^{-2} \propto C_1^2(t) \quad (30)$$

Basically, eq. 30 is not only valid for Rouse dynamics, but for any other spatially isotropic model of polymer dynamics.⁷³⁻⁷⁵ In isotropic models it is assumed that segmental displacements lose correlation with respect to the chain's initial conformation already after short times ($t > \tau_s$). As will be discussed in section 1.7, the intra-molecular relaxation dispersion $R_1^{intra}(\omega)$ is proportional to the Fourier transform of the squared bond vector correlation function (cf. section 1.7).^{6,73-76}

An important difference between the end-to-end vector correlation function $\langle \vec{r}_{ee}(t) \cdot \vec{r}_{ee}(0) \rangle$ (eq. 26) on the one hand and the bond vector correlation function $\langle \vec{b}(t) \cdot \vec{b}(0) \rangle$ (eq. 29) as well as the

segmental MSD $\langle r^2(t) \rangle$ (eq. 28) on the other, is the different weighting of the modes. While $\langle \vec{r}_{ee}(t) \cdot \vec{r}_{ee}(0) \rangle$ is a multi-exponential process governed by the mode numbers with the lowest indices and (essentially) reflects the relaxation time τ_R , $\langle \vec{b}(t) \cdot \vec{b}(0) \rangle$ and $\langle r^2(t) \rangle$ are more sensitive to the whole mode distribution. This results in the sub-diffusive power-law regime.

Concerning stress relaxation, each Rouse mode provides an equitable relaxation pathway. The (normalized) correlation function $\langle X_p^\alpha(t) \cdot X_p^\alpha(0) \rangle \propto \exp[-t/\tau_p]$ corresponds to the probability that the Cartesian component α of the p -th Rouse mode with relaxation time τ_p hasn't relaxed yet after the time t has passed, thus sustaining stress.⁶ Shear stress involves two components (α, β) in the shear-plane, therefore the probability of sustaining the stress is given by $\langle X_p^\alpha(t) \cdot X_p^\alpha(0) \rangle \langle X_p^\beta(t) \cdot X_p^\beta(0) \rangle \propto \exp[-2t/\tau_p]$. After summation over all modes $G(t)$ adopts:

$$G(t) = G_0 \sum_{p=1}^{N-1} e^{-2p^2 \frac{t}{\tau_R}} \propto \begin{cases} G_0 (\tau_R/t)^{-1/2} & t < \tau_R \\ G_0 e^{-2t/\tau_R} & t > \tau_R \end{cases} \quad (31)$$

The static shear modulus (cf. eq. 18) $G_0 = \rho N_A k_B T M^{-1}$ obtained for $t \rightarrow 0$, depends on the mass density ρ and the inverse molar mass M , hence on monomeric properties exclusively.^{6,24,60-62} The zero-shear viscosity is proportional to the molar mass, i.e. $\eta_0 = \int G(t) dt \propto M$. For the complex frequency domain shear modulus $G^*(\omega)$ the following predictions result from the Rouse model which can be deduced by inserting eq. 31 into eq. 12:

$$G'(\omega) \propto \begin{cases} G_0 (\omega \tau_R)^{1/2} \\ G_0 (\omega \tau_R)^2 \end{cases} \quad G''(\omega) \propto \begin{cases} G_0 (\omega \tau_R)^{1/2} & \omega < \tau_R^{-1} \\ G_0 \omega \tau_R & \omega > \tau_R^{-1} \end{cases} \quad (32)$$

In the Rouse regime power-laws result while at long times the behavior of a Newtonian Fluid is obtained. Although phenomena like chain stiffness or torsional energy barriers are not taken into account, the Rouse model is successfully applied to polymer melts and also to concentrated solutions of short chains ($M < M_c$), where entanglement is not yet relevant. Examples will be given in section 2. The Rouse model fails, however, for polymers in dilute solution as neither, hydrodynamic nor excluded volume interactions, are explicitly taken into account. For instance, $D_{cm} \propto M^{-0.6}$ is observed in solution, instead of $D_R \propto M^{-1}$ expected for melts of short chains (cf. eq. 25).⁷⁷ Furthermore, viscosimetric experiments on dilute polymer solutions reveal a weaker M -dependence of the (intrinsic) viscosity of $[\eta] \propto M^{0.5 - 0.75}$, instead of $[\eta] \propto M^1$, expected for Rouse dynamics in the melt.^{78,79} The more general, but non-linear Zimm model for polymers in solution explicitly takes hydrodynamic couplings into account.⁸⁰

1.5 Entangled Polymer Dynamics: the Tube-Reptation Model

The Rouse model is also insufficient for describing the dynamics of longer chains, *e.g.* in the melt state. Above the crossover molar mass M_c , the zero-shear viscosity η_0 and the terminal relaxation time τ_t of a polymer melt obtained by shear rheology, for instance, scale $\propto M^{3.4-3.7}$. The Rouse model, however, predicts much weaker dependences, $\eta_0 \propto M$ and $\tau_R \propto M^2$, respectively (*cf.* section 1.4).^{24,69,81-84} Likewise, the diffusion coefficient is known to scale $D \propto M^{-2.0-2.4}$, instead of $D_R \propto M^{-1}$ predicted for Rouse dynamics.⁸⁵⁻⁸⁷ The Rouse model alone is obviously not appropriate for high M .

The Rouse model doesn't imply any topological constraints underlying the uncrossability of chains, termed entanglements. DeGennes' reptation idea⁸⁸ according to which a polymer chain diffuses back- and forth along its contour in a worm-like motion between fixed obstacles (reptation), together with the tube-concept by Doi and Edwards,^{89,90} led to the phenomenological tube-reptation (TR) model.²⁴ Topological constraints in an entangled polymer melt are assumed to resemble those in an immobile network. Below, the ideas of the TR model are briefly outlined.

At short times $\tau_s < t < \tau_e$ (Rouse regime (I)) where τ_e denotes the entanglement time, segmental displacements are small and not influenced by entanglements yet. The segmental motion is assumed to be describable by the Rouse model, implying $\langle r^2(t < \tau_e) \rangle \propto t^{1/2}$. At $t > \tau_e$ the allowed configuration space for a single "tagged" chain is restricted by the presence of neighboring chains. In the TR model these topological constraints reduce the accessible space to a tube-like region of radius a_0 . The radial extension of the tube, reflected in a_0 , is on the order of the mean distance between entanglements comprising $N_e = M_e/m_0$ Kuhn segments. The average molar mass between adjacent entanglements along a chain is the entanglement molar mass M_e . The crossover molar mass M_c marking the onset of entanglement effects in experiments, is typically 2-4 times higher than M_e .⁶⁰ By introducing the fictitious tube the many-chain problem is reduced to a single chain problem. The tube represents all the possible chain configurations that are compatible with the topological constraints given at a time. The tube contour, called primitive path, is assumed to have a Gaussian configuration with $Z = M / M_e$ steps, evoking the equivalence $\langle r_{ee}^2 \rangle = Nb^2 = Za_0^2$. This readily leads to the relation $a_0 = N_e b^2$.

At times $t > \tau_e$ the MSD approaches the tube dimensions, *i.e.* $\langle r^2(\tau_e) \rangle = a_0^2$. Segmental motion by Rouse dynamics perpendicular to the primitive path becomes constrained, while parallel 1D-motion along the primitive path is still free. Be $s(t)$ the curvilinear displacement of the tagged chain along the primitive path defining the tube, with $s(t) \geq a_0$. Then, the MSD in 3D of a segment confined in the tube is given by $\langle r^2(t > \tau_e) \rangle \approx a_0 \langle s^2(t) \rangle^{0.5}$. In analogy to Rouse diffusion the mean square displacement along the primitive path features a sub-diffusive and a diffusive regime. As a result, the segmental MSD first scales according to $\langle r^2(t) \rangle \propto t^{1/4}$ at times $\tau_e < t < \tau_R$, where $\langle s^2(t) \rangle \propto t^{0.5}$. This regime (II) is called "constrained Rouse" regime. Beyond the Rouse time at $\tau_R < t < \tau_d$, curvilinear 1D diffusion of the whole chain along the primitive path ($\langle s^2(t) \rangle \propto t$) governs the dynamics as the Rouse mode spectrum ends with τ_R . The term "reptation" (*latin: "reptare"; to creep*) was coined for this collective back-and-forth motion constituting regime III, which is accompanied by $\langle r^2(t) \rangle \propto t^{1/2}$. Hence, the dynamics becomes anisotropic and the segmental displacement is strongly correlated with the chain's initial configuration at $t = 0$. The terminal time of the TR model is the disengagement time τ_d , which is determined by the diffusion of the primitive path, *i.e.* of the tube itself. At the ends of the tagged chain the tube is continuously destroyed and renewed. The averaged segmental MSD

obeys the relation $\langle r^2(t) \rangle \propto t$ and is governed by the center-of-mass diffusion of the whole chain in this terminal regime (IV). The dynamics at $t > \tau_d$ finally becomes (normal) diffusive as in any liquid. The associated diffusion constant $D_{TR} = 3D_R a_0^2 / Nb^2 \propto M^{-2}$ scales with the inverse of the squared molar mass.

Altogether, the TR model incorporates the Rouse model and predicts the four hierarchical power-laws mentioned. They are separated by the time constants $\tau_e(T)$, $\tau_R(T)$ and $\tau_d(T)$, respectively, which feature distinct M -dependences and read as follows:

$$\tau_s = \frac{\zeta b^2}{3\pi^2 k_B T} \quad \tau_e = \tau_s \left(\frac{M_e}{M_0} \right)^2 = \tau_s N_e^2 \quad \tau_R = \tau_s \left(\frac{M}{M_0} \right)^2 = \tau_s N^2 \quad \tau_d = 3\tau_s \frac{N^3}{N_e} \quad (33)$$

Those time constants delimit the polymer-specific dynamic regimes I-III, also called Doi/Edwards (DE) limits. The scaling of the MSD in regimes II and III is considered as the “fingerprint” of the tube model. The predictions for the segmental MSD $\langle r^2(t) \rangle$ resulting for the different regimes are illustrated in Fig. 1 and are later on tabulated in Table 1 (section 1.7).

The correlation function of the end-to-end vector at times $\tau_e < t < \tau_d$ reads²⁴

$$\langle \vec{r}_{ee}(t) \cdot \vec{r}_{ee}(0) \rangle = Z a_0^2 \frac{8}{\pi^2} \sum_{p=1,3,5,\dots}^{N-1} \frac{1}{p^2} e^{-p^2 \frac{t}{\tau_d}} := Z a_0^2 \cdot \mu(t) \quad (34)$$

and resembles eq. 26 following from the Rouse model, with τ_R replaced by τ_d . The relaxation described by eq. 34 is again multi-exponential and is dominated by the longest relaxation times, in particular by the tube disengagement time τ_d . As said, the normal mode relaxation in eq. 34 is the relevant correlation function for dielectric spectroscopy as well as for shear rheology in the entanglement regime, *i.e.* for times $\tau_e < t < \tau_d$ (*cf.* section 2).

As in the Rouse model, $\langle \vec{r}_{ee}(t) \cdot \vec{r}_{ee}(0) \rangle$ is less sensitive to the whole mode distribution than $\langle r^2(t) \rangle$. Due to the different weighting of modes the MSD is characterized by two power-law regimes II and III, while the end-to-end vector correlation function on the other hand merely reflects the relaxation of the longest modes, especially the tube disengagement process, as said. In the TR model the normal mode relaxation function (eq. 34) is also interpreted as the tube occupancy function $\mu(t)$.³ The latter reflects the fraction of the initial tube not yet attended by a chain end and thus surviving over time t .²⁴ Otherwise, if a tube segment is visited by a chain end, the tube segment ceases to exist.

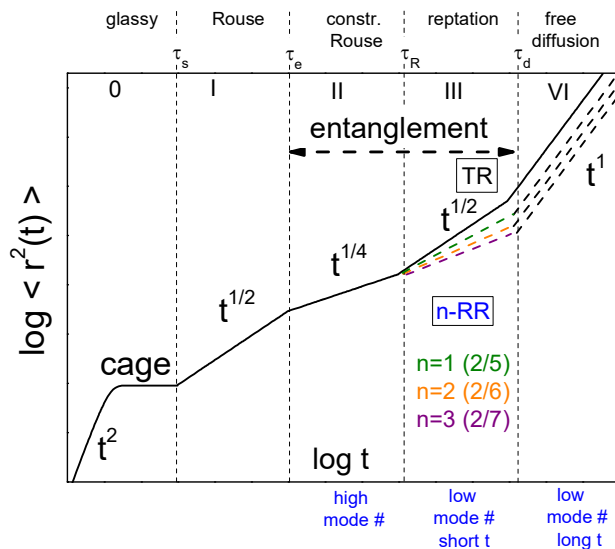


Figure 1: Predictions of the tube-reptation model²⁴ (TR, black) as well as of the n-renormalized Rouse model⁵ (n-RR, blue), respectively, for the segmental mean square displacement $\langle r^2(t) \rangle$. The dynamic regimes I-III are specific for polymers. At shortest times ($t < \tau_s$) and as in any liquid, the dynamics is first ballistic until the caging effect confines translations (“glassy dynamics” (0)).

Concerning the correlation functions $C_{1,2}(t)$ and the bond vector correlation function, the latter being relevant for the intra-molecular relaxation dispersion $R_1^{intra}(\omega)$ in NMR (*cf.* section 1.7), the disengagement process leads to $C_{1,2}(t) \propto \langle \vec{b}(t) \cdot \vec{b}(0) \rangle \propto e^{-t/\tau_d}$ at longest times. Straightforward predictions for regimes II and III of the TR model haven't been derived, yet. Instead, further phenomenological assumptions are made. Specifically, it is argued that the re-orientational correlation function $C_1(t)$ defined in eq. 5 reflects the probability that a segment remains in or returns to its initial tube section after time t .³ Given the Gaussian statistics of the tube axis (primitive path), it follows that $C_1(t) \propto (2\pi \langle s^2(t) \rangle)^{1/2} = p_{RTO}$.^{3,20,88} The right hand side is the so-called return-to-origin probability. Similarly, $C_2(t)$ is interpreted as the probability that the mean square displacement along the primitive path $s(t)$ doesn't exceed the tube radius, *i.e.* that $C_2(t) \propto p(\langle s^2(t) \rangle \leq a_0^2)$.^{3,20,88,128} Ball et al. related this probability to the return-to-origin probability in the sense that $p(\langle s^2(t) \rangle < a_0^2) \propto p_{RTO}$. These considerations lead to the important scaling relation

$$C_1(t) \propto C_2(t) \propto \langle r^2(t) \rangle^{-1} \quad (35)$$

This is the so-called return-to-origin (RTO) hypothesis (*cf.* section 1.7). It states that re-orientation is strongly coupled to translation, if the tube is sufficiently rigid. Orientational correlation survives over time if a segment returns to (or remains in) its original tube segment. Reptation of a chain, *i.e.* its 1D random-walk along the primitive path of the tube, also leads to segmental re-orientation, except for the case that the initial position is attained, the likelihood of which is estimated to be proportional to the inverse MSD. Then, according to the RTO hypothesis, the segmental re-orientation is preserved or regained, respectively. A qualitatively different relation between $C_{1,2}(t)$ and $\langle r^2(t) \rangle$ than eq. 35 follows from isotropic models like the (renormalized) Rouse model. Note for instance, that $C_2(t) \propto \langle r^2(t) \rangle^{-2}$ holds in the Rouse regime (*cf.* eq. 30, section 1.4). The ability of FC NMR relaxometry to probe $C_2(t)$ as well as $\langle r^2(t) \rangle$ predestines the technique for a critical inspection of the RTO hypothesis.

Entanglement causes the so-called rubber plateau in the shear relaxation modulus $G(t)$. Within the TR model this rubber-elastic regime is explained that stress will only relent to an applied strain when the chains completely "reptate" out of their original tube, *i.e.* $G_{tube}(\tau_e < t < \tau_d) \approx G_p \mu(t)$, where $\mu(t)$ is again the tube survival function (eq. 34).⁶ The plateau modulus G_p is an M -independent material constant from which M_e can be estimated explicitly.³ Formally, it has the meaning of a dynamic order parameter. The contribution to the shear relaxation function by reptation is:³

$$G_{tube}(t) \propto G_p \sum_{p=1,3,5,\dots}^{N-1} \frac{1}{p^2} e^{-p^2 \frac{t}{\tau_d}} \quad (36)$$

The zero-shear viscosity, following from integration over $G(t)$, is determined by the disengagement time τ_d ; hence $\eta_0 \propto M^3$. The complex shear modulus in the entanglement regime follows from eq. 36 and again Fourier transform according to eq. 12:

$$G'_{tube}(\omega) \propto \begin{cases} G_p & \tau_e < t, \omega^{-1} < \tau_d \\ G_p \omega^2 & t, \omega^{-1} > \tau_d \end{cases} \quad G''_{tube}(\omega) \propto \begin{cases} G_p \omega^{-1/2} & \tau_e < t, \omega^{-1} < \tau_d \\ G_p \omega^1 & t, \omega^{-1} > \tau_d \end{cases} \quad (37)$$

However, eqs. 36 and 37 don't take Rouse modes into account, yet. The full form of $G(t)$ including free as well as constrained Rouse modes reads according to Likhtman and McLeish:²⁰

$$G(t) = G_p \left(\mu(t) + \frac{1}{5} \sum_{p=1}^{Z-1} \exp(-p^2 t / \tau_R) + \frac{1}{Z} \sum_{p=Z}^N \exp(-2p^2 t / \tau_R) \right) \quad (38)$$

The first term describes the tube relaxation process (regimes III, IV) while the latter two ones represent constrained (II) as well as unconstrained (I) Rouse modes (*cf.* eq. 31), respectively. The Fourier transform of eq. 38 provides the the complex shear modulus $G^*(\omega)$. For an entangled, linear polymer melt the imaginary part of $G^*(\omega)$, the loss modulus $G''(\omega)$, is sketched in Fig. 28 (top) of section 5.5, as it would result from the TR model. Again, four different power-law regimes are obtained.

Experiments in the melt reveal M -dependences of transport coefficients, which are stronger than predicted by the TR model, for instance $\eta_0, \tau_t \propto M^{3.4 - 3.7}$ and $D \propto M^{-2.0 - 2.4}$ (see above and section 2). These deviations led to modifications of the original TR model by adding additional relaxation mechanisms.⁹¹⁻⁹⁴ The most prominent ones are fluctuations of the chain contour length and constraint release.

In real chains the contour length fluctuates with time. Such contour-length fluctuations (CLF), which were already suggested by Doi,^{24,95,96} pose an additional relaxation mechanism for single chains. CLF effectively lead to a loosening of the tube constraints at the chain ends, *i.e.* a_0 increases and the tube effectively widens. Likhtman and McLeish take this effect into account by a modification of the tube survival function at short times ($t < \tau_R$):⁹⁷

$$\mu_{CLF}(t) = 1 - \frac{1.5M_e}{M} \left(\frac{t}{\tau_e} \right)^{1/4} \quad \tau_e < t < \tau_R \quad (39)$$

The long time behavior ($t > \tau_R$) of $\mu(t)$ is described by eq. 34, yet, with an effectively reduced disengagement time according to:⁹⁷

$$\tau_d^{CLF} = \tau_d \left[1 - c_1 (M)^{-0.5} + c_2 (M)^{-1} + \dots \right] \quad (40)$$

The factor of 1.5 in eq. 39 and the constants c_i in eq. 40 arises from a numerical optimization. CLF lead to increased molar mass dependences of τ_d and η_0 , with respect to the original tube model. Thus, CLF explains the experimentally observed exponents. A first direct experimental proof of CLF succeeded via neutron spin echo (NSE) spectroscopy (*cf.* chapter 2) on poly(ethylene) (PE).⁹⁸ The findings were later supported by another NSE work on poly(butadiene) (PB) chains, where only the center section was labelled (protonated) while the ends were disguised by deuteration.⁹⁹ Such pseudo-triblock copolymers are also subject of PUB2 and section 5.2, where FC ^1H NMR results are reported. Yet, CLF can't impact on the diffusion coefficient D , therefore the effect cannot explain the mentioned discrepancies between theory and experiment alone. Graessley suggested that parts of chains can "leak" the strict tube confinement assumed in the original TR model. This enables some lateral movement in regimes II and III.^{100,101} This "constraint release" (CR) is a further relaxation mechanism, taking into account that the tube is actually mobile all over and not only at its ends, as the neighboring chains forming the tube, also move. It is a coherent relaxation process involving many chains, in contrast to CLF. Graessley treated the tube dynamics by a Rouse-like model. As his original ansatz is at variance to some experimental observations,¹⁰² the modelling of CR was refined by Rubinstein and Colby¹⁰³ and later on by Likhtman and McLeish.⁹⁷ The latter propose to add the following relaxation function at short times ($t < \tau_R$):

$$R_{CR}(t) = 1 - \frac{1.8M_e}{M} \left(c_v \frac{t}{\tau_e} \right)^{1/4} \quad \tau_e < t < \tau_R \quad (41)$$

The parameter $0 \leq c_v \leq 1$ characterizes the mobility of the tube. For long times $t > \tau_R$ the Likhtman/McLeish model doesn't apply, which is, however, unproblematic, as here the exponential decay of the tube survival function $\mu(t)$ (eq. 34) dominates anyway. Zamponi et al. provided the first experimental proof of CR using NSE spectroscopy.¹⁰⁴ Summarized, the full form of the end-to-end vector correlation function in the entanglement regime reads:

$$\langle \vec{r}_{ee}(t) \cdot \vec{r}_{ee}(0) \rangle \propto \mu(t) \mu_{CLF}(t) R_{CR}(t) \quad (42)$$

Of course, the corrections appearing in eq. 42 can be applied to $\mu(t)$ in the shear relaxation function (eq. 38) as well. The Likhtman/McLeish theory likely poses the most rigorous treatment incorporating CR as well as CLF. It was successfully applied to fit rheological and dielectric data simultaneously.¹⁰⁵ Graessley conjectured that the predictions of the TR model are approached asymptotically with growing M , so that it becomes appropriate only for $M > M_{rep} \gg M_c$ due to finite length effects.⁶¹ This transition is indeed realized in the Likhtman/McLeish theory when M becomes very large (cf. eqs. 39-41). Experimentally, finite length effects indeed asymptotically disappear for very high $M \gg M_c$, i.e. at a second crossover mass. Then, the predictions of the TR model are essentially reproduced (cf. Figs. 5 and 8).¹⁰⁶⁻¹⁰⁹ It is finally noted that the TR model can also be adapted to semi-dilute polymers using scaling arguments.⁸⁷

1.6 Generalized Rouse Models

As an alternative to the phenomenological TR model, Schweizer adapted a generalized form of the Langevin equation to polymers, which is also known as the polymer mode coupling theory (PMCT, cf. section 1.2).^{45,110,111} The bead-and-spring system of the Rouse model (eq. 21) is extended by a memory matrix intended to take entanglement effects into account, by mimicking a time and position dependent “non-local” friction. A special choice of the memory matrix leads to the renormalized Rouse model (RR) proposed by Kimmich and Fatkullin.⁵ Like the TR model, the RR model predicts a family of four hierarchical power-law regimes for $\langle r^2(t) \rangle$. It incorporates the standard Rouse regime at short times and a diffusive one at long times. At time scales where entanglement is relevant, two further intermediate sub-diffusive power-law regimes in $\langle r^2(t) \rangle$ are predicted, as in the case of the TR model. In the first renormalization, the memory matrix describing entanglement at long times is related to the segmental MSD as provided by the ordinary Rouse model. For the second renormalization, the memory matrix is related to the MSD resulting from the once renormalized Rouse model and so on.⁵ The degree of recursive normalizations is physically only reasonable for $n \leq 3$, thus one distinguishes between once, twice and thrice renormalization.⁵ The regime transition times depend not only on M in a different way than in the TR model, but partially also on the number of recursive renormalizations n . Yet, also the RR model is purely phenomenological. In Fig. 1 (section 1.5) the predictions for $\langle r^2(t) \rangle$ following from the once, twice and thrice RR model are outlined, in comparison to that of the TR model.

In the so-called “high mode number” limit succeeding the ordinary Rouse regime, $\langle r^2(t) \rangle \propto t^{1/4}$ is predicted by the n -RR model, for all degrees of renormalization. As this exponent coincides with that of the constrained Rouse dynamics, this regime is of limited meaningfulness for distinguishing

between the TR and the RR model. In the “low mode number - short time limit” occurring at longer times, $\langle r^2(t) \rangle \propto t^{-2/(n+4)}$ depends on n and values different than that of the reptation regime of the TR model result. Here, both models can indeed be distinguished. Finally, in the terminal regime of the n-RR model called “low mode number - long time limit”, *i.e.* at $t > \tau_t^{nRR}$ the MSD becomes linear in time. It is noted that the n-RR model predicts $\tau_t^{nRR} \propto M^{n/2+2}$ for the M -dependence of the terminal relaxation time and $D^{nRR} \propto M^{-(n/2+1)}$ for the diffusion coefficient. Thus, the forecasts of the thrice RR model conform to experimental observations quite well. In contrast to the TR model, the RR model is isotropic at all times, therefore $\langle \vec{b}(t) \cdot \vec{b}(0) \rangle \propto \langle r^2(t) \rangle^{-1}$ holds in general (*cf.* eq. 30).⁷³⁻⁷⁵ As already mentioned, FC ^1H NMR with its sensitivity to intra- as well as inter-molecular relaxation, allows to confront predictions of the TR vs. the RR model. In PUB 2 and section 5.2 it is discussed that re-orientation of polymers is describable rather in favor of the RR than the TR model. The RR model was already used by Kimmich and co-workers to describe FC NMR relaxation data.^{6,73-76,112,113}

Another generalization of the Rouse model is generalized Gaussian structures (GGs).¹¹⁴ By introducing a connectivity matrix, arbitrary topologies of molecules can be realized via systems of Langevin equations. GGS are used to model complex molecular geometries such as dendrimers, star-like polymers or semi-flexible linear chains, usually based on bead-and spring systems.¹¹⁵⁻¹¹⁷

1.7 Intra- and Inter-Molecular Relaxation in ^1H

In this section it is briefly explained how molecular dynamics in terms of $\langle r^2(t) \rangle$ and $C_2(t/\tau_\alpha)$, is related to the spin-lattice relaxation rate dispersion $R_1(\omega)$ measured by FC ^1H NMR. In particular, it is distinguished between intra- as well as inter-molecular relaxation. The proton (^1H , nuclear spin $I = 1/2$) is the most favorable nucleus for FC NMR for several reasons: with $\gamma = 42.6 \text{ MHz/T}$ it possesses the second largest gyromagnetic factor at all, only that of ^3H is slightly higher.¹¹⁸ Hydrogen is the most abundant atom in the universe and with a share of 99.99%, ^1H is the most abundant isotope. As such, it is omnipresent in organic compounds like polymers. Thus, ^1H offers by far the highest signal, which is beneficial at the still comparatively low detection fields available in FC NMR. The dominating interaction among ^1H is the magnetic dipole-dipole interaction $H_{DD}(t)$, the Hamiltonian of which reads in Cartesian coordinates^{75,119-121}

$$H_{DD}(t) = -\frac{\mu_0}{4\pi} (\hbar\gamma)^2 \cdot \sum_{\substack{\text{spin} \\ \text{pairs}}} |\vec{r}_{ij}(t)|^{-3} \left[3(\vec{I}_i \cdot \vec{e}_{ij}(t))(\vec{I}_j \cdot \vec{e}_{ij}(t)) - \vec{I}_i \cdot \vec{I}_j \right] \quad (43)$$

with $\vec{e}_{ij}(t) = \vec{r}_{ij}/|\vec{r}_{ij}|$ denoting the unit vector connecting two magnetically equivalent spins i and j , respectively, and \vec{I} is the spin vector operator. Higher order interactions involving more than two spins are neglected for simplicity. Nevertheless, the dipolar interaction has many-particle character. The assumed spin pairs display four eigenstates in the Zeeman product basis, two of which are degenerate as both spins are alike. The dipolar interaction acts directly through space. It is sensitive to relative translations and rapidly decreases with the inter-nuclear distance r_{ij} . H_{DD} also depends on the relative orientation of the spins, *i.e.* it also senses rotation. The local magnetic field at the position of each spin generated by its neighbors fluctuates. Thus, the dynamics of molecules bearing the spins leads to a time dependence of $H_{DD}(t)$. H_{DD} generally contains both, secular as well as non-secular components and is considered as a small perturbation to the much stronger Zeeman

interaction $H_z = -\vec{\mu} \cdot \vec{B}$. In liquids H_{DD} is essentially averaged to zero by rapid and isotropic molecular motion, unless the dynamics is sufficiently slowed down, for example during the glass transition at temperatures close to T_g . Then, the dipolar coupling becomes detectable in the spectrum as it leads to line broadening. Otherwise, in systems with spatial long-term order such as liquid crystals, rubbers or entangled polymers, a residual dipolar coupling (RDC) occurs, although motion is rapid. This also leads to spectral line broadening, which can be a valuable source of information (*cf.* section 2). The fluctuations of the non-secular components of H_{DD} do not affect the NMR spectrum but are responsible for spin relaxation.¹²²

The following, well-known expression for the relaxation rate can be derived from time-dependent 2nd order perturbation theory^{75,76,119}

$$R_1(\omega) = \frac{6\pi}{5} \left(\frac{\mu_0}{4\pi} \right)^2 \hbar^2 \gamma^4 \left[\int_0^\infty A_1(t) \cos(\omega t) dt + 4 \int_0^\infty A_2(t) \cos(2\omega t) dt \right] \quad (44)$$

where $A_m(t)$ are second-rank ($l = 2$) autocorrelation functions

$$A_m(t) = n_s^{-1} \sum_{\text{spin pairs}} \left\langle \frac{Y_{2,m}(\vec{e}_{ij}(t))}{r_{ij}^3(t)} \cdot \frac{Y_{2,m}^*(\vec{e}_{ij}(0))}{r_{ij}^3(0)} \right\rangle \quad (45)$$

and n_s is the spin volume density. The occurrence of $A_1(t)$ and $A_2(t)$ in eq. 44 stems from single and double quantum transitions between the four energy states related to the non-secular components of $H_{DD}(t)$.¹²³ In isotropic systems like liquids, the dependence on the index m can be dropped, *i.e.* $A_m(t) = A_0(t)$ and the spherical harmonics reduce to the 2nd rank Legendre polynomial.

$$A_0(t) = \frac{5}{16\pi} n_s^{-1} \sum_{\text{spin pairs}} \left\langle \frac{3\cos^2(\vartheta(t)) - 1}{r_{ij}^3(t)} \cdot \frac{3\cos^2(\vartheta(0)) - 1}{r_{ij}^3(0)} \right\rangle \propto C_{DD}(t) \quad (46)$$

After normalization, the dipolar correlation function $C_{DD}(t) := A_0(t)/A_0(0)$ is gained (*cf.* eq. 4). As it correlates fluctuations with respect spin pairs, $C_{DD}(t)$ is a pair-correlation function. Furthermore, $C_{DD}(t)$ depends on relative translational displacements between nuclei as well as on the alignment in space, *i.e.* the orientation of the inter-nuclear vector. The cos-transformation provides the normalized dipolar spectral density:¹⁸

$$J_{DD}(\omega) = \int_0^\infty C_{DD}(t) \cos(\omega t) dt \quad (47)$$

Hence, eq. 44 can be rewritten to the well-known Bloembergen-Purcell-Pound (BPP) equation,¹²³ with K denoting the dipolar coupling constant:

$$R_1(\omega) = K[J(\omega) + 4J(2\omega)] \approx 5KJ(\omega) \quad (48)$$

As the spectral density $J(\omega)$ encountered in complex liquids is very broad, the difference between the single quantum $J(\omega)$ and the double quantum component $J(2\omega)$ is negligible, *i.e.* $J(\omega) \approx J(2\omega)$ holds in approximation, when discussed on logarithmic scales.^b The coupling constant is related to the second moment M_2 , which reads for $l = 1/2$ nuclei in isotropic systems:¹¹⁹

^b Assuming a power-law behavior for the spectral density for demonstration purposes, *i.e.* $J(\omega) \propto \omega^{-a}$, it follows that $J(\omega)/4J(2\omega) = 2^{a-2}$. For $a < 2$ the term $4J(2\omega)$ dominates over $J(\omega)$. This is practically always the case.

$$M_2 = \frac{9}{20} I(I+1) \left(\frac{\mu_0}{4\pi} \right)^2 \hbar^2 \gamma^4 \sum_{i \neq j} r_{ij}^{-6} \propto \int_0^\infty R_1^{-1}(\omega) d\omega = 5 \frac{\pi}{2} K \quad (49)$$

Besides quantifying the interaction strength, M_2 takes the spatial distribution of interacting spins into account and is formally similar to a lattice sum, like the Madelung constant. The second moment is essentially a system-specific parameter. Yet, as it strongly depends on inter-nuclear distances, it might be affected by density changes, *e.g.* when the temperature is varied. Another advantage of using protons in FC NMR is that the second moments M_2 , and thus the typical relaxation rates, are not too high, so that the switching times encountered in FC NMR (a few *milliseconds*) usually do not compromise the measurements.

The perturbation treatment leading to eqs. 44 and 48, respectively, is only valid if two important conditions are fulfilled.¹²⁴ First, the amplitude of the perturbation $H_{DD}(t)$ in terms of its angular frequency must be small compared to the inverse of the longest correlation time within a given system, *i.e.* $\omega_{DD} \ll \tau_t^{-1}$. This condition is frequently denoted as the Redfield condition.¹²⁵ Only then, the power series of the perturbation ansatz can be restricted to the 2nd order. Second, the time scale of relaxation must be much longer than that of the fluctuations causing it, *i.e.* $R_1 \ll \tau_t^{-1}$.¹²⁴⁻¹²⁶ At very low fields or in viscous systems, respectively, both conditions may be violated. Then, defining a relaxation rate is difficult as it becomes time dependent. A satisfying theoretical treatment appropriate when the common relaxation theory breaks down is still missing.

As mentioned, the dipolar correlation function $C_{DD}(t)$, the dipolar spectral density $J_{DD}(\omega)$ and hence the (total) relaxation rate $R_1(\omega)$ usually probed in FC ¹H NMR, are all superpositions of an intra- and an inter-molecular contribution, which are probed simultaneously:¹¹⁹

$$C_{DD}(t) \propto C_2(t) + C_{\text{inter}}(t) \quad J_{DD}(\omega) \propto J_{\text{intra}}(\omega) + J_{\text{inter}}(\omega) \quad R_1(\omega) = R_1^{\text{intra}}(\omega) + R_1^{\text{inter}}(\omega) \quad (50)$$

The **intra-molecular correlation function** $C_2(t)$ refers to interacting spins situated on the same molecule or segment. As the molecules are assumed to be sufficiently rigid, the inter-nuclear distance r_{ij} is constant, merely leaving the angular dependence in the dipolar correlation function eq. 45. In polymer melts, assuming isotropic dynamics like in the Rouse or the RR model for instance, $C_2(t)$ reflects the bond vector correlation function (*cf.* section 1.4 and eq. 30):

$$C_2(t) \propto \langle \vec{b}(t) \vec{b}(0) \rangle^2 \propto \langle r^2(t) \rangle^{-2} \quad (\text{isotropic dynamics}) \quad (51)$$

This allows for a direct interpretation of the intra-molecular spin-lattice relaxation dispersion in polymer melts as the Fourier transform of the squared bond vector correlation function:⁷³⁻⁷⁵

$$R_1^{\text{intra}}(\omega) \propto \int_{-\infty}^{+\infty} \langle \vec{b}(t) \vec{b}(0) \rangle^2 e^{-i\omega t} dt \quad (\text{isotropic dynamics}) \quad (52)$$

Regarding this relationship, it is understandable, that the power-law regimes occurring in the re-orientational correlation function are mapped in the relaxation dispersion. Intra-molecular relaxation in polymers can actually be subdivided into an intra-segmental and an inter-segment part. The first one originates from neighbored spins, the latter one is associated with spins located on the same molecule but on different segments. Yet, Fatkullin et al.⁷⁶ and later on Kehr et al.¹²⁷ demonstrated, that the inter-segment contribution is negligible (see also PUB2).

In the TR model the dynamics is first isotropic at $t < \tau_e$, *i.e.* in regimes 0 and I. At $\tau_e < t < \tau_d$, however, the dynamics becomes anisotropic due to the tube, meaning that the chain dynamics is correlated to the initial conformation over large times. In this regime, it is difficult to calculate the bond-vector correlation function and hence $R_1^{intra}(\omega)$. Alternatively, deGennes RTO hypothesis is taken up.⁸⁸ According to eq. 35 (section 1.5) it states an inverse proportionality between $C_2(t)$ and $\langle r^2(t) \rangle$ in the constrained Rouse (II) and in the reptation regime (III). As in the case of the shear relaxation modulus $G(t)$, the terminal process is the disengagement from the tube, represented by the tube survival function $\mu(t)$. Neglecting CR/CLF, this produces an exponential cutoff at $t > \tau_d$. Altogether, the following, time scale separation ansatz for $C_2(t)$ in the TR model was proposed by Ball et al., which is currently the most accepted approach, relating entangled polymer dynamics to NMR:¹²⁸

$$C_2(t) \propto \begin{cases} \langle \vec{b}(t) \vec{b}(0) \rangle^2 \propto \langle r^2(t) \rangle^{-2} & t \leq \tau_e \\ \langle r^2(t) \rangle^{-1} & \tau_e \leq t \leq \tau_d \\ \mu(t) \sim e^{-\frac{t}{\tau_d}} & t > \tau_d \end{cases} \quad (\text{TR model}) \quad (53)$$

Note in eq. 53 that $C_2(t \leq \tau_e)$ follows Rouse dynamics. Below in this section, Table 1 summarizes the regimes in $C_2(t)$ and, after Fourier transformation, $R_1^{intra}(\omega)$, as predicted by the TR model. It is again emphasized that, regarding eqs. 51 and 53, the relation between $C_2(t)$ and $\langle r^2(t) \rangle$ in the entanglement regime (at $t > \tau_e$) depends on whether the dynamics is isotropic (like in the Rouse or the RR model) or anisotropic (like in the TR model). In PUB2 FC NMR data is interpreted in this sense.

A somewhat different time scale separation approach was proposed by Kimmich et al.^{5,129} As in Ball's ansatz (eq. 53), the correlation function $C_2(t)$ is phenomenologically decomposed into three independent parts along $C_2(t) := a(t) \times b(t) \times c(t)$. Component $a(t)$ reflects local reorientation of (or within) segments, which is essentially the α -process. Component $b(t)$ comprises chain dynamics. Finally, the terminal relaxation related to diffusion, is represented by $c(t)$. Component $a(t)$ leads to pre-averaging and $c(t)$ to an exponential decay, respectively, as in eq. 53. Concerning component $b(t)$, a relation linking translational and re-orientational motion different from that of eq. 35 is assumed, specifically $C_2(t > \tau_\alpha) \propto d/dt \langle r^2(t) \rangle$. This leads to different exponents in regimes I and II, with respect to eq. 53. Later on, Kimmich and co-workers described the polymer specific component $b(t)$ in the context of the renormalized Rouse model (section 1.6).⁵ Substituting the prediction for the MSD of the RR model into eq. 51, the forecast for the corresponding re-orientational correlation function $C_2(t)$ is calculated. The predictions are outlined in Fig. 19b of section 5.2. Concerning $\langle r^2(t) \rangle$, the TR model and the RR model can only be distinguished in regime III, as mentioned. Yet, due to the fact that $C_2(t) \propto \langle r^2(t) \rangle^{-2}$ results within the RR model, while $C_2(t) \propto \langle r^2(t) \rangle^{-1}$ is assumed in the TR model (RTO hypothesis), one can distinguish both already in regime II, succeeding the Rouse regime.^{PUB2}

The **inter-molecular correlation function** $C_{inter}(t)$ is related to relative translational displacements between protons. Fatkullin et al. derived a theoretical framework relating $C_{inter}(t)$ directly to the segmental MSD in polymers.^{75,127} It is briefly outlined. The conditional probability that two spins (i and j) having an initial distance of $\Delta r = |\vec{r}_i - \vec{r}_j|$ are displaced after time t so that their relative distance becomes $\Delta r' = |\vec{r}_i' - \vec{r}_j'|$, is given by a propagator $W(\Delta r' | \Delta r, t)$. Their relative displacement is given by $\tilde{r} = |\Delta r - \Delta r'|$ and the corresponding propagator by $W(\tilde{r}, t)$. First, the equivalence $W(\Delta r' | \Delta r, t) = W(\tilde{r}, t)$

is assumed, *i.e.* that the propagator only depends on the relative displacement \tilde{r} . In polymer statistics, usually a Gaussian propagator is assumed for long times ($t \gg \tau_s$), specifically:^{5,6,24,75,76,130,131}

$$W(\tilde{r}, t) = \frac{1}{\sqrt{(2\pi)^3 \langle \tilde{r}^2(t) \rangle}} \exp \left[-\frac{\tilde{r}^2(t)}{2 \langle \tilde{r}^2(t) \rangle} \right] \quad (54)$$

For translational correlation to survive requires that the relative displacement during time t is zero, the probability of which is $W(\tilde{r} = 0, t)$. This consideration leads to:^{75,76}

$$C_{\text{inter}}(t) \approx \frac{4\pi}{9} n_s \cdot W(0; t) = n_s \sqrt{\frac{2}{3\pi}} \langle \tilde{r}^2(t) \rangle^{-3/2} + O(\langle \tilde{r}^2(t) \rangle^{-2}) + \dots \quad (55)$$

The relative MSD is related to the absolute one via a factor 2, *i.e.* $\langle \tilde{r}^2(t) \rangle = 2 \langle r^2(t) \rangle$ as it is assumed that chain motion is independent of each other's.^{75,76,PUB4} The expectation for $C_{\text{inter}}(t)$ using the MSD provided by the TR model is included in Table 1 and illustrated in Fig. 21c (section 5.4). Similar predictions result for the RR model; only in regime III a different exponent is expected (*cf.* Fig. 1). Substituting eq. 55 into 44 and reversing the cos-transformation yields:^{75,PUB4}

$$\langle r^2(t) \rangle = \frac{1}{2} \left[\frac{5}{4} \left(\frac{4\pi}{\mu_0} \right)^2 \sqrt{\frac{8}{3\pi^3}} \frac{1}{\gamma_H^4 \hbar^2 n_s} \frac{1}{1 + 2^{25/16}} \int_0^\infty d\omega \cos(\omega t) R_1^{\text{inter}}(\omega) \right]^{-2/3} \quad (56)$$

Equation 56, offers the opportunity to determine the segmental MSD in polymer melts. Inverse Fourier transformation leads to $R_1^{\text{inter}}(\omega)$, the prediction of which by the TR model is also included in Table 1. Equation 54 was tested by atomistic MD simulations (*cf.* also section 5.1).¹³² It was found that the dynamics is not yet Gaussian at times smaller than 1 ns, limiting the range validity of the approach to longer times. Then, higher order corrections have to be added to eq. 56, as indicated. It is further noted that the inter-molecular relaxation doesn't exclusively contain information on translational dynamics. The distance between spins on different molecules will also be modulated by reorientations of the molecules, to which they are attached, a phenomenon called "eccentricity".¹³³ This effect will play a role at small displacements and is neglected in the treatment given here. Equation 56 is exploited in this work to calculate the segmental MSD in poly(butadiene) (PB), poly(dimethyl siloxane) (PDMS) and poly(ethylene propylene) (PEP), of various molar masses from FC NMR relaxation data (*cf.* sections 5.3, 5.4 and PUB4). Explicitly presuming a power-law character $\langle r^2(t) \rangle \propto t^{\alpha < 1}$ of the MSD, eq. 56 can be further simplified to a purely algebraic expression

$$\langle r^2(t) \rangle \propto [\omega R_1^{\text{inter}}(\omega)]^{-2/3} \quad (57)$$

which was used by Herrmann et al.¹³⁴ In the hydrodynamic limit, where the MSD becomes linear in time, $C_{\text{inter}}(t \rightarrow \infty) \propto t^{-3/2}$ adopts a universal, model-independent power-law anticipated in all kinds of liquids.¹³⁵⁻¹³⁷ In the frequency domain

$$R_1(\omega \rightarrow 0) = R_1(0) - BD^{-3/2} \sqrt{\omega} \quad (58)$$

(B is a constant) is found for ^1H spin-lattice relaxation dispersion.¹³⁵⁻¹³⁷ This relation allows to determine the diffusion coefficient D in simple liquids as well as in polymers.¹³⁸⁻¹⁴¹ Computer simulations confirmed this generic low frequency/long time behavior.^{132,142} The presence of inter-molecular relaxation has the important consequence that $R_1(\omega)$ shows dispersion at all ω , hence no "extreme narrowing" exists in ^1H , even at lowest ω . Yet, when D is large, the square root law eq. 57 is

difficult to resolve in the overall dispersion data. Isotope dilution experiments enable a distinction between intra- and inter-molecular components and reveal that the inter-molecular relaxation rate indeed must not be neglected (*cf.* section 4.3 and section 5).¹³⁴ Moreover, it even dominates the shape of $C_{DD}(t)$ at long times as $C_2(t)$ decays exponentially.

regime	$\langle r^2(t) \rangle$	$C_1(t)$	$C_2(t)$	$R_1^{intra}(\omega)$	$C_{inter}(t)$	$R_1^{inter}(\omega)$
Rouse	$t^{1/2}$	$t^{-1/2}$	t^{-1}	$-\tau_0 \ln(\omega \tau_0)$	$t^{-3/4}$	$\omega^{-1/4}$
const. Rouse	$t^{1/4}$	$t^{-1/4}$	$t^{-1/4}$	$\omega^{-3/4}$	$t^{-3/8}$	$\omega^{-5/8}$
reptation	$t^{1/2}$	$t^{-1/2}$	$t^{-1/2}$	$\omega^{-1/2}$	$t^{-3/4}$	$\omega^{-1/4}$
diffusion	t^1	$\exp(-t/\tau_d)$	$\exp(-t/\tau_d)$	<i>const.</i>	$t^{-3/2}$	$R_1(0) - c \omega^{1/2}$

Table 1: Predictions of the TR model for quantities accessible by FC NMR: segmental mean square displacement $\langle r^2(t) \rangle$, re-orientational correlation functions $C_{1,2}(t)$, intra-molecular spin-lattice relaxation dispersion $R_1^{intra}(\omega)$, as well as the respective inter-molecular analogs.

Using the predictions for the TR or the isotropic polymer models, it can be derived that the ratio $A(\omega) := R_1^{inter}(\omega)/R_1^{intra}(\omega) \propto \langle r^2(t=\omega^{-1}) \rangle^{\pm 1/2}$ increases with ω in the TR model (- sign) while isotropic models (like RR) rather predict a decrease (+ sign).^{PUB2} In addition to confronting theoretically predicted power-law exponents to such actually observed in experiments, this can be exploited to test polymer theories (*cf.* Fig. 18, section 5.2).

1.8 Relaxation in ^2H

Deuterons (^2H) possess a nuclear spin of $I = 1$ and thus an electric quadrupole moment Q interacting with an electric field-gradient (EFG). An EFG is induced by the molecular charge distribution, *e.g.* of a C-D single bond.¹¹⁹⁻¹²¹ The quadrupolar Hamiltonian reads¹¹⁹

$$H_Q(t) = \frac{eQ}{2\hbar} \vec{I} \cdot V_{\alpha\beta}(\vec{r}) \cdot \vec{I} \quad (59)$$

The EFG tensor $V_{\alpha\beta} = \partial^2\Phi / \partial\alpha\partial\beta$ (α, β are Cartesian coordinates) comprises the second derivatives of the electric potential Φ and thus information about the charge distribution within a molecule. The quadrupolar interaction is purely local and short ranged. In the case of ^2H also a dipolar interaction exists, but its strength is negligible compared to the much stronger quadrupolar interaction. While the principal moments of $V_{\alpha\beta}$ depend on the charge distribution, the alignment of the EFG tensor fluctuates due to molecular motion; therefore $H_Q(t)$ is a time-dependent perturbation of the Zeeman interaction H_z causing relaxation. The spin-lattice relaxation rate in the case of isotropic motion and an axially symmetric^c EFG tensor reads similar to that of ^1H (*cf.* the BPP-eq. 48)

$$R_1(\omega) = \frac{2}{15} \delta_Q^2 [J(\omega) + 4J(2\omega)] \quad (60)$$

with $\delta_Q = 3e^2qQ/4\hbar$ denoting the ^2H coupling constant. The latter depends on the field-gradient $-eq$ which is, by convention, equal to the maximum principal component V_{zz} of the field gradient tensor.¹¹⁹ Relaxation rates concerning ^2H are significantly higher (typically by a factor of 8-10) when compared to ^1H which, may interfere with the finite switching times emerging in FC NMR. Moreover, the NMR signal is much weaker due to the smaller frequency as the gyromagnetic factor is reduced by $\gamma_{1\text{H}} / \gamma_{2\text{H}} \approx 6.5$. Due to the local character of the quadrupolar interaction, the spectral density $R_1(\omega)$ is exclusively intra-molecular and sensitive to re-orientational dynamics of the segment, *i.e.* $C_2(t)$ is probed. Hence, at low ω under extreme narrowing conditions ($\omega\tau_c \ll 1$), liquids are expected to feature a plateau in the spin lattice relaxation dispersion, *i.e.* $R_1(\omega) = \text{const.}$ (*cf.* Table 1). FC ^2H NMR allows a confirmation of ^1H isotope dilution experiments also revealing the intra-molecular relaxation rate.^{130,134,PUB2} The state-of-the art of FC ^2H NMR on polymers is outlined in section 5.4 and in PUB6.

^c The EFG tensor is axially symmetric if the asymmetry parameter $\eta := (V_{xx} - V_{yy})/V_{zz}$ vanishes, where $|V_{zz}| > |V_{yy}| > |V_{xx}|$ are the principal components.¹⁴³

2. Experiments on Polymer Dynamics Beyond FC NMR – State-of-the-Art

The dynamics in liquids can be studied by a multitude of methods. The most important ones often used to investigate polymer dynamics are outlined in this section, in particular those which also refer to this work. The subsequent section 3 is dedicated to field-cycling (FC) NMR. Figure 2 displays a schematic comparison of the typical dynamic range of the different methods, where the usual domain, time (t) or frequency (f), is indicated.

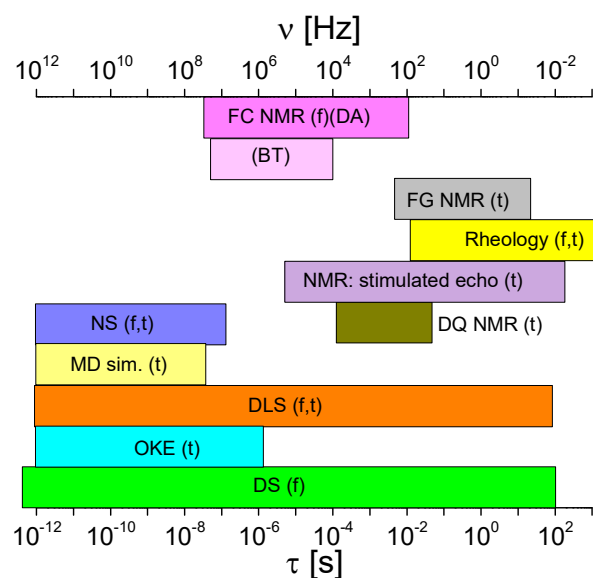


Figure 2: Approximate dynamic range and typical domain (t: time, f: frequency) of various experimental techniques used to study the dynamics in liquids. NS: neutron scattering; MD sim.: molecular dynamics simulations; DQ NMR: double quantum NMR spectroscopy; FG NMR: field-gradient NMR; DLS: dynamic light scattering; OKE: optical Kerr-effect spectroscopy; DS: dielectric spectroscopy.

Translational motion of molecules can be probed by **dynamic scattering methods** involving light¹⁴⁴ (DLS), X-rays, electrons or neutrons^{1,16,145-151} (NS). As outlined in the

Introduction (section 1.1) the dynamic structure factor $S(\vec{q}, \omega)$ or the intermediate scattering function $S(\vec{q}, t)$, respectively, are analyzed. Neutrons yield the highest spatial resolution and selectivity, the latter *e.g.* via $^1\text{H}/^2\text{H}$ labelling. Molecular (segmental) diffusion is reflected in the self-part of the dynamic structure factor accessible from the incoherent contribution of quasi-elastically scattered neutrons, specifically, by measuring the scattering function $S_{\text{inc}}(q, t)$ (*cf.* section 1.1) of a fully protonated liquid.^{16,131,147} Neutron Spin Echo (NSE) spectroscopy, a time-of-flight technique, offers a particularly high energy resolution. Changes in the velocity distribution caused by inelastic scattering in a sample prevent a full refocusing of the phase angles the neutrons accumulate when passing through two magnetic field gradients with opposite directions.^{98,131,148-151} In Fig. 3 the segmental MSD $\langle r^2(t) \rangle$ as derived from NSE measurements on entangled poly(ethylene) (PE) in the melt state is shown. For that purpose, eq. 3 was used.

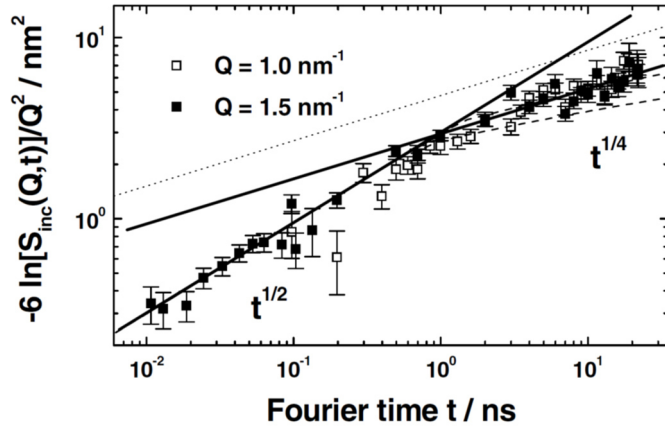


Figure 3: Segmental MSD $\langle r^2(t) \rangle$ of an entangled poly(ethylene) melt. $S_{\text{inc}}(q,t)$ was measured using NSE and related to the MSD via eq. 3 (*cf.* vertical axis). The crossover from Rouse (I) to the constrained Rouse (II) dynamics is observed. Taken from Wischniewski et al.¹³¹

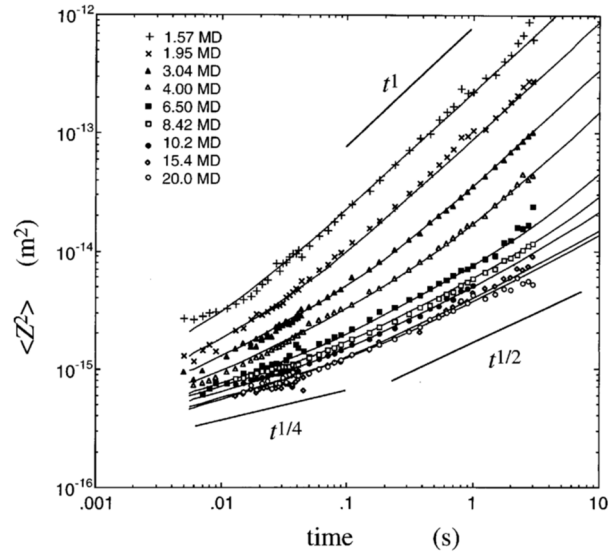
The MSD of PE shown in Fig. 3 features the crossover between the sub-diffusive Rouse and the constrained Rouse power-law regime (*cf.* Table 1).¹³¹ Beyond computer simulations (see below), such NSE experiments have been the only experimental proof of regime II in the segmental MSD of polymers for a long time. In PUB4 as well as in sections 5.3 and 5.4 it is demonstrated that also FC ^1H NMR provides $\langle r^2(t) \rangle$ in polymers, if it succeeds to work out the inter-molecular relaxation dispersion $R_1^{\text{inter}}(\omega)$ from the total ^1H relaxation using the isotope dilution technique. In section 5.4 even a comparison between the MSD of PEP as determined from NSE spectroscopy as well as from FC ^1H NMR relaxometry is carried out.

Moreover, forward recoil spectrometry (FRES),^{83,152-154} scanning infrared microscopy (SIRM),¹⁵⁵ fluorescence recovery after photo bleaching (FRAPP),^{85,86} forced Rayleigh scattering (FRS)¹⁵⁶⁻¹⁵⁹ and fluorescence correlation spectroscopy (FCS)¹⁶⁰⁻¹⁶² can be applied to measure the diffusion coefficient D , *i.e.* translation in the hydrodynamic limit. While the first two techniques are restricted to thin films, the latter three require tracers like dye molecules.

Established as a gold-standard, **field-gradient (FG) NMR**¹⁶³⁻¹⁶⁷ is used to measure diffusion, typically also in the hydrodynamic limit. The loss of phase coherence in a spin system by particle diffusion along an either static or pulsed field-gradient $g = \partial B / \partial z$ is probed via spin-echo techniques, like the stimulated echo. The measured stimulated echo amplitude is formally identical to the (incoherent contribution of the) intermediate scattering function $S_{\text{inc}}(\vec{q}, t)$, when \vec{q} is identified with $g\gamma\tau$. The evolution time is denoted as τ . Indeed, FG NMR and NS are complementary methods.¹⁶⁸ Regarding polymers, under favorable conditions FG NMR is able to advance into the reptation regime, where D becomes time-dependent and the MSD sub-diffusive.^{87,169-176} The lowest diffusion coefficients reliably determinable by FG NMR are on the order of $D \sim 10^{-15} \text{ m}^2/\text{s}$, limited by the NMR specific phenomenon of zero-quantum flip-flop transitions (spin-diffusion)^{5,165,177} and by the strength of the field gradient. Besides the diffusion induced decay, the stimulated echo amplitude is additionally attenuated by longitudinal as well as transversal relaxation, constituting further limitations.^{PUB4} In Fig. 4 the MSD $\langle z^2(t) \rangle$ along the direction of a field-gradient of poly(styrene) (PS) with $1 \leq M/10^6 \leq 20$, well above M_c , is shown as an example.⁸⁷ To match the time scale with the experimental window, the measurements were carried out in concentrated solution and not in the melt. The entanglement

related power-law regimes II and III of the TR model (*cf.* Table 1) are reproduced asymptotically. At longest times, the hydrodynamic limit $\langle z^2(t) \rangle = 2Dt$ is reached. Thus, at least in polymer solutions all regimes of the TR model were reproduced via FG NMR.

Figure 4: FG NMR diffusion data of poly(styrene) with $1 \leq M/10^6 \leq 20$. (MD = megadaltons). MSD $\langle z^2(t) \rangle$ in the direction of a field-gradient. Depending on M , transitions between power-laws $t^{1/4}$ to $t^{1/2}$ and $t^{1/2}$ to t^1 , respectively, conforming to regimes II-IV of the TR model, are indicated (straight lines). From Komlos et al.⁸⁷



The identification of all sub-diffusive regimes of $\langle r^2(t) \rangle$ in a polymer melt by a single technique was still missing. In PUB4 (section 5.3) the complementary time ranges of FG ^1H and FC ^1H NMR are combined to measure the segmental MSD in PB and PDMS melts over a huge time range.

Re-orientational motion in terms of the correlation functions $C_l(t)$ is accessible by **DLS** ($l=2$) using **depolarized detection**.^{29,30,39,55,56,49,144,177-180} Frequency (Raman, $10^{-12} \text{ s}^{-1} < 10^{-8} \text{ s}^{-1}$) and time domain (Photon Correlation Spectroscopy, $10^{-8} \text{ s}^{-1} < 10^1 \text{ s}^{-1}$) techniques provide complementary dynamic ranges. Yet, while DLS is predestined for measuring the α -process and faster dynamics, large scale polymer dynamics is difficult to detect.⁵⁵ Another optical method suitable for measuring the local and fast dynamics in the time domain is **Kerr-effect spectroscopy** (OKE, $l=2$).¹⁸¹⁻¹⁸⁴ **Dielectric spectroscopy** (DS, $l=1$) probes the fluctuating electric polarization, usually in the frequency domain.^{23,185,186} Most polymers merely have (electric) dipole components perpendicular to the chain contour and are classified as type-B.⁷² Such dipole components re-orientate independently with the corresponding monomers and reflect the local α -relaxation $\Phi_\alpha(t)$ solely. In the rare case of type-A polymers⁷² like poly(isoprene) (PI) or poly(propylene glycol) (PPG), there is also a dipolar component parallel to the backbone, accumulating along the chain. Therefore type-A polymers feature two relaxations, $\Phi_\alpha(t)$ and the normal mode $\Phi_{NM}(t)$, the latter posing the correlation function of the end-to-end vector $\langle \vec{r}_{ee}(t) \cdot \vec{r}_{ee}(0) \rangle$ (*cf.* eqs. 26 and 34).^{108,185}

In Fig. 5a master curves of the dielectric loss $\epsilon''(\omega\tau_\alpha)$ of PI plotted vs. the reduced frequency $\omega\tau_\alpha$ are shown.¹⁰⁸ They include the α -process at high as well as a normal mode (NM) at low frequencies. The latter shifts toward lower reduced frequencies with increasing M . Figure 5b shows the ratio of the time constant of the normal mode and of the α -process $\tau_{NM}(M)/\tau_\alpha$. Three power-law regimes $\tau_{NM}(M)/\tau_\alpha \propto M^a$ were identified, the exponents of which slightly differ from the predictions of the Rouse and of the TR model (sections 1.4, 1.5). Specifically, for $M < M_c$ $a_I = 2.6$ was found, while the Rouse model predicts $a_R = 2$. For $M_c < M < M_{rep} \approx 10 M_c$ an intermediate regime with $a_{II} = 4.0$ and for

$M > M_{rep}$ a regime with $a_{III} = 3.0$ was attributed, the latter being in accordance with the TR model. This finding is an indication that finite length effects (like CLF, CR) disappear when M becomes very large. Then the predictions of the TR model for pure reptation are approached (*cf.* section 1.5). Similar observations follow from shear measurements which also suggest such a further crossover molar mass M_{rep} in the M -dependence of the zero shear viscosity $\eta_0(M)$ of polymer melts (see below and Fig. 8).

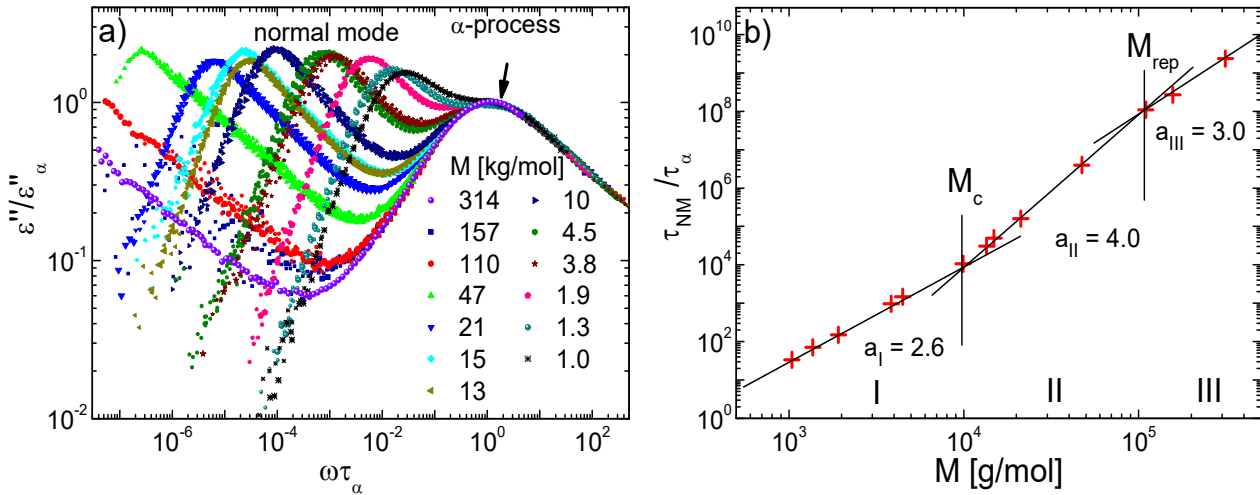


Figure 5: a) Dielectric loss master curves $\epsilon''(\omega\tau_\alpha)$ of poly(isoprene) (PI) evolving with M , as indicated. The amplitude of the α -peak is scaled to 1. Besides the α -process an M -dependent normal mode is observed. b) Ratio $\tau_{NM}(M)/\tau_\alpha$ as a function of M . Three power-law regimes occur, with exponents and crossover molar masses M_c , M_{rep} as indicated. Adapted from Abou Elfadl et al.¹⁰⁸

Computer simulations of molecular dynamics (MD) give access to atomic or segmental trajectories, from which any quantity, like correlation functions or the MSD, can be computed.^{10,187} The virial theorem in combination with eq. 16 is used in simulations to predict mechanic response of complex fluids such as polymer melts.²⁵ As simulations still lack of sufficient computing power, slow dynamics, as they occur in complex liquids like polymers, are impossible to simulate for large scale systems, unless microscopic details are coarsened or the potentials are facilitated. Kremer et al. were the first to discover the transition from Rouse (I) to constrained Rouse (II) dynamics, applying a bead-and-spring model.^{188,189} Since then, numerous simulations revealed further evidence for polymer dynamics in terms of Rouse modes and reptation.^{19,71,97,187-196} In Fig. 6 a state-of-the-art example of simulated polymer dynamics in the entangled melt is given.²⁰ A generic bead-and-spring model was assumed in this work by Wang, Likhtman and Larson which poses a rare example for a simulation addressing both, the segmental MSD as well as re-orientational correlation functions. It can be considered as a reference for FC ^1H relaxometry.

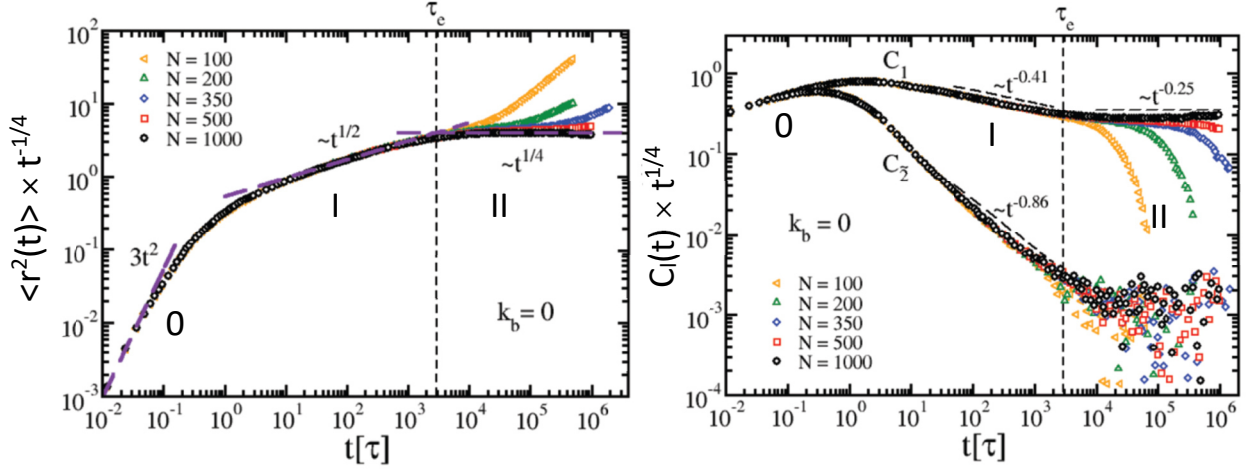


Figure 6: a) Scaled MSD and (b) re-orientational correlation functions $C_1(t)$ and $C_2(t)$, respectively, of central monomers, resulting from coarse-grained computer simulations of entangled polymer melts. Chain lengths N are indicated. Power-law regimes of ballistic (0), Rouse (I) and constrained Rouse (II) dynamics are assigned, as well as the entanglement time τ_e . Taken from Wang et al.²⁰

Specifically, Fig. 6a displays the (rescaled) MSD $\langle r^2(t) \rangle \times t^{-1/4}$, averaged over the ten middle monomers of entangled chains, each consisting of at least $N = 100$ and up to $N = 1000$ segments. Figure 6b shows the corresponding (rescaled) re-orientational correlation functions $C_1(t) \times t^{1/4}$ and $C_2(t) \times t^{1/4}$. This scaling of the abscissae was chosen, as in the constrained Rouse regime (II) on which the work focusses, the TR model predicts plateaus due to $\langle r^2(t) \rangle^{-1} \propto C_1(t) \propto C_2(t) \propto t^{-1/4}$ (cf. section 1.7 and Table 1). Three power-law regimes are apparent in all three quantities. They were assigned to ballistic (0), Rouse (I) and constrained Rouse (II) dynamics. At short times (regime 0), ballistic motion going along with $\langle r^2(t) \rangle \propto t^2$ was observed, but no “cage” effect, which is actually characteristic for “glassy dynamics” (cf. Fig. 1). In the Rouse regime (I), the predicted behavior $\langle r^2(t) \rangle \propto t^{1/2}$ was reproduced essentially. Also the power-law exponents of the functions $C_{1,2}(t)$ slightly differ only slightly from the predicted ones in the Rouse regime: while $C_1(t) \propto t^{-1/2}$ follows from the Rouse model, a value of -0.41 was obtained in the simulation. For the 2nd order correlation function one expects $C_2(t) \propto t^{-1}$, while an exponent of -0.86 followed from the simulation data. The relation between both correlation functions anticipated for Rouse dynamics $C_2(t) \propto C_1^2(t)$ (cf. section 1.4) was also satisfyingly reproduced. In regime II, *i.e.* beyond the entanglement time τ_e , $\langle r^2(t) \rangle^{-1} \propto C_1(t) \propto C_2(t) \propto t^{-1/4}$ behavior is reflected in the long time plateaus turning up in Fig. 6b, although regime II in $C_2(t)$ is poorly resolved within the noise. Thus, also the exponent values of the constrained Rouse regime were reproduced satisfyingly. The extension of regime II along the time axis shrinks with decreasing chain length. While for $N = 1000$ the constrained Rouse regime was observed up to the longest times, it barely extended over one decade for $N = 100$. As said, the findings discussed above resulted from merely averaging over the ten inner monomers of the chains. Wang et al. also evaluated $C_{1,2}(t)$ and $\langle r^2(t) \rangle$ averaged over the whole chains. Increased mobility of chain ends was found, slightly increasing the absolute exponent values in regime II. Thus, significant finite size effects were discovered in the simulation. A comparison of $C_2(t)$ obtained by FC NMR of fully as well as centrally

labelled chains shows similar results, as will be demonstrated in section 5.2. Concluding, Wang and co-workers claim to confirm the RTO hypothesis (eq. 35).²⁰

Finally, it should be noted that in Herrmann et al. carried out a comparison between the dipolar correlation function $C_{DD}(t)$ of PB obtained by FC ^1H NMR, and $C_2(t)$ from another coarse-grained (Monte Carlo) simulation by Kreer et al.¹⁹⁷. Consistent results in the Rouse and the constrained Rouse regime were revealed,¹⁹⁸ although inter-molecular relaxation was not considered in this simulation, which is, however, crucial for ^1H relaxation. In **atomistic MD simulations**, Newton's equations of motion are integrated, using potentials derived from quantum-chemical calculations.¹⁹⁹ In contrast to generic (coarse-grained) simulations it is attempted to pretend a microscopic environment as realistic as possible. With contemporary computational power atomistic MD simulations have become available also for polymeric systems, where time scales on the order of 100ns can be reached.¹³² For the first time, atomistic MD simulation data of a polymer melt of different M is compared to FC ^1H NMR data, practically measured on the same polymer (*cf.* section 5.1 and PUB1).

NMR spectroscopy is mostly performed at a single, high field, generated by a cryo-magnet. The only available parameter for varying the dynamic range is the temperature. Applied to many nuclei, the most prominent ones being ^2H , ^{13}C or ^{31}P , $C_2(t)$ is probed by a variety of pulse sequences. Most methods are sensitive to local and fast dynamics.²⁰⁰⁻²⁰⁸ Polymer dynamics is difficult to detect via spectroscopy since the signal (spectrum), resulting from the secular components of the Hamiltonian, is averaged to zero by rapid, isotropic dynamics.¹²¹ In entangled polymers, liquid crystals or rubbers, however, this averaging may be incomplete, when topological constraints remain on the NMR time scale (inverse Larmor frequency). Then, the so-called order parameter $S = \langle P_2[\cos(\varphi(t))] \rangle$ is larger than zero. Such residual coupling leads to a subtle broadening of the NMR linewidth^{209,210} and the occurrence of pseudo-solid echoes.^{59,211,212}

Besides longitudinal (R_1) relaxation which is the keystone of FC NMR, **transversal (R_2) relaxation** is another source of information about polymer dynamics. Based on previous work of Cohen-Addad and co-workers,²¹³ Brereton et al. derived expressions for the M -dependence of the transversal relaxation rate R_2 in terms of the Rouse²¹⁴ and the TR model,²¹⁵ respectively, using a coarsened scenario of the microscopic chain details. Specifically, R_2 is predicted to feature $\log(M)$ in the Rouse and $M \log(M)$ dependence in the entanglement regime, allowing for a distinction between entangled and un-entangled chains and also for the determination of parameters of the Rouse and of the TR model, respectively. Yet, the treatment is only appropriate in the absence of residual couplings. For large M ($\gg M_e$) the residual coupling renders the transversal magnetization decay multi-exponential and the definition of a single transversal relaxation rate R_2 becomes inappropriate.^{216,217} The transversal relaxation rate R_2 is proportional to the zero-frequency component of the spectral density, which is, by definition, identical to the mean correlation time, *i.e.* $R_2 \propto J(0) = \langle \tau \rangle$. Consequently, there is no ω -dependence in R_2 and the quantity is not of interest for FC NMR.

In proton **double quantum (DQ) NMR** the temporal build-up of double quantum coherences among dipolarly coupled spins is measured.^{218,219} Without major modifications the technique is also applicable to ^2H .^{195,218} The coherence build-up is recorded via a time dependent intensity function, the so-called (normalized) DQ intensity $I_{nDQ}(\tau_{DQ})$. In polymers $I_{nDQ}(\tau_{DQ})$ can be related to the re-orientational auto-correlation function via $C_2(t = \tau_{DQ}) \propto I_{nDQ}(\tau_{DQ}) / \tau_{DQ}^2$.^{195,218-223} Concerning ^1H , also

inter-molecular effects are detected via isotope dilution experiments,¹⁹⁵⁻²²¹⁻²²³ therefore one should rather write $C_{DD}^{DQ}(t)$, as in the case of FC ^1H NMR relaxometry. It is unclear if such evidently relevant inter-molecular effects are still compatible with the assumptions leading to this simple relationship between $I_{nDQ}(\tau_{DQ})$ and the correlation function $C_{DD}^{DQ}(t)$. Indeed, Fatkullin et al. have derived expressions for the DQ build-up curves for different polymer models.²²⁴ They actually demonstrate the relevance of inter-molecular interactions. Also the authors of the mentioned DQ studies state that “Presumably, our simplistic model based on spin dynamics in an isolated chain segment does not take proper account of inter-chain dipolar couplings”.²²² The DQ evolution time τ_{DQ} is varied in a specific pulse sequence²²⁵ within some $10\ \mu\text{s}$, limited by technical aspects, and about $1\ \text{ms}$, providing an almost two decades broad time window. Assuming time-temperature superposition (TTS) the time range can be extended to $\tau_e < t < \tau_e \times 10^5$, which is sufficient to cover the terminal relaxation for polymers up to $M/M_c \approx 100$.^{195,221-223} The first applications of DQ NMR to polymers were reported by Graf et al.²²⁰ and Dollase et al.²²⁶ The authors claimed to confirm the TR model in regimes II and III. The method was later improved by K. Saalwächter²¹⁸ and applied to PB^{195,221,223} and to further polymers (PI, PDMS).²²²

$C_{DD}(t)$ data from DQ ^1H NMR was previously combined with such from FC ^1H NMR by Vaca Chávez et al. and Herrmann et al. (cf. section 4.2).^{221,227} As merely the STELAR device was used at that time, the FC NMR data comprised $\tau_\alpha < t < \tau_e \times 10^3$. Both methods were still complementary, together covering ten decades in time. Using the FC-1 relaxometer in Darmstadt FC NMR nowadays reaches the longest time scales, which were preserved to DQ NMR previously.²²⁷ In Fig. 14 (section 4.2) it is demonstrated that the $C_{DD}(t)$ curves obtained by DQ ^1H NMR coincide with such obtained by FC ^1H NMR almost perfectly. However, when intra- and inter-molecular relaxation is explicitly distinguished via isotope dilution experiments, $C_2(t)$ resulting from FC ^1H NMR doesn't coincide with its analogue from DQ NMR any more, as is addressed in section 5.2 and in PUB2.

As outlined in section 1.1, in **shear rheology** the relaxation of shear stress, as a consequence of applied strain is recorded. Such strain can be step-like and the decay of stress in the time domain is monitored in terms of the relaxation modulus $G(t)$. Applying oscillatory strain, the complex shear modulus $G^*(\omega)$ in the frequency domain is gained.^{6,24,60-62} As examples, master curves of $G'(\omega\tau_\alpha)$ and $G''(\omega\tau_\alpha)$ of the linear, low disperse polymer PB with $M = 130k \gg M_c$ taken from a publication of Colby and co-workers²²⁸ are reprinted in Fig. 7. The measurements were carried out in an extraordinarily broad temperature range. As T reaches as low as T_g the α -process, reflected in the peak in G'' at $\omega\tau_\alpha(T) \approx 1$ is included. This allows determining $\tau_\alpha(T)$, as in the case of DS, DLS and FC NMR (cf. section 5.5). Note that the frequency axis was scaled by the time constant $\tau_\alpha(T)$ subsequently. Rheological measurements which include the local dynamics are rarely reported in the literature.²²⁸⁻²³⁰ In section 5.5 such data will be shown.

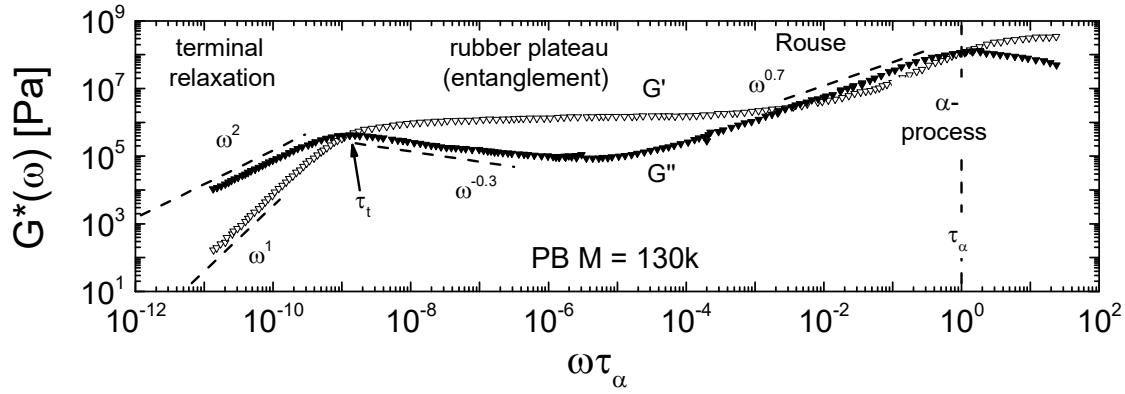


Figure 7: Master curves of the loss and the storage modulus, $G'(\omega\tau_\alpha)$ and $G''(\omega\tau_\alpha)$, respectively, of PB 130k. Going from high to low (reduced) frequencies, the α -process, the polymer specific Rouse and the rubbery regime as well as the terminal regime are covered. Taken from Colby et al.²²⁸, rescaled and complemented by the power-law indicators.

At lowest (reduced) frequencies the terminal power-laws $G' \propto \omega^2$ and $G'' \propto \omega^1$ are observed. Thus, the polymer melt behaves like a Newtonian fluid on long time scales. The intersection between G' and G'' at lowest frequencies is often used as an estimate for the terminal relaxation time τ_t (indicated by the arrow in Fig. 7).⁶² The most obvious feature in entangled polymers is the rubber plateau in $G'(\omega)$ (and $G(t)$) between the Rouse and the terminal regime. Strain and stress are (approximately) proportional (Hooke's law), indicating elastic response. This interplay of temporary rubber-like elasticity and liquid-like flow is called visco-elasticity. At $\omega\tau_\alpha < 1$ the local relaxation is followed by a power-law regime $G' \propto G'' \propto \omega^{0.7}$, referred to Rouse dynamics, although the exponent doesn't match exactly; a value of 0.5 is predicted (*cf.* eq. 32 and Fig. 28 (top)). Up to the authors knowledge, no regime compatible with constrained Rouse dynamics (II, *cf.* Fig. 28 top) was experimentally observed in rheological data. The high frequency flank of the terminal peak in G'' typically has a slope of $-0.3 \div -0.2$ (Fig. 7). The difference to the TR model predicting a slope of -0.5 in the reptation regime (eq. 37) is explained by finite length effects causing further relaxation modes (*cf.* eq. 38 with the modification of $\mu(t)$ via eq. 42).⁶

In contrast to FC NMR, the transition from Rouse (I) to constrained Rouse (II) dynamics occurring at τ_e is difficult to determine from shear data shear rheology. Park et al. recently proposed a procedure according to the which the shear spectra are fitted by the Likhtman/McLeish model⁹⁷ (*cf.* section 1.5), after the α -process was subtracted from shear master curves.²³¹ As will be suggested in this work, FC NMR is indeed capable of determining τ_e in entangled polymers model-independently, as the technique probes different correlation functions than shear rheology. Specifically, in PUB5 and section 5.5, rheological data of PEP and PPG are presented and compared to spin-lattice relaxation data, in which the transition between regime I and II is pronounced. Shear rheology also doesn't allow for a straightforward distinction between the regimes II and III of the TR model (section 5.5).

Unidad et al. recently summarized a multitude of zero-shear viscosity data $\eta_0(M)$ of PI and PB, collected from various rheological works.¹⁰⁹ This data is reprinted in Fig. 8. Three power-law regimes were identified in both species: for $M < M_c$, $\eta_0 \propto M$ is apparent, in accordance with the Rouse model (cf. section 1.4). For entangled systems a first regime with the typical scaling, $\eta_0 \propto M^{3.3 \pm 3.7}$ is observed.^{6,24,60-62} Finally, when even another limit $M_{rep} \gg M_c$ is exceeded, the prediction of the TR model is approached, as finite length effects disappear, *i.e.* $\eta_0 \propto M^3$. This is similar to the dielectric results plotted in Fig. 5b, which also suggest a second crossover at M_{rep} in the M -dependence of the relaxation time of the end-to-end vector.¹⁰⁸ Unidad et al. state that the crossover regime between Rouse and fully established reptation dynamics characterized by $\eta_0 \propto M^3$ shrinks if the packaging length $p := M (\rho N_A \langle r_{ee}^2 \rangle)^{-1}$ increases.¹⁰⁹ The latter is a characteristic of the polymer species.

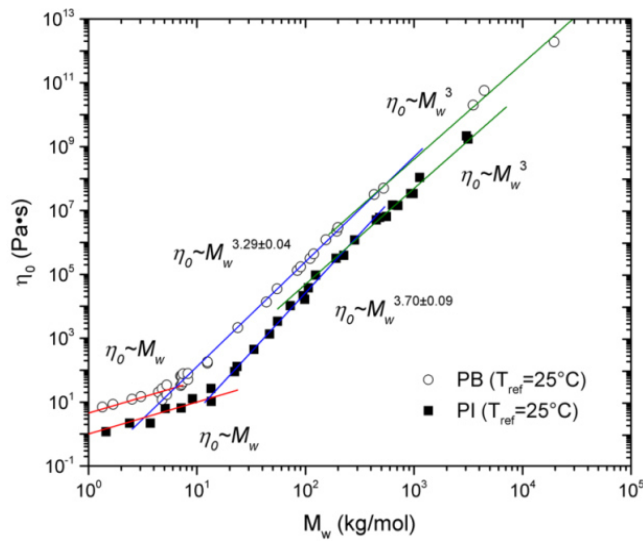


Figure 8: M -dependence of the zero-shear viscosity η_0 of PB and PI, respectively. Three power-law regimes are indicated. Taken from Unidad et al.¹⁰⁹

3. Principles of Field-Cycling NMR Relaxometry

The idea of frequency-dependent NMR, in particular relaxometry, dates back to the origins of NMR in the end of the 1940s.¹²³ Although applications in biomedicine are presented in the literature like the optimization of contrast agents,²³² FC NMR tomography,^{233,234} organic tissue investigations,²³⁵⁻²³⁷ food science²³⁸ or landmine detection,²³⁹ the technique is still quasi-monopolized by academia.

3.1 Overview

Due to the Zeeman interaction $H_z = -\gamma \vec{I} \vec{B}$ a nuclear spin-system features para-magnetism in an external magnetic field B . It can be brought out of equilibrium by manipulation through sequences of radio frequency pulses being resonant with the Larmor frequency $\omega = |\gamma B|$ or by instantaneously switching the magnetic field, which is the idea behind FC NMR. Equilibrium goes along with a diagonal density operator, the elements of which are the Boltzmann populations of the spin-states. The latter depend on T and, in particular, on the magnetic field. In equilibrium, the differences in populations lead to a tiny net longitudinal (z-)magnetization described by the Curie law. Non-equilibrium states go along with populations differing from Boltzmann equilibrium, *i.e.* perturbed z-magnetization, or the existence of coherent superpositions of spin-states. This leads to off-diagonal elements in the density operator and causes transversal magnetization in the x-y plane. Relaxation is the process of re-establishing thermal equilibrium out of a non-equilibrium state.

The mostly encountered application of FC NMR is the frequency dependent measurement of the spin-lattice relaxation rate $R_1(\omega \propto B)$. Modern superconducting (cryo-) magnets typically operate at one single frequency in the high-field range of $100 \text{ MHz} \leq \nu = \omega/2\pi \leq 1 \text{ GHz}$, lacking the possibility of field variation. Moving a sample in the fringe field of a superconducting high-field magnet is an option for varying the field or otherwise, the use of electromagnets. As the naturally already weak NMR signal decreases with the squared magnetic field, conventional detection suffers from weak signals when frequencies below, say, 10 MHz, shall be achieved.^{4,240} This issue can be circumvented by realizing relaxation and signal detection at different fields. This decoupling can be implemented either mechanically or electronically. Mechanical field-cycling (“shuttling”), profits from high and homogeneous fields providing spectral resolution. The technique requires transfer times of about 100 ms, rendering shorter relaxation times inaccessible.²⁴¹⁻²⁴⁶ Electronic (fast) field-cycling draws upon resistive coils generating variable fields, nowadays by FET-controlled currents and typical switching times of about 1-3 ms. Generally, electromagnets are inhomogeneous and provide a poor spectral resolution on the order of 1 kHz. Further technical details are described in the relevant literature.^{4,240,247-252} An interesting design of a superconducting FC NMR device operating between 1kHz and 50MHz and switching times on the order of ms was presented by Schauer et al.²⁵³

Currently, the Spinmaster FFC2000 from STELAR²⁵⁴ is the only commercially available FC relaxometer. One such device is located at the *University of Bayreuth* since 2004. It provides a frequency window of $10 \text{ kHz} \leq \nu \leq 20 \text{ MHz}$ (^1H). The field is upwardly restricted by the maximal applicable current. Downwardly, it is limited by insufficient field-stability as well as interfering magnetic fields such as

the earth-field (which is about 2.5 kHz) and stray fields from other laboratory equipment like NMR magnets. In order to probe the very slow dynamics encountered in high- M polymers, a self-built FC relaxometer located at the *Technical University of Darmstadt* (group of F. Fajara) was used, specifically the device named FC-1.²⁴⁰ It allows for measurements in the range of $100 \text{ Hz} \leq \nu \leq 30 \text{ MHz}$ by employing three different power-sources each appropriate for its own magnetic field range, by shielding external fields in three dimensions and by an active field-drift and fluctuation compensation system. In tilted magnetic fields (such with a component perpendicular to the z -axis), a low-frequency record of 12 Hz (0.3 μT) could be achieved by Kresse et al. recently.^{255,256} The dynamic ranges of both relaxometers are indicated in Fig. 2. The instrumental limitations can be overcome by performing measurements at different temperatures. Assuming FTS dispersion data sets recorded for different T can be assembled to master curves. For that purpose $R_1(\omega)$ is converted to the susceptibility representation (cf. sections 1.1 and 4.1). The temperature can be controlled to $\pm 1 \text{ K}$ in the range of 180 K – 420 K on both, the *Bayreuth* and the *Darmstadt* relaxometer.

3.2 Technical Principles

Initially, an equilibrated Curie magnetization $M_{eq}(B_p)$ aligned in z -direction is generated by exposing a sample to a polarization field B_p . The latter is either zero (non pre-polarized (NP-) experiment) or as high as technically possible (pre-polarized (PP-) experiment) (cf. Figure 9). Within a few ms , the field is quickly switched to the desired relaxation field B_r , which is maintained for the evolution time τ . During the evolution time the magnetization $M(\tau)$ relaxes toward the pertinent equilibrium $M_{eq}(B_r) = M(B_r, \tau \rightarrow \infty)$. The corresponding time scale of the presumed exponential recovery is the spin-lattice relaxation rate R_1 . The magnetization $M(B_r, \tau)$ is probed in the x - y -plane via quadrature detection, after rotation by a $\pi/2$ -radio-frequency pulse. This produces a complex signal $M^*(t) = M_x(t) + iM_y(t)$, termed free induction decay (FID), the initial magnitude of which provides a measure for the evolution of the magnetization. Yet, just before detection, the external field is again switched almost instantaneously to the acquisition field B_{aq} , which is as high as possible to gain maximum signal. The receiver dead-time between the detection pulse and the beginning of the acquisition is about 5 μs . The cycle schematically depicted in Fig. 9, is repeated with incremented τ , providing a magnetization curve $M(B_r, \tau)$. The relaxation dispersion $R_1(B_r)$ is probed by varying B_r .

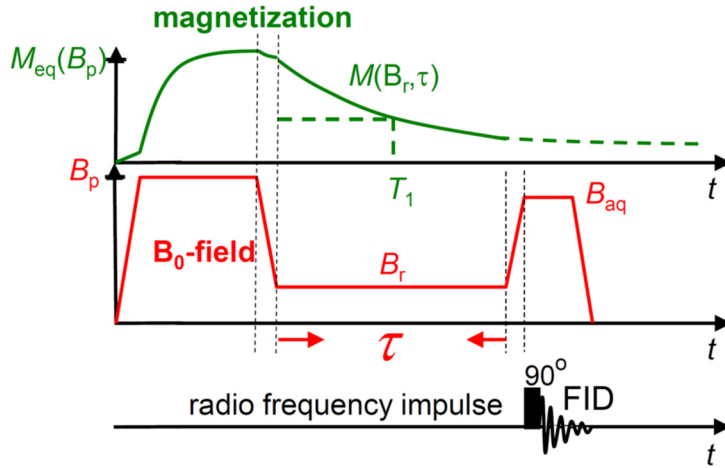


Figure 9: Schematic field-cycle for measuring spin-lattice relaxation at a field B_r using pre-polarization. Middle row: external magnetic field toggled through polarization B_p , evolution B_r and acquisition field B_{aq} . Upper row: corresponding evolution of the magnetization $M(t)$. Lower row: detection of $M(B_r, \tau)$ via a $\pi/2$ -radio-frequency pulse. Switching ramps are indicated by vertical dashed lines.

Generally, the probed magnetization curve has the following form:

$$M(B_r, t) = M_{eq}(B_r) + [M_{eq}(B_p) - M_{eq}(B_r)] \cdot m(t; p(R_1)) \quad (61)$$

The pre-factor $M_{eq}(B_p) - M_{eq}(B_r)$ defined by the field-cycle is decisive whether pre-polarization is profitable or not, where $M_{eq}(B_r)$ is the (apparent) equilibrated magnetization corresponding to B_r . The time-dependent expression $m(t; p(R_1))$ is the normalized relaxation function. By definition, it decays from one to zero. In general, a distribution $p(R_1)$ of relaxation rates has to be considered. Regarding ^1H , however, in most cases $p(R_1)$ gets averaged by rapid cross relaxation, leading to a single (averaged) relaxation time R_1 (cf. below). Then, $m(t; R_1)$ is an exponentially relaxing time function. Figure 10a displays typical magnetization raw data $M(B_r, t)$, here of the entangled, linear and low-disperse polymer PDMS, measured utilizing the FC-1 relaxometer. Pre-polarization was used for $\nu \lesssim 15 \text{ MHz}$, while above, pre-polarization was omitted. This results in the observed built-up and decay curves, respectively, observed in Fig. 10a. The time axis corresponds to the beginning of acquisition.

Instantaneous field switching is an idealization as switching usually takes some few ms . Actually, also during switching some magnetization relaxes, spoiling both equilibrium values $M_{eq}(B_p)$ and $M_{eq}(B_r)$, respectively, between which the progress of relaxation is monitored. When successively going to lower fields, the switching time from B_p to B_r increases, causing a small but growing loss of magnetization at the beginning of $M(t)$, as can be seen in Fig. 10a. This bias causes the weak frequency dependence of $M_{eq}(B_p) = M(t \rightarrow 0)$. Likewise, in the NP case, magnetization already builds-up during the upward field-ramp between zero-field and the relaxation field B_r , therefore $M(t \rightarrow 0)$ is not zero. On the other hand, at $M_{eq}(B_r) = M(B_r, t \rightarrow \infty)$ one would anticipate the Curie law, i.e. $M_{eq}(B_r) \propto \nu$ which is, however, also spoiled by switching effects.

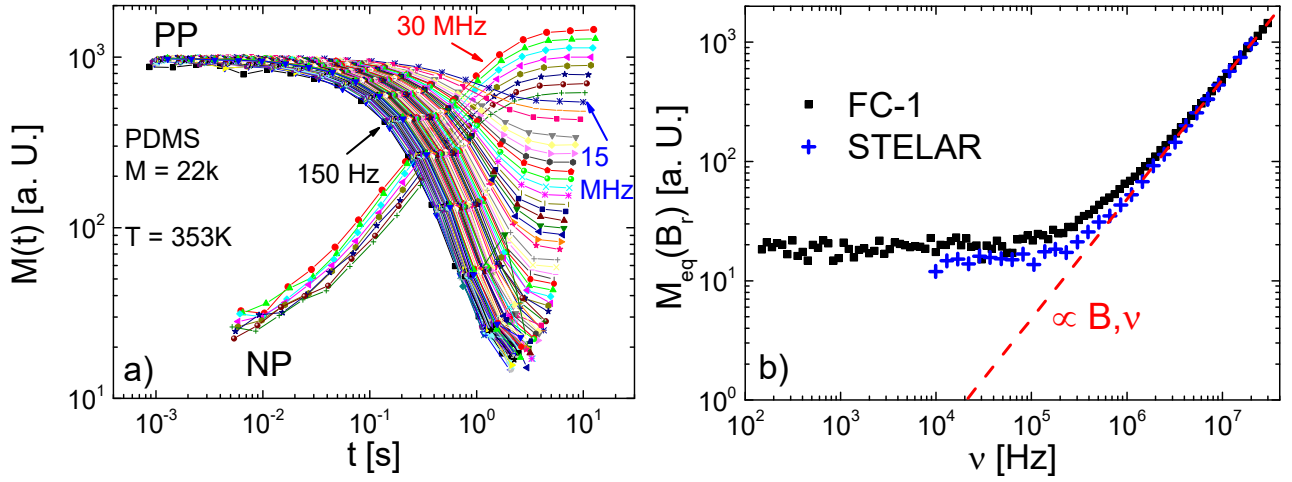


Figure 10: a) Magnetization curves $M(t)$ of PDMS with $M = 22k$, measured on the *Darmstadt* FC-1 relaxometer within relaxation fields B_r corresponding to $150 \text{ MHz} \leq \nu \leq 30 \text{ MHz}$ and at 353 K . The lines are intended to guide the eye. (b) Apparent long-time limit $M_{eq}(B_r)$ as a function of frequency ν for both relaxometers. Only above 1 MHz the Curie-law $M_{eq}(B_r) \propto \nu$ holds, indicated by the red, dashed line.

In order to demonstrate this, the experimentally observed value of $M_{eq}(B_r)$ is plotted in Fig. 10b as a function of ν . For the same sample and temperature data measured on the STELAR device is included for comparison, after vertical scaling to coincide with the FC-1 data. In fact, at high frequencies the expected Curie law is perfectly reproduced by the data measured on both relaxometers and the points lay on an original straight. At lower ν , however, plateaus are observed, which are explained by field-switching between relaxation and acquisition field during which some additional magnetization is built-up prior to detection. The STELAR plateau is somewhat lower than that of the FC-1 relaxometer. This is probably due to the slightly lower switching time of the STELAR machine. The detection field in *Bayreuth* was about 16 MHz while that in *Darmstadt* was 40 MHz . Furthermore, the STELAR data begins to deviate from the Curie law for frequencies below, say, 700 kHz , while the FC-1 data already deviates for $\nu < 3 \text{ MHz}$. The equilibrium value $M_{eq}(B_r)$ is thus an apparent one at low fields. Yet, as long as the magnetization curve $m(t)$ is mono-exponential, field-switching effects merely decrease the signal intensity in terms of the level difference $M_{eq}(B_p) - M^*_{eq}(B_r)$ but do not lead to systematic errors in $R_1(\omega)$.^{166,251,257} Else, if $m(t)$ is not exponential, one has to consider that relaxation components being on the order or even faster than the switching-interval, may relax appreciably during the ramps. Their proportion in the recorded magnetization curve $M(t)$ will be under-represented. Another effect additively contributing to $M(t)$ at long evolution times is the noise, which is always positive due to the magnitude evaluation of the complex NMR signal. Taking the magnitude of the complex signal is necessary due to phase- and field-fluctuations occurring in electronic FC NMR.

3.3 Multi-Exponential Spin-Lattice Relaxation

Indeed, there are some cases, where non-exponential relaxation is observed, namely in dendrimer melts (PUB3, section 5.6) as well as in proteins in aqueous solution.²⁵⁷ Furthermore, it was attempted to explain the mentioned discrepancies between FC and DQ NMR findings regarding polymer dynamics (for details see section 5.2), by handling (supposedly) multi-exponential relaxation in some of the FC magnetization curves negligent. This triggered an in-depth re-analysis of former raw data regarding non-exponential relaxation. Thereby, an instrumental artifact produced by the *Darmstadt* relaxometer, which appears to mimic non-exponential relaxation was revealed.

Magnetical equivalence of spins, which was presumed in section 1.7 for ^1H relaxation, is rarely fulfilled. In practice, spins may be subject to dynamic or spatial inhomogeneities: as an example, consider the simple liquid toluene, where the hydrogen atoms in the molecular backbone and those in the methyl group constitute two different spin subgroups. The dipolar interaction within the latter is dynamically pre-averaged by rapid rotation. One would first anticipate relaxation to be bi-exponential. Another example is polymer chains, where the chain ends move faster than the inner parts. However, if there are several magnetically inequivalent spin subgroups of ^1H , they are, to a certain extent, coupled together as well, due to the long-range, multi-particle character of the dipolar interaction. This leads to cross relaxation among different spin subgroups. While the intrinsic relaxation of each subgroup is associated with energy exchange with the lattice (the “heat bath” in NMR), cross relaxation leads to a continuous, energy conserving distribution of magnetization among the different subgroups. Solomon treated the case of a system consisting of only two different spins I , $S = \frac{1}{2}$, each with a different Larmor frequency ω_I , ω_S , and interacting with each other via dipolar coupling.²⁵⁸ The treatment was later generalized to take many spins in an arbitrary number of subgroups into account.²⁵⁹⁻²⁶³

Here, the model of Zimmerman and Brittin is outlined.²⁵⁹ The deviation from the equilibrium magnetization of the i -th out of N spin subgroups $\Delta m_i(t) := m_i(t) - m_i^{eq.}$ in vector notation follows a system of coupled differential equations $d/dt \Delta \vec{m}(t) = -R \Delta \vec{m}(t)$. The $N \times N$ relaxation matrix R reads $R = \delta_{ij}(\sigma_i + R_1^i) - \sigma_i \rho_{ij}$. Here, R_1^i is the spin-lattice relaxation rate of the i -th spin subgroup in the sense of the BPP-eq. 48, σ_i is the cross relaxation rate of the magnetization leaving the i -th subgroup and entering any other subgroup (but not the lattice), and ρ_{ij} is the conditional probability that magnetization is just transferred from subgroup i to j . If there are only two spin subgroups, $\rho_{12} = \rho_{21} = 1$ and $\rho_{11} = \rho_{22} = 0$. The solution of the system reads $\Delta \vec{m}(t) = e^{-Rt} \Delta \vec{m}(0) = (T e^{-Dt} T^{-1}) \Delta \vec{m}(0)$, where the diagonal matrix $D = T^{-1} R T$ containing the N eigenvalues λ_i , results from principal axes transformation. $\Delta \vec{m}(0)$ are the initial conditions which depend on the preparation of the experiment. Multidimensional NMR experiments allow determining the entries of the matrix R .^{122,263} If it is assumed that all subgroups are fully polarized at the beginning, $\Delta m_i(0)$ is proportional to the fraction p_i of spins in subgroup i with $\sum p_i = 1$. Two limiting cases need to be discussed. The first is that of **rapid cross relaxation**, i.e. $R_1^i \ll \sigma_i$. Setting $R_1^i \rightarrow 0$ yields the trivial result of no relaxation. The net magnetization would stay constant. Thus, Zimmerman and Brittin treated this limit via perturbation theory.²⁵⁹ The result for the total magnetization reads

$$m(t) \propto \exp\left[-t \sum_{i=1}^N p_i R_1^i\right] = \exp[-t \langle R_1 \rangle] \quad , \quad (62)$$

which is a single exponential function decaying with the average rate $\langle R_1 \rangle$. Rapid cross relaxation inherently leads to an averaging over all the different intrinsic rates of the individual spin subgroups, so that the whole system relaxes with a single relaxation time. Thus, information is lost. In the vast majority of ^1H spin-lattice relaxation measurements, rapid cross relaxation is efficient and $m(t)$ mono-exponential. If **cross relaxation is slow** compared to spin-lattice relaxation, i.e. $R_1^i \gg \sigma_i$ or even absent, the eigenvalues of R approach the spin-lattice relaxation rates ($\lambda_i \approx R_1^i$) and the total magnetization function reads²⁵⁹

$$m(t) \propto \sum_{i=1}^N p_i \exp[-t R_1^i] \quad . \quad (63)$$

This is just a linear superposition of independent exponential relaxation processes with the weights corresponding to the relative number of spins within each subgroup. The moments $\langle R_1^n \rangle$ can be calculated model-independently by differentiation. The mean $\langle R_1 \rangle$ is obtained from the initial slope $\langle R_1 \rangle = - \lim_{t \rightarrow 0} d/dt \ln m(t)$.²⁶⁴ Also in the intermediate regime, where R_1^i and σ_i are of the same order and the magnetizations are only partially averaged, the initial slope of the magnetization curve will provide the mean relaxation rate $\langle R_1 \rangle$.²⁶⁵ Thus, the initial decay of $m(t)$ is a universal and reliable measure of $\langle R_1 \rangle$, independent of cross relaxation.

The spin-lattice relaxation rates R_1^i and the cross relaxation rates σ_i depend in different ways on combinations of spectral densities and also on the interaction strengths (essentially determined by the inter-nuclear distances) within or between the spin subgroups. As R_1^i depends on single- and double quantum transitions, the spectral density is evaluated at ω and 2ω (eq. 48). In opposition, σ_i is governed by zero-quantum transitions (flip-flop-processes). Thus, σ_i is evaluated at the zero-frequency value of the spectral density. As $J(0)$ is usually much larger than $J(\omega, 2\omega)$ cross relaxation is practically always expected to be rapid. Indeed, for many systems like low- M liquids,¹³⁸⁻¹⁴¹ ionic liquids,²⁶⁶ rubbers and in particular polymer melts,^{70,74,127,134,140,227,267-275} mono-exponential relaxation is reported in a wide range of T and ω , although different spin subgroups eventually exist therein. Yet, when the frequency ω becomes so low that the inverse terminal relaxation time is reached, the spectral density runs into the plateau ("extreme narrowing"), i.e. $J(\omega \tau_c(T) < 1) = \text{const.}$. Consequently, the spin-lattice relaxation rates always approach the cross rates and the averaging will be incomplete, leading to non-exponential magnetization curves. This case may occur at low ω , at high T and in systems with a relatively short terminal relaxation time. The magnitude of cross relaxation also strongly depends on the distances between the different subgroups. In order to check relaxation data for mono-exponentiality, it is useful to plot the normalized magnetization function following from eq. 60, with time axis scaled by $\langle R_1 \rangle$:

$$m(t \cdot \langle R_1 \rangle) = (M(t \cdot \langle R_1 \rangle) - M_{eq}(B_r)) / (M_{eq}(B_p) - M_{eq}(B_r)) \quad (64)$$

Neither the software provided by the manufacturer of the STELAR relaxometer nor that running on the FC-1 setup is sufficient for that task. Therefore, the raw data in terms of the FID's is analyzed externally, employing a self-written program. If the initial decay of $m(t \cdot \langle R_1(\omega) \rangle)$ concurs with $\exp[-\langle R_1 \rangle t]$, the mean rate $\langle R_1 \rangle$ was determined correctly, irrespective of the method or fit function used for its determination. Furthermore, magnetization data measured at numerous different

frequencies is strongly condensed by plotting $m(t < R_1(\omega) >)$, as master curves are generated. Another benefit of this kind of representation is that non-exponential relaxation can be identified easily. Fig. 11 exemplifies the suggested representation of $m(t < R_1(\omega) >)$, based on selected protonated polymers, specifically PDMS-h 22k (a), PEP-h 200k (b) and PB-h 196k, isotopically diluted in deuterated PB-d 191k (cf. sections 4.3 and 5.2) (c), as well as for (partially) protonated toluene h_8 , h_5 and h_3 (d). The relaxation curves measured with the STELAR relaxometer are shown in blue, while such recorded on the FC-1 device are distinguished in gray. It is emphasized that in the case of the polymers (Figs. 10a-c) only data is included which was measured at about the same temperature and in a common frequency interval, as indicated. This allows for a direct comparison between magnetization curves measured with the STELAR and with the FC-1 relaxometer, respectively. In the case of toluene (Fig. 11c), only FC-1 data was available.^{PUB6}

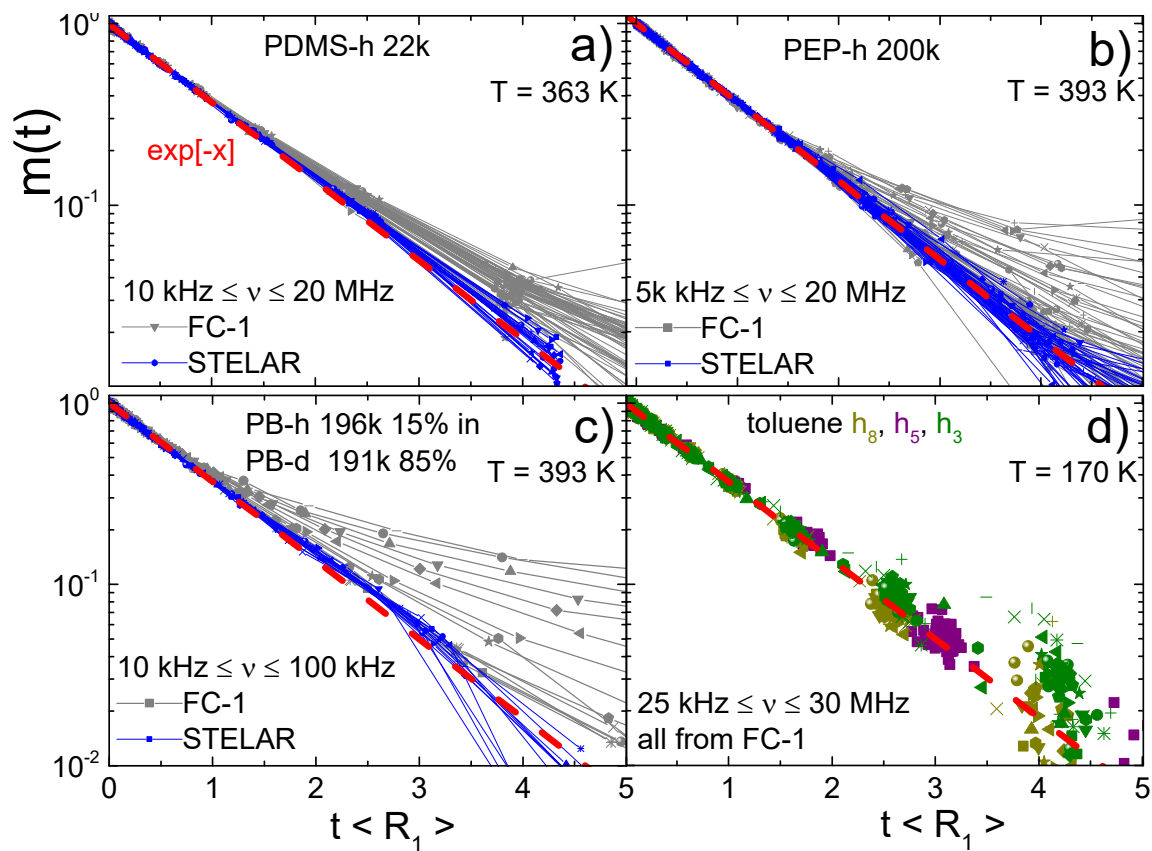


Figure 11: Normalized ^1H relaxation functions $m(t < R_1 >)$ of (a) PDMS-h 22k, (b) PEP-h 200k and (c) PB-h 196k diluted to 15% in PEP-d 191k, resulting from measurements in *Darmstadt* (gray) and *Bayreuth* (blue). d) Same representation for toluene h_3 , h_5 and h_8 (distinguished by different colors), all of which were solely measured in *Darmstadt*.^{PUB6} Frequency intervals and temperatures as indicated. Simulations of single exponentials are also included (red dashed lines).

At least at short times ($t < \langle R_1^{-1} \rangle$), perfect mastering is observed in all cases, from which it is concluded that $\langle R_1(\omega) \rangle$ was always determined correctly. Obviously, at the long evolution times, there is a difference between data measured on the STELAR and on the FC-1 relaxometer, as can be

seen from Figs. 11a-c. While $m(t)$, when measured in *Bayreuth* is clearly mono-exponential over two decades for all frequencies and in all three polymers, the curves measured in *Darmstadt* always bend up at long evolution times, *i.e.* they deviate from mono-exponential behavior indicated by the red dashed lines.

The first example PDMS-h 22k, for which $m(t < R_1(\omega))$ is shown in Fig. 11a, merely contains one group of magnetically equivalent protons, namely those in the methyl side-groups. While relaxation measured with the STELAR device is mono-exponential, as expected, the FC-1 curves bend up at long times. The second example is PEP-h 200k (Fig. 11b), which is alternatingly constituted from ethylene and propylene monomers, imposing the existence of two magnetically inequivalent spin-subgroups. The first comprises seven protons per repeat unit in the backbone, the second one three protons in the methyl side group, respectively. The relaxation rate $R_1^{CH_3}(\omega)$ of the methyl protons subject to rapid rotation, is expected to be significantly smaller than that of the seven protons attached to the chain, $R_1^{chain}(\omega)$. One could be inclined to expect a bi-exponential $m(t)$ (*cf.* section 5.4). The STELAR data is again single exponential, suggesting rapid cross relaxation among the different ensembles of protons. Yet, the *Darmstadt* data is again apparently not exponential. The next example is PB-h 196k diluted to 15% in a matrix of deuterated PB-d 191k, shown in Fig. 11c. This important isotope dilution experiment is crucial, as it is used for determining the pure intra-molecular relaxation contribution $R_1^{intra}(\omega)$ in this polymer (*cf.* sections 4.3 and 5.2). Also in this case, the *Bayreuth* data is clearly mono-exponential, in contrast to that of *Darmstadt*. The dilution goes along with a decrease of the proton signal. This could explain why the *Darmstadt* artifact is more pronounced in the diluted system.

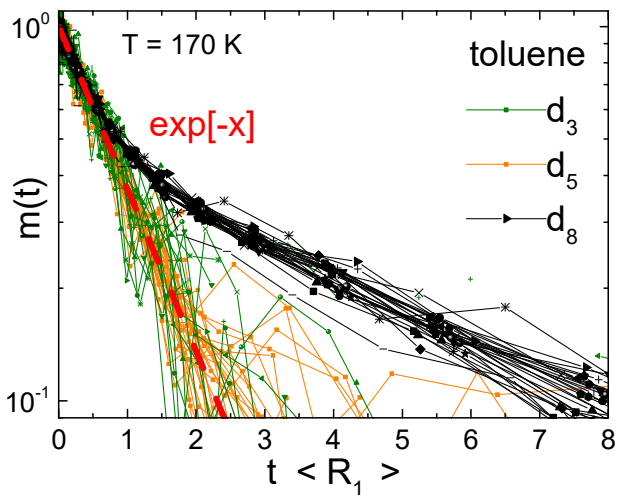
The final example is toluene (Fig. 11d). The fully protonated species toluene h_8 bears five backbone and three methyl protons, *i.e.* again two spin subgroups. Nonetheless, the curves of h_8 highly resemble those of the single spin subgroup systems h_3 and h_5 , respectively. The deviation from mono-exponential behavior observed at long times in all three toluene species is of similar extend compared to that of the (undiluted) polymers. It is thus concluded, that relaxation is actually single exponential in all three cases of toluene labelling, in particular in toluene h_8 , where rapid cross relaxation averages over both spin subgroups. Apparently, all the 1H magnetization curves shown in Fig. 11 which were measured in *Darmstadt*, are superimposed by an instrumental artifact, pretending an apparent multi-exponentiality at long evolution times. A closer inspection of the artifact reveals no systematic trend, like frequency dependence. Considered as a whole, the discovered instrumental artifact occurring on the FC-1 relaxometer is weak and previous measurements are not challenged. It turns out that the un-weighted, mono-exponential fits used so far for determining relaxation rates from *Darmstadt* data, approximate the values determined by initial slope analysis, so well, that there are virtually no differences. The corrections are in the percent area. In particular, they cannot explain the mentioned discrepancies between FC and DQ NMR concerning relaxation in polymers, which will be discussed in detail in section 5.2. Yet, until the artifact is overcome, one should refrain from explicitly including the long-time tail of magnetization curves measured on the FC-1 relaxometer in the analysis.

Counterexamples for actual, multi-exponential longitudinal magnetization decay of 1H are, as said, proteins in aqueous solution^{257,276} and dendrimer melts^{PUB3} (*cf.* section 5.6), but also organic tissues²⁷⁷ and 1-phenylpropyne ($CH_3C\equiv CC_5H_5$).²⁶⁰ Those are also systems with more than one 1H spin subgroup. Nevertheless, cross relaxation may be inefficient here due to weak interaction strength between the

different spin subgroups. As discussed in section 1.7, the strength of the dipolar coupling depends on the inter-spin distance r^{-6} . If different spin subgroups are spatially well-separated, the averaging via cross relaxation is incomplete and the magnetization remains multi-exponential. Phenomenologically, the extent of non-exponentiality can be quantified by fitting experimental data to model-functions. Roos et al. evaluated FC magnetization curves of proteins in concentrated solution measured in *Bayreuth*, assuming a Gaussian distribution of $\ln(R_1)$ (log-normal distribution).²⁵⁷ It contains two parameters, the width σ and the median R_1^{med} . The arithmetic mean follows from $\langle R_1 \rangle = R_1^{med} \exp[\sigma^2/2]$. Yet, the log-normal distribution doesn't feature a maximal cutoff relaxation rate physically required. This issue potentially leads to an overestimation of the obtained mean-value. In PUB3 a stretched exponential was fitted to the magnetization curves of dendrimer melts. Yet, the arithmetic mean rate doesn't exist for the underlying distribution function in this case. Instead, the mean relaxation time $\langle T_1 = R_1^{-1} \rangle^{-1} \neq \langle R_1 \rangle$ was calculated using the stretched exponential. This issue will be revisited in section 5.6.

Regarding ^2H , the situation is different. The relatively short range of the quadrupolar interaction compared to that of the dipole-dipole interaction inhibits cross relaxation among different nuclei, therefore $m(t)$ is expected to obey the limit in eq. 63, and the different relaxation rates are not averaged. As an example, FC ^2H NMR measurements performed on the FC-1 device provide bi-exponential $m(t)$ for toluene d_8 , as shown in Fig. 12, where the mean rate, used for scaling the time axis, was determined from a bi-exponential decomposition.^{PUB6} In the case of toluene d_3 and d_5 , respectively, the expected mono-exponential decay is observed over the first decade in amplitude; beyond, the "FC-1 artifact" again spoils the data.

Figure 12: Normalized relaxation functions $m(t \langle R_1 \rangle)$ of toluene d_3 , d_5 and d_8 , all measured on the FC-1 relaxometer.^{PUB6} The temperature was 170 K.



4. FC NMR: Previous Work

The following chapter is intended to briefly summarize previous work concerning FC NMR relaxometry on polymer melts, a field which was mainly pioneered by Kimmich and co-workers.^{5,6,166} Different linear standard polymers like PB, PDMS and PE were investigated by FC ^1H and ^2H NMR, yet, in limited ranges regarding temperature and molar mass. In particular, no low- M reference systems were investigated, and the evolution from the simple liquid to the polymer melt was not addressed. In accordance with their theoretical time scale separation ansatz^{5,129} (cf. section 1.7), Kimmich et al. ascribed spin-lattice relaxation dispersion in polymer melts to three distinct regimes. The first reflects the local regime (α -process), which they didn't cover as they only measured at rather high temperatures. The second regime is that of polymer dynamics, governed by chain modes. Kimmich et al. focused on this regime and found rich dispersion in form of different power-law regimes, which they explained within the renormalized Rouse model. The third regime is governed by the terminal relaxation.

The subsequent FC relaxometry works on polymer melts of S. Kariyo et al.,^{70,271,273} R. Meier et al.^{140,141} and in particular A. Herrmann et al.^{134,198,227,274,275,278} in the *Bayreuth* group can be considered as a continuation of the studies of Kimmich and co-workers. The low-field capabilities of the FC-1 relaxometer allowed reaching frequencies of a few hundred *Hz*, while previous experiments of Kimmich and also of the *Bayreuth* group were limited to about 10 *kHz*. One of the most important developments in the *Bayreuth* group is the construction of master curves in the so-called susceptibility representation. By measuring relaxation dispersion in a much broader temperature range than Kimmich et al., the effective frequency window is broadened so much, that a transformation into the time domain becomes possible and the dipolar correlation function $C_{DD}(t)$ is gained (cf. below and section 1.1). However, the role of intra- and inter-molecular relaxation in ^1H wasn't fully understood initially.

4.1 Susceptibility Representation and Master Curves

Even with the low-field capabilities of the *Darmstadt* relaxometer, the frequency range is restricted to about five decades (cf. Fig. 2 and section 3.1). In order to study the full hierarchy of polymer dynamics, still a wider frequency interval is required. Assuming frequency-temperature superposition (FTS), this window can be significantly extended by measuring $R_1(\omega)$ in a broad temperature range.

As an example, dispersion data $R_1(\nu)$ of the fully protonated, entangled ($M \gg M_c$) polymer PB 87k is displayed in Fig. 13a. It was measured on the STELAR relaxometer within $10 \text{ kHz} \leq \nu \leq 20 \text{ MHz}$ and at $220 \text{ K} \leq T \leq 400 \text{ K}$.²²⁷ Rich dispersion is found at all temperatures. In Fig. 13b the conversion into the NMR susceptibility representation $\chi''(\omega) = \omega R_1(\omega)$ (eq. 19, section 1.1) is shown. Assuming FTS a master curve $\chi''(\omega a_T)$ from susceptibility data is constructed by applying T -dependent frequency shift factors a_T , a procedure well-known from DS^{57,58,108} and in particular rheology.^{6,60-62,82,228,229} The idea of analyzing spin-lattice relaxation data in terms of $\omega R_1(\omega)$ was first spawned by Cohen-Addad.²⁷⁹ Yet,

not ω was varied as in FC NMR, but the relaxation rate by changing the concentration of a polymer in solution.

Such master curves are shown in Fig. 13c for many different M .²²⁷ It is again emphasized that solely horizontal shifting is required in the susceptibility representation, while the second moment M_2 (eq. 48 in section 1.7) is conserved. An approach for constructing master curves in terms of $R_1^{-1}(\omega a_T)$, where shifting in the two dimensions is necessary to keep M_2 , was proposed by Kariyo et al.^{269,270} In bulk liquids, including polymers, typically a good mastering is observed. Constructing master curves dramatically extends the frequency range from five to up to ten decades and leads to a strong condensation of a large amount of data recorded at many different temperatures. Furthermore, susceptibility master curves allow for a direct comparison between spin-lattice relaxation dispersion and measurements from other techniques, such as DLS, DS and in particular rheology.

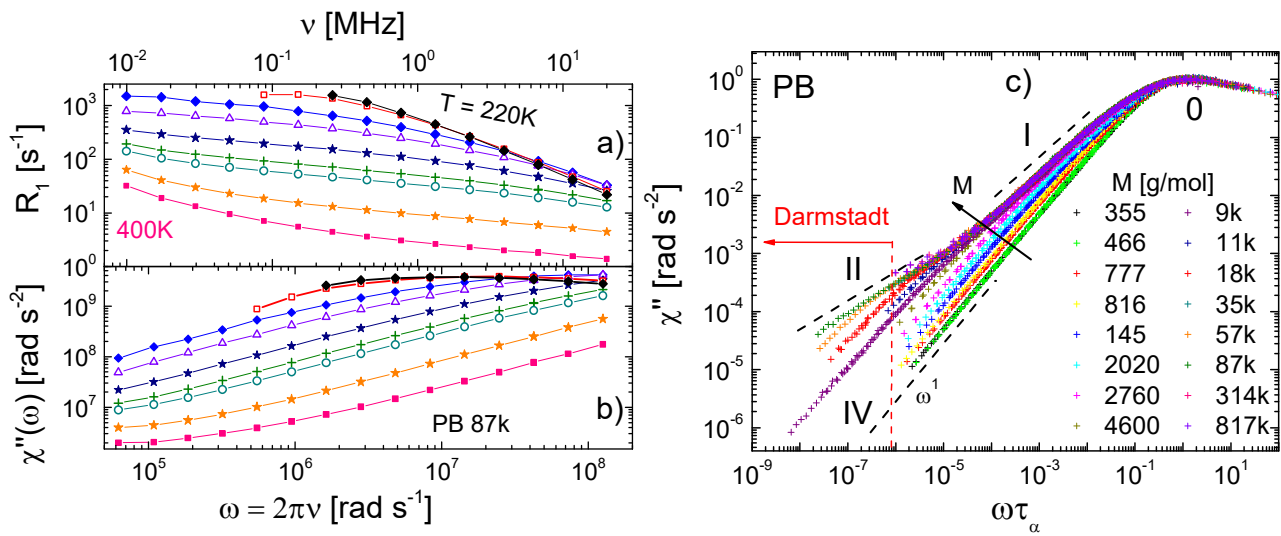


Figure 13: a) $R_1(\omega)$ of PB 87k measured by A. Herrmann on the STELAR relaxometer in the T range as indicated.²²⁷ (b) Same data in the susceptibility representation $\chi''(\omega)$. (c) Evolution of NMR susceptibility master curves $\chi''(\omega\tau_\alpha)$ with M , from the simple liquid (PB 355) to the entangled melt ($M > M_c$). The range solely accessible to the *Darmstadt* relaxometer is marked. Relaxation regimes (0,I,II,IV) are indicated. Fig. 13c was taken from Herrmann et al. and adapted.²²⁷

By measuring down to sufficiently low T it is ensured that the α -relaxation is included in the FC NMR susceptibility spectra. In Figs. 13b and c the α -process is reflected in the dominating peak at high frequencies. Then, the frequency axis of the master curves is scaled according to $\chi''(\omega\tau_\alpha)$. This provides the temperature dependence of τ_α along the way. The values can be compared to those of other techniques like DS and shear rheology (cf. Fig. 32, section 5.5). Master curves $\chi''(\omega\tau_\alpha)$ of the total ^1H relaxation of PB of several M are shown in Fig. 13c. For the first time, Herrmann et al. extended the measurements on PB carried out on the STELAR relaxometer toward lower frequencies employing the FC-1 device.²²⁷ Thus, extremely low fields were accessed (cf. section 3.1). The evolution of the polymer dynamics with increasing chain length M , i.e. from the simple liquid to the

entangled melt, was studied. Starting with the simple liquid PB 355, where essentially just the peak of the α -process (regime 0) is recognized, M is increased, finally exceeding the crossover molar mass significantly, *i.e.* $M \gg M_c \approx 2k$. In the entangled melt, additional amplitude at $\omega\tau_\alpha \ll 1$ arises in $\chi''(\omega\tau_\alpha)$, to which two polymer specific power-law regimes, denoted with I and II, were ascribed. They were referred to Rouse and entanglement dynamics, respectively. In particular in the entanglement regime (II) the shape of the $\chi''(\omega\tau_\alpha)$ curves depends on the molar mass. If M is not too high, the terminal relaxation (regime IV) falls into the frequency window of FC NMR. Yet, the corresponding low-frequency behavior $\chi''(\omega\tau_\alpha) \propto \omega^1$, indicated in Fig. 13c, is actually just apparent. The diffusion-determined inter-molecular relaxation predominant in ^1H at low frequencies leads to a square root behavior in the dispersion (*cf.* section 1.7 and eq. 58). In the susceptibility representation this behavior yields $\chi''(\omega) \propto (\omega R_1(0) - c\omega^{3/2})$. In the limit of small frequencies this expression approaches $\propto \omega^1$ asymptotically. Hence, the inter-molecular relaxation, governing the low-frequency dispersion, is somewhat concealed in the susceptibility representation. In the rate representation, however, the inter-molecular relaxation contribution is more visible and the diffusion coefficient can be determined, typically in the range $10^{-15} < D \text{ m}^2\text{s} < 10^{-9}$ using eq. 58. When compared to reference data from FG NMR, the agreement is striking.¹³⁸⁻¹⁴¹ A more detailed description of how FC relaxation data evolve with increasing M is given in the subsequent section, where it is focused on the time domain.

4.2 FC ^1H NMR in the Time Domain and Comparison to DQ ^1H NMR

As said, the dynamic range of FC susceptibility master curves (like those shown in Fig. 13c) is very broad. Hence, a transformation into the time domain can be performed, yielding the dipolar correlation function $C_{DD}(t/\tau_\alpha)$. After master curve construction the data is arbitrarily spaced over a huge frequency range. Thus, an ordinary discrete Fourier transformation will not work. Instead, a version of Filon's numerical integration method is employed.²⁸⁰ Figure 14 shows the resulting evolution of $C_{DD}(t/\tau_\alpha)$ with M , obtained by transforming the susceptibility master curves of the total ^1H relaxation of PB ($M \geq 2k$) shown in Fig. 13c. Nine decades in time and almost seven in amplitude are covered, and the full form of the dipolar correlation function is monitored by a single technique.²²⁷ Other linear polymers display very similar behavior regarding $C_{DD}(t)$ (*cf.* ref. 272 and section 5.4).

In a methodical comparison, corresponding $C_{DD}^{DQ}(t)$ data of DQ ^1H NMR (*cf.* section 2) is also included in Fig. 14 and marked in red.²²¹ Using the *Darmstadt* relaxometer, FC NMR has approached the long time scales, which were restricted to DQ NMR before.²²⁷ Otherwise, DQ NMR doesn't reach times shorter than τ_e , in contrast to FC NMR. Almost perfect agreement among the both ^1H NMR methods is observed, *i.e.* $C_{DD}(t) \cong C_{DD}^{DQ}(t)$. Yet, the DQ data had to be vertically scaled by a factor of about 0.5 in order to achieve overlap (*cf.* section 5.2).^{223,227}

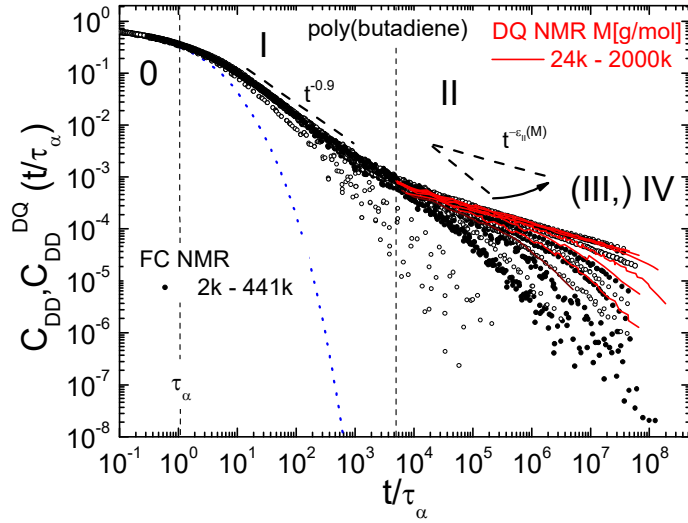


Figure 14: Evolution of $C_{DD}(t/\tau_\alpha)$ of PB with M .²²⁷ DQ ^1H NMR data $C_{DD}^{DQ}(t/\tau_\alpha)$ is included (red lines).²²¹ Dynamic regimes (0-IV) and the entanglement time τ_e are indicated. The extrapolation of the α -process by a (stretched) exponential is also shown (dashed blue line). Adapted from ref. 278.

Beyond the initial stretched exponential decay (regime 0) indicated by the blue dashed line in Fig. 14 and referred to the α -process, two polymer specific power-law regimes

(I,II) where $C_{DD}(t) \propto t^{-\epsilon}$ were attributed by Herrmann et al.²²⁷ At times $\tau_\alpha < t < \tau_e$, the dipolar correlation function of the polymers is first governed by the Rouse regime (I). With increasing M , it emerges from the relaxation behavior of a simple liquid and saturates for M around M_c , finally converging toward a power-law regime with an apparent exponent $\epsilon_I \approx 0.9$, as indicated in Fig. 14. At τ_e a crossover to a second power-law regime (II) occurs. As M increases, regime II also extends toward longer times. The exponent value, *i.e.* the slope depends on M , specifically $0.3 \leq \epsilon_{II}(M) \leq 0.8$. The slope decreases with increasing M and saturates at very high M , say, for $M > 200 M_c$. The values $\epsilon_{II}(M)$ resulting from FC as well as DQ ^1H NMR are summarized in Fig. 20 of section 5.2, again demonstrating the good agreement between FC and DQ NMR, at least at high M .^{221,227} At that time, it was still assumed that inter-molecular relaxation would be negligible, and consequently that $C_{DD}(t)$ agrees with the re-orientational correlation function $C_2(t)$.^{221,227} As the found values for ϵ_{II} at highest M are very close to the one predicted by the TR model regarding re-orientation ($\epsilon_{II}^{TR} = 0.25$, *cf.* Table 1), the findings were interpreted as a validation of the TR model. In other words, for M high enough that finite length effects don't interfere any more, the existence of the constrained Rouse regime of the TR model concerning re-orientation, appeared to be confirmed by two independent NMR techniques (DQ & FC).^{221-223,227} The “highly protracted transition” (refs. 198, 221) to the predicted value of 0.25 was also observed in the computer simulations by Wang et al. (*cf.* section 2).²⁰ It was justified by finite length effects, especially CR.

According to Herrmann et al., regime II is succeeded by a smooth transition to the terminal regime (IV), which can only be observed, if the strongly M -dependent terminal relaxation time still fits into the experimental time window.²²⁷ Yet, it wasn't commented on the terminal behavior of $C_{DD}(t)$ adequately. Neglecting inter-molecular relaxation, one would expect that $C_{DD}(t) \equiv C_2(t)$. The terminal relaxation of $C_2(t)$ is supposed to be an exponential decay, which is, however, not observed in Fig. 14. Subsequent isotopic dilution experiments by Herrmann et al. indeed confirmed that assuming inter-molecular relaxation to be negligible, is grossly wrong,¹³⁴ as will be discussed below in section 4.3. In section 5.4 a re-interpretation of the findings on PB concerning the dipolar correlation function $C_{DD}(t)$ will be given.

4.3 Isotope Dilution Experiments

Due to the fact that in the case of protons the functions $C_{DD}(t)$ and $\chi''(\omega)$, respectively, are time/frequency dependent superpositions of intra- and inter-molecular contributions, a rigorous comparison with theoretical models (like TR) is only reasonable when a separation is performed and both components are studied independently (*cf.* section 1.7). The selectivity of NMR enables a distinction, applying the isotope dilution technique: fully protonated chains are diluted in a matrix consisting of fully deuterated chains of the same species and of similar molar mass.^{112,127,281,282} While the intra-molecular contribution is preserved, the inter-molecular one is suppressed, when approaching zero concentration. It is assumed that such isotope dilution doesn't change anything else, except for the dipolar interaction between spins of different molecules. In practice, isotope dilution experiments are challenging. Isotope effects on T_g are reported,^{134,PUB2} it is often difficult to obtain the same M for deuterated and protonated chains¹⁹⁵ and, due to the low mixing entropy, such polymer blends tend to demix.⁶² Nevertheless, first FC experiments on isotopic polymer blends of PB as well as of PEO were performed by Kehr et al.^{127,130} and later on by Herrmann et al. on protonated PB-h 24k diluted to 11% in a matrix of deuterated PB-d 23k and on PB-h 196k diluted to 15% in a PB-d 191k.¹³⁴ The correlation functions $C_2(t/\tau_\alpha)$ and $C_{inter}(t/\tau_\alpha)$ for PB 196k, resulting from the decomposition of susceptibility master curves and subsequent Fourier transformation, are displayed in Fig. 15.¹³⁴

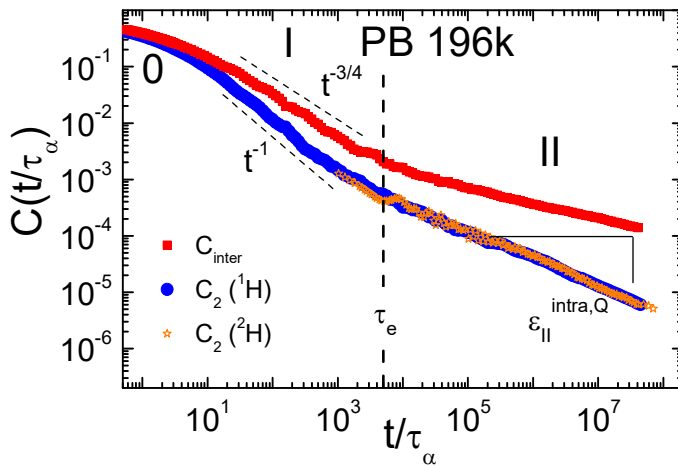


Figure 15: Intra- and inter-molecular correlation functions of PB 196k, as determined by FC ^1H as well as by ^2H relaxometry. Relaxation regimes (0,I,II) are indicated. Adapted from ref. Herrmann et al.¹³⁴

The most important experimental finding of Herrmann et al. was that the inter-molecular relaxation is not negligible at all, as was often assumed before. Instead, it even dominates the

relaxation dispersion at low frequencies/long times. At $\tau_\alpha < t < \tau_e$ (regime I) $C_2(t) \propto t^{-\epsilon}$ features a slightly steeper decay than $C_{inter}(t)$, a subtle fact on which it was not commented on by Herrmann et al. and which will be also revisited in section 5.4. It will be discussed that for $t > \tau_e$ the exponent $\epsilon_{II}^{intra}(M)$ becomes smaller with increasing M , *i.e.* the protracted transition is observed, as in the case of the total relaxation (*cf.* ref. 134, section 4.2 and Fig. 20). The “protracted transition” is consequently also observed in $C_2(t)$. An exponent value of $\epsilon_{II}^{intra}(196 \text{ k}) \approx 0.49$ was estimated by Herrmann et al.¹³⁴ A refined analysis of the derivative of $C_2(t)$ in log-log scaling presented PUB2 (section 5.2) reveals a somewhat smaller value of around $\epsilon_{II}^{intra}(196 \text{ k}) \approx 0.45$. The precise exponent values can be found in Fig. 20 of section 5.2. Nevertheless, the value ϵ_{II}^{intra} of high- M PB differs from the value 0.25 predicted by the TR model significantly (Table 1). This fact challenges the TR model regarding re-orientation, which actually seemed to be essentially confirmed, when the total relaxation was regarded (*cf.* section 4.2). The reliability of this important finding was confirmed by ^2H

dispersion measurements probing intra-molecular relaxation exclusively and yielding $\varepsilon_{II}^{intra} \approx \varepsilon_{II}^Q$ (Q stands for “quadrupolar” ^2H relaxation). This data is also included in Fig. 15 (orange stars) and the corresponding exponent value in Fig. 20 (section 5.2).

The determination of $C_{inter}(t)$ allowed the calculation of the segmental MSD $\langle r^2(t) \rangle$ of PB 24k and PB 196k.¹³⁴ For that purpose still the analytical expression eq. 57 was applied. Good agreement with the TR model for Rouse and constrained Rouse dynamics was found.¹³⁴ The fact that translational motion is in accordance with the TR model while re-orientational motion is not, explicitly challenges the RTO hypothesis and the further investigation of both is part of this PhD work. The $C_2(t)$ data of PB is revisited in section 5.2 and the $C_{inter}(t)$ data in section 5.4. Moreover, a further isotope dilution experiment on the linear polymer PEP was performed recently. It enables to check whether the results on PB indicating a failure of the TR model with respect to re-orientation, can be generalized (*cf.* section 5.4).

5. Results - FC NMR as a Tool of Molecular Rheology

Refraining from chronological order, the following chapter summarizes the major results of this PhD work, which are partially published in the articles reprinted in section 6. Furthermore, the chapter is enriched with recent findings, which are be part of three further publications, which are currently under review (*cf.* also section 6.3).

5.1 FC ^1H Relaxometry vs. Atomistic MD Simulations

PUB1 arose from the unique opportunity of comparing FC ^1H relaxometry results to those of atomistic MD simulations (*cf.* section 2). Already at the end of my Diploma studies preceding the PhD work, I started measuring the polymer dynamics of poly(propylene glycol) (PPG) in a broad M range via FC ^1H relaxometry, using the STELAR machine. At around the same time, atomistic MD simulations of poly(propylene oxide) (PPO) were performed at the *Technische Universität Darmstadt* in the group of M. Vogel. As PPG and PPO are chemically identical except for the end-groups (hydroxyl vs. methyl), the findings of both, experiment and simulation could be confronted. The FC ^1H NMR relaxation data on PPG was published in a preceding article.²⁷² Assuming FTS, susceptibility master curves $\chi''(\omega\tau_\alpha)$ of the total relaxation were constructed for PPG in the range $0.1\text{k} \leq M \leq 18\text{k}$. Fourier transformation yielded the dipolar correlation function $C_{DD}(t/\tau_\alpha)$ (*cf.* section 1.7).

Concerning the MD simulations, a set of atomistic, quantum chemistry-based potentials was applied to PPO chains of different molar masses $0.1\text{k} \leq M \leq 6\text{k}$. The force field comprised Coulomb and Buckingham potentials for non-bonded interactions, as well as stretching, bending and torsion potentials for modelling the chemical bonds between monomers. The number of simulated atoms in the volume was about 4000. The longest chains consisted of $N = 100$ monomers. Atomic trajectories in the time range $1\text{ps} \leq t \leq 30\text{ns}$ and at different temperatures were simulated and recorded using the GROMACS package.²⁸³ In a preceding atomistic simulation work, the M -dependence of the α -relaxation was investigated in terms of the intermediate scattering function.²⁸⁴ For PUB1 the re-orientational autocorrelation function

$$C_2(t) \cong 1/2 \langle 3[\vec{e}_{oo}(t) \cdot \vec{e}_{oo}(0)]^2 - 1 \rangle, \quad (65)$$

with \vec{e}_{oo} denoting the bond vector connecting two consecutive oxygen atoms located in the chain backbone, was calculated. It was assumed that this correlation function is equivalent to the intra-molecular correlation function $C_2(t)$, accessible by NMR relaxometry. In PUB1 the inter-molecular relaxation was first spared out in the evaluation of the simulation data. As also the time range of the simulations was limited by insufficient computational power, TTS (*cf.* section 1.2) was assumed to create master curves $C_2(t/\tau_\alpha)$ of PPO of the different M . Thus, the simulation data was analyzed in the same way as that of NMR relaxometry. Figure 16 shows selected results for the simple liquids di-propylene glycol/di-propylene oxide (a) and for some PPG/PPO polymer melts (b). The dimers were chosen because monomeric PO was not simulated, and second, due to the fact that a pronounced inter-molecular contribution appears in the total relaxation dispersion of PG.²⁷²

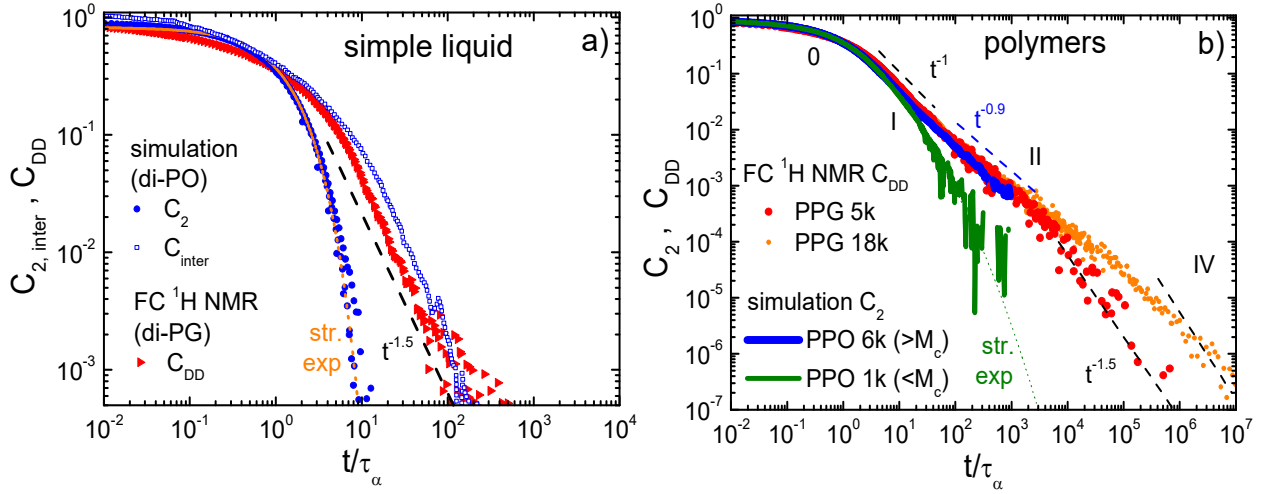


Figure 16: a) Dipolar correlation function $C_{DD}(t/\tau_\alpha)$ of di-PG gained from FC ^1H NMR relaxometry in comparison to $C_2(t/\tau_\alpha)$ and $C_{\text{inter}}(t/\tau_\alpha)$ (ref. 132), obtained from atomistic MD simulations. b) $C_2(t/\tau_\alpha)$ from simulations (thick lines) of un-entangled PPO 1k as well as of entangled PPO 6k, respectively, in comparison to $C_{DD}(t/\tau_\alpha)$ of entangled PPG 5k and PPG 18k, obtained from FC ^1H NMR relaxometry (symbols). Relaxation regimes (0-IV) and power-laws are indicated. The dotted lines represent extrapolations of the α -relaxation via stretched exponential fits. Both figures are adapted and extended from PUB1.

Regarding the simple liquids (Fig. 16a), $C_2(t/\tau_\alpha)$ and $C_{DD}(t/\tau_\alpha)$ are obviously different, which can be explained by the fact that $C_2(t)$, determined from the simulation data, solely refers to re-orientation. It features a stretched exponential decay, as indicated by the dotted orange line. Otherwise, $C_{DD}(t)$ gained from FC NMR, is a superposition of intra- as well as inter-molecular relaxation contributions, the latter dominating the shape of $C_{DD}(t/\tau_\alpha)$ at long times (*cf.* section 1.7). In fact, the long-term behavior of di-PG follows $C_{DD}(t/\tau_\alpha) \propto t^{-1.5}$, as indicated in Fig. 16a. In the course of a subsequent publication by the Vogel group, the inter-molecular correlation function $C_{\text{inter}}(t)$ was explicitly calculated from the trajectories of di-PO.¹³² In Fig. 16a this $C_{\text{inter}}(t/\tau_\alpha)$ data of di-PO is included (blue open symbols). It also features the expected $\propto t^{-1.5}$ behavior at long times, as it was found for the NMR data $C_{DD}(t)$. The good agreement to the FC NMR data on di-PG corroborates the fact that inter-molecular relaxation determines the shape of $C_{DD}(t)$ in this simple liquid. It is noted again that simulations, in particular atomistic ones, rarely address inter-molecular correlation functions. Another notable exception is a simulation of a Lennard-Jones liquid by Odelius and co-workers.¹⁴²

For the polymers (Fig. 16b) PPG 5k (FC NMR, blue) and PPO 6k (simulation, red), $C_2(t)$ and $C_{DD}(t)$ yield a consistent picture in the glassy regime (0) as well as beyond, in regimes I and II, where polymer dynamics is detected. From this good agreement between FC ^1H NMR and simulation regarding PPG 5k vs. PPO 6k, it was concluded that at least in the common time range (glassy and Rouse dynamics) inter-molecular relaxation is not so important, yet. First, a power-law regime is established, where both, $C_2(t)$ as well as $C_{DD}(t)$ are $\propto t^{-1}$. This exponent value is in accordance with the Rouse model concerning intra-molecular relaxation (*cf.* Table 1). Only for curves with $M > M_c \approx 5k$ a second power-law regime (II) appears at $t > \tau_e \approx 300 \tau_\alpha$ in both, $C_2(t)$ as well as in $C_{DD}(t)$.^{PUB1} Note that in the case of PPO (simulation) only $M \approx 6k$ exceeds M_c and an exponent value of $\varepsilon_{II} \approx 0.9$ is assigned. As far as it is known, this could be the first hint of entanglement in atomistic simulations of polymers. In Fig. 16b

also FC NMR data of the higher M polymer PPG 18k is included. Here, the entanglement related regime II is more pronounced and features a lower exponent of around $\varepsilon_{II} \approx 0.7$, *i.e.* also in PPG the exponent value $\varepsilon_{II}(M)$ decreases with increasing M , according to the “protracted transition” (*cf.* section 4.2 and Fig. 20). For the lower M polymer PPO 1k, for which $C_2(t/\tau_\alpha)$ data is also included in Fig. 16b, regime II is not observed, yet. At longest times, only FC NMR reaches the terminal regime (IV) in the case of PPG 5k where $C_{DD}(t/\tau_\alpha) \propto t^{-3/2}$. In order to approach the terminal regime of PPO 6k also by the atomistic simulations, way more computational power is required. Yet, for lower M , the simulation was still able to cover the terminal relaxation, for example in the case of un-entangled PPO 1k (*cf.* Fig. 16b). As expected, and as it is the case of the simple liquid di-PG, $C_2(t/\tau_\alpha)$ of PPO 1k decays (stretched) exponentially at long times (green dashed line).

Atomic trajectories offer the opportunity to calculate $C_2(t)$ for different positions along the chains, enabling to address the dynamics of segments close to the chain ends and of segments in the center separately. In ref. 284 (Vogel group) it was found that the local segmental reorientation (α -process) of terminal and central segments becomes increasingly decoupled when chains become longer, *e.g.* τ_α of the terminal segments in PPO 2k was found to be four times larger when compared to central segments. In the course of PUB1 the long-time behavior in $C_2(t)$ of PPO 6k was investigated position-dependently. It was found that segments close to the ends de-correlate quicker than central ones. Those at the very ends even feature (stretched) exponential correlation decay and no polymer dynamics at all. In contrast, central segments appear to be stronger affected by entanglement, reflected in a decreased exponent $C_2(t) \propto t^{-0.75}$ in regime II instead of $\propto t^{-0.9}$, as resulted from averaging over the whole chain.^{PUB1} Similar findings were already reported by Kremer and Grest, yet, from coarse-grained simulations based on a simple bead-and-spring model.¹⁸⁹ Cohen-Addad et al. also ascribed two regimes to transverse relaxation data, reflecting the dynamics of inner as well as of end-monomers, respectively.⁵⁹ In experiments, such a position resolved analysis of quantities like correlation functions is very difficult. Nevertheless, the selectivity of NMR offers the opportunity of probing only parts of chains by partial isotope labelling. In the course of PUB2, which is discussed in the upcoming section, chains where only the central monomers are labelled while the ends are obscured by deuteration, were investigated.

5.2 Reorientation and Finite Length Effects in Polymer Melts

In this section results on the segmental re-orientational dynamics of entangled poly(butadiene) (PB) are reported. Mainly the correlation function $C_2(t)$, resulting from the Fourier transform of intra-molecular relaxation data was analyzed. The latter was obtained by isotope dilution experiments as well as by FC ^2H NMR relaxometry, already performed by Herrmann et al.¹³⁴ The findings are confronted with predictions of different models as well as with results from the competitive method of double quantum (DQ) NMR (*cf.* section 2). As said, DQ NMR is suitable to probe the dipolar correlation function $C_{DD}^{DQ}(t)$ directly in the time domain, without need of Fourier transformation. Beforehand, almost perfect agreement between FC and DQ ^1H NMR was found in undiluted PB, *i.e.* $C_{DD}(t) \cong C_{DD}^{DQ}(t)$ (*cf.* section 4.2).

In PUB2 the intra-molecular relaxation contribution of entangled polymer melts of PB 196k and PB 24k presented by Herrmann et al.¹³⁴ (cf. section 4.3) was revisited and a refined data analysis in the frequency domain was presented. This became necessary because the direct comparison of these systems regarding $C_2(t)$, as determined from FC NMR as well as measured by DQ NMR, respectively, revealed significant and consequential differences. The DQ NMR data was published in a recent follow-up study.¹⁹⁵

The issue is illustrated in Fig. 17, where $C_2(t)$ of PB 196k is shown again.¹³⁴ Corresponding DQ ^1H NMR results reported by Furtado et al. on the isotopic blend, PB-h 196k diluted to 15% in PB-d 191k, as well as DQ ^2H data on undiluted PB-d 191k, are also displayed in Fig. 17.¹⁹⁵ To be exact, the FC and DQ measurements, which are compared to each other in this section, were done on the same systems, yet, not on the same samples. However, the polymers used were purchased from the same provider.^{PUB2,134,195} The DQ data on $C_2(t)$ was vertically shifted (see below) to coincide with the corresponding correlation function $C_{DD}^{DQ}(t)$ of neat PB-h 196k, which is also displayed (cf. Fig. 14). The power-law exponents of the dipolar as well as the re-orientational correlation function in regime II can be found in Fig. 20, for all M . With one exception they show the mentioned “protracted transition” (cf. section 4.2). A more detailed discussion of the exponents in regime II follows at the end of this section.

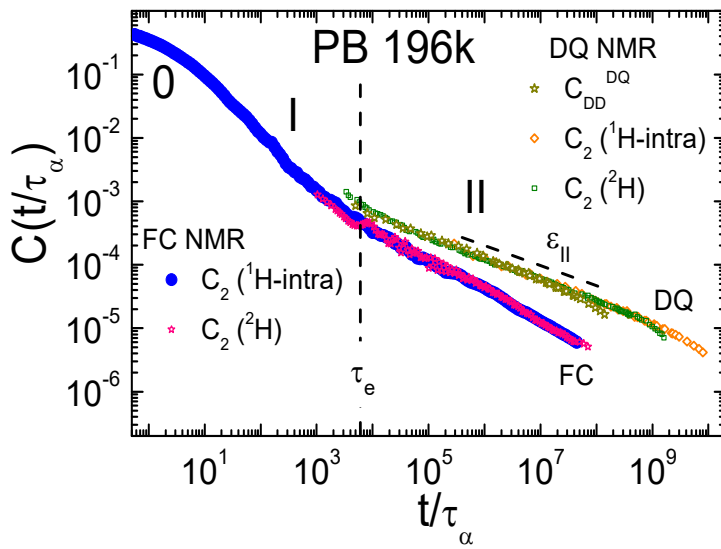


Figure 17: Segmental re-orientational correlation function $C_2(t/\tau_\alpha)$ of PB 196k as measured by FC ^1H NMR¹³⁴ as well as by DQ ^1H NMR (data taken from Furtado et al.¹⁹⁵ and vertically scaled, see text). In the case of DQ NMR the full dipolar correlation function $C_{DD}^{DQ}(t)$ of the undiluted melt is also included. Relaxation regimes (0,I,II) are indicated.

Concerning the FC results it is recalled from section 4.3 that the exponent value in regime II of $C_2(t)$

(at $t > \tau_e \approx 6000\tau_\alpha$) $\epsilon_{II}^{intra}(196\text{ k}) \approx 0.45$ (cf. also Fig. 20) determined by FC ^1H NMR is significantly larger than $\epsilon_{II}(196\text{ k}) \approx 0.3$, found for the corresponding dipolar correlation function $C_{DD}(t)$. This experimental value ϵ_{II}^{intra} doesn't conform to the constrained Rouse regime of the TR model. Hence, the dilution changes the slope in regime II as the inter-molecular relaxation is suppressed. The reliability of the isotope dilution experiment was checked via FC ^2H NMR relaxometry. This data is also included in Fig. 17 (red stars). The found exponent value $\epsilon_{II}^{intra}(196\text{ k}) \approx 0.45$ actually fits better to the (thrice) renormalized Rouse model, for which a value of $4/7 \approx 0.57$ results in the high mode number limit.⁵ Below, in Fig. 19b the prediction of the n-RR models for $C_2(t)$ is shown (cf. sections 1.6 and 1.7). One would expect to observe a similar behavior in the DQ NMR measurements. Instead, a discrepancy between both methods is apparent in Fig. 17, as the FC NMR curves of $C_2(t)$ are clearly steeper than their DQ NMR counterparts. In fact, the DQ power-law exponent values, $\epsilon_{II}^{intra, DQ}$

(isotopic blend) and $\epsilon_{II}^{Q,DQ}$ (deuterated melt), are both about 0.3 and thus smaller than their counterparts from FC NMR (Fig. 20). At first glance, the DQ NMR results on $C_2(t)$ are in favor of the TR model, predicting a value of 0.25 in the constrained Rouse regime (II). Suppressing the inter-molecular relaxation contribution in the DQ experiments by isotope dilution doesn't change the slope in regime II. Almost the same exponent and an identical curve shape as for the undiluted, fully protonated PB-h 196k is obtained, *i.e.* $\epsilon_{II}^{intra, DQ} = \epsilon_{II}^{DQ}$. Furtado et al. backed their DQ results on $C_2(t)$ by a computer simulation.¹⁹⁵ Moreover, the DQ findings on $C_2(t)$ not only conform to the TR model but are also consistent with the generic simulations by Wang et al.²⁰ (*cf.* Fig. 6 of section 2). However, the DQ data on the isotopic blend of PB 196k had to be multiplied by a factor of about ten in amplitude in order to match $C_2(t)$ with $C_{DD}^{DQ}(t)$ in Fig. 17. A similar effect on DQ measurements in a lesser diluted isotopic blend of PB 196k was reported before.²²¹ Consequently, the dilution also has a significant effect on the DQ experiments, *i.e.*, also the DQ ^1H NMR data $C_{DD}^{DQ}(t)$ obtained from fully protonated polymer melts contains intra- as well as inter-molecular contributions (*cf.* section 2).^{195,221-223} In contrast to FC NMR (*cf.* $C_{inter}(t)$ in Fig. 15), however, the inter-molecular contribution in DQ NMR is obviously time independent, a fact contradicting all current theories of polymer dynamics (including TR).

In this light, the good agreement between FC and DQ ^1H NMR concerning fully protonated polymers (Fig. 14, section 4.1) is actually surprising, because $C_{DD}(t)$ determined by FC NMR is a superposition of $C_2(t)$ and $C_{inter}(t)$, both showing pronounced time dependence. FC and DQ NMR, respectively, evidently deliver different results for each of these two correlation functions. Admittedly, it is not necessarily required that $C_{inter}(t)$, as measured by FC ^1H relaxometry and related to the segmental MSD, represents the same (time independent) "inter-molecular effect" occurring in DQ ^1H NMR. If this is true, $C_{DD}(t)$ from FC ^1H NMR and its counterpart $C_{DD}^{DQ}(t)$ from DQ ^1H NMR can not be compared to each other. The good agreement in Fig. 14 would be rather accidental.

In order to resolve the discrepancies between FC and DQ NMR regarding $C_2(t)$, the intra-molecular FC relaxation data on PB 24k and 196k was re-analyzed in PUB2 in the frequency domain, *i.e.* in the susceptibility representation $\chi''(\omega)$, $\chi''_{intra}(\omega)$. Doing so, numerical Fourier transformation was avoided. Additionally, relaxation was studied only at a single, high temperature (393 K), therefore assuming FTS was not necessary. The power-law exponents in regime II were more precisely determined using a derivative method. Instead of extrapolating the relaxation rate $R_1(\omega, c \rightarrow 0)$ of the isotope dilution series to zero concentration, the exponent itself was extrapolated, yielding ϵ_{II}^{intra} . Such a procedure allows skirting possible isotope effects on the local dynamics (τ_α).^{134,281} Indeed, DSC measurements presented in PUB2 revealed that there may be significant differences (> 10 K) in T_g between the deuterated and the protonated component of an isotopic mixture. The thorough re-analysis presented in PUB2 merely led to minor corrections of the exponent values published before and the previous FC NMR results were fully confirmed. The specific exponent values are summarized below in Fig. 20. For the higher M PB 370k proton relaxometry on a further isotopic blend as well as FC ^2H NMR on a fully deuterated sample was performed. Again, $\epsilon_{II}^{intra}(M) > \epsilon_{II}(M)$ was found. Yet, PB 370k was purchased from another manufacturer and features a different micro-structure (a different composition of conformational isomers) than the PB's investigated previously; therefore, it couldn't be compared.^{PUB2}

Given the puzzling discrepancies between FC and DQ NMR, FC measurements on the much better suited polymer PEP were performed recently. Protonated as well as deuterated material of different M was available in sufficient quantities (provided by L. Willner, *Forschungszentrum Jülich*), enabling for a comprehensive investigation. Fully protonated, fully deuterated and isotopic diluted systems were studied. The results on PEP will be addressed in section 5.4. Thus, the findings on PB are checked for another system featuring *i.a.* a well-defined microstructure.

The frequency dependence of the ratio between inter- and intra-molecular relaxation $A(\omega) := R_1^{inter}(\omega)/R_1^{intra}(\omega)$ is an alternative to comparing experimentally observed power-law exponents to such predicted. The quantity offers another way for testing models on a very fundamental level. Neither has FTS to be assumed, nor is Fourier transformation required. $A(\omega)$ follows from experimental raw data directly. Such data is presented in Fig. 18 for the two M of PB.

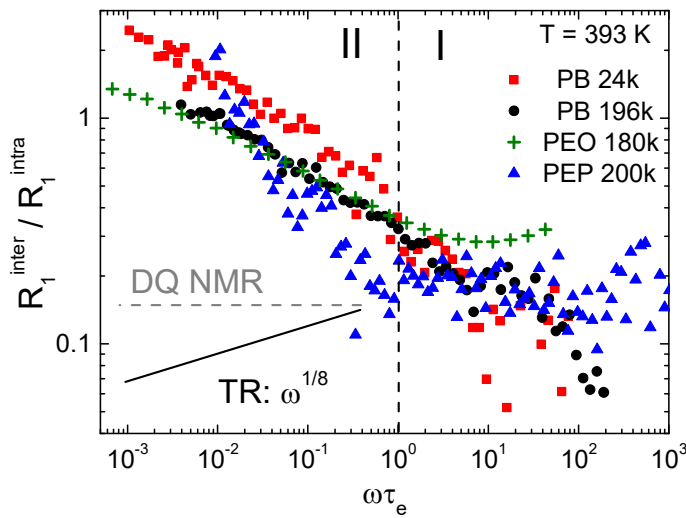


Figure 18: Ratio $A(\omega) = R_1^{inter}/R_1^{intra}$ vs. $\omega\tau_e$ of PB 24k, PB 196k, PEP 200k (*cf.* section 5.4) as well as PEO 180k. The latter data was taken from Kehr et al.¹²⁷ The prediction for constrained Rouse dynamics (TR model) is indicated. Gray: expectation for DQ ^1H NMR.

The ratio $A(\omega)$ in PB of two different M is found to increase with decreasing ω in the entanglement regime (II). Thus, the inter-molecular relaxation becomes increasingly important at low ω . The

same trend is also observed for PEP 200k (*cf.* section 5.4) as well as for poly(ethylene oxide) (PEO 180k, measured by Kehr et al.¹²⁷). Those results are also included in Fig. 18. All $A(\omega)$ data was horizontally scaled to take the different temperatures and entanglement times τ_e into account. As derived in PUB2, this trend, which is now confirmed for three different polymers, contradicts the anisotropic TR model predicting the opposite, a decrease of $A(\omega)$ when going from high to low ω , specifically $A(\omega) \propto \omega^{1/8}$ (*cf.* section 1.7). Instead, the observation, which appears to be universal, is rather in favor of isotropic models like the n-RR model.^{PUB2} At lowest frequencies the square root behavior (eq. 58) is expected to show up in $A(\omega)$, when $R_1^{intra}(\omega)$ becomes a constant and inter-molecular relaxation prevails. Figure 18 suggests that the absolute value $R_1^{inter}(\omega)$ becomes larger than $R_1^{intra}(\omega)$ below, say, $\omega\tau_e < 0.01$. This might be misleading because the dispersion, *i.e.* the frequency dependence of $R_1^{inter}(\omega)$ may of course be stronger than that of $R_1^{intra}(\omega)$. The fact that the correlation decay of $C_{inter}(t)$ is delayed with respect to $C_2(t)$ is not at all in contradiction with the finding that $R_1^{intra}(\omega)$ is still appreciably larger than $R_1^{inter}(\omega)$. Yet, the latter features the stronger dispersion (change with frequency). As the inter-molecular contribution in DQ ^1H NMR is obviously time-independent (see above), the corresponding ratio, tentatively defined as $A^{DQ} = [C_{DD}^{DQ}(t^{-1}=\omega) - C_2^{DQ}(\omega)] / C_2^{DQ}(\omega)$, yields a constant, as schematically indicated by the gray

dashed line in Fig. 18. In other words, the time/frequency independence of the inter-molecular contribution concluded from the DQ NMR measurements on PB¹⁹⁵ shown in Fig. 17 would lead to the proportionality $R_1^{intra}(\omega) \propto R_1^{inter}(\omega)$, which is clearly not observed in Fig. 18.

PB chains composed of deuterated ends and a protonated center section offer the opportunity to study the influence of enhanced chain-end mobility. PB chains labeled this way were synthesized by L. Willner and were provided by the *Forschungszentrum Jülich* (group of D. Richter).^{PUB2} Employing FC ¹H NMR on such samples the more mobile chain ends are obscured and the CLF effect (*cf.* section 1.5) is suppressed. Furthermore, the partial ¹H labelling leads to an isotope dilution, also suppressing inter-molecular relaxation. In the case of PB composed by deuterated/protonated/deuterated sections of $M = 13\text{k} / 6\text{k} / 10\text{k}$ (= PB-dhd 29k), it is consequently assumed that only the intra-molecular relaxation of the center segments is probed. In fact, this scenario comes closest to the generic models that are assumed in polymer theories. While in PUB2 $\chi''(\omega)$ data at just one T was shown, Fig. 19a of this work displays the full correlation function $C_2(t/\tau_\alpha)$ of PB-dhd 29k, in comparison to that of the fully protonated but diluted chains of PB 24k, *i.e.* of a similar M .

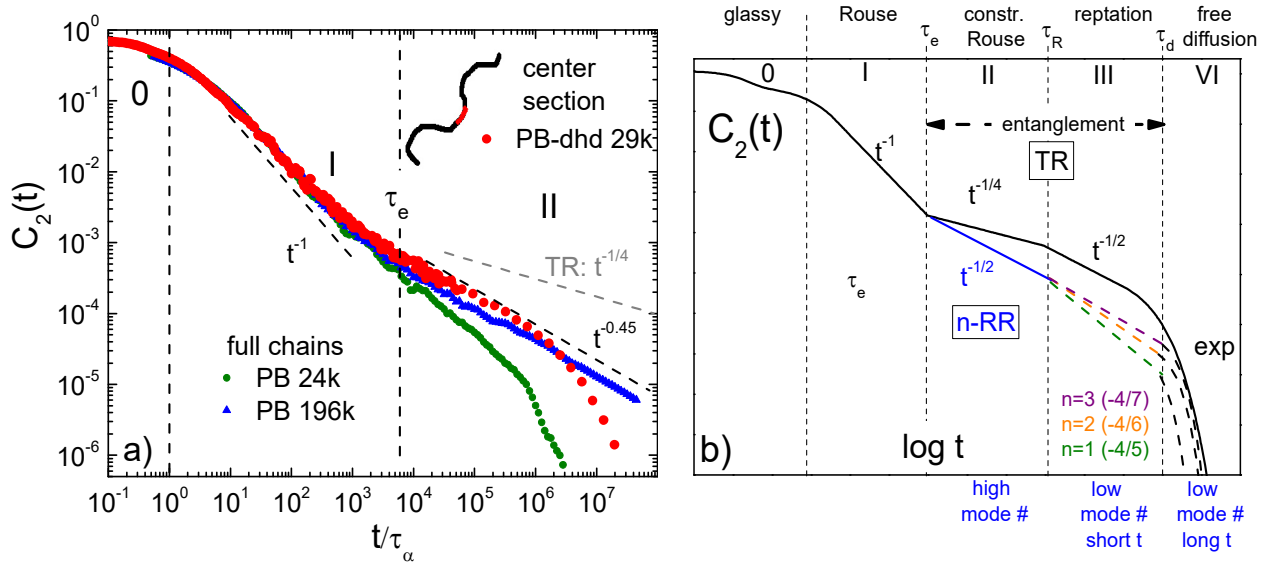


Figure 19: a) Re-orientational correlation function $C_2(t)$ of PB-dhd 29k (red, unpublished). For comparison, $C_2(t)$ of fully protonated but diluted PB 24k and PB 196k is displayed.^{134,PUB2} Relaxation regimes (0, I, II) are indicated, as well as the prediction of the TR model (gray). (b) Prediction of the TR³ (black) as well as of the RR model⁵ (colored).

Differences in $C_2(t/\tau_\alpha)$ with respect to entirely protonated chains only occur at long times in regime II and in the terminal one. Against the trend of the “protracted transition”, ε_{II}^{intra} of PB-dhd 29k agrees with that of the high molar PB 196k ($\varepsilon_{II}^{intra} = 0.45$) well and is significantly lower than that of fully protonated (but diluted) PB 24k (0.66). It is concluded that the “protracted transition” found before by FC as well as DQ NMR (*cf.* Fig. 20) is a finite-length effect involving chain-end relaxation. It

disappears when merely the center sections are regarded. Similar results arose from the atomistic MD simulations discussed in PUB1 (*cf.* section 5.1). Yet, the discrepancy with respect to the TR model predicting a value of 0.25, remains. Still, the thrice-RR model, for which the prediction is plotted in Fig. 19b, fits better. In Fig. 19a the terminal relaxation of PB-dhd 29k, reflected in the (stretched) exponential decay at longest times, appears to be shifted with respect to that of PB 24k by about one decade toward longer times. The shift cannot be explained by the slightly higher M alone as $(29\text{ k} / 24\text{ k})^{3.7} \approx 2$. This finding clearly confirms the idea that the M -dependence of the terminal relaxation time τ_t is significantly decreased by enhanced chain end motion (*cf.* eq. 40, section 1.5). The computer simulations by Wang et al. indicate that $C_2(t)$ is also strongly influenced by the CR process, which is not obfuscated by the partial protonation.²⁰ In order to suppress the CR process, one could mix PB-dhd 29k with deuterated chains with a much larger M . Then, the topological constraints (the “tube”) become immobile.

Figure 20 summarizes all the values of the power-law exponent in regime II of the different correlation functions, gathered for PB via FC as well as DQ NMR. In addition to PB 196k further M are now included in the discussion. For PEP 200k (*cf.* section 5.4) data is also added. Concerning the full dipolar (ϵ_{II}), the pure intra-molecular ($\epsilon_{II}^{\text{intra}}$) and the quadrupolar relaxation (ϵ_{II}^Q) the exponent values are plotted vs. M/M_c , with $M_c(\text{PEP}) = 3k$ and $M_c(\text{PB}) = 2k$. The exponent values $\epsilon_{II}^{\text{DQ}}$, $\epsilon_{II}^{\text{intra,DQ}}$ and $\epsilon_{II}^{\text{Q,DQ}}$ resulting from the DQ NMR studies are also shown for comparison.^{195,221-223}

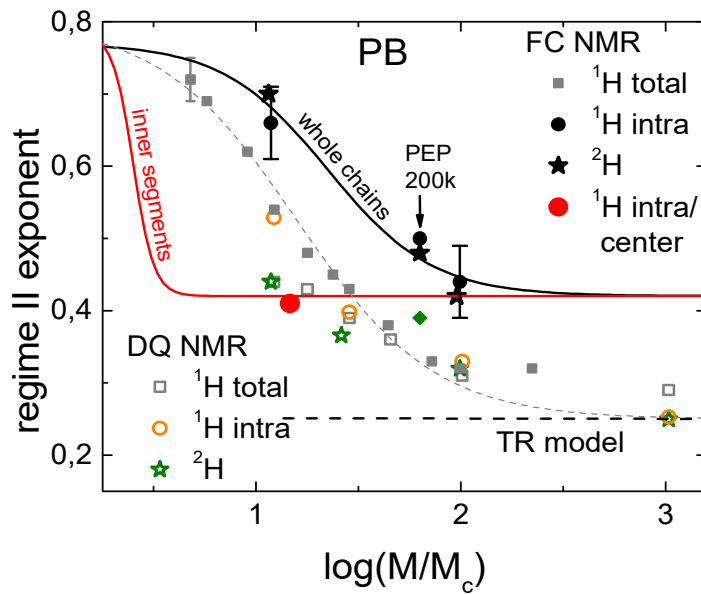


Figure 20: Power-law exponent in regime II of PB as a function of M/M_c . The following values of M_c were used: $M_c(\text{PEP}) = 3k$, $M_c(\text{PB}) = 2k$. Results from FC (closed symbols) and DQ NMR (open symbols), each applied on both, ^1H and ^2H , respectively, are compared. Data points of PEP 200k are also included (*cf.* section 5.4). The protracted transition (represented by the gray and the black line) disappears when just the middle segments are investigated (as suggested by the red line).

First, the total dipolar relaxation of PB is addressed. The “protracted transition” is reflected in the exponent ϵ_{II} decreasing from about 0.8 to about 0.3. As already discussed in section 4.2 and in this section, DQ NMR ($\epsilon_{II}^{\text{DQ}}$, gray open squares) and FC NMR (gray closed squares) provide similar exponent values. When the intra-molecular relaxation is singled out, the exponent values gained from both techniques diverge. As mentioned, the values $\epsilon_{II}^{\text{intra,DQ}}$ (orange open circles) resemble those corresponding to the total correlation function $\epsilon_{II}^{\text{DQ}}$. At least for high M DQ ^2H NMR measurements reveal similar values, *i.e.* $\epsilon_{II}^{\text{Q,DQ}} \approx \epsilon_{II}^{\text{intra,DQ}} \approx \epsilon_{II}^{\text{DQ}}$ (see above). In opposition, the exponent values in FC NMR increase upon isotopic dilution, *i.e.* $\epsilon_{II}^{\text{intra}} > \epsilon_{II}$. The values from isotopic

dilution are also validated by FC ^2H relaxometry. The agreement between the outcomes of the isotope dilution experiments and corresponding ^2H measurements are even better in FC than in DQ NMR. Furthermore, the FC data on PB is confirmed by those on PEP.

In the diluted/deuterated systems the protracted transition is still observable. Compared to the full dipolar data it is less pronounced as the decay goes just down to about 0.45, instead to 0.3. It is illustrated by the black line in Fig. 20. When the partially deuterated sample PB-dhd 29k is regarded, the protracted transition in the power-law exponent $\epsilon_{\text{H}}^{\text{intra}}$ has disappeared. As suggested by the solid red line, the high- M plateau value of about 0.45 for intra-molecular relaxation is reached immediately.

Finally, it is remarked that in the experimental section of PUB2 it was claimed that “*in all investigated systems the magnetization build-up or decay curves were found to be monoexponential*”, which turned out to be wrong after closer inspection. In fact, the magnetization curves $m(t)$ of all data measured on the FC-1 relaxometer are apparently non-exponential at long evolution times (*cf.* Fig. 11c). It was attempted to remedy the mentioned discrepancies between FC and DQ NMR by fitting $m(t)$ under the assumption of a log-normal distribution of relaxation rates.²⁸⁵ Yet, as turned out later, the non-exponentiality results from experimental artifacts of the FC-1 relaxometer and not from a broad distribution of relaxation rates (*cf.* section 3.3). The (unweighted) mono-exponential fits applied by Herrmann et al.¹³⁴ over whole magnetization curves provide practically the same results for $\langle R_1(\omega) \rangle$ as restricting the fit to the initial, artifact-free region at $t \leq \langle R_1(\omega) \rangle^{-1}$. Thus, no results presented in PUB2 have to be revised in this sense.

5.3 Mean Squared Displacements of Segments in Polymer Melts

While in the previous section the focus lies on the re-orientational dynamics in polymer melts, this one is dedicated to translational motion of segments. FC and FG ^1H NMR measurements on the same samples were combined to probe $\langle r^2(t) \rangle$ in two different polymers, namely in PB and in PDMS, over an extremely wide time range, not reached by any other single technique.^{PUB4} Later on, the analysis was repeated with PEP (section 5.4).

By extracting the inter-molecular relaxation dispersion $R_1^{\text{inter}}(\omega)$ from the total one, the segmental MSD $\langle r^2(t) \rangle$ in polymer melts was calculated from FC ^1H NMR data. To this end, the theoretical framework of Fatkullin et al.^{75,130} outlined in section 1.7 was applied. Specifically, a version of the full expression eq. 56 was used (see below), relating the absolute MSD of polymer segments to the cosine-transform of $R_1^{\text{inter}}(\omega)$. Technically, $R_1^{\text{inter}}(\omega)$ was received from isotope dilution experiments (*cf.* sections 4.3 and 5.2) via subtracting the intra-part from the total one, *i.e.* $R_1^{\text{inter}}(\omega) = R_1(\omega) - R_1^{\text{intra}}(\omega)$. For two different molar masses of entangled PB, such data was available from the experiments carried out by Herrmann et al.¹³⁴ (see also section 4.3). In the case of the other polymer PDMS the overall relaxation is inter-molecular dominated already for relatively high frequencies of $\omega\tau_\alpha < 0.1$, as was demonstrated by Herrmann et al.¹³⁴ This peculiarity is related to the fact that PDMS only contains methyl protons that undergo rapid rotations in addition, as mentioned in section 3.3. Those pre-average the intra-molecular dipolar coupling and cause low values of $R_1^{\text{intra}}(\omega)$. Thus,

concerning PDMS no isotope dilution was required as it was focused on the collective polymer dynamics occurring at frequencies $\omega\tau_\alpha \ll 1$. Applying the common FC NMR toolbox of the *Bayreuth* group, susceptibility master curves $\chi''_{inter}(\omega\tau_\alpha)$ were constructed from the inter-molecular relaxation data via subtraction along $\chi''_{inter}(\omega\tau_\alpha) = \chi''_{total}(\omega\tau_\alpha) - \chi''_{intra}(\omega\tau_\alpha)$. While in a first attempt of Herrmann and co-workers the algebraic approximation eq. 57 was used,¹³⁴ the actually required numerical transformation was carried out in PUB4 rigorously. By substituting $d(\ln \omega) = \omega d\omega$, eq. 55 can be re-written in its most convenient form used in PUB4:

$$\langle r^2(t/\tau_\alpha) \rangle = \frac{1}{2} \left[\frac{5}{4} \left(\frac{4\pi}{\mu_0} \right)^2 \sqrt{\frac{8}{3\pi^3}} \frac{1}{\gamma_H^4 \hbar^2 n_s} \frac{1}{1 + 2^{25/16}} \int_0^\infty d(\ln \omega) \cos(\omega t) \chi''_{inter}(\omega\tau_\alpha) \right]^{-2/3} \quad (66)$$

In contrast to the original eq. 56 the above expression has the advantage that it works with susceptibility master curves as input. As $\tau_\alpha(T)$ is known from the master curve construction over a wide range $400 \text{ K} \gtrsim T \gtrsim 200 \text{ K}$, the absolute MSD can be calculated for any reference temperature therein. This is necessary for comparing FC results with that of FG NMR and also NSE spectroscopy (*cf.* section 5.4) as these techniques cover significantly different time ranges (*cf.* Fig. 2).

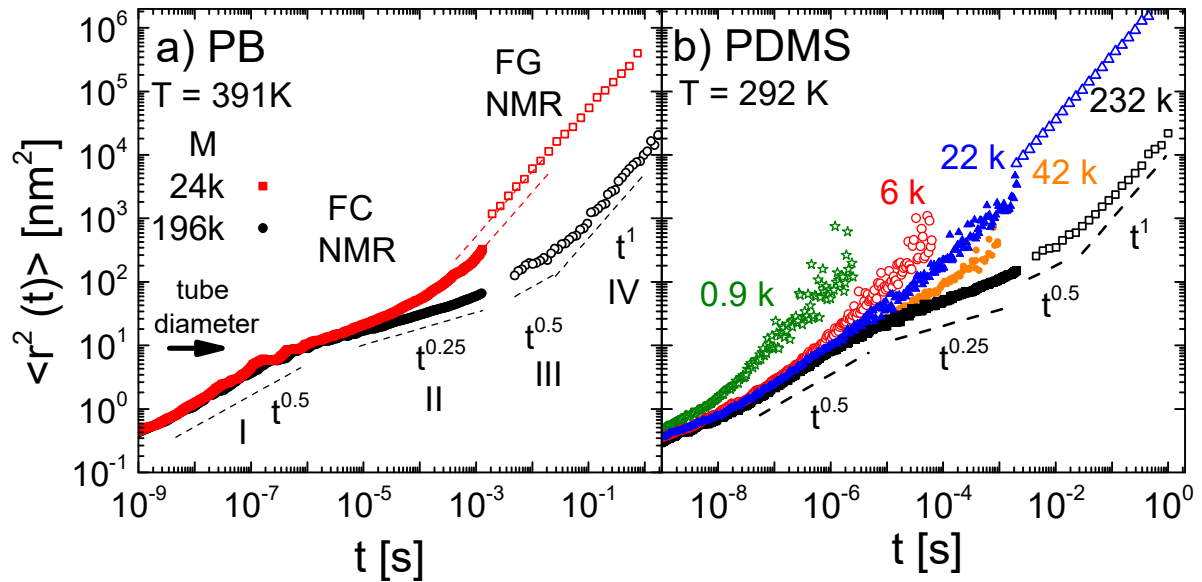


Figure 21: Segmental MSD $\langle r^2(t) \rangle$ in PB (a) and PDMS (b) melts with M and T as indicated. Data from FG ^1H NMR (full symbols) and from FC ^1H NMR (open symbols) is combined, together covering four power-law regimes (I-IV). Adapted from PUB4 and extended. c) Forecast of the TR model.²⁴

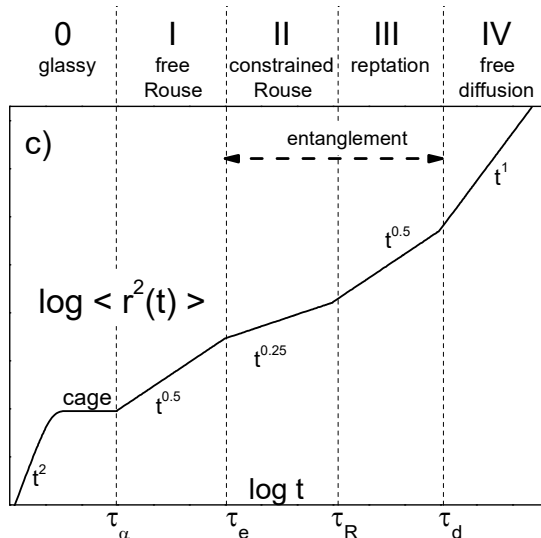


Figure 21a displays the MSD $\langle r^2(t) \rangle$ for two different $M > M_c$ of PB, after scaling the data to the reference temperature $T = 391$ K. In Fig. 21b $\langle r^2(t) \rangle$ of PDMS at 292 K is shown, for which a broader range of M was investigated, ranging from the simple liquid PDMS 860 up to entangled PDMS 232k. Assuming FTS, a time range between *ns* and *ms* is covered by FC NMR, revealing several sub-diffusive regimes, depending on M , which will be discussed below. In order to extend this window toward even longer times, FG ^1H NMR was performed on some M of the same undiluted polymers. FG NMR is a standard method for measuring the diffusion in the hydrodynamic limit, where the diffusion coefficient D is well-defined. Measuring sub-diffusive motion, where $\langle r^2(t) \rangle \propto t^{\alpha < 1}$ or D becomes time-dependent, is difficult with FG NMR but possible. However, experimental data is scarce (cf. section 2). In the course of PUB4 the benefits of a static, very high magnetic field gradient were exploited, allowing for measuring down to such short diffusion times (a few *ms*) that D indeed becomes time-dependent for high M and T . While for long diffusion times $D(t \gtrsim 100 \text{ ms}) = \text{const.}$ holds (hydrodynamic limit), power-laws close to $D(t) \propto t^{0.5}$ are observed at shorter times, associated with chain reptation (regime III). The MSD $\langle r^2(t) \rangle$ is derived using the Einstein relation $\langle r^2(t) \rangle = 6Dt$. For both polymers, PB and PDMS, the data resulting from FG NMR is included in Fig. 21. The MSD data coming from FC and FG NMR is complementary as the data of both techniques doesn't overlap. When the curves are projected (red dashed lines in Fig. 21a), there appears to be a vertical gap of about a factor of two between the absolute values of $\langle r^2(t) \rangle$. Possible explanations for this mismatch, which is marginal regarding the many methodical differences, are proposed in PUB4.

Given the complementary time ranges, both NMR methods cover the complete dynamical hierarchy of $\langle r^2(t) \rangle$ in entangled polymer melts, namely the Rouse regime (I), two entanglement related regimes (II, III) and finally normal diffusion (IV). When compared to the TR model (Fig. 21c), high correspondence is found: all predicted translational power-law regimes are identified. The values of the power-law exponents agree with those predicted within ± 0.1 . When M is decreased below M_c the entanglement related regimes (II, III) disappear, while the hydrodynamic regime $\langle r^2(t) \rangle \propto t^1$ shifts toward shorter times. Going down even further, finally the Rouse regime (I) vanishes. For the shorter polymers PDMS 22k, 6k and 860 and eventually also for PB 24k, the terminal behavior is already observed in the FC NMR data. The constrained Rouse regime (II) with its characteristic exponent of $\langle r^2(t) \rangle \propto t^{0.25}$ is only fully established for the systems with the highest M , i.e. PB 196k and PDMS 232k, respectively. PB 24k and PDMS 42k (the latter is not yet included in PUB4) are also entangled. However, regime II is not fully established yet, and one would assign higher slopes than 0.25. Thus, the protracted transition observed in regime II concerning $C_{DD}(t)$ and $C_2(t)$ (cf. Fig. 20 in section 5.2) is also relevant for the MSD.

The full segmental MSD at hand allowed estimating the Kuhn length b as well as the tube radius a_0 of the TR model. Concerning the Kuhn length, some variance to literature data was found, while the tube radius is essentially in accordance.^{PUB4} Moreover, the extracted values of the translational diffusion coefficient D , the terminal relaxation time τ_t and the entanglement time τ_e were compared to results from the literature in PUB4, mostly to rheological results; good agreement was found. Finally, "relaxation maps" of both PB as well as PDMS including $\tau_\alpha(T)$, $\tau_e(T)$ and $\tau_t(T)$ were presented in PUB4, emphasizing the correspondence between NMR and other methods, in particular between FC NMR and rheology. A further relaxation map will be presented in the next section for the linear polymer PEP (Fig. 32).

Concluding, the combination of FC and FG NMR provides information on the translational motion in polymer melts over a huge time range in terms of the segmental MSD. The results are well described within the TR model, which is essentially confirmed concerning segmental translation. Nevertheless, it is recalled that the re-orientational correlation function $C_2(t)$ also accessible from FC ^1H NMR doesn't match to the TR model, as was discussed in the previous chapter. In the meantime, a further isotope dilution experiment was performed for PEP, enabling the determination of $\langle r^2(t) \rangle$ as well. These unpublished results are part of the next section, which is dedicated to a comprehensive investigation of the polymer dynamics in PEP via FC ^1H and ^2H relaxometry.

5.4 NMR Relaxation in Poly(ethylene propylene)

FC measurements on polymer melts which started with PB in the *Bayreuth* group, were meanwhile extended to a multitude of different linear polymers. The results are published only in parts. In Fig. 22 the total ^1H susceptibility master curves $\chi''(\omega\tau_\alpha)$ of high- M (i.e. $M > M_c$) representatives of PB,²²⁷ PI,²⁷⁴ PDMS,¹³⁴ PPG,²⁷² poly(propylene sulfide) (PPS, sample provided by H. Pletsch, *Universität Bayreuth*), poly(butylene oxide) (PBO, sample provided by L. Willner, *Forschungszentrum Jülich*) and PEP are shown, with M as indicated. In each case, the highest M available was chosen. For comparison, the curve of the simple, low- M liquid di-PG (cf. section 5.1) is also provided.^d Note that the curves are vertically scaled to $\chi''(\omega\tau_\alpha \approx 1) = 1$ at the α -peak, to take small variances in the coupling constants/second moments into account. It turns out that the behavior found for PB (cf. section 4.1) is also observed in other entangled polymers, i.e. power-law regimes reflecting Rouse and entanglement dynamics occur at $\omega\tau_\alpha < 1$, unlike in low- M liquids like di-PG. The shape of $\chi''(\omega\tau_\alpha)$ of linear polymers and its evolution with M appear to be generic.²⁷² It is emphasized that polymers with different ratios of M/M_c are compared. In cases where this ratio is small (PPG 18k, for instance) the entanglement regime is less pronounced and the terminal relaxation already affects the curves at low frequencies. Nevertheless, it is obvious that the amplitude of polymer relaxation strength in relation to the low- M reference di-PG depends on the type of polymer. Possibly, the nature of the monomer, in particular the orientation of the inter-nuclear vectors with respect to the chain contour,²⁷⁴ or differences in chain stiffness²⁰ provide an explanation.

^d Dimeric PG was chosen as the low- M reference in FC ^1H NMR as monomeric PG features more pronounced inter-molecular relaxation (cf. section 5.1 and PUB1).

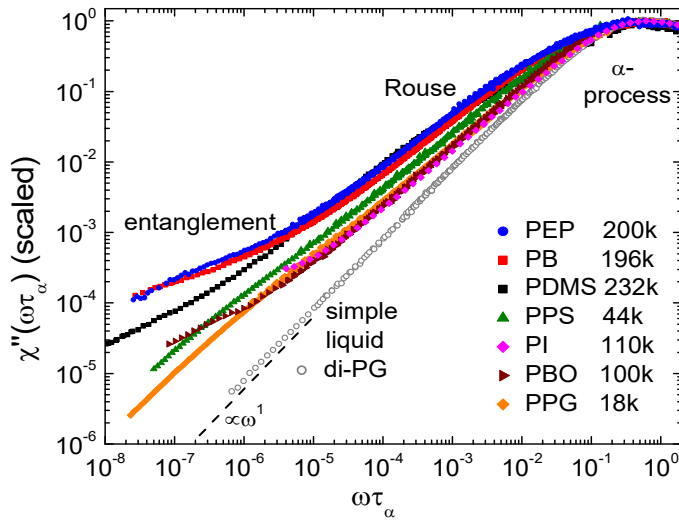


Figure 22: Vertically scaled NMR susceptibility master curves $\chi''(\omega\tau_\alpha)$ of different entangled ($M > M_c$) polymers, in comparison to that of the simple liquid di-propylene glycol (PG). Partially unpublished data (see text).

Although somewhat different M are compared, it is apparent that PB (blue colored) and PEP (red colored) feature the strongest polymer effect among the species investigated so far. Their susceptibility master curves

show the largest amplitudes at low ω , in relation to the α -process. The latter is essentially represented by the curve of the simple liquid di-PG. Actually, the $\chi''(\omega\tau_\alpha)$ curves of PB and PEP are very similar. PEP is a linear co-polymer consisting of alternating ethylene and propylene monomers, the latter bearing each a methyl side group. Unlike PB, PEP contains single bonds exclusively. As a consequence, PEP has no variation in its micro-structure in contrast to PB, for instance, which is known to feature variations in the content of different conformational isomers.²⁰⁶ Furthermore, PEP poses a compromise between the simplest implementation of a linear chain (poly(ethylene)) and a weak tendency to crystallize. Furthermore, PEP features a suitable T_g , *i.e.* low enough that the relevant frequency/time scale of polymer dynamics coincides with the window of the FC NMR technique. This renders PEP as an ideal candidate for further FC NMR investigations. Specifically, the far-reaching conclusions drawn from the previous measurements on PB (sections 4.2, 4.3 and 5.2) can be critically checked for another system. It is reminded that FC and DQ NMR on PB yields contradicting results concerning re-orientational dynamics (*cf.* section 5.2).

Seven batches of protonated PEP with different M within $3k \leq M \leq 200k$ and low polydispersity ($M_w/M_n \leq 1.06$) were provided by the group of D. Richter (*Forschungszentrum Jülich*). In the case of PEP 200k and 50k also deuterated polymer was provided. Unfortunately, no low- M reference was available. The systems were investigated via FC ^1H and ^2H NMR, respectively, as well as by shear rheology. The NMR results are summarized in this section. The subsequent one is dedicated to a methodical comparison between the NMR and the rheological results.

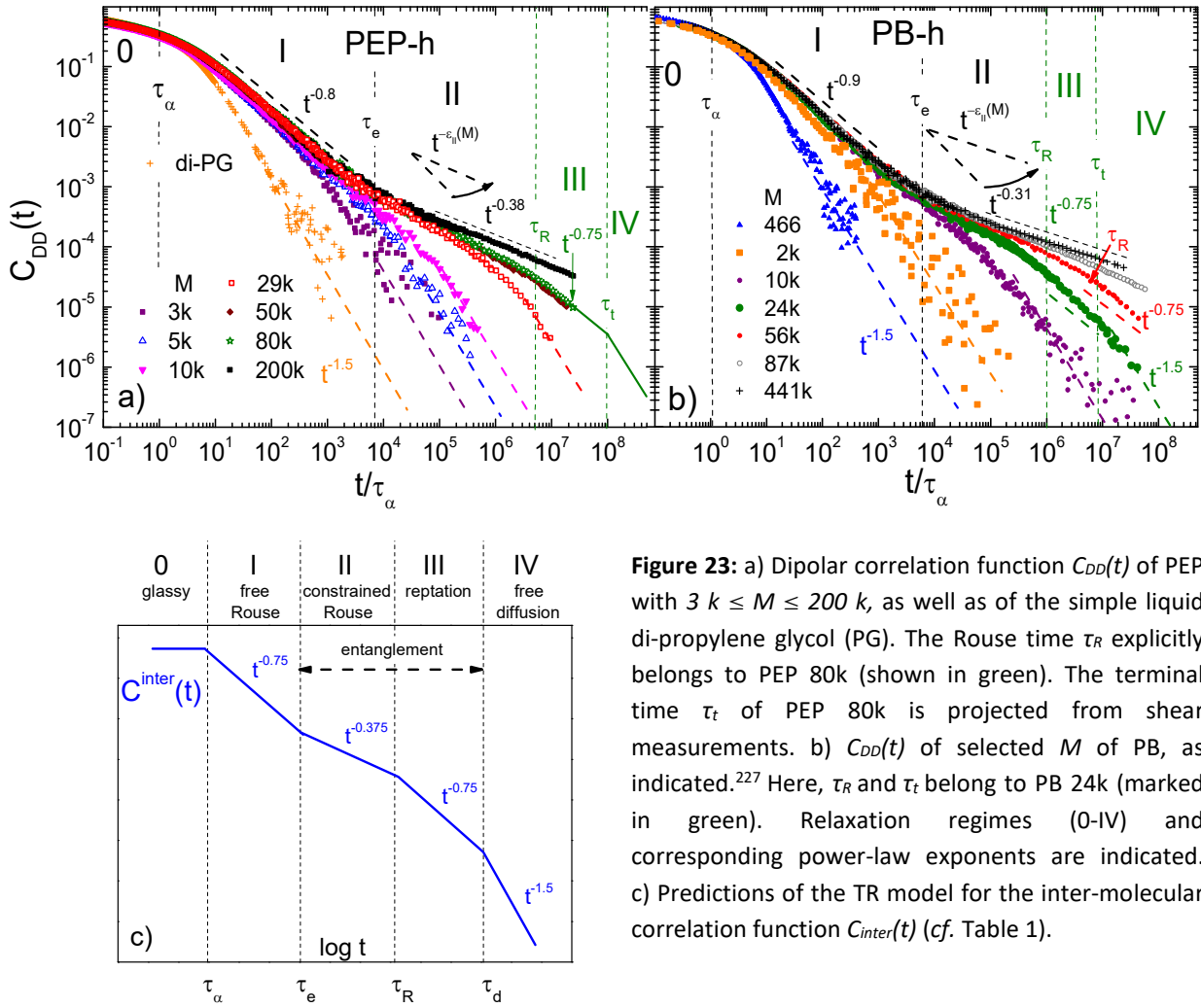


Figure 23: a) Dipolar correlation function $C_{DD}(t)$ of PEP with $3 \leq M \leq 200 \text{ k}$, as well as of the simple liquid di-propylene glycol (PG). The Rouse time τ_R explicitly belongs to PEP 80k (shown in green). The terminal time τ_t of PEP 80k is projected from shear measurements. b) $C_{DD}(t)$ of selected M of PB, as indicated.²²⁷ Here, τ_R and τ_t belong to PB 24k (marked in green). Relaxation regimes (0-IV) and corresponding power-law exponents are indicated. c) Predictions of the TR model for the inter-molecular correlation function $C_{inter}(t)$ (cf. Table 1).

In Fig. 23a the time domain master curves of the dipolar correlation function $C_{DD}(t/\tau_\alpha)$ of PEP are shown, in comparison to that of di-PG. As in the case of PB (section 4.2), they result from Fourier transformation of susceptibility master curves $\chi''(\omega\tau_\alpha)$ of the total (*i.e.* intra- + inter-molecular) ^1H relaxation. The time constant $\tau_\alpha(T)$ of PEP, gained from the master curve construction, is plotted in Fig. 32 (section 5.5) in a “relaxation map”. There, a comparison to results from other techniques, in particular to the shear measurements, is performed. It is anticipated that perfect agreement among the different techniques regarding $\tau_\alpha(T)$ is found. FTS applies perfectly.

As in the case of PB (section 4.2) and other polymers,²⁷² several power-law regimes $C_{DD}(t) \propto t^{-\epsilon}$ are discovered in PEP beyond the α -process (regime 0), *i.e.* at $t \gg \tau_\alpha$. The curves actually highly resemble those of PB, for which $C_{DD}(t)$ of selected M is plotted again in Fig. 23b, for a direct comparison. Remarkably, the found exponent values for the different regimes I-IV in $C_{DD}(t)$ in both, PEP as well as in PB, resemble those predicted by the TR model rather for $C_{inter}(t)$ than for $C_{intra}(t)$ (cf. Table 1). The corresponding forecast concerning $C_{inter}(t)$ is sketched in Fig. 23c. In the case of PB, this fact was actually overseen by Herrmann et al.,²²⁷ where an apparent agreement between the experimentally

determined $C_{DD}(t)$ and the prediction of the TR model concerning $C_2(t)$ was actually claimed. First, in the Rouse regime (I) power-law exponents of $\epsilon_I = 0.8$ (PEP) and $\epsilon_I = 0.9$ (PB) are observed, independent of M . Concerning inter-molecular relaxation, $C_{inter}(t) \propto t^{-0.75}$ is predicted by the Rouse model, following from the relationship between the segmental MSD and $C_{inter}(t)$ given by eq. 56 (cf. section 1.7). For the re-orientational correlation function resulting from the intra-molecular relaxation contribution, $C_2(t) \propto t^{-1}$ is predicted. As the experimentally observed exponent values are in-between the predicted ones concerning $C_2(t)$ and $C_{inter}(t)$, respectively (Table 1), one might speculate that already in the Rouse regime, the shape of $C_{DD}(t)$ is affected by inter-molecular relaxation significantly, although the absolute relaxation rate is still intra-dominated here (cf. Fig. 18, section 5.2 and below).

PEP with molar mass $M \geq 5k$ shows characteristics of entanglement dynamics. Hence, the crossover molar mass is supposed to be in between $3k \leq M_c \leq 5k$, which is in accordance to values reported in the literature.²⁸⁶ The constrained Rouse regime (II) with its exponent $\epsilon_{II}(M)$ decreasing with M , occurs at times $t > \tau_e$. The “protracted transition” in $\epsilon_{II}(M)$ (cf. Fig. 20 and section 5.2) is also observed for PEP. Concerning the longest chains studied, an exponent value of $\epsilon_{II}(PEP\ 200k) = 0.38 \pm 0.03$ is found for the total relaxation (cf. Fig. 23a). The entanglement time $\tau_e/\tau_\alpha \approx 7000$ is estimated from the corresponding power-law intersection in $C_{DD}(t/\tau_\alpha)$. The value is by about 1-2 decades higher than predicted by the TR model (eq. 33), a finding which was also observed for PB and PDMS, respectively.^{PUB4} For PB, a high- M exponent value of $\epsilon_{II}(PB\ 441k) = 0.31 \pm 0.03$ was found. The TR model provides $C_{inter}(t) \propto t^{-0.375}$ for the constrained Rouse regime, which is in between the exponent values of PEP and PB concerning regime II of $C_{DD}(t)$.

For PEP 50k and 80k, respectively, actually a third polymer-related power-law regime is observed at longest times in $C_{DD}(t)$, with an apparent exponent value of $\epsilon_{III} \approx 0.75$. Regime III, which wasn’t identified before, apparently doesn’t show up in PEP for M lower than 50k. Otherwise, in PEP 200k it is already outside the accessible time window. Besides regime II, this could be a second power-law regime characteristic for entanglement dynamics, such as the “reptation” regime forecast by the TR model (cf. section 1.5) or, alternatively, the “low mode number – short time limit” of the RR model (cf. section 1.6). Tentatively interpreting $C_{DD}(t)$ in terms of the TR model, the crossover time $\tau_R/\tau_\alpha \approx 5 \times 10^6$ at which the Rouse mode spectrum ends and reptation becomes dominant, is indicated in Fig. 23a for PEP 80k (green colored). A closer inspection of the dipolar correlation function $C_{DD}(t)$ of PB, which is shown again in Fig. 23b for selected M , also reveals regime III for PB 24k (green colored) and PB 56k (red colored). The corresponding exponent is $\epsilon_{III} \approx 0.75$ also in these cases. It is remarked that also the authors of the DQ 1H NMR studies²²¹⁻²²³ on PB claim the existence of regime III in $C_{DD}^{DQ}(t)$, while Herrmann et al. refrained from a clear statement. The latter rather attribute this regime to a smooth transition toward terminal relaxation.²²⁷ The exponent value $\epsilon_{III} \approx 0.75$ found for PEP as well as for PB, conforms to the prediction of the TR model in the reptation regime, again concerning $C_{inter}(t)$ (cf. Table 1). Notably, regime III doesn’t (yet) show up in the re-orientational correlation function $C_2(t)$ of PB 24k and of partially deuterated PB-dhd 29k (Fig. 19a). This could indicate that segmental translation and re-orientation decouple at long times, in contradiction to the RTO hypothesis (cf. section 1.5).

The terminal regime (IV) in PEP as well as in PB is coined by $C_{DD} \propto t^{-1.5}$ behavior, which is indicated by dashed lines in Figs. 23a and b. Herrmann et al. didn’t sufficiently comment on the terminal behavior

of $C_{DD}(t)$ of PB.²²⁷ In fact, for all PB of molar mass smaller than about 30k, the universal behavior $C_{DD}(t) \propto t^{-1.5}$ is observed at longest times. Here, the inter-molecular relaxation governed by diffusion dictates the form of $C_{DD}(t)$. This circumstance was even exploited by Meier et al. to determine the diffusion coefficient of PB with $M \leq 10k$ and other polymers.¹⁴¹ The terminal correlation decay quickly shifts with $\tau_t \propto M^{3.7}$ (cf. section 5.5) toward longer times and leaves the experimental window.

As said, the exponent values for the different regimes I-IV in $C_{DD}(t)$ in both, PEP as well as in PB, are close to those predicted by the TR model for $C_{inter}(t)$. In the case of PDMS the equivalence of $C_{DD}(t)$ and $C_{inter}(t)$ at long times allowed determining the segmental MSD even without necessity of isotope dilution (cf. section 5.3). Thus, also concerning PDMS the shape of $C_{DD}(t)$ is governed by inter-molecular relaxation. In the case of PB 24k, which is marked in green in Fig. 23b, $C_{DD}(t)$ actually covers all the mentioned translational power-law regimes (I-IV). For PEP, no such molar mass was studied. Yet, the terminal time τ_t can be estimated from the mentioned shear measurements presented below in section 5.5. This allows projecting the further progress of $C_{DD}(t)$ e.g. of PEP 80k, as indicated in Fig. 23a by the solid green lines. In conclusion, the dispersion of the total relaxation and the corresponding dipolar correlation function $C_{DD}(t)$ is much more affected by inter-molecular relaxation than it was perceived before. Consequently, $C_{DD}(t)$ appears to conform to the TR model, yet, not regarding re-orientation but translation.

In the case of PEP 200k deuterated material in sufficient quantity was provided, offering the opportunity to perform a further isotope dilution experiment. This enabled a separation between intra- and inter-molecular relaxation contributions for another polymer than PB (section 5.2). According to the procedure described by Herrmann et al.,¹³⁴ an isotopic blend of fully protonated (PEP-h) and fully deuterated (PEP-d) chains with the same $M = 200k$ was mixed and measured in a broad T range in *Bayreuth* as well as in *Darmstadt*. The concentration was 10 (weight) % of PEP-h 200k in 90% of PEP-d 200k, controlled by thorough weighing. Due to dilution by the deuterated matrix, it is assumed that the inter-molecular relaxation is (mostly) suppressed. An intra-molecular susceptibility curve $\chi''_{intra}(\omega\tau_\alpha)$ was constructed from measurements on the isotopic blend at different temperatures. The result is shown in Fig. 25b, after converting $\chi''_{intra}(\omega\tau_\alpha)$ to the rate representation $R_1^{intra}(\omega)$ (see below). As in the case of PB, the intra-molecular susceptibility curve $\chi''_{intra}(\omega\tau_\alpha)$ was subtracted from the total susceptibility $\chi''(\omega\tau_\alpha)$ of PEP-h 200k, to get the pure inter-contribution $\chi''_{inter}(\omega\tau_\alpha)$. Afterwards, both $\chi''_{intra}(\omega\tau_\alpha)$ and $\chi''_{inter}(\omega\tau_\alpha)$, were transformed into the time domain. Figure 24 shows the resulting correlation functions $C_2(t/\tau_\alpha)$ as well as $C_{inter}(t/\tau_\alpha)$, respectively, of PEP 200k.

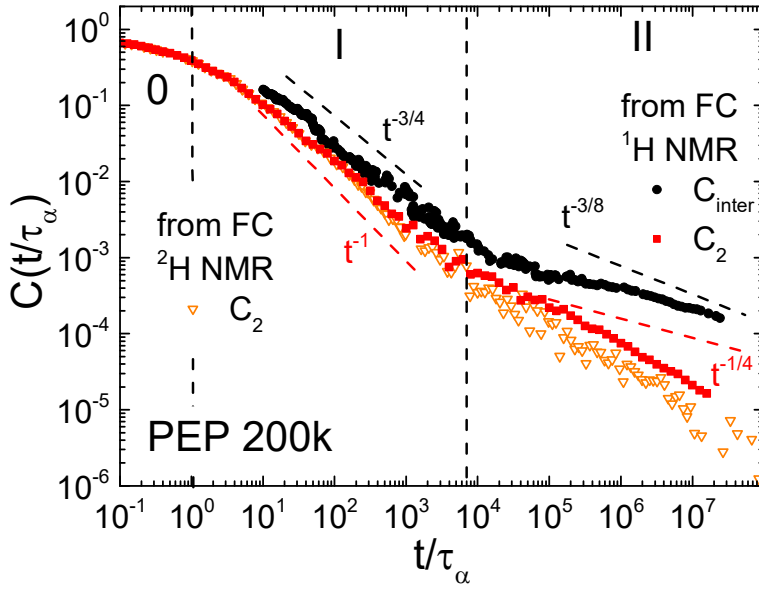


Figure 24: Inter- and intra-molecular correlation functions $C_{inter}(t/\tau_\alpha)$ (black) and $C_2(t/\tau_\alpha)$ (red), respectively, resulting from ^1H FC relaxometry on isotopically diluted PEP 200k. $C_2(t/\tau_\alpha)$ obtained from FC ^2H relaxometry is also included (orange triangles). Dynamic regimes are indicated. Dashed lines: predictions of the TR model³ for $C_{inter}(t)$ and $C_2(t)$ (cf. Table 1).

In regime 0 the intra- and the inter-molecular contribution are barely distinguishable and the noisy $C_{inter}(t)$ data is not shown in Fig. 24. In regime I $C_{inter}(t)$ closely follows $\propto t^{0.75}$, as predicted by the Rouse model (cf. Table 1). For Rouse dynamics $C_2(t) \propto t^{-1}$ is predicted. Experimentally, a somewhat lower slope of around -0.9 is observed. Returning to the results on the isotope dilution experiment concerning PB 196k shown in Fig. 15 (section 4.3), it is noted that $C_2(\tau_\alpha < t < \tau_e)$ features a slightly steeper decay with $\varepsilon_I^{intra} \approx 1$ than $C_{inter}(\tau_\alpha < t < \tau_e)$ with $\varepsilon_I^{inter} \approx 0.75$, a subtle fact that wasn't addressed by Herrmann et al.¹³⁴ As in the case of PEP 200k, both these exponent values in PB are very close to the respective predictions of the Rouse model (cf. Table 1). In regime II $C_{inter} \propto t^{-0.30 \pm 0.05}$ is found for PEP 200k, which is somewhat flatter than the corresponding prediction of $\propto t^{-0.375}$. Otherwise, $C_2 \propto t^{-0.50 \pm 0.05}$ observed in regime II is clearly steeper than $C_2 \propto t^{-0.25}$ predicted by the TR model, just as it was found previously for PB (section 5.2). This exponent is also reproduced by ^2H relaxation dispersion measurements (see below). The resulting $C_2(t)$ data is included in Fig. 24 (orange colored) and fits to that obtained from the dilution experiment well. Both exponent values ε_{II}^{intra} , and ε_{II}^Q , respectively, of PEP 200k are integrated in Fig. 20 of section 5.2; they match and confirm the previous data of PB.

Using the *Darmstadt* FC-1 relaxometer, also the quadrupolar relaxation dispersion $R_1(\omega)$ of the pure, per-deuterated PEP 200k (PEP-d 200k) was measured via FC ^2H NMR at 393 K and within $500 \text{ Hz} \leq \omega/2\pi \leq 5.6 \text{ MHz}$. The results have been published in PUB6 recently. As similar power-law exponents as for the intra-molecular ^1H relaxation are expected, the FC ^2H NMR measurements serve again as a verification of the isotope dilution experiment. Due to the local character of the quadrupolar interaction averaging of the spin-lattice relaxation by cross-relaxation is inefficient, leading to bi-exponential (normalized) magnetization $m(t)$, unlike in fully protonated PEP-h (cf. section 3.3). In Fig. 25a the normalized magnetization curves $m(t < R_1)$ of PEP-d are shown for different frequencies. They can be well fitted to a bi-exponential, where the weights are specified as the number of deuterons $p = 3/10$ and $(1-p) = 7/10$, respectively, as found in the monomer unit. One relaxation component in PEP-d stems from the deuterons directly connected to the chain backbone

(R_1^{chain}), the other one from the deuterons in the methyl groups (R_1^{CD3}). The average rate was calculated via $\langle R_1(\omega) \rangle = p R_1^{CD3} + (1-p) R_1^{chain}$ and is used in Fig. 25a to scale the time axis, yielding a master curve for all frequencies ω in good approximation.

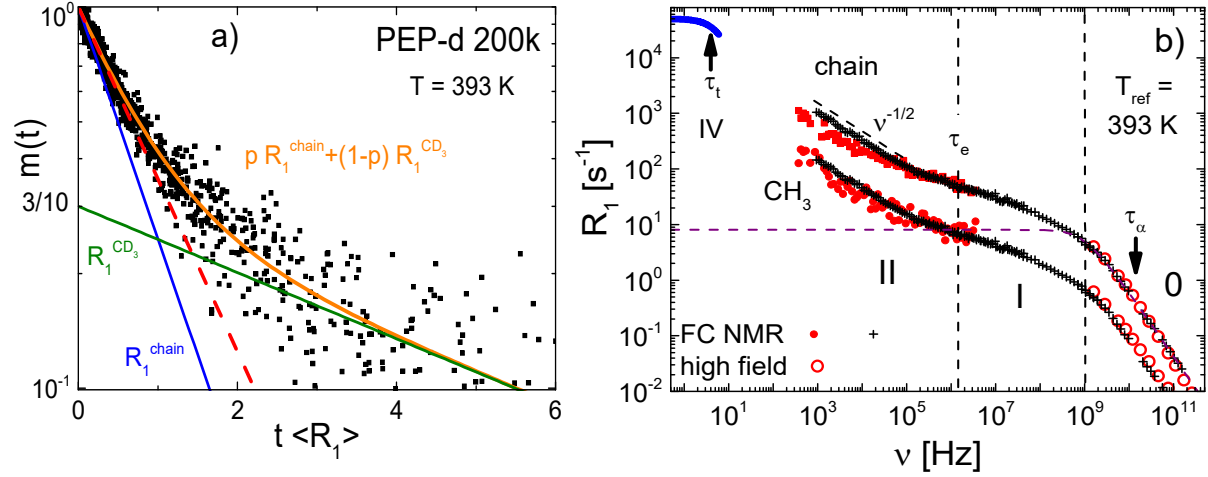


Figure 25: a) Rescaled relaxation function $m(t\langle R_1(\omega) \rangle)$ of PEP-d 200k at 393 K, measured at different frequencies $500 \text{ Hz} \leq \nu = \omega/2\pi \leq 5.6 \text{ MHz}$ (not distinguished). The initial decay reflecting $\langle R_1 \rangle$ is indicated (red dashed line). The decomposition into R_1^{chain} (blue) and R_1^{CD3} (green) is sketched. b) Corresponding relaxation rates of chain and methyl group deuterons. Data measured at $\omega/2\pi = 46 \text{ MHz}$ on a high-field magnet is included. The high-field and FC data is interpolated by the (vertically shifted) intra-contribution $R_1^{intra}(\nu)$ of ^1H relaxation obtained from isotope dilution (black crosses). Relaxation regimes are indicated. Purple dashed line: CD function fitted to the α -process of the chain relaxation and extrapolated to lowest ν . Blue: transition to the plateau for the chain relaxation as predicted from rheological data (cf. section 5.5). Both figures are taken from PUB6.

Although the noise is large due to the technical difficulties of FC ^2H NMR (cf. section 1.8), an initial linear regime at $t \leq \langle R_1 \rangle^{-1}$ is identified for all ω , *i.e.* a master curve is gained. This gives confidence about the reliability of the bi-exponential decomposition. The individual contributions R_1^{chain} and pR_1^{CD3} , respectively, are also indicated in Fig. 25a. The smaller relaxation rate corresponds to the rapidly rotating methyl group. One could raise the question if the long time tail of $m(t)$ rather results from the FC-1 artifact than from the methyl group relaxation. When compared to the relaxation of toluene (Fig. 11d in section 3.3) the data appears to be reliable down to a 10% drop, while methyl group relaxation contributes to 30%, as expected. Thus, chain- and methyl group relaxation are distinguishable, as in the case of deuterated toluene (cf. Fig. 12).

The extracted rates are shown in Fig. 25b, where the relaxation regimes for Rouse (I) and entanglement dynamics (II) are indicated. Additionally, ^2H NMR relaxation measurements on PEP-d 200k at $\omega/2\pi = 46 \text{ MHz}$ were carried out, employing a superconducting high-field magnet.²⁸⁷ These results are included in Fig. 25b (open symbols). In contrast to the FC ^2H NMR measurements, where ω was varied at constant $T_{ref} = 393 \text{ K}$, the temperature was varied within $100 \text{ K} \leq T \leq 330 \text{ K}$ at a constant field. With the full temperature dependence $\tau_\alpha(T)$ known (cf. Fig. 32 in section 5.5) and

under the assumption of FTS, it is possible to include the high-field relaxation data in Fig. 25b, where the time constant τ_α for $T_{ref} = 393\text{ K}$ is indicated. While the α -process (0) is covered in the high-field data, the polymer specific power-law regimes I, II appear in the FC measurements. The purple dashed line indicates the contribution of the α -process in the chain relaxation, extrapolated over the full frequency range. The gap between both methods, FC and high field, is still two decades broad and could be filled in future work by (i) performing FC ^2H NMR measurements at lower T or (ii) higher ω , respectively, (iii) by performing high-field measurements at $T > 330\text{ K}$ or, preferentially, by using further high-field magnets operating within $46\text{ MHz} > \omega/2\pi > 4.6\text{ MHz}$.

A comparison to the results of the ^1H isotope dilution experiment on PEP 200k discussed above (Fig. 24), is worthwhile. The corresponding susceptibility master curve is included in Fig. 25b by proper scaling. For that purpose $R_1^{intra}(\omega) = [\chi''_{intra}(\omega\tau_\alpha)/\omega\tau_\alpha] \times \tau_\alpha(T_{ref} = 393\text{ K})$ is plotted vs. $\omega\tau_\alpha/\tau_\alpha(T_{ref} = 393\text{ K})$. This procedure yields a rate curve $R_1^{intra}(\omega)$ as if it was measured at 393 K, but on a relaxometer pretending an extremely broad frequency range. This data is included as black crosses and interpolates the ^2H data from both, FC and high-field measurements, very well, after vertical scaling. This additional scaling is necessary to compensate the different coupling constants of the dipolar and the quadrupolar interaction. Only at low frequencies, minor deviations between the ^1H and ^2H curves are found.

As in the case of the intra-molecular relaxation resulting from isotopic dilution, also the ^2H dispersion data are transformed into the time domain to gain the re-orientational correlation function $C_2(t)$. For that purpose the gap between the ^2H high-field and the FC data was interpolated by the $\chi''_{intra}(\omega\tau_\alpha)$ data obtained from the isotopic dilution experiment. The resulting re-orientational correlation function $C_2(t)$ is included in Fig. 24 (orange triangles), as mentioned before. Also in this representation, only at long times slight deviations with respect to $C_2(t)$ obtained by isotope dilution are observed. They may result from residual inter-molecular relaxation in the isotopic blend. Specifically, ε_{II}^Q agrees well with $\varepsilon_{II}^{intra} = 0.5$ derived from the isotope dilution experiment but not with the prediction (0.25) of the TR model concerning re-orientation, a fact also found for PB before. This exponent value already shows up in the relaxation rate raw data, where in regime II $R_1^{intra}(\omega) \propto \omega^{-0.5}$ is observed (cf. Fig. 25b). As mentioned, the exponent values ε_{II}^{intra} and ε_{II}^Q of PEP 200k are included in Fig. 20 of section 5.2 and fit well to the FC NMR data on PB. Consequently, the results on PEP fully support the conclusion drawn in PUB2 (cf. section 5.2) that segmental re-orientation is not correctly described within the TR model. Again, also for PEP $\varepsilon_{II}^{intra} > \varepsilon_{II}^{total}$ is found, confirming the previous observations by FC NMR on PB and cementing the discrepancy to the DQ NMR measurements revealing $\varepsilon_{II}^{intra, DQ} = \varepsilon_{II}^{DQ, 195}$.

As also rheological measurements on PEP 200k were carried out, which are presented in section 5.5, the value of the terminal relaxation time $\tau_t(393\text{ K}) \approx 0.1\text{ s}$ is known. It can be read off, from the “relaxation map” in Fig. 32. Furthermore, the so-called “cumulative mode ratio” $F_{NMR}(M)$ which will be introduced in section 5.5, allows to predict the low frequency plateau value of $R_1(\omega)$ of PEP 200k, which is still outside the frequency window of FC NMR for such a high M . Without going into detail yet, the quantity is defined as $F_{NMR}(M) := \langle \tau(M) \rangle / \tau_\alpha = R_1(0) / R_1^\alpha(0)$. It quantifies the mean relaxation time averaged over the whole mode distribution, in relation to τ_α . When M grows, polymer dynamics shows up, causing an increase of $\langle \tau(M) \rangle$. The quantity $F_{NMR}(M)$ as shown in Fig. 31 *i.a.* for PEP, is linearly extrapolated to estimate its value at $M = 200\text{ k}$. Afterwards, the extrapolated value is

multiplied with $R_1^\alpha(\omega \rightarrow 0)$, estimated from a fit of the α -process by a CD function (purple dashed line in Fig. 25b). Doing so, the low frequency plateau of R_1 is estimated to about $R_1(\omega \rightarrow 0) \approx 50000 \text{ s}^{-1}$. Clearly, such a high rate exceeds the limits of FC NMR with respect to the switching time. The plateau representing the terminal regime (IV) of PEP 200k, is included in Fig. 25b as a blue line. This approach yields the pure intra-molecular relaxation dispersion $R_1^{\text{intra}}(\omega)$ of an entangled polymer over more than ten decades in frequency.

Given the inter-molecular correlation function $C_{\text{inter}}(t)$ also provided by the isotope dilution experiment, the segmental MSD $\langle r^2(t) \rangle$ is calculated for PEP 200k as well. For that purpose, eq. 66 was used again, as it was done for PB and PDMS (cf. section 5.3 and PUB4). After scaling to the reference temperature $T_{\text{ref}} = 393 \text{ K}$, the MSD $\langle r^2(t) \rangle$ is shown in Fig. 26.

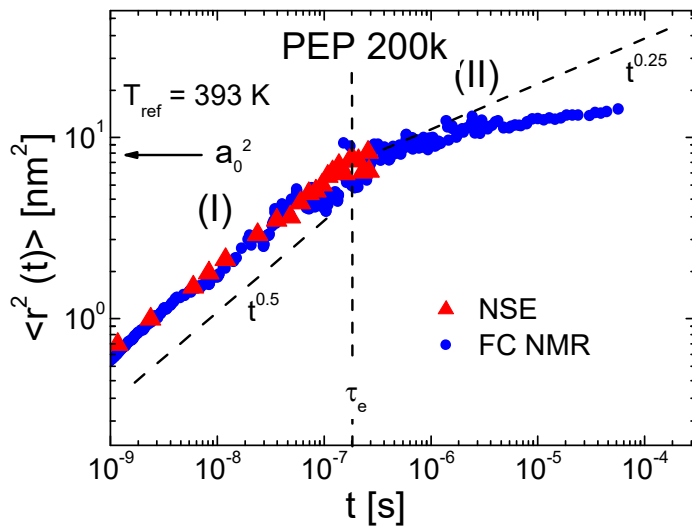


Figure 26: Segmental MSD $\langle r^2(t) \rangle$ at $T_{\text{ref}} = 393 \text{ K}$ of PEP 200k obtained by FC ^1H NMR. Corresponding NSE data from Wischniewski et al.¹³¹ on PEP 80k is also included, after conversion to T_{ref} . Relaxation regimes (I,II) are indicated.

For the somewhat lower M PEP 80k reference data from neutron spin echo (NSE) spectroscopy is available in the literature, which is included in Fig. 26.¹³¹ The NSE data was recorded at 492 K, which exceeds

the range of the FC NMR and the rheological measurements. Thus, the value of $\tau_\alpha(T = 492 \text{ K})$ needs to be projected in order to rescale the time axis of the NSE data to that of the FC NMR data measured at e.g. $T_{\text{ref}} = 393 \text{ K}$. For that purpose, an Arrhenius function fitted to the high- T data of $\tau_\alpha(T)$ collected by FC NMR and rheology is used. The extrapolation to 492 K is shown in Fig. 32 with $\tau_\alpha(492 \text{ K})$ represented as a red star. Accordingly, the NSE data on $\langle r^2(t) \rangle$ has to be horizontally rescaled by the factor $\tau_\alpha(393\text{K})/\tau_\alpha(492 \text{ K}) \approx 12$, to shift the time axis to the reference temperature 393 K. Of course FTS is assumed in this rescaling. It is noted that no vertical shifting had to be employed.

In the common range, absolute agreement between both methods, FC NMR and NSE data, is found. As in high- M PB and PDMS (Fig. 21, section 5.3), the power-law regimes of Rouse (I) and constrained Rouse (II) dynamics are covered by FC NMR, while NSE is restricted to the Rouse regime (I) and the onset of the constrained Rouse regime II. This again highly supports the reliability of the FC measurements on the isotopic blend of PEP and, moreover, the whole idea of determining the MSD from ^1H spin-lattice relaxation dispersion. It is noted that NSE measurements on the different polymer poly(ethylene) also revealed the transition into the constrained Rouse (II) regime.⁹⁸ While in the Rouse regime the predicted slope $\langle r^2(t) \rangle \propto t^{0.5}$ (cf. Table 1) is experimentally reproduced, the exponent in regime II is slightly lower than forecast, $\langle r^2(t) \rangle \propto t^{0.2}$ rather than $\propto t^{0.25}$. The value of the

MSD at the crossover between Rouse and entanglement dynamics occurring at the entanglement time τ_e can be used to estimate the tube radius a_0 , emerging in the TR model: specifically $a_0 = (\langle r^2(\tau_e) \rangle)^{1/2} \approx 3 \text{ nm}$ is found, while Fetters et al. derived a somewhat lower value of 2.4 nm , yet, from rheological data.⁶⁵

As discussed in section 5.2, the ω dependence of the ratio between inter- and intra-molecular relaxation $A(\omega) = R_1^{\text{inter}}/R_1^{\text{intra}}$ provides another source of information about the nature of the molecular dynamics, besides analyzing power-law exponents. Also for PEP 200k $A(\omega)$ is found to increase with decreasing ω in the entanglement regime (Fig. 18, section 5.2). This finding, confirmed now for three different polymers (PEP, PB, PEO¹²⁷), is an indication for the isotropy of the dynamics in the constrained Rouse regime and contradicts the anisotropic TR model predicting the opposite, a decrease of A with decreasing ω (*cf.* section 1.7).⁷⁵

Summarized, the findings on PEP are actually very similar to those on PB (sections 5.2 and 5.3). Hence, the discrepancies concerning $C_2(t)$ between FC NMR on the one hand and DQ NMR, generic simulations and the TR model on the other hand, are reinforced. The fact that translation appears to conform to the TR model, while re-orientation does not may seem surprising and challenges in particular de Gennes' RTO hypothesis (eq. 35), an issue deserving future investigation. The situation is depicted in Fig. 27, where the (normalized) product of the measured functions $C_2(t)$ and $\langle r^2(t) \rangle$ is shown for PB 24k, 196k and PEP 200k.

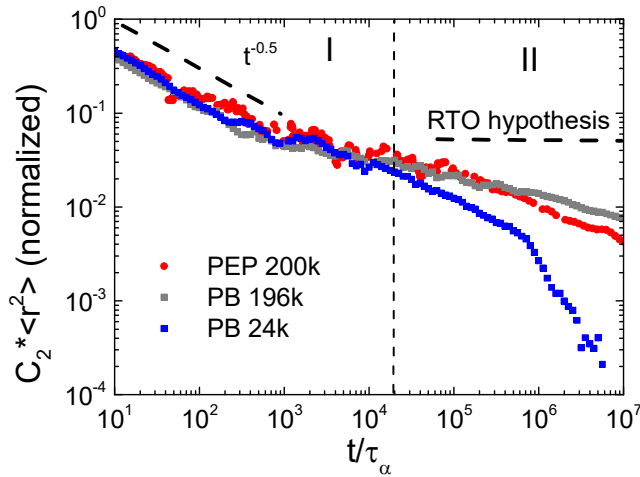


Figure 27: Product of the segmental MSD $\langle r^2(t) \rangle$ and the re-orientational correlation function $C_2(t)$ of PB 24k, 196k, and PEP 200k. The predictions of the TR model for regimes I and II are indicated.

In all three systems, the product is $\propto t^{-0.5}$ at $t < \tau_e$ (regime I) and thus in accordance with the Rouse model (*cf.* section 1.7 and Table 1). In the constrained Rouse regime

(II, $t > \tau_e$) the product is predicted to be a constant (eqs. 35, 53). It is recalled that Wang et al. indeed found $C_2(t) \times \langle r^2(t) \rangle = \text{const.}$ from generic computer simulations in regime II (Fig. 6).²⁰ Experimentally, this is actually not observed due to the fact that $C_2(t)$ decays steeper in regime II than predicted. As this result is now confirmed for two different polymers, PEP and PB, it may be a generic one for entangled polymer melts. Kimmich states that “The topological constraints restricting translational segment diffusion are not necessarily the same as those being responsible for limited rotational reorientations”.⁶ Given the experimental evidence, this statement can be confirmed.

5.5 From NMR Relaxometry to “Molecular Rheology”

This section is dedicated to a comparison between FC ^1H NMR and shear rheology. For that purpose, FC ^1H NMR relaxation and dynamic shear experiments were performed for identical samples, the results of which are compared in the frequency and in the time domain. A first such comparison in the frequency domain was carried out in PUB5 for the linear polymer PPG and for the dendrimer poly(propylene imine) (PPI) (*cf.* also section 5.6.). The most important findings of PUB5 will be included in this section. Yet, the focus lays on new, unpublished results on the linear polymer PEP, for which FC NMR relaxometry (*cf.* section 5.4) as well as rheological measurements were performed, the latter in cooperation with the group of N. Aksel (*Bayreuth*).

The spin-lattice relaxation rate $R_1(\omega)$ measured by FC ^1H NMR is related to the frequency components of the fluctuations of the inter-nuclear vectors between adjacent, magnetically interacting protons. As mentioned in section 1.7 $R_1(\omega)$ is proportional to the spectral density $J(\omega)$, thus quantifying equilibrium fluctuations. It is the Fourier transform of the dipolar correlation function $C_{DD}(t)$ (eqs. 4, 45). Using the fluctuation-dissipation theorem (eq. 14) fluctuation in general can be related to dissipation (section 1.1). This allows comparing the NMR susceptibility (*cf.* section 4.1) given by $\chi''(\omega) = \omega R_1(\omega)$, to its rheological analogue, the dynamic loss modulus $G''(\omega)$. Thus, microscopic and macroscopic rheology are confronted to each other.

The seven (fully protonated) PEP samples, on which the ^1H FC relaxation experiments presented in section 5.4 were performed, were additionally investigated by oscillatory shear rheology. The complex shear modulus $G^*(\omega)$ was measured on a state-of-the-art rheometer *Anton Paar MCR-500*. The frequency window of $0.01 \text{ Hz} \leq \nu = \omega/2\pi \leq 30 \text{ Hz}$ is strongly different than that of FC NMR, where typically several 10 MHz down to some 100 Hz (when using the FC-1 device) are covered. Assuming FTS, both, the discrepancy in the dynamic windows, as well as the instrumental limitations to about three (shear) and to about five decades (FC NMR) are overcome by constructing master curves, a procedure very common in rheology.^{6,60-62} As in the case of the FC NMR experiments the shear measurements were carried out in an extraordinarily broad temperature range of about $200 \text{ K} \leq T \leq 400 \text{ K}$. Thus, the lowest temperatures reach down as low as T_g . Consequently, the α -process is included also in the shear data, a fact rarely found in the literature and a peculiarity of this work. Figure 28 (middle) shows the rheological master curves of $G''(\omega\tau_\alpha)$ of the different samples of PEP with $3 \text{ k} \leq M \leq 200 \text{ k}$. Directly above, the corresponding prediction resulting from the TR model is sketched, *i.e.* the loss modulus resulting from Fourier transform of eq. 38 without finite length effects.⁹⁷ Below, the corresponding susceptibility master curves $\chi''(\omega\tau_\alpha)$ of the total ^1H relaxation are shown. In both cases a low- M reference system lacking of polymer dynamics is included as well, namely propylene glycol (PG) in the rheological data and di-PG in the NMR data.

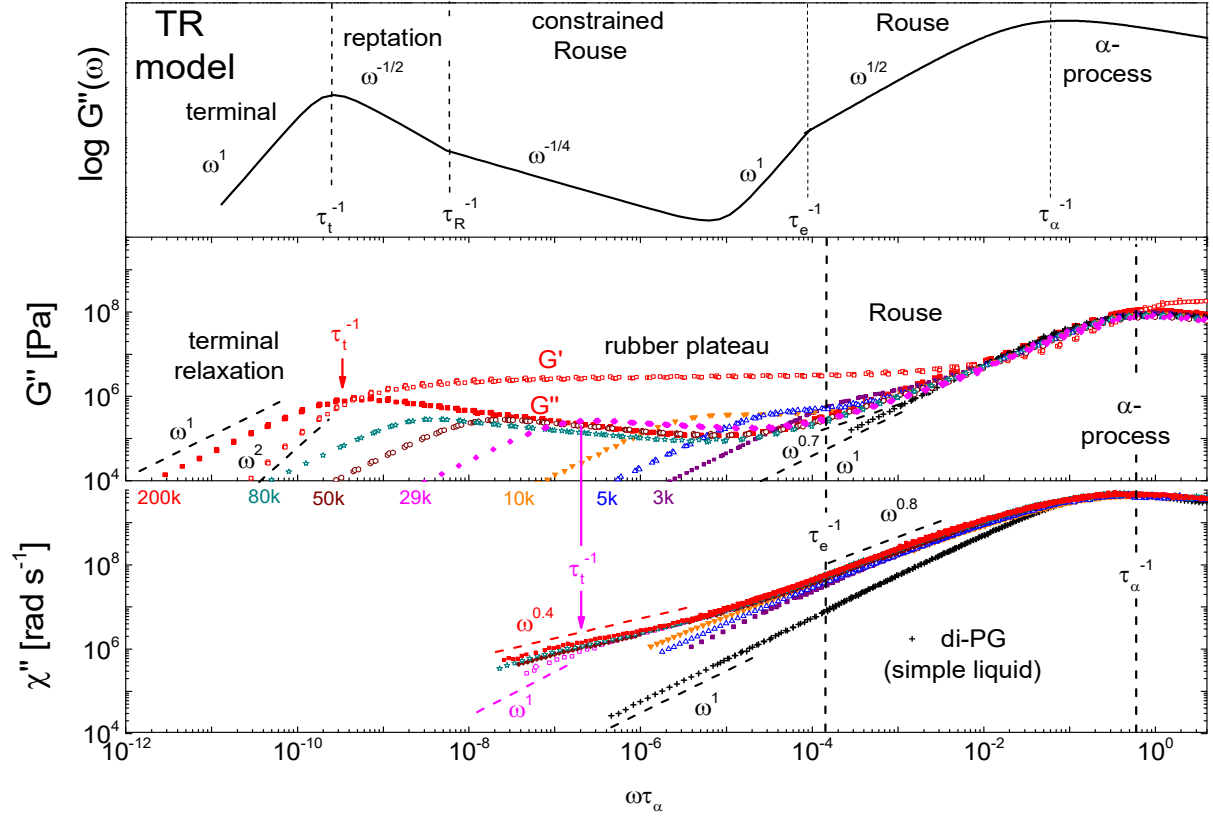


Figure 28: **Top:** Forecast by the TR model for $G''(\omega)$ of a linear entangled polymer melt without finite length effects. **Middle:** Master curves of the loss modulus $G''(\omega\tau_\alpha)$ of PEP of different M , as indicated. For PEP 200k the storage modulus $G'(\omega\tau_\alpha)$ is also shown. **Bottom:** Master curves of the NMR susceptibility $\chi''(\omega\tau_\alpha)$. Relaxation regimes, power-law behavior (dashed lines) and crossover times are indicated. The entanglement time (represented by the vertical dashed line) $\tau_e/\tau_\alpha \approx 7000$ was determined from the corresponding time domain data $C_{DD}(t)$ (cf. section 5.4).

Despite the mentioned differences between both methods, the master curves $G''(\omega\tau_\alpha)$ and $\chi''(\omega\tau_\alpha)$ show certain correspondences, not only in the case of PEP presented in Fig. 28, but also for PPG, as well as for dendritic PPI (cf. PUB5). The α -process reflected in the peak at $\omega\tau_\alpha \approx 1$ dominates both types of spectra at high frequencies. Going toward lower frequencies the α -process in the simple liquid PG is directly succeeded by the terminal relaxation obeying $\propto \omega^1$ in the results of both techniques. Indeed, concerning PG/di-PG (black crosses) $G''(\omega)$ and $\chi''(\omega)$ feature similar shapes and both data can be well interpolated by a CD function, for instance. In the polymer PEP the α -peak is succeeded by the Rouse regime, where a power-law common for all M is apparent, with exponents of $\propto \omega^{0.7}$ concerning the shear and $\propto \omega^{0.8}$ concerning the FC NMR data. Thus, the slope in $G''(\omega\tau_\alpha)$ is somewhat steeper than predicted by the Rouse model ($\omega^{0.5}$, cf. Fig. 28 (top)). In $\chi''(\omega\tau_\alpha)$ a crossover to entanglement dynamics is observed, *i.e.* a transition to a second, polymer specific power-law for $M > M_c$. The entanglement time τ_e was estimated to $\tau_e/\tau_\alpha \approx 7000$ from the time domain data, specifically from the intersection between the power-laws of regime I and II in $C_{DD}(t)$. A similar

extraction in the frequency domain $\chi''(\omega\tau_e)$ yields a different entanglement time.^e Determining τ_e from the power-law intersection in the frequency domain would yield a value which is by a factor of about five higher than the value estimated from $C_{DD}(t)$. In this work, the value of τ_e determined from the time domain is considered. The rheological data shows no distinct feature at τ_e and actually no signs of the constrained Rouse regime at all, *i.e.* the descent with $\omega^{-1/4}$ and the subsequent ascend with ω^1 predicted by the TR model in regime II (*cf.* Fig. 28 top) are not observed. Here, $G'(\omega)$ is governed by the rubber plateau at frequencies $\omega\tau_e \approx 1$. The estimation of τ_e from rheological data using the onset frequency of the rubber plateau as proposed by Kimmich for instance⁶, is questioned. The frequency, where the FC data fulfills the condition $\omega\tau_e \approx 1$, indicated by the dashed vertical line in Fig. 28, appears to agree with the frequency where the minimum in $G''(\omega\tau_e)$ occurs for high M . However, this frequency also depends on M slightly, *i.e.* $G''(\omega\tau_{min}) = \text{Min}[G''(\omega\tau_e)]$ with $\tau_{min}(M) \propto M^{-0.7 \pm 0.05}$. Per definition, τ_e is M -independent (eq. 33) and determining τ_e this way is not correct. Finally, the fact that τ_e determined by FC NMR agrees with the terminal decay of PEP 3k in $G''(\omega\tau_e)$ supports the reliability of the value. PEP 3k is supposed to be very close to M_e .¹⁰⁵ The terminal time of a polymer with $M \approx M_e$ is a reasonable approximation for τ_e . Unlike FC NMR, rheology appears to be not appropriate for a straightforward determination of τ_e due to the absence of the constrained Rouse regime.

At lowest frequencies the terminal power-laws $G' \propto \omega^2$ and $G'' \propto \omega^1$ characteristic for a Newtonian liquid are observed in the shear data, which quickly shift to higher frequencies with decreasing M . As a consequence, the Rouse regime and the rubber plateau, both being specific for polymers, successively disappear and finally leave the behavior of a simple liquid like PG. FC ^1H NMR reaches the terminal relaxation, where $\chi'' \propto \omega^1$ is observed (*cf.* section 4.1), only up to $M = 29\text{k}$. The transition to the terminal regime in the FC data of PEP 29k (colored in pink) concurs with the terminal peak position in the corresponding G'' curve.

As mentioned, rheology and FC NMR detect different correlation functions: while FC ^1H NMR probes the dipolar correlation function $C_{DD}(t)$, shear rheology probes the shear relaxation modulus $G(t)$ related to the fluctuation of the stress tensor (*cf.* eq. 16, section 1.1). In Fig. 29 both correlation functions are compared for (di-)PG as a low- M reference (green), for un-entangled PEP 3k (blue) and for entangled PEP 50k (red). For that purpose, the corresponding FC NMR and shear master curves shown in Fig. 28 were transformed into the time domain. $G(t)$ was normalized by dividing out G_0 .

^e The asymptotes of the time function $f(t) = t^{-a} + t^{-b}$ intersect at $t = 0$ per construction, for all $0 < a, b < 1$. After Fourier transformation $g(\omega) = \pi/2[\Gamma(a)]^{-1} \sec(a\pi/2)\omega^{a-1} + \pi/2[\Gamma(b)]^{-1} \sec(b\pi/2)\omega^{b-1}$ is gained. The intersection point of the asymptotes of $g(\omega)$, however, depends on the exponents a, b . As a consequence, the determination of τ_e in the time and in the frequency domain will provide different values.

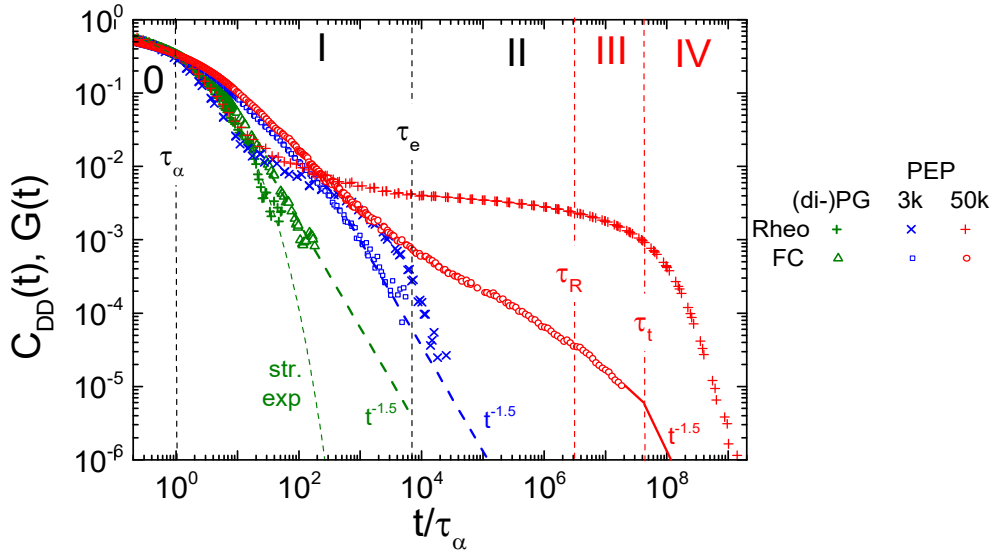


Figure 29: Normalized correlation functions $C_{DD}(t/\tau_\alpha)$ (open symbols) and $G(t/\tau_\alpha)$ (crosses) of selected M of PEP, as well as of (di-)PG. Relaxation regimes and transition times are indicated. Here, τ_R and τ_t explicitly belong to PEP 50k. Red solid line: projection for $C_{DD}(t)$ of PEP 50k after estimating τ_t from shear measurements.

Regarding the simple liquid (di-)PG, for which the α -process is directly succeeded by the terminal regime, $G(t/\tau_\alpha)$ and $C_{DD}(t/\tau_\alpha)$ are barely distinguishable. At shorter times the decay of both quantities is first stretched exponential. The functions only differ in the terminal behavior, as $G(t)$ remains (multi-)exponential, whereas $C_{DD}(t) \propto t^{-3/2}$ holds due to the dominance of inter-molecular relaxation. The curves of the polymer PEP differ in the Rouse regime insofar as the amplitude of $C_{DD}(t)$ is somewhat larger when compared to $G(t)$. An explanation might be the factor of 2 appearing in the exponentials (modes) contributing to $G(t)$ (eqs. 31, 38), which doesn't appear in the quantities relevant for $C_{DD}(t)$, specifically the segmental MSD (eq. 27) and $C_2(t)$ (eq. 29). Otherwise, the slopes are quite similar and close to -0.8 in both cases. Yet, in the absence of entanglement in PEP 3k $C_{DD}(t)$ and $G(t)$ still resemble each other as both functions probe the same regimes, namely the glassy, the Rouse and the terminal one.

The shapes of $G(t)$ and $C_{DD}(t)$ become increasingly different when going from the simple liquid to the entangled melt. For PEP 50k ($M \gg M_c$) in the region where $G(t)$ remains on the rubber plateau, $C_{DD}(t)$ continues decaying and has a richer structure: the transitions between regime I (Rouse) and II (constrained Rouse) occurring at τ_e as well as between II and III (reptation) at τ_R , respectively, are resolved (cf. section 5.4). In PEP 50k and for higher M the terminal regime, where $C_{DD}(t) \propto t^{-3/2}$ is expected, exceeds the time window of current FC ^1H NMR. Taking the terminal time τ_t of the shear data the further progress of $C_{DD}(t)$ is projected in Fig. 29 by the red solid line. Clearly, the area under the curve of $C_{DD}(t)$ is significantly lower than that of the corresponding $G(t)$, thus, the mean correlation time averaged over the whole mode distribution is significantly lower in $C_{DD}(t)$ than in $G(t)$. This discrepancy strongly increases with growing chain length. This is a consequence of the different weighting factors of the relaxation modes as will be discussed below.

A full quantitative spectral analysis of both, shear as well as NMR relaxation data in terms of a detailed mode analysis is difficult as the contributions of intra- and inter-molecular relaxation need to be disentangled. Nevertheless, some quantitative analysis can be performed. A novel scaling is presented in PUB5 and applied to linear PPG as well as dendritic PPI. From susceptibility master curves the master curve $J(\omega\tau_\alpha)/\tau_\alpha = \chi''(\omega\tau_\alpha)/\omega\tau_\alpha$ can be calculated. After multiplication with $\tau_\alpha(T)$ the spectral density $J(\omega)$ is gained for any reference temperature T , if $\tau_\alpha(T)$ is known. Likewise, the dynamic viscosity master curve follows from $\eta'(\omega\tau_\alpha)/\tau_\alpha = G''(\omega\tau_\alpha)/\omega\tau_\alpha$. It is formally similar to a spectral density (*cf.* section 1.1). While master curves are most easily constructed from susceptibility data (*cf.* section 4.1), collective dynamics occurring at very low ω are more emphasized in the spectral density representation. The curves are divided by the respective zero-frequency values of the local dynamics (α -process) contributions $R_1^\alpha(\omega\tau_\alpha \rightarrow 0)$ and $\eta_\alpha'(\omega\tau_\alpha \rightarrow 0)$, respectively, for the sake of comparability. Those reference spectra ($R_1^\alpha(\omega\tau_\alpha)$ and $\eta_\alpha'(\omega\tau_\alpha)$) are obtained by extrapolating the α -relaxation with a CD function. The rescaling provides iso-frictional (T_g independent) spectra, which is important for low- M systems.^{55-59,272} The rescaling also removes possible M -dependences of the dipolar coupling constant K , as well as of G_0 , respectively. Figure 30 exemplifies the rescaled relaxation rates $R_1(\omega\tau_\alpha)/R_1^\alpha(0)$ and dynamic viscosities $\eta'(\omega\tau_\alpha)/\eta_\alpha'(0)$ for PPG of different M as indicated.^{PUB5} The respective contribution by the α -process (R_1^α , η_α) to which both types of spectra are normalized, is marked by the black dashed lines.

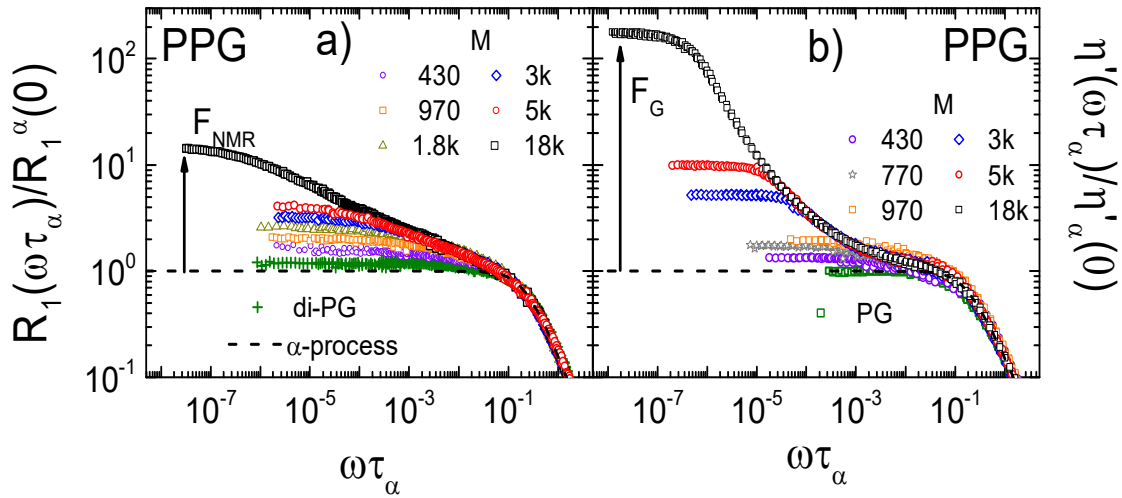


Figure 30: Evolution of the re-scaled spin lattice relaxation rate (a) and the dynamic viscosity (b) of PPG with M . Black dashed lines: contribution of the α -process. The cumulative mode ratios F_{NMR} and F_G denote the corresponding plateau values at zero frequency. Both figures are adapted from PUB5.

Qualitatively, the shapes of the curves obtained by both methods are similar, also in this kind of representation. Most prominent is the low-frequency plateau quickly increasing with growing M . This effect is clearly more pronounced in the rheological data. The FC data of PPG 18k shows a kink at around $\omega\tau_\alpha \approx 10^{-4}$, marking the frequency where entanglement becomes relevant. In the corresponding rheological data, again no such feature is observed. A quantitative analysis of

$R_1(\omega\tau_\alpha)/R_1^\alpha(0)$ and $\eta'(\omega\tau_\alpha)/\eta_\alpha'(0)$ is performed by determining the M dependent zero-frequency limits ($\omega\tau_\alpha \rightarrow 0$). These quantities were termed “cumulative mode ratios” $F_{NMR}(M)$ and $F_G(M)$.^{PUB5} Basically, $F(M) := \langle \tau(M) \rangle / \tau_\alpha$ measures the increase of the mean relaxation time, resulting from averaging over the whole mode distribution, with respect to the reference time scale τ_α . The increase of $F(M)$ is caused by slow molecular dynamics emerging at $\omega\tau_\alpha < 1$ with growing M . In the case of type-A polymers like PPG or PI, the normal mode relaxation measured via DS can be included in such a comparison.^{PUB5} The corresponding cumulative mode ratio is similarly defined as $F_{DS}(M) := \varepsilon''(\omega\tau_\alpha \rightarrow 0) / \omega\tau_\alpha$. In PUB5 predictions for $F(M)$ were derived, assuming the Rouse, the TR and, in the case of NMR, also the RR model. Table 2 summarizes the TR predictions resulting within the Rouse and the TR model, respectively. Mostly, power-law behavior is anticipated. A peculiarity occurs in (^1H) NMR, where different predictions arise for intra- and inter-molecular relaxation.

cumulative mode ratio	Rouse	TR
$F_{NMR}^{\text{intra}}(M) \propto R_1^{\text{intra}}(0)$	$\ln(M)$	M^2
$F_{NMR}^{\text{inter}}(M) \propto R_1^{\text{inter}}(0)$	$M^{1/2}$	$M^{3/2}$
$F_G(M) \propto \eta'(0)$	M^1	M^3
$F_{DS}(M) \propto \frac{\varepsilon''(0)}{\omega\tau_\alpha}$	M^2	M^3

Table 2: M -dependences of the cumulative mode ratios F_{NMR} , F_G and F_{DS} as predicted by the Rouse and the TR model, respectively.^{PUB5} In the case of ^1H NMR the intra- and inter-molecular relaxation rates contribute separately.

For this Extended Abstract the analysis of $F(M)$ was extended to include the data of PEP, PB and PI. The dielectric data of the latter two are taken from ref. 108. Figure 31 shows the resulting cumulative mode ratios $F(M)$, plotted vs. M/M_c . The respective M_c values are given in the figure caption.

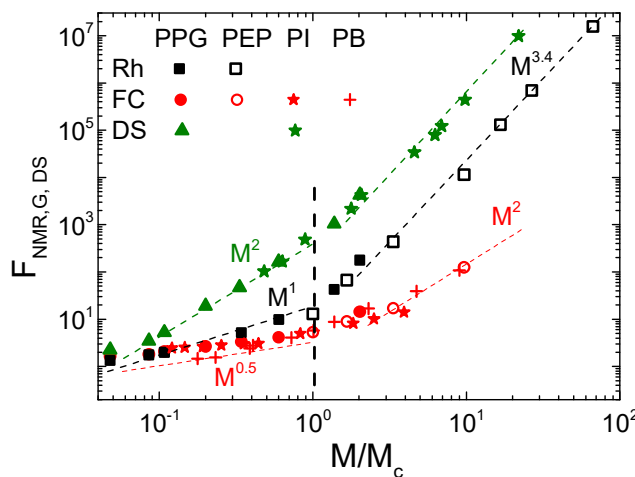


Figure 31: Cumulative mode ratios $F(M)$ of different polymers vs. M/M_c . Power-law behavior suggested by the Rouse and the TR model is indicated. The following values of M_c were used: $M_c(\text{PPG}) = 9k$, $M_c(\text{PEP}) = 3k$, $M_c(\text{PI}) = 14k$, $M_c(\text{PB}) = 2k$. Adapted from PUB5 and extended.

Two specific regimes, referred to un-entangled and entangled dynamics, respectively, are observed in all investigated polymers. The crossover in

experimental data occurs at M_c . In both regimes the exponents are different for the different methods: while behaviors close to $F_{NMR} \propto M^{0.5}$, $F_G \propto M^1$ and $F_{DS} \propto M^2$, respectively, are found in the un-entangled regime, the ascends of $F(M)$ above M_c follow $F_{NMR} \propto M^2$, $F_G \propto M^{3.4}$ and $F_{DS} \propto M^{3.4}$. Thus,

the forecasts for DS and rheology are reproduced (cf. Table 2). As said, in the case of FC NMR different scaling relations for the intra- and the inter-molecular relaxation are expected. In particular, in the un-entangled regime ($M < M_c$), a distinction between the square root law and the log-scaling is difficult. Also in the entangled regime the values are somewhat ambiguous because $R_1^{inter}(\omega)$ shows dispersion down to lowest ω due to inter-molecular relaxation. Therefore, the plateau values are possibly somewhat underestimated. Comparing the different techniques, the M -dependences of F_{NMR} , F_G and F_{DS} are different and increase in this order, explaining why DS provides the highest sensitivity with respect to polymer dynamics. Rheology provides the second largest sensitivity and FC ^1H NMR shows the lowest among those three methods. The methodical sensitivity diverges in particular above M_c , explaining why $G(t)$ and $C_{DD}(t)$ increasingly disperse the higher M becomes (see Fig. 29).

The large differences in the quantity $F(M)$ between the different methods in entangled polymers can be immediately understood by the different correlation functions monitored. For example, $R_1^{intra}(\omega)$ probes the bond-vector correlation function (eqs. 29, 51) to which all chain modes count equally. The same argument holds for the segmental MSD. In contrast, the quantities $\eta_\alpha'(\omega)$ and $\varepsilon''(\omega)/\omega$ are related to the end-to-end vector correlation function governed by the longest (terminal) mode τ_t (cf. eqs. 26, 34). In the quantities relevant for NMR relaxation ($\langle r^2(t) \rangle$, $C_2(t)$), the modes with $\tau_i \leq \tau_t$ and integers $i = 1, \dots, N$ are equally weighted. Otherwise, the correlation function relevant for DS and rheology is that of the end-to-end vector (eq. 34). To this correlation function, only odd mode numbers (indices 1,3,5...) contribute and the modes are weighted by the inverse of the squared mode index. This difference immediately explains the slower evolution of $F(M)$ in FC NMR, when compared to rheology and DS. The different weighting leads to different mean correlation times. In other words, in DS and rheology the amplitude in the normalized spectral density is concentrated at lowest frequencies thus yielding higher amplitude there. In contrast, the intensity in the NMR spectral density is distributed over a broad frequency range. In conclusion, FC NMR provides superior spectral information, for example in terms of well-resolved polymer-specific power-laws, yet, on cost of sensitivity, i.e. the decay of the probed correlation function is faster overall. In un-entangled polymers like PEP 3k the difference between rheology and FC NMR is smaller. Here, the weighting of the exponentials (modes) in the shear response function $G(t)$ (eq. 38, third term) is similar to that of the NMR quantities $\langle r^2(t) \rangle$ and $C_2(t)$, given by eqs. 28 and 29. The only difference is the factor of 2 appearing in the exponents of $G(t)$ but not in $\langle r^2(t) \rangle$ and $C_2(t)$.

Combining FC NMR, shear rheology and other techniques, a “relaxation map” was drawn.^{PUB4} The values for the time constant $\tau_\alpha(T)$ in PEP, determined from master curve construction for temperatures well above T_g , are shown in Fig. 32. They feature a super-Arrhenius temperature dependence, as typical for glass forming liquids. The results for the two methods, rheology and FC NMR, overlap over about eight decades almost perfectly. No M -dependence of τ_α is found in the investigated M -range. Reference data obtained from ^2H solid state NMR²⁸⁷, DS^{288,289} and DSC²⁸⁷ included in Fig. 32 is also highly consistent. Altogether, the slowdown of the α -process during the glass transition is probed over 15 decades in amplitude and within a temperature range of $200\text{ K} \leq T \leq 420\text{ K}$. The $\tau_\alpha(T)$ data in Fig. 32 is well interpolated by a three parameter function proposed by Schmidtke et al.,³⁹ intended to guide the eye. DSC measurements were done on deuterated PEP-d 50k (courtesy of T. Körber²⁸⁷) as well as on protonated PEP-h 50k. Both measurements yield similar results for the calorimetric glass transition temperature. $T_g^{DSC} = (212 \pm 1)\text{ K}$ was determined for

PEP-h 50k, while $T_g^{DSC} = (209 \pm 1) \text{ K}$ was found for PEP-d 50k. In contrast to PB (*cf.* PUB2) only a weak isotope effect on T_g is observed in PEP.

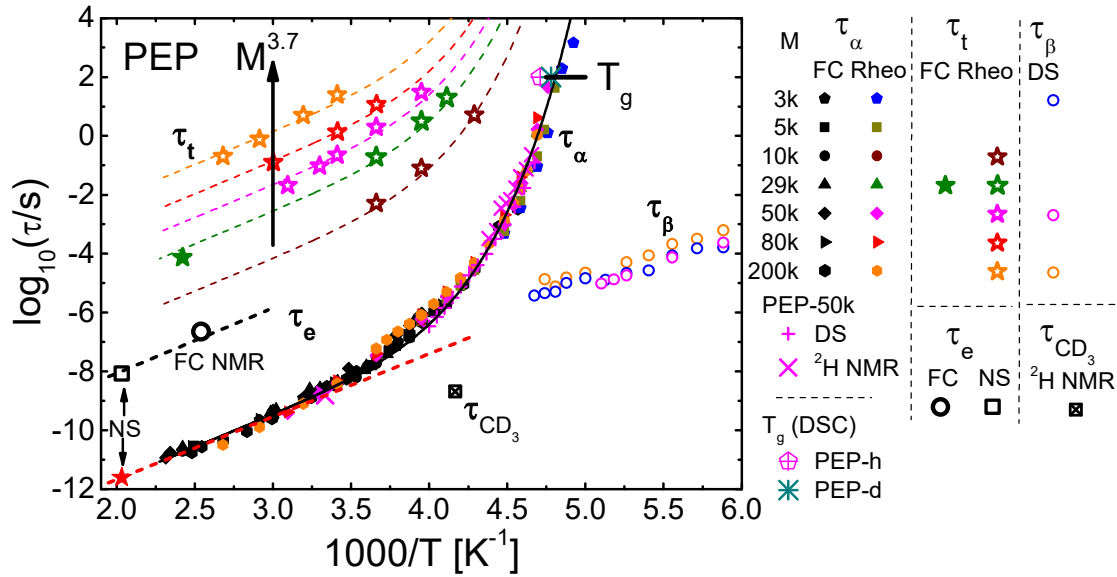


Figure 32: Relaxation map of PEP: $\tau_\alpha(T)$ determined by FC 1H NMR and rheology for various M , as indicated. For PEP 50k also data from DS,²⁸⁸ 2H solid state NMR²⁸⁷ and DSC (on PEP-h as well as on PEP-d) is shown (crosses). Red star: extrapolation of $\tau_\alpha(T = 492 \text{ K})$ (*cf.* section 5.4) using an Arrhenius law (red dashed line) for the high T data. The $\tau_\alpha(T)$ data is interpolated by a three-parameter function³⁹ (black solid line), versions of which are vertically shifted to intersect $\tau_t(T)$ values determined by rheology (closed symbols) as well as the entanglement time $\tau_e(T)$, determined by FC NMR. Concerning τ_e a value reported from a neutron scattering study is added (open black square).⁹⁸ Time constants of methyl group rotation τ_{CH_3} and of the β -process $\tau_\beta(T)$ are also added.^{287,288} All data is unpublished.

The low-frequency intersection between the $G'(\omega)$ and $G''(\omega)$ raw data observed at highest T provides a measure for the terminal relaxation time τ_t .⁶² It is found to scale as $\tau_t(M) \propto M^{3.7}$ (see Fig. 32), in accordance with numerous studies on linear polymers.^{6,60-62,81,82} This estimation is only possible for $M \geq 10k$ as below, G' and G'' do not cross at lowest ω . The $\tau_t(M, T)$ values are included in the plot and coincide quite well with vertically shifted versions of the interpolation function used for $\tau_\alpha(T)$. For PEP 29k τ_t determined from the FC data is included in Fig. 32 at around $1000 \text{ K}/T \approx 2.5$. It was estimated from the intersection between the entanglement (regime II) and the terminal power-law. The value extracted from FC NMR fits well to the extrapolation of the rheological data $\tau_t(T, M = 29k)$ (green dashed line). The fact that τ_α and τ_t feature the same temperature dependence justifies the assumption of FTS, meaning that the α -process, relevant for the glass transition, also drives the collective, non-local polymer dynamics and even the terminal relaxation. Also included in the relaxation map is the value of τ_e as estimated from the power-law intersection between the Rouse and the constrained Rouse regime in $\chi''(\omega)$, through which the interpolation function of $\tau_\alpha(T)$ is also placed. Otherwise, τ_e can experimentally only be determined via scattering methods.¹⁵⁰ A further

τ_e value of PEP 80k taken from a NSE study⁹⁸ is included in Fig. 32. It essentially confirms the value obtained by FC NMR, as the temperature dependence $\tau_e(T)$ appears to be consistent with $\tau_\alpha(T)$. Thus, FC NMR provides an alternative way for detecting the transition between Rouse and entanglement dynamics in a model-independent way. For the sake of completeness $\tau_\beta(T)$ of a secondary (β -) relaxation detected in PEP via DS²⁸⁸ as well as τ_{CH3} of the methyl group rotation in the propylene monomers determined from solid state ^2H NMR spectroscopy²⁸⁷ is included in Fig. 32. The β -process is observed below T_g and features an Arrhenius-like temperature dependence. It is furthermore M -independent. Similar relaxation maps as the one shown in Fig. 32 are published in PUB4 for PB and PDMS.

5.6 Molecular Dynamics in Dendrimers

Many simple liquids and linear polymers were investigated by FC NMR in the *Bayreuth* group. Dendrimers (*greek: "dendron"; tree*), self-similar cascade molecules *aka. "starburst molecules"*, pose a continuation toward more complex molecular topologies. Dendrimers were first synthesized by Buhleier et al. in 1978.²⁹⁰ They potentially face applications *e.g.* as carriers for MRI contrast agents, in drug-delivery or as catalysts.²⁹¹⁻²⁹⁴ MD simulations revealed "...a compact (space filling) structure under solvent conditions, with the radius of gyration which scales with the number of monomers as $R_g \propto N^{1/3}$ ".²⁹⁵ The number of generations G of dendrimers is inherently limited due to the divergence going along with the exponential growth of the density. The dynamics of dendrimers is subject of quite a number of simulations,²⁹⁶⁻³⁰⁴ often based on Rouse-like models and generalized Gaussian structures (*cf.* section 1.6). Difficulties in the interpretation of simulation results arise from the degeneracy of the eigenmodes, as a consequence of the topological self-similarity. A multitude of experimental works address the structure³⁰⁵⁻³⁰⁷ or the dynamics in solution.³⁰⁷⁻³¹⁸ Yet, the highly concentrated or the melt state is rarely investigated; some shear data³¹⁹⁻³²¹ as well as dielectric data³²² is reported. The present spin-lattice relaxation dispersion measurements on dendrimers are a novelty.

Employing FC NMR, the ^1H relaxation dispersion of the frequently investigated dendrimer poly(propylene imine) (PPI) of generations $G \in \{2,3,4,5\}$ in the melt state was measured in a broad temperature range of $230 \text{ K} \leq T \leq 400 \text{ K}$.^{PUB3, PUB5} In the case of G4 and G5, respectively, STELAR (*Bayreuth*) data was complemented by measurements carried out on the FC-1 relaxometer in *Darmstadt*, in order to reach extraordinarily low fields. Furthermore, solid state ^2H NMR, DS and in particular shear rheology were applied.^{PUB3,PUB5} PPI is commercially available in bulk quantities since the early 90's.³²³ It is characterized by a di-aminobutane core, a functionality of 3 at the branching points formed by nitrogen, and terminal NH_2 groups. In the melt state, PPI dendrimers constitute transparent, viscous, low- T_g ($\approx 200 \text{ K}$, *cf.* PUB3) glass-forming liquids. For the solid state ^2H NMR measurements, the protons in the terminal amino-groups were exchanged by deuterons.

Concerning the ^1H magnetization, non-exponential relaxation was observed at high temperatures ($> 300\text{K}$), for all G , at all frequencies and in the data of both relaxometers. As an example normalized magnetization curves $m(t < R_1(\omega) >)$ of PPI G2 and G5 measured on the STELAR relaxometer are plotted in Fig. 35. Below, the non-exponentiality will be addressed in more detail. Tentatively, $<T_1>^{-1}$ was

determined from stretched exponential fits of the magnetization curves.^{PUB3,PUB5} The inverse mean relaxation time is not equal to the mean relaxation rate in general, *i.e.* $\langle T_1 \rangle^{-1} \neq \langle R_1 \rangle$. Nevertheless, master curves $\chi''(\omega\tau_\alpha)$ were constructed from $\omega\langle T_1(\omega) \rangle^{-1}$ data measured at different temperatures, which are shown in Fig. 33a. For comparison, $\chi''(\omega\tau_\alpha)$ curves of the simple liquid di-PG as well as of entangled linear PEP 200k and of un-entangled PEP 3k (*cf.* section 5.4) are also integrated in Fig. 33a.

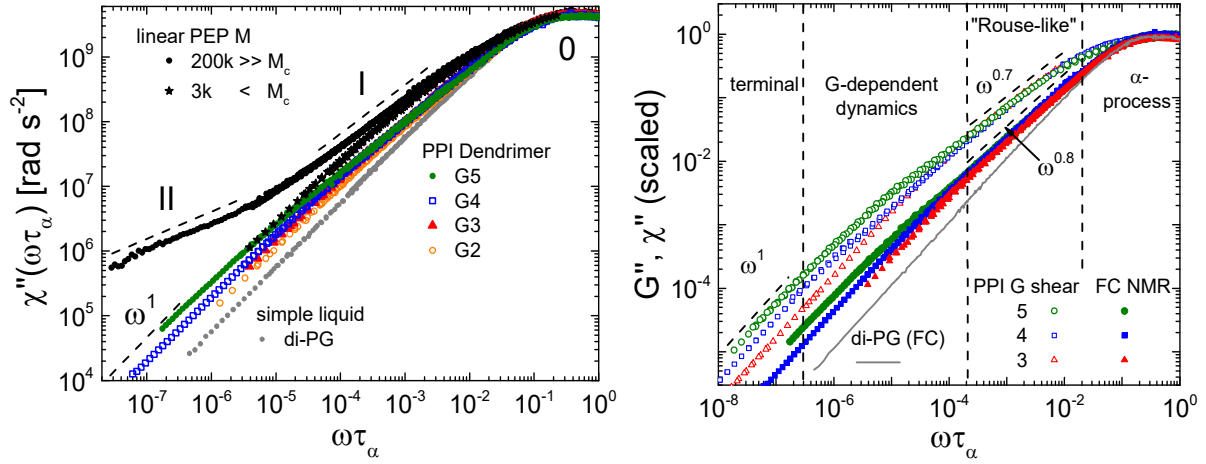


Figure 33: a) NMR Susceptibility master curves $\chi''(\omega\tau_\alpha)$ of PPI dendrimer melts of G2-G5, in comparison to di-PG and entangled (200k) as well as un-entangled linear PEP 3k. Adapted from PUB3 and extended. b) $\chi''(\omega\tau_\alpha)$ in comparison to the shear loss modulus $G''(\omega\tau_\alpha)$ of PPI dendrimer melts G3, G4 and G5. The data was taken from PUB5 and is vertically scaled to $\chi''(\omega\tau_\alpha \approx 1) = G''(\omega\tau_\alpha \approx 1) = 1$. Dynamic regimes are indicated in both figures.

With respect to the simple liquid di-PG, excess contribution is found in the dendrimers at $\omega\tau_\alpha < 1$. It systematically increases with G. This is a clear evidence for collective, G-dependent dynamics slower than the α -process. The curves of PPI resemble that of an un-entangled, linear polymer like PEP 3k (black stars in Fig. 33a). In contrast to entangled PEP 200k, the dendrimer lacks of a pronounced second, polymer-specific power-law regime. Based on Fig. 33b, the collective dynamics of the PPI dendrimer is inspected more deeply in a comparison to $G''(\omega\tau_\alpha)$, included in Fig. 33b. As also for PPI the shear measurements were carried out in a broad temperature window ranging as low as T_g , the α -process is covered, as in the case of FC NMR (see below). A high level of similarity between $\chi''(\omega\tau_\alpha)$ and $G''(\omega\tau_\alpha)$ is found in Fig. 33b, where all master curves are vertically scaled along $\chi''(\omega\tau_\alpha \approx 1) = G''(\omega\tau_\alpha \approx 1) = 1$. At reduced frequencies about $2 \times 10^{-4} < \omega\tau_\alpha < 2 \times 10^{-2}$, both $\chi''(\omega\tau_\alpha)$ as well as $G''(\omega\tau_\alpha)$, are obviously G-independent in the case of G3-G5. Power-laws $\chi''(\omega\tau_\alpha)$, $G''(\omega\tau_\alpha) \propto \omega^\epsilon$ are observed in this two decades broad regime, with similar exponent values of around 0.8 (NMR) and 0.7 (rheology), respectively. Thus, this regime shows some reminiscence of the Rouse regime observed in linear polymers, where (above a certain chain length) molar mass dependence is observed neither. In G2 (not shown in Fig. 33b) this regime is not established, yet.^{PUB3} For even lower reduced frequencies ($\omega\tau_\alpha < 2 \times 10^{-4}$) both, $\chi''(\omega\tau_\alpha)$ and $G''(\omega\tau_\alpha)$, split up and the curves become G-dependent. Both quantities systematically increase in amplitude with growing number of generations G. In entangled polymer melts like PEP (Fig. 28, section 5.5) one would expect that the Rouse regime

is succeeded by the rubbery regime, where $G''(\omega\tau_\alpha)$ features a pronounced minimum. Such a minimum in $G''(\omega\tau_\alpha)$ is not observed in the dendrimers and no signs of a rubber plateau are apparent in $G'(\omega\tau_\alpha)$.^{PUB5} Also in the FC data, a pronounced second power-law regime, usually characteristic for entangled polymer dynamics, is not observed. At lowest reduced frequencies, the terminal relaxation with the asymptotical ω^{-1} -behavior takes over in $G''(\omega)$ as well as in $\chi''(\omega)$, the transition being increasingly retarded as G increases. Note again that, as the total ^1H relaxation is studied, the terminal behavior in the FC data actually follows $\chi''(\omega) \propto (\omega R_1(0) - c\omega^{3/2})$ due to inter-molecular relaxation (cf. section 4.1).

Summarized, concerning the slow, collective dynamics PPI dendrimers resemble polymers without entanglement.^{PUB3,PUB5} The collective dynamics was ascribed to “breathing modes”, i.e. whole dendrimer arms move against each other’s collectively.^{PUB5} Experimentally, such slow, collective dynamics was first detected by NSE spectroscopy in star polymers^{324,325} and later on, also in dendrimers³¹⁸. It is also noted that in the mentioned DS measurements no normal mode showed up in the spectra. Therefore, no information about collective dynamics is gained by this technique. This again demonstrates the enormous potential of FC NMR in probing slow, collective dynamics.

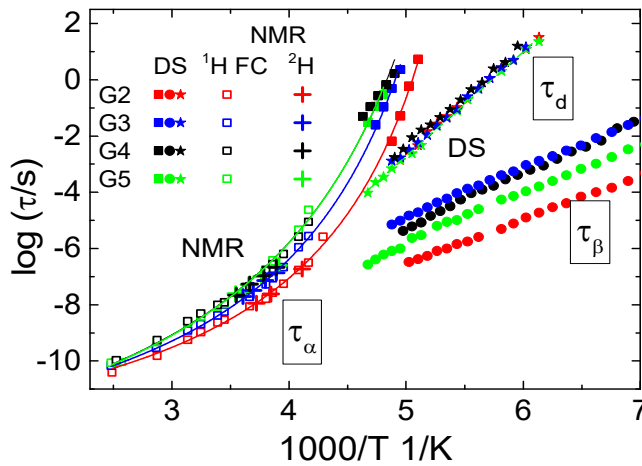


Figure 34: Relaxation map of PPI dendrimer melts of generations G 2-5, encompassing three local relaxation processes, termed α , β , and d , as found by DS, solid state ^2H and FC ^1H NMR.^{PUB3} To guide the eye, τ_α is interpolated by the VFT equation (lines). Adapted from PUB3.

Besides the collective dynamics, three local relaxations were found by FC NMR, by solid state ^2H NMR and in particular by DS. The α -process, as well as two secondary relaxations, termed β - and d -process, respectively, were detected.^{PUB3} The corresponding time constants are displayed in Fig. 34 in an Arrhenius representation. In the case of FC NMR, the temperature dependence of τ_α followed from master curve construction. The FC NMR technique covers the temperature range well above T_g , where good agreement to the solid state ^2H NMR data is found. At low T $\tau_\alpha(T)$ was determined by DS (closed symbols). The α -relaxation features the characteristic super-Arrhenius behavior of a glass former and $\tau_\alpha(T)$ can be well interpolated by a VFT equation (solid lines in Fig. 34). A slight tendency that τ_α increases with G is recognizable. The two secondary relaxations termed, β - and d -process, respectively, were detected in the dielectric spectra for temperatures below $T_g \approx 200\text{K}$ (measured by DSC), the corresponding time constants (τ_β , τ_d) both showing an Arrhenius temperature dependence. Mijovic et al. even found three secondary processes in PAMAM dendrimer melts below T_g via DS.³²² Actually, their dielectric results on PAMAM highly resemble those on PPI.

Investigating the sample of PPI G5 with the deuterated terminal amino groups used for the solid state ^2H NMR measurements reveals a significant decrease of the inverse mean relaxation time with respect to the fully protonated system at low frequencies.^{PUB3} This indicates the relevance of intermolecular relaxation which is supposed to be partially suppressed by exchanging the topologically outermost ^1H by ^2H . Exploiting the square root law eq. 58, the translational diffusion coefficient D was estimated from the low frequency dispersion, where intermolecular relaxation dominates.^{PUB3} It obeys $D(T) \propto \tau_\alpha^{-1}(T)$ approximately. Furthermore, the scaling-relation $D(M) \propto M^{-1}$ was estimated, yet, only from the four data points (number of generations) available. In the course of the subsequent work $D(T, M)$ was determined by pulsed FG NMR, providing $D(M) \propto M^{-1.6}$.^{PUB5} From the shear measurements another important scaling relation for the zero-shear viscosity was determined, namely $\eta_0(M) \propto M^{1.9}$, which is in good agreement to the exponent of 2.1 reported by Rietveld et al.³¹³

As an addendum, which is not included in the publications PUB3 and PUB5, a closer inspection of the magnetization curves was performed. The aim was to study the nature of the non-exponentiality. It is revealed that also a bi-exponential function interpolates the magnetization curves of the dendrimers well. In Fig. 35 $m(t)$ of fully protonated PPI G5 (a) and G2 (b) measured at around 400 K is shown. The evolution time axis is again scaled by the individual $\langle R_1(\omega) \rangle$ value, determined from the weighted sum of the two components, resulting from the bi-exponential fits.

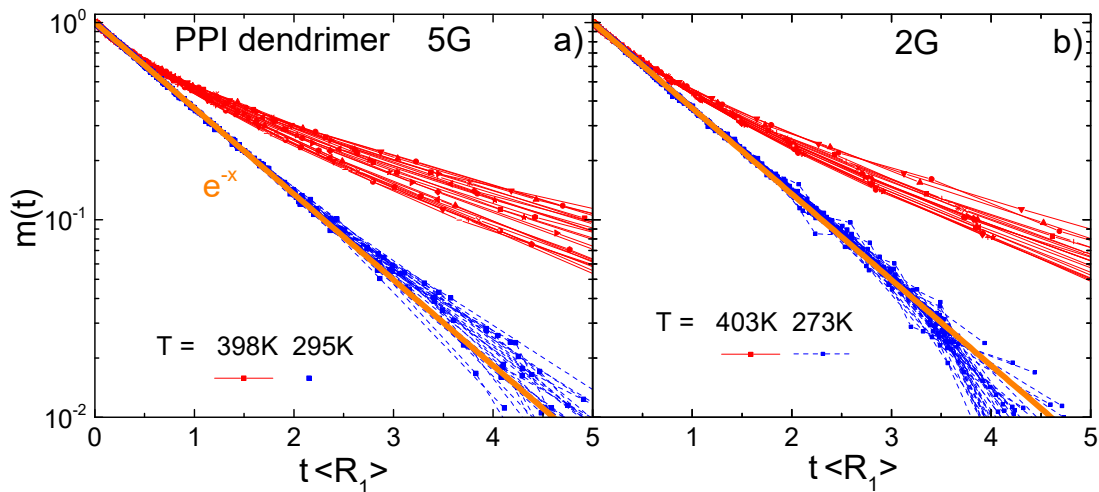


Figure 35. ^1H magnetization function, $m(t)$ horizontally scaled with $\langle R_1(\omega) \rangle$ for dendritic PPI of G5 (a) and G2 (b). In both cases, data measured at a high T (red) and at a lower T (blue) is shown. Mono-exponential behavior is indicated by orange lines. All data was measured in *Bayreuth* and all this magnetization data is unpublished.

The initial decay to around 0.5 is mono-exponential as indicated by the orange line, giving confidence that $\langle R_1(\omega) \rangle$ was always determined correctly. All curves measured at different fields coincide. At longer times the curves begin to deviate from the exponential. As those measurements were exclusively done in *Bayreuth*, $m(t)$ should be artifact-free (*cf.* section 3.3). When T is lowered below 295 K in the case of G5 and below 273 K in the case of G2, $m(t)$ becomes purely mono-exponential

and a master curve is gained, as can be seen from Fig. 35. The non-exponentiality vanishes with decreasing T . Obviously, cross-relaxation is not efficient enough at higher T to average over the different R_1 of the ^1H located at different sites within the dendrimer molecules.

Two following explanations for the occurrence of significantly different relaxation rates R_1 within PPI dendrimers are reasonable: applying selective labelling, ^2H and ^{13}C NMR relaxation experiments with spectral resolution on PAMAM by Meltzer et al. revealed a gradient in the spin-lattice relaxation rate, which decreases from the core to the outermost shells. The authors demonstrate that "...segmental motion is most rapid at the chain terminus and slower at interior sites..."^{326,327} Besides such dynamic heterogeneities, the apparent bi-exponential $m(t)$ may also be caused by the fact that protons close to nitrogen atoms situated at the branching points as well as in the terminal amino groups face quadrupole enhanced relaxation, induced by heteronuclear cross-relaxation. As a $I = 1$ nucleus ^{14}N has three energy levels if the asymmetry of the electronic field gradient tensor $\eta \neq 0$.¹⁴³ When the ^1H Larmor frequency matches one of the three ^{14}N Larmor frequencies the ^1H relax via the ^{14}N spin system, which acts as a relaxation sink. The condition is fulfilled if $\omega_1 = \omega_{14\text{N}}2/3\eta$, $\omega_{2,3} = \omega_{14\text{N}}(1 \pm \eta/3)$, where $\omega_{14\text{N}} = 3/2\pi\delta_Q$ and δ_Q denotes the quadrupolar coupling constant.³²⁸ The energy level-crossing leads to the so-called quadrupolar peaks ("Q-peaks") in systems where protons are coupled to quadrupolar nuclei. FC NMR is predestined to detect this phenomenon which is only detectable at very low T .^{4,240,329,330} In Fig. 36 $R_1(\omega)$ of ^1H is shown for PPI G5, measured in Bayreuth at 209 K. This is close to T_g , i.e. the dynamics is very slow.

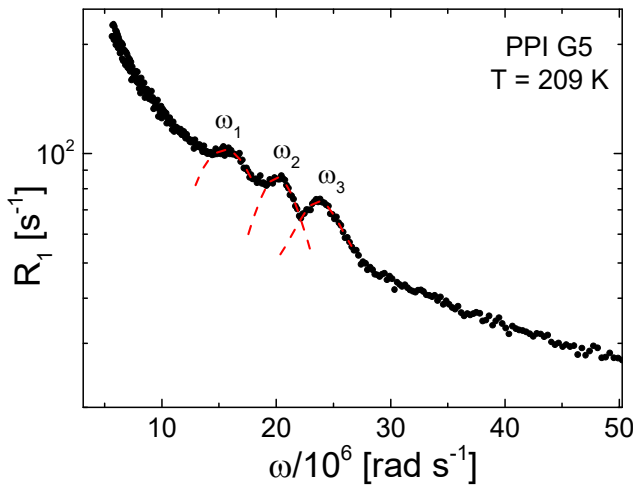


Figure 36: Dispersion of the ^1H relaxation rate of dendritic PPI G5, measured on the STELAR relaxometer at 209 K. Three peaks at frequencies $\omega_{1,2,3}$ appear. Red dashed lines: Lorentzian fitting functions used to estimate $\omega_{1,2,3}$. Unpublished data.

Indeed, three peaks are resolved in Fig. 36 at frequencies $\omega_1/2\pi=2.47$ MHz, $\omega_2/2\pi=3.19$ MHz and $\omega_3/2\pi=3.78$ MHz, which are estimated by Lorentzian fit functions (red dashed lines). Given the three experimental

peak frequencies ω_i , the coupling constant $\delta_Q=4.6$ MHz as well as $\eta=0.79$ are determined. While the first is in good agreement to values reported in the literature, the latter is larger. For amino groups values of $\eta=0.25\div0.35$ are reported.³³¹ Yet, as mentioned, ^1H - ^{14}N couplings may also arise at the nitrogen atoms at the branching points within the dendrimer, i.e. in the topological interior. The occurrence of the Q-peaks demonstrates the relevance of ^{14}N - ^1H cross relaxation, at least for such protons in the vicinity of nitrogen. When going to higher T the Q-peaks disappear as the correlation time $\tau_c(T)$ becomes smaller, i.e. $\omega\tau_c \ll 1$, and the interaction is averaged out. Yet, it was shown by Westlund³²⁸ that the relaxation dispersion as a whole will be distorted by ^{14}N - ^1H cross relaxation,

leading to stretched ^1H dispersion profiles of affected protons. This may provide another explanation for the bi-exponential decay, besides dynamic heterogeneities.

6. Publications

6.1 List of Included Publications as Referred to in this Thesis

The most important publications contributing to this PhD work are listed in chronological order. They are also reprinted below.

PUB 1 “Chain-Length Dependence of Polymer Dynamics: A Comparison of Results from Molecular Dynamics Simulations and Field-Cycling ^1H NMR.”

Bormuth, A.; Hofmann, M.; Henritzi, P.; Vogel, M.; Rössler, E. A.
Macromolecules **2013**, 46, 7805-7811.

PUB 2 “Field-Cycling NMR Relaxometry Probing the Microscopic Dynamics in Polymer Melts.”

Hofmann, M.; Kresse, B.; Privalov, A. F.; Willner, L.; Fatkullin, N.; Fujara, F.; Rössler, E. A.
Macromolecules **2014**, 47, 7917-7929.

PUB 3 “Dynamics of PPI Dendrimers: A Study by Dielectric and ^2H NMR Spectroscopy and by Field-Cycling ^1H NMR Relaxometry.”

Mohamed, F.; Hofmann, M.; Pötzschner, B.; Fatkullin, N.; Rössler, E. A.
Macromolecules **2015**, 48, 3294-3302.

PUB 4 “All Polymer Diffusion Regimes Covered by Combining Field-Cycling and Field-Gradient ^1H NMR.”

Kresse, B.; Hofmann, M.; Privalov, A. F.; Fatkullin, N.; Fujara, F.; Rössler, E. A.
Macromolecules **2015**, 48, 4491-4502.

PUB 5 “Field-Cycling Relaxometry as a Molecular Rheology Technique: Common Analysis of NMR, Shear Modulus and Dielectric Loss Data of Polymers vs. Dendrimers.”

Hofmann, M.; Gainaru, C.; Cetinkaya, B.; Valiullin, R.; Fatkullin, N.; Rössler, E. A.
Macromolecules **2015**, 48, 7521-7534.

PUB 6 “Perspectives of ^2H Field-Cycling NMR Relaxometry for Probing Molecular Dynamics in Soft Matter.”

Flämig, M.; Becher, M.; Hofmann, M.; Körber, T.; Kresse, B.; Privalov, A. F.; Willner, L.; Kruk, D.; Fujara, F.; Rössler, E. A.

6.2 Individual Contributions to Joint Publications

PUB 1: I performed some of the FC NMR measurements on PPG during my diploma thesis, the results of which are published in ref. 272. PG was measured by R. Meier.³³² The low-field measurements on PPG 18k were performed by me during my PhD work, with the technical assistance of B. Kresse. The simulations on PPO were performed by the co-authors from the *Technische Universität Darmstadt*. I constructed all the master curves (including those concerning the simulation data) and performed the Fourier transformations during my PhD time. I performed all further analyses (simulation and FC NMR), except for the position-resolved investigation of segmental relaxation, which was done in *Darmstadt*.

PUB 2: I performed the FC $^1\text{H}/^2\text{H}$ measurements on PB-h 380k, PB-d 364k, on the corresponding isotopic blend, on PB-h 441k and on the two partially labeled polymers PB-dhd 29k in *Darmstadt*, with the technical assistance of B. Kresse. The other FC measurements on the PB samples summarized in Table 1 of PUB2 were done by A. Herrmann, B. Kresse and S. Kariyo.^{70,134,227} The refined analysis of all the PB data was performed by me during my PhD studies. I also did the DSC measurements at the *Lehrstuhl für Makromolekulare Chemie I* at the *Universität Bayreuth* with the technical assistance of P. Knauer.

PUB 3: I performed all the FC measurements on the dendrimer melts in *Bayreuth* and in *Darmstadt* during my PhD time. For the measurements in *Darmstadt*, I had technical assistance by B. Kresse. Furthermore, I performed all analyses related to the FC NMR measurements.

PUB 4: The FG NMR measurements were performed in *Darmstadt*. The FC measurements were done by B. Kresse, A. Herrmann and S. Kariyo, respectively, and were published in parts previously.^{70,134,227} I performed the data analysis, except for the determination of the diffusion coefficient from the stimulated echo data. All work was done during my PhD studies.

PUB 5: I performed all the FC measurements some of which were published in parts previously,^{272,PUB3} except for PG, which was measured by R. Meier.³³² The oscillatory shear measurements on PPI were performed by B. Cetinkaya at the *Technische Universität Dortmund* (group of R. Böhmer), except for the generation 2 dendrimer, which I measured by myself at the *Lehrstuhl für Technische Mechanik und Strömungsmechanik* (*Universität Bayreuth*, group of N. Aksel). The pulsed field-gradient NMR measurements were done by R. Valiullin at the *Universität Leipzig*. All work, including the data analysis, was done by me during my PhD studies.

PUB 6: I measured PEP-d 200K via FC ^2H NMR on the FC-1 relaxometer, together with B. Kresse (*Darmstadt*). I also measured the isotopic blend employing both, the STELAR and the FC-1 relaxometer. I performed all analyses concerning PEP. All work was done during my PhD time.

Furthermore, I performed all other FC measurements on PEP (*cf.* sections 5.4, 5.5) in *Bayreuth* and in *Darmstadt*, respectively, the latter in close collaboration with F. Fajara's group. I also conducted the shear measurements on PEP in N. Aksel's group and carried out the data analysis regarding PEP. I had

technical assistance of L. Heymann who introduced me to the Rheometer. The DS measurements on PEP were carried out by A. Lichtinger (*Bayreuth*) and F. Mohamed (*Bayreuth*). The solid state ^2H NMR measurements were done by T. Körber (*Bayreuth*), as well as the DSC measurement on PEP-d 50k. The DSC measurement on PEP-h 50k was performed by me at the *Lehrstuhl für Makromolekulare Chemie I* at the *Universität Bayreuth*. PBO and PPS (Fig. 22) were also measured by me in *Bayreuth* and in *Darmstadt* via FC NMR. Some of the FC measurements on proteins in solution presented in ref. 257 were done by me in *Bayreuth*. Finally, I did all analyses of FC NMR data in terms of the normalized magnetization curves $m(t)$ presented throughout this extended abstract.

6.3 Further Publications

- “Polymer Dynamics of Polybutadiene in Nanoscopic Confinement As Revealed by Field Cycling ^1H NMR.”
Hofmann, M.; Herrmann, A.; Ok, S.; Franz, C.; Kruk, D.; Saalwächter, K.; Steinhart, M.; Rössler, E. A.
Macromolecules **2011**, 44, 4017-4021.
- “Glassy, Rouse, and Entanglement Dynamics As Revealed by Field Cycling ^1H NMR Relaxometry.”
Hofmann, M.; Herrmann, A.; Abou Elfadl, A.; Kruk, D.; Wohlfahrt, M.; Rössler, E. A.
Macromolecules **2012**, 45, 2390-2401.
- „From boiling point to glass transition temperature: Transport coefficients in molecular liquids follow three-parameter scaling.”
Schmidtke, B.; Petzold, N.; Kahlau, R.; Hofmann, M.; Rössler, E. A.
Phys. Rev. E **2012**, 86, 0451508.
- “Iso-Frictional Mass Dependence of Diffusion of Polymer Melts Revealed by ^1H NMR Relaxometry.”
Meier, R.; Herrmann, A.; Hofmann, M.; Schmidtke, B.; Kresse, B.; Privalov, A. F.; Kruk, D.; Fujara, F.; Rössler, E. A.
Macromolecules **2013**, 46, 5538-5548.
- “Simultaneous measurement of very small magnetic fields and spin-lattice relaxation.”
Kresse, B.; Privalov, A. F.; Herrmann, A.; Hofmann, M.; Rössler, E. A.; Fujara, F.

Solid State Nucl. Magn. Reson. **2014**, 45, 56-60.

- “Proton spin dynamics in polymer melts: New perspectives for experimental investigations of polymer dynamics.”
Fatkullin, N.; Stapf, S.; Hofmann, M.; Meier, R.; Rössler, E. A.
J. Non-Cryst. Solids **2015**, 407, 309.
- “Temperature Dependence of the Segmental Relaxation Time of Polymers Revisited.”
Schmidtke, B.; Hofmann, M.; Lichtinger, A.; Rössler, E. A.
Macromolecules **2015**, 48, 3005-3013.
- “The “long tail” of the protein tumbling correlation function: observation by ^1H NMR relaxometry in a wide frequency and concentration range.”
Roos, M.; Hofmann, M.; Link, S.; Ott, M.; Baalbach, J.; Rössler, E. A.; Sallwächter, K.; Kuschelnitzky, A.
J. Biomol. NMR **2015**, 63, 403-415.
- "Protein anisotropy modulates the coupling between rotational and translational diffusion under crowding conditions."
Roos, M.; Ott, M.; Hofmann, M.; Link, S.; Rössler, E.; Balbach, J.; Krushelnitsky, A.; Saalwächter, K.
J. Am. Chem. Soc. USA **2016**, 138, 10365-10372.
- Poly(ethylene-alt-propylene): Main and secondary relaxation studied by dielectric and ^2H NMR spectroscopy.
Körber, T.; Mohamed, F.; Hofmann, M.; Pötzschner, B.; Lichtinger, A.; Bingemann, D.; Willner, L.; Rößler, E. A.
Macromolecules **2016** (submitted).
- “Segmental Mean Square Displacement: Field-Cycling NMR Relaxometry vs. Neutron Scattering”.
Hofmann, M.; Kresse, B.; Privalov, A. F.; Heymann, L.; Willner, L.; Aksel, N.; Fujara, F., Rößler, E. A.
Macromolecules **2016** (in print).

- “Dynamics of a Paradigmatic Linear Polymer: a Proton Field-Cycling NMR Relaxometry Study on Poly(ethylene-alt-propylene)”.
Hofmann, M.; Kresse, B.; Privalov, A. F.; Heymann, L.; Willner, L.; Aksel, N.; Rössler, E. A. Macromolecules **2016** (submitted).
- „Field-Cycling NMR vs. Rheology“.
Hofmann, M.; Kresse, B.; Heymann, L.; Willner, L.; Privalov, A. F.; Fatkullin, N.; Aksel, N.; Rössler, E. A.
Macromolecules **2016**, (in preparation).

6.4 Oral and Poster Presentations

- 2nd International Workshop on Dendrimers and Hyperbranched Polymers
23.11. – 24.11.2015, Haus zur Lieben Hand (Freiburg, Germany)

Talk: “Molecular dynamics in poly(propylene imine) dendrimer melts studied by ^1H field-cycling NMR and rheology”.

- Gesellschaft dt. Chemiker – Fachgruppe Magnetische Resonanz: 37th Annual Meeting
07. 09. – 10. 09. 2015, Technische Universität Darmstadt (Germany)

Talk: “Segmental Mean Square Displacement in Polymer Melts revealed by Field-Cycling ^1H NMR Relaxometry and Field-Gradient ^1H NMR”.

- 9th Conference on Fast Field-Cycling NMR Relaxometry
27. 07. – 30. 07. 2015, University of Aberdeen (Scotland, UK)

Talk: “Sub-diffusion in polymer melts revealed by FC and FG ^1H NMR”.

- 7th International Discussion Meeting on Relaxation in Complex Liquids
21. 07. – 26. 07. 2013, Universitat Politècnica de Catalunya (Spain)

Invited talk: “Segmental reorientation and diffusion in polymer melts revealed by field-cycling ^1H NMR”.

- 7th Conference on Fast Field-Cycling NMR Relaxometry
02. 06. – 04. 06. 2011, Turin (Italy)

Poster presentation: „Tracing the „Corset-Effect“: Polybutadiene in nanoscopic confinement“.

- International Workshop on Dynamics in Viscous Liquids
30. 03. – 02. 04. 2011, Accademia dei Lincei, (Rome, Italy)

Poster presentation: „Glassy and polymer dynamics in confining geometry as revealed by ^{31}P and field-cycling ^1H -NMR“.

Publication 1

Chain-Length Dependence of Polymer Dynamics:
A Comparison of Results from Molecular Dynamics
Simulations and Field-Cycling ^1H NMR

Bormuth, A.; Hofmann, M.; Henritzi, P.; Vogel, M.; Rössler, E. A.

Macromolecules **2013**, 46, 7805-7811.

DOI: 10.1021/ma401198c

(Copyright 2013 by The American Chemical Society)

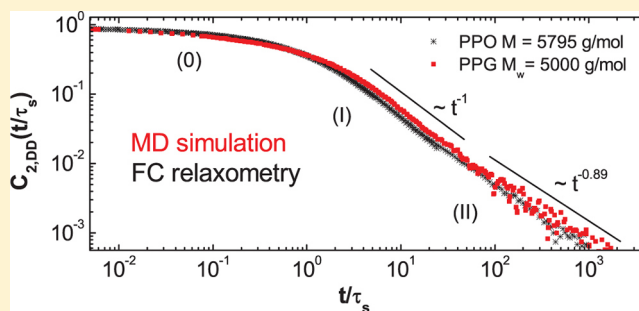
Chain-Length Dependence of Polymer Dynamics: A Comparison of Results from Molecular Dynamics Simulations and Field-Cycling ^1H NMR

André Bormuth,[†] Marius Hofmann,[‡] Patrick Henritzi,[†] Michael Vogel,^{*,†} and Ernst A. Rössler^{*,‡}

[†]Institut für Festkörperphysik, Technische Universität Darmstadt, D-64289 Darmstadt, Germany

[‡]Experimentalphysik II, Universität Bayreuth, D-95440 Bayreuth, Germany

ABSTRACT: Molecular dynamics simulations are performed for poly(propylene oxide) with molecular masses between $M = 104$ and 5795 g/mol using an atomistic force field. From atomic trajectories extending well into the nanoseconds regime, we calculate rank-two orientational correlation functions, providing access to segmental motion, to free Rouse dynamics, and even to the onset of entanglement dynamics, depending on the molecular mass. The simulation results are directly compared with experimental data for poly(propylene glycol) from field-cycling ^1H NMR relaxometry. We find that simulation and experiment are in very good agreement for high values of M . For low values of M , some deviations result from the fact that the present analysis of the simulation results focuses on intramolecular behavior while the experimental data are influenced by both intramolecular and intermolecular relaxation contributions, particularly at longer time scales. Exploiting that the computational data allow us to separately study polymer motions at different positions along the polymer backbone, it is shown that free Rouse dynamics and constrained Rouse dynamics are modified for a few and a few dozen monomers at the chain ends, respectively. We discuss implications of such chain-end effects for the interpretation of experimental results, which are obtained from an ensemble average over all monomers along the backbone.



INTRODUCTION

Molecular dynamics simulations provide important insights into the microscopic nature of polymer dynamics.^{1–5} For example, simulations using generic polymer models, such as the bead-and-spring model, have given early confidence to the concept of tube reptation rationalizing the rheological behavior of melts of entangled linear polymers, i.e., for long chains.⁶ With progress of computing power, atomistic simulations have become available, which are expected to draw a more realistic picture of microscopic dynamics in a given polymer. Yet, comparison with experimental data is not straightforward as only few techniques are capable of probing the microscopic polymer dynamics over many orders of magnitude of time needed to cover the loss of correlation caused by glassy and polymer dynamics. More precisely, in terms of the Doi–Edwards tube-reptation model,⁷ polymer dynamics are expected to exhibit four relaxation regimes: free Rouse (I), constrained Rouse (II), reptation (III), and disentanglement dynamics reflecting free diffusion (IV). In addition, glassy dynamics (0) have to be considered at shortest times.^{8,9} Regarding the mean-squared displacement, neutron scattering studies confirmed a crossover from the free to the constrained Rouse regime.^{10,11} At the long time end, a crossover from regime (III) to free diffusion, i.e., regime (IV), was observed in field gradient NMR studies.¹²

Recently, the application of field-cycling (FC) ^1H NMR relaxometry has gained new momentum for the investigation of polymer dynamics due to the availability of commercial spectrometers.^{8,9,13} The method measures the frequency dependence (dispersion) of the spin–lattice relaxation time T_1 by cycling the magnetic field between polarization, relaxation, and detection fields. In the present contribution we exclusively refer to ^1H relaxation data. By applying frequency–temperature superposition (FTS), as often done in rheological studies,^{14,15} master curves can be constructed which, in the case of proton relaxation, directly yield the dipolar correlation function after Fourier transformation and which typically cover 6 decades in amplitude and 8 decades in time.^{16–21} The accessible frequency window can be further extended by 2 orders of magnitude if earth field compensation is applied to reach frequencies down to about 100 Hz.^{22,23} The obtained correlation functions disclose glassy dynamics, Rouse dynamics, and entanglement dynamics, thus enabling tests of current polymer theories as well as comparison with simulation data. First experiments show a highly protracted transition to tube reptation; i.e., a trend to reptation is found only at a

Received: June 11, 2013

Revised: August 19, 2013

Published: September 16, 2013

molecular mass much larger than the entanglement mass M_e , a result also confirmed by double quantum NMR studies.^{24,25}

Because of the short-range character of the magnetic dipole–dipole interaction among protons, it is usually assumed that intramolecular relaxation reflecting segmental reorientation dominates ^1H spin–lattice relaxation. Then, the dipolar correlation function $C_{\text{DD}}(t)$ obtained from FC ^1H NMR is expected to follow the rank-two reorientational correlation function $C_2(t)$ closely. However, as was demonstrated recently,^{23,26} intermolecular relaxation leads to a failure of this assumption, in particular, in the entanglement regime, i.e., at low frequencies or long times. It turns out that the agreement with the tube-reptation theory is not satisfactory when neglecting the intermolecular relaxation and considering only the intramolecular relaxation, which is given by $C_2(t)$. The latter contribution can be determined by isotope dilution experiments, which permit a suppression of the intermolecular contribution. Here, we will directly compare the dipolar correlation function $C_{\text{DD}}(t)$ with the rank-two correlation function $C_2(t)$ obtained from atomistic simulations. As we essentially encompass the Rouse regime at intermediate time scales, we expect that the intermolecular contribution is still negligible in the experiments.

In the present experiments, we focus on poly(propylene glycol) (PPG), which was investigated by FC ^1H NMR for a series of molecular masses in previous work.²¹ The atomistic simulations are carried out for poly(propylene oxide) (PPO) for which a reliable force field is available.²⁷ The glassy dynamics of this polymer model was ascertained in previous computational studies.^{28–30} PPG and PPO differ with respect to their end groups. Specifically, PPG and PPO chains are terminated by hydroxyl groups and methyl groups, respectively (see Figure 1). This difference is relevant for small molecular

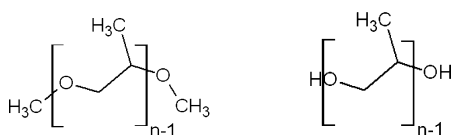


Figure 1. Chemical structure of (left) PPO featuring methyl end groups as simulated and (right) PPG featuring hydroxyl end groups as measured by FC ^1H NMR.

weights, but it can be neglected for high ones. Following a previous analysis²¹ of NMR dispersion data, which included the correlation function $C_{\text{DD}}(t)$ as well as the corresponding spectral density $J_{\text{DD}}(\omega)$, we will discuss the molecular-weight dependence of the FC ^1H NMR (PPG) and MD simulation (PPO) results against the background of the tube-reptation model, which enables calculation of not only the segmental mean-square displacement but also the rank-two correlation function $C_2(t)$. In particular, a relation $C_l(t) \propto \langle R^2(t) \rangle^{-1}$, which was first derived based on rather general arguments,³¹ is also assumed in regime II of the tube-reptation model.^{8,23} These aspects were discussed in some detail in previous work.³² We will show that there is a remarkable agreement between experimental and computational results in the dynamic regimes typical of polymers. In our analyses, we will exploit that atomistic simulations reach the entanglement regime for the first time and that such approach provides access to position-resolved correlation functions.

METHODOLOGICAL AND EXPERIMENTAL SECTION

Field-Cycling Relaxometry. Electronic FC ^1H NMR measures the (Larmor) frequency dependence of the longitudinal relaxation time, $T_1(\omega)$, by cyclically switching the magnetic field in a solenoid coil.¹³ In doing so, it is exploited that the frequency ω and the magnetic field strength B are related via $\omega = \gamma_{\text{H}}B$, where γ_{H} is the gyromagnetic ratio of the proton. In the framework of the relaxation theory by Bloembergen, Purcell, and Pound³³ (BPP), the relaxation dispersion $T_1(\omega)$ is related to a spectral density $J(\omega)$ describing the fluctuations of the magnetic dipole–dipole interactions between each pair of proton spins. As the spectral density and the corresponding susceptibility are connected via the fluctuation–dissipation theorem, $\chi''(\omega) = J(\omega)\omega$, multiplication of the BPP equation with the frequency ω yields the susceptibility representation $\chi''_{\text{DD}}(\omega)$:

$$\frac{\omega}{T_1(\omega)} = K[\omega J(\omega) + 4\omega J(2\omega)] = K[\chi''(\omega) + 2\chi''(2\omega)] \\ =: 3K\chi''_{\text{DD}}(\omega) \quad (1)$$

Here, K is an effective coupling constant. The subscript “DD” refers to the dipole–dipole interaction between proton spins, which includes both intra- and intermolecular contributions.^{23,26} Strictly speaking, $\chi''_{\text{DD}}(\omega)$ is a weighted sum of two separate susceptibilities evaluated at single- and double-quantum transitions, but both are hardly distinguishable when considering broad relaxation dispersions on a logarithmic scale.

Under the assumption that FTS is valid, the accessible frequency window of the FC experiment can be effectively extended from 3 to 7 or even more orders of magnitude.^{16–21} In summary, this approach involves that several susceptibility curves $\omega/(T_1(\omega,T))$ obtained for different temperatures T are subsequently shifted horizontally along the frequency axis by applying temperature-dependent shift factors a_T in order to create a susceptibility master curve. The thus obtained master curve can then be scaled to the correlation time of segmental motion, τ_s , by fitting to a Cole–Davidson function.³⁴ This yields the NMR susceptibility master curve $\chi''_{\text{DD}}(\omega\tau_s)$. Fourier transformation of $\chi''_{\text{DD}}(\omega\tau_s)$ provides access to the dipolar correlation function $C_{\text{DD}}(t/\tau_s)$. Here, we discuss the molecular mass dependence of this correlation function against the background of the tube-reptation theory of polymer dynamics by Doi–Edwards and de Gennes.⁷ This theory predicts various characteristic power law decays $C_2(t) \propto t^{-\epsilon}$ in the above-mentioned dynamic regimes, called Doi–Edwards limits.

The experiments are performed on a STELAR FFC 2000 relaxometer working in a proton Larmor frequency range of 10 kHz $\leq \nu \leq$ 20 MHz. The accuracy of the temperature was better than ± 1 K within an accessible range of 180–420 K. FC ^1H NMR is used to investigate PPG with molecular masses M_w between 134 and 18 200 g/mol. The samples are denoted as PPG followed by the value of M_w , e.g., PPG 134, to indicate the respective molecular mass. Based on M_w , the number of segments (monomers) N constituting a chain can be estimated according to

$$M_w(N) \approx 2m_{\text{H}} + m_{\text{O}} + [N(3m_{\text{C}} + 6m_{\text{H}} + m_{\text{O}})] \quad (2)$$

where m_{C} , m_{H} , and m_{O} denote the respective atomic masses. The PPG compounds were purchased from PSS Mainz except PPG 18200, which was kindly provided by R. Böhmer (TU Dortmund). We would appreciate provision of PPG with higher molecular masses.

Molecular Dynamics Simulations. In MD simulations, Newton’s equations of motion are numerically solved for multiparticle systems, interacting via classical interaction potentials. Here, MD simulations are performed for PPO, where the number of monomer units N varies between $N = 2$ and $N = 100$. The corresponding molecular masses

$$M(N) = 2m_{\text{C}} + 6m_{\text{H}} + m_{\text{O}} + [N(3m_{\text{C}} + 6m_{\text{H}} + m_{\text{O}})] \quad (3)$$

range between 104 and 5795 g/mol. The studied models will be denoted as PPO followed by the value of M in the following.

The interatomic interactions of the model are described by a quantum-chemistry-based all-atom force field, which enables good

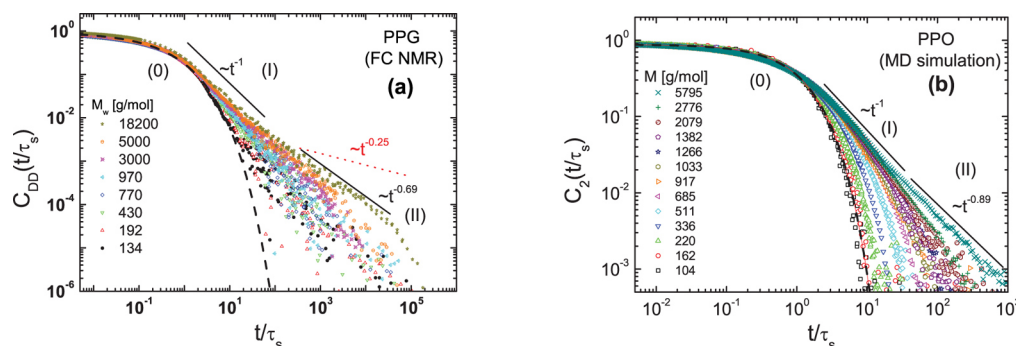


Figure 2. (a) Dipolar correlation functions $C_{DD}(t/\tau_s)$ for PPG from FC ^1H NMR relaxometry and (b) reorientational correlation functions $C_2(t/\tau_s)$ for PPO from MD simulations. The molecular masses are indicated. Dashed lines: short-time stretched exponential decay typical of reorientation in simple liquids (regime 0). Solid lines: power laws in relaxation regimes I and II. Red dotted line in (a): prediction for Doi–Edwards regime II (constrained Rouse dynamics).

reproduction of structural and dynamical properties of PPO melts.²⁷ In addition to nonbonded interactions, which are considered via Buckingham and Coulomb potentials, the force field contains terms adjusting bond lengths, bond angles, and dihedral angles. These MD simulations provide us with the trajectories of all atoms of the PPO models, i.e., with the full microscopic information. The studied PPO systems comprise ca. 4000 atoms, and the time window extends from 10^{-15} s to about 10^{-7} s, limited by computing power. Further details of our simulations can be found in previous publications.^{28,29} To enable comparison with NMR data, we calculate the rank $l = 2$ rotational correlation function

$$C_2(t) = \frac{1}{2} \langle 3[\vec{e}_{OO}(t + t_0) \cdot \vec{e}_{OO}(t_0)]^2 - 1 \rangle \quad (4)$$

Here, the unit vector $\vec{e}_{OO}(t)$ describes the orientation of the internuclear vector connecting two consecutive oxygen atoms along the polymer backbone at a time t . The brackets $\langle \dots \rangle$ denote the ensemble average over all neighboring oxygen atoms in all polymer molecules and the time average over various time origins t_0 . The relation between correlation functions that characterize the reorientation of internuclear vectors connecting different pairs of atomic species within a PPO molecule was investigated in previous simulation work.³⁰

RESULTS AND DISCUSSION

Analysis in the Time Domain. In Figure 2, we show correlation functions from FC ^1H NMR relaxometry on PPG and from MD simulations on PPO for the indicated molecular masses. Specifically, we display master curves $C_{DD}(t/\tau_s)$ and $C_2(t/\tau_s)$ obtained from results at various temperatures. For details about the construction of master curves in the frequency and time domains and about the determination of the segmental relaxation times τ_s , the interested reader is referred to previous publications.^{16,17,21,29,30} Depending on the molecular mass, several dynamic regimes are distinguishable for both the measured and computed data. In the following, we argue that these dynamic regimes can be identified with local, “glassy” dynamics (regime 0) and the Doi–Edwards limits I and II.

At shortest times, $t \leq \tau_s$, $C_{DD}(t/\tau_s)$ and $C_2(t/\tau_s)$ are well described by stretched exponential (Kohlrausch) functions, as expected for the structural relaxation of viscous liquids (see Figure 2). Therefore, we identify this dynamic regime with glassy dynamics. In this regime, the experimental data for PPG do not depend on M . In particular, the stretched exponential decays of all studied samples can be described with the same stretching parameter $\beta = 0.41$. The stretching parameters obtained from the simulated data for PPO are somewhat

higher. They decrease from $\beta = 0.87$ for $M = 104$ g/mol to $\beta = 0.57$ for $M > 2000$ g/mol. The origin of the molecular mass dependent stretching for PPO was studied in a previous simulation work.²⁹ Partly, it is due to a higher relevance of chain-end effects for shorter chains. The different stretching of the experimental and computational correlation functions can have several origins. First, it is necessary to consider that the computed data exclusively monitor intramolecular dynamics, while the measured data additionally probe intermolecular dynamics. Moreover, one should take into account the fact that the experimental and simulated correlation functions are sensitive to motions of H–H and O–O internuclear vectors, respectively, which involve different length scales. Finally, the different end groups of PPG and PPO can play a role in particular, for small molecular masses.

At longer times, $t > \tau_s$, the measured and simulated correlation functions show pronounced and characteristic molecular mass dependencies, which highly resemble each other. When the molecular weight increases, the decays of the correlation functions become more and more delayed. In the following, we discuss the molecular mass dependent long-time behavior in more detail. First, we focus on the time range $\tau_s < t < 100\tau_s$. In this regime, the number of Rouse modes grows with increasing chain length resulting in a retardation of the dynamics until the behavior saturates (see Figure 2). Specifically, for PPG, the loss of correlation slows down until a common (i.e., essentially M_w independent) power law is observed at intermediate time scales for $M_w \geq 3000$ g/mol. The power law exponent amounts to $\varepsilon_1 = 1$, in perfect agreement with the prediction for the Doi–Edwards regime (I), the free Rouse dynamics.³⁵ For the simulation data of PPO, free Rouse dynamics saturates at a molecular mass of $M \geq 2079$ g/mol. Thus, the behavior saturates at a somewhat smaller molecular weight in the simulation than in the experiment, but we cannot determine whether this difference is significant as PPG specimen with $M_w \approx 2000$ g/mol were not studied in NMR. Consistent with our experimental results, the behavior of the simulation data is well described by a power law with an exponent of $\varepsilon_1 = 1$ and extends over at least $1\frac{1}{2}$ orders of magnitude in time, enabling clear identification of the Rouse regime in our simulations, too.

Now, we move on to the time range $t > 100\tau_s$. For these times in both experiments and simulations, a further power law is evident for specimen with highest molecular masses, yet with an exponent $\varepsilon < 1$ (see Figure 2). The observation of such crossover is taken as evidence for an existence of chain

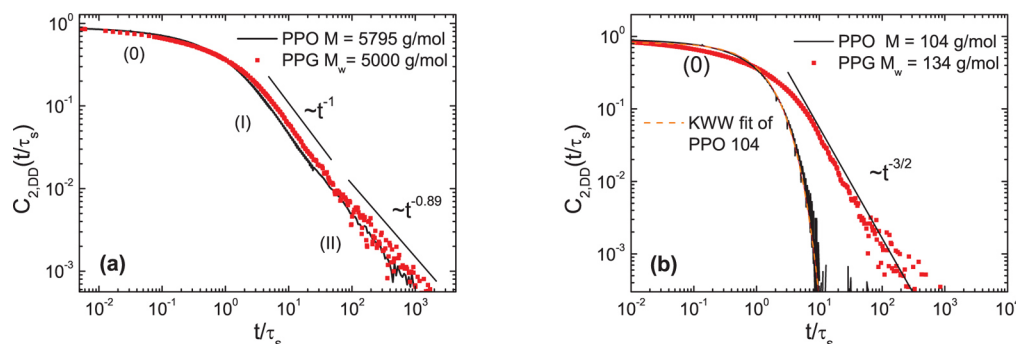


Figure 3. Comparison of correlation functions $C_{DD}(t/\tau_s)$ and $C_2(t/\tau_s)$ as obtained for (a) PPG 5000/PPG 5795 and for (b) PPG 134/PPG 104. The resulting power laws are indicated as straight lines. In panel b, $C_2(t/\tau_s)$ of PPO 104 is fitted to a Kohlrausch function yielding $\beta = 0.87$.

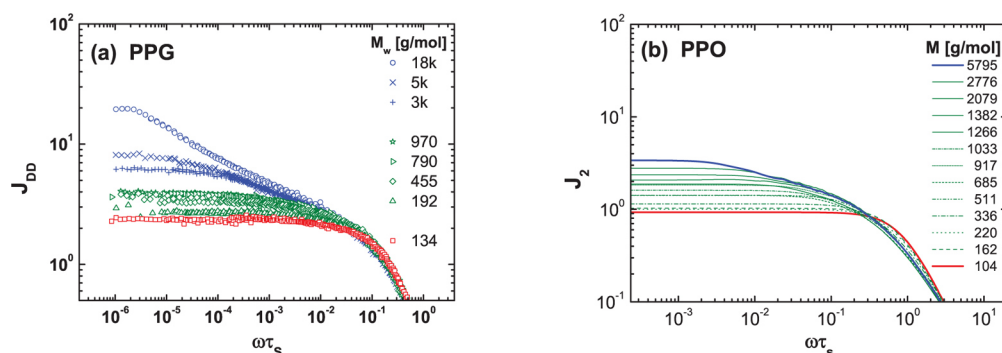


Figure 4. Spectral densities (a) $J_{DD}(\omega\tau_s)$ of PPG from FC ^1H NMR relaxometry and (b) $J_2(\omega\tau_s)$ of PPO from MD simulations. The molecular masses are indicated. In panel a, the color code distinguishes di(propylene glycol) showing only glassy dynamics (red) from nonentangled (green) and entangled (blue) polymers. In panel b, an analogous color code is used for the simulated PPO models.

entanglement. In the case of PPG, the decays start to develop a power law beyond the Rouse regime for $M_w \geq 3000$ g/mol, which led us to the conclusion that the entanglement molecular mass amounts to $M_e \approx 3000$ g/mol in our previous publication.²¹ Unlike ε_I , the exponent in the long-time regime depends on the molecular mass, i.e., $\varepsilon_{II} = \varepsilon_{II}(M_w)$. It decreases steadily from 1 to 0.69 for PPG 18200. The latter value is still very different from the prediction $\varepsilon_{II} = 0.25$ for the Doi–Edwards regime (II), the constrained Rouse regime. However, it was argued in previous studies^{22,24,32} that ε_{II} is expected to approach the value of 0.25 only for highest molecular masses of $M \geq 50M_e$ which were not available to us in the case of PPG. Concerning the simulation data of PPO, we also observe a second power law regime extending over more than an order of magnitude. Specifically, for PPO 5795, we find a power law exponent of $\varepsilon_{II} = 0.89$, which is practically identical with the experimental finding for PPG 5000. As the studied molecular mass of $M = 5795$ g/mol is larger than the entanglement molecular mass $M_e \approx 3500$ g/mol for PPO,³⁶ it is reasonable to conclude that the long-time power law results from entanglement effects. These observations are remarkable since, to the best of our knowledge, it is the first time that MD simulations using a fully atomistic force field reach entanglement dynamics. We note that the time window of FC NMR is still about 2 orders of magnitude larger, enabling observation of the terminal relaxation for the highest molecular mass $M_w = 18200$ g/mol on the basis of an exponential cutoff.

In Figure 3a, the correlation functions $C_{DD}(t/\tau_s)$ and $C_2(t/\tau_s)$ for PPG 5000 and PPO 5795 are compared in more detail. We see that the experimental and computational results agree very well. Some minor deviations exist in the regime of glassy

dynamics where the stretching of the measured correlation function is more pronounced than that of the simulated one, as discussed above. Moreover, the crossover between the power law regimes is located at $t \approx 50\tau_s$ in the simulation, while it is found at $t \approx 100\tau_s$ in the experiment. Notwithstanding, the good agreement between measured and simulated data provides strong evidence that the observed dynamic regimes are generic features of the relaxation behavior shown by linear polymers in bulk melts. In previous work, it was reported that poly(ethylene glycol) and poly(ethylene oxide) show different end-group effects as a consequence of hydrogen bonding.³⁷ Here, the good agreement between experimental data on PPG and computational data on PPO implies that the differences are largely removed when considering rescaled times t/τ_s .

For the dimer PPO 104, the decay of the MD correlation function $C_2(t/\tau_s)$ follows a stretched exponential function, as expected for the reorientational dynamics in simple liquids (see Figure 3b). The NMR correlation function $C_{DD}(t/\tau_s)$ of the corresponding low-molecular-weight reference system PPG 134 exhibits a different long-time behavior. Specifically, a power law with an exponent $\varepsilon = 1.5$ is observed for $t/\tau_s \gg 1$, in harmony with predictions from the theory of intermolecular relaxation,^{23,38} which yields $C_{\text{inter}} \propto \langle R^2 \rangle^{-3/2} \approx t^{-3/2}$ for Fickian diffusion. Thus, the differences between the experimental and computational data at long times can be attributed to the fact that the former and the latter do and do not probe intermolecular contributions, providing further evidence that it is very important to consider intermolecular relaxation in ^1H NMR, particularly at long time scales. These effects were addressed in some detail in previous experimental and computational studies.^{23,26,30}

Analysis in the Frequency Domain. Next, we study the manifestation of the different relaxation regimes in the frequency domain. Specifically, the spectral density $J_2(\omega\tau_s)$ is determined from the simulated correlation functions $C_2(t/\tau_s)$ by means of Fourier transformation. To deal with data nonuniformly distributed on a linear scale, the Filon algorithm³⁹ is used for this conversion. In the experimental counterpart, we divide the susceptibility master curves by ω to obtain $J_{DD}(\omega\tau_s)$. In Figure 4, we compare the spectral density master curves for (a) PPG and (b) PPO, as obtained by FC ^1H relaxometry and MD simulation studies, respectively. To allow for straightforward comparison, all data sets fulfill the normalization condition:

$$\int_0^\infty J_{DD,2}(\omega) d\omega = \frac{\pi}{2} \quad (5)$$

Consistent with our results for the correlation functions, the experimental and computational spectral densities exhibit similar behaviors. For PPG and PPO dimers, we observe the characteristics of glassy dynamics (red data in Figure 4) with a plateau at lowest frequencies ($\omega\tau_s \ll 1$). For higher molecular masses, J_2 and J_{DD} exhibit additional contributions in the low-frequency range, which can be attributed to dynamics characteristic for polymers. For unentangled chains (green data in Figure 4), a successive emergence of Rouse modes with increasing chain length leads to a strong molecular mass dependence of the spectral density at low frequencies (regime I), in particular, the plateau shifts to higher values. Beyond the entanglement molecular mass M_e , the plateau height increases even more strongly with increasing chain length and dispersion is found down to lowest frequencies (in regime II). This behavior is expected due to an onset of even slower entanglement dynamics. Specifically, for entangled chains (blue data in Figure 4), a pronounced dispersion of the spectral density extends to lowest values of $\omega\tau_s$.

A quantitative analysis can be achieved when the molecular-mass dependence of the low-frequency plateaus $J_{DD,2}(\omega \rightarrow 0)$ is determined. Such an analysis has been done before using experimental results for several polymers^{18,21} in order to identify the Rouse regime and the crossover to entanglement dynamics. The low-frequency limit ($\omega\tau_s \ll 1$) for the contribution of Rouse dynamics to the spectral density has been given as¹⁸

$$J_{DD,2}^{\text{Rouse}}(\omega \rightarrow 0) = \frac{\tau_0\pi}{2} \ln(N_G) \quad (6)$$

where τ_0 is the shortest Rouse time and N_G is the number of Gaussian chain segments. This analysis of the low-frequency behavior of the spectral densities resembles in a way that performed by other authors who studied the molecular-weight dependence of ^2H spin–spin relaxation times T_2 for polybutadiene and observed the crossover to entanglement dynamics by plotting $1/T_2$ as a function of $\ln M$.⁴⁰

In Figure 5, we see that the height of the low-frequency plateau obtained from the simulation data of PPO well agrees with the prediction for the Rouse regime (see eq 6), over almost 2 decades in chain length, when identifying N_G with N and τ_0 with τ_s obtained from the reorientation of the O–O internuclear vectors. For $N_e > 50$, the chain-length dependence of the plateau height deviates from the prediction for Rouse dynamics. This discrepancy can be attributed to the crossover to entanglement dynamics, providing further evidence that the onset of such polymer motion is observed in the present

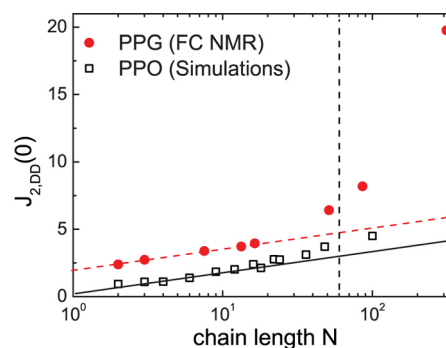


Figure 5. Extrapolated values $J_{DD}(\omega \rightarrow 0)$ for the experimental data of PPG (red circles) and $J_2(\omega \rightarrow 0)$ for the simulated data of PPO (black squares). Straight black line: prediction for Rouse dynamics, as obtained using $N = N_G$ and $\tau_0 = \tau_s$ in eq 6. Red dashed line: guide for the eye resulting from adding a constant value to this prediction. Vertical dashed line: entanglement molecular mass $M_e = 3500$ g/mol ($N \approx 60$).³⁶

atomistic simulations. Concerning the experimental results for PPG, a logarithmic molecular mass dependence is also found for sufficiently short chains. As larger N are covered in the experiments, stronger deviations are found in the entanglement regime, in particular for PPG 18200. The crossover occurs in the vicinity of $N_e \approx 60$, corresponding to an entanglement molecular mass $M_e = 3500$ g/mol reported in previous work.³⁶ The discrepancy between our computational and experimental data can be rationalized based on the outcome of a previous simulation study,³⁰ which ascertained the role of intermolecular contributions and the relation between different correlation functions in some detail.³⁰ It was found that, unlike the computational data, the experimental data are affected by intermolecular contributions, which are particularly important at low frequencies and that the rotational correlation functions of the H–H vectors can decay an order of magnitude faster than that of the O–O vectors. The latter effect means that the present analysis does not provide straightforward access to the value of τ_0 , and hence, the observed agreement between data and prediction for the PPO model does not necessarily indicate that N_G equals N ; i.e., it is not possible to conclude that the Gaussian chain segment can be identified with the PPO monomer.

Chain-End Effects. When elaborate isotopic labeling strategies are not available, experimental techniques usually probe a superposition of signals from all segments along the polymer backbone. In particular, there are contributions from monomers in the backbone centers and from monomers at the chain ends, which are expected to exhibit somewhat different dynamical behaviors. In simulation studies, it is straightforward to separately ascertain the motions of segments at different positions along the polymer backbone. In previous work, we found for PPO 1382 at 300 K that the correlation times of segmental motion τ_s differ by up to a factor of 5 within a chain.²⁹ In this contribution, we investigate whether Rouse dynamics is different for monomers in the backbone centers and at chain ends. For this purpose, we separately determine the correlation functions for O–O vectors at different positions n along the polymer backbone. Here, n is the distance of an O–O vector from the nearest chain end, starting with $n = 1$. Figure 6 shows these position-resolved correlation functions $c_2(t, n)$ for PPO 5795 at 450 K. We see that the dynamical behavior of a segment strongly depends on its position along the polymer

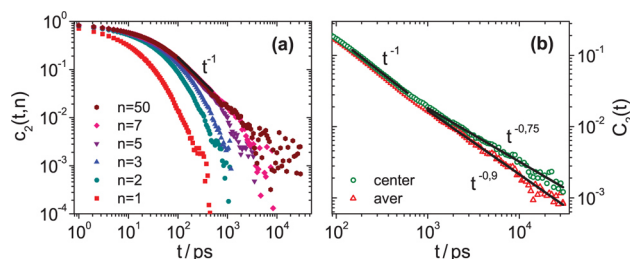


Figure 6. Correlation functions from MD simulations for PPO 5795 ($N = 100$) at 450 K: (a) position-resolved correlation functions $c_2(t, n)$, which separately characterize the dynamical behaviors of O–O vectors at different positions n in the polymer backbone ($n = 1$: chain end, $n = 50$: chain center) and (b) comparison of correlation functions $C_2(t)$ resulting from a superposition of the contributions from all O–O vectors along the polymer backbone and from the O–O vectors in the chain center, respectively. In the latter case, O–O vectors near the chain ends ($n = 1–29$ and $n = 70–99$) are excluded from the average. In both panels, the straight lines mark power laws with the indicated exponents.

backbone. In particular, monomers at chain ends ($n \leq 3$) do not exhibit Rouse dynamics. When moving from the end to the center of a chain, Rouse dynamics continuously develop, but the findings differ in the relaxation regimes I and II. In regime I, the n dependence of the curves ceases at $n \approx 7$, while such saturation is not observed in regime II. Thus, free Rouse dynamics is common to all but the outermost monomers of a chain, while constrained Rouse dynamics is diverse for a few dozen monomers near a chain end. To further demonstrate the latter effect, we compare correlation functions $C_2(t)$, which are obtained when we average the contributions from all monomers along the backbone and when we exclusively average the contributions from those monomers in the center of the chain. In Figure 6, we see that the power law exponent of regime II, ε_{II} , changes from -0.90 to -0.75 when excluding contributions from the chain ends.

The results of experimental studies of polymer dynamics are affected by this diversity of motions at various positions in the polymer backbone. In regime 0, the stretching of the correlation functions increases due to the difference of glassy dynamics in the backbone centers and at the chain ends. Also, the crossover between the dynamic regimes I and II is smeared out due to the position-dependent free and constrained Rouse dynamics. In particular, the strong variation of the latter motion along the polymer backbone complicates a comparison of experimental findings and theoretical predictions. Specifically, a precise determination of the entanglement molecular mass M_e can be difficult since first indications of entanglements are masked by strong contributions from outer monomers, which show less pronounced entanglement dynamics and constitute a significant fraction at the relevant chain lengths. Furthermore, meaningful determination of the power law exponent in regime II requires use of very high molecular masses, as mentioned in the preceding sections, so that it is possible to neglect contributions from outer monomers, which exhibit steeper correlation functions in this regime.

CONCLUSIONS

We combined FC ^1H NMR relaxometry results for poly(propylene glycol) and MD simulation results for poly(propylene oxide) to investigate the molecular mass dependence of polymer dynamics in the melt. To enable

straightforward comparison, time domain data and frequency domain data were transformed into one another. In both domains, it was found that the experimental results for PPG and the computational findings for PPO yield a consistent picture not only in regime 0 of glassy dynamics on short time scales but also in the Doi–Edwards regimes I and II characteristic for polymer dynamics occurring on long time scales, namely, free Rouse and constrained Rouse dynamics, respectively.

For low molecular masses, the correlation functions are well described by stretched exponentials; i.e., glassy dynamics is observed, corresponding to regime 0. In this simple-liquid limit, differences between experimental and computational results were observed at times $t \gg \tau_e$. On such time scales, the experimental correlation functions are governed by intermolecular dynamical effects, which give rise to a power law with an exponent of $-3/2$, in harmony with intermolecular relaxation theory. By contrast, the computational correlation functions of the present approach are of purely intramolecular nature, and hence, they are not sensitive to these intermolecular contributions. However, the long-time behavior of measured and simulated data for small molecules can be reconciled when including both intra- and intermolecular contributions into the calculation of correlation functions from simulation data.³⁰ When the molecular mass is increased, Rouse dynamics slows down the loss of correlation at long times. Free Rouse dynamics, i.e., the Doi–Edwards regime I, is fully established at $M_w = 2000–3000$ g/mol, as indicated by our finding of a power law with exponent $\varepsilon_I = 1$ in both experiment and simulation. Constrained Rouse dynamics, i.e., Doi–Edwards regime II, starts to develop when the chain length is further increased. However, for the studied molecular masses $M_w \leq 18\,200$ g/mol, the theoretically predicted power law exponent of 0.25 is not observed, but rather significantly larger values of ε_{II} are found. In the frequency domain, we compared master curves of spectral densities obtained from our NMR and MD studies. It was found that these frequency-domain data are also highly comparable. Analysis of $J(\omega \rightarrow 0)$ provided clear evidence for the existence of free Rouse dynamics, and it enabled an estimation of the entanglement molecular mass, yielding $M_e \approx 3000$ g/mol for measured and computed data, in agreement with a literature value of $M_e = 3500$ g/mol.³⁶ The described dynamical behaviors appear to be common to all linear homopolymers. Specifically, we obtained similar FC ^1H NMR results for poly(butadiene), poly(isoprene), and poly(dimethylsiloxane) in recent work.²¹

In addition, our combined experimental and computational approaches revealed that different molecular dynamics at the backbone centers and at the chain ends affect the results of experimental studies, which usually probe a superposition of signals from monomers at different positions along the polymer backbone. In particular, we found that a few dozen monomers near the chain ends show modified constrained Rouse dynamics so that their contributions affect the value of the observed power law exponent in regime II unless polymers with very high molecular masses are investigated. Thus, the present approach yielded interesting insights into polymer dynamics by probing entanglement dynamics, up to our knowledge, for the first time in MD simulations of an all-atom polymer model.

AUTHOR INFORMATION

Corresponding Authors

*E-mail: michael.vogel@physik.tu-darmstadt.de.

*E-mail: ernst.roessler@uni-bayreuth.de.

Notes

The authors declare no competing financial interest.

ACKNOWLEDGMENTS

Financial support of the Deutsche Forschungsgemeinschaft through grants FU 308/14, RO 907/16-1 (SPP 1369), and VO 905/5-1 (PAK 553) is gratefully acknowledged. We also thank the Freistaat Bayern for a fellowship for M. Hofmann within the framework of the BayEFG.

REFERENCES

- (1) Faller, R.; Müller-Plathe, F.; Doxastakis, M.; Theodorou, D. *Macromolecules* **2001**, *34*, 1436–1448.
- (2) Smith, G. D.; Paul, W.; Monkenbusch, M.; Willner, L.; Richter, D.; Qiu, X. H.; Ediger, M. D. *Macromolecules* **1999**, *32*, 8857–8865.
- (3) Smith, G. D.; Borodin, O.; Bedrov, D.; Paul, W.; Qiu, X. H.; Ediger, M. D. *Macromolecules* **2001**, *34*, 5192–5199.
- (4) Paul, W.; Smith, G. D. *Rep. Prog. Phys.* **2004**, *67*, 1117.
- (5) Kremer, K.; Grest, G. S. *J. Chem. Phys.* **1990**, *92*, 5057–5086.
- (6) Kremer, K.; Grest, G. S.; Carmesin, I. *Phys. Rev. Lett.* **1988**, *61*, 566–569.
- (7) Doi, M.; Edwards, S. F. *The Theory of Polymer Dynamics*; Oxford Science Publication: Oxford, UK, 1986.
- (8) Kimmich, R.; Fatkullin, N. *Adv. Polym. Sci.* **2004**, *1*, 170.
- (9) Kruk, D.; Herrmann, A.; Rössler, E. *Prog. Nucl. Magn. Reson. Spectrosc.* **2012**, *63*, 33–64.
- (10) Richter, D.; Butera, R.; Fetters, L. J.; Huang, J. S.; Farago, B.; Ewen, B. *Macromolecules* **1992**, *25*, 6156–6164.
- (11) Wischniewski, A.; Monkenbusch, M.; Willner, L.; Richter, D.; Kali, G. *Phys. Rev. Lett.* **2003**, *90*, 058302.
- (12) Pahl, S.; Fleischer, G.; Fujara, F.; Geil, B. *Macromolecules* **1997**, *30*, 1414–1418.
- (13) Kimmich, R.; Anardo, E. *Prog. Nucl. Magn. Reson. Spectrosc.* **2004**, *44*, 257–320.
- (14) Ferry, J. D. *Viscoelastic Properties of Polymers*, 3rd ed.; Wiley: New York, 1980.
- (15) Graessley, W. W. *Polymeric Liquids & Networks: Dynamics and Rheology*; Taylor and Francis: New York, 2008.
- (16) Kariyo, S.; Herrmann, A.; Gainaru, C.; Schick, H.; Brodin, A.; Novikov, V. N.; Rössler, E. A. *Phys. Rev. Lett.* **2008**, *100*, 109901.
- (17) Kariyo, S.; Brodin, A.; Gainaru, C.; Herrmann, A.; Schick, H.; Novikov, V. N.; Rössler, E. A. *Macromolecules* **2008**, *41*, 5313–5321.
- (18) Kariyo, S.; Brodin, A.; Gainaru, C.; Herrmann, A.; Hintermeyer, J.; Schick, H.; Novikov, V. N.; Rössler, E. A. *Macromolecules* **2008**, *41*, 5322–5332.
- (19) Herrmann, A.; Novikov, V. N.; Rössler, E. A. *Macromolecules* **2009**, *42*, 2063–2068.
- (20) Herrmann, A.; Kariyo, S.; Abou Elfadl, A.; Meier, R.; Gmeiner, J.; Novikov, V. N.; Rössler, E. A. *Macromolecules* **2009**, *42*, 5236–5243.
- (21) Hofmann, M.; Herrmann, A.; Abou Elfadl, A.; Kruk, D.; Wohlfahrt, M.; Rössler, E. A. *Macromolecules* **2012**, *45*, 2390–2401.
- (22) Herrmann, A.; Kresse, B.; Gmeiner, J.; Privalov, A. F.; Kruk, D.; Fujara, F.; Rössler, E. A. *Macromolecules* **2012**, *45*, 1408–1416.
- (23) Herrmann, A.; Kresse, B.; Wohlfahrt, M.; Bauer, I.; Privalov, A. F.; Kruk, D.; Fatkullin, N.; Fujara, F.; Rössler, E. A. *Macromolecules* **2012**, *45*, 6516–6526.
- (24) Chávez, F. V.; Saalwächter, K. *Phys. Rev. Lett.* **2010**, *104*, 198305.
- (25) Chávez, F. V.; Saalwächter, K. *Macromolecules* **2011**, *44*, 1549–1559.
- (26) Kehr, M.; Fatkullin, N.; Kimmich, R. *J. Chem. Phys.* **2007**, *126*, 094903.
- (27) Smith, G. D.; Borodin, O.; Bedrov, D. *J. Phys. Chem. A* **1998**, *102*, 10318–10323.
- (28) Vogel, M. *Macromolecules* **2008**, *41*, 2949–2958.
- (29) Bormuth, A.; Henritzi, P.; Vogel, M. *Macromolecules* **2010**, *43*, 8985–8992.
- (30) Henritzi, P.; Bormuth, A.; Vogel, M. *Solid State Nucl. Magn. Reson.* **2013**, *54*, 32–40.
- (31) Ball, R.; Callaghan, P.; Samulski, E. J. *J. Chem. Phys.* **1997**, *106*, 7352–7361.
- (32) Wang, Z.; Likhtman, A. E.; Larson, R. G. *Macromolecules* **2012**, *45*, 3557–3570.
- (33) Bloembergen, N.; Purcell, E. M.; Pound, R. V. *Phys. Rev.* **1948**, *73*, 679–712.
- (34) Beckmann, P. A. *Phys. Rep.* **1988**, *171*, 85–128.
- (35) Rouse, P. E. *J. Chem. Phys.* **1953**, *21*, 1273.
- (36) Smith, B. A.; Samulski, E. T.; Yu, L. P.; Winnik, M. A. *Macromolecules* **1985**, *18*, 1901–1905.
- (37) Wick, C. D.; Theodorou, D. N. *Macromolecules* **2004**, *37*, 7026–7033.
- (38) Scholl, C. A. *J. Phys. C: Solid State Physics* **1981**, *14*, 447–464.
- (39) Filon, L. N. G. *On a quadrature formula for trigonometric integrals*, 1928.
- (40) Klein, P.; Adams, C.; Brereton, M.; Ries, M.; Nicholson, T.; Hutchings, L.; Richards, R. *Macromolecules* **1998**, *31*, 8871–8877.

Publication 2

Field-Cycling NMR Relaxometry Probing the Microscopic Dynamics in Polymer Melts

Hofmann, M.; Kresse, B.; Privalov, A. F.; Willner, L.; Fatkullin, N.;

Fujara, F.; Rössler, E. A.

Macromolecules **2014**, 47, 7917-7929.

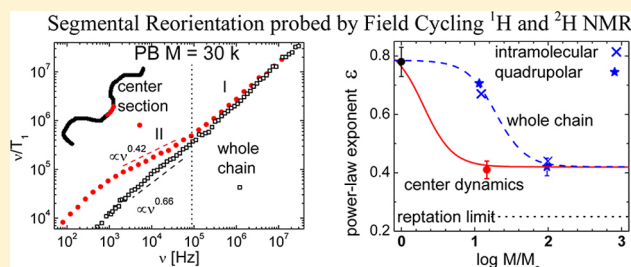
DOI: 10.1021/ma501520u

(Copyright 2014 by The American Chemical Society)

Field-Cycling NMR Relaxometry Probing the Microscopic Dynamics in Polymer Melts

M. Hofmann,[†] B. Kresse,[‡] A. F. Privalov,[‡] L. Willner,[§] N. Fatkullin,[#] F. Fujara,[‡] and E. A. Rössler^{*,†}[†]Experimentalphysik II, Universität Bayreuth, D-95440 Bayreuth, Germany[‡]Institut für Festkörperphysik, TU Darmstadt, Hochschulstrasse 6, D-64289 Darmstadt, Germany[§]Institute of Complex Systems, Forschungszentrum Jülich, D-52425 Jülich, Germany[#]Institute of Physics, Kazan Federal University, Kazan 420008, Tatarstan Russia

ABSTRACT: Field-cycling (FC) ^1H and ^2H NMR relaxometry is applied to linear polybutadiene (PB) of different molar mass (M) in order to test current polymer theories. Applying earth field compensation, five decades in the frequency dependence of the spin–lattice relaxation rate $T_1^{-1}(\nu) = R_1(\nu)$ are accessed (200 Hz – 30 MHz), and we focus on the crossover from Rouse to entanglement dynamics. A refined evaluation is presented, which avoids application of frequency–temperature superposition as well as Fourier transformation. Instead, the power-law exponent ε in the entanglement regime is directly determined from the susceptibility representation $\chi''_{\text{NMR}}(\omega) = \omega/T_1(\omega) \propto \omega^\varepsilon$ by a derivative method. Correspondingly, a power-law $t^{-\varepsilon}$ characterizes the decay in the time domain, i.e., the dipolar correlation function. For the total ^1H relaxation, comprising intra- and intermolecular relaxation, a high- M exponent $\varepsilon_{\text{total}} = 0.31 \pm 0.03$ is found. An isotope dilution experiment, which yields the intramolecular relaxation reflecting solely segmental reorientation, provides an exponent $\varepsilon_{\text{intra}} = 0.44 \pm 0.03$. It agrees with that of FC ^2H NMR ($\varepsilon_Q = 0.42 \pm 0.03$) probing only segmental reorientation. The fact that $\varepsilon_{\text{intra}} > \varepsilon_{\text{total}}$ demonstrates the relevance of intermolecular relaxation in the entanglement regime (but not in the Rouse regime), and $\varepsilon_{\text{intra}}$ is significantly higher than predicted by the tube-reptation (TR) model ($\varepsilon_{\text{TR}} = 0.25$) and, the latter being supported also by recent simulations. The ratio of inter- to intramolecular relaxation grows with decreasing frequency, again in contradiction to the TR model and results from double quantum ^1H NMR. We conclude that no clear evidence of a tube is found on the microscopic level and the so-called return-to-origin hypothesis is not confirmed. Studying the influence of chain end dynamics by FC ^1H NMR we compare differently chain end deuterated PB. For the dynamics of the central part of the polymer the exponent drops from $\varepsilon_{\text{intra}} = 0.66 \pm 0.03$ down to $\varepsilon_{\text{cent}} = 0.41 \pm 0.03$ for $M = 29\text{k}$ which is very close to the high- M value $\varepsilon_{\text{intra}}$. Thus, the protracted transition to entanglement dynamics reported before is not found when the polymer center is probed; instead full entanglement dynamics appears to set in directly with $M > M_e$.



1. INTRODUCTION

The tube-reptation (TR) model,¹ a combination of the Rouse model² for nonentangled chains (with molar mass M below the entanglement mass M_e) and de Gennes' reptation idea³ for $M > M_e$, is a widely accepted model describing the dynamics of melts of entangled linear polymers. The model predicts four different power-law regimes (I–IV) for the microscopic dynamics, more specifically for the time dependence of the segmental mean square displacement $\langle r^2(t) \rangle \propto t^\alpha$, summarized in Figure 1. Molecular dynamics (MD) simulations,^{4,5} neutron scattering experiments⁶ as well as recently field-cycling (FC) ^1H NMR,^{7,8} have essentially confirmed parts of the model by identifying the predicted crossover from $\langle r^2(t) \rangle \propto t^{0.5}$ to $\langle r^2(t) \rangle \propto t^{0.25}$ for the transition from free Rouse (regime I) to constrained Rouse dynamics (regime II). On long time scales the final crossover from $\langle r^2(t) \rangle \propto t^{0.5}$ typical of reptation (regime III) to $\langle r^2(t) \rangle \propto t^1$ of the terminal regime of free diffusion (regime IV) has been observed by field gradient (FG) NMR.^{9,10} Another regime (regime 0) usually not included in polymer theories reflects glassy dynamics at very short times,

i.e., local motions on the time scale of the segmental correlation time τ_s .^{11,12} Given the large range of different relaxation regimes, characterization by essentially a single experiment is still missing. Also, the connection of diffusion with segmental reorientation described in a coarse grained model by the tangent vector correlation function is not accessed experimentally. Cast in rank- l reorientational correlation functions (e.g., $l = 2$ accessible by NMR) a corresponding set of power-laws $C_2(t) \propto t^{-\varepsilon}$ is provided by the TR model (cf. Figure 1).^{3,11,12} In regimes II and III the motion of polymer chains is confined inside a tube and the correlation function $C_l(t)$ for any l is $C_l(t) \propto \langle r^2(t) \rangle^{-1}$, whereas in regime I $C_l(t)$ is l -dependent with $C_2(t) = [C_1(t)]^2 \propto t^{-1}$ and $C_1(t) \propto \langle r^2(t) \rangle^{-1}$ (the so-called return-to-origin hypothesis).^{3,11–14}

For comparison, we also included the prediction of the n -renormalized Rouse model,^{11,15–18} an alternative approach

Received: July 24, 2014

Revised: October 23, 2014

Published: November 12, 2014

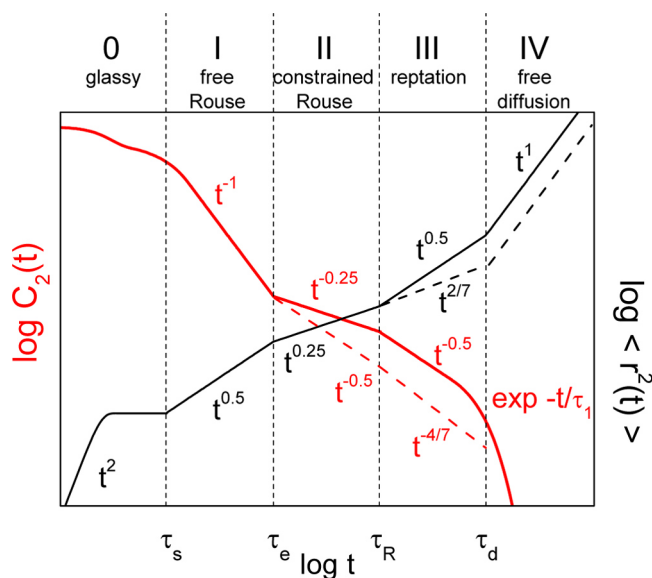


Figure 1. Predictions of the tube-reptation model for the segmental mean square displacement $\langle r^2(t) \rangle$ (black solid line, right scale) and the rank-two reorientational correlation function $C_2(t)$ (red solid line, left scale).¹² Relaxation regimes are indicated (adapted from ref 8). Dashed lines: predictions for the thrice-renormalized Rouse model.^{11,15–18}

describing entanglement dynamics in Figure 1. We have chosen the thrice ($n = 3$) renormalized Rouse model as it reproduces the well-known scaling relations for the diffusion coefficient ($D \propto M^{-2.3}$) and the terminal relaxation time ($\tau_t \propto M^{3.4}$) best. Concerning the mean square displacement $\langle r^2(t) \rangle$ in regimes I ($\alpha = 1/2$) and II ($\alpha = 1/4$) the exponents predicted by the renormalized Rouse models and those of the TR agree, only in regime III discrepancies are expected. In the case of $C_2(t)$, however, differences are found even in regime II. Here the TR theory provides $C_2(t) \propto t^{-1/4}$ (constraint Rouse regime) while the n -renormalized Rouse models provide a $t^{-1/2}$ scaling in the so-called high-mode number limit. In regime III the TR theory provides $\propto t^{-1/2}$ while the n -renormalized Rouse models predict $\varepsilon = 4/(4 + n)$. Thus, only by measuring segmental reorientation the two theoretical models can be distinguished in regime II and this can be achieved by FC NMR.^{11,19,20}

Recent progress by two different NMR methods has provided new insights. While FC ^1H NMR relaxometry gives access to the frequency dependence of the spin–lattice relaxation time,^{8,11,19–23} double quantum (DQ) ^1H NMR probes the correlation function directly in the time domain.^{24–27} The quantities accessed are correlation functions probing the fluctuations of the nuclear magnetic dipole–dipole interaction. Usually, it is argued that the relaxation is dominated by intramolecular relaxation, and thus segmental reorientational dynamics in terms of the rank-two reorientational correlation function $C_2(t)$ (tensorial segmental orientational autocorrelation function as used by Saalwächter et al.²⁷) is probed. Both methods usually extend their effective frequency/time range by applying frequency–temperature superposition (FTS), a procedure well-known from rheological studies.^{28–30} Discussing the power-law exponent of regime II, both techniques so far provide clear indications for a highly protracted crossover from Rouse to reptation dynamics. Concerning the dipolar correlation function, $C_{DD}(t/\tau_e) \propto t^{-\varepsilon}$, the results on 1,4-polybutadiene (PB) agree even quantitatively.^{8,22,26,27} At high molar masses the exponent in regime II is found to be $\varepsilon_{\text{total}} = 0.31$ (FC ^1H NMR)

and 0.29 (DQ ^1H NMR) and almost reaches the theoretical prediction of the TR model, $\varepsilon_{\text{TR}} = 0.25$.¹

Yet, it has been shown that the assumption of intramolecular relaxation dominating the total spin–lattice relaxation does not hold.^{7,8,20,31–34} In particular, at low frequencies in the regime of terminal relaxation, the intermolecular relaxation reflecting translational dynamics becomes the dominant contribution, actually allowing to extract the self-diffusion coefficient as an alternative method to FG NMR.^{20,32–34} Thus, the correlation function probed by ^1H NMR is expected to be a superposition of intra- and intermolecular contributions. Intermolecular contributions are also expected for the correlation function probed by DQ NMR.³⁵ Isotope dilution experiments, i.e., mixing a protonated species with its deuterated counterpart allows for separating both relaxation contributions.^{35,36} In the case of PB, such experiments were carried out in a recent publication.⁸ The exponent $\varepsilon = \varepsilon_{\text{intra}}$ of $C_2(t)$ in regime II, represented by the isolated intramolecular relaxation, turned out to be significantly larger than the prediction $\varepsilon_{\text{TR}} = 0.25$ of the TR model. Explicitly, while the long-time exponent in the total dipolar correlation function $C_{DD}(t)$ was reported to be $\varepsilon_{\text{total}} = 0.31 \pm 0.03$, it becomes $\varepsilon_{\text{intra}} = 0.49 \pm 0.03$ for the intramolecular correlation function $C_2(t)$. In addition, the exponent agrees essentially with the one found from ^2H NMR relaxation, the latter probing only reorientational dynamics. We concluded that the relation $C_2(t) \propto \langle r^2(t) \rangle^{-1}$, as predicted by the TR model, is not confirmed.

Very recently, in a DQ ^1H NMR study by Saalwächter and co-workers,²⁷ experiments on PB in deuterated matrices have also been performed, and regarding the power-law exponents, virtually no difference was reported for fully protonated melts and those diluted in deuterated chains, although a strong intermolecular contribution was identified, yet with apparently the same time dependence as the intramolecular contribution. This result is at variance with our FC ^1H NMR finding.⁸ It is the purpose of the present publication to dwell on this discrepancy by thoroughly reanalyzing our previous data and by presenting new FC NMR data. Clarifying this issue is of great importance since in one case (DQ NMR) the TR model is confirmed while in the present case (FC NMR) it is not. Again we emphasize that only by comparing reorientational and translational dynamics the return-to-origin hypothesis underlying the TR model can be tested.

We will reanalyze relaxation data of PB already presented⁸ but refrain from constructing master curves and directly analyze the relaxation dispersion $R_1(\omega) = T_1^{-1}(\omega)$ measured at highest temperatures for which the slowest polymer dynamics appear. Moreover, applying the isotope dilution technique in order to characterize the intramolecular relaxation contribution, we do not extrapolate the rate to zero concentration but the power-law exponents instead. Both approaches avoid possible sources of errors. As we apply active earth and stray field compensation a large frequency range of $200 \text{ Hz} \leq \nu \leq 30 \text{ MHz}$ is covered. In addition, the existing data are complemented by new FC ^1H and ^2H NMR measurements involving a novel low-field stabilization system.^{37,38} Saalwächter and co-workers extracted the exponents from the flattest part of the measured correlation function by applying a derivative procedure.²⁷ This avoids an overestimation of the exponent in the case when some influence of the terminal relaxation leads to a higher exponent at longest times. Indeed, reinspect our FC ^1H NMR results for $C_2(t)$ for the highest M , a possible influence of terminal relaxation may be anticipated for the intra part. The actual

exponent reported in our previous FC NMR studies resulted from averaging over one to two decades at lowest frequencies; thus, such effects were not taken into account. In the present contribution we also stick to a derivative method allowing a consistent comparison between the two NMR methods. Yet, we will show that the newly obtained high- M exponent $\varepsilon_{\text{intra}}$ is still higher than that reported by DQ ^1H NMR and does not agree with that of the TR model as well as simulation data. We emphasize that in both FC and DQ NMR studies PB from the same source was investigated.

From a theoretical perspective^{7,11,18,39,40} the relative weights of intra- and intermolecular contributions are expected to be time (or frequency) dependent and sensitive to details of the chain dynamics. Quite different expressions result for the ratio $A(\omega) = R_1^{\text{inter}}(\omega)/R_1^{\text{intra}}(\omega)$ when isotropic models of polymer dynamics, like the renormalized Rouse^{11,15} or the mode coupling model,^{15,16,41} in which already at short times, yet longer than segmental relaxation time, $t > \tau_s$, the segmental displacements are not correlated with the polymer chain's initial conformation, are compared to the "anisotropic" TR model for which the polymer chain is confined to a tube at times $\tau_e \leq t \leq \tau_1$. Here τ_1 denotes the terminal relaxation time of the polymer chain equivalent to the disengagement time τ_d in the TR model and τ_e the entanglement time.¹ Thus, the actually measured ratio $A(\omega)$ provides important information on the microscopic dynamics in polymer melts. First attempts in this direction have already been undertaken by Kimmich and co-workers,^{7,31} we will extend such studies. Furthermore, we will discuss the influence of the chain end dynamics by investigating protonated PB with differently deuterated chain ends. In a neutron spin echo study on poly(ethylene) dynamics the results have been explained by contour length fluctuations (CLF).⁴² Yet, such experiments are still rare.

All in all, our analysis will show that the discrepancy to the DQ ^1H NMR cannot be resolved, and our experiments do not confirm the return-to-origin hypothesis assumed in the TR model. Microscopically, the dynamics is rather isotropic than anisotropic. However, the previously claimed "protracted transition" to reptation dynamics has to be revised in the light of studying only the polymer centers.

2. THEORETICAL BACKGROUND: INTRA- AND INTERMOLECULAR RELAXATION

Field-cycling ^1H NMR probes the segmental polymer dynamics in the frequency domain by measuring the dispersion, i.e., the frequency dependence, of the spin–lattice relaxation rate $R_1(\omega = \gamma \cdot B) = T_1^{-1}(\omega)$ where B is the magnetic field and γ the gyromagnetic ratio. The rate probes the segmental dynamics via the fluctuations of the magnetic dipole–dipole interaction of proton pairs. The dipolar couplings comprise two contributions, such acting between protons located each on the same molecule, causing intramolecular relaxation, and such located on different molecules, causing intermolecular relaxation. The total relaxation rate measured by FC ^1H NMR can consequently be separated:⁴³

$$R_1 = R_1^{\text{intra}} + R_1^{\text{inter}} \quad (1)$$

Both contributions follow the Bloembergen, Purcell, and Pound (BPP) equation⁴⁴

$$R_1^{\text{intra,inter}}(\omega) = K^{\text{intra,inter}} [J_2^{\text{intra,inter}}(\omega) + 4J_2^{\text{intra,inter}}(2\omega)] \quad (2)$$

with K denoting the corresponding coupling constant. The intramolecular rate R_1^{intra} has to be split into an intrasegment contribution referring to spin pairs within a polymer segment, and an intersegment contribution implying pairs of spins in different segments of the same macromolecule. Yet, the intersegment contribution can be neglected^{18,31,39} wherefore R_1^{intra} reflects segmental reorientational dynamics described by the rank-two correlation function $C_2(t)$ which is linked to the spectral density $J_2^{\text{intra}}(\omega)$ via Fourier transformation. We again refer to Figure 1 where the predictions for $C_2(t)$ by the different polymer models are displayed.

The TR model is a so-called anisotropic polymer model.^{7,11,15} Here, in the time interval $\tau_e \leq t \leq \tau_d$, spatial displacements of polymer segments are confined within a tube and polymer conformations are strongly correlated with the polymer chain initial conformation. In this scenario the ratio of inter- to intramolecular relaxation contribution is connected to the segmental root-mean-square displacement $\langle r^2(t = \omega^{-1}) \rangle^{1/2}$ for times $\tau_s \leq t \leq \tau_1$ in the following way:^{18,39}

$$A_{\text{TR}}(\omega) = \frac{R_1^{\text{inter}}(\omega)}{R_1^{\text{intra}}(\omega)} \propto \frac{1}{\langle r^2(1/\omega) \rangle^{1/2}} \quad (3)$$

In the case of the isotropic polymer models like the n -renormalized Rouse or the polymer mode–mode coupling model, it is assumed that already at short times $t > \tau_s$ the segmental displacements are not correlated with the polymer chain initial conformation. Assuming that the relative mean square displacement of two segments from different chains (actually measured by FC NMR) scale with time like the polymer segment mean square displacement, the inverse connection with $\langle r^2(t) \rangle^{1/2}$ is derived, explicitly:^{18,39}

$$A_{\text{iso}}(\omega) = \frac{R_1^{\text{inter}}(\omega)}{R_1^{\text{intra}}(\omega)} \propto \langle r^2(1/\omega) \rangle^{1/2} \quad (4)$$

Thus, the different models of polymer dynamics can be distinguished by their relation between inter- and intramolecular relaxation $A(\omega)$; quite distinct frequency dependencies are expected. Separation of both contributions becomes feasible by isotopic dilution experiments where protonated chains are successively diluted in a fully deuterated matrix constituted by chains of the same molar mass.^{7,8,11,32,45} Extrapolating the concentration of the protonated species to zero the intermolecular relaxation contribution is removed since dipolar couplings between ^1H and ^2H are negligible.⁷ In addition, FC ^2H NMR can be applied to probe solely segmental reorientation. In this case the relaxation is caused by fluctuations of the electric field gradient (EFG) which interacts with the electric quadrupole moment of the $I = 1$ nucleus ^2H .⁴³ Since in organic systems the EFG is caused by the inhomogeneous charge distribution of the carbon–hydrogen bond, solely reorientation of the latter is probed, i.e., the correlation function $C_2(t)$ is explored. The quadrupolar relaxation rate follows an analogous equation like eq 2 with an appropriate coupling constant K_Q .⁴³

In order to stress the similarity with rheological experiments, the dispersion data are given in the susceptibility representation, $\chi''(\nu = \omega/2\pi) = \nu \cdot R_1(\nu)$.^{20–23} Note that the power-law exponent ε in $C(t) \propto t^{-\varepsilon}$ reappears in $\chi''(\omega) \propto \omega^\varepsilon$. We once again emphasize that we refrain from constructing master curves by applying frequency–temperature superposition.

3. EXPERIMENTAL SECTION AND DATA ANALYSIS

3.1. Samples. Linear, either fully protonated (*-h*) or fully deuterated (*-d*), 1,4-polybutadienes (PB) with low polydispersity and with various molar masses between $M_w = 4.6$ kg/mol (=4.6k) and $M_w = 441$ k, all being well above the entanglement mass $M_e \approx 2$ k,^{29,46} were purchased from Polymer Standards Service (PSS), Mainz, Germany. The molar mass refers to the weight-average molar mass M_w . The PSS polymers are stabilized by 0.1% butylated hydroxytoluene. The microstructures of selected PB samples from PSS were determined from ¹³C NMR spectra.⁴⁷ For $M > 11$ k, all samples contain around 50% cis-isomers and 40% trans-isomers; the rest refers to 1,2-PB (cf. Table 1). In order to excerpt the intramolecular

Table 1. Properties of the Investigated Poly(butadiene) Samples^a

sample code	M_w [g/mol]	PDI = M_w/M_n	1,2-PB content in %	T_g [K] (± 1 K)
PB-h 4.6k	4600	1.03		
PB-h 9.5k	9470	1.02	8	
PB-h 11k	11400			
PB-h 18k	18200	1.01	7	176
PB-d 23k	22800	1.02		187
PB-h 24k	24300	1.01	7	177
PB-h 35k	35300	1.02		
PB-h 47k	47000	1.04	24	187
PB-h 57k	56500	1.02		
PB-h 88k	87500	1.05		
PB-h 143k	143000	1.02		
PB-d 191k	191000	1.03		176
PB-h 196k	196000	1.02		177
PB-d 364k* (PS)	364000	1.08	5	190
PB-h 380k* (PS)	380000	1.12	5	177
PB-h 441k*	441000	1.07	6	174

^aThe sample code reflects the isotope labeling and the mass average molar mass M_w . Whenever known, the polydispersity (PDI), the 1,2-PB (vinyl) content and the glass transition temperature T_g (in K) is given. Samples marked with the asterisk (*) were measured in the present work, those without in the context of ref 8. Samples from Polymer Source were labeled with PS, the others are obtained from Polymer Standards Service.

relaxation contribution, two isotope dilution series were set up, namely PB-h with $M = 24$ k with mole fractions x of 76%, 53%, 22% and 11% in PB-d 23k, and 16% PB-h 196k in PB-d 191k.⁸ In addition, protonated 1,4-PB with $M_w = 380$ k (PB-h 380k) and fully deuterated 1,4-PB with $M_w = 364$ k (PB-d 364k) were purchased from another source, namely from Polymer Source (PS), Dorval, Canada. According to the datasheet the protonated species contains 68% cis- and 27% trans-isomers, thus differing somewhat from that of the PSS polymers (cf. Table 1). The 1,2-PB content is given as 5%.

Differential scanning calorimetry (DSC) using a DSC 7 device (PerkinElmer Inc., Waltham, MA) was applied in order to determine the glass transition temperatures T_g of selected systems. Thermal cycles between 153 K and 213 K were run at a cooling/heating rate of 10 K/min and T_g listed in Table 1, were determined from the intersection of the two tangents applied to the DSC curves at the endothermic step. Exemplarily, two DSC curves are shown in Appendix A, which demonstrate that, in the case of PB-d 23k, we find a T_g which is by 11 K higher than that of PB-h 24k. This will be further discussed, below.

In order to investigate end group effects, two different triblock PB copolymers consisting of two fully deuterated blocks at the chain ends and a protonated center were investigated. These systems are abbreviated with the term PB-dhd. The triblock polymers, PB-dhd 13/6/10 and PB-dhd 5/20/4, were prepared by living anionic polymerization of butadiene at room temperature under high vacuum. Benzene was used as solvent and *s*-butyllithium as initiator. The techniques and purification applied were similar to those specified

in ref 48. The triblock structure was achieved by sequentially polymerizing butadiene-*d*₆, butadiene-*h*₆, and butadiene-*d*₆. Termination of the polymerization reaction was done by adding a small amount of degassed methanol. After each polymerization step, a small sample was removed from the polymerization mixture for separate characterization. The PB was isolated by precipitation in methanol and dried in high vacuum.

The polymers and the individual blocks were characterized by size exclusion chromatography. Tetrahydrofuran (THF) was used as eluant at a flow rate of 1 mL/min. Molar masses and molar mass distributions were determined relative to polystyrene standards taking into account the Mark–Houwink–Sekurada relationship between PS and 1,4-PB in THF: $M_{PB} = 0.581 M_{PS}^{0.997}$. The chromatograms showed a single peak indicating that no termination occurred during the addition of new monomer for the individual blocks. Polydispersities were found to be smaller than 1.03 for the final triblocks as well as for the intermediate homo- and diblocks. Absolute molar masses of the triblocks were additionally determined by light scattering in *n*-heptane and membrane osmometry in toluene at 310 K. The microstructure of the polybutadienes consists of 7% 1,2, 52% trans-1,4, and 41% cis-1,4 as calculated from ¹H NMR spectra. Therefore, the microstructure of the triblocks agrees with that of the samples from PSS and are identical to those discussed in ref 42 and their characteristics are summarized in Table 2.

Table 2. Properties of the Poly(butadiene) Tri-Block Copolymers^a

sample code	M_w [g/mol]	composition [kg/mol]	1,2-PB content in %
PB-dhd 13/6/10	29500	13.2–6.2–10.1	7
PB-dhd 5/20/4	28300	4.7–19.6–4.0	7

^aThey consist of protonated center sections and deuterated chain ends.

All PB samples were filled into standard 5 mm NMR sample tubes without further purification. Subsequently the samples were degassed under vacuum for 2 days to remove paramagnetic oxygen impurities and finally sealed.

3.2. Spin–Lattice Relaxation Measurements. The ¹H and ²H spin–lattice relaxation experiments were carried out on a home-built FC NMR relaxometer located at the Technische Universität Darmstadt (Germany).^{8,37,38,49} With respect to protons, a Larmor frequency range of $200 \text{ Hz} \leq \nu = \omega/2\pi \leq 30 \text{ MHz}$ was accessible. In the case of ²H, the Larmor frequency is reduced by a factor of $\gamma_H/\gamma_D = 6.51$. That is, extremely low frequencies are achieved by actively compensating the earth magnetic field and other stray fields caused by surrounding laboratory equipment. A novel field stabilization system was applied.³⁷ The lower limit for the spin–lattice relaxation time is determined by the time needed for electronic field-stabilization which is around 2 ms. In all investigated systems the magnetization build-up or decay curves were found to be monoexponential. Since this study focuses on the slow entanglement dynamics, the experiments were performed at a temperature as high as 393 K where the spectral density of entanglement dynamics coincides with the accessible frequency range of the FC spectrometer.

The relaxation behavior of a polymer melt shows up in form of different power-law regimes (cf. Figure 1). A power-law $t^{-\alpha}$ with $0 < \alpha < 1$ is transformed as $\int dt t^{-\alpha} e^{-i\omega t} \propto \omega^{\alpha-1}$ to the spectral density. Hence, one gets equal magnitudes of the exponent, yet with opposite sign when the susceptibility representation $\chi''(\omega) = \omega R_1(\omega)$ is used.^{8,21–23} In order to reliably characterize the power-law behavior of the relaxation data we applied the derivative method as was also done in ref 27. On a double-logarithmic scale, an interval with length of one decade is shifted pointwise along the frequency axis. All data points comprised by the actual interval were linearly interpolated providing the corresponding (window-averaged) apparent power-law exponent $\alpha(\omega)$. Each data point of $\alpha(\omega)$ belongs to the center (on a log-scale) of the corresponding frequency interval.

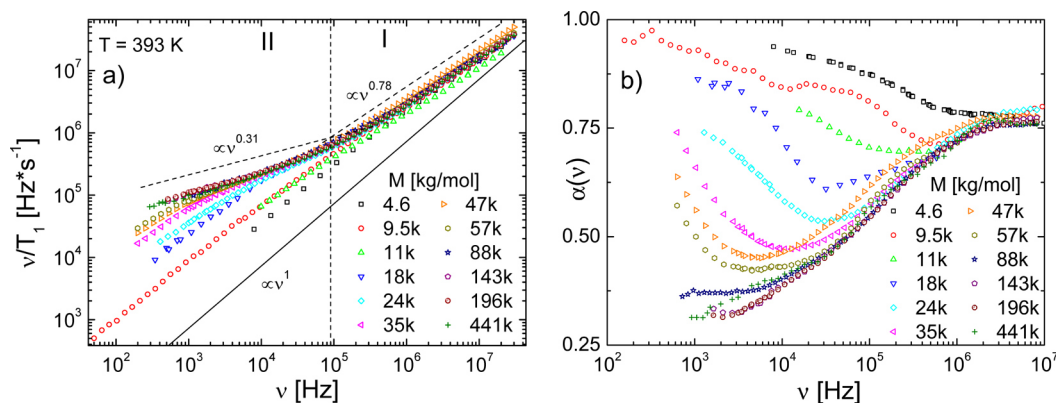


Figure 2. (a) Susceptibility representation of the relaxation data recorded at $T = 393$ K obtained from FC ^1H NMR of PB-h of different molar masses $M > M_e$. Two relaxation regimes (I, II) are observed. For the highest M the corresponding power-laws ($\nu^{0.78}$ and $\nu^{0.31}$) and the intersection point at around 90 kHz are indicated providing an estimate of the entanglement time τ_e . The low-frequency behavior of a simple liquid $\chi''(\nu) \propto \nu^{-1}$ is added (solid line). (b) Apparent power-law exponent $\alpha(\nu)$ of the curves calculated by a derivative method.

4. RESULTS

This section is divided as follows: We start with the FC ^1H NMR results obtained for PB containing intra- and intermolecular contributions, i.e., the total relaxation (eq 1) is discussed (section 4.1). Then we proceed with the analysis of the intramolecular relaxation obtained by isotope dilution experiments (section 4.2) and FC ^2H NMR results for selected systems (section 4.3). Finally we prove the significance of finite length effects by measuring partially labeled chains (section 4.4).

4.1. Results from FC ^1H NMR. Figure 2a summarizes the dispersion data in the susceptibility representation $\nu R_1(\nu)$ recorded for different molar masses of (fully protonated) PB as indicated, each at 393 K, over five decades in frequency range. The rate $R_1(\nu) = T_1^{-1}(\omega/2\pi)$ contains intra- and intermolecular contributions. Since all molar masses are higher than the entanglement molar mass $M_e \approx 2k^{29,46}$ entanglement effects are anticipated. As going from high to low frequencies all curves in Figure 2a essentially coincide for $\nu \geq 1$ MHz except for PB-h 11k and PB-h 47k which appear to be slightly shifted toward higher/lower frequencies, respectively. This can be explained by somewhat different microstructures changing slightly the segmental time constants τ_s (different T_g). Indeed, PB-h 47k features larger vinyl content and a by 10 K higher T_g than most other systems (cf. Table 1) while actually no changes in T_g are expected at such high M .⁵⁰ This effect, however, is of minor relevance for the present discussion as we are mainly interested in the power-law behavior of the susceptibility, i.e., in the corresponding exponents.

As in our previous publications,^{8,21–23} two regimes of polymer dynamics are identified. Applying the derivative method (cf. Experimental Section) a common power-law with an exponent $\varepsilon_I = 0.78 \pm 0.05$ (cf. exponents in Figure 2b) independent of M is observed at high frequencies ($\nu > 90$ kHz) and attributed to Rouse dynamics (regime I). This value agrees well with 0.76 found in ref 22 in the frequency domain but differs slightly from 0.85 reported in ref 8 after transformation to the time domain. One theoretically expects an exponent of $\varepsilon_{\text{Rouse}} = 1$; thus, our result is close to this. It is well-known that the so-called free Rouse regime in entangled polymers never agrees perfectly with the Rouse theory, the latter designed to describe dynamics of unentangled polymers.⁵ At lower frequencies ($\nu < 90$ kHz) one observes a crossover to a second power-law with a smaller exponent reflecting entanglement dynamics; it extends to lower

and lower frequencies for increasing M . For M below 88k, the terminal relaxation is reached signaled by an apparent exponent asymptotically returning to one at longest times. The exact determination of the exponent in regime II is most important for answering the question whether it can be explained by the TR model, for which an exponent of $\varepsilon_{\text{TR}} = 0.25$ (constrained Rouse dynamics) is predicted.

The crossover frequency from regime I to regime II can be defined as the intersection of the two power-law extrapolations located at around 90 kHz and which we associate with the entanglement time τ_e via $\tau_e 2\pi\nu = 1$ yielding $\tau_e \approx 1.8 \mu\text{s}$ (cf. Figure 2(a)). In contrast, one calculates $\tau_e = \tau_s \times N_e^2 \approx 10$ ns (using $\tau_s(393 \text{ K}) = 32$ ps taken from ref 23 and $N_e = M_e/M_0 = 2000/113 \approx 18^{29,46}$) for the theoretically expected value which is by 2 orders of magnitude shorter. Up to our knowledge, in most rheological experiments τ_e is not explicitly determined and a systematic test has not been carried out so far. For other polymers investigated by FC ^1H NMR similar much higher ratios are found as well, i.e., $\tau_e/\tau_s \approx 50000$. We postpone the discussion of this issue to a forthcoming publication.

The value of the exponent $\varepsilon_{\text{total}}$ in the entanglement regime displayed in Figure 3 is defined by the minimum value of the

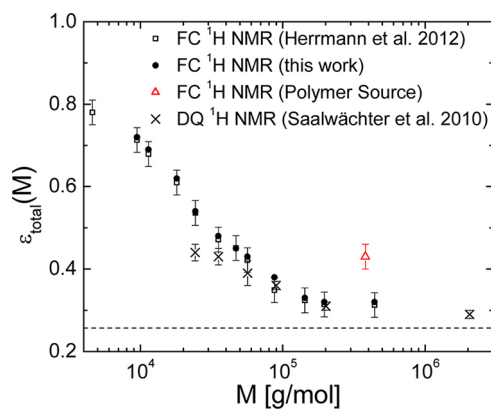


Figure 3. Power-law exponent $\varepsilon_{\text{total}}$ in regime II as a function of molar mass M obtained via a derivative method in the frequency domain (open squares), in the time domain by Herrmann et al.⁸ (black filled circles) and by DQ ^1H NMR²⁷ (crosses). All samples are from Polymer Standards Service except one (from Polymer Source).

apparent frequency dependent exponent $\alpha(\nu)$ (cf. Figure 2b). The index “total” refers to the total relaxation including intra- and intermolecular relaxation contributions. As long as a local minimum is recognized in $\alpha(\nu)$, it defines the crossover from the Rouse regime at high frequencies to regime II and further to the terminal relaxation at low frequencies. The minimum observed for all curves except that of PB-h 4.6k (which is very close to M_e) becomes deeper and shifts toward lower frequencies when M is increased (again one realizes that the curve $\alpha(\nu)$ for $M = 47k$ is shifted with respect to the other curves). At highest M no such minimum is found as the terminal relaxation is well beyond the frequency window and only a plateau is observed as first anticipated for $M = 57k$. For $M = 143k$, $M = 196k$, and $M = 441k$, the plateau value saturates at a level of $\epsilon_{\text{total}} = 0.31 \pm 0.03$ while it is 0.78 ± 0.03 for $M = 4.6k$ for which Rouse dynamics dominate. The exponents $\epsilon_{\text{total}}(M)$ are in very good agreement with those of our previous work⁸ where the exponents were determined after Fourier transformation into the time domain. We take the saturation of the exponent at the highest three M as an indication that the final exponent in regime II is reached eventually, i.e., no further decrease is expected. The M -dependence $\epsilon_{\text{total}}(M)$ is shown in Figure 3 together with data from DQ ^1H NMR²⁷ obtained in the time domain, which matches our data for $M \geq 30k$. From these results, a “protracted transition” to the power-law behavior predicted by the TR model was concluded,^{22,25,26} i.e., the exponent approaches the theoretical value $\epsilon_{\text{TR}} = 0.25$ asymptotically only for highest M . At the present $\epsilon_{\text{total}} = 0.29$ is the lowest exponent found by DQ ^1H NMR in PB-h $M = 2000k$.²⁷

In order to test the reliability of the FC NMR dispersion data at very high M and low frequencies, the sample PB-h 441k was measured once again using the new field stabilization system (cf. Experimental). As shown in Figure 4 an almost perfect

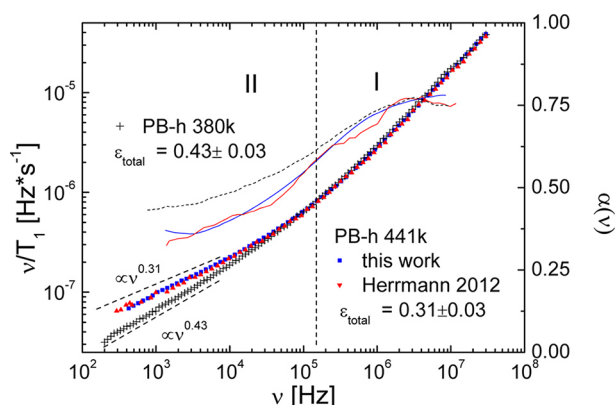


Figure 4. FC ^1H NMR dispersion data (symbols) and corresponding apparent exponent $\alpha(\nu)$ (lines, corresponding to the right scale) of PB-h 441k (from Polymer Standards Service) at $T = 393\text{ K}$ newly measured using the field stabilization system (blue squares) in comparison to previous data from ref 8 (red triangles). Included: data for PB-h 380k (black crosses) from Polymer Source.

agreement with our previous measurement is found, yet with improved signal-to-noise ratio. In addition to the PB systems (PB-h) which were invariably purchased from PSS, another high- M PB, specifically PB-h 380k, was obtained from Polymer Source (Canada), which allows for testing the comparability of the polymer provided by different manufacturers. The susceptibility curve recorded at 393 K and its derivative

for that system is added to Figure 4 in comparison to PB-h 441k from PSS. Above $\nu = 20\text{ kHz}$ the curves agree well. Therefore we conclude that relaxation in the regimes of glassy dynamics and Rouse dynamics agrees. Indeed, the T_g measured by DSC differ only by 3 K (Table 1). At lower frequencies in the entanglement regime, however, PB-h 380k features a significantly steeper increase leading to an exponent $\epsilon_{\text{total}} = 0.43 \pm 0.03$. This is about 0.1 higher than one might expect with respect to the other high- M exponents shown in Figure 3 and far off from the TR limit. With vinyl contents being similar (Table 1), the varying cis-/trans-ratios might cause the differences. Similar differences are found when the FC ^2H NMR results are compared (Appendix B). As Saalwächter and co-workers exclusively run their DQ ^1H NMR experiments on PSS samples, comparison between both NMR techniques remains unchallenged. Yet, the results emphasize the importance of investigating polymers (at least in the case of PB with its varying microstructure) obtained from a common source when comparing the results from different techniques.

4.2. Intra- and Intermolecular Relaxation. In selected cases, deuterated and protonated PB samples of similar molar masses were available (cf. Table 1) allowing for the separation of the intra- and intermolecular relaxation contributions via the application of the isotope dilution technique. Mixing the protonated species with its deuterated counterpart leads to a suppression of the intermolecular relaxation contribution. Figure 5a shows the proton dispersion data of PB-h 24k and PB-h 196k diluted by PB-d 23k and PB-d 191k, respectively. For $\nu \geq 1\text{ MHz}$, the Rouse regime is probed and all susceptibility curves coincide on an absolute scale independently of molar mass and dilution and the exponent of $\epsilon_I = 0.78 \pm 0.05$ is again observed in all cases. This clearly demonstrates that virtually no intermolecular relaxation contribution is present in the Rouse regime. In contrast, at low frequencies, i.e., in the entanglement regime II, the relaxation rates decrease systematically upon dilution with respect to the undiluted reference curves leading to a strong separation of the susceptibilities at lowest frequencies. In the case of the low- M system PB-h 24k the exponent in regime II is changed and also the terminal relaxation which becomes apparently faster at high dilution. As mentioned, in the regime of the terminal relaxation, i.e., at lowest frequencies, the total relaxation in polymers as well as in simple liquids is determined by the intermolecular relaxation reflecting Fickian diffusion of the entire polymer chain (cf. Theoretical Background).^{20,32–34} The apparent faster relaxation at high dilution, however, does not mean that the translational diffusion coefficient D changes. Instead, the proton spin-density decreases upon dilution.

The apparent exponents $\alpha(\nu)$ observed in Figure 5a are displayed in Figure 5b. They qualitatively follow the behavior described in the previous section for the total relaxation (cf. Figure 2b). However, in the entanglement regime, the value of the exponent increases upon dilution with respect to the undiluted case. In Figure 6, for both concentration series, the minimum values of $\alpha(\nu)$ are shown. This exponent $\epsilon(x)$ appears to follow a linear behavior with the same slope. Although this linearity of the exponent cannot be easily explained we take it as a first approach to extract the intercept for $x \rightarrow 0$ which yields the infinite-dilution limit $\epsilon(x \rightarrow 0) = \epsilon_{\text{intra}}$ representing the exponent of the intramolecular relaxation contribution and which, as mentioned, is solely determined by segmental reorientational dynamics. One finds $\epsilon_{\text{intra}} = 0.44 \pm 0.03$ for PB-h 196k and $\epsilon_{\text{intra}} = 0.66 \pm 0.03$ for PB-h 24k, which is about 0.1 higher than the exponents obtained for the corresponding total relaxation,

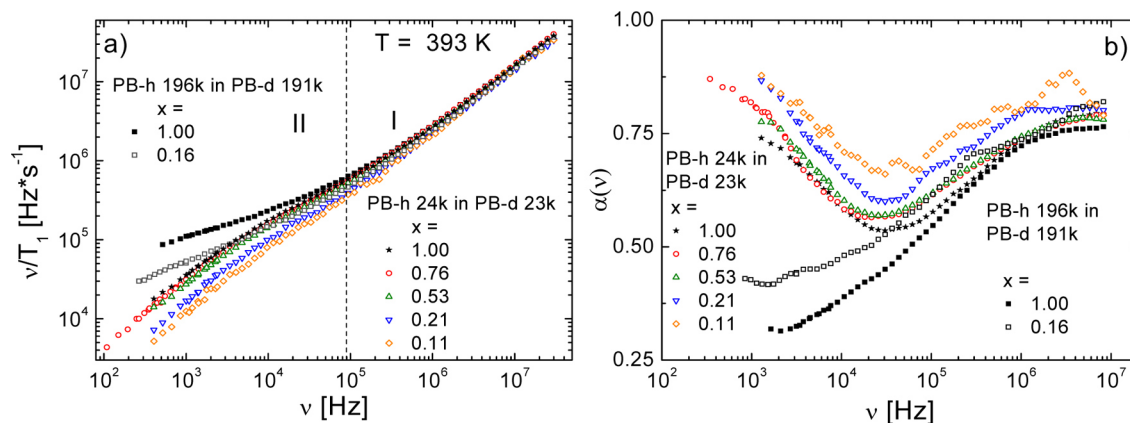


Figure 5. (a) Susceptibility curves measured by FC ^1H NMR at 393 K of PB-h 24k diluted in PB-d 23k and PB-h 196k diluted in PB-d 191k, respectively. The mole fractions of PB-h are indicated. (b) Apparent exponent $\alpha(\nu)$ calculated from FC ^1H NMR relaxation data of the isotope dilution series PB-h 24k in PB-d 23k and PB-h 196k in PB-d 191k, respectively; mole fractions of the protonated species are indicated.

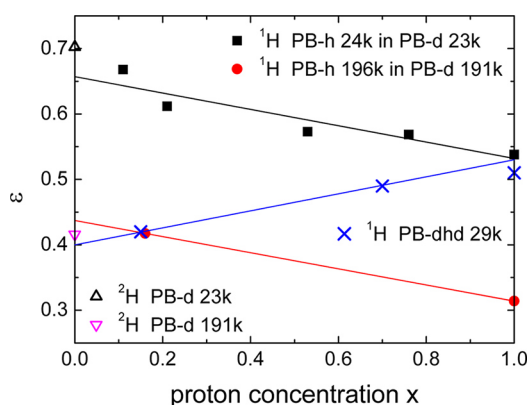


Figure 6. Concentration dependence of the power-law exponent $\varepsilon(x)$ in relaxation regime II for both dilution series (closed symbols); straight lines reflect linear interpolations. Open triangles: exponents ε_Q from FC ^2H NMR on PB-d 23k and PB-d 191k; crosses: exponents $\varepsilon_{\text{dhd}}(x)$ for center-labeled PB-dhd $M = 30\text{k}$ (cf. Table 2) and the corresponding interpolation to zero proton concentration.

i.e., $\varepsilon_{\text{total}} = 0.31 \pm 0.03$ and $\varepsilon_{\text{total}} = 0.54 \pm 0.03$, respectively. The fact that $\varepsilon_{\text{intra}} > \varepsilon_{\text{total}}$ demonstrates the relevance of intermolecular relaxation in the entanglement regime (but not in the Rouse regime), and $\varepsilon_{\text{intra}}$ is significantly higher than predicted by the TR model ($\varepsilon_{\text{TR}} = 0.25$). Here, we emphasize that the determination of $\varepsilon_{\text{intra}}$ was done without taking recourse to extrapolating the original relaxation $R_1(\nu, x)$ data to $x \rightarrow 0$. Thereby, one avoids isotope effects discussed previously⁸ and effects of possibly different τ_s of the protonated and the deuterated polymers (see below).

In order to obtain the intermolecular rate $R_1^{\text{inter}}(\nu)$ one has to extrapolate $R_1(\nu, x)$ down to $x \rightarrow 0$ and subtract the thereby obtained $R_1^{\text{intra}}(\nu)$ from the total relaxation rate $R_1(\nu)$. This procedure was carried out in our previous publication.⁸ The extrapolation relies on the assumption that the dynamics of the mixed (protonated and deuterated) polymers does not change. This, however, is usually not the case. For example, T_g of the protonated and deuterated species may differ. Here, the T_g contrast of PB-h 24k and PB-d 23k is 10 K whereas the T_g of PB-h 196k and PB-d 191k practically agree (cf. Table 1). In addition, mixing different polymers may lead to additional “isotope effects” like a trend toward demixing. In order to remove such effects, we previously constructed master curves applying

FTS. Yet, as we want to avoid this procedure, we are left with the assumption that the lowest concentration of the dilution series reflects the best estimate for the pure intramolecular contribution. The thus extracted rates $R_1^{\text{intra}}(\nu)$ and $R_1^{\text{inter}}(\nu)$ are shown in the Appendix C. In Figure 7 the ratio

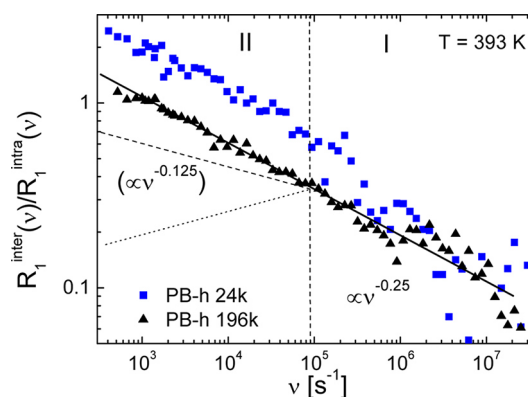


Figure 7. Frequency dependence of the ratio $A(\omega)$ of inter- and intramolecular relaxation rate for PB-h 24k and PB-h 196k at 393 K as calculated from the data shown in Figure 6a and Appendix C. The prediction of eq 4 for isotropic models (dashed line) is indicated; for comparison, also the prediction of the anisotropic TR model for regime II is shown (dotted line).

$A(\omega) = R_1^{\text{inter}}(\nu)/R_1^{\text{intra}}(\nu)$ is displayed for both M . As in the case of $M = 23\text{k}/24\text{k}$ the values of T_g are different such that the results for this system have to be taken with some care.

Obviously the ratio $A(\omega)$ is frequency dependent and increases with decreasing frequency. At high frequencies ($\nu \geq 90\text{ kHz}$), i.e., in the Rouse regime, R_1^{intra} dominates over R_1^{inter} and the ratio is small, i.e., as already seen in Figure 5a, essentially no intermolecular contribution is observed. Below, in the entanglement regime (II) the rate increases in favor of R_1^{inter} which becomes equal to R_1^{intra} at around $\nu \approx 30\text{ kHz}$ for PB-h 24k and at $\nu \approx 1\text{ kHz}$ for PB-h 196k. At lower frequencies R_1^{inter} becomes even dominating. The effect is stronger for the low- M PB sample PB-h 24k. In this case the terminal relaxation is reached at lowest frequencies. Here the intermolecular contribution always becomes dominating as it is controlled by translational diffusion being slower than reorientation.^{32–34} A ratio $A(\omega)$ increasing with decreasing frequency clearly supports the isotropic polymer models. For $\nu \geq 90\text{ kHz}$ the

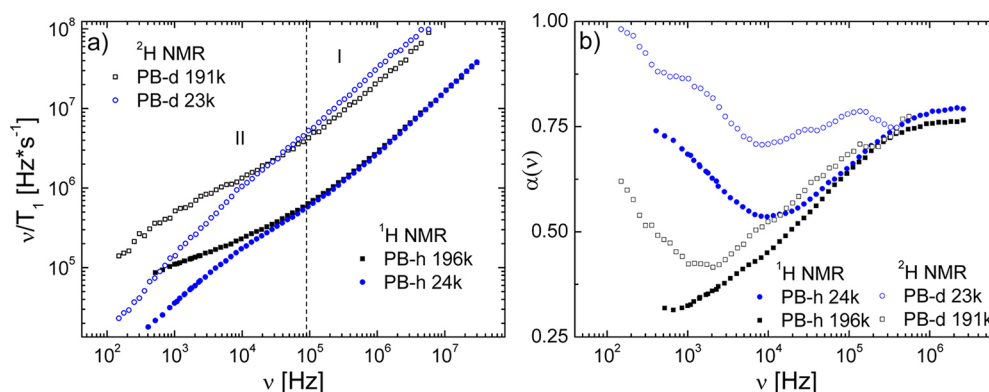


Figure 8. (a) Comparison between the susceptibility curves ($T = 393$ K) of PB-d 23k and PB-h 24k as well as between PB-d 191k and PB-h 196k measured by FC ²H and FC ¹H NMR, respectively. The two power-law regimes (I, II) are indicated. (b) Corresponding apparent exponents $\alpha(\nu)$.

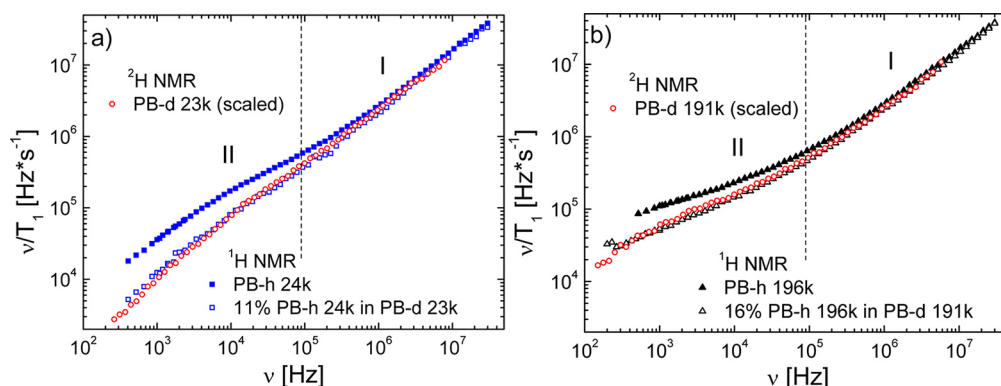


Figure 9. (a) FC ¹H NMR relaxation dispersion data of PB-h 24k ($x = 1.00$) and PB-h 24k ($x = 0.11$) diluted in PB-d 23k compared to the FC ²H NMR data of neat PB-d 23k (circles) after proper scaling (see text). (b) Proton relaxation data of PB-h 196k ($x = 1.00$) and PB-h 196k ($x = 0.16$) in PB-d 191k (open squares), respectively; circles: FC ²H NMR data after vertical scaling (see text).

ratio follows a power-law behavior $\propto \nu^{-0.25}$ as suggested by the (isotropic) Rouse model (eq 4) provided that the mean square displacement of the Rouse model $\langle r^2(t) \rangle \propto t^{0.5}$, which has essentially been confirmed experimentally,^{4–6,8,52} is used. At lower frequencies a crossover to $\propto \nu^{-0.125}$ is expected for isotropic models if the scaling $\langle r^2(t) \rangle \propto t^{0.25}$ in regime II, which again can be taken as experimentally granted, is used in eq 4. However, this is not observed in $A(\omega)$. Instead, for both M , the whole curves continue with $\propto \nu^{-0.25}$. Below 90 kHz, i.e., in regime II the frequency dependence of $A(\omega)$ appears to be even stronger than predicted by the isotropic models.

4.3. Quadrupolar Relaxation. The intramolecular part R_1^{intra} contains an intra- and an intersegment contribution, the latter implying spin pairs located on different segments of the same macromolecule. Yet, the intersegment contribution can be neglected.^{18,31,39} This can be demonstrated by comparing the intramolecular relaxation contribution with the quadrupolar relaxation measured by FC ²H NMR. By its very nature the quadrupolar interaction measures solely the fluctuation of the C–²H bond probing the reorientational correlation function $C_2(t)$. Figure 8a shows a comparison between the relaxation data of PB-d 23k and PB-d 191k, respectively, obtained by FC ²H NMR and their protonated counterparts of similar molecular masses (PB-h 24k and PB-h 196k) measured by FC ¹H NMR. The comparison of the samples from PS is found in Appendix B. The curves measured by FC ²H NMR, for which the accessible frequency range is reduced by a factor $\gamma_H/\gamma_D = 6.51$, resemble those of FC ¹H NMR as two power-law

regimes are recognized. The differences in magnitude result from the different coupling constants ($K_Q > K_{\text{intra}}$). However, the curve of PB-d 23k appears to be shifted by a factor of around 2 toward lower frequencies with respect to PB-d 191k (as a consequence of different T_g , cf. Table 1), a fact which is not observed for the combination PB-h 196k and PB-h 24k. In regime I at $\nu \geq 90$ kHz the (M -independent) exponent $\epsilon_I = 0.78 \pm 0.05$ obtained by FC ¹H NMR (section 4.1) is well reproduced by both PB-d 23k and PB-d 191k. In regime II, $\epsilon_Q = 0.70 \pm 0.03$ and $\epsilon_Q = 0.42 \pm 0.03$ are observed for PB-d 23k and PB-d 191k (cf. Figure 8b), respectively, being in good agreement with $\epsilon_{\text{intra}} = 0.66 \pm 0.03$ and $\epsilon_{\text{intra}} = 0.44 \pm 0.03$ found by the isotope dilution technique (section 4.2). We note that no indications for a third power-law regime (III) are found in Figure 8 as one could expect from Figure 1.

Parts a and b of Figure 9 show direct comparisons between the FC ²H and the intramolecular ¹H NMR relaxation data, the latter being represented by the results for the lowest concentrations of the isotope dilution series. In the case of PB-d 23k, the data were shifted along the frequency axis first by applying a factor of 1.75, in order to coincide with those of PB-d 191k in regime I to compensate the slightly different segmental dynamics. Afterwards, the curve has been divided by a factor of 8.4, taking the different coupling constant K_Q into account, to achieve best overlap. After scaling, the FC ²H and ¹H intramolecular relaxation data agree well. Thus, we not only confirm that intersegment relaxation is negligible in FC ¹H NMR but also that the rather high power-law exponents in regime II concur for both techniques ($\epsilon_{\text{intra}} \cong \epsilon_Q$).

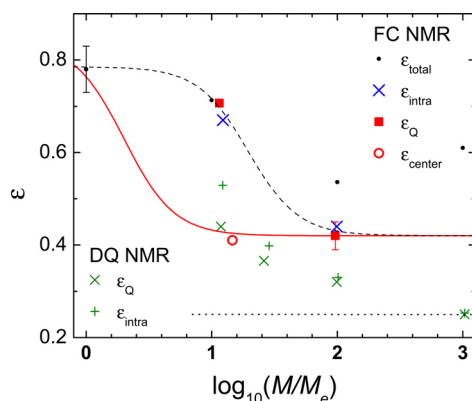


Figure 10. Power-law exponents in the entanglement regime (II) ϵ_{total} , ϵ_{intra} , ϵ_Q and ϵ_{cent} vs reduced molar mass M/M_e . Exponents from DQ ^1H NMR of PB-h diluted to $x = 0.15$ by PB-d and from DQ ^2H NMR are included for comparison.²⁷ Key: red line, suggested behavior of $\epsilon_{\text{cent}}(M)$; dashed line, $\epsilon_{\text{intra}}(M)$ guide-for-the-eye; dotted line, prediction of the TR model.

Figure 10 summarizes the exponents in regime II for the total relaxation ϵ_{total} (see also Figure 3), the intramolecular contribution ϵ_{intra} and ϵ_Q for the quadrupolar relaxation. The latter is compared to that from DQ ^1H and DQ ^2H NMR. When the pure intramolecular relaxation is considered, a clear discrepancy between both methods becomes obvious. The intramolecular exponents obtained by DQ ^1H NMR data resemble the values obtained for the total relaxation and appear to approach $\epsilon_{\text{TR}} = 0.25$ while the FC NMR data saturate at around $\epsilon_{\text{intra}}(M \rightarrow \infty) = 0.44 \pm 0.03$. Thus, although a strong intermolecular contribution (of about 50%) was found in the DQ ^1H NMR data, it appears not to be frequency dependent.²⁷ Moreover, ϵ_{intra} and ϵ_Q from DQ NMR only agree within a high error margin, while the FC NMR data are consistent here. In any case, a protracted crossover from the Rouse to the entanglement regime is revealed by both techniques.

4.4. Finite Length Effects. In order to investigate the effect of chain end dynamics we have studied the FC ^1H NMR relaxation dispersion of PB chains partially deuterated at their ends. The effect of deuterating the end sections of the polymer is 2-fold. First, the dynamics in the center of the chain is probed and, second, the intermolecular relaxation contribution is partially suppressed as spin-density is decreased. In Figure 11a,

we present the results for the two PB samples PB-dhd 5/20/4 and PB-dhd 13/6/10 (cf. Table 2) in comparison to that of PB-h 24k. Correcting for slight changes of the segmental time constant τ_s and assuming that the relaxation in the Rouse regime is not expected to be altered, shift factors of $a_T = 0.7$ for PB-dhd 5/20/4 and $a_T = 0.4$ for PB-dhd 13/6/10 have been applied along the frequency axis in order to match the curves of PB-h 24k at high frequencies. The resulting wide overlap over more than three decades in the frequency range where Rouse dynamics is probed demonstrates that it is irrelevant in this regime whether the whole chain is regarded or just the central section. Below $\nu \cdot a_T \leq 10$ kHz the dispersion curves and their corresponding apparent exponents $\alpha(\nu)$ (cf. Figure 11b) differ increasingly. In addition, the terminal relaxation becomes gradually slower. As demonstrated above (Figure 5a) the decreasing spin-density should result in accelerated terminal relaxation. However, the opposite is observed.

Neglecting the effect of the inhomogeneous distribution of protons and deuterons in the dhd polymers, the exponents $\epsilon_{\text{dhd}}(x)$ are plotted against the overall proton concentration, i.e., $x = 0.70$ in PB-dhd 5/20/4 and $x = 0.15$ in PB-dhd 13/6/10 in Figure 6. As a reference for the fully protonated system, we took the average of the exponents of PB-h 24k and PB-h 35k yielding $\epsilon_{\text{total}}(x = 1.0) \approx 0.51$ as no data for PB-h 29k were available. In strong difference to our results of the isotope dilution experiment on the fully protonated PB the exponent decreases with increasing dilution. This effect is understood such that in the case of the short chain PB the chain end dynamics strongly influence the relaxation of the fully protonated polymer. It actually overcompensates the dilution effect suppressing the intermolecular interaction. A linear extrapolation to $x \rightarrow 0$ as suggested by the observed concentration dependence provides the limit of chain dynamics not influenced by the chain end dynamics as well as by intermolecular contributions. A value $\epsilon_{\text{cent}} = 0.41 \pm 0.03$ is found; it is in very good agreement with the value obtained for the intramolecular part of PB-h 196k. In other words, the high- M limit of $\epsilon_{\text{intra}} = 0.44 \pm 0.03$, reflecting the relaxation behavior of the pure reorientational dynamics, is already reached at $M = 29\text{k}$ when solely polymer centers are considered. The effect of a protracted transition observed for the full chain dynamics again displayed in Figure 10 is not present. Thus, a rather sharp drop of the exponent from $\epsilon_i = 0.78 \pm 0.05$ in the Rouse regime to $\epsilon_{\text{intra}} = 0.44 \pm 0.03$ in regime II is

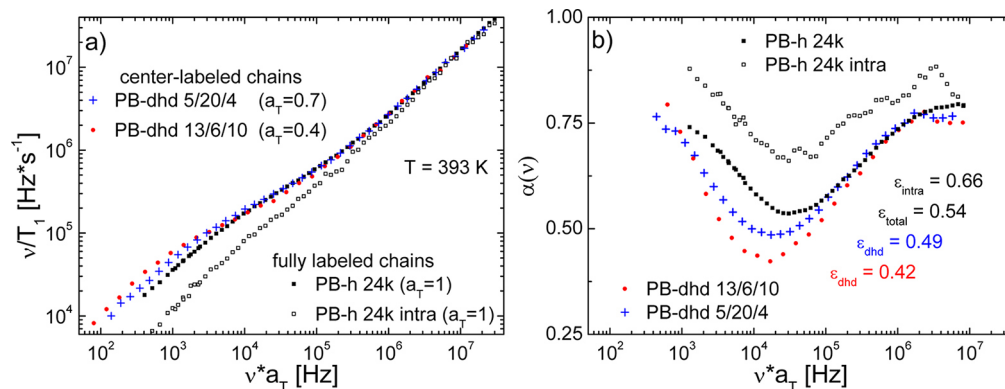


Figure 11. (a) Dispersion curves from FC ^1H NMR of partially proton labeled PB-dhd samples with similar molar masses ($M \approx 29\text{k}$) with protonated center fractions of 6.2k (red circles) and 19.6k (blue crosses). The data of fully labeled PB-h 24k and PB-h 24k in PB-d23k ($x = 0.11$) reflecting intramolecular relaxation are included. The PB-dhd data are horizontally scaled by shift factors a_T to coincide with those of PB-h 24k at high frequencies (see text). (b) Corresponding apparent power-law exponents $\alpha(\nu)$.

anticipated for the dynamics of the center sections (red solid line).

5. DISCUSSION

Field-cycling NMR relaxation dispersion data of linear, either fully protonated or fully deuterated PB bulk melts of various molar masses were reinvestigated and supplemented by new measurements. All PB samples discussed in what follows (as well as those studied by DQ NMR^{25–27}) were obtained from the same source. Refraining from the application of FTS, five decades in frequency were covered by a home-built relaxometer. Two power-laws are identified in the frequency domain. They are associated with the free Rouse (I) and the entanglement regime (II), the latter being of particular interest as a comparison with different polymer theories is to be attempted. In the case of the total relaxation (including intra- and intermolecular relaxation), it has turned out that the M -dependent exponent of regime II $\epsilon_{\text{total}}(M)$ coincides with that previously obtained by analyzing the time domain.^{8,22} The derivative method provides small corrections with respect to some of the exponents reported before.⁸ The found high- M exponent $\epsilon_{\text{total}} = 0.31 \pm 0.03$ (at $M/M_e \cong 100$) is close to the prediction of the TR model for regime II (constrained Rouse dynamics) and agrees with reports from DQ ^1H NMR.^{25–27}

Investigating a high- M polymer obtained from a different manufacturer, however, a significant difference is observed by FC ^1H as well as FC ^2H NMR. This stresses the problem of controlling the microstructure in the case of PB. Also, as learned from DSC results, deuterated and protonated polymers may show different values of T_g and thus render a direct application of the isotope dilution technique partly obsolete. Therefore, we have avoided the extrapolation of original relaxation data $R_1(\nu, x)$ to zero concentration. Instead, we have extrapolated the corresponding power-law exponents to attain the exponents of the intramolecular relaxation contribution. Still, in order to estimate the intermolecular relaxation, the isotope dilution technique is essential, and we consider the good agreement between intramolecular and quadrupolar relaxation as a support of our decomposition of the relaxation.

The intermolecular relaxation contribution is accessed for low and high M . In both cases a strong contribution is revealed in the entanglement and in the terminal relaxation regime but virtually not in the Rouse regime. In contrast to the assumption of most relaxation studies, the intermolecular contribution must not be ignored; at lowest frequencies it even becomes dominant, a fact already demonstrated by the pioneering work of Kimmich and co-workers^{7,18,31} and recently by ourselves extracting the diffusion coefficient.^{33,34,51} Concerning the intramolecular relaxation, which probes only segmental reorientation, a high- M exponent $\epsilon_{\text{intra}} = 0.44 \pm 0.03$ is found. It well agrees with that of FC ^2H NMR ($\epsilon_Q = 0.42 \pm 0.03$), yet is somewhat lower than previously obtained due to applying the derivative method for the determination of the exponent. The value, however, is significantly higher than that for the correlation function $C_2(t)$ predicted by the TR model ($\epsilon_{\text{TR}} = 0.25$). It is close to the value $\epsilon_{3RR} = 0.5$ predicted for the so-called high-mode-number limit (regime II) of the thrice-renormalized Rouse theory (cf. Figure 1).^{11,15} Any corrections of the TR model in terms of taking into account additional relaxation modes like contour length fluctuations and constraint release effects will render the model more isotropic and thus closer to the n -renormalized Rouse models. Yet, such

modified TR approaches become more and more phenomenological and more nonanalytical.

Employing coarse-grained simulations, Wang et al.⁵² accessed the rank-one and rank-two reorientational correlation functions $C_1(t)$ and $C_2(t)$, respectively, for chain lengths reaching well into the entanglement regime. They found a prolonged cross-over for $C_2(t)$ (as compared to $C_1(t)$) from the free Rouse to the entangled state. Still, for highest N an exponent $\alpha = 0.27 \pm 0.03$ has been found for flexible and $\alpha = 0.29 \pm 0.03$ for semiflexible chains. Finding at the same time that the segmental mean square displacement $\langle r^2(t) \rangle$ follows the prediction of the TR model, the authors concluded that the return-to-origin hypothesis, which leads to the proportionality of $C_{1,2}(t) \propto \langle r^2(t) \rangle^{-1}$ is well confirmed for long chains. In another recent simulation study²⁷ a similar result was reported, i.e., the exponent of $C_2(t)$ in the entanglement regime was found to follow the prediction of the TR model. As mentioned, recent DQ ^1H NMR findings also appear to be in agreement with these simulation results in clear contrast to our present findings (cf. Figure 10). The result of the DQ ^1H NMR study is particularly surprising as good agreement between FC and DQ NMR is found for the total relaxation. Here, we note that the result $\epsilon_{\text{intra}} > \epsilon_{\text{total}}$ is also confirmed for a polymer investigated from a different manufacturer (Figure 13) as well as by Kehr et al.^{7,31} The failure of the TR model when compared to the FC NMR result could be explained by assuming that the return-to-origin hypothesis applies only when microscopic details of the dynamics can be ignored. Future atomistic simulations may give an answer here.

As theoretically discussed^{18,19,39} the ratio $A(\omega) = R_1^{\text{inter}}(\omega)/R_1^{\text{intra}}(\omega)$ can reveal details of the microscopic dynamics in polymer melts. Quite different expressions result when isotropic models of polymer dynamics, like the renormalized Rouse model, are considered in opposition to the (anisotropic) TR model (cf. Theoretical Background). In accordance with Kimmich and co-workers³¹ the present study finds that the ratio grows with decreasing frequency. This is in clear contradiction to the TR model where an inverse trend is expected in regime II. The found frequency dependence of $A(\omega)$ in regime I (Rouse) is described quantitatively by the isotropic model as expected, since the Rouse model is an isotropic model. However, in the entanglement regime II, $A(\omega)$ further decreases. Again, our findings do not agree with the results from the recent DQ ^1H NMR. As mentioned, in this case no difference in the frequency dependence of total and intramolecular relaxation has been reported although actually about 50% of the correlation was attributed to the intermolecular contribution (at high M), yet apparently with the same time dependence as the total correlation function.²⁷ Here we emphasize that in any case at long times the intermolecular correlation function follows a power-law $t^{-3/2}$ being characteristic for free diffusion^{20,36,53,54} in contrast to an essentially exponential decay for the intramolecular or reorientational dynamics. This will always lead to a predominance of the intermolecular contribution at longest times. Here, the DQ NMR results appear to reveal some inconsistencies.

Investigating the influence of chain end dynamics we compare the relaxation of fully protonated and differently chain end deuterated PB for a relatively short PB chain with $M = 29k$. A strong effect is observed, i.e., an enhanced chain end mobility becomes relevant for low M . Extrapolating for solely center dynamics an exponent $\epsilon_{\text{cent}} = 0.41 \pm 0.03$ is found which is very close to the high- M value of fully protonated PB ($\epsilon_{\text{intra}} = 0.44 \pm 0.03$). Thus, the previously discussed protracted

transition^{8,23,25} to the final exponent occurring at highest M , say above $M = 500k$, observed for the total as well as for the intramolecular relaxation in the recent FC¹¹ as well as DQ ^1H NMR²⁷ studies, disappears when the polymer centers are considered. The exponent ϵ_{cent} quickly drops from its Rouse value $\epsilon_1 = 0.78 \pm 0.05$ at $M > M_e$ to the apparently M independent value $\epsilon_{\text{intra}} = 0.44 \pm 0.03$ (cf. Figure 10). As already mentioned, neutron scattering studies came to the same result and the effect was explained by contour length fluctuations.^{42,55} The relevance of chain end dynamics spoiling the TR dynamics has already been emphasized ever since the first simulation data.^{4,5,56,57}

CONCLUSIONS

Our study demonstrates that FC ^1H and ^2H NMR provide a unique opportunity to reveal details of the microscopic dynamics of polymer melts. In particular, the frequency dependence of the ratio of inter- to intramolecular relaxation rate can discriminate between different microscopic models of polymer dynamics. In the case of polybutadiene (PB), by accessing the exponent ϵ of the dipolar correlation function in the entanglement regime II, a strong influence of intermolecular relaxation is revealed. The TR model does not correctly describe the relation between segmental diffusion and reorientation, i.e., the so-called return-to-origin hypothesis fails. The found frequency dependence of the ratio of inter- to intramolecular relaxation does not support the existence of a strong restriction of the dynamics by a tube-like region. The derived exponent ϵ_{intra} is closer to the prediction of the

isotropic n-renormalized Rouse theory. Currently, the experimental disagreement between FC and previous DQ ^1H NMR regarding the exponent ϵ_{intra} cannot be resolved. The consistent results of FC ^1H and ^2H NMR provide confidence in the robustness of our findings. The previously discussed protracted transition to the final high- M exponent occurring only at highest M observed in the recent FC⁸ as well as DQ ^1H NMR²⁷ studies disappears when the polymer centers of chain end deuterated PB are considered; i.e., entanglement dynamics sets in directly at $M > M_e$. Future experiments have to be extended to other polymers in order to check whether the relaxation features revealed for PB can be generalized or whether the ratio of intra- and intermolecular relaxation might depend on the particular structure of the monomer.

APPENDIX

A. DSC Measurements

Figure 12 shows two exemplifying DSC curves measured for PB-h 24k (a) and PB-d 23k (b). Both polymers were purchased from PSS. The heating rate was 10 K/min. The T_g which have been determined at the intersection of both tangents differ by about 10 K. The T_g values of further systems are summarized in Table 1.

B. Relaxation of PB Samples from Different Suppliers

For sake of completeness, Figure 13a shows proton and deutron relaxation data of PB-h 380k and PB-d 364k, respectively, both purchased from Polymer Source, Canada. Figure 13b shows the corresponding derivatives $\alpha(\nu)$ providing $\epsilon_{\text{total}} = 0.43 \pm 0.03$ for PB-h 380k and $\epsilon_Q = 0.56 \pm 0.03$ for PB-d 364k. Again, as in the case of the other PB studied, the power-law exponent of the

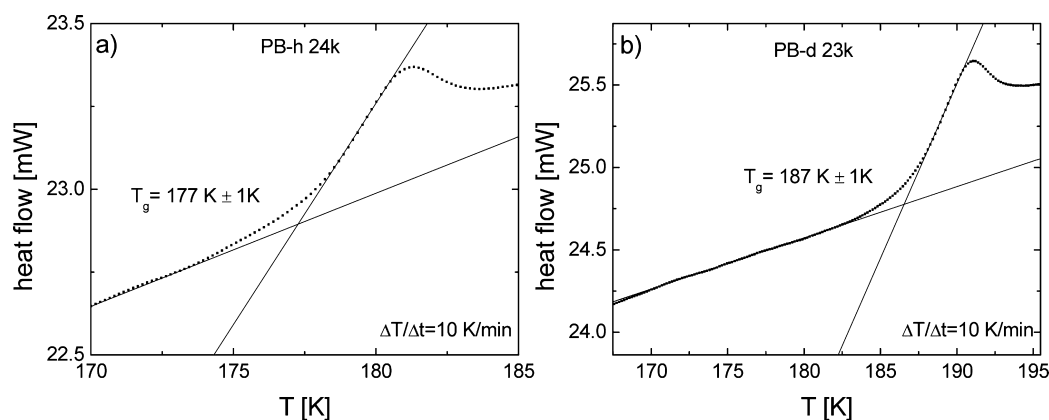


Figure 12. Selected DSC curves recorded with a heating rate of 10 K/min of PB-h 24k (a) and PB-d 23k (b) showing the glass transition.

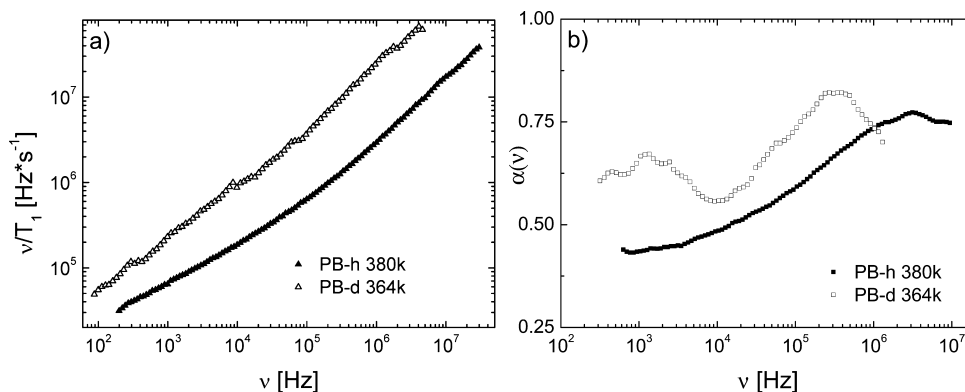


Figure 13. (a) Susceptibility curves of samples purchased from Polymer Source, namely PB-h 380k and PB-d 364k as measured by FC ^1H NMR and FC ^2H NMR, respectively. (b) Corresponding apparent exponents $\alpha(\nu)$.

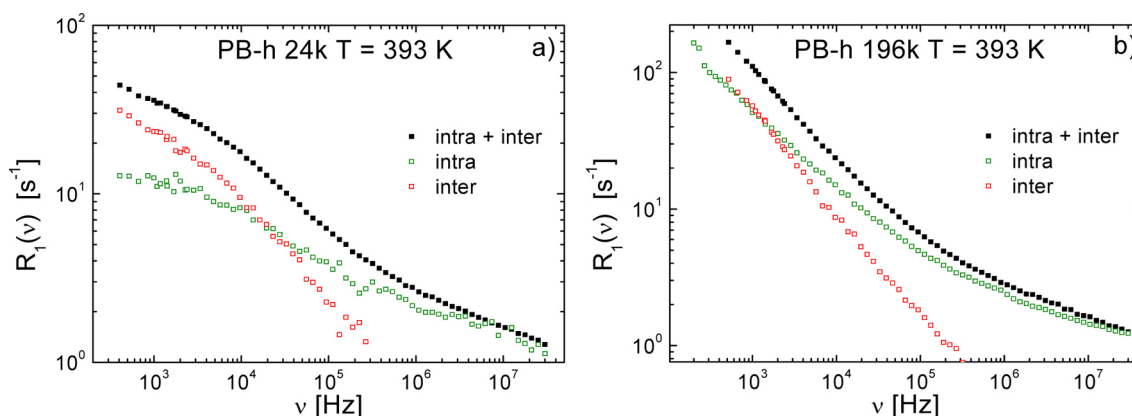


Figure 14. Intra-, inter-, and total relaxation dispersions of PB-h 24k (a) and PB-h 196k (b).

intramolecular relaxation contribution (reflected by ε_Q) is significantly higher than that of the total relaxation. Yet, the absolute values are in both cases significantly higher than for those purchased from Polymer Standards Service. Hence, it does not fit in the series.

C. Intra- and Intermolecular Relaxation Rates in PB-h

Figure 14 shows the decomposition of the total relaxation rates of PB-h 24k (a) and PB-h-196k (b), respectively, into their intra- and intermolecular contributions. The intra-parts were equated with the lowest concentrations of the dilution series. The inter-part results from subtraction from the total rate after linear interpolation of the measured frequencies. From these data the ratios $R_1^{\text{inter}}(\nu)/R_1^{\text{intra}}(\nu)$ in Figure 8 were calculated.

AUTHOR INFORMATION

Corresponding Author

*(E.A.R.) E-mail: ernst.roessler@uni-bayreuth.de.

Notes

The authors declare no competing financial interest.

ACKNOWLEDGMENTS

The authors appreciate funding through the Deutsche Forschungsgemeinschaft (DFG) in the projects SFB 481, RO 907/13, RO 907/16 (SPP 1369) and FU 308/14 and through the Elitenetzwerk Bayern. Thanks are also given to D. Richter (Jülich) for providing the partially deuterated PB. We are grateful for the opportunity of performing the DSC measurements at the Department of Macromolecular Chemistry I at the University of Bayreuth.

REFERENCES

- (1) Doi, M.; Edwards, S. F. *The Theory of Polymer Dynamics*; Oxford Sci. Publication: London, 1986.
- (2) Rouse, P. E. *J. Chem. Phys.* **1953**, *21*, 1272.
- (3) de Gennes, P. G. *J. Chem. Phys.* **1971**, *55*, 572.
- (4) Kremer, K.; Grest, G. S. *J. Chem. Phys.* **1990**, *92*, 5057.
- (5) Paul, W.; Smith, G. D. *Rep. Prog. Phys.* **2004**, *67*, 1117.
- (6) Wischniewski, A.; Monkenbusch, M.; Willner, L.; Richter, D.; Kali, G. *Phys. Rev. Lett.* **2003**, *90*, 058302.
- (7) Kehr, M.; Fatkullin, N.; Kimmich, R. *J. Chem. Phys.* **2007**, *126*, 094903.
- (8) Herrmann, A.; Kresse, B.; Gmeiner, J.; Privalov, A. F.; Kruk, D.; Fujara, F.; Rössler, E. A. *Macromolecules* **2012**, *45*, 1408.
- (9) Pahl, S.; Fleischer, G.; Fujara, F.; Geil, B. *Macromolecules* **1997**, *30*, 1414.
- (10) Callaghan, P. T.; Coy, A. *Phys. Rev. Lett.* **1992**, *68*, 3176.
- (11) Kimmich, R.; Fatkullin, N. *Adv. Polym. Sci.* **2004**, *170*, 1.

- (12) Ball, R. C.; Callaghan, P. T.; Samulski, E. T. *J. Chem. Phys.* **1997**, *106*, 7352.
- (13) Fatkullin, N.; Kimmich, R.; Weber, H. W. *Phys. Rev. E* **1993**, *47*, 4600.
- (14) Kimmich, R.; Weber, H.; Stapf, S.; Fatkullin, N. *J. Non Cryst. Solids* **1994**, *172*, 689.
- (15) Schweizer, K. S. *J. Chem. Phys.* **1989**, *91*, 5802.
- (16) Schweizer, S. J. *J. Chem. Phys.* **1989**, *91*, 5822.
- (17) Krutyeva, M. A.; Fatkullin, N. F.; Kimmich, R. *Polym. Sci., Ser. A* **2005**, *47*, 1716.
- (18) Fatkullin, N.; Gubaidullin, A.; Stapf, S. *J. Chem. Phys.* **2010**, *132*, 094903.
- (19) Rössler, E. A.; Stapf, S.; Fatkullin, N. *Curr. Opin. Colloid Interface Sci.* **2013**, *18*, 173.
- (20) Meier, R.; Kruk, D.; Rössler, E. A. *ChemPhysChem* **2013**, *14*, 3071.
- (21) Kariyo, S.; Gainaru, C.; Schick, H.; Brodin, A.; Rössler, E. A. *Phys. Rev. Lett.* **2006**, *97*, 207803. Erratum: Kariyo, S.; Herrmann, A.; Gainaru, C.; Schick, H.; Brodin, A.; Rössler, E. A. *Phys. Rev. Lett.* **2008**, *100*, 109901.
- (22) Herrmann, A.; Kresse, B.; Gmeiner, J.; Privalov, A. F.; Kruk, D.; Fujara, F.; Rössler, E. A. *Macromolecules* **2012**, *45*, 6516.
- (23) Hofmann, M.; Herrmann, A.; Abou Elfadl, A.; Kruk, D.; Wohlfahrt, M.; Rössler, E. A. *Macromolecules* **2012**, *45*, 2390.
- (24) Saalwächter, K. *Prog. Nucl. Magn. Reson. Spectrosc.* **2007**, *51*, 1.
- (25) Vaca Chávez, F.; Saalwächter, K. *Phys. Rev. Lett.* **2010**, *104*, 198305.
- (26) Vaca Chávez, F.; Saalwächter, K. *Macromolecules* **2011**, *44*, 1549.
- (27) Furtado, F.; Damron, J.; Trutschel, A. L.; Franz, C.; Schröter, K.; Ball, R. C.; Saalwächter, K.; Panja, D. *Macromolecules* **2014**, *47*, 256.
- (28) Strobl, G. *Condensed Matter Physics*; Springer Verlag: Berlin and Heidelberg, Germany, 2004.
- (29) Rubinstein, M.; Colby, R. H. *Polymer Physics*; Oxford University Press: Oxford, U.K., 2003.
- (30) Graessley, W. W. *Polymeric Liquids & Networks: Dynamics and Rheology*; Taylor and Francis: New York, 2008.
- (31) Kehr, M.; Fatkullin, N.; Kimmich, R. *J. Chem. Phys.* **2007**, *127*, 084911.
- (32) Meier, R.; Kruk, D.; Gmeiner, J.; Rössler, E. A. *J. Chem. Phys.* **2012**, *136*, 034508.
- (33) Kruk, D.; Meier, R.; Rössler, E. A. *Phys. Rev. E* **2012**, *85*, 020201.
- (34) Meier, R.; Herrmann, A.; Hofmann, M.; Schmidtke, B.; Kresse, B.; Privalov, A. F.; Kruk, D.; Fujara, F.; Rössler, E. A. *Macromolecules* **2013**, *46*, 5538.
- (35) Fatkullin, N.; Mattea, C.; Stapf, S. *J. Chem. Phys.* **2013**, *139*, 194905.
- (36) Henritzi, P.; Bormuth, A.; Vogel. *Solid State Nucl. Magn. Reson.* **2013**, *54*, 32.
- (37) Kresse, B.; Privalov, A. F.; Fujara, F. *Solid State Nucl. Magn. Reson.* **2011**, *40*, 134.

- (38) Kresse, B.; Privalov, A. F.; Hofmann, M.; Rössler, E. A.; Fujara, F. *Solid State Nucl. Magn. Reson.* **2014**, *59–60*, 45.
- (39) Fatkullin, N.; Stapf, S. J.; Hofmann, M.; Meier, R.; Rössler, E. A. *J. Non-Cryst. Solids* **2014**, submitted.
- (40) Kimmich, R.; Fatkullin, N.; Seitter, R. O.; Gille, K. J. *J. Chem. Phys.* **1998**, *108*, 2173.
- (41) Fuchs, M.; Schweizer, K. S. *Macromolecules* **1997**, *30*, 5133.
- (42) Zamponi, M.; Monkenbusch, M.; Willner, L.; Wischniewski, A.; Farago, B.; Richter, D. *Europhys. Lett.* **2005**, *72*, 1039.
- (43) Abragam, A. *The Principles of Nuclear Magnetism*; Clarendon Press: Oxford, U.K., 1961.
- (44) Bloembergen, N.; Purcell, E. M.; Pound, R. V. *Phys. Rev.* **1948**, *73*, 679.
- (45) Zeidler, M. D. *Ber. Bunsen-Ges. Phys. Chem.* **1965**, *69*, 659.
- (46) Fetters, L. J.; Lohse, D. J.; Richter, D.; Witten, T. A.; Zirkel, A. *Macromolecules* **1994**, *27*, 4630.
- (47) Lusceac, S. A.; Gainaru, C.; Vogel, M.; Koplin, C.; Medick, P.; Rössler, E. A. *Macromolecules* **2005**, *38*, 5625.
- (48) Hadjichristidis, N.; Iatrou, H.; Pispas, S.; Pitsikalis, M. *J. Polym. Sci., Part A: Polym. Chem.* **2000**, *38*, 3211.
- (49) Lips, O.; Privalov, A. F.; Dvinskikh, S. V.; Fujara, F. *J. Magn. Reson.* **2001**, *149*, 22.
- (50) Hintermeyer, J.; Herrmann, A.; Kahlau, R.; Goiceanu, C.; Rössler, E. A. *Macromolecules* **2008**, *41*, 9335.
- (51) Meier, R.; Herrmann, A.; Kresse, B.; Privalov, A. F.; Kruk, D.; Fujara, F.; E.A. Rössler, E. A. *ACS Macro Lett.* **2012**, *1*, 1339.
- (52) Wang, Z.; Likhtman, A. E.; Larson, R. G. *Macromolecules* **2012**, *45*, 3557.
- (53) Sholl, C. A. *J. Phys. C: Solid State Phys.* **1981**, *14*, 447.
- (54) Belorizky, E.; Fries, P. H. *Chem. Phys. Lett.* **1988**, *145*, 33.
- (55) Wischniewski, A.; Monkenbusch, M.; Willner, L.; Richter, D.; Likhtman, A. E.; McLeish, T. C. B.; Farago, B. *Phys. Rev. Lett.* **2002**, *88*, 058301.
- (56) Likhtman, A. E.; McLeish, T. C. B. *Macromolecules* **2002**, *35*, 6332.
- (57) Bormuth, A.; Hofmann, M.; Henritzi, P.; Vogel, M.; Rössler, E. A. *Macromolecules* **2013**, *46*, 7805.

Publication 3

Dynamics of PPI Dendrimers: A Study by Dielectric
and ^2H NMR Spectroscopy and by
Field-Cycling ^1H NMR Relaxometry

*Mohamed, F.; Hofmann, M.; Pötzschner, B.; Fatkullin, N.;
Rössler, E. A.*

Macromolecules **2015**, 48, 3294-3302.

DOI: 10.1021/acs.macromol.5b00486

(Copyright 2015 by The American Chemical Society)

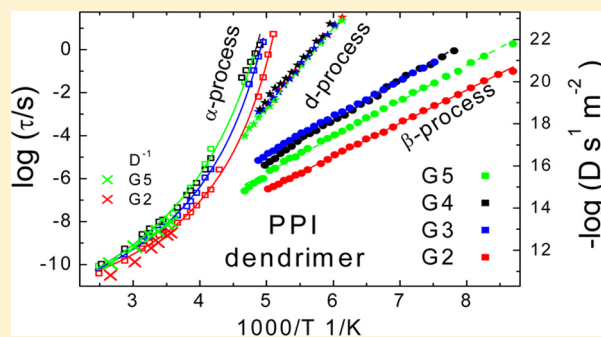
Dynamics of PPI Dendrimers: A Study by Dielectric and ^2H NMR Spectroscopy and by Field-Cycling ^1H NMR Relaxometry

F. Mohamed,[†] M. Hofmann,[†] B. Pötzschner,[†] N. Fatkullin,[‡] and E. A. Rössler^{*,†}

[†]Experimentalphysik II, Universität Bayreuth, 95440 Bayreuth, Germany

[‡]Institute of Physics, Kazan Federal University, Kazan 420008, Tatarstan Russia

ABSTRACT: We investigate bulk poly(propyleneimine) dendrimers of generation (G) 2–5 by dielectric spectroscopy (DS), solid-state ^2H NMR, and field-cycling ^1H NMR relaxometry (FC ^1H NMR) in a large temperature range (120–400 K). Three relaxation processes are identified by DS: a main (α -) relaxation ($T > T_g$) and two secondary processes ($T < T_g$). The α -process exhibits a super-Arrhenius temperature dependence typical of glass-forming liquids and changes only weakly with G , yielding $T_g \sim 200$ K. The temperature dependence of the secondary relaxations is governed by an Arrhenius law. While one secondary process exhibits features characteristic for glasses, the other is atypical. Its time constant is virtually independent of G , and its spectral width does not increase with lowering temperature as is usually observed for sub- T_g relaxations. Regarding FC ^1H NMR probing the dispersion of the spin–lattice rate R_1 in the frequency range 200 Hz–30 MHz, transformation to the susceptibility representation, $\chi''(\omega) \equiv \omega R_1(\omega)$, and applying frequency–temperature superposition, an effective frequency range of 9 decades is covered by a master curve $\chi''(\omega\tau_\alpha)$. In addition to the segmental time $\tau_\alpha(T)$, which complements the results from DS up to high temperatures, a longer terminal relaxation $\tau_t(T)$ is identified. In between, an intermediate power-law regime is observed in $\chi''(\omega\tau_\alpha)$ with an exponent of about 0.8. The broad relaxation spectrum is attributed to local dynamics, breathing modes, and overall tumbling and diffusion of the dendrimer molecule. In the low-frequency limit, $R_1(\omega)$ is determined by intermolecular relaxation from which the molar mass dependence of the translational diffusion coefficient can be estimated. We find $D(M) \propto M^{-1.2 \pm 0.2}$.



1. INTRODUCTION

Dendrimers as a special type of macromolecular architecture offer an interesting field of investigations in physics and chemistry.^{1–5} Starting from a central point with a functionality f , segments of uniform length again with functionality f are attached. Thereby “shells” of segments are created, and each shell defines a generation starting with $G = 0$ for the functional center. Dendrimers are thus perfectly monodisperse, and as mass grows faster than volume, the number of generations G is limited. Yet, the actual maximum depends on the chemistry of the segment. The latter also strongly determines structure and dynamics of the dendrimers.

Here we focus on bulk poly(propyleneimine) (PPI) dendrimers with $f = 3$. Generations 2–5 can be synthesized and purchased commercially. At room temperature they constitute liquids of high viscosity, and cooling below the glass transition temperature T_g (around 200 K) yields transparent glasses. The dendrimer structure is soft enough to allow for partial interpenetration, however, the extent of which decreases with generation.⁶ Entanglement effects, as in the case of long-chain polymers, do not occur.^{7,8} Correspondingly, the viscosity is significantly lower than in entangled linear polymers.⁷ According to MD simulations, the dendrimers become more compact and spherical as the generation number grows, and also dendra turn

inward.^{6,9} Thus, the end amine groups are spread more and more uniformly over the entire dendrimer volume. The overall density profile decreases gradually from the center to the surface of the molecule while the radius of gyration scales approximately with the cubic root of the number of segments. This structural picture sketched by simulation data essentially agrees with experimental studies.^{3,6,9}

While several studies on the solution behavior were published, up to our knowledge not many experiments were done attempting to unravel the dynamics in bulk dendrimers. Values of T_g for neat and end group modified PPI, linear and nonlinear rheological behavior, and the M dependence of the zero-shear viscosity were reported.⁸ Detailed rheological results were also reported for polyamidoamine (PAMAM) dendrimers.⁷ No entanglement (rubber) plateau was observed in the dynamic modulus, indicating, as mentioned, the absence of entanglement effects. Altogether, one finds a relaxation behavior showing some reminiscence of melts of polymer chains below their entanglement molar mass. That is, in addition to segmental dynamics determined by the glass transition phenomenon,⁴ a

Received: March 6, 2015

Revised: April 17, 2015

Published: May 4, 2015

spectrum of slower modes appears. Indeed, the Rouse model¹⁰ was applied to reproduce the rheological behavior, yet deviations were found.⁷ Also, secondary relaxation processes as usually observed in molecular glasses were reported for other dendrimers.^{11,12} A number of MD simulations as well as theoretical approaches deal with the dynamics of particular dendrimer models.^{4–6,9,13–17}

In the present work we investigate the dynamics of PPI dendrimers by dielectric and NMR spectroscopy. A large temperature range is covered (120–400 K) comprising the melt ($T > T_g$) as well as the glassy state ($T < T_g$). In the case of NMR we present results from solid-state ^2H NMR and from field-cycling (FC) ^1H NMR relaxometry. The latter technique has gained new momentum with the availability of commercial spectrometers.^{18–22} In contrast to existing NMR studies on dendrimers mostly in solution,^{23–26} which characterize the spin–lattice relaxation time T_1 at a few frequencies (magnetic fields), the FC method probes the frequency dependence of the relaxation rate $1/T_1 = R_1(\omega)$ usually in the frequency ($\omega/2\pi$) range 10 kHz–20 MHz. Taking recourse to a self-built FC relaxometer,²⁸ we were able to reach a low-frequency limit of 200 Hz. Converting the relaxation data to the susceptibility representation $\chi''(\omega) \equiv \omega R_1(\omega)$ and applying frequency–temperature superposition (FTS), an approach well-known from rheological studies,²⁷ a large effective frequency range is covered by a master curve $\chi''(\omega\tau_\alpha)$. It reveals both local and collective segmental dynamics.^{29–33} Here $\tau_\alpha = \tau_\alpha(T)$ denotes the time scale of the local segmental dynamics. The evolution of $\chi''(\omega\tau_\alpha)$ with molar mass M will be compared to that of linear polymers. Moreover, as the low-frequency dispersion is determined by translational dynamics, we are able to extract the diffusion coefficient $D(M)$.

2. EXPERIMENTAL SECTION

2.1. Systems. We investigated the dynamics of PPI dendrimers in bulk, which were purchased from SyMO-Chem BV (University of Eindhoven) and used without further treatment. In the case of FC ^1H NMR the samples were degassed to remove paramagnetic oxygen. The chemical structure of generation 2 is shown in Figure 1. For each further

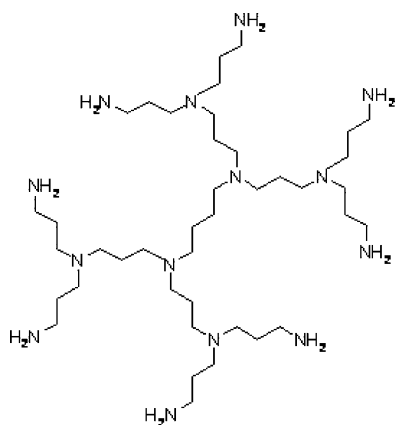


Figure 1. Idealized structure of the PPI dendrimer of generation 2.

generation the number of amine end groups doubles. We investigated dendrimers of generation 2 (G2), 3 (G3), 4 (G4), and 5 (G5); higher generations are not available for this type of dendrimer. For the ^2H NMR investigations, the amine end groups were deuterated by dissolving the dendrimers in deuterated water and evaporating the water again. The procedure was repeated twice. The glass transition temperature T_g was determined by DSC experiments (cf. Table 1).

2.2. Dielectric Spectroscopy. Dielectric measurements were carried out with an Alpha-A Analyzer by Novocontrol, which allows for frequency-resolved measurements of the dielectric permittivity in the range 10^{-2} – 10^6 Hz. Temperature stability was ± 0.2 K controlled by a Quatro-H temperature controller (Novocontrol). The absolute accuracy is better than ± 0.5 K. The sample cell is designed as described in ref 34 and guarantees constant plate distance while cooling.

In most of the PPI dendrimer samples a pronounced dc conductivity is observed in the dielectric loss $\epsilon''(\omega)$ ($T > T_g$), which is subtracted by using the expression $\epsilon_{dc}''(\omega) = \sigma_{dc}/(\epsilon_0\omega)$ (cf. Figure 12). All time constants were estimated by “peak picking”; i.e., the condition $\tau_i = 1/(2\pi\nu_{\max})$ was applied. In the case of the two secondary processes (“d” and “b”) a sum of a distribution of correlation times $G(\ln \tau)$ appropriate for thermally activated relaxation processes³⁵ was chosen for interpolating the dielectric spectra, explicitly

$$\epsilon^*(\omega) = \Delta\epsilon \int_{-\infty}^{\infty} \frac{G(\ln \tau)}{1 + i\omega\tau} d \ln \tau + \epsilon_{\infty} \quad (1)$$

with

$$G(\ln \tau) = AN_{\beta} \frac{1}{b_{\beta} \left(\frac{\tau}{\tau_{\beta}} \right)^{a_{\beta}} + \left(\frac{\tau}{\tau_{\beta}} \right)^{-a_{\beta} b_{\beta}}} + (1 - A)N_d \frac{1}{b_d \left(\frac{\tau}{\tau_d} \right)^{a_d} + \left(\frac{\tau}{\tau_d} \right)^{-a_d b_d}} \quad (2)$$

and the normalization factors

$$N_{i \in \{d, \beta\}}(a_i, b_i) = \frac{a_i(1 + b_i)}{\pi} b_i^{b_i/(1+b_i)} \sin \left(\frac{\pi b_i}{1 + b_i} \right) \quad (3)$$

The coefficients A and $(1 - A)$ define the relative weight of the individual contributions. The parameter a causes a symmetric broadening of the distribution while the “asymmetry parameter” b only affects its short time flank. After Laplace transformation, the resulting susceptibility peak is symmetrically broadened by a , which is also the exponent of the power-law asymptotically approached by the peak’s low-frequency flank. The exponent of the power-law asymptote of the high-frequency flank is given by the product ab .

2.3. ^2H NMR. Solid-state ^2H NMR spectra of the end group deuterated dendrimers are dominated by the interaction of the nuclear quadrupolar moment with the electric field gradient (EFG), and the NMR angular frequency depends on the spherical angles (θ, ϕ) between the EFG tensor axis and the magnetic field direction³⁶

$$\omega_Q(\theta, \phi) = \pm \delta_Q/2(3 \cos^2 \theta - 1 - \eta \sin^2 \theta \cos(2\phi)) \quad (4)$$

where $\omega_Q(\theta, \phi)$ is the shift of the resonance frequency with respect to the Larmor frequency ω . The parameter δ_Q is the anisotropy and η the asymmetry parameter of the EFG tensor. In the case of an isotropic distribution of tensor orientations and $\eta = 0$, a so-called Pake spectrum is observed, which is measured with a solid-echo pulse sequence.³⁶ At high temperatures the two-site reorientation of the dendrimer’s amine groups becomes faster than the NMR time scale ($\tau_{\text{jump}} \ll 1/\delta_Q$), which leads to a motion-averaged powder spectrum with $\bar{\eta}$ close to one (cf. below and Figure 6). In the case of an isotropic reorientation occurring at even higher temperatures a Lorentzian line typical for a liquid results. Under the condition $1/\delta_Q \gg \tau_\alpha \gg \omega^{-1}$, for which effects from the crossover to a solid-state spectrum and from field inhomogeneity, respectively, can be ignored, the full half-width $\Delta\nu$ of the line is related to the transversal relaxation time T_2 via $\Delta\nu = 1/\pi T_2$, and one can estimate the reorientational correlation time τ_α from³⁷ $1/T_2 = (1/5)\bar{\delta}_Q^2(1 + \bar{\eta}^2/3)\tau_\alpha$ where $\bar{\delta}_Q = 2\pi \cdot 90$ kHz is the motionally averaged anisotropy parameter and $\bar{\eta} = 0.9$ due to the fast 180° two-site jumps.

The ^2H NMR experiments were performed on an upgraded Bruker Avance DSX spectrometer and a 300 MHz Oxford cryomagnet. The ^2H Larmor frequency is $\omega = 46.067$ MHz for a magnetic field of 7 T. The pulse length of a $\pi/2$ pulse was 2.8 μs . The recovery delay after applying a saturation sequence of 5 $\pi/2$ pulses was at least $4T_1$ and 8-fold phase

Table 1. Properties of the Investigated PPI Dendrimers: Molecular Formula, Molar Mass, Number of Amine Groups, Glass Transition Temperature (T_g) from DSC and Dielectric Relaxation (DS), Activation Energy E_A/R , and Attempt Time τ_∞ of the β -Process

generation	molecular formula	molar mass [g/mol]	no. of amine end groups	T_g [K] (DSC)	T_g [K] (DS)	$E_A/R(\beta)$ [K]	$\tau_\infty(\beta)$ [s]
2	$C_{40}N_{14}H_{96}$	773.3	8	195	196	3522	5×10^{-15}
3	$C_{88}N_{30}H_{208}$	1686.8	16	198	200	3914	2×10^{-14}
4	$C_{184}N_{62}H_{432}$	3513.9	32	204	204	4282	5.2×10^{-15}
5	$C_{372}N_{126}H_{880}$	7198.1	64	200	200	3868	5.5×10^{-16}

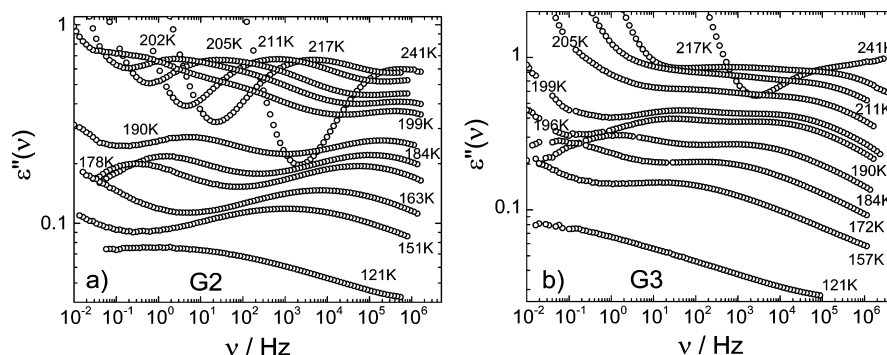


Figure 2. (a) Dielectric spectra of PPI dendrimer G2 as measured for temperatures 121 to 241 K as indicated. (b) Analogous spectra of PPI dendrimer G3 from 121 to 241 K.

cycling was applied for collecting the solid-echo spectra with a pulse delay of 10 μ s. The home-built 2H NMR probe was cooled by liquid nitrogen with a CryoVac Konti cryostat and an Oxford ITC-503 temperature controller with temperature accuracy better than ± 1 K and temperature stability better than ± 0.2 K.

2.4. Field Cycling 1H NMR. The spin–lattice relaxation time T_1 describes the recovery of the nuclear magnetization toward its equilibrium value. Its frequency dependence can be studied by applying the FC technique where the external magnetic field is switched between a variable relaxation field B and a constant detection field.¹⁸ The angular frequency is given by the Larmor frequency $\omega = \gamma B$, where γ denotes the gyromagnetic ratio. Usually, T_1 reflects intra- and intermolecular relaxations contributions, and the measured rate $R_1 = 1/T_1$ is given by $R_1(\omega) = R_1^{\text{intra}}(\omega) + R_1^{\text{inter}}(\omega)$.^{18,37} The role of the two relaxation paths was elucidated by not only measuring the fully protonated system but also the dendrimer with the protons at the amine groups exchanged by deuterons used for the 2H NMR experiments (cf. above).

Rewriting the Bloembergen–Purcell–Pound (BPP) expression in the susceptibility representation yields^{29–33,37}

$$\omega R_1(\omega) = C[\chi''(\omega) + 2\chi''(2\omega)] \equiv 3C\omega J_{\text{NMR}}(\omega) = 3C\chi''_{\text{NMR}}(\omega) \quad (5)$$

where $\chi''(\omega) = \omega J(\omega)$ is the susceptibility with the spectral density $J(\omega)$, and C denotes the coupling constant of the magnetic dipole–dipole interaction. In the case of intramolecular relaxation $J(\omega)$ is given by the Fourier transform of the rank-two reorientational correlation function $C_2(t)$ of a dendrimer segment, more precisely of the internuclear vectors of the proton spin pairs in the segment. Although $\chi''_{\text{NMR}}(\omega)$ and $J_{\text{NMR}}(\omega)$ are actually weighted sums, in the case of a broad distribution of correlation times, both quantities are essentially indistinguishable on logarithmic scales from $\chi''(\omega)$ and $J(\omega)$, respectively, besides the factor of 3.

As said, the actually measured relaxation rate contains both intra- and intermolecular contributions and follows a similar equation like eq 5. Thus, the spectral density splits up into two parts. While the intra part reflects segmental reorientation, the inter part probes translational motion. The correlation functions $C_2(t)$ and $C_{\text{trans}}(t)$ exhibit quite different long-time behavior. While $C_2(t)$ decays stretched exponentially for long times, $C_{\text{trans}}(t)$ follows a power law $t^{-3/2}$ reflecting Fickian diffusion and therefore will always dominate the total correlation function in the limit of long times.^{38–40} Thus, at low frequencies the relaxation dispersion $R_1(\omega)$ follows a square root law, explicitly

$$R_1(\omega) = R_1^{\text{intra}}(\omega) + R_1^{\text{inter}}(\omega) = R_1(0) - \frac{B}{D^{3/2}}\sqrt{\omega} \quad (6)$$

with

$$B = \frac{\pi}{30}(1 + 4\sqrt{2})\left(\frac{\mu_0}{4\pi}\hbar\gamma_H^2\right)^2 n_s$$

and the spin density $n_s = 7.3 \times 10^{28} \text{ m}^{-3}$ in the case of the dendrimers. This relation was recently exploited to determine the diffusion coefficient $D(T)$ in simple liquids⁴⁰ as well as in polymers,⁴¹ and it will be employed here to estimate the $D(T, M)$ of the PPI dendrimers.

As a large temperature range is covered, local segment dynamics as well as dendrimer specific dynamics are probed and one is able to construct master curves $\chi''_{\text{NMR}}(\omega\tau_a)$ extending over many decades in time by assuming frequency–temperature superposition (FTS). Specifically, the individual data sets measured at different temperatures are shifted solely horizontally to obtain best overlap.^{30–33} The master curves $\chi''_{\text{NMR}}(\omega\tau_a)$ thus combine $R_1(\omega)$ results from a broad temperature range and yield “isofrictional” spectra which allow comparing the results for different dendrimer generations. As the high-frequency part reflects the α -dynamics, which is interpolated by a Cole–Davidson function, the construction of the master curves provides the time constants $\tau_a(T)$.^{29–33} For simple liquids, no spectral contribution at $\omega\tau_a < 1$ in excess to the Debye behavior $\chi''(\omega) \propto \omega^{-1}$ is observed except for some weak intermolecular contributions. Any additional low-frequency relaxation thus reflects dendrimer specific dynamics.

The dispersion of the spin–lattice relaxation time T_1 was monitored by a STELAR FFC 2000 relaxometer, which allows measurements in the temperature range 160–420 K and in (Larmor) frequency range 10 kHz $\leq \nu \leq 20$ MHz.^{18,30} The accuracy and stability of the temperature measurements are typically ± 1 K. Concerning G4 and G5 the $T_1(\omega)$ measurements performed in Bayreuth were complemented by two data sets obtained at the Technical University of Darmstadt. There, a home-built relaxometer allows for extremely low frequencies via active field stabilization and stray field compensation.²⁸ The lower limit is 200 Hz being well below the limitations of the STELAR machine and even below the earth’s magnetic field. This gives access to extremely slow dendrimer dynamics.

The magnetization curves for all dendrimers investigated feature a monoexponential decay at $T < 300$ K. With temperature growing the decay curves develop an increasingly stretched form which is well describable by a stretched exponential function $\propto \exp[-(t/T_1^K)^\beta]$. The

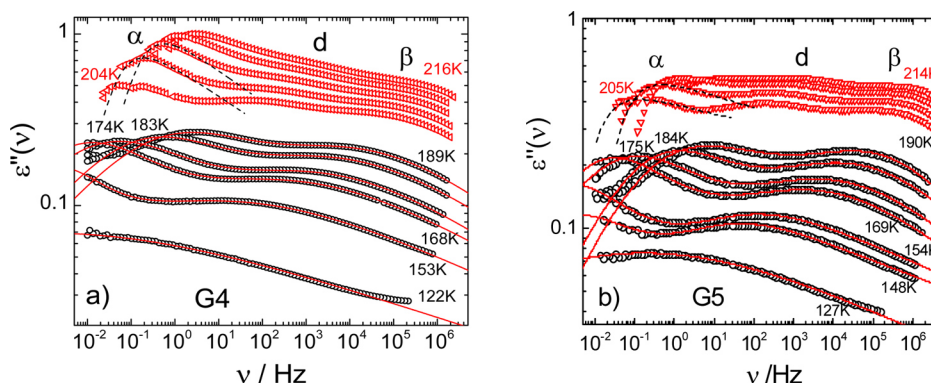


Figure 3. Dielectric loss after subtracting the dc conductivity contribution of PPI dendrimer G4 (a) and G5 (b); red triangles: $T > T_g$ in 3 K steps; black circles: $T < T_g$ (selected data); solid red lines: fits by a sum of two subspectra along eq 2 corresponding to d - and β -processes; dashed black lines: Cole–Davidson fits of the α -relaxation.

(mean) relaxation time follows from $\langle T_1 \rangle = T_1^K \beta^{-1} \Gamma(\beta^{-1})$ which is generally used in this work. The stretching parameter decreases only slightly between $\beta = 1$ at low temperatures and $\beta \approx 0.8$ at $T \approx 400$ K.

3. RESULTS

3.1. Dielectric Spectra. Figure 2 shows dielectric spectra as measured at different temperatures for the generation G2 and G3 of the PPI dendrimer. In Figure 11 we display the corresponding spectra of G4 and G5. Three rather broad and barely separated relaxation processes are recognized at high temperatures. The relaxation peak at lowest frequencies is partly covered by a dc conductivity contribution, most obviously for G3, G4, and G5 (cf. Figures 11 and 12). With decreasing temperature the low-frequency peak leaves the acquisition window and the other two relaxations become better resolved while shifting to lower frequencies. In addition, below T_g their amplitudes appear to decrease and their widths to broaden. This is typical for secondary processes in molecular glasses.⁴² Figure 3 shows the DS spectra of G4 and G5 after subtracting the dc contribution (see Figure 12). Above T_g (data marked in red) the three relaxation processes can be distinguished. Inspecting also the corresponding spectra of G2 (Figure 2) and G3 (Figure 12), one can conclude that relaxation patterns are rather similar for all generations: PPI dendrimers show three relaxation processes which we call, for reasons becoming clear below, α , d (d for dendrimer), and β , according to the order of their appearance in the DS frequency window upon cooling. At lowest temperatures only the β -relaxation can be probed in the given frequency window.

In order to extract time constants for α , d , and β -relaxation, we take the estimate $\tau_i = 1/(2\pi\nu_{\max})$. The results for all generations are shown in Figure 4. Close to T_g (measured by DSC, cf. Table 1) the segmental time constant $\tau_\alpha(T)$ exhibits a strong temperature dependence and reaches values of the order of seconds. This is typical of the structural relaxation (α -process) in supercooled liquids or polymer melts and justifies this assignment. Moreover, the time constants fit well to the high-temperature data compiled by the NMR techniques (cf. below) included in Figure 4. Considering all data the temperature dependence is describable by a Vogel–Fulcher–Tammann (VFT) law. Because of quite similar T_g the different $\tau_\alpha(T)$ almost coincide around 200 K. In Table 1, T_g values obtained via the condition $T_g = T(\tau_\alpha = 100 \text{ s})$ are compared to those from DSC experiments; very good agreement is found. We note that also the dc conductivity $\sigma(T)$ extracted from the original data

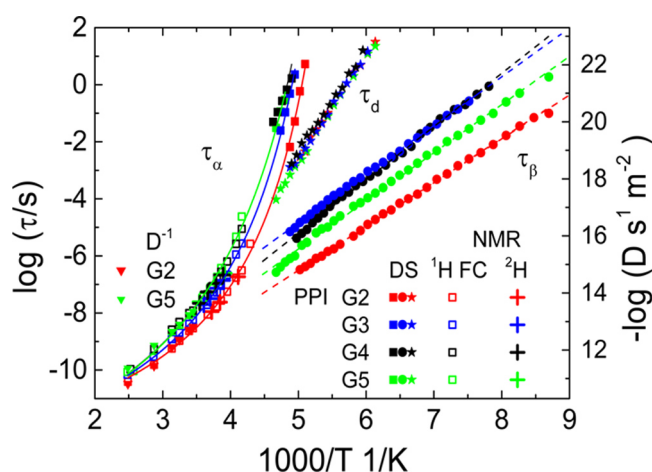


Figure 4. Time constants of the PPI dendrimers for the different relaxations identified by the different techniques. Structural relaxation times τ_α : dielectric spectroscopy (DS, filled squares), FC ^1H NMR (open squares), solid-state ^2H NMR (crosses). Time constants τ_d and τ_β of the d - and the β -process as provided by DS (stars and circles, respectively); the color code for the generations is given in the legend. Solid lines: VFT interpolations for $\tau_\alpha(T)$; dashed lines: Arrhenius fits for d - and β -process. Triangles: diffusion coefficient $D(T)^{-1}$ referred to the right ordinate.

exhibits a temperature dependence similar to that of $\tau_\alpha(T)$. Usually, dc conduction in molecular liquids or polymers originates from diffusion of ionic impurities. Thus, conductivity is coupled to the viscosity of the host. Concerning the stretching parameter of the α -relaxation, we find a value $\beta_{\text{CD}} = 0.3$ when applying a Cole–Davidson function.⁴³

The other two relaxations (d and β) show an Arrhenius temperature dependence of their time constants characteristic for secondary processes in glasses ($T < T_g$) (cf. Figure 4). The d -relaxation displays a time constant which is virtually independent of the number of generations while that of the β -relaxation shows some differences. Yet, no systematic trend can be identified. The Arrhenius law for the d -process yields a rather high activation energy $E_A/R = 8520 \text{ K}$ ($E_A/RT_g \cong 42$) and an attempt time $\tau_\infty = 5.3 \times 10^{-22} \text{ s}$, which is exceptionally low. Regarding the β -process, E_A and τ_∞ are listed in Table 1. Its activation energy is found in the range $18 < E_A/RT_g < 21$. The corresponding τ_∞ values range within $5 \times 10^{-16} - 2 \times 10^{-14} \text{ s}$, which is typical for β -processes in glasses.⁴²

Below T_g a quantitative interpolation of the DS spectra is possible using the distribution $G(\ln \tau)$ defined in eq 2. The asymmetry parameter b was kept constant. The corresponding fits are included in Figure 3 and well reproduce the spectra. As demonstrated in Figure 5, the parameter ab of the β -process

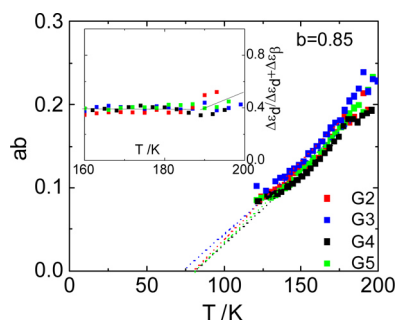


Figure 5. Temperature dependence of the spectral shape parameter ab (cf. eq 2) of the β -process; asymmetry parameter b is kept constant. Inset: temperature dependence of the dielectric strength of the d -process with respect to that of the sum of both β - and d -processes.

decreases essentially linearly upon cooling, which is the typical trend of a β -process in glasses,⁴² while the parameter ab of the d -process is temperature-independent for all generations. Thus, this relaxation is atypical. In order to illustrate directly the spectral changes of the secondary relaxations, we display in Figure 13a rescaled spectra of G2, for which $\epsilon''(\omega)/\epsilon''_{d,\max}$ is plotted versus $\nu/\nu_{d,\max}$ with $\epsilon''_{d,\max}$ and $\nu_{d,\max}$ denoting the height and frequency of the d -relaxation peak, respectively. Figure 13b shows the analogous scaling for the β -process. It is apparent that FTS applies for the d -process while the β -relaxation broadens upon cooling, so FTS does not hold for the latter. Finally, the inset of Figure 5 displays the temperature dependence of the relative dielectric strength of the d -process. The ratio does not change and is temperature independent below T_g while it tends to increase above T_g .

3.2. Solid-State NMR. Figure 6 shows the ^2H NMR spectra for all the generations of PPI dendrimers beginning with G2 in the left column to G5 in the right column in a temperature range from 110 to 240 K. The temperature at which the spectra were

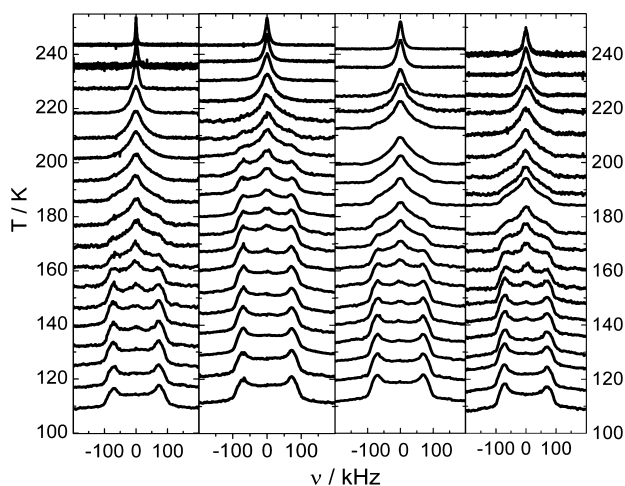


Figure 6. ^2H NMR spectra for generation G2 to G5 (from left to right). The baseline of each spectrum indicates the temperature at which the spectrum was measured.

measured is given by the baseline of the spectra. At lowest temperatures a typical Pake spectrum with a small asymmetry parameter $\eta \approx 0.15$ is observed for all G (cf. Figure 7). At highest temperatures a Lorentzian line shows up characteristic of fast isotropic (liquid-like) reorientation. In between features of spectra with an anisotropy parameter close to one are discovered, indicating fast 180° two-site jumps of the ND_2 groups according to their symmetry. Concerning the transition to the liquid line the spectra of different G essentially agree. Thus, the liquid dynamics do not significantly change, in agreement with very similar T_g values (cf. Table 1). Yet, some differences are observed for the transition from the low-temperature Pake spectrum to the motionally averaged spectrum of the fast amine group jumps.

In order to quantitatively describe the solid-state spectra ($T \leq 180$ K), a weighted superposition of two subspectra, namely a Pake spectrum and a motionally averaged spectrum due to the fast jumps of the amine group, is assumed. Examples of calculated spectra are shown in Figure 7. An angle of 104° between the two ND_2 bond directions has to be assumed to reproduce the experimental subspectrum with the motion-averaged anisotropy parameter $\bar{\eta} \approx 0.92$. The large temperature range 120–180 K (G2, G4, G5) (130–190 K for G3) in which the spectra must be described by a superposition of the two subspectra indicates dynamical heterogeneities regarding the two-site jump of the ND_2 group. In other words, the jump process, actually taking place also below T_g , is determined by a broad distribution of jump times. This behavior is typical of glasses that exhibit static density fluctuations.^{44,45} Figure 7 shows such a “two-phase” spectrum for G2 at 153.9 K and a fit with a superposition of a 50% solid state spectrum and a 50% motionally averaged spectrum due to the ND_2 jumps. At higher temperatures (180–210 K for G2, G4, G5; 190–220 K for G3) the solid-state line collapses to a liquid-like Lorentzian line. The width $\Delta\nu$ of the Lorentzian line at high temperatures is taken to estimate the time constant of the α -process (cf. Experimental Section). The extracted time constants $\tau_\alpha(T)$ fit well to those from FC ^1H NMR as is shown in Figure 4.

3.3. Field-Cycling ^1H NMR. Figure 8a shows typical relaxation rates $R_1(\omega) = 1/T_1(\omega)$ for the PPI dendrimer G5 as a function of frequency $\nu = \omega/2\pi$. For all temperatures one recognizes pronounced dispersion, becoming stronger at low temperatures where the local dynamics determines the relaxation. At $T = 393$ K the measurements for G4 and G5 were extended to lower frequencies by applying a home-built spectrometer which covers significantly lower frequencies (cf. Experimental Section). As described, the relaxation rates are transformed into the susceptibility representation via $\omega/T_1 = \chi''(\omega)$. Then master curves $\chi''_{\text{NMR}}(\omega\tau_\alpha)$ are constructed by applying FTS which collapses different data sets collected at several temperatures in the range 220–400 K.³² The resulting master curves for G2–G5 are shown in Figure 8b and can be characterized by three relaxation regimes. At frequencies around the relaxation maximum ($\omega\tau_\alpha \cong 1$) the glass transition determines the segmental relaxation. Here, by construction, all master curves agree. In the regime $\omega\tau_\alpha \ll 1$ excess relaxation is observed when compared to the susceptibility of a low- M liquid (oligo-butadiene $M = 460$ g/mol,³⁰ cf. Figure 8b) which does not exhibit any polymer dynamics. The excess relaxation becomes more pronounced with growing generation number G . It can be specified by a power law ω^ϵ with an apparent exponent ϵ weakly changing from 0.87 (G2) to 0.76 (G5). At even lower frequencies the curves turn back to a behavior with an exponent very close to one. This is typical for the terminal relaxation. The $\chi''_{\text{NMR}}(\omega\tau_\alpha)$

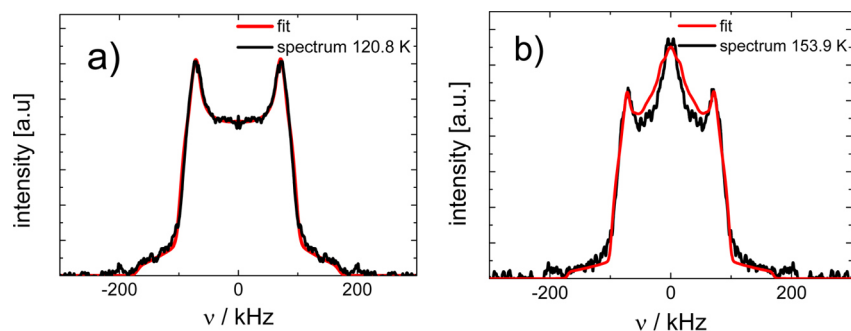


Figure 7. Examples of ^2H NMR spectra (symmetrized) fitted to a “two-phase” model. (a) Spectrum of PPI dendrimer G3 at $T = 120.8\text{ K}$ (black line) and fit with a solid-state spectrum with $\eta = 0.15$ (red line). (b) Spectrum of G2 at $T = 153.9\text{ K}$ (black line) and fit (red line) with a superposition of a 50% solid-state and 50% motionally averaged spectrum ($\eta \approx 0.9$).

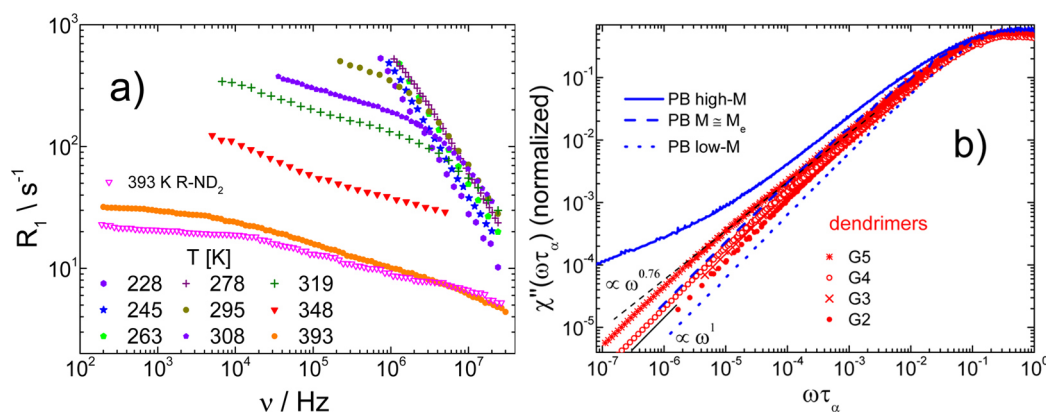


Figure 8. (a) Spin–lattice relaxation rate $R_1(\nu)$ of the fully protonated dendrimer G5 as a function of frequency ν , obtained by FC ^1H NMR; in addition, at $T = 393\text{ K}$ data for the end group-deuterated dendrimer G5. (b) Normalized (by area) susceptibility master curves of the (fully protonated) PPI dendrimers of different generations; for comparison master curves of polybutadiene for $M = 460\text{ g/mol}$ (simple liquid, dotted blue line), $M = 2000\text{ g/mol} \approx M_e$ (unentangled, dashed blue line), and for $M = 87\,000\text{ g/mol}$ (entangled, blue line) are shown.

curves show some similarity with the FC ^1H NMR results for unentangled (linear) polymers like polybutadiene (PB, $M = 2000\text{ g/mol}$,³³ data included in Figure 8b), i.e., PB with M below the entanglement molar mass M_e . However, high- M (entangled) PB³³ displays a quite different behavior (PB, $M = 87\text{ kg/mol} \gg M_e$, data included in Figure 8b). In the latter case a second power-law regime with an even lower exponent is recognized at lowest frequencies, a finding which is typical for entanglement polymer dynamics.³³ This second power-law is absent for the dendrimers; that is, they do not show entanglement effects, a fact well-known from rheological studies.⁷ Upon constructing the master curves $\chi''_{\text{NMR}}(\omega\tau_\alpha)$ the time constants $\tau_\alpha = \tau_\alpha(T)$ are obtained and included in Figure 4. They well extend the data sets from DS to high temperatures and also agree perfectly with those from solid-state ^2H NMR.

As discussed in the Experimental Section, performing ^1H NMR always raises the question to what extent the spin–lattice relaxation is actually determined by the intramolecular reorientation-mediated relaxation and whether there is some significant contribution from intermolecular relaxation reflecting also translational diffusion. In order to address this question, we compare in Figure 9 the FC ^1H susceptibility master curves for the fully and the partially deuterated dendrimer G5 (original $R_1(\omega)$ data is shown in Figure 8a). Indeed, differences are observed, in particular at low frequencies; the susceptibility of the end group deuterated dendrimer is reduced due to the suppression of some of the intermolecular relaxation contributions. Thus, the relaxation rate of the fully protonated samples

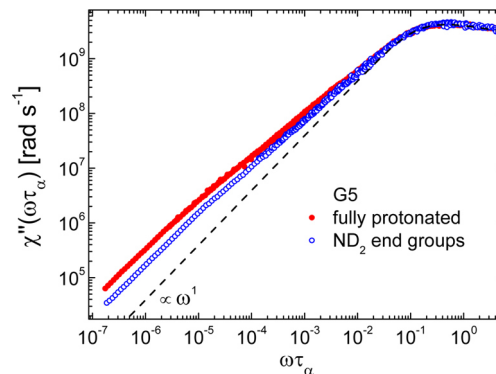


Figure 9. Comparing the FC ^1H NMR susceptibility master curve for fully and end group deuterated dendrimer G5. Dashed line: simple liquid (Debye) limit.

contains a significant intermolecular contribution. This can be exploited to estimate the diffusion coefficient $D(T, M)$ for the different generations along eq 6.

Figure 10 presents the relaxation rates measured at the highest temperature $T = 393\text{ K}$ as a function of the square root of angular frequency. At the lowest frequencies a linear behavior is observed from which $D(M)$ is extracted when inserting the spin density $n_s = 7.3 \times 10^{28}\text{ m}^{-3}$ in eq 6. The latter is calculated from the molecular structure and mass density $\rho \approx 1\text{ g cm}^{-3}$ (from the supplier) and only slightly depends on G . The inset of Figure 10 shows the change of D with M . We find $D(M) \propto M^{-1.2 \pm 0.2}$ (cf.

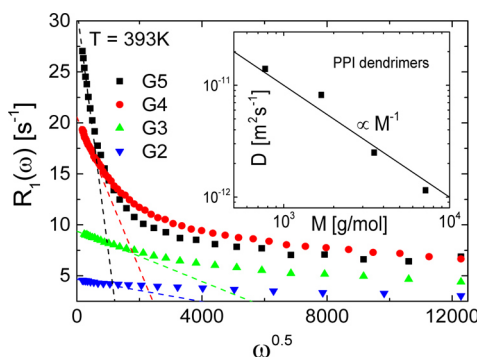


Figure 10. Spin–lattice rate $R_1(\omega)$ at 393 K as a function of the square root of angular frequency. The slope of the linear part at lowest frequencies (dashed line) yields the diffusion coefficient D (cf. eq 6). Inset: D as a function of M with corresponding power-law fit.

inset). This result will be reconsidered in the Discussion. The temperature dependence of D closely follows, as expected, that of the reciprocal segmental time $1/\tau_\alpha(T)$ (see Figure 4).

4. DISCUSSION

The dynamics of PPI dendrimers is investigated by several techniques addressing segmental (“local”) and polymer specific (“collective”) dynamics. Concerning the local dynamics, as revealed by DS and ^2H NMR, the dendrimers show features well-known from amorphous polymers and molecular glass-formers.^{42,46} The main (structural or α -) relaxation only weakly changes with generation and follows a super-Arrhenius temperature dependence. Correspondingly, T_g is virtually independent of G , in agreement with previous studies,⁸ but in contrast to other dendritic macromolecules.⁴⁷ The spectral width of the α -process is broad but similar to polymers.⁴⁸ Yet, some influence of heterogeneous dynamics within the dendrimers reflecting different mobilities in different “shells”, as documented by NMR studies^{23–26} as well as theoretical work,^{5,16,17} may additionally broaden the α -relaxation. This fact may also explain the weak nonexponential relaxation observed in the present study, yet most of the dynamic heterogeneities are averaged out due to spin diffusion in the present case of ^1H NMR. Secondary relaxations occur, which appear to merge with the structural relaxation above T_g . Below T_g their time constants follow an Arrhenius law. One of the secondary relaxations (d -process) displays time constants that virtually do not change with G and its spectral shape does not change with temperature. In addition, the attempt frequency is unphysically high. A temperature-independent spectral shape of the relaxation is usually found

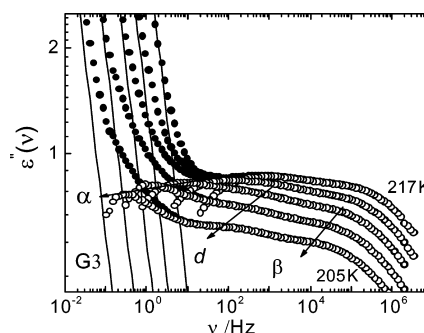


Figure 12. Dielectric spectra of PPI dendrimer G3 (filled symbols) for temperatures $T = 217, 214, 211, 208$, and 205 K. Lines: dc conductivity contribution. Open symbols: susceptibility after subtracting the conductivity contribution.

for cooperative processes like the α -process.⁴⁶ Thus, we may speculate whether the d -process is of cooperative nature and reflects internal motion of the dendrimers which still can proceed in the structurally frozen state, i.e., below T_g . As proven by ^2H NMR, the amine end groups undergo a two-site jump governed by a broad distribution of jump times reflecting (static) density fluctuations in the glass state.^{44,45} The latter process is not probed by DS as the dipole moment does not change by a 180° jump. We plan to run ^2H NMR experiments on PPI dendrimers deuterated only in the core. Then the amine group reorientation will not obscure the ^2H spectral features characteristic of main and secondary relaxations.

The other secondary process displays features typical of a β -process (also Johari–Goldstein process) in amorphous systems.⁴² Although there are conflicting interpretations of its nature,⁴⁹ according to ^2H NMR investigations in molecular glasses ($T < T_g$) it is attributed to small-angle displacements of the segments, and a wobbling-on-a-cone model reproduces the salient NMR findings.^{50,51} Secondary processes in dendrimers were also reported by other research groups.^{11,12} For example, a quite similar relaxation scenario with an α -process and two secondary relaxations virtually not changing with generation was found in PAMAM dendrimers.¹² Also, hyperbranched polymers show a relaxation time map highly resembling that of the present PPI dendrimers, in particular, also two secondary relaxations are observed.^{52–54}

The collective polymer dynamics, in addition to local dynamics, are revealed by FC ^1H NMR ($T > T_g$). Here we note that the collective dynamics are not probed by dielectric measurements since already the local segmental dynamics (α -process) leads to a complete loss of the correlation as is the case

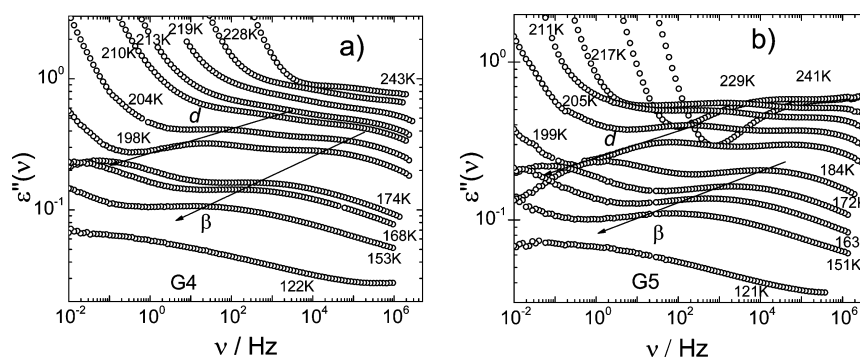


Figure 11. Dielectric spectra of PPI dendrimer G4 (a) and G5 (b) including the dc conductivity masking the structural relaxation (α -process).

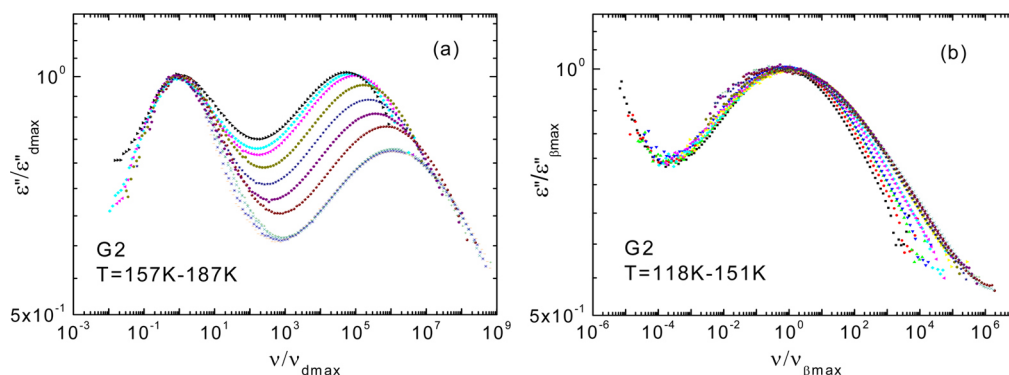


Figure 13. (a) Rescaled dielectric spectra of PPI dendrimer G2; dielectric permittivity ϵ'' is rescaled by maximum height $\epsilon''_{d,\max}$ and frequency ν by $\nu_{d,\max}$ of the d -relaxation peak in a temperature range $T = 157\text{--}187\text{ K}$. (b) Dielectric data are rescaled with respect to the β -relaxation peak in $T = 118\text{--}151\text{ K}$.

of so-called type B polymers (Stockmayer notation⁵⁵). Frequency–temperature superposition works well and susceptibility master curves $\chi''(\omega\tau_\alpha)$ extending over 9 decades in (reduced) frequency are obtained. Clear evidence of additional dynamics much slower than the local dynamics is found. The construction of the master curves provides $\tau_\alpha(T)$ which complements the data from dielectric spectroscopy and ^2H NMR; summarized, 12 decades in $\tau_\alpha(T)$ are covered. Between the local dynamics (α -process) and the terminal relaxation time τ_t of the collective dynamics an intermediate relaxation regime can be approximated by a power-law with an exponent around 0.8 depending weakly, yet systematically on G . When compared with results for linear polymers, some resemblance with Rouse dynamics is recognized. Entanglement can be excluded, a fact well-known also from rheological studies.⁷ The FC ^1H NMR susceptibility also shows some features that were recently reported by theory¹⁴ as well as simulations.^{5,13–17} Yet, quantitative comparison is not possible since no fully realistic models were considered. Qualitatively, local dynamics at high, breathing modes at intermediate, and overall tumbling and diffusion of the whole dendrimer molecule at low frequencies can be distinguished in accordance with our experimental findings.

Exploiting the universal low-frequency dispersion law, the diffusion coefficient $D(M)$ is estimated from the low-frequency relaxation rate $R_1(\omega)$, a relation $D(M) \propto M^{-1.2 \pm 0.2}$ is found. Of course, having only four generations at hand the change with M is small, and the extracted exponent should be taken with caution. Nevertheless, to our knowledge this is the first report of $D(M)$ for bulk PPI dendrimers. We note that our approach extracting D from the low-frequency dispersion of T_1 was recently applied for linear polymers⁴¹ as well as simple liquids,⁴⁰ and good agreement with field gradient NMR was found. Again, attempting to understand the M dependence appears somewhat speculative as only five generations of PPI generations can be synthesized. Nevertheless, we want to propose some scaling arguments, the details of which will be discussed in a forthcoming publication. They are meant to provide a semiquantitative understanding. In any case, the rheological behavior of dendrimers certainly depends on details of their structure.

In first approximation, a dendrimer can be considered as a viscoelastic ball with constant density and a radius scaling as $R \propto N^{1/3}$ with N denoting the number of segments. In a coordinate system fixed within the dendrimer any segment has a well-defined average position \vec{r} with respect to which thermal fluctuations lead to a displacement $\vec{u}(\vec{r};t)$. The vector $\vec{u}(\vec{r};t)$ satisfies a diffusion equation with adequate boundary conditions and a diffusion coefficient D_α being on the order of the segmental

diffusion coefficient. The thus derived (longest) relaxation time of such breathing modes scales as $\tau_{\text{breath}} \propto R^2/D_\alpha \propto N^{2/3}$ with $\tau_\alpha \ll \tau_{\text{breath}} \ll \tau_t$. In order to estimate the longest relaxation connected with translational diffusion, the friction coefficient of a (large) dendrimer with its environment is assumed to be proportional to the number f of surface segments for N going to ∞ , i.e., $f \propto R^2 \propto N^{2/3}$. Hence, self-diffusion scales as $D \propto (k_B T/f) \propto D_\alpha N^{-2/3} \propto (b^2/\tau_\alpha) N^{-2/3}$, where b is a characteristic segment length. Hence, the time during which the dendrimer diffuses over a distance of about its linear size will scale as $\tau_{\text{trans}} \propto (R^2/D) \propto \tau_\alpha N^{4/3}$. Regarding rotation the same M scaling is expected within this model. The spin–lattice relaxation at $\omega\tau_\alpha \leq 1$ is determined by these three types of motions. It appears that the breathing time τ_{breath} cannot be resolved from the experimental susceptibility (cf. Figure 9); only an intermediate power-law regime is found. Yet, in any case, the low-frequency part of spin–lattice relaxation is determined by translations and rotations of the entire dendrimer molecule. Given this coarse-grained description for $D(M)$, the actually observed M dependence $D(M) \propto M^{-1.2 \pm 0.2}$ can be explained by finite size effects due to the rather small M range investigated. In addition, for these small molar masses the extent of penetration is large, i.e., comparable with the radius, which will increase the exponent of $D(M)$. Qualitatively, our mathematically simple model may be regarded as continuous limit of the discrete viscoelastic models recently proposed.^{5,13–17} Its advantage is that it takes into account excluded volume interactions between the dendrimer's arms.

5. CONCLUSIONS

We investigated bulk PPI dendrimers of generation (G) 2–5 by dielectric spectroscopy (DS), solid-state ^2H NMR, and field-cycling (FC) ^1H NMR relaxometry in a large temperature range of 120–400 K, above and below the glass transition temperature $T_g = 200\text{ K}$. Three relaxation processes are identified by DS; a main (α -) relaxation ($T > T_g$) and two secondary processes ($T < T_g$). The α -process exhibits a super-Arrhenius temperature dependence typical of glass-forming liquids. The secondary relaxations are governed by an Arrhenius temperature law. While one secondary process exhibits features characteristic of a β -process in amorphous systems, the other one is atypical and thus possibly specific to dendrimers. Its spectral width does not vary with temperature and exhibits time constants independent of G . Regarding FC ^1H NMR probing the dispersion of the spin–lattice relaxation rate $R_1(\omega)$, applying susceptibility representation, $\chi''(\omega) \equiv \omega R_1(\omega)$, and frequency–temperature superposition a large effective frequency range is covered by the master curve $\chi''(\omega\tau_\alpha)$. Its construction yields $\tau_\alpha(T)$; thereby, together

with results from DS, 12 decades in $\tau_\alpha(T)$ are covered. The obtained master curve $\chi''(\omega\tau_\alpha)$ provides evidence of dynamics much slower than the local dynamics. An intermediate power-law regime is identified which covers the frequency range between the terminal relaxation and local relaxation. In accordance with theoretical models and computer simulations reported in the literature, we identify three processes: local reorientations at high, breathing modes at intermediate, and overall tumbling of the dendrimer at low frequencies. Estimating the diffusion coefficient $D(M)$ from the universal low-frequency dispersion law of $R_1(\omega)$, the $D(M) \propto M^{1.2 \pm 0.2}$ is found. Discussing some scaling arguments, we derive $D(M) \propto M^{-2/3}$. This deviation may be connected to the relatively small range of molar masses that can be investigated in the case of PPI dendrimers.

AUTHOR INFORMATION

Corresponding Author

*E-mail: ernst.roessler@uni-bayreuth.de (E.A.R.).

Notes

The authors declare no competing financial interest.

ACKNOWLEDGMENTS

The authors are indebted to F. Fujara and B. Kresse (Technical University Darmstadt) for giving the opportunity to measure the $R_1(\omega)$ dispersion at extremely low frequencies. We also thank Maxim Dolgushev (University of Freiburg) for providing unpublished results where he shows the relevance of intermolecular relaxation contribution. Financial support by Deutsche Forschungsgemeinschaft (DFG) through grant RO 907/17 is appreciated.

REFERENCES

- Bosman, A. W.; Janssen, H. M.; Meijer, E. W. *Chem. Rev.* **1999**, *99*, 1665.
- Jean, M. J.; Fréchet, D. A. T. *Dendrimers and Other Dendritic Polymers*; John Wiley & Sons, Ltd.: New York, 2002.
- Ballauff, M.; Likos, Ch. N. *Angew. Chem., Int. Ed.* **2004**, *43*, 2998.
- Karatasos, K. *Macromolecules* **2006**, *39*, 4619.
- Markelov, D. A.; Lyulin, S. V.; Gotlib, Y. Y.; Lyulin, A. V.; Matveev, V. V.; Lahderanta, E.; Darinskii, A. A. *J. Chem. Phys.* **2009**, *130*, 044907.
- Zacharopoulos, N.; Economou, L. G. *Macromolecules* **2002**, *35*, 1814.
- Uppuluri, S.; Morrison, F. A.; Dvornic, P. R. *Macromolecules* **2000**, *33*, 2551.
- Tande, B. M.; Wagner, N. J.; Kim, Y. H. *Macromolecules* **2003**, *36*, 4619.
- Götze, I. O.; Likos, C. N. *Macromolecules* **2003**, *36*, 8189.
- Doi, M.; Edwards, S. F. *The Theory of Polymer Dynamics*; Oxford Science Publications: Oxford, 1986.
- Trahasch, B.; Stühn, B.; Frey, H.; Lorenz, K. *Macromolecules* **1999**, *32*, 1962.
- Mijovic, J.; Ristic, S.; Kenny, J. *Macromolecules* **2007**, *40*, 5212.
- Gotlib, Y. Y.; Markelov, D. A. *Polym. Sci., Ser. A* **2007**, *49*, 1137.
- Markelov, D. A.; Lähderanta, E.; Gotlib, Y. Y. *Macromol. Theory Simul.* **2010**, *19*, 158.
- Dolgushev, M.; Berezovska, G.; Blumen, A. *Macromol. Theory Simul.* **2011**, *20*, 621.
- Kumar, A.; Biswas, P. *Phys. Chem. Chem. Phys.* **2013**, *15*, 20294.
- Markelov, D. A.; Dolgushev, M.; Gotlib, Y. Y.; Blumen, A. *J. Chem. Phys.* **2014**, *140*, 244904.
- Kimmich, R.; Anardo, E. *Prog. Nucl. Magn. Reson. Spectrosc.* **2004**, *44*, 257.
- Kruk, D.; Herrmann, A.; Rössler, E. A. *Prog. Nucl. Magn. Reson. Spectrosc.* **2012**, *63*, 33.
- Kimmich, R. *Principles of Soft-Matter Dynamics*; Springer: Berlin, 2012.
- Meier, R.; Kruk, D.; Rössler, E. A. *ChemPhysChem* **2013**, *14*, 3071.
- Fujara, F.; Kruk, D.; Privalov, A. F. *Prog. Nucl. Magn. Reson. Spectrosc.* **2014**, *82*, 39.
- Meltzer, A. D.; Tirrell, D. A.; Jones, A. A.; Inglefield, P. T.; Hedstrand, D. M.; Tomalia, D. A. *Macromolecules* **1992**, *25*, 4541.
- Meltzer, A. D.; Tirrell, D. A.; Jones, A. A.; Inglefield, P. T. *Macromolecules* **1992**, *25*, 4549.
- Malveau, C.; Baille, W. E.; Zhu, X. X.; Ford, W. T. *J. Polym. Sci., Part B: Polym. Phys.* **2003**, *41*, 2969.
- Pinto, L. F.; Correa, J.; Martin-Pastor, M.; Riguera, R.; Fernandez-Megia, E. *J. Am. Chem. Soc.* **2013**, *135*, 1972.
- Rubinstein, M.; Colby, R. H. *Polymer Physics*; Oxford University Press: New York, 2003.
- Kresse, B.; Privalov, A. F.; Herrmann, A.; Hofmann, M.; Rössler, E. A.; Fujara, F. *Solid State Nucl. Magn. Reson.* **2014**, *59*, 45.
- Kariyo, S.; Gainaru, C.; Schick, H.; Brodin, A.; Novikov, V. N.; Rössler, E. A. *Phys. Rev. Lett.* **2006**, *97*, 207803.
- Kariyo, S.; Brodin, A.; Gainaru, C.; Herrmann, A.; Schick, H.; Novikov, V. N.; Rössler, E. A. *Macromolecules* **2008**, *41*, 5313.
- Herrmann, A.; Kariyo, S.; Abou Elfadl, A.; Meier, R.; Gmeiner, J.; Novikov, V. N.; Rössler, E. A. *Macromolecules* **2009**, *42*, 5236.
- Hofmann, M.; Herrmann, A.; Abou Elfadl, A.; Kruk, D.; Wohlfahrt, M.; Rössler, E. A. *Macromolecules* **2012**, *45*, 2390.
- Herrmann, A.; Kresse, B.; Gmeiner, J.; Privalov, A. F.; Kruk, D.; Fujara, F.; Rössler, E. A. *Macromolecules* **2012**, *45*, 1408.
- Wagner, H.; Richert, R. *J. Phys. Chem. B* **1999**, *103*, 4071.
- Blochowicz, T.; Gainaru, C.; Medick, P.; Tschirwitz, C.; Rössler, E. A. *J. Chem. Phys.* **2006**, *124*, 134503.
- Spiess, H. W.; Sillescu, H. *J. Magn. Reson.* **1981**, *42*, 381.
- Abragam, A. *The Principles of Nuclear Magnetism*; Clarendon Press: Oxford, 1961.
- Harmon, J. F.; Muller, B. H. *Phys. Rev.* **1969**, *182*, 400.
- Sholl, C. A. *J. Phys. C: Solid State Phys.* **1981**, *14*, 447.
- Kruk, D.; Meier, R.; Rössler, E. A. *Phys. Rev. E* **2012**, *85*, 020201.
- Meier, R.; Herrmann, A.; Hofmann, M.; Kresse, B.; Privalov, A. F. *Macromolecules* **2013**, *46*, 5538.
- Kudlik, A.; Benkhof, S.; Blochowicz, T.; Tschirwitz, C.; Rössler, E. A. *J. Mol. Struct.* **1999**, *479*, 201.
- Böttcher, C. J. F.; Bordewijk, P. *Theory of Electronic Polarization*; Elsevier Scientific Polarization: Amsterdam, 1978.
- Rössler, E. A.; Taupitz, M.; Börner, K.; Schulz, M.; Vieth, H.-M. *J. Chem. Phys.* **1990**, *92*, 5847.
- Böhmer, R.; Diezemann, G.; Hinze, G.; Rössler, E. A. *Prog. Nucl. Magn. Reson. Spectrosc.* **2001**, *39*, 191.
- Petzold, N.; Schmidtke, B.; Kahlau, R.; Bock, D.; Meier, R.; Micko, B.; Kruk, D.; Rössler, E. A. *J. Chem. Phys.* **2013**, *138*, 12A510.
- Wooley, K. L.; Hawker, C. J.; Pochan, J. M.; Frechet, J. M. J. *Macromolecules* **1993**, *26*, 1514.
- Abou Elfadl, A.; Kahlau, R.; Herrmann, A.; Novikov, V. N.; Rössler, E. A. *Macromolecules* **2010**, *43*, 3340.
- Johari, G. P. *J. Non-Cryst. Solids* **2002**, *307*, 317.
- Vogel, M.; Rössler, E. A. *J. Chem. Phys.* **2001**, *115*, 10883.
- Micko, B.; Tschirwitz, C.; Rössler, E. A. *J. Chem. Phys.* **2013**, *138*, 154501.
- Garcia-Bernabe, A.; Diaz-Calleja, R.; Haag, R. *Macromol. Chem. Phys.* **2006**, *207*, 970.
- Turky, G.; Sangoro, J. R.; Rehim, M. A.; Kremer, F. *J. Polym. Sci., Part B: Polym. Phys.* **2010**, *48*, 1651.
- Sangoro, J. R.; Turkey, G.; Rehim, M. A.; Jacob, C.; Naumov, S.; Ghoneim, A.; Kaerger, J.; Kremer, F. *Macromolecules* **2009**, *42*, 1648.
- Stockmayer, W. H. *Pure Appl. Chem.* **1967**, *15*, 539.

Publication 4

All Polymer Diffusion Regimes Covered by Combining Field-Cycling and Field-Gradient ^1H NMR

Kresse, B.; Hofmann, M.; Privalov, A. F.; Fatkullin, N.;

Fujara, F.; Rössler, E. A.

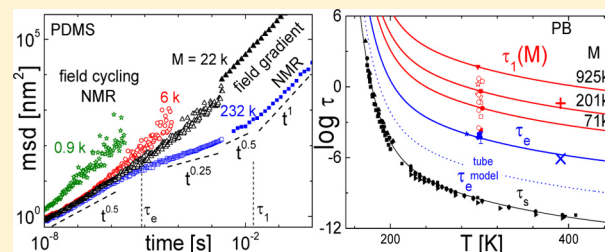
Macromolecules **2015**, 48, 4491-4502.

DOI: 10.1021/acs.macromol.5b00855

(Copyright 2015 by The American Chemical Society)

All Polymer Diffusion Regimes Covered by Combining Field-Cycling and Field-Gradient ^1H NMRB. Kresse,[‡] M. Hofmann,[†] A. F. Privalov,[‡] N. Fatkullin,[§] F. Fujara,[‡] and E. A. Rössler^{*,†}[†]Experimentalphysik II, Universität Bayreuth, D-95440 Bayreuth, Germany[‡]Institut für Festkörperphysik, TU Darmstadt, Hochschulstr. 6, D-64289 Darmstadt, Germany[§]Institute of Physics, Kazan Federal University, Kazan 420008 Tatarstan, Russia

ABSTRACT: Field-cycling and field-gradient ^1H NMR experiments were combined to reveal the segmental mean-square displacement as a function of time for polydimethylsiloxane (PDMS) and polybutadiene (PB). Together, more than 10 decades in time are covered, and all four power-law regimes of the tube-reptation (TR) model are identified with exponents rather close to the predicted ones. Characteristic polymer properties like the tube diameter a_0 , the Kuhn length b , the mean-square end-to-end distance $\langle R_0^2 \rangle$, the segmental correlation time $\tau_s(T)$, the entanglement time $\tau_e(T)$, and the disengagement time $\tau_d(T)$ are estimated from the measurements and compared to results from literature. Concerning $\tau_d(T)$, fair agreement is found. In the case of τ_e , agreement with rheological data is achieved when the time constant is extracted from the minimum in the shear modulus $G''(\omega)$. Concerning the TR predictions the molar mass (M) dependence of τ_d is essentially reproduced. Yet, calculating τ_e from τ_d for PDMS yields agreement with experimental data while for PB it gets by 2 orders of magnitude too short. In no case τ_e is correctly reproduced from $\tau_s(T)$. Segmental and shortest Rouse times appear to coincide for PB, while in the case of PDMS the latter turns out to be longer by 1 decade.



1. INTRODUCTION

The tube-reptation (TR) model¹ is a widely accepted approach to describe the microscopic dynamics of entangled polymer melts. The model predicts four different power-law regimes (I–IV) for the time dependence of the segmental mean-square displacement $\langle r^2(t) \rangle \propto t^\alpha$ (cf. inset of Figure 5b). Molecular dynamics simulations^{2,3} and neutron scattering (NS) experiments⁴ essentially confirmed parts of the model by identifying the predicted crossover from $\langle r^2(t) \rangle \propto t^{0.5}$ to $\langle r^2(t) \rangle \propto t^{0.25}$ for the transition from free Rouse (regime I) to constrained Rouse dynamics (regime II). On long time scales the crossover from $\langle r^2(t) \rangle \propto t^{0.5}$, characteristic for reptation (regime III), to $\langle r^2(t) \rangle \propto t^1$, for the terminal regime of free diffusion (regime IV), was observed by field gradient (FG) NMR.^{5–8} However, the agreement was only qualitative since numerical discrepancies with respect to the TR model occurred. Another regime (regime 0) reflects local motions connected with fluctuations for times on the order of the segmental correlation time τ_s determined by structural relaxation of the glass transition dynamics. Given the large range of relaxation regimes, characterization by essentially a single experiment is still missing.

Recently, field-cycling (FC) ^1H NMR relaxometry^{9,10} confirmed the crossover between the power-law behavior of regime I and II and has thus become a complementary method to FG NMR and a competing one to NS. The method, which measures the frequency dependence (dispersion) of the spin–lattice relaxation rate $R_1 = 1/T_1$, gained momentum with the

availability of advanced FC relaxometers.^{9–16} Commercial machines typically cover a frequency range of 10 kHz–20 MHz. Using a home-built relaxometer, where we applied active earth and stray field compensation, we are able to achieve a low-frequency limit of about 100 Hz (in ^1H Larmor frequency units).^{10,14–16} In the case of ^1H NMR the relaxation originates from fluctuations of the magnetic dipole–dipole interaction. Here one has to distinguish contributions from spins belonging to the same polymer molecule constituting the intramolecular contribution, and spins from different molecules, representing the intermolecular contribution.¹⁷ As a consequence, the total relaxation rate is given by the sum of both contributions, i.e., $R_1 = R_1^{\text{intra}} + R_1^{\text{inter}}$. In polymer melts $R_1^{\text{inter}}(\omega)$ is dominated by translational dynamics and hence reflects the relative msd of segments from different macromolecules.¹⁷ Assuming subdiffusive power-law governed translational dynamics for times $t < \tau_1$, where τ_1 is the terminal relaxation time,¹ it was demonstrated that $\langle r^2(t) \rangle$ can be estimated from the intermolecular relaxation rate $R_1^{\text{inter}}(\omega)$ by a simple analytical expression (cf. Theoretical Background).^{9,10,18} Note that in the framework of the TR theory the terminal relaxation time τ_1 is equivalent to the tube disengagement time τ_d . The intermolecular relaxation rate was singled out from the total relaxation by applying isotope dilution experiments for which

Received: April 23, 2015

Revised: June 12, 2015

Published: June 24, 2015



protonated chains are successively diluted in a perdeuterated polymer matrix.^{9,10,19–21}

A more general relationship connecting $\langle r^2(t) \rangle$ directly with the Fourier transform of $R_1^{\text{inter}}(\omega)$ was derived^{9,18} which does not rely on any assumptions (cf. Theoretical Background). It is the purpose of the present contribution to test this approach and to compare it with results measured by FG ^1H NMR which provides absolute values of the segmental msd in the regime III and IV. The method is a well-established technique to access translational diffusion; $\langle r^2(t) \rangle$ is usually probed in the hydrodynamic limit (regime IV in the case of polymers).⁶ Yet, in order to access also shorter times $t < \tau_1$, where the diffusion coefficient becomes time dependent, special experimental efforts have to be undertaken. In particular, the so-called dipolar correlation effect due to reorientational motion has to be accounted for.^{6,22} We will demonstrate, for the first time, that all four regimes of polymer diffusion are covered by combining data of two NMR methods for polybutadiene (PB) and polydimethylsiloxane (PDMS). Moreover, a comparison with rheological data is carried out and discussed within the frame of the TR model.

2. THEORETICAL BACKGROUND

2.1. Mean-Square Displacement Derived from ^1H FC NMR. Here we provide a derivation of the relationship between the intermolecular spin–lattice relaxation time $T_1(\omega)$ accessible by FC ^1H NMR and the segmental msd. Proton relaxation is determined by fluctuations of the magnetic dipole–dipole interaction, specifically, by the following correlation function:

$$A_p(t) = \frac{1}{N_s} \sum_{k \neq m} \left\langle \frac{Y_{2p}(\vec{e}_{km}(t)) Y_{2p}^*(\vec{e}_{km}(0))}{r_{km}^3(t) r_{km}^3(0)} \right\rangle \quad (1)$$

$Y_{lp}(\vec{e}_{km})$ is component p of the spherical function of rank l , N_s is the total number of spins in the system, r_{km} is the internuclear distance, and $\vec{e}_{km}(t) = \vec{r}_{km}(t)/r_{km}(t)$ is the corresponding unit vector. In isotropic systems the correlation function becomes independent of p , yielding $A_0(t) = A_1(t) = A_2(t) \equiv A(t)$.^{11,17} The correlation function includes intra- and intermolecular contributions; i.e., it comprises correlations between spins belonging to the same macromolecule and to spins from different macromolecules, respectively. We note that we use the nomenclature $A(t)$ in the present context denoting the reorientational correlation function while we usually chose $C(t)$.^{10,13,19}

The relaxation rate $R_1 = T_1^{-1}$ is a linear combination of Fourier transforms of $A(t)$ evaluated at the frequencies ω and 2ω .¹⁷

$$\frac{1}{T_1(\omega)} = \left(\frac{\mu_0}{4\pi} \right)^2 \frac{6\pi}{5} \gamma_H^4 \hbar^2 \int_0^\infty dt \{ A(t) \cos(\omega t) + 4A(t) \cos(2\omega t) \} \quad (2)$$

Note that this expression is only correct as long as the so-called Redfield condition is satisfied, i.e., $T_1(\omega) \gg 2\pi\omega^{-1}$. At very low frequencies ($\nu = \omega/2\pi < 400$ Hz) this limit is approached for high M in the present case. A violation of the Redfield condition would go along with a pseudo-Gaussian magnetization decay, which is actually not (yet) observed. Instead, all magnetization curves encountered in the course of this work are monoexponential. Furthermore, a common spin temperature has to be established by fast flip-flop processes (spin diffusion) which also applies well within the frequency window $\nu = 200$ Hz–30 MHz covered by our experiments.

Equation 2 can be rewritten

$$\frac{1}{T_1(\omega)} = \left(\frac{\mu_0}{4\pi} \right)^2 \frac{6\pi}{5} \gamma_H^4 \hbar^2 \int_0^\infty dt \cos(\omega t) \{ A(t) + 2A(t/2) \} \quad (3)$$

The Fourier transform in eq 3 connects the total dipolar correlation function, including intra- and intermolecular contributions, with the dispersion of the relaxation rate:

$$\hat{A}(t) = A(t) + 2A(t/2) = \left(\frac{4\pi}{\mu_0} \right)^2 \frac{5}{3\pi^2} \frac{1}{\gamma_H^4 \hbar^2} \int_0^\infty d\omega \frac{\cos(\omega t)}{T_1(\omega)} \quad (4)$$

The total dipolar correlation function can be decomposed into a sum of inter- and intramolecular parts:^{11,17}

$$\hat{A}(t) = \hat{A}^{\text{inter}}(t) + \hat{A}^{\text{intra}}(t) \quad (5)$$

The intermolecular part reads

$$\begin{aligned} \hat{A}^{\text{inter}}(t) &= A^{\text{inter}}(t) + 2A^{\text{inter}}(t/2) \\ &= \left(\frac{4\pi}{\mu_0} \right)^2 \frac{5}{3\pi^2} \frac{1}{\gamma_H^4 \hbar^2} \int_0^\infty d\omega \frac{\cos(\omega t)}{T_1^{\text{inter}}(\omega)} \end{aligned} \quad (6)$$

For times $t \gg \tau_s$, $A^{\text{inter}}(t)$ assumes a universal form valid for all models of polymer dynamics, explicitly

$$A^{\text{inter}}(t) = \frac{4\pi}{9} n_s \tilde{W}(0; t) \quad (7)$$

where n_s is the proton spin density and $\tilde{W}(\vec{r}; t) = \tilde{W}(\vec{r}' - \vec{r}; t)$ the propagator of relative displacements of two spins from different macromolecules, i.e., the probability density for two spins separated by a vector \vec{r} initially and by a vector \vec{r}' at later time t . For times $t \gg \tau_s$, the $A^{\text{inter}}(t)$ is proportional to the probability density to recover the initial spatial separation at time t , i.e., the vector $\vec{r} = \vec{r}'$.¹⁸ Next, the propagator in eq 7 can be approximated by a Gaussian distribution:²³

$$\tilde{W}(\vec{r}; t) = ((2\pi/3) \langle \tilde{r}^2(t) \rangle)^{-3/2} \exp \left\{ -\frac{3}{2} \frac{r^2}{\langle \tilde{r}^2(t) \rangle} \right\} \quad (8)$$

Here $\langle \tilde{r}^2(t) \rangle = \langle ((\vec{r}_i(t) - \vec{r}_i(0)) - (\vec{r}_j(t) - \vec{r}_j(0)))^2 \rangle$ is the relative msd of two arbitrary spins (i, j) located on different macromolecules. Combining eqs 7 and 8 and setting $\vec{r} = 0$ yields

$$A^{\text{inter}}(t) = \sqrt{\frac{2}{3\pi}} \frac{n_s}{(\langle \tilde{r}^2(t) \rangle^{1/2})^3} \quad (9)$$

Thus, for times $t \gg \tau_s$, one is left with two parameters governing the intermolecular correlation function: the spin density n_s and the relative msd $\langle \tilde{r}^2(t) \rangle$. In this case $\langle \tilde{r}^2(t) \rangle^{1/2} \gg \sigma^*$ holds with $\sigma^* \propto (b^2 \rho_s)^{-1}$ being a microscopic quantity characterizing the spatial separation of nearest segments; b is the Kuhn length, and ρ_s is the concentration of Kuhn segments. Otherwise, if the time scale approaches the segmental correlation time $t \cong \tau_s$, the relative msd becomes of the order of the segmental packaging length, i.e., $\langle \tilde{r}^2(t) \rangle^{1/2} \cong \sigma^*$, and eq 9 needs to be corrected:

$$A^{\text{inter}}(t) = \sqrt{\frac{2}{3\pi}} \frac{n_s}{(\sigma^* + \langle \tilde{r}^2(t) \rangle^{1/2})^3} \quad (10)$$

We emphasize that the Gaussian approximation (8) does not necessarily assume that diffusion has Brownian character, i.e.,

$\langle \tilde{r}^2(t) \rangle \propto t$, but also applies for subdiffusive motion. By substituting eq 9 into eq 6, a connection between the relative msd and the relaxation rate ($1/(T_1^{\text{inter}}(\omega))$) can be established:

$$\frac{1}{\langle \tilde{r}^2(t) \rangle^{3/2}} + \frac{2}{\langle \tilde{r}^2(t/2) \rangle^{3/2}} = \frac{5}{4n_s} \left(\frac{4\pi}{\mu_0} \right)^2 \sqrt{\frac{8}{3\pi^3}} \frac{1}{\gamma_H^4 \hbar^2} \int_0^\infty d\omega \frac{\cos(\omega t)}{T_1^{\text{inter}}(\omega)} \quad (11)$$

In polymer melts translational motion is subdiffusive on time scales $\tau_s \leq t \leq \tau_1$ and the msd scales as $\langle r^2(t) \rangle \propto t^\alpha$, where the exponent $\alpha \in [0.25, 1]$, depending on the regime of the underlying polymer dynamics ($\alpha = 1$ reflects isotropic diffusion). Exploiting this power-law character of the msd, the left-hand side of eq 11 can be rewritten

$$\frac{1}{\langle \tilde{r}^2(t) \rangle^{3/2}} + \frac{2}{\langle \tilde{r}^2(t/2) \rangle^{3/2}} = \frac{1 + 2^{1+3\alpha/2}}{\langle \tilde{r}^2(t) \rangle^{3/2}} \quad (12)$$

Note that the α -dependent factor (which is denoted as δ from now on) in eq 12 changes rather slowly for $\alpha \in [0.25, 1]$, thus varying within $3.6 \leq \delta := 1 + 2^{1+3\alpha/2} \leq 6.6$. Finally, to convert the actually measured relative msd $\langle \tilde{r}^2(t) \rangle$ into the absolute displacement $\langle r^2(t) \rangle$, one assumes that motion of chains is essentially independent of each other. Then the relative segmental msd can be estimated as twice as large as the absolute msd yielding the final result

$$\begin{aligned} \langle r^2(t) \rangle &= \frac{1}{2} \langle \tilde{r}^2(t) \rangle \\ &= \frac{1}{2} \left[\frac{5}{4} \left(\frac{4\pi}{\mu_0} \right)^2 \sqrt{\frac{8}{3\pi^3}} \frac{1}{\gamma_H^4 \hbar^2 n_s} \frac{1}{\delta} \int_0^\infty d\omega \frac{\cos(\omega t)}{T_1^{\text{inter}}(\omega)} \right]^{-2/3} \end{aligned} \quad (13)$$

This expression will be applied in the present study to derive the msd.

For a constant $\alpha < (2/3)$ eq 13 is equivalent to

$$\begin{aligned} \langle r^2(t = \omega^{-1}) \rangle &= \frac{1}{2} \langle \tilde{r}^2(t = \omega^{-1}) \rangle \\ &= \frac{1}{2} \left[\frac{5}{12} \left(\frac{4\pi}{\mu_0} \right)^2 \sqrt{\frac{6}{\pi}} \frac{1}{\gamma_H^4 \hbar^2 n_s} \frac{1}{f(a)} \frac{\omega}{T_1^{\text{inter}}(\omega)} \right]^{-2/3} \end{aligned} \quad (14)$$

which was originally derived in ref 9 with

$$f(\alpha) = \frac{\pi\delta}{2 \cos\left(\frac{3\pi\alpha}{4}\right) \Gamma\left(\frac{3\alpha}{2}\right)} \quad (15)$$

Assuming $\langle r^2(t) \rangle \propto t^\alpha$, eq 14 directly leads to

$$\frac{1}{T_1^{\text{inter}}(\omega)} \propto \frac{1}{\omega^{3/2\alpha-1}} \quad (16)$$

For calculating the msd as a function of time, $R_1^{\text{inter}}(\omega)$ is required over a wide range of frequencies. The long-time diffusion coefficient D , however, can be obtained from the low-frequency limit of the total relaxation dispersion $R_1(\omega)$.^{24,25} This was recently demonstrated for simple liquids²⁶ as well as

for polymers.²⁷ The low-frequency dispersion of the rate $R_1(\omega)$ is always dominated by the intermolecular relaxation contribution mediated by translational motion, while at higher frequencies both inter- and intramolecular contributions are relevant. In a liquid, self-diffusion at long times is Fickian, yielding a power-law $A^{\text{inter}}(t) \propto t^{-3/2}$. Therefore, the total relaxation rates (including intra- and intermolecular contributions) can be expanded at low frequencies, providing a universal dispersion law:^{24–27}

$$R_1(\omega) = R_1^{\text{intra}}(\omega) + R_1^{\text{inter}}(\omega) = R_1(0) - \frac{B}{D^{3/2}} \sqrt{\omega} \quad (17)$$

with

$$B = \frac{\pi}{30} (1 + 4\sqrt{2}) \left(\frac{\mu_0}{4\pi} \hbar \gamma_H^2 \right)^2 n_s$$

The intramolecular (reorientational) contribution is included in $R_1(0)$ as the rotational contribution is frequency independent at low frequencies ($\omega\tau_{\text{rot}} \ll 1$). The corresponding spectral density is constant here. Thus, at sufficiently high temperatures $R_1(\omega)$ is indeed expected to follow eq 17 at low frequencies. With given spin density²⁷ n_s (cf. Table 1), the diffusion coefficient D can be directly extracted from $R_1(\omega)$ measured at different temperatures. Important to note, this approach yields absolute $D(T, M)$ values without resorting to a master curve construction.

2.2. Mean-Square Displacement Derived from FG NMR. A stimulated echo FG NMR experiment measures an autocorrelation function, $S_{\text{Dif}}(\tau, t)$, which is essentially equivalent to the intermediate incoherent scattering function in neutron scattering.²⁸ The evolution time τ is proportional to the size of the scattering vector $Q = \tau\gamma g$ (gyromagnetic ratio γ , magnetic field gradient g), and the mixing time t is the dynamic time variable. Since FG NMR always deals with the hydrodynamic regime (Q^{-1} small compared to intermolecular distances) for isotropic diffusion this correlation function is in the limit $t \gg \tau$ given by^{6,29}

$$S_{\text{Dif}}(\tau, t) = \exp[-g^2 \gamma^2 \tau^2 D(t)t] \quad (18)$$

The time-dependent diffusion coefficient $D(t)$ accounts for cases where a possibly sublinear time dependence of the mean-square displacement is mapped onto $D(t)$ via

$$\langle r^2(t) \rangle = 6D(t)t \quad (19)$$

By measuring in two different gradients, G and g , at the same Larmor frequency, the same evolution times τ and mixing times t , it is possible to divide the stimulated echo signals, in the following equations named S_G and S_g , by each other to eliminate all other contributions to the time-dependent NMR signal:

$$S(\tau, t) \equiv \frac{S_G(\tau, t)}{S_g(\tau, t)} = \exp[-(G^2 - g^2) \gamma^2 \tau^2 D(t)t] \quad (20)$$

For the case of anomalous diffusion with a Gaussian propagator (eq 8) the corresponding expression is more involved but can, for arbitrary values of τ and t , be derived from eq 29 of ref 30:

$$S(\tau, t) = \exp \left[-(G^2 - g^2) \gamma^2 \frac{\{D(t+2\tau)(t+2\tau)^{\alpha+2} + D(t)t^{\alpha+2} - 2D(t+\tau)(t+\tau)^{\alpha+2} - 2D(\tau)\tau^{\alpha+2}\}}{(1+\alpha)(2+\alpha)} \right] \quad (21)$$

For $t \gg \tau$, the right-hand side can be expanded and approximated leading to

$$S(\tau, t) = \exp \left[-(G^2 - g^2) \gamma^2 D(t) \tau^2 t \right] \times \left\{ 1 - \frac{2}{(1+\alpha)(2+\alpha)} \left(\frac{\tau}{t} \right)^\alpha + \alpha \left(\frac{\tau}{t} \right) \dots \right\} \quad (22)$$

For the case of normal diffusion, $\alpha = 1$, and in the limit $t \gg \tau$ this expression is exactly equal to eq 20. If the condition $t \gg \tau$ does not hold, eq 22 will lead to an equation quite similar to eq 20 but t being replaced by $t + \frac{2}{3}\tau$.³¹

Note also that the initial decay of the expression (eq 21) is the same for any model of anomalous diffusion.¹¹ Obviously, when deriving $D(t)$ from a full experimental decay curve according to eq 21, some ambiguity prevails due to the lacking knowledge of α . This ambiguity is subsequently transferred, via eq 19, to $\langle r^2(t) \rangle$. As pointed out in the Introduction in the relevant regimes III and IV, $\frac{1}{2} < \alpha < 1$ is expected. This point and its implications will be discussed in more detail further below.

3. EXPERIMENTAL SECTION

3.1. Polymers. The polymers investigated are polybutadiene (PB) with molar masses $M_w = M = 232k$ and $M = 196k$ and polydimethylsiloxane (PDMS) with $M = 0.9k$, $M = 0.6k$, $M = 22k$, and $M = 232k$. The entanglement molar masses are $M_e = 1.9k$ for PB and $M_e = 12k$ for PDMS.³² All polymers were purchased from Polymer Standards Service (Mainz, Germany) and used without further purification. They were filled into standard 5 mm NMR tubes and kept under vacuum for 48 h to remove paramagnetic oxygen gas.

3.2. Extraction of the Intermolecular Relaxation Rate from FC NMR. The 1H NMR spin-relaxation data analyzed in this paper were measured over the temperature interval of 200–400 K using two different electronic FC relaxometers: a commercial one (Stelar Spinmaster FFC 2000) at Bayreuth University covering the 1H Larmor frequency range between $\nu = \omega/2\pi$ of 10 kHz and 20 MHz and a home-built one at Darmstadt University reaching further down to about 100 Hz and up to 30 MHz. For further technical details of the Darmstadt relaxometer we refer to previous publications.^{14–16}

The intermolecular relaxation rate of the measured set of $R_1^{inter}(\omega)$ was determined in our previous publications in terms of a susceptibility master curve $\chi''_{inter}(\omega\tau_s)$,^{10,12,19} with the susceptibility representation given by $\chi''(\omega) \equiv \omega R_1(\omega)$. In order to isolate the inter part from the total relaxation, protonated PB was successively diluted in deuterated PB which suppresses the intermolecular relaxation, since the dipolar interaction between protons and deuterons can be neglected.⁹ Extrapolating to $c \rightarrow 0$ consequently yields $R_1^{intra}(\omega)$, and the intermolecular relaxation rate follows from subtraction $R_1^{inter}(\omega) = R_1^{total}(\omega) - R_1^{intra}(\omega)$. For PDMS we showed that for $\omega\tau_s \ll 1$ the total relaxation is dominated by the intermolecular relaxation.¹⁰ Hence, the total relaxation can be directly used in eq 13. Next, as in the case of many rheological experiments³² frequency–temperature superposition (FTS) is exploited to cover an effectively larger frequency window compared to a single experiment.³³ As the segmental relaxation (α -process) is also covered by our NMR experiments the susceptibility master curve is scaled according to $\chi''(\omega\tau_s)$. Using $\tau_s(T)$ values³³ obtained from the construction of the master curves, the rate $R_1^{inter}(\omega, T)$ for any desired temperature T can be calculated via

$$R_1^{inter}(\omega, T) = \frac{\chi''_{inter}(\omega\tau_s)}{\omega\tau_s} \tau_s(T) \quad (23)$$

Transforming the relaxation data into the msd a cosine transformation of $R_1^{inter}(\omega)$ has to be performed according to eq 13. For that purpose a Filon-type algorithm³⁴ was applied.

3.3. Field-Gradient Experiments. All FG measurements were performed in a (static) superconducting gradient magnet at a 1H Larmor frequency of 99.5 MHz. The magnet provides two different gradients at this frequency: A large one of $G = 168(T/m)$ and a smaller one of $g = 60(T/m)$.³⁵ The magnet resides on an air cushion, so that building and ground vibrations are strongly damped. Thereby, motion of the sample relative to the magnet is effectively avoided which otherwise could easily be misinterpreted in term of molecular diffusion inside the sample.³⁶ The position of the probe head in the magnet can be adjusted by a stepper motor. In this way, measurements in the different gradients can be performed directly after each other without removing the sample from the cryostat nor changing tuning or matching of the probe. The temperature is stabilized in a cryostat, where the temperature drift is less than 0.1 K with an absolute uncertainty of about 1 K. A 2 kW amplifier was used in order to get short ($\pi/2$) pulses of 0.4 μs length. A stimulated echo pulse sequence ($90^\circ - \tau - 90^\circ - t - 90^\circ - \tau -$) was used to measure the time-dependent diffusion coefficient $D(t)$. The stimulated echo signal $S_{StE}(\tau, t)$ with the initial amplitude S_0 may be decomposed along

$$S_{StE}(\tau, t) = S_0 S_{SSR}(\tau) S_{SLR}(\tau) S_{Dip}(\tau, t) S_{Dif}(\tau, t) \quad (24)$$

where $S_{SSR}(\tau)$ and $S_{SLR}(\tau, t)$ describe the spin–spin and the spin–lattice relaxation, respectively, $S_{Dip}(\tau, t)$ denotes the dipolar correlation, and $S_{Dif}(\tau, t)$ is the diffusion-induced decay.^{6,22,29} The only factor depending on the magnetic field gradient is the diffusion factor $S_{Dif}(\tau, t)$. Therefore, when dividing experimental data $S_{StE}(\tau, t)$ gained at a large gradient G by those gained in a small gradient g , we are left with $S(\tau, t)$ given by eqs 21 and 22.

Figure 1 exemplarily shows data taken at 292 K of the two normalized decay curves $S_G(\tau, t = 51 \text{ ms})$ and $S_g(\tau, t = 51 \text{ ms})$,

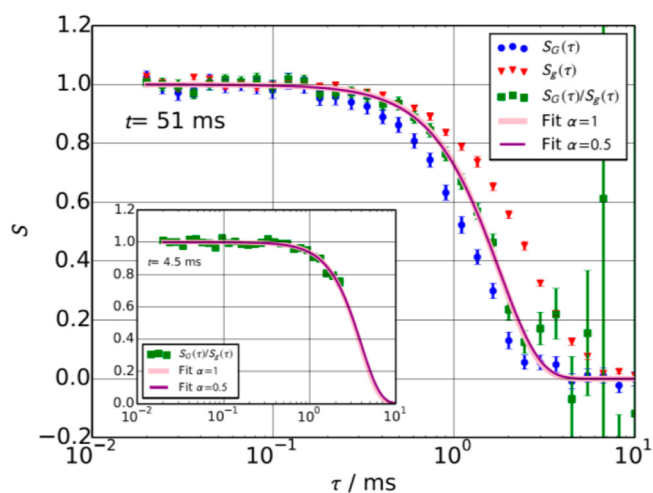


Figure 1. Stimulated echo amplitude of PDMS 232k at $T = 292$ K in two different gradients $G = 168 \text{ T m}^{-1}$ and $g = 60 \text{ T m}^{-1}$ at a 1H Larmor frequency of 99.5 MHz and a fixed mixing time $t = 51 \text{ ms}$. In addition, the ratio of both curves is shown. The fits of $S(\tau) = (S_G(\tau)/S_g(\tau))$ with eq 22 for $\alpha = 0.5$ and $\alpha = 1$ are almost indistinguishable (drawn curves). Inset: same experiment using $t = 4.5 \text{ ms}$.

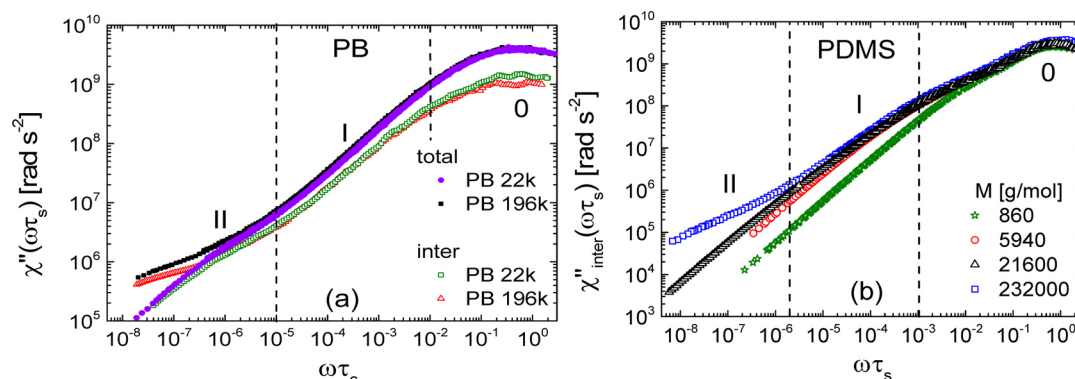


Figure 2. (a) Susceptibility master curves of polybutadiene (PB) with two different molar masses as obtained from field-cycling ^1H NMR relaxometry. Both the intermolecular, $\chi''_{\text{inter}}(\omega\tau_s)$, and total susceptibilities, $\chi''(\omega\tau_s)$, are shown. Different relaxation regimes (0, I, II) and molar masses (M) are indicated. (b) Susceptibility master curves $\chi'' \cong \chi''_{\text{inter}}$ of PDMS with different M .

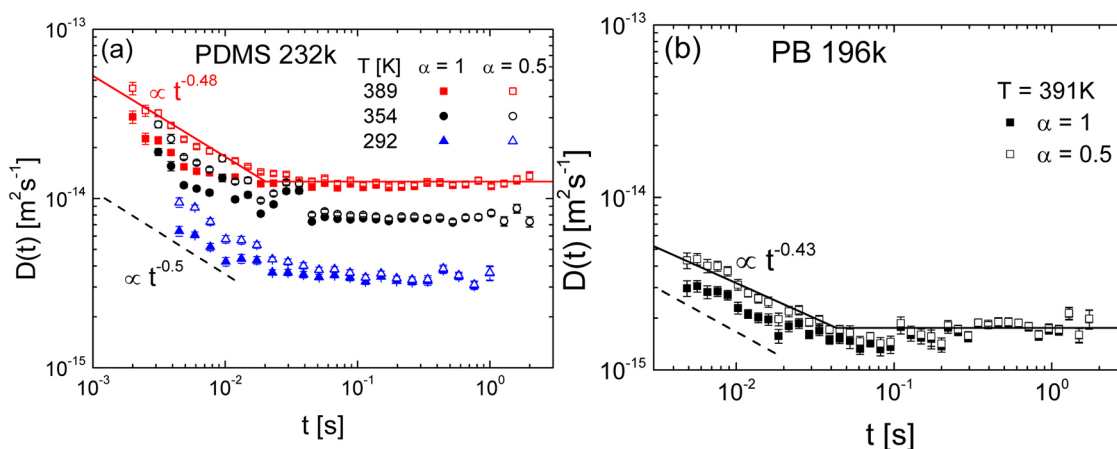


Figure 3. Time-dependent diffusion coefficients of PDMS 232k (a) and of PB 196k (b) as deduced from fits of eq 22 to the measured decay curves $S(\tau)$ as exemplified in Figure 1. For small diffusion times the resulting $D(t)$ depends on the choice of α . The solid lines show fits for highest temperatures and $\alpha = 0.5$ used in eq 22 (see text) with a power-law decay (resulting exponents are indicated) at short and a constant regime D at long times. The dashed lines illustrate a power law $D(t) \propto t^{-0.5}$ (regime III) predicted by the TR model.

measured in the two gradients G and g , respectively. Also, the ratio $S(\tau, 51 \text{ ms}) = (S_G(\tau, 51 \text{ ms})/S_g(\tau, 51 \text{ ms}))$ is plotted.

Note that the condition $t \gg \tau$ is fulfilled for this example as S reaches almost zero at $\tau \approx 5 \text{ ms} \ll t = 51 \text{ ms}$. If this condition was not fulfilled, the diffusion time t would not be defined accurately since the molecules significantly diffuse during the evolution time τ . In order to accounting for the condition $t \gg \tau$, we decided to evaluate the data only for evolution times $\tau < 0.5t$. In this limiting case, the “true” diffusion time may still be approximated by t as a lower limit. An upper limit for the diffusion time can be approximated by $t + \tau_{\text{max}}$. Here τ_{max} is taken either to be the longest evolution time used for the fit or the half decay time of the magnetization, depending on which one is shorter. The inset of Figure 1 shows the diffusion decay at the shortest chosen diffusion time, $t = 4.5 \text{ ms}$, of PDMS 232k at $T = 292 \text{ K}$. According to the above condition only the beginning of the decay curve is shown and fitted. From these fits time-dependent (apparent) diffusion coefficients $D(t)$ are gained which will be discussed in section 4.2.

4. RESULTS

4.1. Susceptibility Master Curves from FC NMR. Figure 2 displays the susceptibility master curves of PB (a) and PDMS (b), both extending over about 9 decades in frequency, as obtained from FC ^1H NMR relaxometry comprising relaxation data in the temperature range of around 200–400 K (cf. ref 10). In the case of PB both the total relaxation data $\chi''(\omega\tau_s)$ and the pure intermolecular contributions $\chi''_{\text{inter}}(\omega\tau_s)$ are shown, the

latter being extracted previously by isotope dilution experiments.^{10,19} The susceptibility shows three relaxation regimes denoted by 0, I, and II. Regime 0 reflects the (fast) segmental dynamics and manifests itself in a relaxation peak at $\omega\tau_s \cong 1$. For $\omega\tau_s \ll 1$ regime I features a M -independent power-law regime reflecting Rouse dynamics while regime II at lowest frequencies ($\omega\tau_s \ll 10^{-5}$ in PB and $\omega\tau_s \ll 2 \times 10^{-6}$ in PDMS) is characteristic for entanglement dynamics and has a significantly smaller and M -dependent power-law exponent.^{10,19,37} We note that the crossover from regime 0 to I, i.e. the beginning of the Rouse regime, is somewhat difficult to define. It works better for the transition between I and II occurring at $\omega\tau_s \approx 1$ (see below). As far as PDMS is concerned, it was shown that the relaxation is dominated by intermolecular relaxation over the whole frequency range $\omega\tau_s \ll 1$,¹⁰ implying $\chi'' \cong \chi''_{\text{inter}}$. Another peculiarity is that for PDMS the power-law regime I first appears at frequencies ($\omega\tau_s < 10^{-3}$) of 1 decade smaller than for PB ($\omega\tau_s < 10^{-2}$). Actually, some kind of shoulder is recognized. We will return to this point below.

4.2. Time-Dependent Diffusion Coefficients Gained from FG NMR. Let us proceed with the results from FG NMR. For all temperatures the diffusion coefficients depicted in Figure 3 for both PDMS 232k and PB 196k clearly show a time dependence at short times. One subtlety has to be taken care of while fits with eq 22 lead to decay curves which cannot

Table 1. Collected Properties of PB and PDMS at 390 K^a

property	PDMS 232k (<i>T</i> = 389 K)		PB 196k (<i>T</i> = 391 K)	
τ_1 [ms]	20		43	
D [m ² s ⁻¹]	1.3×10^{-14}		1.8×10^{-15}	
$\langle r^2(\tau_1) \rangle$ [nm ²]	1500		450	
$\langle R_0^2 \rangle$ [nm ²]	1100 ⁴⁰		1700 ⁴⁰	
	experimental (present work)	from literature	experimental (present work)	from literature
a_0 [nm]	4.8 ⁴¹	7.9, ⁴⁰ 7.2 ⁴²	3.2	3.2, ⁴³ 4.4 ⁴⁰
b [nm]	1.6	1.3 ³²	0.5	1.0 ³²
M_0 [g mol ⁻¹]	381 ³²		113 ³²	
M_e [g mol ⁻¹]	12k ³²		1.9k ³²	
$N_e = M/M_e$	31		17	
$N = M/M_0$	609		1735	
T_g [K]	150 ⁴⁴		180, ⁴⁵ 177, ¹⁹ 175 ⁴⁶	
n_s [10 ²⁸ m ⁻³]	4.70 ²⁷		5.75 ²⁷	

^aTerminal relaxation time τ_1 and $D = D(t \rightarrow \infty)$ determined from Figure 3; the msd $\langle r^2(\tau_1) \rangle$ and the mean-square end-to-end distance $\langle R_0^2 \rangle$ taken from ref 40. Estimates for the tube diameter a_0 and the Kuhn length b and in comparison to values given in the literature (as indicated); for their uncertainties see text. Other parameters used were taken from the literature: the Kuhn molar mass M_0 , the entanglement molar mass M_e , the ratios $N_e = M/M_e$ and $N = M/M_0$, the glass transition temperature T_g and the spin density n_s .

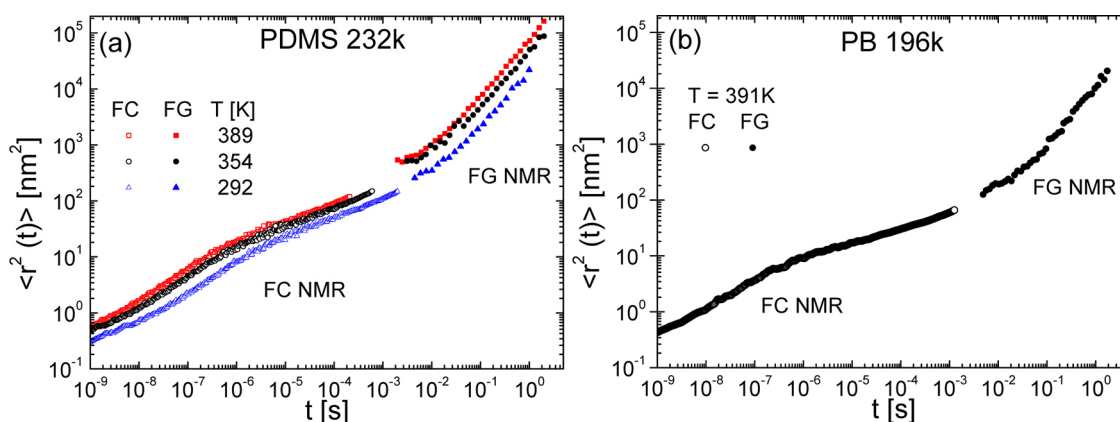


Figure 4. (a) Segmental mean-square displacements obtained from field-cycling (FC) and field-gradient (FG) ¹H NMR for PDMS 232k at temperatures as indicated. (b) Corresponding results for PB 196k.

distinguish between $\alpha = 0.5$ (TR regime III) and $\alpha = 1$ (TR regime IV); for small diffusion times the resulting apparent diffusion coefficients $D(t)$ do differ and for $\alpha = 0.5$ being above those for $\alpha = 1$ by up to a factor of 2 (Figure 3).

The short-time regime in both polymers can be acceptably described by a power law $D(t) \propto t^{-0.5 \pm 0.1}$ which is expected for regime III of the TR model (cf. the inset of Figure 5b). At long times the diffusion coefficient becomes time-independent when the terminal relaxation of free diffusion (regime IV) is finally reached. For highest temperatures we exemplarily included fit curves for both polymers in Figure 3 consisting of an initial power-law decay regime and a constant long time regime $D(t \rightarrow \infty) = D$ the transition occurring at the terminal relaxation time τ_1 . The resulting D and τ_1 are included in Table 1. Although the transition between regimes III and IV is clearly discernible, the experimental errors are significant. We emphasize again the experimental difficulties of reaching such low diffusion coefficients by FG NMR, especially in the case of PB (cf. Experimental Section). At this point a comment on the validity range of FG measuring time-dependent diffusion coefficients is appropriate: A competing process which may eventually feign segmental diffusion or at least contribute to $D(t)$ is spin diffusion. The validity criterion chosen by us requires the long time diffusion coefficient to scale with the inverse segmental relaxation time, i.e., $D \propto \tau_s^{-1}$. If we do so, it turns out that data

only at those temperatures shown in Figure 3 can be trusted; at lower temperatures spin diffusion gradually takes over.

As stated, in regime IV the evaluated $D(t)$ does not depend on the choice of the parameter α in eq 22, but it does in regime III. Here, $\alpha = 0.5$ is expected from the TR model for which we will base the evaluation of the msd on those $D(t)$ data obtained with $\alpha = 0.5$. According to eq 19 the time-dependent msd, to be discussed later, can now be directly evaluated from these $D(t)$.

4.3. Mean-Square Displacements from Combination of FC and FG Data. In Figure 4 the msd of both PDMS 232k (a) and PB 196k (b) is displayed for several temperatures as obtained from the application of eq 13 (FC NMR data) and via $\langle r^2(t) \rangle = 6D(t)t$ (FG NMR data). For the FC NMR data we employed $\alpha = 3/8$ being the average of $\alpha = 0.5$ and $\alpha = 0.25$ predicted for the regimes I and II of the TR theory, respectively, which are usually covered by the FC method for high M . We once again emphasize that the influence of the parameter α is marginal here. About 10 decades in diffusion time is covered, and the data obtained from FC NMR agree well with the absolute values derived from FG NMR. Several power-law regimes are identified in both polymers and will be discussed below. We note that at shortest times, say, at $t < 10^{-9}$ s, eq 13 does no longer apply as the spatial extension of the monomer unit is not taken into account. Thus, our analysis holds for times $t \gg \tau_s$.

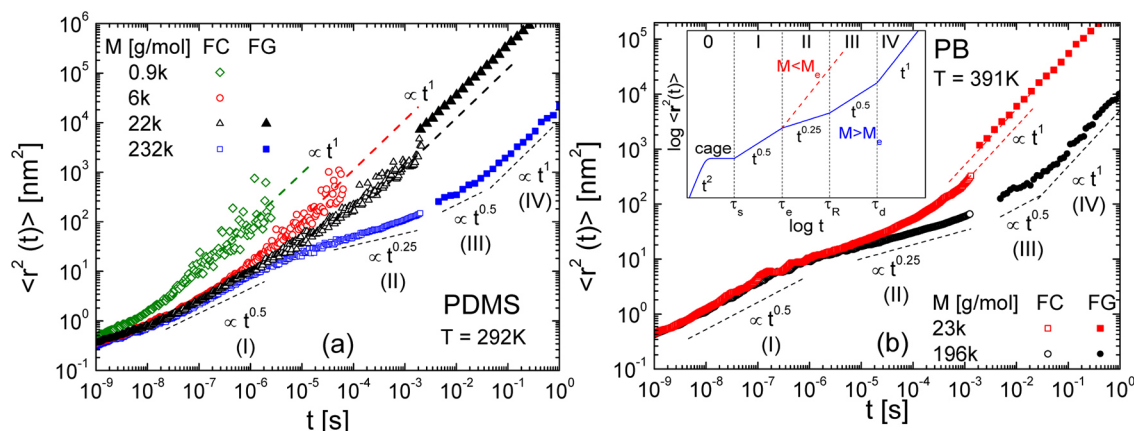


Figure 5. Segmental mean-square displacement of PDMS (a) and PB (b) obtained from FC and FG NMR; data for a single temperature are shown. In both, data for short-chain systems are included. Dashed lines represent corresponding power-law regimes. The inset in (b) illustrates the prediction of the TR theory.

Figure 5 shows the msd of PDMS at 292 K (a) and PB (b) at 391 K and for different molar masses. First, we discuss the case of highest M , PDMS 232k and PB 196k, both being well above M_e . Starting with the FC NMR data at short times, the msd of both polymers follows a power-law which matches the prediction of (free) Rouse dynamics with $\alpha_R = 0.5 \pm 0.1$ well (regime I). At succeeding times, in regime II a power-law exponent of $\alpha_{II} = 0.3 \pm 0.1$ is observed in PDMS 232k while $\alpha_{II} = 0.2 \pm 0.1$ is found in PB 196k. Both values are consistent with 0.25 of the constraint Rouse regime (II) predicted by the TR model. On even longer times, a further power-law with $\alpha_{III} = 0.5 \pm 0.1$ for both PDMS 232k and PB 196k appears in the FG NMR data. This relaxation regime is quite limited in time and actually difficult to be unambiguously identified. However, it can be well estimated from the diffusion data shown in Figure 3. Finally, at longest times the free diffusion limit (regime IV) with an exponent $\alpha_{IV} = 1.0 \pm 0.1$ is reached in both polymers. Thus, for the first time all four power-law regimes of the TR model are discovered in two high- M polymers by combining two NMR techniques, and the power-laws are close to those predicted by the TR model.

When going to lower M the regimes II and III, which reflect the entanglement dynamics, shrink and the free diffusion regime (IV) directly succeeds the Rouse regime (I). PDMS 22k and PDMS 6k, for instance, are close to $M_e = 12k$. While the Rouse regime (I) is still fully established with $\alpha_R = 0.5 \pm 0.1$ in the FC NMR data, regime II disappears in both cases, and already the FC NMR measurements reach the regime of terminal relaxation, i.e., $\langle r^2(t \gg \tau_1) \rangle \propto t^1$. Regime III is completely absent in the FG NMR data of PDMS 22k. Although FC NMR and FG NMR data show virtually the same exponent in the terminal regime (IV), they do not fully agree on an absolute scale provided by the FG data; a discrepancy of a factor 3–4 prevails. We will discuss possible reasons for this mismatch below. For PDMS 0.9k even the Rouse regime is missing. In this case essentially no polymer dynamics is discovered as this oligomer actually behaves like a simple liquid. For PB just one further molar mass with $M = 23k$ is studied by FC NMR as an isotope dilution experiment is necessary here in order to isolate the intramolecular relaxation.^{9,10,19–21} Although regime II is significantly less pronounced, it can still be identified. Regime III appears to be absent in the corresponding FG NMR data. While for $M \gg M_e$ only the combination of FG

and FC NMR provides the full msd, FC NMR already suffices to probe the translational dynamics for $M \leq M_e$.

In Figure 6, we compare the msd for PB 196k and PDMS 232k at virtually the same temperature ($T \cong 390$ K) in a

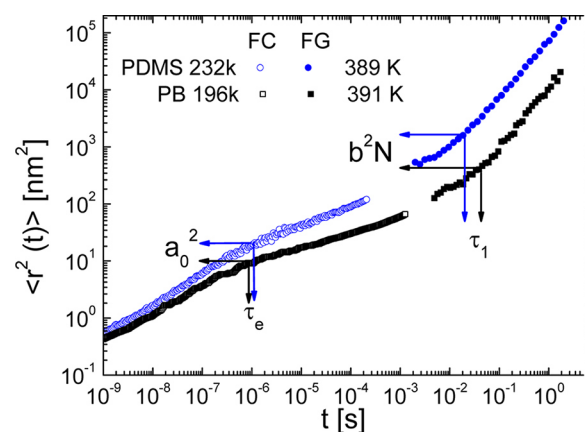


Figure 6. Segmental mean-square displacement (msd) of polydimethylsiloxane (PDMS) and polybutadiene (PB) for a similar temperature. Entanglement time τ_e and disengagement time $\tau_d = \tau_1$ referred to the intersection points of the power-law transitions between regimes I to II and III to IV, respectively, are indicated. The msd evaluated at τ_e and τ_1 provide an estimate of the tube diameter a_0 and segment length b , respectively (cf. Table 1).

common presentation. From the intersection points of the power-law regimes I and II we extract rough estimates of the tube diameter¹ $a_0 = \langle r^2(t = \tau_e) \rangle^{1/2}$ and the entanglement time τ_e . We read from the plot $a_0 = 4.8$ nm for PDMS and $a_0 = 3.2$ nm for PB (cf. also Table 1). A comparison with literature data follows in the Discussion. Moreover, the Kuhn length b can be estimated via¹ $\langle r^2(\tau_1) \rangle = Nb^2$, i.e., from the intersection points between regimes III and IV. In order to get b the number of Kuhn segments $N = M/M_0$ with M_0 being the Kuhn segment mass has to be known. We tentatively adopt M_0 from the literature³² (cf. Table 1). The extracted proxies are $b = 1.6$ nm for PDMS and $b = 0.5$ nm for PB. The uncertainties of both a_0^2 and b^2 , as read from Figure 6, are estimated to be of about a factor of 2.

Recently,²⁷ in the case of PDMS absolute (long-time) diffusivities $D(M)$ were determined by applying eq 17; i.e., the

total relaxation rate was analyzed in the low-frequency limit for various temperatures without applying FTS. In Figure 7 we

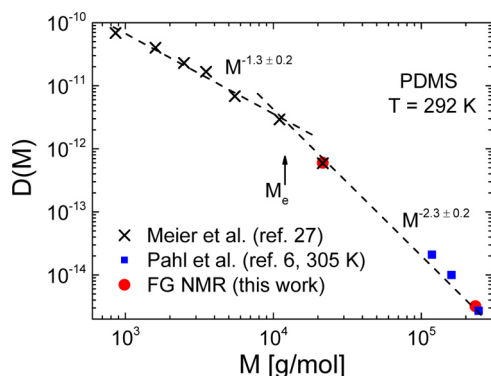


Figure 7. Molar mass dependence of the (long-time) diffusion coefficient D of PDMS at 292 K obtained from FG NMR (red disks). For comparison, values of Meier et al.,²⁷ derived from FC ^1H NMR relaxometry (black crosses) and from Pahl et al.,⁶ also obtained by FG NMR (blue squares), yet, at a slightly higher temperature of 305 K, are included. Two power-law regimes are indicated while the crossover molecular mass agrees well with the entanglement molar mass $M_e \approx 12\text{k}$ (cf. Table 1 and refs 32 and 40).

compare those data with the ones from the present FG NMR work and with literature data⁶ at about 292 K. All three data sets match very well. While FG NMR covers the entanglement regime $M > M_e$ and a power-law with the exponent $\alpha = 2.3 \pm 0.2$ is found in agreement with literature data,^{5,6,38,39} FC NMR cannot cover high M with the present low-frequency limit of some 100 Hz. In any case, the crossover from Rouse to entanglement dynamics can be well identified. We emphasize that the low- M D values are not corrected for the M -dependent monomeric friction coefficient as it was done before.²⁷ In the case of PB we measured only at a single M value and literature data at this temperature is not available.

5. DISCUSSION

The complementary frequency/time windows of FC ^1H NMR and static FG ^1H NMR experiments were combined in order to measure the segmental msd in two different polymers, namely PDMS and PB, over almost 10 decades. While the msd can be easily obtained from the (time dependent) diffusion coefficient measured by FG NMR, it is calculated from FC ^1H NMR intermolecular relaxation data involving Fourier transformation (eq 13). In general, the intermolecular contribution must be isolated from the total ^1H spin–lattice relaxation data by applying an isotope dilution experiment.^{9,10,19–21} Only in favorable cases like PDMS the total ^1H relaxation at $\omega\tau_s \ll 1$ is dominated by the intermolecular relaxation since the fast methyl group rotation reduces the intramolecular relaxation. Thus, the data can directly be used for obtaining the msd.¹⁰ As the time windows of FC and FG NMR do not overlap, the experiments need to be performed at different temperatures; thus, a direct comparison of the msd relies in the construction of the master curve $\chi''_{\text{inter}}(\omega\tau_s)$ which assumes the validity of FTS. With $\tau_s(T)$ known from the master curve construction, $\chi''_{\text{inter}}(\omega)$ can be calculated for any temperature. As will be discussed below, there are strong indications that FTS indeed applies well for both polymers.

At time scales longer than the segmental relaxation time ($t \gg \tau_s$) four different relaxation regimes, each showing power-law

behavior, can be identified for the msd in the high- M limit and compared to the TR model.¹ While regimes I and II are covered by FC NMR, FG NMR traces the transition from regime III to IV (Figure 5). The four regimes can be associated with those from the TR model, namely that of the (free) Rouse (I), the constrained Rouse (II), the reptation (III), and finally the free diffusion (IV) regime at longest times. All found power-law exponents agree well, within ± 0.1 , with the predicted ones. On an absolute scale, it appears that there is some mismatch between the msd measured by FC and FG NMR, in particular for $M = 22\text{k}$ for both PDMS as well as PB (cf. Figure 5). Field-gradient NMR yields absolute msd values within an uncertainty of a factor of 2 at most which is due to the lacking knowledge of the power law exponent α . The corresponding msd data of FC ^1H NMR relies on several assumptions: (i) Adopting $\tau_s(T)$ from master curves assumes FTS to hold. Any correction will shift the FC ^1H NMR msd along the time axis (cf. Figure 5). (ii) The choice of the numerical factor δ in eq 13 weakly influences the value of the msd. It is actually time dependent due to the different diffusion regimes covered. (iii) The assumed relation between relative and absolute msd may not strictly hold (cf. Theoretical Background). In general, it may vary according to $\langle r^2(t) \rangle = (1/q)\langle \tilde{r}^2(\tau_1) \rangle$ with $0 \leq q \leq 2$, the limits representing the cases of rigidly bonded segments and completely uncorrelated segmental motion, respectively. However, when regime IV is reached, $q = 2$, precisely. (iv) The Gaussian approximation is assumed for deriving the connection between the msd and $R_1(\omega)$ (eq 8). If it does not fully apply an additional numerical factor would appear. (v) Fast dynamics (β -process, methyl group rotation in PDMS, etc.) also may slightly affect the results. Given these various sources of possible corrections of the FC ^1H NMR data, we think the present results provide a fair agreement between the two NMR methods. So, within these limitations, for the first time, all four diffusion regimes of the msd are covered and confirm the TR model. We note that the power-law regimes I and II were also covered by NS experiments.⁴ Here, FC NMR and NS are competing techniques, yet according to our knowledge no msd data from NS addressing the regime I to II transition are available for PDMS and PB.

The TR model also provides predictions⁴⁷ regarding the segmental reorientation correlation function $A_l(t)$ of rank l . According to the so-called return-to-origin hypothesis,^{47,48} the model predicts an inverse proportionality between $A_l(t)$ and $\langle r^2(t) \rangle$ in regimes II and III independent of rank l , specifically, $A_l(t) \propto \langle r^2(t) \rangle^{-1}$. This relation was tested by FC ^1H and ^2H NMR and found to be violated.¹⁰ However, in a recent publication by Furtado et al. applying also isotope dilution and double quantum (DQ) NMR together with MD simulations the TR predictions were confirmed essentially.³⁷ Yet, in a succeeding publication¹⁹ we reanalyzed our results together with new measurements. We critically assessed the findings and once again reproduced our previous results. For example, in the case of PB the exponent of $A_2(t)$ in regime II turns out to be $\alpha_{11} \approx 0.44$, which is in strong disagreement with the prediction 0.25 given by the TR model, although finite chain length effects were taken into account. We emphasize that $A_2(t)$ can only be obtained from isolating the intramolecular ^1H relaxation contribution or, more directly, by FC ^2H NMR. Although the discrepancy among the results from DQ and FC NMR still needs to be settled, given our FC NMR results, it appears that the inverse proportionality between $A_2(t)$ (probing reorientation) and the msd (probing translation) does not apply.

Possibly, the relation depends on the microscopic details of the polymer chain, i.e., the chemical structure of the monomer.

At 390 K the tube diameter is obtained from the condition $a_0 = \langle r^2(\tau_e) \rangle^{1/2}$, and τ_e is defined as the crossover time between the regimes I and II. In the case of PDMS the deduced diameter, $a_0 = 4.8$ nm, is smaller than reported from rheological experiments which gave $a_0 = 7.9$ nm⁴⁰ while $a_0 = 7.2$ nm was found in NS experiments (cf. Table 1 and Figure 6).⁴² We note that in the case of PDMS our value differs somewhat from the one reported previously.^{10,41} Regarding PB, our value of $a_0 = 3.2$ nm is in good accordance with reference values derived from rheological experiments (cf. Table 1).^{40,43} It appears, however, that a_0 slightly depends on temperature.^{40,49}

The FG NMR data also allow estimating the Kuhn lengths b from the transition time between regime III and IV using $\langle r^2(\tau_1) \rangle = (M/M_0)b^2$.¹ The value $b = 1.6$ nm obtained for PDMS agrees reasonably well with literature data (cf. Table 1). In PB, for which $b = 0.5$ nm is found, there is a deviation by a factor of 2. Of course, M_0 and b are not independent of each other, and therefore only a proxy for b can be given. On the other hand, within the TR model,^{1,50} at τ_1 the msd is expected to be equal to the mean-square end-to-end distance $\langle R_0^2 \rangle$, i.e., $\langle R_0^2 \rangle \approx \langle R^2(\tau_1) \rangle$. It can be determined by small-angle neutron scattering (SANS) and compared to our results (cf. Table 1). Given the molar masses of PB and PDMS investigated in this work the SANS results reported in ref 40 provide $\langle R_0^2 \rangle = 1100$ nm² for PDMS and $\langle R_0^2 \rangle = 1700$ nm² for PB, while we obtain $\langle R^2(\tau_1) \rangle = 1500$ nm² and $\langle R^2(\tau_1) \rangle = 450$ nm². Again, the discrepancy is much less for PDMS than for PB. Here one has to keep in mind that data from experiments characterizing the dynamics (FG NMR) and the structure (SANS) may not necessarily agree.

Next, we compare the time constants $\tau_s(T)$, $\tau_e(T)$, and $\tau_1(T)$ from our work with data found in the literature. As far as PB is concerned, we first display the segmental time constant $\tau_s(T)$ in Figure 8 as obtained from combining FC ¹H NMR and dielectric spectroscopy^{33,51} (DS) for various high- M samples. In this limit $\tau_s(T)$ is independent of M which goes along with a saturation of T_g . Usually in polymers, $\tau_s(T)$ is interpolated by a Vogel–Fulcher–Tammann equation. Alternatively, we use a recently introduced four-parameter function^{52,53} (cf. Appendix). Experimental data of high-temperature segmental time constants are scarce. Here, FC NMR offers a unique opportunity to provide $\tau_s(T)$. The values $\tau_s(T)$ can be checked against those from rheological experiments which usually provide the temperature dependence in terms of the shift factor a_T . In ref 46, $a_T(T)$ is given for PB ($M = 130$ k), and together, with $\tau_s(298$ K) = 0.3 ns,³² it is referred to $\tau_s(T)$ as described in the Appendix. The thus calculated curve (green dashed line) reproduces our data almost perfectly. Alternatively, $\tau_s(T)$ (more precisely the fastest Rouse time $\tau_0(T)$) can be calculated from the monomeric friction coefficient $\xi(T)$ given in ref 45 (cf. eq 27, Appendix). This leads again to a fair agreement with our results (cf. purple dashed line in Figure 8).

Rheological experiments are well established for determining the terminal time τ_1 . We follow ref 32 and estimate τ_1 from the intersection of the storage and loss shear moduli at lowest frequencies. The red (open and full) symbols in Figure 8 represent τ_1 values obtained in this way from a multitude of rheological results.^{32,46,54–57} A large range of molar masses $21\text{k} \leq M \leq 925\text{k}$ is covered, essentially at room temperature. Assuming FTS, our interpolation (black solid line) of the FC NMR and DS data along eq 25 for $\tau_s(T)$ is shifted to intersect

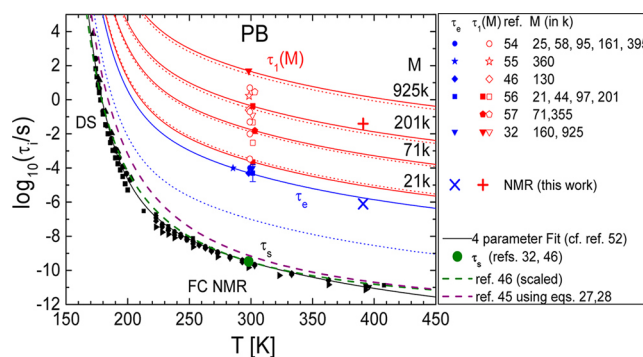


Figure 8. Temperature and M dependence of the time constants of PB: $\tau_s(T)$ for several high- M samples ($M > M_e$) (distinguished from each other by the different black symbols) as obtained from FC NMR and DS,^{33,51} respectively, interpolated by the black solid line in comparison to rheological data reported in the literature as indicated (green and purple dashed lines). Terminal relaxation time $\tau_1(T)$ as obtained by FG NMR (red cross) and by rheology (other red symbols). Solid red lines: same interpolation of $\tau_s(T)$ but shifted for hitting selected M values (represented by solid red symbols) suggesting the behavior of $\tau_1(T)$. Red dashed lines: prediction for $\tau_d(T)$ by the TR model for the selected M . $\tau_e(391$ K) as obtained by FC NMR (blue cross) in comparison to rheological data (other blue symbols). The solid blue line is another shifted version of the interpolation of $\tau_s(T)$. Dashed blue line: prediction by the TR model for $\tau_e^{DE}(T)$. Molar masses M are indicated.

selected data points (solid red symbols in Figure 8) obtained from rheology providing the solid red lines. Obviously, our FG NMR measurement, yielding $\tau_1(391$ K) = 43 ms (cf. Figure 3b) in the case of PB 196k, is in fair agreement with the behavior suggested by shifting $\tau_s(T)$ through the value given by the rheological data given in ref 56 for the similar molar mass of 201k. The M dependence $\tau_1(M)$ is further discussed below.

Field-cycling NMR also provides τ_e (cf. Figure 6); actually, this crossover from regime I to II is well documented in all FC NMR experiments.^{10,19,33} We are not aware of any work which attempts to estimate τ_e in a model-independent way. In rheological spectra and according to the ideal TR model, τ_e should be given by the beginning of the rubber plateau in $G'(\omega)$ or $G(t)$ or likewise from the end of the Rouse power-law regime. This implies that τ_e is also given by the minimum in $G''(\omega)$ (cf. ref 50). However, experimentally the position of the minimum depends weakly on M , which appears not to be the case for τ_e as probed by FC NMR. Notwithstanding, we estimated τ_e from the minimum in $G''(\omega)$ and included it in Figure 8 (blue symbols) together with an error bar indicating the spread with M . A version of the interpolation of $\tau_s(T)$ is once again shifted to intersect (the average of) those τ_e data. Our value of $\tau_e(391$ K) = 0.8 μ s (cf. Figure 3a) is in good agreement with these rheological results. Thus, it appears that the time constants τ_e obtained from NMR agree rather well with those obtained from rheology when taking τ_e from the minimum, ignoring its weak M dependence. As will be shown below this also holds for PDMS.

The results collected for PB and shown in Figure 8 can be checked against the predictions of the TR model according to which the disengagement time τ_d is related to τ_s via^{1,11} $\tau_d(T) = 3\tau_s(T)(N^3/N_e)$. Such calculated curves for selected molar masses (red solid symbols) using the interpolation of $\tau_s(T)$ and N_e given in Table 1 are included in Figure 8 as red dashed lines. Fair agreement with the experimental results (τ_1) is found.

However, experimentally $\tau_1(M)$ rather scales with $M^{3.4}$.^{32,44,46} Therefore, deviations between τ_1 and τ_d are anticipated. With respect to the entanglement time τ_e the TR model provides^{1,11} $\tau_e^{DE} = \tau_s N_e^2$. This prediction is also included in Figure 8 as a blue dashed line. Likewise, it can be expressed and estimated in terms of the disengagement time along $\tau_e^{DE} = (\tau_d/3)(N_e/N)^3$. A very similar result (and thus not shown) is found to that obtained using $\tau_e^{DE} = \tau_s N_e^2$. Apparently, in the case of PB the TR prediction for τ_e^{DE} is more than 2 decades shorter than suggested by FC NMR and by the minimum of the rheological spectra, even if the more realistic $\tau_e^{DE} \propto \tau_1(N_e/N^{3.4})$ (instead of -3.0) scaling is used. As indicated in ref 32 τ_e , when calculated from the TR model, appears to be close to the crossing of $G'(\omega)$ and $G''(\omega)$ at high frequencies which indeed is much higher than the minimum in $G''(\omega)$. Yet, it is not obvious what the physical meaning of this intersection is.

The comparison of the different time constants $\tau_s(T)$, $\tau_e(T)$, and $\tau_1(T, M)$ can be carried out for PDMS as well, which is done in Figure 9. When compared to rheological data⁴⁴ (cf.

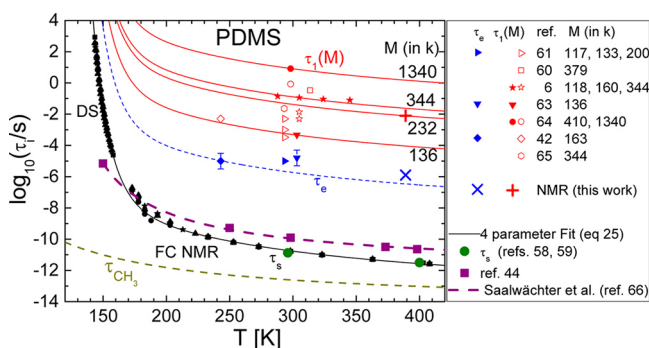


Figure 9. Temperature and M dependence of the time constants in PDMS: $\tau_s(T)$ for several high- M samples ($M > M_e$) (distinguished by the black solid symbols) as obtained from FC NMR and DS fitted with a four-parameter function⁵² (black solid line, cf. Appendix) in comparison to rheological data (see text). $\tau_e(389\text{ K})$ as obtained by FC NMR (blue cross) in comparison to rheological data (other blue symbols). Dashed blue line: prediction by the TR model for τ_e^{DE} . Red: $\tau_1(T)$ as obtained from our FG NMR results (red cross) and from reference data (also FG NMR⁶ and rheology, other red symbols). Solid red lines: several versions of the interpolation of our $\tau_s(T)$ data shifted for intersecting selected M values (solid red symbols) suggesting the behavior of $\tau_1(T)$. The molar masses studied in each reference are indicated. Also indicated: time constant $\tau_{CH_3}(T)$ of methyl group rotation.⁶⁰

Appendix) our high-temperature values for $\tau_s(T)$ appear to be faster by 1 decade. Two values for $\tau_s(T)$ were reported,⁵⁸ which were originally deduced from NS⁵⁹ confirming our result (green disks in Figure 9). As a note of caution: we were unable to retrace these values to the original work.⁵⁹ As the $\tau_s(T)$ values determined by FC ^1H NMR could be spoiled by the influence of the methyl group rotation, we included in Figure 9 the corresponding values $\tau_{CH_3}(T)$; they are significantly shorter.⁶⁰ As another possibility we suggest the following: FC NMR and DS actually probe reorientations on molecular level (so-called α -process). This must not necessarily be identical with the shortest Rouse time τ_0 reflecting reorientation of the Kuhn element, a finding deserving further investigations. As in the case of PB $\tau_s \approx \tau_0$ is found from the consistency between eq 28 (Appendix) and the experiments, we conclude that rather $\tau_0 \approx 10\tau_s$ holds for PDMS. Reinspecting Figure 2b the power-law

regime I (characteristic of free Rouse dynamics) sets in at $\omega\tau_s < 10^{-3}$ while in the case of PB this crossover is already observed at $\omega\tau_s < 10^{-2}$ (Figure 2a).

The terminal relaxation time $\tau_1(T = 389\text{ K}) = 20\text{ ms}$ obtained by FG NMR for PDMS 232k essentially agrees with reference data: the value is somewhat lower than anticipated from the FG NMR data in ref 6 for PDMS 344k and somewhat larger than that of PDMS 200k measured by rheology.⁶¹ The value $\tau_e(389\text{ K}) = 1.3\text{ }\mu\text{s}$ obtained by FC NMR is in fair agreement with data obtained from rheological experiments^{42,61,63} (blue symbols in Figure 9) extrapolated to 389 K when again taking the minimum in $G''(\omega)$. As we lack of a reliable source of τ_0 we calculate τ_e^{DE} from τ_1 applying $\tau_e^{DE} = (\tau_1/3)(N_e/N)^3$ for PDMS 232k. Unlike in PB our value τ_e agrees acceptably with τ_e^{DE} predicted by the TR theory. Otherwise, the estimation along $\tau_e^{DE} = \tau_s N_e^2$ provides, as in the case of PB, values, which are by more than 2 orders of magnitude too short when compared to the experimental τ_e , even when $\tau_0 \approx 10\tau_s$ is taken into account.

Finally, the M -dependence of τ_1 evaluated at around 300 K is plotted in Figure 10. In the case of PB we included a fit with a

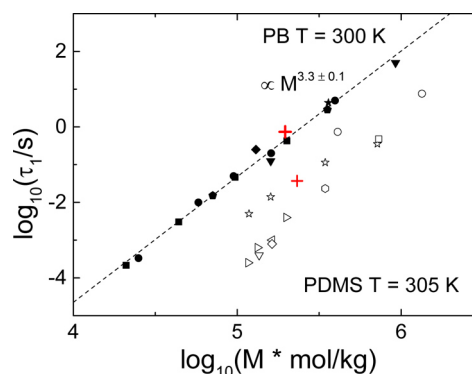


Figure 10. M -dependence of the terminal relaxation time τ_1 obtained from rheological experiments, evaluated at 300 K for PB (solid symbols) and PDMS at 305 K (open symbols). Red crosses: τ_1 as obtained from the transition between regime III and IV in Figure 6. The symbol style reflects the various references given in Figures 8 and 9, respectively. A fit with a power-law provides $\tau_1 \propto M^{3.3 \pm 0.1}$ for PB (dashed black line).

power-law providing $\tau_1 \propto M^{3.3 \pm 0.1}$ which, in accordance with other authors^{44,46} and our FG NMR data point, fits in perfectly. Since for PDMS the data scatter more we omit a fit. Our data point, however, fits well to FG NMR results reported elsewhere.⁶

CONCLUSIONS

By combining field-cycling (FC) and field-gradient (FG) NMR experiments, the segmental mean-square displacement (msd) is determined covering 10 decades of time for PB and PDMS. While the msd can directly be obtained by FG NMR, it is calculated from the dispersion of the FC ^1H NMR intermolecular relaxation rate $R_1^{\text{inter}}(\omega)$ involving Fourier transformation. The quantity $R_1^{\text{inter}}(\omega)$ was isolated from the total ^1H spin-lattice relaxation rate by applying isotope dilution experiments. As the FG and FC NMR experiments, when performed at the same temperature, cover completely different time/frequency ranges, FTS has to be applied to convert the FC data to temperatures covered by the FG experiments. For the first time all four power-law regimes of the

tube-reptation (TR) model are identified in the msd with the exponents rather close to the predicted ones. Even on absolute scale the msd extracted from FC NMR agrees fairly well with that from FG NMR. The estimates of the Kuhn length b and the tube diameter a_0 resemble those found in the literature. Comparing the temperature dependence of segmental time $\tau_s(T)$ and disengagement time $\tau_d(T)$ to literature data, we find satisfying agreement. In the case of PDMS we find indications that the segmental time is not identical with the shortest Rouse time; i.e., the Rouse regime I sets in about 1 decade later in time as compared to PB. In the case of τ_e , agreement with rheological data is achieved when the time constant is extracted from the minimum in the shear modulus $G''(\omega)$. Concerning the TR predictions the molar mass (M) dependence of τ_d is essentially reproduced. Yet, calculating τ_e from τ_d for PDMS yields agreement with experimental data while this is not the case for PB, for which the prediction yields times by 2 orders of magnitude too short. In no case τ_e is correctly reproduced from $\tau_s(T)$.

Altogether, we have demonstrated that with advanced equipment FC ^1H NMR relaxometry, which can probe the frequency dependence of the spin–lattice relaxation in a frequency range of 100 Hz–40 MHz, has become a powerful tool not only to unravel segmental reorientation as previously shown but also translational diffusion.

APPENDIX

An Interpolation Formula Used To Describe $\tau_s(T)$

As shown earlier,^{52,53} the temperature dependence of the segmental correlation time $\tau_s(T)$ can be decomposed into an Arrhenius-like high- T part and in a cooperative part along

$$\tau_s(T) = \tau_\infty \exp[T^{-1}(E_\infty + E_{\text{coop}}(T))] \quad (25)$$

with

$$E_{\text{coop}}(T) = E_\infty \exp\left[-\frac{\mu}{E_\infty}(T - T_A)\right]$$

The parameters denote the high- T activation energy E_∞ , an attempt time τ_∞ , a generalized fragility parameter μ , and a characteristic temperature T_A . In contrast to the VFT equation it also covers temperatures well above T_g .

Extracting Segmental Time Constants from Rheological Data

In the context of discussing Figure 8, we compare $\tau_s(T)$ obtained by FC NMR and DS with rheological data. Assuming FTS,⁴⁶ shear modulus measurements on PB ($M = 130\text{k}$) span a broad (reduced) frequency range. This allows mapping the shift factors a_T given in ref 46 in form of a Williams–Landel–Ferry (WLF) equation

$$\log a_T = -\frac{C_1(T - T_0)}{C_2 + T - T_0} \quad (26)$$

with $C_1 = 3.48$ and $C_2 = 163\text{ K}$, to absolute values of $\tau_s(T)$: From ref 46 we estimate $\tau_s(298\text{ K}) = 0.3\text{ ns}$ corresponding to $a_{298\text{ K}} = 1$. This value is also in accordance with that given in ref 32 (green disk in Figure 8). Finally, $\tau_s(T)$ is calculated from eq 26 according to $\log \tau_s(T) = \log \tau_s(298\text{ K}) + \log a_T$.

In ref 45, the monomeric friction coefficient $\xi(T)$ of high- M PB is also given as the expression

$$\log \xi(T) = \log \xi_0 + \frac{C_1^s C_2^s}{T - T_g + C_2^s} \quad (27)$$

with $\xi_0(T) = 10^{-13.8}\text{ N s m}^{-1}$, $C_1^s = 13.9$, and $C_2^s = 44\text{ K}$. Inserting $\xi(T)$ into the definition of the segmental correlation time¹

$$\tau_0(T) = \frac{b^2 \xi(T)}{3\pi^2 k_B T} \quad (28)$$

yields the purple dashed line in Figure 8. Concerning PDMS (Figure 10) $\xi(T)$ is given in ref 44 for several temperatures. Inserting these values into eq 28 yields the purple squares in Figure 9. We note that the thereby obtained $\tau_0(T)$ values for PDMS are consistent with those used by Chávez et al.⁶⁶ but differ from those obtained by FC NMR and DS (cf. Discussion).

AUTHOR INFORMATION

Corresponding Author

*E-mail: ernst.roessler@uni-bayreuth.de (E.A.R.).

Notes

The authors declare no competing financial interest.

ACKNOWLEDGMENTS

The authors appreciate funding by the Deutsche Forschungsgemeinschaft (DFG) through the projects FU 308/15 and/16 (Darmstadt) and RO 907/17 (Bayreuth) as well as the Elitenetzwerk Bayern.

REFERENCES

- (1) Doi, M.; Edwards, S. F. *The Theory of Polymer Dynamics*; Oxford Science Publication: London, 1986.
- (2) Kremer, K.; Grest, G. S. *J. Chem. Phys.* **1990**, *92*, 5057.
- (3) Binder, K.; Baschnagel, J.; Paul, W. *Prog. Polym. Sci.* **2003**, *28*, 115.
- (4) Richter, D.; Monkenbusch, M.; Arbe, A.; Colmenero, J. *Neutron Spin Echo in Polymer Systems*; Springer: Berlin, 2005.
- (5) Callaghan, P. T.; Coy, A. *Phys. Rev. Lett.* **1992**, *68*, 3176.
- (6) Pahl, S.; Fleischer, G.; Fujara, F.; Geil, B. *Macromolecules* **1997**, *30*, 1414.
- (7) Fischer, E.; Kimmich, R.; Fatkullin, N. *J. Chem. Phys.* **1996**, *104*, 9174.
- (8) Fischer, E.; Kimmich, R.; Fatkullin, N. *J. Chem. Phys.* **1997**, *106*, 9883.
- (9) Kehr, M.; Fatkullin, N.; Kimmich, R. *J. Chem. Phys.* **2007**, *126*, 094903.
- (10) Herrmann, A.; Kresse, B.; Gmeiner, J.; Privalov, A. F.; Kruk, D.; Fujara, F.; Rössler, E. A. *Macromolecules* **2012**, *45*, 6516.
- (11) Kimmich, R.; Fatkullin, N. *Adv. Polym. Sci.* **2004**, *170*, 1.
- (12) Kruk, D.; Herrmann, A.; Rössler, E. A. *Prog. Nucl. Magn. Reson. Spectrosc.* **2012**, *63*, 33.
- (13) Meier, R.; Kruk, D.; Rössler, E. A. *ChemPhysChem* **2013**, *14*, 3071.
- (14) Kresse, B.; Privalov, A. F.; Fujara, F. *Solid State Nucl. Magn. Reson.* **2011**, *40*, 134.
- (15) Kresse, B.; Privalov, A. F.; Herrmann, A.; Hofmann, M.; Rössler, E. A.; Fujara, F. *Solid State Nucl. Magn. Reson.* **2014**, *59*, 45.
- (16) Fujara, F.; Kruk, D.; Privalov, A. F. *Prog. Nucl. Magn. Reson. Spectrosc.* **2014**, *82*, 39.
- (17) Abragam, A. *The Principles of Nuclear Magnetism*; Clarendon Press: Oxford, UK, 1961.
- (18) Fatkullin, N.; Stapf, S.; Hofmann, M.; Meier, R.; Rössler, E. A. *J. Non-Cryst. Solids* **2015**, *407*, 309.
- (19) Hofmann, M.; Kresse, B.; Privalov, A. F.; Willner, L.; Fatkullin, N.; Fujara, F.; Rössler, E. A. *Macromolecules* **2014**, *47*, 7917.

- (20) Zeidler, M. D. *Ber. Bunsen-Ges. Phys. Chem.* **1965**, 69, 659.
- (21) Henritzi, P.; Bormuth, A.; Vogel, M. *Solid State Nucl. Magn. Reson.* **2013**, 54, 32.
- (22) Kimmich, R.; Fischer, E.; Callaghan, P.; Fatkullin, N. *J. Magn. Reson., Ser. A* **1995**, 117, 53.
- (23) Fatkullin, N.; Gubaidullin, A.; Stapf, S. J. *Chem. Phys.* **2010**, 132, 094903.
- (24) Harmon, J. F.; Muller, B. H. *Phys. Rev.* **1969**, 182, 400.
- (25) Sholl, C. A. *J. Phys. C* **1981**, 14, 447.
- (26) Kruk, D.; Herrmann, A.; Rössler, E. A. *Phys. Rev. E* **2012**, 85, 020201.
- (27) Meier, R.; Herrmann, A.; Hofmann, M.; Schmidtke, B.; Kresse, B.; Privalov, A. F.; Kruk, D.; Fujara, F.; Rössler, E. A. *Macromolecules* **2013**, 46, 5538.
- (28) Fleischer, G.; Fujara, F. NMR as a Generalized Incoherent Scattering Experiment. In *Solid-State NMR I Methods*; Blümich, B., Ed.; Springer: Berlin, 1994; Vol. 30, p 159.
- (29) Fleischer, G.; Fujara, F. *Macromolecules* **1992**, 25, 4210.
- (30) Kärger, J.; Pfeifer, H.; Vojta, G. *Phys. Rev. A* **1988**, 37, 4514.
- (31) Stejskal, E. O.; Tanner, E. J. *Chem. Phys.* **1965**, 42, 288.
- (32) Rubinstein, M.; Colby, R. H. *Polymer Physics*; Oxford University Press: Oxford, UK, 2003.
- (33) Hofmann, M.; Herrmann, A.; Abou Elfadl, A.; Kruk, D.; Wohlfahrt, M.; Rössler, E. A. *Macromolecules* **2012**, 45, 2390.
- (34) Filon, L. N. *Proc. R. Soc. Edinburgh* **1928**, 49, 38.
- (35) Chang, I.; Fujara, F.; Geil, B.; Hinze, G.; Sillescu, H.; Tölle, A. J. *Non-Cryst. Solids* **1994**, 172, 674.
- (36) Feiweier, T.; Geil, B.; Isfort, O.; Fujara, F. *J. Magn. Reson.* **1997**, 131, 203.
- (37) Furtado, F.; Damron, J.; Trutschel, M. L.; Franz, C.; Schröter, K.; Ball, R. C.; Saalwächter, K.; Panja, D. *Macromolecules* **2014**, 47, 256.
- (38) Appel, M.; Fleischer, G. *Macromolecules* **1993**, 26, 5520.
- (39) Bartels, C. R.; Crist, B.; Graessley, W. W. *Macromolecules* **1984**, 17, 2702.
- (40) Fetters, L. J.; Lohse, D. J.; Richter, D.; Witten, T. A.; Zirkel, A. *Macromolecules* **1994**, 27, 4639.
- (41) In our previous publication with participation of one of us (ref 8) a factor of 2π erroneously occurred along the ordinate in Figure 8b rendering the extracted a_0 by a factor of $(2\pi)^{1/2}$ too large.
- (42) Ewen, B.; Maschke, U.; Richter, D.; Farago, B. *Acta Polym.* **1994**, 45, 143.
- (43) Graessley, W. W. *Polymeric Liquids & Networks: Dynamics and Rheology*; Taylor & Francis Group: New York, 2008.
- (44) Ferry, J. D. *Viscoelastic Properties of Polymers*; John Wiley & Sons Ltd.: New York, 1980.
- (45) Klopffer, M. H.; Bokobza, L.; Monnerie, L. *Polymer* **1998**, 39, 3445.
- (46) Colby, R. H.; Fetters, L. J.; Graessley, W. W. *Macromolecules* **1987**, 20, 2226.
- (47) Ball, R. C.; Callaghan, R. T.; Samulski, E. T. *J. Chem. Phys.* **1997**, 106, 7352.
- (48) Wang, Z.; Likhtman, A. E.; Larson, R. G. *Macromolecules* **2011**, 45, 3557.
- (49) Mark, J. E., Ed. *Physical Properties of Polymers Handbook*; Springer: New York, 2007.
- (50) Kimmich, R. *Principles of Soft-Matter Dynamics*; Springer: Dordrecht, 2012.
- (51) Hintermeyer, J.; Herrmann, A.; Kahlau, R.; Goiceanu, C.; Rössler, E. A. *Macromolecules* **2008**, 41, 9335.
- (52) Schmidtke, B.; Petzold, N.; Kahlau, R.; Hofmann, M.; Rössler, E. A. *Phys. Rev. E* **2012**, 86, 041507.
- (53) Schmidtke, B.; Hofmann, M.; Lichtinger, A.; Rössler, E. A. *Macromolecules* **2015**, 48, 3005.
- (54) Archer, L. J. *Rheol.* **2001**, 45, 691.
- (55) Pearson, D. S. *Rubber Chem. Technol.* **1987**, 60, 439.
- (56) Baumgaertel, M.; De Rosa, M. E.; Machado, J.; Masse, M.; Winter, H. H. *Rheol. Acta* **1992**, 31, 75.
- (57) Rubinstein, M.; Colby, R. H. *J. Chem. Phys.* **1988**, 89, 5291.
- (58) Ding, Y.; Kisiuk, A.; Sokolov, A. P. *Macromolecules* **2004**, 37, 161.
- (59) Arrighi, V.; Gagliardi, S.; Zhang, C.; Ganazzoli, F.; Higgins, J. S.; Occone, R.; Telling, M. T. *Macromolecules* **2003**, 36, 8738.
- (60) Litvinov, V. M.; Spiess, H. W. *Makromol. Chem.* **1991**, 192, 3005.
- (61) Verdier, C.; Longin, P.-Y.; Piau, M. *Rheol. Acta* **1998**, 37, 234.
- (62) Fan, Y.; Liao, H. *J. Appl. Polym. Sci.* **2008**, 110, 1520.
- (63) Barlow, A. J.; Harrison, G.; Lamb, J. *Proc. R. Soc. London, Ser. A* **1964**, 282, 228.
- (64) Plazek, D. J.; Dannhauser, W.; Ferry, J. D. *J. Colloid Sci.* **1961**, 16, 101.
- (65) Peirrotti, M. B.; Deiber, J. A.; Ressia, J. A.; Villar, M. A.; Vallés, E. M. *Rheol. Acta* **1998**, 37, 449.
- (66) Vaca Chávez, F.; Saalwächter, K. *Macromolecules* **2011**, 44, 1549.

Publication 5

Field-Cycling Relaxometry as a Molecular Rheology
Technique: Common Analysis of NMR, Shear Modulus
and Dielectric Loss Data of Polymers vs. Dendrimers

Hofmann, M.; Gainaru, C.; Cetinkaya, B.; Valiullin, R.;

Fatkullin, N.; Rössler, E. A.

Macromolecules **2015**, 48, 7521-7534.

DOI: 10.1021/acs.macromol.5b01805

(Copyright 2015 by The American Chemical Society)

Field-Cycling Relaxometry as a Molecular Rheology Technique: Common Analysis of NMR, Shear Modulus and Dielectric Loss Data of Polymers vs Dendrimers

M. Hofmann,[†] C. Gainaru,[‡] B. Cetinkaya,[‡] R. Valiullin,[§] N. Fatkullin,[⊥] and E. A. Rössler^{*,†}

[†]Experimentalphysik II, Universität Bayreuth, D-95440 Bayreuth, Germany

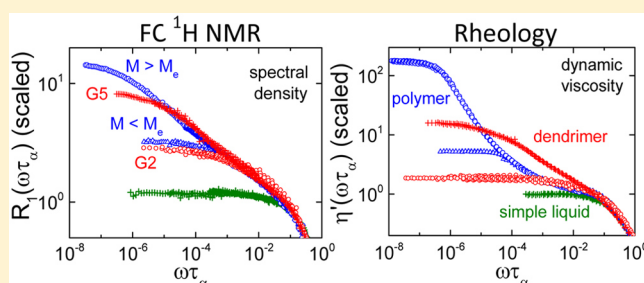
[‡]Fakultät Physik, Technische Universität Dortmund, D-44221 Dortmund, Germany

[§]Faculty of Physics and Earth Sciences, Leipzig University, D-04103 Leipzig, Germany

[⊥]Institute of Physics, Kazan Federal University, Kazan 420008, Tatarstan, Russia

ABSTRACT: Linear poly(propylene glycol) (PPG) as well as a poly(propyleneimine) (PPI) dendrimer with different molar masses (M) are investigated by field-cycling (FC) ^1H NMR, shear rheology (G) and dielectric spectroscopy (DS). The results are compared in a reduced spectral density representation: the quantity $R_1(\omega\tau_\alpha)/R_1^a(0)$, where $R_1(\omega\tau_\alpha)$ is the master curve of the frequency dependent spin–lattice relaxation rate with τ_α denoting the local correlation time, is compared to the rescaled dynamic viscosity $\eta'(\omega\tau_\alpha)/\eta'_a(0)$. The quantities $R_1^a(0)$ and $\eta'_a(0)$, respectively, are the zero-frequency limits of a simple liquid reference system.

Analogously, the dielectric loss data can be included in the methodological comparison. This representation allows quantifying the sensitivity of each method with respect to the polymer-specific relaxation contribution. Introducing a “cumulative mode ratio” $F_i(M)$ for each technique i , which measures the zero-frequency plateau of the rescaled spectral density, characteristic power-law behavior $F_i(M) \propto M^{\alpha_i}$ is revealed. In the case of PPG, $F_{\text{NMR}}(M)$, $F_G(M)$, and $F_{\text{DS}}(M)$ essentially agree with predictions of the Rouse model yielding characteristic exponents α_i . The crossover to entanglement dynamics is identified by a change in α_i around $M \cong 10$ kg/mol. The analysis is extended to the dendrimer which exhibits a relaxation behavior reminiscent of Rouse dynamics. Yet, clear evidence of entanglement is missing. The M -dependencies of the dendrimer diffusion coefficient D obtained by pulsed field-gradient NMR and the zero-shear viscosity are found to be $D(M) \propto M^{-1.6 \pm 0.2}$ and $\eta(M) \propto M^{1.9 \pm 0.2}$, respectively, in good agreement with our theoretical prediction $\eta(M) \propto M^{1/3} D^{-1}(M)$. The close correspondence of $R_1(\omega\tau_\alpha)$ with $\eta'(\omega\tau_\alpha)$ establishes FC NMR as a powerful tool of “molecular rheology” accessing the microscopic processes underlying macroscopic rheological behavior of complex fluids.



1. INTRODUCTION

Field-cycling (FC) NMR relaxometry provides important information on molecular dynamics in condensed matter.^{1–5}

In contrast to conventional NMR relaxation studies, which measure the spin–lattice relaxation rate R_1 (inverse relaxation time, T_1^{-1}) at a single frequency, usually as a function of temperature, the FC method allows probing its frequency dependence (dispersion) by varying the relaxation field. Since the end of the nineties a commercial FC relaxometer has become available which covers a frequency range of 10 kHz–20 MHz (for protons).¹ By employing earth field compensation, frequencies down to some 100 Hz can be reached.^{5–8} Achieving such low frequencies, the method is particularly suited to study slow dynamics in complex liquids.

FC experiments are most often performed for protons, although studies of other nuclei like ^2H , ^{13}C , or ^{19}F are possible.^{5,9,10} In the case of ^1H , relaxation is caused by fluctuations of the magnetic dipole–dipole interactions and one has to distinguish intra- and intermolecular relaxation path-

ways.^{1,4,8} While the intramolecular contribution $R_1^{\text{intra}}(\omega)$ originates from interactions between nuclei belonging to one molecule, the intermolecular relaxation $R_1^{\text{inter}}(\omega)$ stems from interactions between nuclei belonging to different molecules. Thus, the intramolecular relaxation is associated with reorientational dynamics while the intermolecular part provides information on translational motion. However, it is difficult to distinguish both pathways, in particular, determining the ratio of both relaxation contributions as a function of frequency. Yet, by applying isotope dilution experiments intra- and intermolecular relaxation can be separated and individually analyzed.^{8,11–14} From general arguments, it can be shown that intermolecular relaxation, mediated by translation, dominates at lowest frequencies^{15,16} which was exploited recently to extract the translational diffusion coefficient $D(T, M)$ in simple liquids,

Received: August 14, 2015

Revised: October 2, 2015

Published: October 13, 2015

polymers and dendrimers,^{17–19} with M denoting the molar mass. Having $R_1^{\text{inter}}(\omega)$ at hand, even the mean square displacement as a function of time is available.^{11,13,20}

In a series of papers we demonstrated that the effective frequency window of FC NMR can be significantly extended by applying frequency–temperature superposition (FTS),^{20–24} a procedure well-known from rheological studies.^{25–27} For this purpose, the FC relaxation data are first converted to the susceptibility representation $\chi''(\omega) = \omega R_1(\omega)$. By shifting the data sets obtained at different T along the frequency axis, in good approximation a susceptibility master curve is revealed covering local as well as collective dynamics, i.e., glassy, Rouse, and entanglement dynamics in the case of polymers. Subsequently, the master curve can be scaled along $\chi''(\omega\tau_\alpha)$ with $\tau_\alpha(T)$ denoting the local correlation time controlled by the glass transition phenomenon. Such master curves typically cover about 10 decades in frequency and allow transformation into the time domain yielding the corresponding correlation function.^{4,13,23} Applying these procedures for polymers a picture emerged which confirms the tube-reptation model only in parts.^{8,13}

Recently, we also investigated the dynamics of poly(propyleneimine) (PPI) dendrimer of different generations by different techniques.¹⁹ The bulk dendrimer constitutes highly viscous liquids at room temperature that undergo a glass transition with a glass transition temperature T_g of around 200 K, virtually independent of the number of generations. The local (α -) dynamics was probed by dielectric spectroscopy (DS) and solid state ^2H NMR. In addition to the α -relaxation, two secondary processes were identified persisting below T_g . The existence of collective dynamics slower than the local dynamics ($T > T_g$) was revealed by FC ^1H NMR. Specifically, an intermediate relaxation regime between the α -dynamics and the terminal relaxation of the collective dynamics was identified. When compared with results for linear polymers, some resemblance with Rouse dynamics is recognized. Yet, entanglement was excluded for dendrimers, a fact also known from rheological studies.²⁸ Tentatively, in accordance with theoretical and simulation work,^{29–33} local dynamics at high, breathing modes at intermediate, and overall tumbling and diffusion of the dendrimer at low frequencies were attributed.

For characterizing the rheological behavior of soft matter, oscillatory shear relaxation in terms of the complex shear modulus $G^*(\omega)$ is an important source of information.^{25–27} In the case of polymers, the data are usually discussed in the frame of the Rouse model (short chains) and the tube-reptation model²⁷ (long chains) while a detailed understanding of dendrimers is still missing. In the present contribution we report on $G^*(\omega)$ of linear poly(propylene glycol) (PPG) and a poly(propyleneimine) (PPI) dendrimer with different molar masses M collected in a large temperature interval, allowing to cover both polymer-specific as well as local dynamics. In addition, for the dendrimer we provide the diffusion coefficient $D(M)$ as obtained from pulsed field gradient (PFG) NMR. The rheological results are compared to the corresponding relaxation spectra provided by FC ^1H NMR, published in part previously.^{19,24} We note that there already exist rheological studies of PPG³⁴ as well as of PPI dendrimer,²⁸ yet, in smaller M and T ranges. Our main goal is to demonstrate that providing master curves of the spectral density (instead of the susceptibility) in terms of $R_1(\omega\tau_\alpha)$, a direct comparison with the frequency dependent viscosity $\eta'(\omega\tau_\alpha)$ derived from $G^*(\omega)$ becomes possible. As a type A polymer,³⁵ PPG reveals a normal

mode relaxation in the dielectric spectra and the data extracted from ref 36 can be included in the methodical comparison. As will be demonstrated, with increasing M qualitatively similar evolution of the low-frequency, polymer-specific contribution is disclosed in $R_1(\omega\tau_\alpha)$ and $\eta'(\omega\tau_\alpha)$, respectively. Without need of describing the full relaxation spectra our analysis allows testing predictions of the Rouse theory being taken as a reference also for the dendrimer. The close correspondence with shear relaxation establishes FC NMR as a powerful tool of “molecular rheology”, directly accessing the microscopic processes underlying the (macroscopic) rheological behavior in complex liquids, here of linear PPG and dendritic PPI.

2. THEORETICAL BACKGROUND: M DEPENDENCE OF FC ^1H NMR, SHEAR, AND DIELECTRIC RELAXATION IN POLYMERS

Field-Cycling NMR. Field-cycling ^1H NMR relaxometry provides the frequency dependence of the spin–lattice relaxation rate $R_1(\omega) = T_1(\omega)^{-1}$ giving access to a spectral density $J(\omega)$ characterizing the fluctuations of the magnetic dipole–dipole interaction among protons. In the case of intramolecular relaxation, it is given by the Fourier transform of a rank-two reorientational correlation function $C_2(t)$ of a monomer, more precisely of the internuclear vectors of the spin pairs within a monomer.^{1,4} In the case of intermolecular relaxation, a translational correlation function $C_{\text{trans}}(t)$ is probed, the long-time behavior of which follows a power-law due to Fickian diffusion, specifically $C_{\text{trans}}(t) \propto t^{-3/2}$.^{4,15–18} The actually measured (total) relaxation is given by the sum of the rates

$$R_1(\omega) = R_1^{\text{intra}}(\omega) + R_1^{\text{inter}}(\omega) \quad (1)$$

The Bloembergen, Purcell, and Pound expression connects rate and spectral density^{1,37}

$$R_1^{\text{intra/inter}} = K^{\text{intra/inter}} [J_{\text{NMR}}^{\text{intra/inter}}(\omega) + 4J_{\text{NMR}}^{\text{intra/inter}}(2\omega)] \quad (2)$$

where $K^{\text{intra/inter}}$ is the NMR coupling constant of intra- and intermolecular relaxation, respectively. The Larmor frequency is given by the magnetic field, i.e., $\omega = \gamma B$, where $\gamma = \gamma_H$ is the gyromagnetic ratio of the proton. The spectral density is normalized, $\int_0^\infty J(\omega) d\omega = \pi/2$. Then, by definition $J(0) = \langle \tau \rangle$, where $\langle \tau \rangle$ denotes a mean correlation time. In simple liquids the latter is just the structural (rotational) correlation time τ_α determined by the so-called α -process (ignoring intermolecular relaxation). In the case of polymers or dendrimers featuring further relaxation contributions at low frequencies ($\omega\tau_\alpha \ll 1$), the average is taken over all modes appearing between the terminal relaxation time τ_1 and the much faster time scale τ_α .

For the present context discussing the evolution of the polymer specific dynamics we take the Rouse model²⁷ as a reference. In polymer theories it is usually assumed that the shortest Rouse mode τ_s can be identified with that of the α -process ($\tau_s = \tau_\alpha$). Yet, this is not always a proper description when compared to experimental results.²⁰ This is not surprising, because the concept of Kuhn segments mainly reflects the equilibrium statistics of long polymer chains in the melt. For flexible chains the Kuhn segment roughly corresponds to a chain segment containing 3–10 monomers, which have a large number of internal degrees of freedom and internal mobility. Therefore, the shortest Rouse time τ_s is usually somewhat longer than τ_α , which characterizes the

dynamics of the smallest unit of a polymer chain. The spectral shape of the latter relaxation is essentially M -independent. Thus, as a heuristic approximation, we describe the (total) spectral density in terms of a sum of three contributions:

$$J_{\text{NMR}}(N; \omega) = f(1-p)J_{\text{NMR}}^{\text{intra}}(N; \omega) + (1-f)(1-p)J_{\text{NMR}}^{\alpha}(\omega) + pJ_{\text{NMR}}^{\text{inter}}(N, \omega) \quad (3)$$

The functions $J_{\text{NMR}}^{\text{intra}}(N; \omega)$ and $J_{\text{NMR}}^{\text{inter}}(N; \omega)$ represent polymer-specific dynamics, thus depending on the number of Kuhn segments N (or M), while $J_{\text{NMR}}^{\alpha}(\omega)$ reflects “glassy” (or intrasegmental) dynamics being N independent. The quantity f specifies the fraction of the decay of the reorientational correlation function induced by polymer dynamics, which is related to the order parameter S by $f = S^2$. It depends on the chemical structure of the monomer and is on the order of $f = 0.01$.^{1,38,39} The parameter p gives the fraction of the intermolecular relaxation in the total NMR correlation function. It is actually unknown but may be estimated to be around $p \approx 0.1$ – 0.2 .⁸ Both f and p are assumed to be temperature independent, which is of course an approximation. In accordance with recent findings,^{8,12–14} we assume in eq 3 that the contribution of the α -process is essentially of intramolecular nature. While the polymer specific contributions

are described within the Rouse model (short chains),²⁷ that of the α -process is phenomenologically interpolated by a Cole-Davidson (CD) function accounting for the non-Debye character of the spectral density of dense simple liquids.⁴⁰

Next, we discuss the low-frequency limit of eq 3 and assume Rouse dynamics for describing intra- and intermolecular spin-lattice relaxation

$$J_{\text{NMR}}(N; 0) = f(1-p)\frac{\pi}{2}\tau_s \ln(2N/\sqrt{\pi}) + p\pi^{3/2}(3/2)(a_0/b)^3\tau_s N^{1/2} + (1-f)(1-p)\tau_\alpha \quad (4)$$

The first (intramolecular) term is obtained in accordance with refs 3 and 22. The second term reflecting the intermolecular relaxation contribution is derived in the Appendix A eq 30. The parameter a_0 denotes a characteristic length reflecting the local packing of the protons from different chains and b the Kuhn length; as a rule $a_0 < b$. We note that, neglecting the intermolecular term, eq 4 was tested previously,^{22,24} but succeeding experiments revealed that the intermolecular relaxation has to be taken into account, in particular, when low-frequency dispersion is discussed.^{8,12,13}

Next, we define the cumulative mode ratio $F_{\text{NMR}}(N)$:

$$F_{\text{NMR}}(N) := J_{\text{NMR}}(N; 0)/J(1; 0) = \frac{\left(f(1-p)\frac{\pi}{2}\ln(2N/\sqrt{\pi}) + p3\pi^{3/2}/2(a_0/b)^3N^{1/2} + (1-f)(1-p)\frac{\tau_\alpha}{\tau_s}\right)}{\left(f(1-p)\frac{\pi}{2}\ln(2/\sqrt{\pi}) + p3\pi^{3/2}/2(a_0/b)^3 + (1-f)(1-p)\frac{\tau_\alpha}{\tau_s}\right)} \propto N^{1/2} \quad (5)$$

It is a measure how much the mean correlation time (averaged over a particular mode distribution) of the dynamics of a macromolecule has increased with respect to that of a melt of segments, i.e., a chemically equivalent simple liquid. The denominator of eq 5 is a number of the order of one and the ratio $\tau_\alpha/\tau_s \leq 1$ is assumed to be temperature independent. Usually, the second term in the nominator dominates, resulting in a $N^{1/2}$ dependence expected for Rouse dynamics.

In the case of long chains ($M > M_c$), the tube-reptation (TR) model²⁷ and the n -renormalized Rouse model^{41–44} (n -RR) (discussed for NMR, only) provide the following expressions as given by scaling arguments (for details see Appendix A)

$$J_{\text{NMR}}(0) \propto f(1-p)\tau_s(N/N_c)^2 + p\tau_s(a_0/b)^3N^{3/2} \text{ (TR)} \quad (6)$$

$$J_{\text{NMR}}(0) \propto f(1-p)\tau_s(N/N_c)^{n/2} + p\tau_s(a_0/b)^3(N)^{(n+1)/2} N_c^{-n/2} \text{ (n-RR)} \quad (7)$$

including intra- (first term) as well as intermolecular relaxation (second term). Here, we have neglected the contribution from intrasegmental dynamics (α -process) as its influence is irrelevant for high N .¹¹ For the cumulative mode ratio one thus expects for $M > M_c$:

$$F_{\text{NMR}}(N) \propto N^{1.5 \cdots 2.0} \text{ (TR)} \quad (8)$$

$$F_{\text{NMR}}(N) \propto N^{1.5 \cdots 2.0} \text{ (3-RR)} \quad (9)$$

Note that TR and thrice-renormalized Rouse (3-RR) model predict very similar N dependences for $F_{\text{NMR}}(N)$. Yet there is a qualitative difference: in the TR model the term proportional to $N^{1.5}$ results from the intermolecular while the term proportional

to N^2 arises from the intramolecular contribution. Within the 3-RR model the situation is opposite.

When the quantity

$$J_{\text{NMR}}(\omega\tau_\alpha)/J_{\text{NMR}}^\alpha(0) = R_1(\omega\tau_\alpha)/R_1^\alpha(0) = F_{\text{NMR}}(N) \quad (10)$$

is plotted, $F_{\text{NMR}}(N)$ can directly be read off from the low-frequency plateau ($\omega\tau_\alpha \rightarrow 0$). Here $J_{\text{NMR}}^\alpha(0)$ (or $R_1^\alpha(0)$) denotes the low-frequency limit of the relaxation contribution attributed to the local (glassy) dynamics. It may be extracted from the spectral density master curve $J_{\text{NMR}}(\omega\tau_\alpha)$ by interpolating the high-frequency peak region with a CD function or by directly taking data from a low- M reference system. The master curve for the spectral density itself is derived from the susceptibility master curve $\chi''_{\text{NMR}}(\omega\tau_\alpha) = \omega\tau_\alpha J_{\text{NMR}}(\omega\tau_\alpha)$ which is the most reliable way to get a master curve just by shifting the spectra solely along the frequency axis (cf. Experimental Section).

Shear Modulus. The rheological experiments provide the complex shear modulus $G^*(\omega) = G'(\omega) + iG''(\omega)$. Its imaginary part is connected to the real part of the dynamic viscosity by²⁶

$$\eta'(\omega) = G''(\omega)/\omega = G_\infty \frac{G''}{G_\infty \omega} = G_\infty J_G(\omega) \quad (11)$$

The quantity $G_\infty = G'(\omega \rightarrow \infty)$ is the high frequency modulus and $J_G(\omega)$ the spectral density in terms of rheology. Although quite different fluctuation phenomena with respect to NMR are considered—in the case of $G^*(\omega)$ fluctuations of off-diagonal elements of the stress tensor are monitored^{27,34} (cf. Appendix B)—eq 11 represents a kind of spectral density representation. Consequently, we compare the results of the NMR and rheological measurements in this representation.

Again, we again split the total rheological response into two parts, in analogy to eq 3:

$$\eta'(\omega) = G_{\infty}^{\text{pol}} J_G^{\text{pol}}(\omega) + G_{\infty}^{\alpha} J_G^{\alpha}(\omega) \quad (12)$$

The quantities G_{∞}^{pol} and G_{∞}^{α} are the high-frequency shear moduli for the polymer-specific and the α -dynamics, respectively. Assuming Rouse dynamics in the continuum limit, the corresponding cumulative mode ratio $F_G(N)$ (cf. eq 5) reads^{3,26}

$$F_G(N) = \eta'(0)/\eta'_\alpha(0) = \frac{G_{\infty}^{\text{pol}}(\pi^2/6)\tau_s N^2 + G_{\infty}^{\alpha}\tau_\alpha}{G_{\infty}^{\alpha}\tau_\alpha} \propto N \text{ (Rouse)} \quad (13)$$

Here, $\eta'_\alpha(0) = G_{\infty}^{\alpha}\tau_\alpha$ (Maxwell relaxation) denotes the zero-frequency limit in the case of a simple liquid. The proportionality with N in the case of Rouse dynamics follows from the relation $G_{\infty}^{\text{pol}} = \rho RT/M \propto 1/N$ ^{3,26} with ρ being the mass density. For long chains ($M > M_c$), the TR model predicts $F_G(N) \propto N^3$.^{25–27}

Dielectric Relaxation. In the case of type A polymers (Stockmayer classification³⁵) to which PPG belongs, a normal mode relaxation is observed in addition to the α -relaxation, which probes the fluctuation of the end-to-end vector. The N -dependence of its correlation time is well-known.^{45–47} The scaled spectral density is defined in analogy to eqs 10 and 13 as

$$J_{\text{norm}}(\omega\tau_\alpha)/J_\alpha(0) = \frac{\varepsilon_{\text{norm}}''(\omega\tau_\alpha)/\varepsilon_\alpha''(0)}{\omega\tau_\alpha} = F_{\text{DS}}(N) \quad (14)$$

with

$$F_{\text{DS}}(N) \propto N^2 \text{ (Rouse)} \quad (15)$$

$$F_{\text{DS}}(N) \propto N^3 \text{ (TR)} \quad (16)$$

We note that the normal mode relaxation solely probes polymer dynamics. It vanishes for $N \rightarrow 0$. Thus, in eq 14 we take the α -relaxation, usually measured in addition in the DS spectrum of a type A polymer, as reference.

In conclusion, quite different scaling relations are expected for the cumulative mode ratio $F_{\text{NMR}}(N)$, $F_G(N)$, and $F_{\text{DR}}(N)$ provided by NMR, mechanical and dielectric relaxation, respectively, when considering linear polymers. For bulk dendrimer melts, to our knowledge, theoretical predictions are not available so far. Nevertheless, we can compare the results collected for the dendrimer with those for linear polymers in the way sketched above.

3. EXPERIMENTAL SECTION

A series of linear poly(propylene glycole) (PPG) melts with several, narrowly distributed ($M_w/M_n \leq 1.06$) molar masses $134 \leq M_w$, mol $\text{g}^{-1} \leq 18200$ was investigated by FC ^1H NMR relaxometry, oscillatory shear rheology, and dielectric spectroscopy. It was obtained from Polymer Standards Service PSS, Mainz (Germany), except the species $M_w = 18200$ g mol^{-1} (PPG 18k, kindly provided by Roland Böhmer, TU Dortmund) characterized via MALDI-TOF and investigated previously^{36,48} as well as $M_w = 1800$ g mol^{-1} (PPG 1.8k) which was bought from Polymer Source, Dorval (Canada). Henceforth, the name code reflects the (rounded) values of M_w . The different generations of PPI dendrimer were purchased from SyMo-Chem BV (University of Eindhoven) and feature monodisperse molar masses of 773 g mol^{-1} , 1687 g mol^{-1} , 3514 g mol^{-1} and 7198 g mol^{-1} , corresponding to generation numbers $G \in \{2, 3, 4, 5\}$. For the NMR measurements the

polymers/dendrimers were used as delivered and filled into standard 5 mm NMR glass tubes. After thoroughly degassing under vacuum for 48h the tubes were sealed.

The dispersion of the spin-lattice relaxation rate $R_1(\omega)$ was measured by an electronic FC relaxometer STELAR FFC 2000, located at the University Bayreuth, allowing for measurements in a frequency range of $10 \text{ kHz} \leq \nu \leq 20 \text{ MHz}$. Measurements are possible in a temperature range of 150–420 K enabling to extend the frequency window assuming FTS. In order to probe very slow molecular dynamics, the data were supplemented by measurements on a home-built FC relaxometer situated at the TU Darmstadt reaching extremely low frequencies of $200 \text{ Hz} \leq \nu \leq 40 \text{ MHz}$, achieved by actively compensating the earth's magnetic field.⁶⁷ For PPG we always observed monoexponential build-up/decay of the longitudinal magnetization extending over almost two decades in amplitude. Concerning the dendrimers the build-ups/decays are slightly stretched at high temperatures wherefore we determined the (mean) relaxation rate from a stretched exponential function $M(t) \propto \exp[-(t/T_1^k)^\beta]$ ($0.8 \leq \beta \leq 1$).

The dielectric spectra were published before³⁶ and supplemented by own measurements of dipropylene glycol (DPG). The shear experiments on the polymers and the dendrimers G3, G4, and G5 were performed in plate-plate geometry with diameters of 8 mm, 25 mm and 50 mm at low, medium and high temperatures, respectively, on a MCR-502 rheometer from Anton Paar located at the Technical University Dortmund.⁴⁹ The G2 dendrimer was measured on an MCR-500 rheometer at the University of Bayreuth (group of Nuri Aksel). The gap was 1 mm in all cases. All mechanical measurements were done under linear response conditions.

Diffusion measurements on the dendrimers were performed using pulsed field gradient⁵⁰ (PFG) ^1H NMR on a 400 MHz spectrometer located at the University of Leipzig. It is equipped with a home-built PFG unit allowing for gradients up to 35 T/m. The measurements were conducted with a 13-interval pulse sequence allowing for an efficient compensation of the disturbing eddy currents upon the application of the strong magnetic field gradient pulses.⁵¹ Typical parameters of the pulse sequence were: $\tau = 2$ ms for the separation between the $\pi/2$ and π pulses, $\Delta = 50$ ms for the separation between the $\pi/2$ pulses defining the diffusion time, $\delta = 1$ ms for the duration of the gradient pulses, and $R_d = 5$ s for the delay between repetitions of the pulse sequence. The temperature was controlled to ± 0.2 K.

Figure 1 displays typical normalized spin-echo attenuations showing the signal intensities obtained for different values of q^2t_d .

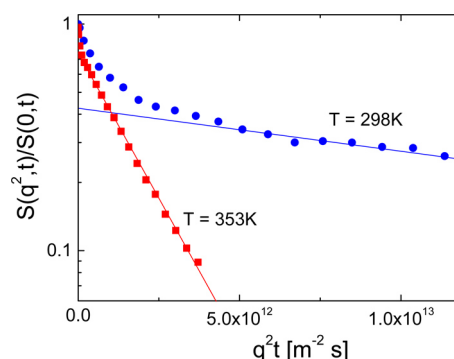


Figure 1. Normalized spin-echo decay for PPI dendrimer G4 at two temperatures as indicated. The solid lines show eq 17 interpolating the slowly decaying parts of the experimental data with their slopes yielding $D(T)$.

where $q = \gamma\delta g$ is the wave vector (with γ being the gyromagnetic ratio) and $t_d = \Delta + 7\tau/2 + \delta/6$ is the diffusion time, measured at two different temperatures for the dendrimer G4. Most notably, the decay curves appear to deviate from the exponential behavior characteristic of normal diffusion,

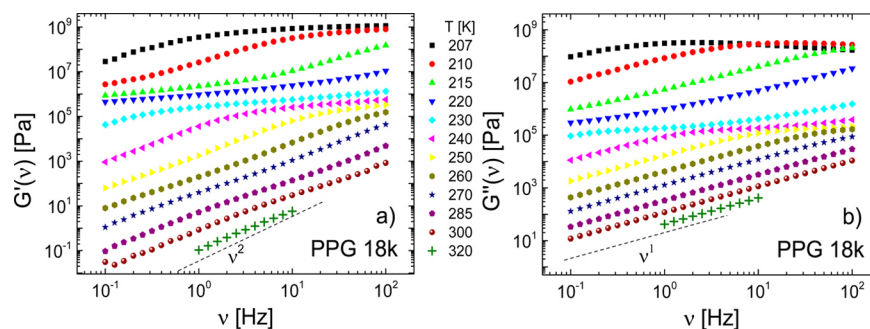


Figure 2. (a) Real $G'(\nu)$ and (b) imaginary part $G''(\nu)$ of the complex shear modulus for poly(propylene glycol) (PPG) with $M = 18k$ at several temperatures as indicated. Dashed lines: power-laws reflecting the terminal relaxation.⁴⁹

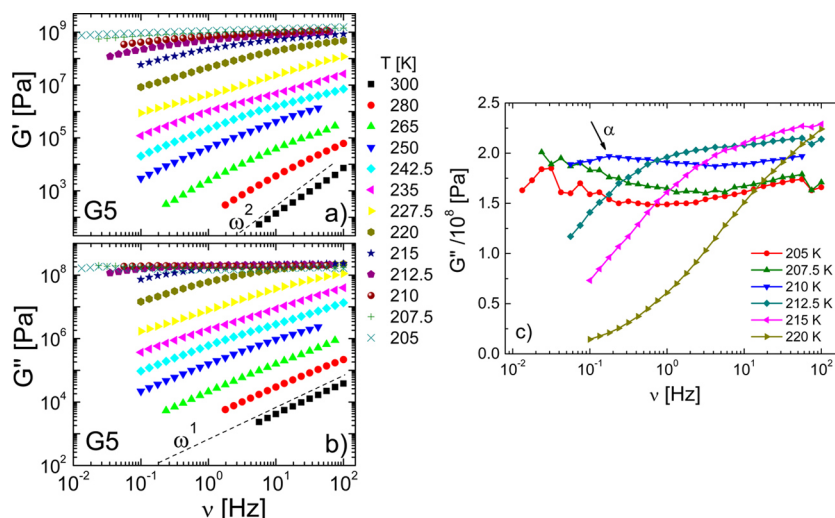


Figure 3. (a) Storage $G'(\nu)$ and (b) loss modulus $G''(\nu)$ of PPI dendrimer G5 for several temperatures as indicated. Terminal power-laws are indicated. (c) $G''(\nu)$ at temperatures close to T_g on linear scale. The α -process (arrow) is observed in addition to some secondary relaxation at higher frequencies.

$$S(q, t_d) = S(q = 0, t_d) \exp\{-q^2 t_d D\} \quad (17)$$

where D is the self-diffusion coefficient. Hence, the curves were described biexponentially

$$S(q, t_d) = S(q = 0, t_d) [p_f \exp\{-4\tau/T_{2f}\} \exp\{-q^2 t_d D_f\} + p_s \exp\{-4\tau/T_{2s}\} \exp\{-q^2 t_d D_s\}] \quad (18)$$

with components weighted by the spin–spin relaxation time T_2 . Measurements using the CPMG pulse sequence indicate the occurrence of two proton fractions having different T_2 . The component slower diffusing with D_s has a much shorter T_2 than the faster diffusing one. This indicates that the slowly diffusing component can be associated with the dendrimer molecules. The origin of the faster diffusing component is not clear so far. Applying eq 17 to the long-time tail of the echo decays, the D values of the dendrimer molecules were obtained as indicated in Figure 1.

4. RESULTS

Shear Modulus. Parts a and b of Figure 2 display the real $G'(\nu = \omega/2\pi)$ and the imaginary part $G''(\nu)$, respectively, of PPG 18k in double logarithmic presentation as collected in a temperature interval of 200–320 K.⁴⁹ The spectra show all the features typical of entangled polymer melts. At lowest frequencies and highest temperatures the terminal relaxation characteristic of a liquid is identified based on the power-laws $G'(\omega) \propto \omega^2$ and $G''(\omega) \propto \omega^1$, respectively, (dashed lines in Figure 2, cf. also Figure 4). At intermediate temperatures (e.g.,

230 K) a rubber plateau is suggested in $G'(\omega)$ indicating entanglement effects. At low temperatures the high-frequency plateau value G_∞ is found in $G'(\omega)$, while in $G''(\omega)$ the main relaxation peak associated with local dynamics (α -process) is displayed. Regarding the α -relaxation, similar spectra are found for the lower M values investigated while the mentioned features characteristic of polymer dynamics continuously disappear with decreasing M . As our experiments cover the α -relaxation the shift factors a_T usually applied for constructing master curves can be allocated to the correlation time $\tau_\alpha = \tau_\alpha(T)$: for that purpose the peak region of the master curve of $G''(a_T \omega)$ is fitted by a Cole–Davidson (CD) function⁵² allowing one to refer the a_T to time constants $\tau_\alpha(T)$. The resulting $\tau_\alpha(T)$ are displayed in Figure 7a and will be discussed below. Density changes caused by temperature variation eventually impacting the amplitudes cannot be resolved within experimental accuracy.

The master curves $G'(\omega \tau_\alpha)/G_\infty$ and $G''(\omega \tau_\alpha)/G_\infty$ of PPG are shown in Figure 4 for the different M investigated, where they are compared to those obtained for the dendrimers (cf. below). As mentioned, PPG was rheologically investigated by Nicolai and Floudas.³⁴ The authors reported that segmental and normal mode do not exhibit the same temperature dependence close to T_g . A deviation of about a factor of 10 was found at T_g . Yet, 30 K above $T_g \approx 205$ K,¹⁹ this effect disappeared, and they were able to construct master curves. In

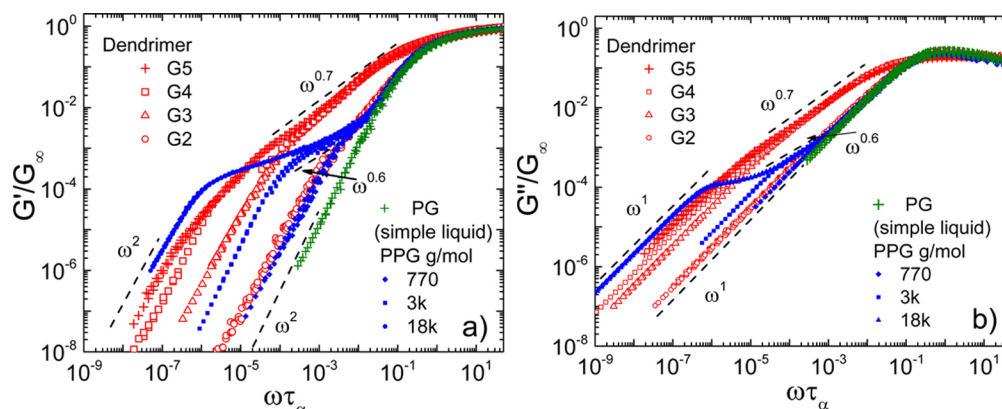


Figure 4. (a) Master curves of the dynamic moduli $G'(\omega\tau_\alpha)$ and (b) $G''(\omega\tau_\alpha)$ of selected M (as indicated) of PPG (blue symbols) as well as of the PPI dendrimers G2–G5 (red symbols) as a function of reduced frequency. For comparison the corresponding data of the simple liquid propylene glycol (PG) is shown. Terminal and intermediate (Rouse) power-laws are indicated by dashed lines. Data for PPG are from ref 49.

our case, FTS works in good approximation over the whole temperature range and for all systems investigated.

Parts a and b of Figure 3 present $G'(\nu)$ and $G''(\nu)$, respectively, for the PPI dendrimer G5 within a temperature range of 200–300 K. Broad dispersion curves are observed. Figure 3c shows $G''(\nu)$ of G5 for several temperatures around T_g on a linear scale, where the main (α -) relaxation is identified (arrow); at high frequencies a crossover to some secondary process is recognized. The corresponding time constant τ_α is again extracted via fitting the peak region with a CD function. A terminal relaxation typical of a liquid is identified at low frequencies, i.e., $G'(\omega) \propto \omega^2$ and $G''(\omega) \propto \omega^1$ (dashed lines in Figure 3) are observed at low frequencies and high temperatures, as in the case of PPG. The master curves of the dendrimers G2–G5 are included in Figure 4 and the resulting time constants $\tau_\alpha(T)$ are displayed in Figure 7b and will be discussed below.

In Figure 4 the master curves of PPG and PPI dendrimers in terms of $G'(\omega)$ and $G''(\omega)$, respectively, are compared to each other as well as to a reference, namely the simple liquid propylene glycol (PG). Clearly, with respect to the dynamics of PG, the terminal relaxation for both polymers and dendrimers shifts to lower reduced frequencies the higher M becomes. In the case of PPG, polymer-specific and α -dynamics appear to be well separated, i.e., an intermediate power-law $G'(\omega) \propto G''(\omega) \propto \omega^{0.6}$ fairly close to that predicted for Rouse dynamics²⁷ ($G'(\omega) \propto G''(\omega) \propto \omega^{1/2}$) is suggested at $\omega\tau_\alpha < 10^{-2}$ (dashed line). In the case of the dendrimers G3, G4, and G5 an intermediate power-law regime $G'(\omega) \cong G''(\omega) \propto \omega^{-0.7}$ extending over at least two decades in amplitude and three in frequency succeeds the α -relaxation more closely for $\omega\tau_\alpha < 1$ with an exponent actually slightly decreasing from G3 (0.72) to G5 (0.65). At intermediate frequencies $10^{-5} < \omega\tau_\alpha < 10^{-1}$ the rescaled moduli $G'(\omega\tau_\alpha)/G_\infty$ and $G''(\omega\tau_\alpha)/G_\infty$ of these dendrimers obviously exceed their counterparts of PPG by more than one decade. Concerning G2 the intermediate power-law regime is not observed and the curves highly resemble that of the polymer PPG 770 attended by a low-frequency shoulder for $\omega\tau_\alpha < 10^{-1}$. Note also that high- M PPG features indications of a rubber plateau in G' intimating entanglement while this is not the case for the dendrimers.

Field-Cycling ^1H NMR. Some FC ^1H NMR relaxation data of PPG were published before.²⁴ They are supplemented by new measurements on PPG 1.8k. In the case of the high- M

PPG 18k we collected new data at extremely low-frequencies ($200 \text{ Hz} < \nu < 10 \text{ kHz}$) obtained from a home-built relaxometer (cf. Experimental Section) as shown in Figure 5.

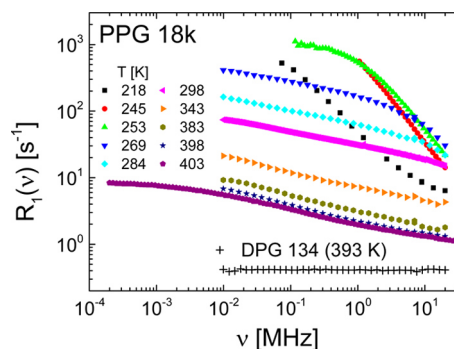


Figure 5. FC ^1H NMR relaxation dispersion of poly(propylene glycol) (PPG) with $M = 18\text{k}$ at different temperatures (as indicated). Also shown for comparison: dispersion of di(propylene glycol) (DPG) at 393 K representing the simple liquid.

While at high temperatures comparatively weak dispersion due to polymer dynamics is recognized in $R_1(\nu)$, strong frequency dependence is found at low temperatures reflecting the α -process. For comparison the data of the simple liquid reference system di(propylene glycol) (DPG, $M = 134$) is also shown for a high temperature.²⁴ Note that in the case of FC ^1H NMR we use DPG instead of PG as low- M reference as it turned out that the latter is stronger influenced by intermolecular relaxation contributions.¹⁴ As polymer dynamics are absent in DPG, an (almost) dispersion free behavior is observed. The master curves $\chi''(\omega\tau_\alpha)$ (cf. Theoretical Background) belonging to various M are shown in Figure 6a. As in the rheological spectra (cf. Figures 2 and 3) the FC NMR spectra also cover low temperatures where the α -process determines the relaxation. Analogously, its time constant can be determined from a fit of the susceptibility maximum by a CD function.

Inspecting the evolution of the low-frequency contribution $\chi''(\omega\tau_\alpha < 1)$ of PPG 18k (Figure 6a) one observes an apparent power-law regime with $\chi''(\omega\tau_\alpha) \propto \omega^{0.8}$ for $10^{-4} < \omega\tau_\alpha < 10^{-2}$. It is also present in the other PPG systems 5k, 3k, and 1.8k while the extension to low frequencies decreases with decreasing M and a crossover to the terminal relaxation is found at the lowest frequencies. This intermediate power-law is attributed to Rouse

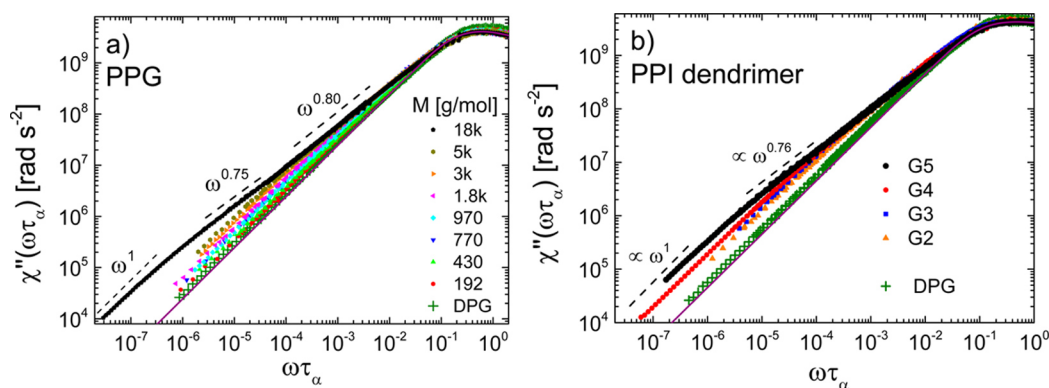


Figure 6. (a) FC NMR susceptibility master curves $\chi''(\omega\tau_\alpha)$ for PPG of molar mass M as indicated and (b) for the PPI dendrimer of generations G2–G5. Terminal and intermediate power-law regimes are indicated (dashed lines). Solid lines: Fit of the α -peak with a Cole-Davidson function indicating simple liquid dynamics.

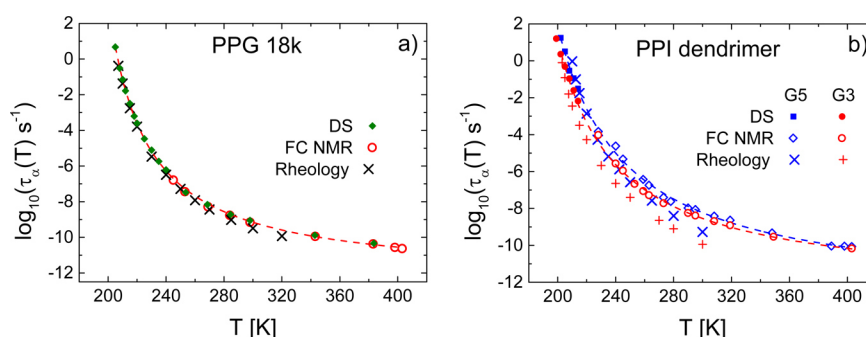


Figure 7. (a) Temperature dependent time constant $\tau_\alpha(T)$ of the α -process in PPG 18k as obtained by FC NMR, DS and rheology.⁴⁹ (b) Same plot for the PPI dendrimers G3 and G5. The dashed lines are interpolations by the Vogel–Fulcher–Tammann law intended to guide the eye.

dynamics. Here, a note of caution has to be given: In the Rouse model, one actually expects $\chi''(\omega\tau_\alpha) \propto \omega \ln \omega$ for intramolecular relaxation dominating instead of a power-law.^{22,45} Yet, this is difficult to be distinguished from a power-law with an exponent somewhat smaller than 1. For $M = 18k$ at even lower frequencies an inflection point appears at $\omega\tau_\alpha \approx 5 \times 10^{-5}$ and a crossover to a second power-law with a slightly lower exponent $\chi''(\omega\tau_\alpha) \propto \omega^{0.75}$ is suggested. This is typical of entanglement dynamics emerging for $M > M_e$.²⁴ Finally, the terminal relaxation sets in and $\chi''(\omega\tau_\alpha)$ asymptotically approaches $\chi''(\omega\tau_\alpha) \propto \omega^1$. We note that no PPG with higher M was available. In the case of high- M poly(butadiene) the low-frequency exponent in the entanglement (or constraint Rouse) regime decreases down to 0.3.^{8,13}

Concerning the dendrimer, the original NMR dispersion data were published previously.¹⁹ In Figure 6b, we present the master curves for the different generations. The relaxation maximum at around $\omega\tau_\alpha = 1$ reflects the α -process. At $\omega\tau_\alpha < 1$ an excess relaxation with respect to the data of the simple liquid DPG becomes more pronounced with growing generation. It yields an intermediate power-law $\chi''(\omega\tau_\alpha) \propto \omega^\varepsilon$ the apparent exponent ε of which changes from 0.87 (G2) to 0.76 (G5). At even lower frequencies the curves return to a power-law behavior with an exponent close to one. This again reflects the terminal relaxation, and the corresponding terminal relaxation time τ_1 grows with the number of generations, i.e., the time scale separation between τ_1 and τ_α increases.

Figure 7 shows the time constant $\tau_\alpha(T)$ of PPG 18k (a) and of the PPI dendrimers G3 and G5 (b) as obtained from master curve construction of the data of FC NMR and rheology, respectively. In addition, we included DS data.^{19,24,36} The time

constants for PPG of lower M coincide with those of PPG 18k as T_g already saturates at low M . For PPG 18k the time constants obtained from the rheological data agree with those obtained by FC NMR and DS within a factor of 3. In the case of the dendrimers there is some variance between FC NMR and DS on the one hand and rheology on the other. As reported,¹⁹ T_g of the dendrimers is essentially independent of G within 5K which is well recognized in Figure 7b: no strong difference is observed between the different G .

Common Representation of FC ^1H NMR, Shear Modulus, and Dielectric Data. As discussed in the Theoretical Background, formally, the real part $\eta'(\omega)$ of the complex dynamic viscosity is a spectral density representation and can thus directly be compared to the spectral density provided by FC NMR. Depending on the particular macromolecular architecture (linear polymer or dendrimer) as well as on the experimental probe (NMR, rheology, DS), quite different mode distributions are expected, spanning between the local time τ_α and the terminal relaxation time τ_1 . Although the polymer-specific effects appear rather weak in the NMR susceptibility representation, it is actually most suitable for constructing master curves as merely horizontal shifting is required while normalization of the spectral density (cf. Theoretical Background) is conserved. Yet, in the spectral density representation, which can be recalculated from the susceptibility via $J_{\text{NMR}}(\omega\tau_\alpha) \propto \chi''_{\text{NMR}}(\omega\tau_\alpha)/\omega\tau_\omega$ low-frequency features are more pronounced and $J_{\text{NMR}}(\omega\tau_\alpha)$ can be directly compared to the dynamic viscosity $\eta'(\omega\tau_\alpha)$. Moreover, this representation of the relaxation spectra allows a quantitative analysis without carrying out a full spectral fitting (cf. below).

In Figure 8a, the reduced NMR spectral density $R_1(\omega\tau_\alpha)/R_1^\alpha(0)$ eq 10 for PPG (blue symbols) as well as for the

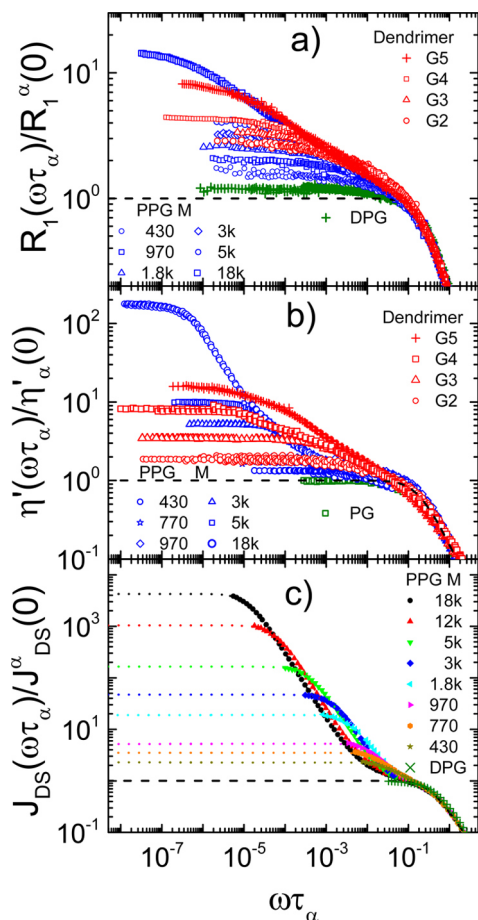


Figure 8. (a) Scaled spectral density from FC ^1H NMR of the PPI dendrimers (red) in comparison with that of the simple liquid DPG (green) and of poly(propylene glycol) (PPG, blue, ref 49). (b) Scaled dynamic viscosity of the dendrimers (red) in comparison with that of the simple liquid propylene glycol (PG, green) and that of PPG (blue). (c) Scaled spectral density obtained from dielectric normal mode spectra of PPG.^{24,36} At low frequencies the DS spectra are obscured by DC conductivity contribution, therefore they are extrapolated (dashed lines). Molar masses and number of generations, respectively, are indicated.

dendrimer (red symbols) are shown, while in Figure 8b the corresponding rescaled dynamic viscosities $\eta'(\omega\tau_\alpha)/\eta_\alpha'(0)$ are presented. Finally, Figure 8c shows the dielectric PPG data taken from ref 36. Note that for the PPI dendrimer, no normal mode relaxation is observed. In the case of DS, the experimental frequency range is sufficient so that one can omit constructing master curves. Indeed, rather similar relaxation patterns are observed for the three techniques for both PPG and the PPI dendrimer, respectively. As M (or G) increases, the low-frequency plateau rises indicating a growing polymer-specific relaxation contribution. By construction, the plateau value for the simple liquid limit represented by PG and DPG, respectively, is set to yield 1. In the case of the FC ^1H NMR data we take the CD fit as the simple liquid limit; due to a weak intermolecular relaxation contribution of DPG its plateau value is slightly above that of the CD limit. Generally, one finds that the plateau value grows fastest with M in the DS and weakest in the NMR data.

In Figure 9 the cumulative mode ratio $F_{\text{NMR}}(M)$, $F_G(M)$, and $F_{\text{DS}}(M)$ for PPG (a) and dendrimers (b), respectively, are displayed (cf. Theoretical Background). The values can be directly read off from the low-frequency plateau values in Figure 8. Generally, as already mentioned, the ratio is weakest in NMR while strongest in DS. For PPG in the Rouse regime ($M < 10\text{k}$) the data are compatible with power-laws of $F_{\text{DS}}(M) \propto M^2$ for the dielectric data, $F_G(M) \propto M^1$ for the dynamic viscosity, and $F_{\text{NMR}}(M) \propto M^{0.5}$ for FC ^1H NMR, in accordance with the predictions of the Rouse model eqs 15, 13 and 5. We note that in the case of FC ^1H NMR the weak M dependence of $F_{\text{NMR}}(M)$ can also be described by $F_{\text{NMR}}(M) \propto \ln M$ which is expected for the case that exclusively intramolecular relaxation contributes in the Rouse regime (cf. eq 4).^{22,24} The M range of the Rouse regime is too small for deciding this question. For $M > 10\text{k}$ the M -dependences of $F_{\text{DS}}(M)$ and $F_G(M)$ strongly increase with power-law exponents compatible to 3.3, in agreement with well-known experimental observations regarding entanglement dynamics.^{25–27} In the case of NMR, a weaker M dependence is indicated, yet being close to the predictions of $F_{\text{NMR}}(M) \propto M^{1.5–2.0}$ eqs 8,9 expected for the TR as well as the renormalized Rouse model. The crossover mass M_e between Rouse and entanglement dynamics is estimated to $M_e \approx 10\text{k}$.

In the case of the dendrimers, we find the shear data being close to $F_G(M) \propto M^1$ (cf. eq 13) while $F_{\text{NMR}}(M)$ shows again a weaker M -dependence, yet close to $\propto M^{0.5}$. We indicated the Rouse limits of each technique in Figure 9b (dashed lines).

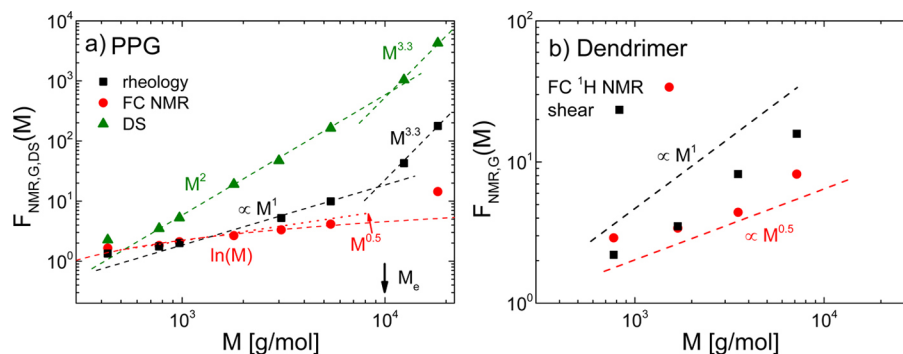


Figure 9. (a) Cumulative mode ratio $F_{\text{NMR}}(M)$, $F_G(M)$ and $F_{\text{DS}}(M)$ as a function of molar mass M for poly(propylene glycol) (PPG); expected power-law behavior is indicated (dashed and dotted lines) assuming Rouse ($M < 10\text{k}$) and tube-reptation ($M > 10\text{k}$), respectively. In the case of FC NMR, both cases, intra- (dashed) and intermolecular (dotted) relaxation, are compatible with the data. (b) Corresponding data for PPI dendrimers; Rouse limits for each method are included (dashed lines).

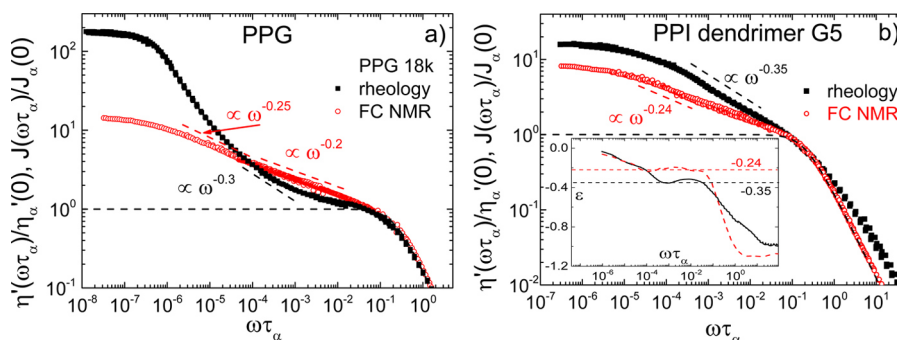


Figure 10. (a) Scaled dynamic viscosity⁴⁹ of PPG in comparison with the scaled spectral density from FC NMR calculated from the data shown in Figure 6a). (b) Same representation for the PPI dendrimer G5. The inset shows the corresponding apparent exponent as a function of frequency (derivative of the curves). The dashed lines indicate power-law behavior corresponding to that observed in Figures 4 and 5.

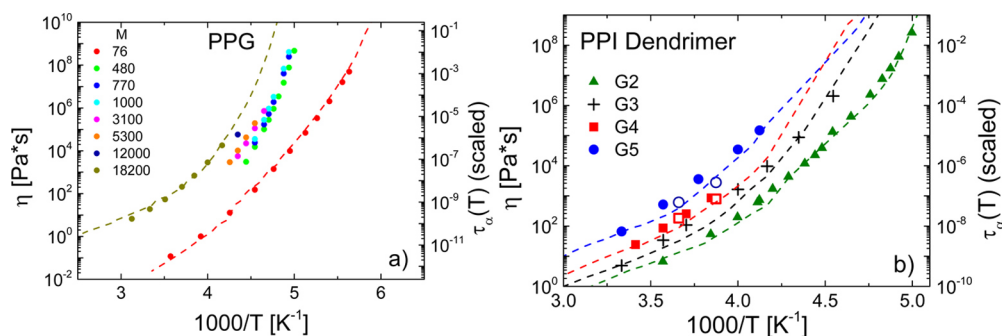


Figure 11. (a) Zero-shear viscosity of the liquid propylene glycol (PG) and the polymer PPG (colored circles). For PG and PPG 18k (cf. Figure 7a) the time constants $\tau_\alpha(T)$ obtained from combining FC NMR and DS measurements are also included (dashed lines) after vertical scaling to coincide with the viscosity data points. (b) The same plot for the PPI dendrimers with the dashed lines again reflecting (scaled) $\tau_\alpha(T)$ values (cf. Figure 7b). Open symbols: literature data for G4 and G5.²⁸

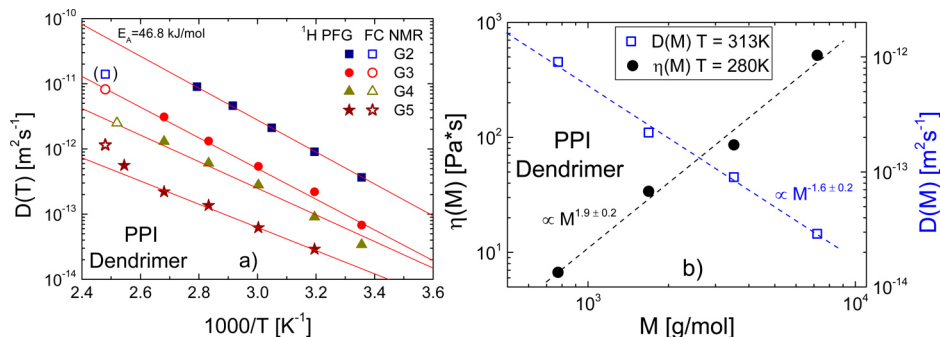


Figure 12. (a) Arrhenius plot of the diffusion coefficient D for the different generations (G2–G5) of the PPI dendrimer as obtained by PFG ¹H NMR (solid symbols) and previously by FC ¹H NMR (open symbols). (b) Molar mass dependence of the zero shear viscosity η and the diffusion coefficient D of the PPI dendrimer; power-laws are suggested by dashed lines with apparent exponents (as indicated).

Tentatively, one can state that the dendrimer displays a behavior reminiscent of Rouse dynamics. As said, the dielectric spectra of the PPI dendrimer do not show normal mode relaxation, thus no information on collective dynamics can be extracted.

A direct comparison between a FC ¹H NMR and a shear relaxation spectrum is done in Figure 10a for PPG 18k and in 10b for PPI dendrimer G5. In the case of the dendrimers, the NMR curve was horizontally shifted to coincide with the rheological data at high frequencies where the local dynamics dominates the spectra. This is justified by the fact that the time constants obtained by FC NMR and rheology do not fully coincide (cf. Figure 7b). In the case of PPG, the shapes of the spectral densities agree well at high frequencies where local

dynamics are probed. The low-frequency plateau values reflecting the polymer-specific relaxation is significantly different, and also the exponents of the intermediate power-law spanning between the terminal τ_1 and local time τ_α . In the case of the dendrimers both techniques provide rather similar curves. Yet, the agreement at high frequency is less manifested and the corresponding exponents in the intermediate regime differ (cf. inset of Figure 10b showing the apparent, frequency dependent exponent).

Temperature and Mass Dependence of Viscosity and Diffusion. In Figure 11, we present the temperature dependence of the (zero-frequency) viscosity η of PPG and the PPI dendrimers of different M . In both cases, super-Arrhenius dependence is observed being characteristic of glass

forming systems. It agrees well with that of the (vertically scaled) $\tau_\alpha(T)$ as obtained from constructing the NMR master curves and directly from DS, i.e. $\eta(T) \propto \tau_\alpha(T)$ holds for both kinds of systems. Up to our knowledge there is only one other report²⁸ which provides the viscosity for PPI dendrimers G4 and G5 at just two temperatures (open symbols); the data agree well (cf. Figure 11b).

In Figure 12a the temperature dependence of the diffusion coefficient $D(T)$ of the dendrimer as determined by PFG NMR is displayed and tentatively interpolated by an Arrhenius law being appropriate at such high T . We also included the previously reported D values as estimated by FC ^1H NMR.¹⁹ While the agreement among PFG and FC ^1H NMR is fair for the dendrimers G3–G5, stronger deviations are found for G2 for which the D value is highest and apparently exceeds the resolution limit of FC NMR.

Finally, in Figure 12b we show the M dependence of the diffusion coefficient and the viscosity, for the investigated dendrimers. We estimate $D(M) \propto M^{-1.6 \pm 0.2}$ and $\eta(M) \propto M^{1.9 \pm 0.2}$, respectively, via linear fitting on double-logarithmic scales. The latter is in accordance with $\eta(M) \propto M^{2.1}$ obtained by other authors employing low-shear rotational viscosimetry.⁵³ The expected $\eta(M) \propto M^{1/3} D^{-1}(M)$ thus holds in good approximation, which is derived in Appendix B eq 44 and discussed below.

DISCUSSION

Poly(propylene glycol) with different M and PPI dendrimers of different generations G were investigated by FC ^1H NMR, shear and dielectric relaxation experiments. By application of FTS, master curves were constructed covering polymer-specific as well as local dynamics. Although quite different fluctuations are probed, qualitatively similar spectral evolution with M (or G) is observed. Between the local dynamics (α -process) and the terminal relaxation (depending on M) an intermediate frequency regime $1/\tau_t < \omega < 1/\tau_\alpha$ is found, which can be approximated by at least one power-law with exponents depending on the macromolecular architecture (polymer or dendrimer) as well as on the probing method.

It is the purpose of the present contribution to demonstrate that the results of the methods are most conveniently compared in the spectral density (NMR) and the dynamic viscosity (rheology) representation, where the polymer-specific effects appear most pronounced. However, it is suitable to construct master curves in the susceptibility representation as merely frequency shifting is required while the integral over the spectral density is conserved. Without performing a full description of the corresponding spectral densities (covering polymer and α -relaxation), which is not easily possible, the evolution of the polymer-specific modes with M can be quantified in the zero-frequency limit and tested against theoretical predictions. We note that, beyond the search for characteristic power-laws in the dispersion data, this is currently the only reliable way to extract quantitative, model-free information in the case of FC ^1H NMR. Although a different kind of correlation function is involved, dielectric relaxation can be included in the methodological comparison.

For the zero-frequency limit considered here, a “cumulative mode ratio” $F_i(M)$ (with $i = \text{NMR, G, and DS}$) is introduced, which measures the ratio of a mean relaxation time, averaged over the mode distribution probed by the particular technique, with respect to the local time scale τ_α . It can be directly read off when the relaxation spectra are scaled to that of the low- M limit

system. The ratio $F_i(M)$ reflects a “structure factor”, i.e., it does not depend on a possible M dependence of τ_α (reflecting a possible M dependence of T_g), what is usually observed for short-chain polymers. In other words, “iso-frictional” dynamics are compared. For the different methods, the function $F_i(M)$ displays different M dependences, usually in terms of a power-law. Generally, while the M dependence is strongest for DS, it is weakest for FC ^1H NMR. In the case of PPG, the different $F_i(M)$ follow the predictions of the Rouse model in good approximation, and clear indications are found that entanglement dynamics sets in around $M_e \approx 10$ kg/mol, which is higher than reported elsewhere: values from the literature span between $M_e \approx 3$ kg mol⁻¹ (ref 54), $M_e \approx 5.3$ kg mol⁻¹ (ref 36), and $M_e \approx 7$ kg mol⁻¹ (ref 55). For a more reliable determination additional M need to be investigated. In the case of FC ^1H NMR intra- as well as intermolecular relaxation contributions control the M dependence of $F_{\text{NMR}}(M)$. Given the small M range for which Rouse dynamics applies and the weak M dependence of $F_{\text{NMR}}(M)$, it cannot be decided so far what contribution dominates. Here, future FC measurements by ^2H NMR may settle the question. We note that while the low-frequency dispersion, i.e., the change of the relaxation rate R_1 with frequency, is always determined by the intermolecular relaxation,^{15–17} the absolute contribution depends on the particular polymer system.

Regarding the PPI dendrimer, similar relaxation spectra are observed as well, when NMR and rheological data are compared. Again, $F_{\text{NMR}}(M)$ grows weaker with M and a behavior reminiscent of Rouse dynamics is observed. Reinspecting the relaxation spectra of the highest generation (G5) in detail, indication of an inflection point can be recognized instead of a well-defined intermediate power-law, as first anticipated in our analysis. Indeed, some bimodal spectral shape is observed when the derivative, i.e., the apparent exponent is considered (cf. inset of Figure 10b) suggesting that actually two slow relaxation processes appear ($\omega\tau_s \ll 1$). Three relaxation processes were also identified by Brownian simulations,³² namely (i) rotation of the dendrimer as whole, (ii) rotation of the dendrimer’s branches, a kind of breathing modes, and (iii) local reorientation of the segment. However, the bimodal structure of the polymer-specific relaxation spectrum may also be interpreted as reminiscence of weak entanglement effects, i.e., the dendrimers could interpenetrate each other to some extent. For the PPI dendrimer addressed in this study, only five generations can be synthesized, wherefore the three processes are difficult to separate—essentially a single apparent intermediate power-law is safely identified. Thus, future work should focus on a dendrimer class which allows studying more generations.

Measuring both $\eta(T, M)$ and $D(T, M)$, the latter by FC as well as FG NMR, the corresponding M dependencies, specifically $D(M) \propto M^{-1.6 \pm 0.2}$ and $\eta(M) \propto M^{1.9 \pm 0.2}$, closely follow an interrelation, which can be derived from rather general arguments, explicitly $\eta(M) \propto M^{1/3} D^{-1}(M)$ (Appendix B). Within the “elastic ball” model presented in our previous publication¹⁹ providing $D \propto M^{-2/3}$ interpenetration is considered as a surface effect referring to the case of large dendrimers, the linear size of which being much larger than the segment length, i.e., $R_g \gg b$. In our case, however, $R_g \approx 15$ Å and $b \approx 5$ Å are comparable and nearly 50% of all segments are situated in a surface layer of depth b . Therefore, the limit of strong interpenetration is more appropriate: if the dendrimer molecules strongly interpenetrate themselves, i.e., the character-

istic length of interpenetration is on the order of $R_g \propto bN^{1/3}$ and breathing modes start to play a key role for translational displacements. Indeed, due to the uncrossability of different dendrimer branches from different interpenetrating dendrimers, breathing modes can create free space for performing large scale translation. The breathing modes of a given dendrimer provide space for the segments of neighboring dendrimers for translating on a distance of the segment length b . As was discussed in ref 19, the typical breathing time scales as $\tau_{br} \propto \tau_s N^{2/3}$. Provided that the translations of the N monomers of the dendrimer due to the breathing mode of its neighbors are uncorrelated, the diffusion coefficient can be estimated as $D \propto ((b^2/\tau_{br}) \cdot (1/N)) \propto N^{-5/3}$, which is close to the experimental observation.

CONCLUSIONS

We investigated the polymer PPG and dendritic PPI of different M by dynamic shear experiments and by field-cycling ^1H NMR relaxometry in a large temperature range at $T > T_g$. In both cases, the α -process exhibits a super-Arrhenius temperature dependence typical of glass forming liquids. In order to provide a direct comparison, we propose to plot the relaxation data in the spectral density representation, i.e., the rescaled spectral density $R_1(\omega\tau_\alpha)/R_1^0(0)$ is compared to the rescaled dynamic viscosity $\eta'(\omega\tau_\alpha)/\eta'_0(0)$, where $R_1^0(0)$ and $\eta'_0(0)$ are the corresponding zero-frequency limits for a simple liquid reference system. Dielectric data are included in this comparison. In both, the polymer as well as the dendrimer, this representation shows qualitatively similar evolution with M among the techniques. The quantitative differences can be brought out by introducing a cumulative mode ratio $F_i(M)$ (with $i = \text{NMR, rheology, and DS}$) which measures the zero-frequency plateau of the spectral density with respect to that of the simple liquid limit. In the case of PPG each technique provides a different power-law behavior which essentially agrees with the prediction of the Rouse model ($M < M_e$). For PPG with its normal mode relaxation, dielectric spectra can be included in the comparison. Actually, $F_{\text{DS}}(M)$ shows the strongest while $F_{\text{NMR}}(M)$ shows the weakest M dependence. Moreover the crossover to entanglement dynamics is estimated to $M_e \approx 10k$.

In the case of the PPI dendrimer again systematic differences are observed for the rescaled spectral density as well as for $F_{\text{NMR}}(M)$ and $F_G(M)$, yet, the interpretation is still preliminary. An extensive, intermediate power-law regime is identified covering the frequency range between the terminal relaxation and the local (segmental) relaxation, yet, with the exponent differing among the techniques. Qualitatively the spectra show some reminiscence of Rouse dynamics.

Without performing a full interpolation of the relaxation spectra, the analysis allows for testing theoretical predictions. The correspondence of $J_{\text{NMR}}(\omega)$ with $\eta'(\omega)$ spectra establishes FC NMR as a powerful tool of “molecular rheology” accessing the microscopic processes underlying the (macroscopic) rheological and dielectric behavior of soft matter

Measuring both $\eta(T, M)$ and $D(T, M)$, the latter by FC as well as field gradient NMR, the M dependences are revealed, specifically $D(M) \propto M^{-1.6 \pm 0.2}$ and $\eta(M) \propto M^{1.9 \pm 0.2}$ is observed in accordance with the relation $\eta(M) \propto M^{1/3} D^{-1}(M)$ derived from general arguments. Improving our recent “elastic ball” model by assuming interpenetration of the dendrimers we find $D(M) \propto M^{-5/3}$, again in nice agreement with the experiment.

APPENDIX A

Derivation of low-Frequency Limits of the Spin–Lattice Relaxation Rate in Polymers

The most general expression for the proton spin–lattice relaxation rate, when determined by fluctuations of the magnetic dipole–dipole (DD) interaction, is given by^{37,56}

$$R_1(\omega) = \frac{8\pi}{5} \gamma^4 \hbar^2 I(I+1) \int_0^\infty \{ \cos(\omega t) A_1(t) + 4 \cos(2\omega t) A_2(t) \} dt \quad (19)$$

with

$$A_p(t) = \frac{1}{N_s} \sum_{k \neq m} \left\langle \frac{Y_{2p}(\vec{e}_{km}(t))}{r_{km}^3(t)} \frac{Y_{2p}(\vec{e}_{km}(0))}{r_{km}^3(0)} \right\rangle \quad (20)$$

where $Y_{2p}(\vec{e}_{km})$ is the component p of the spherical harmonic of rank 2, N_s the number of spins and $\vec{e}_{km}(t) = ((\vec{r}_{km}(t))/(r_{km}(t)))$ the unit vector with $\vec{r}_{km}(t)$ being the internuclear vectors. For isotropic systems $A_p(t)$ does not depend on p . The correlation function (20) contains information about the dynamics of all spins and will be called the total DD correlation function. Its initial value depends on the spatial distribution of spins

$$\begin{aligned} A_p(t=0) &= \frac{1}{N_s} \sum_{k \neq m} \left\langle \frac{Y_{2p}(\vec{e}_{km}(0))}{r_{km}^3(0)} \frac{Y_{2p}^*(\vec{e}_{km}(0))}{r_{km}^3(0)} \right\rangle \\ &= \frac{1}{4\pi} \frac{1}{N_s} \sum_{k \neq m} \left\langle \frac{1}{r_{km}^6} \right\rangle \end{aligned} \quad (21)$$

Introducing the second moment

$$M_2 = \frac{3}{5} \gamma^4 \hbar^2 I(I+1) \frac{1}{N_s} \sum_{k \neq m} \left\langle \frac{1}{r_{km}^6} \right\rangle \quad (22)$$

the relaxation rate can be written as

$$R_1(\omega) = \frac{2}{3} M_2 \int_0^\infty \{ \cos(\omega t) C_2(t) + 4 \cos(2\omega t) C_2(t) \} dt \quad (23)$$

where $C_2(t) = ((A(t))/(A(0)))$ is the normalized DD correlation function with the corresponding spectral density

$$J_{\text{NMR}}(\omega) \equiv \int_0^\infty \cos(\omega t) C_2(t) dt \quad (24)$$

Then, the relaxation rate can be expressed as

$$R_1(\omega) = \frac{2}{3} M_2 (J_{\text{NMR}}(\omega) + 4J_{\text{NMR}}(2\omega)) \quad (25)$$

The total DD correlation function contains both intra- and intermolecular contributions and can be decomposed in a sum of intra- and intermolecular spectral densities

$$J_{\text{NMR}}(\omega) = (1-p) J_{\text{NMR}}^{\text{intra}}(\omega) + p J_{\text{NMR}}^{\text{inter}}(\omega) \quad (26)$$

where p is the fraction of the intermolecular DD interactions contributing to M_2 .

As derived,⁵⁶ the zero-frequency limit of the intermolecular rate is given by

$$R_1^{\text{inter}}(0) = \sqrt{\frac{\pi}{6}} \frac{\gamma_H^4 \hbar^2}{R_g D} n_s \quad (27)$$

where R_g is the radius of gyration, D the diffusion coefficient, and n_s the spin density. In the Rouse model ($M < M_e$), D can be expressed through the segmental relaxation time τ_s and the number of Kuhn segments N , explicitly $D^R = (1/3\pi^2)(b^2/\tau_s N)$.²⁷ Together with $R_g = (bN^{1/2}/\sqrt{6})$ it follows:

$$R_1^{\text{inter}}(0) = 3\pi^{5/2} \frac{\gamma_H^4 \hbar^2}{b^3} n_s \tau_s N^{1/2} \text{ (Rouse)} \quad (28)$$

The intermolecular second moment can be estimated along

$$M_2^{\text{inter}} = \frac{3}{5} \gamma_H^4 \hbar^2 I(I+1) \frac{1}{N_s} \sum_{l \neq k} \frac{1}{r_{lk}^6} \cong \frac{3}{5} \gamma_H^4 \hbar^2 I(I+1) 4 \pi \int_{a_0}^{\infty} \frac{dr}{r^6} n_s r^2 = \frac{3\pi \gamma_H^4 \hbar^2 n_s}{5a_0^3} \quad (29)$$

where a_0 is a characteristic cut-off length on the order of the distance between nearest spins on different macromolecules. We can now combine eq 28 and $M_2^{\text{inter}} = pM_2$ with

$$R_1(0) = 5\pi^{3/2} \left(\frac{a_0}{b}\right)^3 M_2^{\text{inter}} \tau_s N^{1/2} = 10/3 M_2 \left[p(3/2) \pi^{3/2} \left(\frac{a_0}{b}\right)^3 \tau_s N^{1/2} \right] \quad (30)$$

which enters in eq 4. The corresponding intramolecular relaxation rate $R_1^{\text{intra}}(0)$ yielding a logarithmic N dependence under the condition of Rouse and entering also in eq 4 is well known from literature.^{22,45}

Concerning the TR model ($M > M_e$), one again applies eq 27, which holds universally. For the TR model one consequently finds

$$D^{\text{rep}} \propto \frac{b^2}{\tau_s} \frac{N_e}{N^2} \quad (31)$$

together with R_g leading to

$$J_{\text{NMR}}^{\text{rep,inter}}(0) \propto p \frac{N^{3/2}}{N_e} \left(\frac{a_0}{b}\right)^3 \tau_s \quad (32)$$

For the n -renormalized Rouse models, one finds⁴³

$$D^{\text{nRR}} \propto \frac{b^2}{N\tau_s} \left(\frac{N_e}{N}\right)^{n/2} \quad (33)$$

yielding

$$J_{\text{NMR}}^{\text{nRR,inter}}(0) \propto p \frac{N^{(n+1)/2}}{N_e^{n/2}} \left(\frac{a_0}{b}\right)^3 \tau_s \quad (34)$$

eqs 33 and 34 are used in eqs 6 and 7.

The intramolecular part of $J_{\text{NMR}}(0)$ for the TR as well as the n -RR models can be derived from the following expression

$$R_1(\omega) \propto f(1-p) \frac{M_2}{b^4} \int_0^\infty dt \langle b_k^z(t) b_k^z(0) b_k^x(t) b_k^x(0) \rangle (\cos(\omega t) + 4 \cos(2\omega t))$$

For $t \ll \tau_1$ the correlation function $\langle b_k^z(t) b_k^z(0) b_k^x(t) b_k^x(0) \rangle$ is exponentially decaying for all models, where τ_1 is the terminal relaxation time. For the zero-frequency limit one gets:

$$\begin{aligned} R_1(\omega = 0) &\propto f(1-p) \frac{M_2}{b^4} \int_0^\infty dt \langle b_k^z(t) b_k^z(0) b_k^x(t) b_k^x(0) \rangle \\ &\times (\cos(0) + 4 \cos(0)) \\ &= f(1-p) \frac{M_2}{b^4} \int_0^{\tau_1} dt \langle b_k^z(t) b_k^z(0) b_k^x(t) b_k^x(0) \rangle \\ &\propto f(1-p) \frac{M_2}{b^4} \langle b_k^z(\tau_1) b_k^z(0) b_k^x(\tau_1) b_k^x(0) \rangle \tau_1 \end{aligned} \quad (35)$$

The decay of the four-point dynamical correlation function $\langle b_k^z(\tau_1) b_k^z(0) b_k^x(\tau_1) b_k^x(0) \rangle$ is essentially different for the TR and n -renormalized Rouse model, respectively. For the TR model one finds⁵⁶

$$\langle b_k^z(\tau_1) b_k^z(0) b_k^x(\tau_1) b_k^x(0) \rangle^{\text{rep}} \propto \frac{b^4}{N_e^2} \frac{bN_e^{1/2}}{bNN_e^{-1/2}} \propto \frac{b^4}{N_e N} \quad (36)$$

Here (b^4/N_e^2) is the remaining correlation after (free) Rouse dynamics and $(bN_e^{1/2}/bNN_e^{-1/2})$ the probability for polymer segment to return at initial part of the tube at times on the order of τ_1 . Furthermore, $bN_e^{1/2}$ is the size of the tube and $bNN_e^{-1/2}$ the tube length.

For the n -renormalized Rouse model, which is spatially isotropic, one can derive⁵⁶

$$\langle b_k^z(\tau_1) b_k^z(0) b_k^x(\tau_1) b_k^x(0) \rangle^{\text{isot}} \propto \frac{b^4}{N^2} \quad (37)$$

With the expressions for the terminal relaxation times

$$\tau_1^{\text{nRR}} \propto \tau_s \frac{N^{4+n/2}}{N_e^{n/2}} \quad \text{and} \quad \tau_1^{\text{rep}} \propto \tau_s \frac{N^3}{N_e} \quad (38)$$

we can get the final estimates used in eqs 6 and 7:

$$\begin{aligned} J_{\text{NMR}}^{\text{rep,intra}}(0) &\propto (1-p) f \left(\frac{N}{N_e} \right)^2 \tau_s \\ J_{\text{NMR}}^{\text{nRR,inter}}(0) &\propto (1-p) f \left(\frac{N}{N_e} \right)^{n/2} \tau_s \end{aligned} \quad (39)$$

APPENDIX B

Connection between Zero-Frequency Viscosity and the Diffusion Coefficient

The connection between $\eta = \eta'(\omega \rightarrow 0)$ and the diffusion coefficient D can be derived from general arguments.^{57–59} The viscosity is the integral over shear-stress tensor correlation function⁶⁰ and formally reads

$$\eta = \frac{V}{k_B T} \int_0^\infty \langle \sigma_0^{\alpha\beta}(t) \sigma_0^{\alpha\beta}(0) \rangle_{\text{eq}} dt \quad (40)$$

The stress tensor $\sigma_0^{\alpha\beta}$ has the following structure:

$$\sigma_0^{\alpha\beta}(t) = -\frac{1}{V} \left\{ \sum_i \left[\frac{1}{M} P_i^\alpha(t) P_i^\beta(t) + \frac{1}{2} \sum_j R_{ij}^\alpha(t) F_{ij}^\beta(t) \right] \right\} \quad (41)$$

Here V denotes the volume of the system and M the molar mass, respectively. $P_i^\alpha(t)$ is the component $\alpha \in \{x, y, z\}$ of the total momentum of molecule i at moment t , $R_{ij}^\alpha(t)$ is the component α of the vector connecting the centers-of-mass of molecules i and j . The component $\beta \in \{x, y, z\}$ of the total force exerted on molecule j by molecule i is $F_{ij}^\beta(t)$. After neglecting the kinetic part of the stress tensor, one can write

$$\eta = \frac{1}{4k_B T V} \int_0^\infty \sum_{i,j} \langle R_{ij}^\alpha(t) F_{ij}^\beta(t) R_{ij}^\alpha(0) F_{ij}^\beta(0) \rangle dt \quad (42)$$

Assuming further dynamical correlations of all dendrimer pairs to be equivalent, the expression can be rewritten

$$\eta = \frac{n_s}{N} \frac{1}{4k_B T} \int_0^\infty \sum_j \langle R_{ij}^\alpha(t) F_{ij}^\beta(t) R_{ij}^\alpha(0) F_{ij}^\beta(0) \rangle dt \quad (43)$$

where n_s is the segment concentration. A final reasonable assumption is that the dynamical correlation function decays with the translational relaxation time $\tau_{tr} \propto R_g^2 D^{-1}$. Then, eq 43 can be simplified further:

$$\begin{aligned} \eta &= \frac{n_s}{N} \frac{1}{4k_B T} \sum_j \langle R_{ij}^\alpha(t) F_{ij}^\beta(t) R_{ij}^\alpha(0) F_{ij}^\beta(0) \rangle \tau_{tr} \\ &\propto z \frac{n_s k_B T}{D} \frac{R_g^4}{N b^2} \end{aligned} \quad (44)$$

Here $z \sim 10$ is the number of nearest dendrimer molecules. As the radius of gyration scales like $R_g \propto N^{1/3}$,⁶¹ the relation between viscosity and diffusion coefficient becomes

$$\eta \propto \frac{n_s k_B T}{D} \frac{R_g^4}{N b^2} \propto \frac{N^{1/3}}{D} \quad (45)$$

which is very close to the experimental observation.

AUTHOR INFORMATION

Corresponding Author

*(E.A.R.) E-mail: ernst.roessler@uni-bayreuth.de.

Notes

The authors declare no competing financial interest.

ACKNOWLEDGMENTS

The authors appreciate funding through the Deutsche Forschungsgemeinschaft (DFG) for Projects SFB 481, RO 907/13, RO 907/16 (SPP 1369), and FU 308/14 and through the Elitenetzwerk Bayern. The authors are also indebted to Roland Böhmer (Fakultät Physik, Technische Universität Dortmund) for enabling the rheological measurements of the polymer PPG and the PPI dendrimer of generations G3, G4, and G5 as well as helpful comments. We thank Nuri Aksel (Department of Applied Mechanics and Fluid Dynamics, University of Bayreuth) for giving the possibility of supplementing measurements on G2 and Lutz Heymann for his assistance. Thanks are also given to Franz Fujara and Benjamin Kresse (Technical University of Darmstadt, Germany) for making it possible to collect FC NMR data down to extremely low frequencies and assistance. Finally, the authors

are grateful for a fruitful discussion with Maxim Dolgushev (University of Freiburg).

REFERENCES

- (1) Kimmich, R.; Anoardo, E. *Prog. Nucl. Magn. Reson. Spectrosc.* **2004**, *44*, 257.
- (2) Kruk, D.; Herrmann, A.; Rössler, E. A. *Prog. Nucl. Magn. Reson. Spectrosc.* **2012**, *63*, 33.
- (3) Kimmich, R. *Principles of Soft-Matter Dynamics*; Springer: Dordrecht, The Netherlands, 2012.
- (4) Meier, R.; Kruk, D.; Rössler, E. A. *ChemPhysChem* **2013**, *14*, 3071.
- (5) Fujara, F.; Kruk, D.; Privalov, A. F. *Prog. Nucl. Magn. Reson. Spectrosc.* **2014**, *82*, 39.
- (6) Kresse, B.; Privalov, A. F.; Rössler, E. A.; Fujara, F.; Herrmann, A.; Hofmann, M. *Solid State Nucl. Magn. Reson.* **2014**, *59*, 45.
- (7) Kresse, B.; Privalov, A. F.; Herrmann, A.; Hofmann, M.; Rössler, E. A.; Fujara, F. *Solid State Nucl. Magn. Reson.* **2014**, *59*, 45.
- (8) Hofmann, M.; Kresse, B.; Privalov, A. F.; Willner, L.; Fatkullin, N.; Fujara, F.; Rössler, E. A. *Macromolecules* **2014**, *47*, 7917.
- (9) Kruk, D.; Meier, R.; Rachocki, A.; Korpala, A.; Singh, R. K.; Rössler, E. A. *J. Chem. Phys.* **2014**, *140*, 244509.
- (10) Ordikhani Seyedlar, A.; Stapf, S.; Mattea, C. *Phys. Chem. Chem. Phys.* **2015**, *17*, 1653.
- (11) Kehr, M.; Fatkullin, N.; Kimmich, R. *J. Chem. Phys.* **2007**, *126*, 094903.
- (12) Meier, R.; Kruk, D.; Gmeiner, J.; Rössler, E. A. *J. Chem. Phys.* **2012**, *136*, 034508.
- (13) Herrmann, A.; Kresse, B.; Wohlfahrt, M.; Privalov, A. F.; Kruk, D.; Fujara, F.; Rössler, E. A.; Bauer, I.; Fatkullin, N. *Macromolecules* **2012**, *45*, 6516.
- (14) Meier, R.; Schneider, E.; Rössler, E. A. *J. Chem. Phys.* **2015**, *142*, 034503.
- (15) Harmon, J. F.; Muller, B. H. *Phys. Rev.* **1969**, *182*, 400.
- (16) Sholl, C. A. *J. Phys. C: Solid State Phys.* **1981**, *14*, 447.
- (17) Kruk, D.; Meier, R.; Rössler, E. A. *Phys. Rev. E* **2012**, *85*, 020201.
- (18) Meier, R.; Herrmann, A.; Hofmann, M.; Kresse, B.; Privalov, A. F.; Schmidtke, B.; Kruk, D.; Fujara, F.; Rössler, E. A. *Macromolecules* **2013**, *46*, 5538.
- (19) Mohamed, F.; Hofmann, M.; Pötzschner, B.; Fatkullin, N.; Rössler, E. A. *Macromolecules* **2015**, *48*, 3294.
- (20) Kresse, B.; Hofmann, M.; Privalov, A. F.; Fatkullin, N.; Rössler, E. A.; Fujara, F. *Macromolecules* **2015**, *48*, 4491.
- (21) Kariyo, S.; Gainaru, C.; Schick, H.; Brodin, A.; Novikov, V. N.; Rössler, E. A. *Phys. Rev. Lett.* **2006**, *97*, 207803. Erratum: Kariyo, S.; Herrmann, A.; Gainaru, C.; Schick, H.; Brodin, A.; Novikov, V. N.; Rössler, E. A. *Phys. Rev. Lett.* **2008**, *100*, 109901.
- (22) Kariyo, S.; Brodin, A.; Gainaru, C.; Herrmann, A.; Schick, H.; Novikov, V. N.; Rössler, E. A. *Macromolecules* **2008**, *41*, 5313.
- (23) Herrmann, A.; Kariyo, S.; Abou Elfadl, A.; Meier, R.; Gmeiner, J.; Novikov, V. N.; Rössler, E. A. *Macromolecules* **2009**, *42*, 5236.
- (24) Hofmann, M.; Herrmann, A.; Abou Elfadl, A.; Kruk, D.; Wohlfahrt, M.; Rössler, E. A. *Macromolecules* **2012**, *45*, 2390.
- (25) Rubinstein, M.; Colby, R. H. *Polymer Physics*; Oxford University Press: Oxford, U.K., 2003.
- (26) Graessley, W. W. *Polymeric Liquids & Networks: Dynamics and Rheology*; Taylor & Francis Group: New York, 2008.
- (27) Doi, M.; Edwards, S. F. *The Theory of Polymer Dynamics*; Oxford Science Publication: London, 1986.
- (28) Tande, B. M.; Wagner, N. J.; Kim, Y. H. *Macromolecules* **2003**, *36*, 4619.
- (29) Gotlib, Y. Y.; Markelov, D. A. *Polym. Sci., Ser. A* **2007**, *49*, 1137.
- (30) Markelov, D. A.; Lähderanta, E.; Gotlib, Y. Y. *Macromol. Theory Simul.* **2010**, *19*, 158.
- (31) Dolgushev, M.; Berezovska, G.; Blumen, A. *Macromol. Theory Simul.* **2011**, *20*, 621.
- (32) Kumar, A.; Biswas, P. *Phys. Chem. Chem. Phys.* **2013**, *15*, 20294.
- (33) Markelov, D. A.; Dolgushev, M.; Gotlib, Y. Y.; Blumen, A. *J. Chem. Phys.* **2014**, *140*, 244904.

- (34) Nicolai, T.; Floudas, G. *Macromolecules* **1998**, *31*, 2578.
- (35) Stockmayer, W. H. *Pure Appl. Chem.* **1967**, *15*, 539.
- (36) Gainaru, C.; Hiller, W.; Böhmer, R. *Macromolecules* **2010**, *43*, 1907.
- (37) Abragam, A. *The Principles of Nuclear Magnetism*; Clarendon Press: Oxford, U.K., 1961.
- (38) Gubaidullin, A.; Shakirov, T.; Fatkullin, N.; Kimmich, R. *Solid State Nucl. Magn. Reson.* **2009**, *35*, 147.
- (39) Vaca Chávez, F.; Saalwächter, K. *Macromolecules* **2011**, *44*, 1549.
- (40) Petzold, N.; Schmidtke, B.; Kahlau, R.; Bock, D.; Meier, R.; Micko, B.; Kruk, D.; Rössler, E. A. *J. Chem. Phys.* **2013**, *138*, 12A510.
- (41) Schweizer, K. S. *J. Chem. Phys.* **1989**, *91*, 5802.
- (42) Schweizer, K. S. *J. Chem. Phys.* **1989**, *91*, 5822.
- (43) Kimmich, R.; Fatkullin, N. *Adv. Polym. Sci.* **2004**, *170*, 1.
- (44) Krutyeva, M. A.; Fatkullin, N. F.; Kimmich, R. *Polym. Sci. Ser. A* **2005**, *47*, 1716.
- (45) Khazanovich, T. N. *Polym. Sci. U.S.S.R.* **1963**, *4*, 727.
- (46) Kremer, F.; Schönhals, A. *Broadband Dielectric Spectroscopy*; Springer: Berlin, 2003.
- (47) Abou Elfadl, A.; Kahlau, R.; Herrmann, A.; Novikov, V. N.; Rössler, E. A. *Macromolecules* **2010**, *43*, 3340.
- (48) Gainaru, C.; Böhmer, R. *Macromolecules* **2009**, *42*, 7616.
- (49) Cetinkaya, B.; Böhmer, R.; Gainaru, C. Unpublished data.
- (50) Callaghan, P. T. *Translational Dynamics & Magnetic Resonance: Principles of Pulsed Gradient Spin Echo NMR*; Oxford University Press: New York, 2011.
- (51) Wu, D. H.; Chen, A. D.; Johnson, C. S. *J. Magn. Reson., Ser. A* **1995**, *115*, 260.
- (52) Böttcher, C. J. F.; Bordewijk, P. *Theory of electric polarization*; Elsevier: Amsterdam, 1973; Vol. 2.
- (53) Rietveld, I. B.; Bedeaux, D. *J. Colloid Interface Sci.* **2001**, *235*, 89.
- (54) Fetters, L. J.; Lohse, D. J.; Richter, D.; Witten, T. A.; Zirkel, A. *Macromolecules* **1994**, *27*, 4639.
- (55) Smith, B. A.; Samulski, E. T.; Yu, L.-P.; Winnik, M. A. *Macromolecules* **1985**, *18*, 1901.
- (56) Fatkullin, N.; Stapf, S.; Hofmann, M.; Meier, R.; Rössler, E. A. *J. Non-Cryst. Solids* **2015**, *407*, 309.
- (57) Fatkullin, N. *J. Non-Cryst. Solids* **2002**, *307*, 824.
- (58) Curtis, C. F.; Bird, R. B. *J. Chem. Phys.* **1981**, *74*, 2016.
- (59) Fixman, M. *J. Chem. Phys.* **1965**, *42*, 3831.
- (60) Kubo, R. *J. Phys. Soc. Jpn.* **1957**, *12*, 570.
- (61) Scherrenberg, R.; Coussens, B.; van Vliet, P.; Edouard, G.; Brackman, J.; de Brabander, E.; Mortensen, K. *Macromolecules* **1998**, *31*, 456.

Publication 6

Perspectives of ^2H field-cycling NMR relaxometry
for probing molecular dynamics in soft matter

Flämig, M.; Becher, M.; Hofmann, M.; Körber, T.; Privalov A. F;

Willner, L.; Kruk, D.; Fujara, F.; Rössler, E. A.

*The Journal of Physical Chemistry Part: Part B: Biophysical Chemistry,
Biomaterials, Liquids, and Soft Matter* **2016**, (submitted)

Perspectives of Deuteron Field-Cycling NMR Relaxometry for Probing Molecular Dynamics in Soft Matter

M. Flämig,[†] M. Becher,[‡] M. Hofmann,[†] T. Körber,[†] B. Kresse,[‡] A. F. Privalov,[‡] L. Willner,[§] D. Kruk,^{||} F. Fujara,[‡] and E. A. Rössler^{*,†}

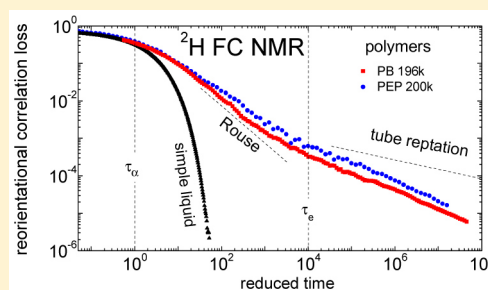
[†]Experimentalphysik II, Universität Bayreuth, 95440 Bayreuth, Germany

[‡]Institut für Festkörperphysik, TU Darmstadt, Hochschulstrasse 6, 64289 Darmstadt, Germany

[§]Institute of Complex Systems, Forschungszentrum Jülich, D-52425 Jülich, Germany

^{||}Faculty of Mathematics and Computer Science, University of Warmia & Mazury, Słoneczna 54, 10-710 Olsztyn, Poland

ABSTRACT: Due to the single-particle character of the quadrupolar interaction in molecular systems, ^2H NMR poses a unique method for probing reorientational dynamics. Spin–lattice relaxation gives access to the spectral density, and its frequency dependency can be monitored by field-cycling (FC) techniques. However, most FC NMR studies employ ^1H ; the use of ^2H is still rare. We report on the application of ^2H FC NMR for investigating the dynamics in molecular liquids and polymers. Commercial as well as home-built relaxometers are employed accessing a frequency range from 30 Hz to 6 MHz. Due to low gyromagnetic ratio, high coupling constants, and finite FC switching times, current ^2H FC NMR does not reach the dispersion region in liquids (toluene and glycerol), yet good agreement with the results from conventional high-field (HF) relaxation studies is demonstrated. The pronounced difference at low frequencies between ^2H and ^1H FC NMR data shows the relevance of intermolecular relaxation in the case of ^1H NMR. In the case of the polymers polybutadiene and poly(ethylene-*alt*-propylene), very similar relaxation dispersion is observed and attributed to Rouse and entanglement dynamics. Combination with HF ^2H relaxation data via applying frequency–temperature superposition allows the reconstruction of the full spectral density reflecting both polymer as well as glassy dynamics. Transformation into the time domain yields the reorientational correlation function $C_2(t)$ extending over nine decades in time with a long-time power law, $C_2(t) \propto t^{-0.45 \pm 0.05}$, which does not conform to the prediction of the tube-reptation model, for which $\propto t^{-0.25}$ is expected. Entanglement sets in below $C_2(t = \tau_e) \cong S^2 = 0.001$, where τ_e is the entanglement time and S the corresponding order parameter. Finally, we discuss the future prospects of the ^2H FC NMR technique.



INTRODUCTION

NMR relaxometry, i.e., measuring the spin–lattice relaxation time T_1 or the spin–spin relaxation time T_2 , is a well established method for probing the dynamics in condensed matter. In particular, with the availability of a commercial field-cycling (FC) relaxometer since about 2000, NMR relaxometry received new momentum, as it is now routinely possible to measure the dispersion of the spin–lattice relaxation in a frequency range of 10 kHz to 30 MHz (^1H).^{1–5} With the use of a home-built relaxometer, even frequencies down to, say, 10 Hz are nowadays accessible.^{6,7} The technique “cycles” the magnetic field produced by a resistive electromagnet from a (high) polarization field down to a (low) relaxation field and back to a (high) detection field. As in the case of dielectric spectroscopy (DS), relaxation spectra are collected for various temperatures and motional models in terms of their spectral density or susceptibility, respectively, are tested.

Most of the FC studies employed ^1H NMR. Due to the rather low detection field (about half a Tesla), protons with their high gyromagnetic ratio provide the most convenient way to get relaxation profiles within a reasonable time. Without

taking recourse to isotope labeling, ^1H FC NMR is well suited to study in particular the collective dynamics in soft matter, for example, in polymers, dendrimers, or liquid crystals. Here, collective dynamics is governed by frequency–temperature superposition (FTS); that is, the spectral shape of the dynamic susceptibility virtually does not change with temperature.^{8–12} As in the case of shear stress relaxation,^{13,14} collecting NMR relaxation data at different temperatures allows master curves to be constructed, which significantly extend the still narrow frequency range of the FC technique. Regarding polymers, different power-law dispersions were identified,^{2–4,15–23} allowing the tube-reptation model to be tested,²⁴ for instance. The high similarity of such “broad band” NMR relaxation spectra with the corresponding shear relaxation spectra may establish FC NMR as a method of molecular rheology.²⁵

The relaxation mechanism of ^1H NMR is provided by the fluctuation of the magnetic dipole–dipole interaction, which by

Received: May 24, 2016

Revised: July 15, 2016

Published: July 15, 2016



its very nature is a many-particle interaction.²⁶ For example, there is an intra- as well as an intermolecular relaxation pathway, and it is not easy to attribute both contributions in the total relaxation. For simple liquids and polymers, it is well-known that intermolecular contribution caused by translational dynamics (molecular diffusion) dominates the low-frequency dispersion of the total relaxation and allows the diffusion coefficient to be extracted,^{26–29} while reorientational dynamics yields the dispersion at higher frequencies. However, this fact was only recently exploited in a systematic way^{30–36} and also verified by molecular dynamics simulations.^{37,38} However, molecular reorientations also yield an intermolecular ¹H relaxation contribution (the so-called eccentricity effect).^{32,39} An ultimate approach to disentangle both intra- and intermolecular relaxation is given by the isotope dilution technique; first FC experiments were reported only recently.^{35,40–43} Here, by dilution with the same but deuterated molecule, the intermolecular relaxation is suppressed. However, such FC experiments are time-consuming, as one has to measure the relaxation spectra for different concentrations (and temperatures). In the case of polymers, there are additional problems due to the necessity of having at hand deuterated and protonated polymers with the same molar mass and glass transition temperature T_g . Moreover, polymer blends tend to demix. Nevertheless, such experiments provide the intermolecular relaxation contribution, in addition to the intramolecular part. From the former, the mean square displacement as a function of time can be extracted in addition to that from field gradient NMR experiments.^{44–47} Combining both methods discloses all the diffusion regimes of long-chain polymers predicted by the tube-reptation model.⁴³

With its multiparticle interaction, another problem is inherent to ¹H NMR, in particular, to ¹H FC NMR with its low spectral resolution. It is not easily possible to distinguish between the relaxation of chemically different groups, for example, between the methyl group and chain protons in a polymer. In the worst case, the simple Bloch equations do not apply and nonexponential relaxations result, rendering it difficult to define a relaxation time.^{48,49} Fortunately, in many cases, the different groups are strongly coupled due to fast cross relaxation and relax with a common time constant, yet the quantitative interpretation may still not be straightforward. These problems led many researchers to investigate the relaxation of other nuclei like ¹³C or ²H, for instance, where a single-particle interaction dominates. However, here relaxation rates for only a few frequencies were accessible, so far.

Applying ²H NMR on (labeled) compounds does not suffer from many of the problems mentioned above, and the power of the techniques, in particular, regarding multidimensional solid-state investigations has been demonstrated in innumerable publications.^{50–53} First of all, the relaxation is controlled by the quadrupolar interaction, which in molecular systems is of purely intramolecular origin; for example, the reorientation of the C–²H bond is probed. Each chemical group exhibits its own relaxation rate, and by appropriate (partial) isotope labeling, the dynamics of a specific group can be singled out. Even in the case when, e.g., two chemically different groups are deuterated and spectral resolution is lost due to molecular slowdown, the resulting (total) relaxation becomes biexponential and can be well measured in conventional high-frequency (HF) spectrometers. Thus, extending the FC technique to include also the ²H nuclei is highly desired, yet several challenges have to be

mastered. Due to the by a factor of 6 lower gyromagnetic ratio, the detection field of the employed commercial electromagnets is below 5 MHz, and thus, the signal-to-noise ratio is very low. Moreover, the quadrupolar interaction is stronger than the ¹H dipolar coupling, and faster relaxation results. This may interfere with the switching time of the FC magnet, even more than in the case of ¹H FC NMR. Nevertheless, first ²H FC NMR studies on polymers were used to check the reliability of the isotope dilution ¹H FC NMR experiments.^{22,40–42,54,55} Intramolecular ¹H and ²H relaxation are expected to essentially display the same dispersion. Indeed, this was found experimentally.

Performing experiments on a commercial as well as on a home-built relaxometer, in the present contribution, we further explore the potential of ²H FC NMR for studying the dynamics in liquids and polymers. Provided that crystallization does not interfere, liquids like glycerol or toluene undergo the glass transition upon cooling, which results in a strong molecular slowdown. As shown by ¹H FC NMR (as well as by conventional high-field ²H relaxation studies), strong dispersion is expected at low temperatures approaching T_g . As will be demonstrated, ²H FC NMR with the current technical possibilities does not reach the dispersion region, but a comparison with results from high-field (HF) relaxation experiments on simple liquids yields good agreement. A direct comparison between the results of ²H and ¹H FC NMR will confirm the relevance of intermolecular relaxation in the case of ¹H NMR, often ignored in conventional ¹H NMR studies. Considering polymers like poly(ethylene-*alt*-ethylene) (PEP) and polybutadiene (PB) collective, polymer-specific dynamics lead to pronounced dispersion well above T_g . By applying FTS, the full spectral density or reorientational correlation function, extending over many decades in frequency or time, respectively, can be revealed. The results will be discussed in the frame of the tube-reptation model describing Rouse and entanglement dynamics of long chain polymers.^{2,15,24,56} Finally, we will discuss the future prospects of ²H FC NMR relaxometry.

THEORETICAL BACKGROUND

Field-cycling NMR is applied to monitor the frequency dependence of the spin–lattice relaxation time T_1 . The latter is determined by the evolution of the nuclear magnetization toward its equilibrium value. The frequency is given by the Larmor frequency depending on the magnetic relaxation field B via $\omega = \gamma B$, where γ denotes the gyromagnetic ratio of the nucleus. In the case of ²H NMR, fluctuations of the quadrupolar interaction cause the relaxation, which in molecular systems is strictly of intramolecular origin.^{50–53} Specifically, the present study focuses on the motional narrowing regime where the NMR spectrum of a more or less viscous liquid (or polymer melt) is given by a Lorentzian line shape with its width reflecting the inverse of the spin–spin relaxation time T_2 . In the case of (high molar mass) polymers, due to slow polymer specific dynamics, some very small residual coupling may still be present. The ²H spin–lattice relaxation rate $R_1 = 1/T_1$ of an ensemble of chemically identical deuterons reorienting presumably isotropically is connected to the spectral densities $J_m(\omega)$ by a “BPP-type” equation^{26,56}

$$R_1(\omega) = K[J_1(\omega) + 4J_2(2\omega)] \quad (1)$$

where K is given by

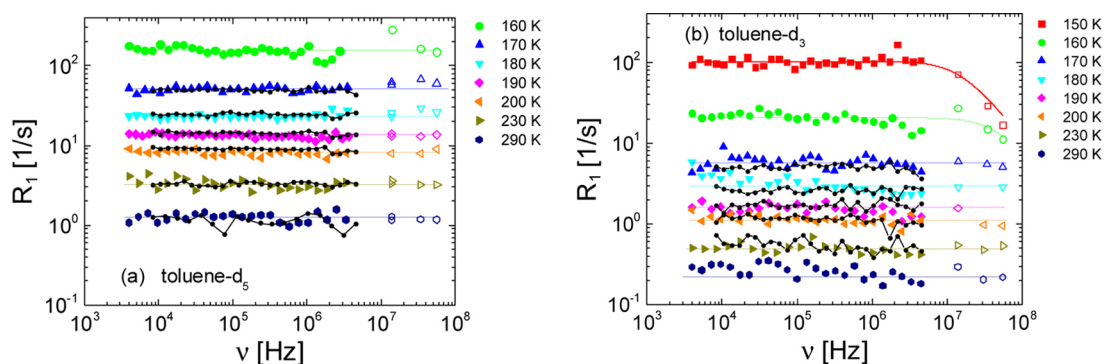


Figure 1. (a) ^2H spin–lattice relaxation rate R_1 of toluene- d_5 as a function of frequency at various temperatures as revealed by FC NMR. Conventional, high-field data measured at 14 MHz (present work), 13.8 MHz,⁷⁵ 34.4 MHz,⁷⁵ and 55.8 MHz⁷⁵ are included (open symbols). (b) Corresponding ^2H relaxation rate of toluene- d_3 : HF data measured at 14 MHz (present work), 30.7 MHz,⁷⁷ 34.4 MHz,⁷⁰ and 55.2 MHz⁵⁹ are added (open symbols). For the two lowest temperatures, we show an interpolation with a Cole–Davidson spectral density. In both figures, the connected black points show the results of toluene- d_8 and the straight lines denote the average rate (cf. text).

$$K = \frac{3\pi^2}{10} \left(\frac{e^2 Q q}{h} \right)^2 \quad (2)$$

Here $\frac{e^2 Q q}{h} = \text{QCC}$ is the ^2H quadrupolar coupling constant, a quantity easily accessible from the solid-state spectrum of a liquid, i.e., in the glass state $T < T_g$ when all large-angle motion has ceased. For the systems investigated, the coupling constant is known (cf. below). In the case of isotropic systems, all the quadrupolar spectral densities are m -independent and $J_m(\omega) = J(\omega)$ is the Fourier transform of the second order reorientational correlation function $C_2(t)$, i.e., the correlation function of the second Legendre polynomial. We note that DS probes $C_1(t)$ in good approximation, i.e., the first Legendre polynomial correlation function.⁵⁷

In liquids or polymers, due to the collective nature of molecular dynamics, quite generally, the shape of the fluctuation spectrum in terms of the susceptibility representation $\chi''(\omega) = \omega J(\omega)$ virtually does not change with temperature; i.e., frequency–temperature superposition (FTS) applies. One can write the susceptibility as a function of a reduced frequency, explicitly $\chi''(\omega\tau)$, where τ denotes a characteristic correlation time, which drives the temperature dependence of the dynamics, for example, the time τ_α determined by the glass transition phenomenon (α -process). Thus, measuring at different temperatures, one can construct master curves, which effectively extend the covered frequency range. Actually, this is quite important for FC NMR as the currently accessible frequency range is still narrow (3–5 decades). In order to allow for such master curve construction, we rewrite eq 1 in the susceptibility representation^{3,4,17–19}

$$\omega R_1(\omega) = K[\chi''(\omega) + 2\chi''(2\omega)] \equiv 3K\chi''(\omega) \quad (3)$$

Although $\chi''(\omega)$ is a weighted sum of two susceptibilities, both quantities are essentially indistinguishable for broad relaxation dispersion monitored on logarithmic scales. We note that the susceptibility representation of NMR relaxation data was already used by Cohen-Addad and co-workers.⁵⁸ In many cases, for example, in rheological studies as well as in ^2H FC NMR studies, the time constant τ_α cannot be obtained directly, since the susceptibility maximum linked to the main relaxation (α -) process is not observable; i.e., the condition $\omega\tau_\alpha \cong 1$ is difficult to match experimentally. However, the temperature dependence of the shift factor a_T is that of τ_α .

Assuming isotropic reorientation in the extreme narrowing, the simple relation $R_1 = 5K\tau_2$ holds, which yields $\tau_2(T)$ from $R_1(T)$ provided that K is known from the solid-state spectrum accessible at low temperatures. Here, τ_2 is the time constant of the second Legendre correlation function.

In viscous liquids not too close to T_g , the reorientational spectral density is well interpolated by a Cole–Davidson (CD)⁵⁷ distribution of correlation times $G(\ln \tau)$ (or equivalently by a Kohlrausch decay in the time domain), a fact extensively demonstrated by dielectric and light scattering studies^{8–12} as well as by many ^2H HF NMR relaxation investigations, which jointly analyzed $T_1(T)$ and $T_2(T)$.^{59–62} This distribution will also be applied in the case of toluene and glycerol- d_5 . Actually, choosing $G(\ln \tau)$ is nothing else than introducing a nonexponential correlation function $C_2(t)$ reflecting the collective dynamics.

EXPERIMENTAL SECTION

Parts of the ^2H spin–lattice relaxation experiments (toluene: methyl deuterated: $-d_3$, phenyl deuterated: $-d_5$, fully deuterated: $-d_8$ and PEP- d_{10}) were carried out on a home-built FC NMR relaxometer located at the Technische Universität Darmstadt. For the measurements on PEP- d_{10} , a home-built main current source^{5–7} was used with a polarization field of 4.5 MHz and a detection frequency of about 6 MHz for deuterons. The earth and other stray magnetic fields from the surrounding laboratory equipment were compensated, and the evolution fields were calibrated carefully.^{6,7,63} The temperature was stabilized by a thermally controlled gas flow across the probe. The measurements on toluene- d_3 , $-d_5$, and $-d_8$ were performed using a commercial gradient pulse amplifier instead of the home-built one, namely, the model Avanto SQ from Siemens. All three channels of this amplifier were used in parallel to set up a detection field of 2 T (12 MHz), but for purposes of a stable coil temperature, the polarization field was kept at 4.5 MHz. In order to reach also lower temperatures (down to 80 K), a commercial cryostat was used. This cryostat contains unavoidable metal parts in which during field switching eddy currents are induced so that the switching time is about 4 ms and the minimum evolution field is limited to 4 kHz. The absolute accuracy of temperature is ± 1.5 K and its stability ± 1 K.

The measurements for glycerol- d_5 were carried out on a STELAR relaxometer FFC 2000 located in Bayreuth, which

allows measurements in the temperature range from 180 to 420 K and in a ^2H Larmor frequency range $800\text{ Hz} \leq \nu \leq 3\text{ MHz}$. The temperature is maintained by evaporating liquid nitrogen, which passes through a glass Dewar carrying the NMR coil with the sample; accuracy and stability of temperature is comparable with that of the home-built relaxometer.

RESULTS AND DISCUSSION

1. Molecular Liquids Undergoing the Glass Transition.

High-field ^2H NMR relaxation studies are well established for investigating the dynamics in liquids, in particular in such systems which undergo the glass transition. Here, a strong molecular slowdown is observed upon cooling, provided that crystallization is avoided. Prominent examples are glycerol,^{61,64–67} propylene carbonate,⁶⁸ salol,^{69,70} *o*-terphenyl,^{60,61,71} and toluene.^{59,72–78} Typically, the spin–lattice relaxation rate is monitored as a function of temperature and at a few frequencies. The major aim is to extract correlation times which characterize the glass transition. In order to achieve this goal, an appropriate spectral density has to be assumed. As discussed (cf. Theoretical Background), a CD spectral density is well suited to describe $R_1(T)$ (and $R_2(T)$) in the modestly viscous regime of the liquid; it provides correlation times which agree with those reported by other methods. At lower temperatures close to T_g , secondary processes become relevant, and a straightforward analysis relying solely on HF NMR relaxation data is elusive. This, of course, makes ^2H FC NMR a promising tool for overcoming the limits of conventional (HF) NMR studies. Here, we discuss the ^2H FC NMR results for differently deuterated toluene ($-d_3$, $-d_5$, $-d_8$) and glycerol- d_5 . As mentioned, ^2H NMR solely probes a single-particle reorientational correlation function which can easily be interpreted.

In Figure 1, we show a few examples of the ^2H relaxation dispersion of toluene- d_5 (Figure 1a) and toluene- d_3 (Figure 1b), respectively, as revealed by FC NMR. They were measured with a home-built relaxometer covering a ^1H frequency range of 4–4500 kHz (cf. Experimental Section). Note that, due to the different gyromagnetic ratio, for ^2H NMR, the frequencies available are by a factor of 6 lower than those for ^1H FC NMR. All relaxation decays are exponential and thus provide a well-defined relaxation rate $R_1(\nu)$. Starting with toluene- d_5 , no frequency dependence is observed down to the lowest temperature (160 K). Even including results from HF NMR experiments taken from refs 59 and 75, no dispersion is found, yet the agreement between the results from FC and HF experiments is very satisfactory. In the case of the toluene- d_3 (Figure 1b), data down to somewhat lower temperature (150 K) can be collected due to the fact that the fast methyl group reorientation reduces the effective QCC (cf. eq 2 and below) and thus decreases the relaxation rate compared to that of toluene- d_5 . Again, no dispersion is recognized for the FC NMR data; however, the HF data^{59,70,77} clearly show the onset of dispersion. The onset can be reproduced by a CD spectral density with a stretching parameter of $\beta = 0.32$ (taken from refs 59 and 75) and included in Figure 1b. For completeness, in Figure 2, the currently available ^2H relaxation rates for toluene are displayed as a function of temperature.

We also measured the spin–lattice relaxation of toluene- d_8 . Figure 3 shows the normalized relaxation function plotted versus a rescaled time $t\langle R_1 \rangle$ for some frequencies and temperatures measured. Here, $\langle R_1(\omega) \rangle$ denotes the initial slope, i.e., the average rate. Essentially, master curves are found; however, small deviations occur for the different temperatures,

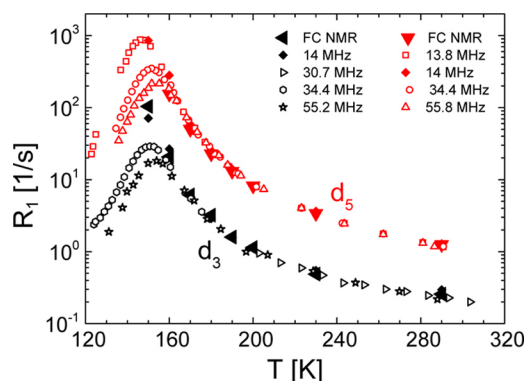


Figure 2. ^2H spin–lattice relaxation rate of toluene as a function of temperature. Closed symbols, present work; open symbols, literature data (13.8, 34.4,⁷⁵ 30.7,⁷⁷ 34.4,⁷⁰ 55.2,⁵⁹ and 55.8 MHz⁷⁵).

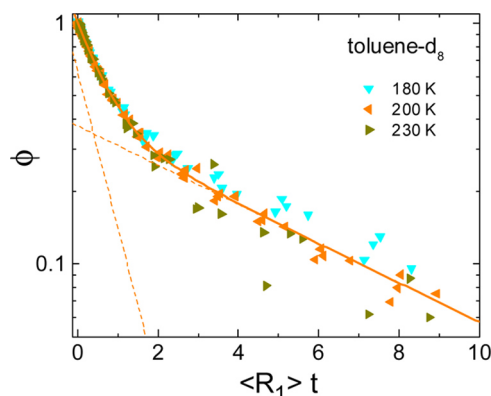


Figure 3. Normalized magnetization decay ϕ of toluene- d_8 for selected frequencies and temperatures displayed as a function of the rescaled time. A biexponential fit is shown for 200 K (straight line) as well as the decomposition in its monoexponential components (dashed lines).

since the ratio of the two relaxation times is not constant (cf. below). The nonexponential relaxation can be well fitted to a sum of two exponentials with weighting factors of 5/8 and 3/8, respectively, reflecting the number of different deuterons in the molecule. Here, we note that the correct weighting factors can only be retained in a limiting temperature range. While at low temperatures, due to the not ignorable switching time, the fast relaxation gets partly lost, at high temperatures and long relaxation times (\sim seconds), the stability of the detection field due to thermal expansion of the main coil decreases. The resulting relaxation rates $R_1^{d_5}(\nu)$ and $R_1^{d_3}(\nu)$ are included in parts a and b of Figure 1, respectively (black connected symbols). Satisfying agreement is observed with the data obtained for toluene- d_5 and toluene- d_3 .

Given the rigid-lattice QCC values for toluene- d_5 as well as for toluene- d_3 and taking $R_1(\omega) = 5K\tau_2$ (cf. Experimental Section), one can extract the correlation time $\tau_2(T)$ from both data sets in Figure 1. For toluene- d_5 , a value of $\text{QCC}_{d_5} = 180\text{ kHz}$ was reported,^{59,79} and for toluene- d_3 , with its fast reorienting methyl group, the motionally averaged coupling is $\text{QCC}_{d_3} = 52\text{ kHz}$ ($T < T_g$).⁵⁹ In Figure 4, the extracted correlation times are compared to a compilation of time constants collected by other techniques like DS and depolarized light scattering.⁸⁰ Overall, satisfying agreement is found; at high temperatures, some deviations are observed. As discussed below, they may be explained by some extent of anisotropic

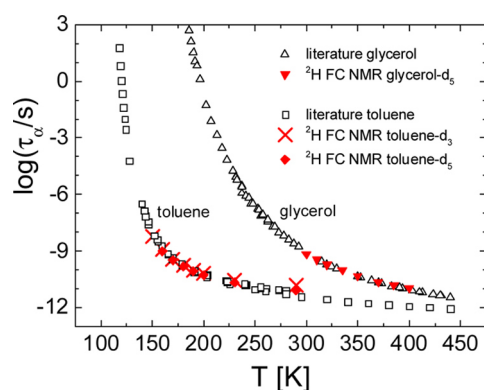


Figure 4. Reorientational correlation times τ_α for toluene and glycerol as a function of temperature as determined from ^2H FC NMR (closed symbols) and from several other techniques (open symbols⁸⁰).

reorientation. As typical of the glass transition in molecular liquids, reorientational time constants revealed by the various methods agree well, i.e., $\tau_2(T) \equiv \tau_\alpha(T)$.

As discussed, collective dynamics in condensed matter usually exhibits FTS; i.e., the shape of the susceptibility virtually does not change with temperature, and it can be expressed as a system specific susceptibility function $\chi''(\omega\tau_\alpha)$. However, when measurements cover a very large temperature range, including temperatures close to T_g FTS may fail. In the present case, we stick to high temperatures only. The simplest way to construct master curves is by transforming the data to the susceptibility representation ωR_1 (cf. Theoretical Background) and taking $\tau_\alpha(T)$ from independent experiments. Another possibility is to produce susceptibility master curves by shifting different data sets solely along the ω -axis and check the extracted shift factor in terms of $\tau_\alpha(T)$ against independent measurements of the latter. Shifting along the frequency axis without any vertical shift conserves the integral over the susceptibility; the latter is given by the QCC, which is temperature independent in good approximation. Such susceptibility master curves are easily compared to results from DS, for instance.

In Figure 5, we constructed a master curve $\chi''(\omega\tau_\alpha)$ for the toluene- d_5 data (NMR and DS) by taking recourse to the time constants plotted in Figure 4. The maximum of $\chi''(\omega\tau_\alpha)$ is

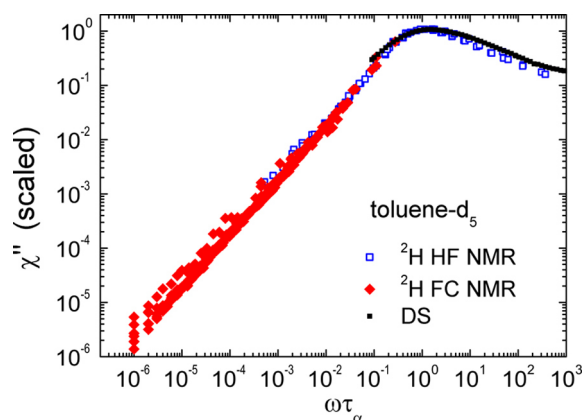


Figure 5. Susceptibility master curve for toluene- d_5 as obtained from ^2H FC and high field (HF) NMR relaxometry;⁷⁵ in addition, the corresponding dielectric spectrum (DS) is included (unpublished results, cf. also ref 9).

scaled to one. First, we discuss the ^2H FC NMR results, which are extended by HF data.⁷⁵ In the latter case, $R_1(T)$ data, measured at a single frequency, is taken, and in order to get the reduced frequency $\omega\tau_\alpha$ for each temperature, the time constant $\tau_\alpha(T)$ is picked off from Figure 4. For both data sets (FC and HF data), the same scaling factor of the amplitude is applied. While the ^2H FC data follow a straight line, i.e., $\omega R_1 \propto \omega^1$, as expected as a consequence of the dispersion-free data of the spectral density representation in Figure 1, the HF data exhibit a relaxation maximum which fits into the trend of the ^2H FC data. We added also the dielectric curve $\chi''(\omega\tau_\alpha)$ of toluene (unpublished results, see also ref 9). Good agreement between DS and ^2H NMR is revealed. In the case of toluene with its low electric dipole moment, DS can only probe a small amplitude range on the low-frequency side of the relaxation maximum. In addition, in most dielectric spectra of liquids (and polymers), the low-frequency flank is spoiled by the presence of parasitic contribution of a dc conductivity. Here, FC experiments provide access to a much larger susceptibility range, and dynamics slower than the α -process (for instance, polymer dynamics, see below) contributes here.

The master curve in Figure 5 can be interpolated by a CD susceptibility⁵⁷ (not shown), as typically done for dielectric spectra of glass forming liquids.^{10,12} Moreover, the master curves demonstrate that in the temperature range (160–290 K) investigated by ^2H NMR no influence of another process like the β -process is recognized. Actually, from analyzing the dielectric spectra close to $T_g = 117$ K,⁹ it is known that a pronounced β -process emerges at low temperatures. In other words, the α - and β -process have merged at temperatures, say, above 160 K, a phenomenon well-known in glass forming liquids.^{9,81} We repeat that ^2H FC NMR with its current instrumentation cannot reach lower temperatures, as the rate becomes too high to be resolved. The master curve displayed in Figure 5 can be Fourier transformed to yield the reorientational correlation function $C_2(t/\tau_\alpha)$, which is included in Figure 11, for comparison (cf. below).

As already mentioned in the context of discussing the data in Figure 4, when extracting correlation times from the relaxation rates, one implicitly assumes isotropic reorientation. However, the deviations observed at high temperatures with respect to the literature data may originate from anisotropic reorientation of the toluene molecule. For example, given that the methyl group rotation is fast⁷⁷ and assuming overall isotropic reorientation, the ratio of the relaxation times $R_1^{d_5}(\nu)/R_1^{d_3}(\nu) = r$ is expected to be $r = (\text{QCC}_{d_5}/\text{QCC}_{d_3}) = (180/52)^2 = 12.0$, thus independent of temperature. Actually, the ratio decreases above 160 K reaching values around 6 at ambient temperature, and this may be explained by the presence of anisotropic reorientation as suggested in the literature.^{82–84} Taking the Woessner model of anisotropic reorientation,⁸⁵ in the Appendix, we extract from $r(T)$ the anisotropy parameter $\delta = D_{||}/D_{\perp}$.

Next, we consider the liquid glycerol- d_5 ; the corresponding relaxation rate $R_1(\omega)$, measured with the commercial relaxometer FFC 2000, is displayed for different temperatures in Figure 6. Compared to Figure 1, the frequency range extends to somewhat lower frequencies, but also the upper limit is smaller (800 Hz to 3 MHz). Again, no dispersion is revealed in the frequency range covered by ^2H FC NMR, and good agreement is found with HF relaxation data. For completeness, we note that at the highest temperatures a very weak dispersion

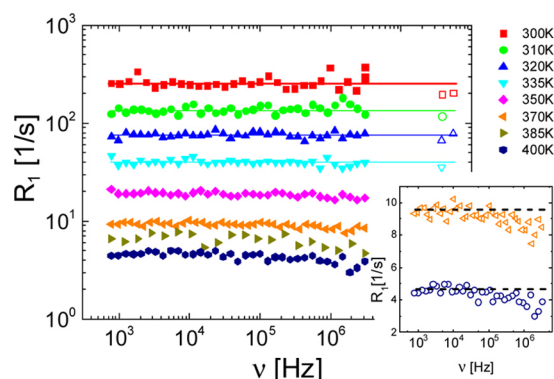


Figure 6. ^2H spin–lattice relaxation rates of glycerol- d_5 from FC NMR (closed symbols) and for comparison high field NMR data (55⁶¹ and 38 MHz⁶⁷). Inset: dispersion at high temperatures on linear scale.

is found (cf. inset in Figure 6), which is actually close to the error margin of the measurement and for which we currently have no explanation. Possibly, the finding is related to hydrogen exchange processes, like those found by ^1H FC NMR in water.¹ Taking the average rate from the ^2H FC data and $\text{QCC}_{\text{glyc}} = 165 \text{ kHz}$,⁶¹ we again get very satisfying agreement with the time constants reported by other techniques (cf. Figure 4).

Figure 7 shows a master curve constructed by taking recourse to $\tau_\alpha(T)$, as given in Figure 4. For the ^2H FC and HF NMR

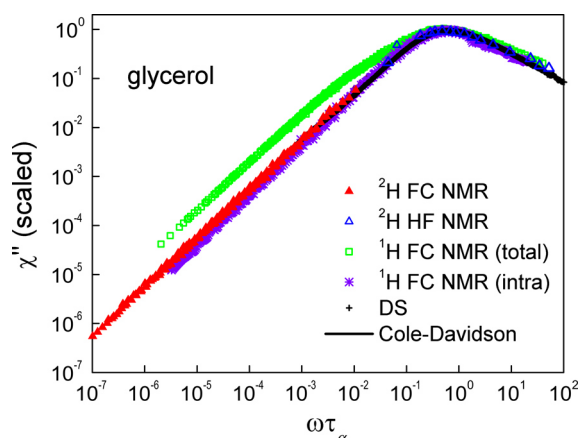


Figure 7. Susceptibility master curve constructed from taking $\tau_2 = \tau_\alpha$ in Figure 4: High field (HF) NMR, ^1H FC NMR (total and intra),³⁰ and data from dielectric spectroscopy (DS)⁸⁶ were added for comparison. Solid line: interpolation by the Cole–Davidson function.

data (cf. ref 61), again the same scaling factor for the relaxation values is applied. While the ^2H FC NMR data follows a straight line, i.e., $\omega R_1 \propto \omega^1$, the HF NMR data exhibits a relaxation maximum which fits into the ^2H FC NMR data. We included the curve provided by our DS measurement,⁸⁶ which follows the HF ^2H NMR data. Moreover, comparing the ^2H NMR results with those from the intramolecular ^1H relaxation dispersion studies obtained by performing isotope dilution experiments,³⁰ complete agreement is recognized. As in the case of ^2H NMR, the ^1H intramolecular rate probes solely the reorientational dynamics. Thus, ^2H , $^1\text{H}(\text{intra})$, and DS all probe essentially the same susceptibility, which can be well interpolated by the same CD function. In contrast, the total ^1H relaxation (taken from ref 30 and included in Figure 5) exhibits a low-frequency shoulder, which thus has to be

attributed to the intermolecular relaxation contribution. As established long ago,^{27–29} the intermolecular correlation function shows a long-time power-law behavior, $C(t) \propto t^{-d/2}$, with d being the spatial dimension. With respect to the more or less exponential decay of $C_2(t)$ in liquids, this long-time power law in $d = 3$ will always dominate the response at long times or at low frequencies, respectively. This implies that for the total ^1H relaxation the extreme narrowing condition (R_1 becoming frequency independent) never applies, while in the ^2H case it is essentially found at high temperatures, as demonstrated in Figures 1 and 7. For $d = 3$, a square root frequency dependence is predicted for $R_1(\omega)$ at low frequencies, which directly allows the translational diffusion coefficient to be determined in liquids as well as polymers.^{4,31–36}

2. Polymer Dynamics. High-field ^2H spin–lattice relaxation studies on polymer melts were conducted by several groups.^{87–95} Focus was on characterizing the “local” segmental relaxation (α -process) determined by the glass transition phenomenon. In contrast, ^2H FC NMR investigations are still rare. For example, in the case of poly(butadiene) (PB) and poly(ethylene oxide) (PEO), first results were reported by the Kimmich group^{2,15,41,54} and by our group.^{22,42} In these systems, the ^2H spin–lattice relaxation is exponential, and in contrast to simple liquids, ^2H FC NMR probes pronounced dispersion at high temperature well above T_g , reflecting polymer-specific (collective) dynamics. They were interpreted in terms of Rouse and entanglement dynamics. Below we will discuss these results on PB in the context of new measurements performed on fully deuterated poly(ethylene-*alt*-propylene) (PEP) with molar mass $M = 200 \text{ k}$ ($\gg M_e$) and $T_g = 206 \text{ K}$.

The low- T_g polymer PEP is well suited to probe the collective dynamics of linear chain polymers over a large temperature interval, as it provides a good compromise between avoiding crystallization and introducing minimal structural complexity. In contrast, structurally simpler polymers like poly(ethylene), poly(ethylene oxide), or poly(dimethylsiloxane) show a strong tendency to crystallize, and thus do not allow the dynamics to be probed from high temperatures down to T_g . In the case of PB, the microstructure strongly influences T_g as well as the polymer-specific dynamics. Hence, any study has to rely on identically prepared polymer samples, which is actually not an easy task.

Poly(ethylene-*alt*-propylene) with a narrow molar mass distribution is synthesized via hydrogenation from standard polyisoprene; the latter is obtained from anionic polymerization.⁹⁶ Concerning the deuterated samples, we had only access to the fully deuterated polymer PEP- d_{10} , which at first glance complicates the situation, as methyl group dynamics as well as chain dynamics are probed by ^2H NMR. However, this is actually not the case, as the methyl and the chain deuterons yield different ^2H relaxation rates which can be resolved when the total relaxation is measured as is done in a FC NMR experiment. In other words, the total ^2H relaxation is biexponential, which was first tested by HF ^2H relaxation (unpublished results). The relaxation dispersion was measured by employing the home-built relaxometer in Darmstadt. However, in comparison to the toluene measurements, we are able to measure to higher relaxation rates R_1 by using a different home-built power supply with a shorter switching time, which covered a frequency range of 30 Hz to 6 MHz (cf. Experimental Section).

In Figure 8, the normalized ^2H relaxation decay plotted as a function of the reduced time $t\langle R_1 \rangle$ is presented for different

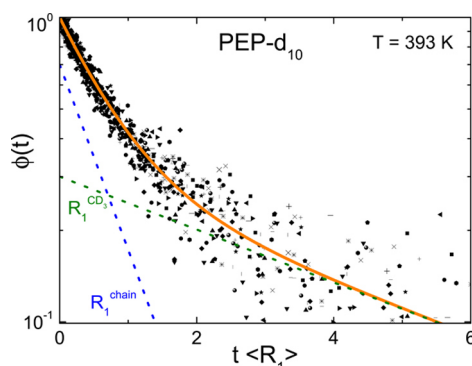


Figure 8. Normalized relaxation decay of PEP- d_{10} as a function of reduced time at $T = 393$ K for all frequencies investigated; $\langle R_1 \rangle$ is the mean relaxation rate derived from the initial slope of the relaxation decay. Decomposition into two exponentials is shown (dotted lines).

frequencies. Here, again, $\langle R_1 \rangle$ is the mean relaxation time taken from the initial slope of the relaxation curve. Comprising the relaxation functions measured at all frequencies, a master curve is found. The scatter for the long-time decay is rather high. Nonetheless, this result indicates that the ratio of these rates as well as the relative weight of the two exponentials are frequency independent—and temperature independent as confirmed by HF measurements (unpublished results). The decay can be fitted to a sum of two exponentials with the relative weights fixed by the ratio 3/10 and 7/10 as given by the numbers of the chemically different deuterons (solid line in Figure 8). The two extracted relaxation rates $R_1^{\text{methyl}}(\nu)$ and $R_1^{\text{chain}}(\nu)$ are shown in Figure 9a. Clearly, pronounced dispersion is identified for both rates, which reflects polymer-specific relaxation. The ratio $R_1^{\text{chain}}/R_1^{\text{methyl}} = 6.5 \pm 0.3$ is found, as said, independent of temperature, yet it is smaller than expected from the ratio of the QCCs. We note that in addition to the fast methyl group reorientation a nonmerging secondary (β -) relaxation process has to be taken into account (unpublished results). For the present discussion, these details are irrelevant.

As revealed by the ^2H FC data (red symbols), two dispersion regimes (I and II, as indicated) can be identified in Figure 9a. Rather similar dispersion is observed for PB which is plotted in Figure 9b, for comparison. In addition, we added our HF NMR results of PEP- d_{10} (unpublished results), which were converted from the temperature axis to the frequency axis by assuming

FTS. As discussed, collective dynamics in polymers (and liquids) usually follows FTS.^{13,14} Showing an even stronger dispersion, the HF relaxation data reflects a third relaxation regime (regime 0), namely, the local dynamics (α -process). Furthermore, we included our results for the intramolecular ^1H relaxation rate of PEP and PB, respectively, obtained from an isotope dilution experiment, and which cover a much larger frequency range (again, a result of applying FTS; unpublished results). In contrast to ^2H , the magnetization recovery is exponential, yielding a single relaxation rate. Regarding the spectral shape, the ^1H (intra) and ^2H data are expected to agree, as was demonstrated above for glycerol. Indeed, the data, appropriately scaled in amplitude (due to different coupling constants), agree so well that the ^1H (intra) data can serve as a guide for the eye interpolating the ^2H dispersion of PEP. Only at lowest frequency some difference appears. Here one has to keep in mind that the nominal “intramolecular” relaxation data are obtained from measuring a sample with 10% protonated PEP in a deuterated matrix and we refrained to extrapolate to zero concentration. Very good agreement is also found for PB; however, HF ^2H relaxation data are missing here. More than nine decades in frequencies are effectively covered and encompassing all the different relaxation regimes of polymer melts, which are discussed in detail next.

In the rate representation (Figure 9), a plateau characteristic of the terminal relaxation is expected at lowest frequencies; this frequency range constitutes the terminal relaxation regime IV in the tube-reptation (TR) model. The plateau value was calculated with the help of the terminal relaxation time, which was determined from shear stress relaxation experiments (unpublished results). For high- M polymers, this regime cannot be covered by ^2H FC NMR but shows up for short chains, as seen for PB in Figure 9b. At higher frequencies, two regimes II and I (with increasing frequency) are well recognized. Presently, it is unclear whether another dispersion regime (reptation in terms of the TR model; III) shows up between regimes II and IV (cf. ref 43). In the frame of the TR model, regime II is attributed to entanglement dynamics, more precisely to the constraint Rouse regime for which a power law $R_1 \propto \nu^{-3/4}$ is predicted; however, a behavior close to $R_1 \propto \nu^{-1/2}$ is actually observed for both PEP and PB, while for the Rouse regime $R_1 \propto \ln(1/\nu)$ is predicted.^{2,15,18,97–99} The latter is difficult to distinguish from a power-law behavior with a rather small exponent, what we could rather attribute. The crossover

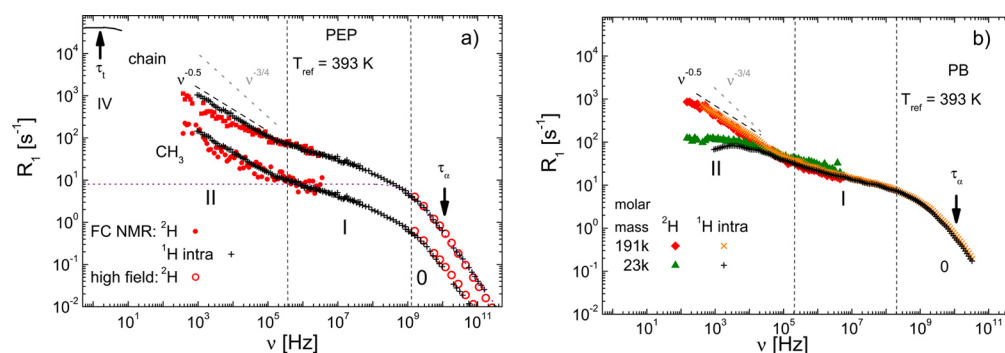


Figure 9. (a) Spin–lattice relaxation rates of PEP (200k) as a function of frequency at 393 K: ^2H FC data (solid symbols) comprising rates for the methyl and the polymer chain; intramolecular ^1H FC data (crosses, shifted; unpublished results), high field data (open symbols); relaxation regimes are indicated; the plateau value at the lowest frequencies (regime IV) is estimated from rheological experiments (unpublished results), dotted line: α -process. (b) Corresponding relaxation rates for polybutadiene (PB) with two molar masses. In both figures, the expectation of the TR model for regime II is indicated as a gray dotted line.

between the two regimes defines the entanglement time τ_e , which is a measure at which time the reorientational fluctuations of the segments “feel” the “tube”,²⁴ and which can thus be extracted easily from FC NMR relaxation spectra. The Rouse regime (I) continues to high frequencies until at highest frequencies the local dynamics with its strong dispersion sets in (regime 0). At even higher frequencies not covered by our experiments, secondary relaxation processes will appear as proven for both PEP and PB by dielectric spectroscopy and HF ^2H NMR (unpublished results and ref 8).

As already demonstrated for toluene and glycerol, instead of the rate representation, the susceptibility representation of data may be of interest for polymers, too—see Figure 10. As

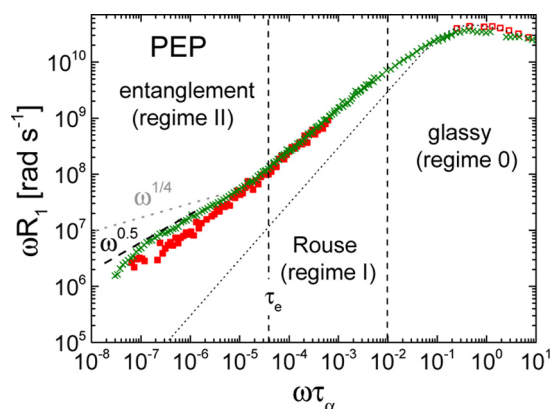


Figure 10. Susceptibility master curve of the chain dynamics of PEP- d_{10} obtained from ^2H FC NMR (filled squares) as well as intramolecular ^1H FC NMR data (crosses, scaled in amplitude); in addition, we added high-field data (open squares; unpublished results); dashed line: Cole–Davidson function representing the glassy relaxation. Gray dotted line: expectation of the TR model for regime II.

discussed, this representation is the starting point for constructing master curves by exploiting FTS. The dispersion profiles measured at different temperatures are solely shifted along the frequency axis to achieve best overlap. In Figure 10, the relaxation peak reflects the α -process, while at lower frequencies ($\omega \tau_\alpha \ll 1$) the polymer-specific contributions starting with the Rouse contribution (regime I) and followed at lower frequencies by another power law reflecting constraint reptation (regime II) is recognized. The dotted line represents a CD function interpolating solely the α -process as it appears in simple liquids. As mentioned before, in the case of the high- M PEP, the terminal relaxation leading to $\chi''(\omega) \propto \omega^1$ is only expected at even lower frequencies not covered by ^2H NMR, yet it shows up for shorter polymer chains. In the susceptibility representation, it is directly seen that ^2H FC NMR data does not cover the relaxation regime 0 (“local” or “glassy” dynamics), which leads to the relaxation maximum at high frequencies. Upon cooling, the value of T_1 quickly becomes too short to be resolved in a ^2H FC NMR experiment, a boundary which limits the analysis in the case of simple liquids as demonstrated above.

Finally, we show in Figure 11, the reorientational correlation function $C_2(t/\tau_\alpha)$ of PEP as well as of PB as obtained from Fourier transformation of the spectral density in Figure 9. The ^1H FC (intra) data were taken for interpolating the ^2H data. We added the corresponding function for toluene- d_5 and glycerol- d_5 (from Figures 5 and 7). This representation of the relaxation data, covering six decades in amplitude and nine

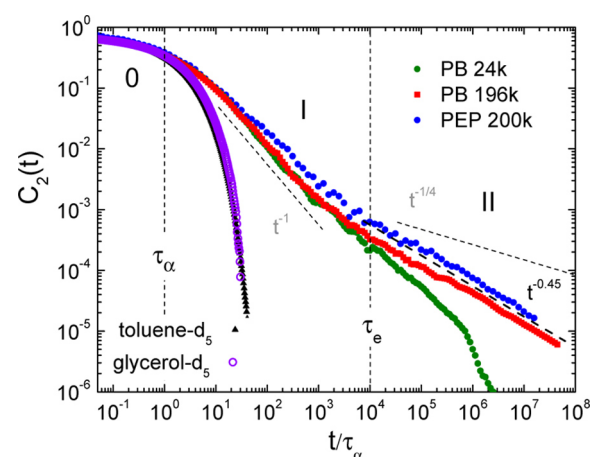


Figure 11. Segmental reorientational correlation function $C_2(t)$ of PEP and PB vs reduced time t/τ_2 as obtained from Fourier transforming relaxation master curves in Figure 9; relaxation regimes are indicated; numbers give the molar mass of polymers; gray dotted lines: prediction of the tube-reptation model;^{15,19,100,101} for comparison, the decay for two simple liquids toluene and glycerol is given.

decades in time, is actually most convenient to illustrate the different relaxation regimes of a high- M polymer melt. Comparing polymer and simple liquid, a strong retardation of $C_2(t/\tau_\alpha)$ is obvious for the polymers. Moreover, the decays for PEP and PB are virtually indistinguishable, which emphasizes the conclusion that generic, polymer-specific relaxation is observed. While for the simple liquids $C_2(t/\tau_\alpha)$ can be interpolated by a Kohlrausch function (the time domain equivalent to the CD function), in the case of the polymers, at least two power-law decays are observed for the high- M samples, in addition to the short-time behavior attributed to glassy dynamics. In regime I, a power-law decay is recognized which closely follows the Rouse prediction, $C_2(t) \propto t^{-1}$. At the longest time, in regime II, a power-law behavior, $C_2(t) \propto t^{-0.45 \pm 0.05}$, is found which does not conform to the TR prediction for the constraint Rouse regime for which one expects a power-law exponent $\alpha = 0.25$. Possibly, the strong rotational–translational coupling assumed in the TR model in terms of the so-called return-to-origin hypothesis^{15,100,101} does not apply in real polymers. Here, atomistic simulations will deliver further insight provided that they reach the entanglement regime which is still difficult with the current computer power.¹⁰² In the case of PB, we added also our results for shorter chains, yet still entangled ($M > M_e$). Here the terminal relaxation appears within the frequency window of ^2H FC NMR featuring an essentially exponential cutoff of the power-law regime II. We note that entanglement dynamics sets in below $C_2(t_e) = S^2 \cong 0.001$, where τ_e is the entanglement time and S the corresponding order parameter, which is on the order of a few percent and thus very small.

CONCLUSION

As shown by the novel examples of ^2H FC NMR relaxometry studying molecular motions in glass forming liquids and polymers, the technique constitutes another dynamic susceptibility method thereby complementing traditional ones such as dielectric spectroscopy, dynamic light scattering, quasi-elastic neutron scattering, and rheology, for example. In the case of dielectric spectroscopy with its broad frequency window, however, only in favorable cases, i.e., for so-called type A

polymers,¹⁰³ the polymer-specific dynamics is accessible in the form of a normal mode relaxation.

Thus, the whole toolbox of susceptibility analyses (e.g., FTS allowing for the construction of master curves) can fruitfully be applied to FC relaxometry irrespective of which nuclear spin species is used. At the same time, one profits from the selectivity of NMR which in many cases allows data to be interpreted in a much more specific way compared to other methods. As this and some of our previous papers demonstrated,^{17–22} there may be a lot of important physics hidden in the FC dynamic range, i.e., at frequencies below the range of typical high field NMR spectrometers. The simplest case (e.g., toluene), when ²H FC relaxometry yields dispersionless rates, gives the nontrivial information that there is no slow process. Another case discussed in this paper dealt with glycerol and the time scale separation of molecular rotation and translation, which is revealed when ²H and ¹H relaxation dispersion is compared. We recall that in ¹H FC NMR translational dynamics leads to a characteristic low-field behavior of the rates.^{29–33} In even other cases, e.g., in network forming monoalcohols,^{104,105} there are dynamics reflecting the reorganization of the hydrogen bonding network, which exhibits characteristic dynamics slower than the structural relaxation. Thus, FC relaxometry should be ideally applicable to address this problem; characteristic low field dispersion is anticipated. A prominent case, discussed in some detail in this paper, is long chain polymer motion. FC relaxometry has been able, partly in concert with other methods, to test grand theories of polymer dynamics.^{19,22,23,25,42} Not too much prophecy is required that more physical cases of slow molecular dynamics, e.g., hydrogen exchange processes¹ or the dynamics of supramolecular structures, wait for being detected by ²H FC NMR.

As the title tells, this paper is meant to draw the attention of the reader to the perspectives of ²H FC NMR relaxometry for studying molecular motions in soft matter. The central question is, why should one use deuterons? By dealing with selected experimental examples, our paper really has proposed some answers, which here we will try to recall in order to finally formulate a couple of summarizing take-home messages. A critical comparison of ¹H and ²H FC relaxometry with respect to certain key properties may be instructive. The first two properties to be mentioned render ²H FC relaxometry a very attractive method:

Reorientations measured exclusively: The dominant relaxation mechanism is the fluctuation of quadrupolar interaction, i.e., in the case of organic systems with covalent CD bonds: molecular reorientations only. Translational motions, which in the case of ¹H NMR contribute at low frequencies, do not contribute. In consequence, theoretical understanding as well as computer simulation is less demanding.

No cross relaxation effects: Deuteron quadrupolar interactions are much stronger than dipole–dipole interactions. This implies that cross relaxation effects, that in the case of ¹H NMR always tend to couple all system protons to each other, do not interfere. Thus, each subgroup of deuterons represents its own thermodynamic system and relaxes independently, and specific isotope labeling allows highly selective studies.

Of course, ²H FC also encounters limitations:

Sensitivity problems: Due to the ²H Larmor frequency being about a factor of 6 below that of the ¹H one is more seriously confronted with a poor signal-to-noise ratio. This stresses the point that high detection fields are essential for a broader

application of the method. Currently, the most advanced home-built relaxometers may reach a detection field of about 12 MHz.

Short relaxation times: Due to the relatively strong (as compared to dipole–dipole interactions among protons) quadrupole interaction, the relaxation times are correspondingly short. This may lead to a limitation for low fields, especially in FC where field switching times are notoriously long anyway. Thus, even if evolution fields down to 10^{−6} T⁶ (corresponding to ²H frequencies of less than 10 Hz) may have become feasible, they cannot always be made use of.

Phase sensitive pulses: Even if in this paper we have not encountered a situation where we would have desired to apply phase sensitive high-frequency pulses and detection, we would like to use the occasion to stress that meeting the slow motion regime (nonaveraged static quadrupole interaction) one will have to measure solid-echo amplitudes. This will then require a highly stable detection field. At present, we have achieved a ²H frequency drift in the detection field of about 500 Hz. This gradually starts to be sufficient for the first applications, and is a work in progress.

Concluding the conclusions: In view of the great potential of applying ²H FC NMR relaxometry, especially at low fields, one should continue to invest in further instrumental improvements, i.e., among others, improving signal-to-noise ratio, increasing and stabilizing detection fields, and shortening field switching times.

■ APPENDIX

Here we discuss the ratio $r(T) = R_1^{d_5}(\nu)/R_1^{d_3}(\nu)$ in the case of toluene which allows one to estimate the extent of anisotropic reorientation. Given that the methyl group reorientation is fast with respect to the overall tumbling of the molecule,⁷⁷ a naïve picture would assume isotropic rotation, which would yield a ratio $R_1^{d_5}(\nu)/R_1^{d_3}(\nu) = r = 12.0$ (cf. above and eq 8). Figure 12

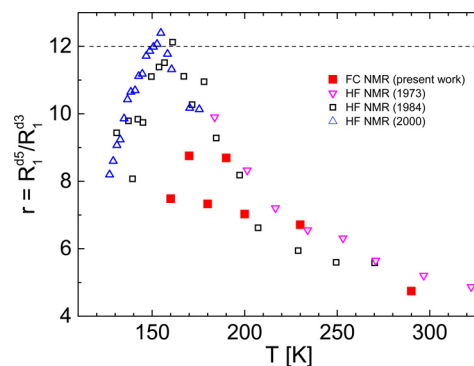


Figure 12. Ratio $r = R_1^{d_5}/R_1^{d_3}$ for toluene plotted versus temperature; conventional high-field (HF) data were taken from the literature: 1973,⁷⁷ 1984,⁵⁹ 2000;⁷⁰ dashed line: isotropic reorientation.

presents the experimentally observed value $r(T)$ taken from the present FC as well as from different HF NMR relaxation data (cf. Figure 2). The expected value (dashed line) is only reached around 160 K; below 160 K as well as above, the ratio drops. As the toluene-*d*₅ and toluene-*d*₃ relaxation rates are usually measured at different temperatures, some interpolation is necessary and may explain the scatter of the ratio. In addition, since the temperature coefficient of the relaxation rates is high at low temperatures, small differences in the absolute temperature may enhance the scatter. We also stress that the

comparison is now done on a linear scale, while in Figures 2 and 4 a logarithmic scale was chosen.

The strong temperature dependence of the ratio r above 160 K is explained by assuming that the reorientation of toluene becomes significantly anisotropic, an indication of which was already reported in the literature,^{75,82–84} where the Woessner model of anisotropic diffusion⁸⁵ was applied. The decrease observed below 160 K is probably due to the emergence of the β -process. While the extension of the Woessner approach to viscous liquids with their nonexponential reorientational correlation functions is not straightforward, the situation under extreme narrowing conditions is more favorable—and it holds for the present analysis of the toluene data at $T > 160$ K.

The toluene molecule is an asymmetric top molecule described by three rotational diffusion coefficients, yet as our experiments cannot discriminate between the rotation around the two axes perpendicular to the C_2 axis, we approximate the molecular reorientation by assuming a symmetric top molecule with only two diffusion constants, D_{\parallel} and D_{\perp} , and an anisotropy parameter given by $\delta = D_{\parallel}/D_{\perp}$. The quantity D_{\parallel} represents the rotation around and D_{\perp} the reorientation perpendicular to the pseudo C_2 axis. Then, given that the methyl group rotation is very fast,⁷⁷ and assuming extreme narrowing conditions, the spectral density of toluene- d_3 —as well as that of the para (p) deuteron in toluene- d_5 —reflects solely $\tau_{\perp} = 1/6D_{\perp}$; one gets

$$J_{d_3} = J_p = \tau_{\perp} \quad (4)$$

For the deuterons in ortho (o) and meta (m) position in toluene- d_5 , it follows⁸⁵

$$J_{o,m} = A(\cos \vartheta)(6D_{\perp})^{-1} + B(\cos \vartheta)(D_{\parallel} + 5D_{\perp})^{-1} + C(\cos \vartheta)(4D_{\parallel} + 2D_{\perp})^{-1} \quad (5)$$

where the coefficients A , B , and C depend on the cosine of the angle ϑ between the C–D bond and the C_2 axis, which is 60° in the case of toluene. These deuterons are sensitive to both D_{\parallel} and D_{\perp} , while the para (p) deuteron—like the methyl group deuterons—reflects only D_{\perp} . As the spin–lattice relaxation rates of o , m , and p deuterons are not expected to be largely different, we assume that the essentially exponential relaxation of toluene- d_5 is described by an average rate and a uniform coupling for each relaxation for o and m , and p , respectively. Thus, we can write

$$J_{d_5} = 0.8J_{o,m} + 0.2J_p \quad (6)$$

With eq 5, this leads to

$$J_{d_5} = 0.8\tau_{\perp} \left[\frac{1}{64} + \frac{81}{64(2\delta + 1)} + \frac{27}{8(\delta + 5)} \right] + 0.2 \cdot \tau_{\perp} \quad (7)$$

Here, the anisotropy parameter δ appears. It can be extracted from the ratio r of the relaxation rates.

$$r(\delta) \equiv \frac{R_1^{d_5}}{R_1^{d_3}} = \frac{J_{d_5} \text{QCC}_{d_5}^2}{J_{d_3} \text{QCC}_{d_3}^2} = \frac{\text{QCC}_{d_5}^2 \cdot (17\delta^2 + 350\delta + 353)}{\text{QCC}_{d_3}^2 \cdot (80\delta^2 + 440\delta + 200)} \quad (8)$$

Figure 13 presents $r(\delta)$. As the dependence of r on δ becomes very flat for low r values, the uncertainty of δ becomes quickly large at high temperatures.

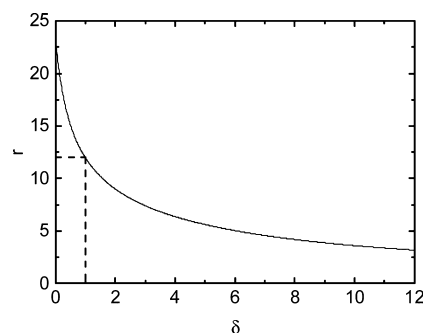


Figure 13. Ratio of the relaxation rates $r = R_1^{d_5}/R_1^{d_3}$ of toluene as a function of δ (cf. eq 8). The isotropic case $r = 1$ is indicated (dashed lines).

Figure 14 displays the anisotropy ratio δ as a function of temperature. While at low temperatures the toluene molecule

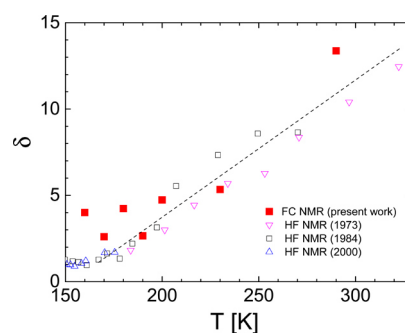


Figure 14. Anisotropy parameter δ versus temperature as given by ^2H FC NMR as well as by HF NMR from the literature: 1973,⁷⁷ 1984,⁵⁹ 2000.⁷⁰ Dashed line: guide for the eye.

essentially reorients isotropically, in the high temperature range, anisotropic reorientation is observed, the extent of which grows upon heating. In the literature, δ values between 2 and 3 were reported for ambient temperature;^{75,82,83} the present study reveals values around 10 at room temperature. A completely different scenario was reported in ref 84 and thus can be questioned. As said, concerning the δ value, the error bars become quickly large when low r values are involved (cf. Figure 12). Importantly, the anisotropy disappears when the glass transition sets in. Hence, the suppression of anisotropic reorientation may be taken as a signature of glassy dynamics becoming strongly cooperative at low temperatures approaching T_g , a phenomenon already suggested a while ago.¹⁰⁶

AUTHOR INFORMATION

Corresponding Author

*E-mail: ernst.roessler@uni-bayreuth.de. Phone: +49 921 553 164.

Notes

The authors declare no competing financial interest.

ACKNOWLEDGMENTS

The authors appreciate financial support through the Deutsche Forschungsgemeinschaft (DFG) through grant RO 907/17 and RO 907/18. Thanks are also given to D. Richter (Jülich) for providing the deuterated PEP and N. Fatkullin (Kazan) for fruitful discussions.

REFERENCES

- (1) Noack, F. NMR Field-Cycling Spectroscopy: Principles and Applications. *Prog. Nucl. Magn. Reson. Spectrosc.* **1986**, *18*, 171–276.
- (2) Kimmich, R.; Anzardo, E. Field-Cycling NMR Relaxometry. *Prog. Nucl. Magn. Reson. Spectrosc.* **2004**, *44*, 257–320.
- (3) Kruk, D.; Herrmann, A.; Rössler, E. A. Field-Cycling NMR Relaxometry of Viscous Liquids and Polymers. *Prog. Nucl. Magn. Reson. Spectrosc.* **2012**, *63*, 33–64.
- (4) Meier, R.; Kruk, D.; Rössler, E. A. Intermolecular Spin Relaxation and Translation Diffusion in Liquids and Polymer Melts: Insight from Field-Cycling ^1H NMR Relaxometry. *ChemPhysChem* **2013**, *14*, 3071–3081.
- (5) Fujara, F.; Kruk, D.; Privalov, A. F. Solid state Field-Cycling NMR relaxometry: Instrumental improvements and new applications. *Prog. Nucl. Magn. Reson. Spectrosc.* **2014**, *82*, 39–69.
- (6) Kresse, B.; Privalov, A. F.; Fujara, F. NMR Field-Cycling at Ultralow Magnetic Fields. *Solid State Nucl. Magn. Reson.* **2011**, *40*, 134–137.
- (7) Kresse, B.; Privalov, A. F.; Herrmann, A.; Hofmann, M.; Rössler, E. A.; Fujara, F. Simultaneous measurement of very small magnetic fields and spin-lattice relaxation. *Solid State Nucl. Magn. Reson.* **2014**, *59–60*, 45–47.
- (8) Götz, W. J. Recent tests of the mode-coupling theory for glassy dynamics. *J. Phys.: Condens. Matter* **1999**, *11*, A1.
- (9) Kudlik, A.; Benkhof, S.; Tschirwitz, T.; Blochowicz, T.; Rössler, E. The dielectric response of simple organic glass formers. *J. Mol. Struct.* **1999**, *479*, 201–218.
- (10) Lunkenheimer, P.; Schneider, U.; Brand, R.; Loidl, A. Glassy dynamics. *Contemp. Phys.* **2000**, *41*, 15–36.
- (11) Wolynes, P. G.; Lubchenko, V. *Structural Glasses and Supercooled Liquids*; Wiley: Oxford, 2012.
- (12) Petzold, N.; Schmidtke, B.; Kahlau, R.; Bock, D.; Meier, R.; Micko, B.; Kruk, D.; Rössler, E. A. Evolution of the Dynamic Susceptibility in Molecular Glass Formers: Results from Light Scattering, Dielectric Spectroscopy, and NMR. *J. Chem. Phys.* **2013**, *138*, 12A510.
- (13) Rubinstein, M.; Colby, R. H. *Polymer Physics*; Oxford University: New York, 2003.
- (14) Graessley, W. W. *Polymeric Liquids & Networks: Dynamics and Rheology*; Taylor and Francis: New York, 2008.
- (15) Kimmich, R.; Fatkullin, N. Polymer Chain Dynamics and NMR. *Adv. Polym. Sci.* **2004**, *170*, 1–113.
- (16) Kariyo, S.; Stapf, S. Restricted Molecular Dynamics of Polymer Chains γ means of NMR Field Cycling Relaxometry. *Macromol. Chem. Phys.* **2005**, *206*, 1300–1310.
- (17) Kariyo, S.; Gainaru, C.; Schick, H.; Brodin, A.; Rössler, E. A. From a Simple Liquid to a Polymer Melt: NMR Relaxometry Study of Polybutadiene. *Phys. Rev. Lett.* **2006**, *97*, 207803. Erratum: Kariyo, S.; Herrmann, A.; Gainaru, C.; Schick, H.; Brodin, A.; Rössler, E. A. *Phys. Rev. Lett.* **2008**, *100*, 109901.
- (18) Kariyo, S.; Brodin, A.; Gainaru, C.; Herrmann, A.; Schick, H.; Novikov, V. N.; Rössler, E. A. From Simple Liquid to Polymer Melt. Glassy and Polymer Dynamics studied by Fast Field Cycling NMR Relaxometry: low and high Molecular Weight Limit. *Macromolecules* **2008**, *41*, 5313–5321.
- (19) Herrmann, A.; Kariyo, S.; Abou Elfadl, A.; Meier, R.; Gmeiner, J.; Novikov, V.; Rössler, E. A. Universal Polymer Dynamics Revealed by Field Cycling ^1H NMR. *Macromolecules* **2009**, *42*, 5236–5243.
- (20) Herrmann, A.; Kresse, B.; Gmeiner, J.; Privalov, A. F.; Kruk, D.; Fujara, F.; Rössler, E. A. Protracted Crossover to Reptation Dynamics: A Field Cycling ^1H NMR Study Including Extremely Low Frequencies. *Macromolecules* **2012**, *45*, 1408–1416.
- (21) Hofmann, M.; A.; Herrmann, A.; Abou Elfadl, A.; Kruk, D.; Wohlfahrt, M.; Rössler, E. A. Glassy, Rouse, and entanglement dynamics as revealed by field cycling ^1H NMR relaxometry. *Macromolecules* **2012**, *45*, 2390–2401.
- (22) Hofmann, M.; Kresse, B.; Privalov, A.; B.; Willner, L.; Fatkullin, N.; Fujara, F.; Rössler, E. A. Field-Cycling NMR Relaxometry Probing the Microscopic Dynamics in Polymer Melts. *Macromolecules* **2014**, *47*, 7917–7929.
- (23) Fatkullin, N.; Stapf, S.; Hofmann, M.; Meier, R.; Rössler, E. A. Proton Spin Dynamics in Polymer Melts: New Perspectives for Experimental Investigations of Polymer Dynamics. *J. Non-Cryst. Solids* **2015**, *407*, 309–317.
- (24) Doi, M.; Edwards, S. F. *The Theory of Polymer Dynamics*; Oxford Sci. Publication: Hoboken, New Jersey, 1986.
- (25) Hofmann, M.; Gainaru, C.; Cetinkaya, B.; Valiullin, R.; Fatkullin, N.; Rössler, E. A. Field-Cycling Relaxometry as a Molecular Rheology Technique: Common Analysis of NMR, Shear Modulus and Dielectric Loss Data of Polymers vs Dendrimers. *Macromolecules* **2015**, *48*, 7521–7534.
- (26) Abragam, A. *The Principles of Nuclear Magnetism*; Clarendon Press: Oxford, U.K., 1961.
- (27) Torrey, H. C. Nuclear Spin Relaxation by Translational Diffusion. *Phys. Rev.* **1953**, *92*, 962.
- (28) Harmon, J. F.; Muller, B. H. Nuclear Spin Relaxation by Translational Diffusion in Liquid Ethane. *Phys. Rev.* **1969**, *182*, 400.
- (29) Sholl, C. A. Nuclear Spin Relaxation by Translational Diffusion in Liquids and Solids: High-and Low-Frequency Limits. *J. Phys. C: Solid State Phys.* **1981**, *14*, 447.
- (30) Meier, R.; Kruk, D.; Gmeiner, J.; Rössler, E. A. Intermolecular relaxation in glycerol as revealed by field cycling ^1H NMR relaxometry dilution experiments. *J. Chem. Phys.* **2012**, *136*, 034508.
- (31) Kruk, D.; Meier, R.; Rössler, E. A. Nuclear Magnetic Resonance Relaxometry as a Method of Measuring Translational Diffusion Coefficients in Liquids. *Phys. Rev. E* **2012**, *85*, 020201.
- (32) Meier, R.; Kruk, D.; Bourdick, A.; Schneider, E.; Rössler, E. A. Inter- and Intramolecular Relaxation in Molecular Liquids by Field Cycling ^1H NMR Relaxometry. *Appl. Magn. Reson.* **2013**, *44*, 153–168.
- (33) Meier, R.; Herrmann, A.; Hofmann, M.; Schmidtke, B.; Kresse, B.; Privalov, A. F.; Kruk, D.; Fujara, F.; Rössler, E. A. Iso-Frictional Mass Dependence of Diffusion of Polymer Melts Revealed by ^1H NMR Relaxometry. *Macromolecules* **2013**, *46*, 5538–5548.
- (34) Kruk, D.; Meier, R.; Rössler, E. A. Determining Diffusion Coefficients of Ionic Liquids by Means of Field Cycling Nuclear Magnetic Resonance Relaxometry. *J. Chem. Phys.* **2014**, *140*, 244509.
- (35) Meier, R.; Schneider, E.; Rössler, E. A. Change of Translational-Rotational Coupling in Liquids Revealed by Field-Cycling ^1H NMR. *J. Chem. Phys.* **2015**, *142*, 034503.
- (36) Ordikhani Seyedlar, A.; Stapf, S.; Mattea, C. Dynamics of the Ionic Liquid 1-Butyl-3-Methylimidazolium Bis (Trifluoromethylsulfonyl) Imide Studied by Nuclear Magnetic Resonance Dispersion and Diffusion. *Phys. Chem. Chem. Phys.* **2015**, *17*, 1653–1659.
- (37) Odelius, M.; Laaksonen, A.; Levitt, M. H.; Kowalewski, J. Intermolecular dipole-dipole relaxation. A molecular dynamics simulation. *J. Magn. Reson., Ser. A* **1993**, *105*, 289–294.
- (38) Henritzi, P.; Bormuth, A.; Vogel, M. Interpretation of 1 and 2 H Spin–Lattice Relaxation Dispersions: Insights from Molecular Dynamics Simulations of Polymer Melts. *Solid State Nucl. Magn. Reson.* **2013**, *54*, 32–40.
- (39) Ayant, Y.; Belorizky, E.; Fries, P.; Rosset, J. Effet des Interactions Dipolaires Magnétiques Intermoléculaires sur la Relaxation Nucléaire de Molécules Polyatomiques dans les Liquides. *J. Phys. (Paris)* **1977**, *38*, 325–337.
- (40) Kehr, M.; Fatkullin, N.; Kimmich, R. Molecular Diffusion on a Time Scale between Nano- and Milliseconds Probed by Field-Cycling NMR Relaxometry of Intermolecular Dipolar Interactions: Application to Polymer Melts. *J. Chem. Phys.* **2007**, *126*, 094903.
- (41) Kehr, M.; Fatkullin, N.; Kimmich, R. Deuteron and Proton Spin-Lattice Relaxation Dispersion of Polymer Melts: Intrasegment, Intrachain, and Interchain Contributions. *J. Chem. Phys.* **2007**, *127*, 084911.
- (42) Herrmann, A.; Kresse, B.; Wohlfahrt, M.; Bauer, I.; Privalov, A. F.; Kruk, D.; Fatkullin, N.; Fujara, F.; Rössler, E. A. Mean Square Displacement and Reorientational Correlation Function in Entangled

Polymer Melts Revealed by Field Cycling 1H and 2H NMR Relaxometry. *Macromolecules* **2012**, *45*, 6516–6526.

(43) Kresse, B.; Hofmann, M.; Privalov, A. F.; Fujara, F.; Fatkullin, N.; Rössler, E. A. All Polymer Diffusion Regimes Covered by Combining Field-Cycling and Field-Gradient 1H NMR. *Macromolecules* **2015**, *48*, 4491–4502.

(44) Fischer, E.; Kimmich, R.; Fatkullin, N. NMR field gradient diffusometry of segment displacements in melts of entangled polymers. *J. Chem. Phys.* **1996**, *104*, 9174–9178.

(45) Fischer, E.; Kimmich, R.; Fatkullin, N. Spin Diffusion in Melts of Entangled Polymers. *J. Chem. Phys.* **1997**, *106*, 9883–9888.

(46) Pahl, S.; Fleischer, G.; Fujara, F.; Geil, B. Anomalous Segment Diffusion in Polydimethylsiloxane Melts. *Macromolecules* **1997**, *30*, 1414–1418.

(47) Komlos, M. E.; Callaghan, P. T. Segmental motion of entangled random coil polymers studied by pulsed gradient spin echo nuclear magnetic resonance. *J. Chem. Phys.* **1998**, *109*, 10053–10067.

(48) Solomon, I. Relaxation Processes in a System of two Spins. *Phys. Rev.* **1955**, *99*, 559.

(49) Kowalewski, J.; Maler, L. *Nuclear Spin Relaxation in Liquids: Theory, Experiments, and Applications*; CRC Press: Boca Raton, FL, 2006.

(50) Spiess, H. W. Molecular Dynamics of Solid Polymers as Revealed by Deuteron NMR. *Colloid Polym. Sci.* **1983**, *261*, 193–209.

(51) Hoatson, G. L.; Vold, R. L. 2H-NMR Spectroscopy of Solids and Liquid Crystals. In *Solid-State NMR III Organic Matter*; Blümich, B., Ed.; Springer: Berlin, 1994; pp 1–67.

(52) Schmidt-Rohr, K.; Spiess, H. W. *Multidimensional Solid-State NMR and Polymers*; Academic Press: Mainz, Germany, 1994.

(53) Böhmer, R.; Diezemann, G.; Hinze, G.; Rössler, E. A. Dynamics of Supercooled Liquids and Glassy Solids. *Prog. Nucl. Magn. Reson. Spectrosc.* **2001**, *39*, 191–267.

(54) Kimmich, R.; Fatkullin, N.; Seitter, R. O.; Gille, K. Chain Dynamics in Entangled Polymers: Power Laws of the Proton and Deuteron Spin-Lattice Relaxation Dispersions. *J. Chem. Phys.* **1998**, *108* (5), 2173–2177.

(55) Kariyo, S.; Stapf, S.; Blümich, B. Site specific Proton and Deuteron NMR Relaxation Dispersion in Selectively Deuterated Polyisoprene Melts. *Macromol. Chem. Phys.* **2005**, *206*, 1292–1299.

(56) Kimmich, R. *Principles of Soft-Matter Dynamics*; Springer Science & Business Media: Heidelberg, Germany, 2012.

(57) Böttcher, C. J. F.; Bordewijk, P. *Theory of Electric Polarization*; Elsevier Scientific Polarization: Amsterdam, The Netherlands, 1978.

(58) Cohen-Addad, J. P.; Messa, J. P. Concentration Frequency Dependence of Short Range Chain Fluctuations Observed in Concentrated Polymer Solutions from Nuclear Magnetic Resonance Rates. *J. Phys., Lett.* **1976**, *37*, 193.

(59) Rössler, E.; Sillescu, H. 2 H NMR Study of Supercooled Toluene. *Chem. Phys. Lett.* **1984**, *112*, 94–98.

(60) Dries, T.; Fujara, F.; Kiebel, M.; Rössler, E.; Sillescu, H. 2H-NMR Study of the Glass Transition in Supercooled ortho-Terphenyl. *J. Chem. Phys.* **1988**, *88*, 2139–2147; *J. Chem. Phys.* **1989**, *90*, 7613.

(61) Schnauss, W.; Fujara, F.; Sillescu, H. The Molecular Dynamics around the Glass Transition and in the Glassy State of Molecular Organic Systems: A 2H– Nuclear Magnetic Resonance Study. *J. Chem. Phys.* **1992**, *97*, 1378–1389.

(62) Rössler, E. A.; Eiermann, P. Reorientational Dynamics in Supercooled m-Tricresyl Phosphate: Its Relation to Main and Secondary Relaxation—31P Nuclear Magnetic Resonance Study of Relaxation, Line Shape, and Stimulated Echo. *J. Chem. Phys.* **1994**, *100* (7), 5237–5248.

(63) Lips, O.; Privalov, A. F.; Dvinskikh, S. V.; Fujara, F. Magnet Design with high B 0 Homogeneity for Fast-Field-Cycling NMR Applications. *J. Magn. Reson.* **2001**, *149*, 22–28.

(64) Drake, P. W.; Meister, R. Rotational Spin–Lattice and Spin–Spin Quadrupole Relaxation in Perdeuterated Glycerol. *J. Chem. Phys.* **1971**, *54*, 3046–3050.

(65) Wolfe, M.; Jonas, J. Reorientational Motions in Compressed Viscous Fluids: Selectively Deuterated Glycerol. *J. Chem. Phys.* **1979**, *71*, 3252–3262.

(66) Diehl, R.; Fujara, F.; Sillescu, H. 2H-NMR-Stimulated Echo Study of Ultraslow Reorientational Motion in Viscous Glycerol near its Glass Transition Temperature. *Europhys. Lett.* **1990**, *13*, 257–262.

(67) Friedrich, A.; Dölle, A.; Zeidler, M. D. Reorientational Dynamics of Glycerol Derived from Temperature-Dependent Multi-Nuclear Magnetic Resonance Relaxation Data. *Magn. Reson. Chem.* **2003**, *41*, 813–818.

(68) Qi, F.; Böhmer, R.; Sillescu, H. The Methyl Group as a built-in Probe of the Glassy Dynamics in Propylene Carbonate. *Phys. Chem. Chem. Phys.* **2001**, *3* (18), 4022–4028.

(69) Döb, A.; Hinze, G.; Böhmer, R.; Sillescu, H.; Kolshorn, H.; Vogel, M.; Zimmermann, H. Deuteron and Carbon Magnetic Resonance Studies of Supercooled Liquid and Glassy Salol. *J. Chem. Phys.* **2000**, *112*, 5884–5892.

(70) Qi, F.; Hinze, G.; Böhmer, R.; Sillescu, H.; Zimmermann, H. Slow and Fast Methyl Group Rotations in Fragile Glass-Formers Studied by NMR. *Chem. Phys. Lett.* **2000**, *328*, 257–262.

(71) Jörg, T.; Böhmer, R.; Sillescu, H.; Zimmermann, H. Isotope Effects on the Dynamics of a Supercooled van der Waals Liquid. *Europhys. Lett.* **2000**, *49* (6), 748.

(72) Woessner, D. E.; Snowden, B. S., Jr. Magnetic Relaxation under Hindered Rotation in Fluids. *Adv. Mol. Relax. Processes* **1972**, *3*, 181–197.

(73) Parker, R. G.; Jonas, J. Spin-Lattice Relaxation in Several Molecules Containing Methyl Groups. *J. Magn. Reson.* **1972**, *6*, 106–116.

(74) Wilbur, D. J.; Jonas, J. Fourier Transform NMR in Liquids at High Pressure. III. Spin–Lattice Relaxation in Toluene-d8. *J. Chem. Phys.* **1975**, *62*, 2800–2807.

(75) Hinze, G.; Sillescu, H. 2H Nuclear Magnetic Resonance Study of Supercooled Toluene: Slow and Fast Processes above and below the Glass Transition. *J. Chem. Phys.* **1996**, *104*, 314–319.

(76) Hinze, G.; Sillescu, H.; Fujara, F. Anisotropic Motion of Toluene above and below the Glass Transition Studied by 2 H NMR. *Chem. Phys. Lett.* **1995**, *232*, 154–158.

(77) Spiess, H. W.; Schweitzer, D.; Haeberlen, U. Molecular Motion in Liquid Toluene from a Study of 13 C and 2 D Relaxation Times. *J. Magn. Reson.* **1973**, *9*, 444–460.

(78) NaNagara, B.; O'Connor, R. D.; Blum, D. Mobility of Toluene in Polystyrene-Toluene Solutions: A NMR Study. *J. Phys. Chem.* **1992**, *96*, 6417–6423.

(79) Barnes, R. G. Deuteron Quadrupole Coupling Tensors in Solids. *Advances in Nuclear Quadrupole Resonance* **1972**, *1*, 335–355.

(80) Schmidtke, B.; Petzold, N.; Kahlau, R.; Rössler, E. A. Reorientational Dynamics in Molecular Liquids as Revealed by Dynamic Light Scattering: from Boiling Point to Glass Transition Temperature. *J. Chem. Phys.* **2013**, *139*, 084504.

(81) Ngai, K. L.; Paluch, M. Classification of Secondary Relaxation in Glass-Formers based on Dynamic Properties. *J. Chem. Phys.* **2004**, *120*, 857–873.

(82) Sturz, L.; Dölle, A. Anisotropic Reorientational Dynamics of Toluene in Neat Liquid. A 13C Nuclear Magnetic Relaxation Study. *J. Phys. Chem. A* **2001**, *105*, 5055–5060.

(83) Lambert, J. B.; Nienhuis, R. J.; Finzel, R. B. The Influence of Anisotropic Motion on the Barrier to Methyl Rotation in p-Toluenes. *J. Phys. Chem.* **1981**, *85*, 1170–1172.

(84) Bauer, D. R.; Alms, G. R.; Brauman, J. I.; Pecora, R. Depolarized Rayleigh Scattering and 13C NMR Studies of Anisotropic Molecular Reorientation of Aromatic Compounds in Solution. *J. Chem. Phys.* **1974**, *61*, 2255–2261.

(85) Woessner, D. E. Nuclear Spin Relaxation in Ellipsoids undergoing Rotational Brownian Motion. *J. Chem. Phys.* **1962**, *37*, 647–654.

(86) Blochowicz, Th.; Tschirwitz, Ch.; Benkhof, St.; Rössler, E. A. Susceptibility Functions for Slow Relaxation Processes in Supercooled

Liquids and the Search for Universal Relaxation Patterns. *J. Chem. Phys.* **2003**, *118*, 7544–7555.

(87) Rössler, E. A.; Sillescu, H.; Spiess, H. W. Deuteron NMR in relation to the glass transition in polymers. *Polymer* **1985**, *26*, 203–207.

(88) Litvinov, V. M.; Spiess, H. W. 2H NMR Study of Molecular Motions in Polydimethylsiloxane and its Mixtures with Aerosils. *Makromol. Chem.* **1991**, *192*, 3005–3019.

(89) Pschorn, U.; Rössler, E.; Sillescu, H.; Kaufmann, S.; Schaefer, D.; Spiess, H. W. Local and Cooperative Motions at the Glass Transition of Polystyrene: Information from one- and two-dimensional NMR as Compared with other Techniques. *Macromolecules* **1991**, *24*, 398–402.

(90) Rössler, E. A.; Sokolov, A. P.; Eiermann, P.; Warschewske, U. Dynamical Phase Transition in Simple Supercooled Liquids and Polymers – an NMR Approach. *Phys. A* **1993**, *201*, 237–256.

(91) Hansen, M. T.; Kulik, A. S.; Prins, K. O. Effect of High Hydrostatic Pressure on the Phenylene Motion in Polycarbonate as Revealed by 2H Spin-Lattice Relaxation. *Polymer* **1992**, *33*, 2231–2233.

(92) Döss, A.; Hinze, G.; Diezemann, G.; Böhmer, R.; Sillescu, H. Spatial heterogeneity in glassy polystyrene detected by deuteron NMR relaxation. *Acta Polym.* **1998**, *49*, 56–58.

(93) O'Connor, R. D.; Ginsburg, E. J.; Blum, F. D. Solid-State Deuterium Nuclear Magnetic Resonance of the Methyl Dynamics of Poly(Alpha-methylstyrene) and Polymethylphenylsilane. *J. Chem. Phys.* **2000**, *112*, 7247–7259.

(94) Lutz, T. R.; He, Y.; Ediger, M. D.; Cao, H. H.; Lin, G. X.; Jones, A. A. Rapid Poly(ethylene oxide) Segmental Dynamics in Blends with Poly(methyl methacrylate). *Macromolecules* **2003**, *36*, 1724–1730.

(95) Nozairov, F.; Nazirov, A.; Jurga, S.; Fu, R. Q. Molecular Dynamics of Poly(l-lactide) Biopolymer Studied by Wide-Line Solid-State 1 and 2 H NMR Spectroscopy. *Solid State Nucl. Magn. Reson.* **2006**, *29*, 258–266.

(96) Perez Aparicio, A.; Arbe, A.; Colmenero, J.; Frick, B.; Willner, L.; Richter, D.; Fetters, L. J. Quasielastic Neutron Scattering Study on the Effect of Blending on the Dynamics of Head-to-Head Poly(propylene) and Poly(ethylene-propylene). *Macromolecules* **2006**, *39*, 1060–1072.

(97) Khazanovich, T. N. Theory of Nuclear Magnetic Relaxation in Liquid-Phase Polymers. *Polym. Sci. U.S.S.R.* **1963**, *4*, 727–736.

(98) Ullman, R. Nuclear Magnetic Relaxation of Polymer Solutions. *J. Chem. Phys.* **1965**, *43*, 3161–3177.

(99) Kariyo, S.; Brodin, A.; Gainaru, C.; Herrmann, A.; Hintermeyer, J.; Schick, H.; Novikov, V. N.; Rössler, E. A. From Simple Liquid to Polymer Melt. Glassy and Polymer Dynamics Studied by Fast Field Cycling NMR Relaxometry: Rouse Regime. *Macromolecules* **2008**, *41*, 5322–5332.

(100) deGennes, P. G. Reptation of a Polymer Chain in the Presence of Fixed Obstacles. *J. Chem. Phys.* **1971**, *55*, 572–579.

(101) Ball, R. V.; Callaghan, P. T.; Samulski, E. T. A Simplified Approach to the Interpretation of Nuclear Spin Correlations in Entangled Polymeric Liquids. *J. Chem. Phys.* **1997**, *106*, 7352–7361.

(102) Bormuth, A.; Hofmann, M.; Henritzi, P.; Vogel, M.; Rössler, E. A. Chain-Length Dependence of Polymer Dynamics: A Comparison of Results from Molecular Dynamics Simulations and Field-Cycling 1H NMR. *Macromolecules* **2013**, *46*, 7805–7811.

(103) Kremer, F.; Schönhals, A. *Broad Band Dielectric Spectroscopy*; Springer: Berlin, 2002.

(104) Gainaru, C.; Gainaru, C.; Meier, R.; Schildmann, S.; Lederle, C.; Hiller, W.; Rössler, E. A.; Böhmer, R. Nuclear-Magnetic-Resonance Measurements Reveal the Origin of the Debye Process in Monohydroxy Alcohols. *Phys. Rev. Lett.* **2010**, *105*, 258303.

(105) Gainaru, C.; Figuli, R.; Hecksher, T.; Jakobsen, B.; Dyre, J. C.; Wilhelm, M.; Böhmer, R. Shear-Modulus Investigations of Monohydroxy Alcohols: Evidence for a Short-Chain-Polymer Rheological Response. *Phys. Rev. Lett.* **2014**, *112*, 098301.

(106) Rössler, E. A. Corresponding States Concept for Simple Supercooled Liquids Identifying a Change of Diffusion Mechanism

Above the Glass Transition Temperature. *Ber. Bunsenges. Phys. Chem.* **1990**, *94*, 392–399.

Acknowledgement

Hereby, I want to express deep gratitude to all people who supported me in the course of my studies and my PhD work, in particular to my doctor father Ernst Rößler, whose outstanding scientific expertise, inventiveness and kindness always motivated me. Looking back, I can say that I have learned a great deal during the time in his group and that I have had a lot of joy.

I thank all my fellow students I got to know, who always created a very pleasant atmosphere. Axel Herrmann and Roman Meier helped me getting started with the relaxometer in Bayreuth. I also sincerely thank Franz Fajara for giving me the opportunity to research in his lab in Darmstadt and his scientific advice. Benjamin Kresse and Alexei Privalov introduced me to the world's most powerful FC relaxometer and helped me with the measurements. I esteem Nail Fatkullin for sharing his broad knowledge on relaxation theory and polymer science. For fruitful discussion and very constructive criticism, I thank the people from Halle, namely Kay Saalwächter, Matthias Roos and Alexey Krushelnitsky. I am also indebted to Nuri Aksel for enabling me the rheological investigations in his department, and Lutz Heymann for introducing me to the rheometer.

Finally, I want to thank my family and, in particular, my beloved wife Lea, who supported me greatly.

Thank you all.

References

1. García Sakai, V.; Alba-Simionesco, C.; Chen, S.-H. *Dynamics of Soft Matter – Neutron Applications*; Springer, **2012**.
2. Williams, M. C. *AIChE J.* **1975**, 21, 1-25.
3. Doi, M. *J. Polym. Sci., Part B: Polym. Phys.* **1980**, 18, 1005-1020.
4. Noack, F. *Prog. Nucl. Magn. Reson. Spectrosc.* **1986**, 18, 171-276.
5. Kimmich, R.; Fatkullin, N. *Adv. in Polym. Sci.* **2004**, 170,1-113.
6. Kimmich, R. *Principles of Soft-Matter Dynamics: Basic Theories, Non-Invasive Methods, Mesoscopic Aspects*; Springer: Dordrecht (NL), **2012**.
7. Hansen, J.-P.; McDonald, I. R. *Theory of Simple Liquids*; Elsevier: London, **2006**.
8. March, N. H.; Tosi, M. P. *Introduction to Liquid State Physics*; World Scientific Pub. Co.: Singapore, **2002**.
9. Yarnell, J. L.; Katz, M. J.; Wenzel, R. G. *Phys. Rev. A* **1973**, 7, 2130-2144.
10. Rahman, A. *Phys. Rev. E* **1964**, 136, 405-411.
11. Frenkel, Y. *Kinetic Theory of Liquids*; Clarendon Press: Oxford, **1946**.
12. Kubo, R. *J. Phys. Soc. Jpn.* **1957**, 12, 570-586.
13. Kubo, R. *Rep. Prog. Phys.* **1966**, 28, 255-284.
14. Einstein, A. *Ann. Phys.* **1905**, 322, 549-560.
15. Smoluchowski, M. *Ann. Phys.* **1906**, 326, 756-780.
16. Colmenero, J.; Arbe, A. *J. Polym. Sci., Part B: Polym. Phys.* **2013**, 51, 87-113.
17. Hokin, P.; Fortini, A.; Archer, A. J.; Schmidt, M. *J. Chem. Phys.* **2010**, 133, 224505.
18. Khintchine, A. *Math. Ann.* **1934**, 109, 604-615.
19. Ottochian, A.; Molin, D.; Barbieri, A.; Leporini, D. *J. Chem. Phys.* **2009**, 131, 174902.
20. Wang, Z.; Likhtman, A. E.; Larson, L. G. *Macromolecules* **2012**, 45, 3557-3570.
21. Callen, H. C.; Welton, T. A. *Phys. Rev.* **1951**, 83, 34-40.
22. Marconi, U. M. B.; Puglisi, A.; Rondoni, L.; Vulpiani, A. *Phys. Rep.* **2008**, 461, 111-195.
23. Böttcher, C. I. F.; Borderwijk, P. *Theory of Electric Polarization (Vol2)*; Elsevier: Asmterdam **1987**.
24. Doi, M.; Edwards, S. F. *The Theory of Polymer Dynamics*; Oxford University Press: New York, **1986**.
25. Likhtman, A. E.; Sukumaran, S. K.; Ramirez, J. *Macromolecules* **2007**, 40, 6748-6757.
26. Swenson, R. J. *Am. J. Phys.* **1983**, 51, 940-942.
27. Ediger, M. D.; Angell, C. A.; Nagel, S. R. *J. Phys. Chem.* **1996**, 100, 13200-13212.

28. Colmenero, J. J. *Phys.: condens. Matter* **2015**, 27, 103101.
29. Petzold, N.; Rössler, E. A. *J. Chem. Phys.* **2010**, 133, 124512, 1-6.
30. Schmidtke, B.; Petzold, N.; Kahlau, R.; Rössler, E. A. *J. Chem. Phys.* **2013**, 139, 084504, 1-10.
31. Davidson, D. W.; Cole, R. H. *J. Chem. Phys.* **1951**, 19, 1484-1490.
32. Beckmann, P. A. *Phys. Rep.* **1988**, 171, 85-128.
33. Kahlau, R.; Kruk, D.; Blochowicz, T.; Novikov, V. N.; Rössler, E. A. *J. Phys.: Condens. Matter* **2010**, 22, 365101.
34. Angell, C. *Proc. Natl. Acad. Sci. U.S.A.* **1995**, 92, 6675-6682.
35. Gutzow, I. S.; Schmelzer, J. W. P. *The Vitreous State: Thermodynamics, Structure, Rheology and Crystallization*; Springer: Berlin, **1995**.
36. Angell, C. A. *Science* **1995**, 267, 1924-1935.
37. Wunderlich, B. *Thermal Analysis*; Academic Press Inc.: San Diego (CA, USA), **1990**.
38. Williams, M. L.; Landel, R. F.; Ferry, J. D. *J. Am. Chem. Soc.* **1955**, 77, 3701-3707.
39. Schmidtke, B.; Petzold, N.; Kahlau, R.; Hofmann, M.; Rössler, E. A. *Phys. Rev. E* **2012**, 86, 041507.
40. Schmidtke, B.; Hofmann, M.; Lichtinger, A.; Rössler, E. A. *Macromolecules* **2014**, 48, 3005-3013.
41. Kawasaki, K.; Gunton, J. *Phys. Rev. B* **1976**, 13, 4658-4671.
42. Götze, W.; Sjörgen, L. *Rep. Prog. Phys.* **1992**, 55, 241-376.
43. Cummins, H. Z. *J. Phys.: Condens. Matter* **1999**, 11, A95-A117.
44. Götze, W.; Sjörgen, L. *J. Phys. C: Solid State Phys.* **1988**, 21, 3407-3421.
45. Schweizer, K. S.; Saltzman, E. J. *J. Chem. Phys.* **2004**, 121, 1984-2000.
46. Krakowiak, V.; Alba-Simioneso, C.; Krauzman, M. *J. Chem. Phys.* **1997**, 3417-3427.
47. Franosch, T.; Götze, W.; Mayr, M. R.; Singh, A. P. *Phys. Rev. E* **1997**, 55, 3183-3190.
48. Götze, W.; Voigtmann, T. *Phys. Rev. E* **2000**, 61, 4133-4147.
49. Domschke, M.; Marsilius, M.; Blochowicz, T.; Voigtmann, T. *Phys. Rev. E* **2011**, 85, 031506.
50. Dudowics, J.; Freed, K. F.; Douglas, J. F. *Adv. Chem. Phys.* **2008**, 137, 125-222.
51. Freed, K. F. *Acc. Chem. Res.* **2011**, 44, 194-203.
52. Xu, W.-S.; Freed, K. F. *Macromolecules* **2015**, 48, 2333-2343.
53. Kirkpatrick, T. R.; Thirumalai D.; Wolynes, P. G. *Phys. Rev. A* **1989**, 40, 1045-1053.
54. Anderson, P. W. *Science* **1995**, 267, 1615-1616.
55. Ding, Y.; Kisliuk, A.; Sokolov, A. P. *Macromolecules* **2004**, 37, 161-166.
56. Ding, Y.; Novikov, V. N.; Sokolov, A. P.; Cailiaux, A.; Dalle-Ferrier, C.; Alba-Simionesco, C.; Frick, B. *Macromolecules* **2004**, 37, 9254-9272.

57. Hintermeyer, J.; Herrmann, A.; Kahlau, R.; Goiceanu, C.; Rössler, E. A. *Macromolecules* **2008**, *41*, 9335-9344.
58. Gainaru, C.; Hiller, W.; Böhmer, R. *Macromolecules* **2010**, *43*, 1907-1914.
59. Cohen Addad, J.-P.; Guillermo, A. *Macromolecules* **2003**, *36*, 1609-1615.
60. Ferry, J. D. *Viscoelastic Properties of Polymers*; John Wiley & Sons: New York, **1980**.
61. Graessley, W. W. *Polymeric Liquids and Networks: Dynamics and Rheology*; Garland Science, London and New York, **2008**.
62. Rubinstein, M.; Colby, R. H. *Polymer Physics*; Oxford University Press: Oxford (UK), **2003**.
63. Daoud, M.; Cotton, J. P.; Farnoux, B.; Jannik, G.; Sarma, G.; Benoit, H.; Duplessix, R.; Picot, C.; de Gennes, P. G. *Macromolecules* **1975**, *8*, 804-818.
64. Kirste, R. G.; Kruse, W. A.; Schelten, J. *Makromol. Chem.* **1973**, *162*, 299-303.
65. Fetters, L. J.; Lohse, D. J.; Richter, D.; Witten, T. A.; Zirkel, A. *Macromolecules* **1994**, *27*, 4639-4647.
66. Londono, J. D.; Habenschuss, A.; Curro, J. G.; Rajasekaran, J. J. *J. Polym. Sci., Part B: Polym. Phys.* **1996**, *34*, 3055-3061.
67. Krishnamoorti, R.; Graessley, W. W.; Zirkel, A.; Richter, D.; Hadjichristidis, N.; Fetters, L. J.; Lohse, D. J. *J. Polym. Sci., Part B: Polym. Phys.* **2002**, *40*, 1768-1776.
68. Flory, P. J. *J. Chem. Phys.* **1949**, *17*, 303-310.
69. Rouse Jr., P. E. *J. Chem. Phys.* **1953**, *21*, 1272-1280.
70. Kariyo, S.; Brodin, A.; Gainaru, C.; Herrmann, A.; Hintermeyer, J.; Schick, H.; Novikov, V. N.; Rössler, E. A. *Macromolecules* **2008**, *41*, 5322-5332.
71. Meyer, H.; Wittmer, J. P.; Kreer, T.; Beckrich, P.; Johnner, A.; Farago, J.; Baschnagel, J. *Eur. Phys. J. E* **2008**, *26*, 25-33.
72. Stockmayer, W. H. *Pure Appl. Chem.* **1967**, *15*, 539-554.
73. Fatkullin, N.; Kimmich, R.; Weber, H. W. *Phys. Rev. E* **1993**, *47*, 4600-4603.
74. Fatkullin, N.; Kimmich, R. *J. Chem. Phys.* **1994**, *101*, 822-832.
75. Fatkullin, N.; Stapf, S.; Hofmann, M.; Meier, R.; Rössler, E. A. *J. Non-Cryst. Solids* **2015**, *407*, 309-317.
76. Fatkullin, N.; Gubaidullin, A.; Stapf, S. *J. Chem. Phys.* **2010**, *132*, 094903.
77. Adam, M.; Delsanti, M. *Macromolecules* **1977**, *10*, 1229-1237.
78. Einaga, Y.; Miyaki, Y.; Fujita, A. *J. Polym. Sci., Polym. Phys.* **1979**, *17*, 2103-2109.
79. Kniewske, R.; Kulicke, W.-M. *Makromol. Chem.* **1983**, *184*, 2173-2186.
80. Zimm, B. *J. Chem. Phys.* **1956**, *24*, 269-278.
81. Barlow, A. J.; Harrison, G.; Lamb, J. *Proc. R. Soc. London, Ser. A* **1964**, *282*, 228-251.

82. Gotro, J. T.; Graessley, W. W. *Macromolecules* **1984**, 17, 2767-2775.
83. Green, P. F.; Mills, P. J.; Palmstroem, C. J.; Mayer, J. W.; Kramer, E. J. *Phys. Rev. Lett.* **1984**, 53, 2145-2148.
84. Baumgaertel, M.; De Rosa, M. E.; Machado, J.; Masse, M.; Winter, H. H. *Rheol. Acta* **1992**, 31, 75-82.
85. Smith, B. A. *Macromolecules* **1981**, 15, 469-472.
86. Smith, B. A.; Samulski, E. T.; Yu, L.-P.; Winnik, M. A. *Macromolecules* **1985**, 1901-1905.
87. Komlos, M. E.; Callaghan, P. T. *J. Chem. Phys.* **1998**, 109, 10053-10067.
88. de Gennes, P. G. *J. Chem. Phys.* **1971**, 55, 572-579.
89. Edwards, S. F. *Proc. Phys. Soc.* **1967**, 92, 9-16.
90. Edwards, S. F. *Polymer* **1977**, 9, 140-143.
91. Read, D. J.; Jagannathan, K.; Likhtman, A. E. *Macromolecules* **2008**, 41, 6843-6853.
92. des Cloizeaux, J. *Macromolecules* **1990**, 23, 3992-4006.
93. Milner, S. T.; McLeish, T. C. B. *Phys. Rev. Lett.* **1998**, 81, 725-728.
94. Liu, C.-Y.; Keunings, R.; Bailly, C. *Phys. Rev. Lett.* **2006**, 97, 246001.
95. Doi, M. *J. Polym. Sci.: Lett. Ed.* **1981**, 19, 265-273.
96. Doi, M. *J. Polym. Sci.: Lett. Ed.* **1983**, 21, 667-684.
97. Likhtman, A. E.; McLeish, T. C. B. *Macromolecules* **2002**, 35, 6332-6343.
98. Wischnewski, A.; Monkenbusch, M.; Willner, L.; Richter, D.; Likhtman, A. E.; McLeish, T. C. B.; Farago, B. *Phys. Rev. Lett.* **2002**, 88, 058301.
99. Zamponi, M.; Monkenbusch, M.; Willner, L.; Wischnewski, A.; Farago, B.; Richter, D. *Europhys. Lett.* **2005**, 72, 1039-1044.
100. Graessley, W. W. *J. Pol. Sci.* **1980**, 18, 27-34.
101. Graessley, W. W. *Adv. Polym. Sci.* **1982**, 47, 67-117.
102. von Seggern, J.; Klotz, S.; Cantow, H.-J. *Macromolecules* **1991**, 24, 3300-3303.
103. Rubinstein, M.; Colby, R. H. *J. Chem. Phys.* **1988**, 89, 5291-5306.
104. Zamponi, M.; Wischnewski, A.; Monkenbusch, M.; Willner, L.; Richter, D.; Likhtman, A. E.; Kali, G.; Farago, B. *Phys. Rev. Lett.* **2006**, 238301 (1-4).
105. Glomann, T.; Schneider, G. J.; Brást, A. R.; Pyckhout-Hintzen, Wischnewski, A.; Zorn, R.; Allgaier, J.; Richter, D. *Macromolecules* **2011**, 44, 7430-7437.
106. Green, P.; Kramer, E. J. *Macromolecules* **1986**, 19, 1108-1114.
107. Vega, J. F.; Rastogi, S.; Peters, G. W. m.; Meijer, H. E. H. *J. Rheol.* **2004**, 48, 663-678.
108. Elfadl, A.; Kahlau, R.; Herrmann, A.; Novikov, V. N.; Rössler, E. A. *Macromolecules* **2010**, 43, 3340-3351.

109. Unidad, H. J.; Abdel Goad, M.; Bras, A. R.; Zamponi, M.; Faust, R.; Allgaier, J.; Pyckhout-Hintzen, W.; Wischniewski, A.; Richter, D.; Fetters, L. J. *Macromolecules* **2015**, 48, 6638-6645.
110. Schweizer, K. S. *J. Chem. Phys.* **1989**, 91, 5802-5821.
111. Schweizer, K. S. *J. Chem. Phys.* **1989**, 91, 5822-5839.
112. Kimmich, R.; Fatkullin, N.; Seitter, R.-O.; Gille, K. *J. Chem. Phys.* **1998**, 108, 2173-2177.
113. Krutyeva, M. A.; Fatkullin, N. F.; Kimmich, R. *Polym. Sci. Ser. A* **2005**, 47, 1022-1031.
114. Gurtovenko, A. A.; Blumen, A. *Adv. in Pol. Sci.* **2005**, 182, 171-282.
115. Dolgushev, M.; Blumen, A. *Macromolecules* **2009**, 42, 5378-5387.
116. Blumen, A.; Dolgushev, M.; Blumen, A. *J. Chem. Phys.* **2009**, 131, 044905.
117. Fürstenberg, F.; Dolhushev, M.; Blumen, A. *J. Chem. Phys.* **2012**, 136, 154904.
118. *Bruker Almanac, Analytical Tables and Product Overview*, **2012** (ISBN-13 978-3-929431-25-4).
119. Abragam, A. *The Principles of Nuclear Magnetism*; Oxford Clarendon Press: Oxford (UK), **1961**.
120. Kowalwewski, J.; Mäler, L. *Nuclear Spin Relaxation in Liquids: Theory, Experiments, and Applications*; Taylor & Francis: New York, **2006**.
121. Levitt, M. *Spin Dynamics: Basics of Nuclear Magnetic Resonance*; John Wiley & Sons Ltd. Chichester (UK), **2008**.
122. Ernst, R.; Bodenhausen, G.; Wokaun, A. *Principles of Nuclear Magnetic Resonance in One and Two Dimensions*; Clarendon Press: Oxford, **1989**.
123. Bloembergen, N.; Purcell, E. M.; Pund, R. V. *Phys. Rev.* **1948**, 73, 679-715.
124. Kruk, D. *Theory of Evolution and Relaxation of Multi-Spin Systems – Application to Nuclear Magnetic Resonance and Electron Spin Resonance*; arima publishing: Suffolk (UK), **2007**.
125. Redfield, A. G. *IBM Journal* **1957**, 1, 19-31.
126. Kruk, D. *Understanding Spin Dynamics*; Taylor & Francis: Boca Raton (FL, USA), **2016**.
127. Kehr, M.; Fatkullin, N.; Kimmich, R. *J. Chem. Phys.* **2007**, 127, 084911.
128. Ball, R. C.; Callaghan, P. T.; Samulski, E. T. *J. Chem. Phys.* **1997**, 106, 7352-7361.
129. Kimmich, R.; Weber, H. W. *J. Chem. Phys.* **1993**, 98, 5847-5854.
130. Kehr, M.; Fatkullin, N.; Kimmich, R. *J. Chem. Phys.* **2007**, 126, 094903.
131. Wischniewski, A.; Monkenbusch, M.; Willner, L.; Richter, D.; Kali, G. *Phys. Rev. Lett.* **2003**, 90, 058302 (1-4).
132. Henritzi, P.; Bormuth, P.; Vogel, M. *Solid State Nucl. Magn. Reson.* **2013**, 54, 32-40.
133. Albrand, J. P.; Taieb, M. C.; Fries, P.; Belorizky, E. *J. Chem. Phys.* **1981**, 75, 2141-2146.
134. Herrmann, A.; Kresse, B.; Wohlfahrt, M.; Bauer, I.; Privalov, A. F.; Kruk, D.; Fatkullin, N.; Fujara, F.; Rössler, E. A. *Macromolecules* **2012**, 45, 6516-6525.
135. Harmon, J. F.; Muller, B. H. *Phys. Rev.* **1969**, 182, 400-410.

136. Sholl, C. A. *J. Phys. C: Solid State Phys.* **1981**, 14, 447-464.
137. Belorizky, E.; Fries, P. H. *Chem. Phys. Lett.* **1988**, 145, 33-38.
138. Kruk, D.; Meier, R.; Rössler, E. A. *J. Phys. Chem. B* **2011**, 115, 951-957.
139. Kruk, D.; Meier, R.; Rössler, E. A. *Phys. Rev. E*, **2012**, 85, 020201.
140. Meier, R.; Herrmann, A.; Kresse, B.; Privalov, A. F.; Kruk, D.; Fujara, F.; Rössler, E. A. *ACS Macro Lett.* **2013**, 2, 96-99.
141. Meier, R.; Herrmann, A.; Hofmann, M.; Schmidtke, B.; Kresse, B.; Privalov, A. F.; Kruk, D.; Fujara, F.; Rössler, E. A. *Macromolecules* **2013**, 46, 5538-5548.
142. Odelius, M.; Laaksonen, A.; Levitt, M. H.; Kowalewski, J. *J. Magn. Reson., Ser. A* **1993**, 105, 289-294.
143. Smith, J. A. S. *J. Chem. Educ.* **1971**, 48, 39-48.
144. Berne, B. J.; Pecora, R. *Dynamic Light Scattering: With Applications to Chemistry, Biology and Physics*; Wiley: New York, **1976**.
145. Lovesey, S. W. *Theory of Neutron Scattering from Condensed Matter (Vol. 1)*; Clarendon Press: Oxford, **1986**.
146. Squires, G. L. *Introduction to the Theory of Thermal Neutron Scattering (3rd Ed.)*; Cambridge University Press: Cambridge (UK), **2012**.
147. Schleger, P.; Farago, B.; Lartigue, C.; Kollmar, A.; Richter, D. *Phys. Rev. Lett.* **1998**, 81, 124-127.
148. Richter, D.; Butera, R.; Fetters, L. J.; Huang, J. S.; Farago, B.; Ewen, B. *Macromolecules* **1992**, 25, 6156-6164. (
149. Ewen, B.; Maschke, U.; Richter, D.; Farago, B. *Acta Polym.* **1994**, 45, 143-147. (NSE)
150. Richter, D.; Monkenbusch, M.; Arbe, A.; Colmenero, J. *Adv. in Pol. Sci.* **2005**, 174, 1-221.
151. Pérez-Aparicio, R.; Alvarez, F.; Arbe, A.; Willner, L.; Richter, D.; Falus, P.; Colmenero, J. *Macromolecules* **2010**, 44, 3129-3139.
152. Green, P.; Kramer, E. J. *Macromolecules* **1986**, 19, 1108-1114.
153. Green, P. F.; Mills, P. J.; Kramer, E. J. *Polym.* **1986**, 27, 1063-1066.
154. Crist, B.; Green, P. F.; Jones, R. A. L.; Kramer, E. J. *Macromolecules* **1989**, 22, 2857-2858.
155. von Seggern, J.; Klotz, S.; Cantow, H.-J. *Macromolecules* **1991**, 24, 3300-3303.
156. Pohl, D. W.; Schwarz, S. E.; Irniger, V. *Phys. Rev. Lett.* **1973**, 31, 32-35.
157. Léger, L.; Hervet, H.; Rondelez, F. *Macromolecules* **1984**, 14, 1732-1738.
158. Köhler, W. *J. Chem. Phys.* **1993**, 98, 660-668.
159. Veniaminov, A. V.; Sillescu, H. *Chem. Phys. Lett.* **1999**, 303, 499-504.
160. Magde, D.; Elson, E.; Webb, W. W. *Phys. Rev. Lett.* **1972**, 29, 705-708.

161. Zettl, H.; Häfner, W.; Böker, A.; Schmalz, H.; Lanzendörfer, M.; Müller, A. H. E.; Krausch, G. *Macromolecules* **2004**, 37, 1917-1920.
162. Wöll, D. *RSC Adv.* **2014**, 4, 2447-2465.
163. Stejskal, E.; Tanner, J. E. *J. Chem. Phys.* **1965**, 42, 288-292.
164. Callaghan, P.T. *Principles of Nuclear Magnetic Resonance Microscopy*; Oxford University Press: Oxford (UK) **1993**.
165. Fischer, E.; Kimmich, R.; Fatkullin, N. *J. Chem. Phys.* **1997**, 106, 9883-9888.
166. Kimmich, R. *NMR Tomography, Diffusometry, Relaxometry*; Springer: Berlin, **1997**.
167. Callaghan, P. T. *Translational Dynamics and Magnetic Resonance: Principles of Pulsed Gradient Spin Echo NMR*; Oxford University Press: Oxford (UK) **2011**.
168. Geil, B. *Concepts Magn. Reson.* **1998**, 10, 299-321.
169. Callaghan, P. T.; Coy, A. *Phys. Rev. Lett.* **1992**, 68, 3176-3179.
170. Appel, M.; Fleischer, G. *Macromolecules* **1993**, 26, 5520-5525.
171. Appel, M.; Fleischer, G.; Kärger, J.; Fujara, F.; Chang, I. *Macromolecules* **1994**, 27, 4274-4277.
172. Pearson, D. S.; Fetters, L. J.; Graessley, W. W.; Ver Strate, G.; von Meerwall, E. *Macromolecules* **1994**, 27, 711-719.
173. Fleischer, G.; Appel, M. *Macromolecules* **1995**, 28, 7281-7283.
174. Fischer, E.; Kimmich, R.; Fatkullin, N. *J. Chem. Phys.* **1996**, 104, 9174-9178.
175. Pahl, S.; Fleischer, G.; Fujara, F.; Geil, B. *Macromolecules* **1997**, 30, 1414-1418.
176. Appel, M.; Fleischer, G.; Kärger, J.; Chang, I.; Fujara, F.; Schönhals, A. *Colloid Polym. Sci.* **1997**, 275, 187-191.
177. Fischer, E.; Kimmich, R.; Fatkullin, N. *J. Chem. Phys.* **1996**, 104, 9174-9178. Tao, N. J.; Li, G.; Cummins, H. Z. *Phys. Rev. Lett.* **1991**, 66, 1334-1337.
178. Bergmann, R.; Börjesson, L.; Torell, L.M.; Fontana, A. *Phys. Rev. B* **1997**, 56, 11619-11628.
179. Wiedersich, J.; Surotsev, N. V.; Rössler, E. *J. Chem. Phys.* **2000**, 113, 1143-1153.
180. Brodin, A.; Rössler, E. A. *Eur. Phys. J. B* **2005**, 44, 3-14.
181. Torre, R.; Bartolini, P.; Pick, R. M. *Phys. Rev. E* **1998**, 57, 1912-1920.
182. Hinze, G.; Brace, D. D.; Gottke, M. D.; Fayer, M. D. *J. Chem. Phys.* **2000**, 113, 3723-3733.
183. Cang, H.; Novikov, V. N.; Fayer, M. D. *Phys. Rev. Lett.* **2003**, 90, 197401.
184. Partesi, G.; Bartolini, P.; Senatra, D.; Ricci, M.; Righini, R.; Barocci, F.; Torre, R. *Phys. Rev. E* **2003**, 67, 021505.
185. Watanabe, H. *Prog. Polym. Sci.* **1999**, 24, 1253-1403.
186. Kremer, F.; Schönhals, A. *Broadband Dielectric Spectroscopy*; Springer: Berlin, **2003**.

187. Binder, K. *Monte Carlo and Molecular Dynamics Simulations in Polymer Science*; Oxford University Press: New York and Oxford: **1995**.
188. Kremer, K.; Grest, G. S.; Carmesin, I. *Phys. Rev. Lett.* **1988**, 61, 566-569.
189. Kremer, K.; Krest, G. S. *J. Chem. Phys.* **1990**, 92, 5057-5086.
190. Smith, G. D.; Paul, W.; Monkenbusch, M.; Willner, L.; Richter, D.; Qiu, X. H.; Ediger, M. D. *Macromolecules* **1999**, 32, 8857-8865.
191. Smith, G. D.; Paul, W. *Rep. Prog. Phys.* **2004**, 67, 1117-1185.
192. Peter, S.; Meyer, H.; Baschnagel, J. *Eur. Phys. J.* **2009**, 28, 147-158.
193. Pérez-Aparicio, R.; Colmenero, J.; Alvarey, F.; Padding, J. T.; Briels, W. J. *J. Chem. Phys.* **2010**, 132, 024904 (1-11).
194. Ramírez-Hernández, A.; Detcheverry, F. A.; Peters, B. L.; Chappa, V. C.; Schweizer, K. S.; Müller, M.; Pablo, J. J. *Macromolecules* **2013**, 46, 6287-6299.
195. Furtado, F.; Damron, J.; Trutschel, M.-L.; Franz, C.; Schröter, K.; Ball, R. C.; Saalwächter, K.; Panja, D. *Macromolecules* **2014**, 47, 256.
196. Likhtman, A. E.; Ponmurugan, M. *Macromolecules* **2014**, 47, 1470-1481.
197. Kreer T.; Baschnagel, J.; M. Müller, Binder, K. *Macromolecules* **2001**, 34, 1105-1117.
198. Herrmann, A.; Novikov, V. N.; Rössler, E. A. *Macromolecules* **2009**, 42, 2063-2068.
199. Smith, G. D.; Borodin, O.; Bedrov, D. *J. Phys. Chem. A* **1998**, 102, 10318-10323.
200. Schnauss, W.; Fujara, F.; Sillescu, H. *J. Chem. Phys.* **1992**, 97, 1378-1389.
201. Schmidt-Rohr, K.; Kulik, A. S.; Beckham, H. W.; Ohlemacher, A.; Pawelzik, U.; Boeffel, C.; Spiess, H. W. *Macromolecules* **1994**, 27, 4733-4745.
202. Rössler, E.; Eiermann, P. *J. Chem. Phys.* **1994**, 100, 5237-5248.
203. Qiu, X. H.; Moe, N. E.; Ediger, M. D. *J. Chem. Phys.* **2000**, 113, 2918-2926.
204. Böhmer, R.; Diezemann, G.; Hinze, G.; Rössler, E. *Prog. Nucl. Magn. Reson. Spectrosc.* **2001**, 39, 191-267.
205. Klein, P. G.; Ries, M. E. *Prog. Nucl. Magn. Reson. Spectrosc.* **2003**, 42, 31-52.
206. Luseac, S. A.; Gainaru, C.; Vogel, M.; Koplin, C.; Medick, P.; Rössler, E. A. *Macromolecules* **2005**, 38, 5625-5633.
207. Chernov, V. M.; Krasnopol'skii, G. S. *J. Exp. Theor. Phys.* **2008**, 107, 354-366.
208. Herbers, C. R.; Sauer, D.; Vogel, M. *J. Chem. Phys.* **2012**, 136, 124511.
209. Cohen-Addad, J. P.; Faure, J. P. *J. Chem. Phys.* **1974**, 61, 1571-1580.
210. English, A. D. *Macromolecules* **1985**, 18, 178-181.
211. Cohen-Addad, J. P.; Vogin, R. *Phys. Rev. Lett.* **1974**, 33, 940-943.
212. Collignon, J.; Sillescu, H.; Spiess, H. W. *Colloid. Polym. Sci.* **1981**, 259, 220-226.

213. Cohen-Addad, J.P.; Dupeyre, R. *Macromolecules* **1985**, *18*, 1101-1109.
214. Brereton, M. G. *Macromolecules* **1989**, *22*, 3667-3674.
215. Brereton, M. G. *Macromolecules* **1990**, *23*, 1119-1131.
216. Brereton, M. G.; Ward, I. M.; Boden, N.; Wright, P. *Macromolecules* **1991**, *24*, 2068-2074.
217. Klein, P. G.; Adams, C. H.; Brereton, M. G.; Ries, M. E.; Nicholson, T. M.; Hutchings, L. R.; Richards, R. W. *Macromolecules* **1998**, *31*, 8871-8877.
218. Saalwächter, K. *Prog. Nucl. Magn. Reson. Spectrosc.* **2007**, *51*, 1-35.
219. Ries, M. E.; Brereton M. G. *Phys. Chem. Chem. Phys.* **2009**, *11*, 6918-6924.
220. Graf, R.; Heuer, A.; Spiess, H. W. *Phys. Rev. Lett.* **1998**, *80*, 5738.
221. Vaca Chávez, F.; Saalwächter, K. *Phys. Rev. Lett.* **2010**, *104*, 198305 (1-4).
222. Vaca Chávez, F.; Saalwächter, K. *Macromolecules* **2011**, *44*, 1549-1559.
223. Vaca Chávez, F.; Saalwächter, K. *Macromolecules* **2011**, *44*, 1560-1569.
224. Fatkullin, N.; Mattea, C.; Stapf, S. *J. Chem. Phys.* **2013**, *139*, 194905
225. Baum, J.; Pines, A. *J. Am. Chem. Soc.* **1986**, *108*, 7447-7454.
226. Dollase, T.; Graf, R.; Heuer, A.; Spiess, H. W. *Macromolecules* **2001**, *34*, 298-309.
227. Herrmann, A.; Kresse, B.; Gmeiner, J.; Privalov, A. F.; Kruk, D.; Fujara, F.; Rössler, E. A. *Macromolecules* **2012**, *45*, 1408-1416.
228. Colby, R. H.; Fetters, L. J.; Graessley, W. W. *Macromolecules* **1987**, *20*, 2226-2237.
229. Benallal, A.; Marig, G.; Montfort, J.P.; Derail, C. *Macromolecules* **1993**, *26*, 7229-7235.
230. Palade, L. I.; Verney, V.; Attané, P. *Macromolecules* **1995**, *28*, 7051-7057.
231. Park, S. J.; Desai, P. S.; Chen, X.; Larson, R. G. *Macromolecules* **2015**, *48*, 4122-4131.
232. Kruk, D.; Korpala, A.; Mehdizadeh Taheri, S.; Rössler, E. *J. Chem. Phys.* **2014**, *140*, 174504.
233. Lurie, D. J.; Foster, M. F.; Yeung, D.; Hutchinson, J. M. S. *Phys. Med. Biol.* **1998**, *43*, 1877-1886.
234. Lurie, D.; Aime, S.; Baroni, S.; Booth, A.; Broche, L.M.; Choi, C.-H.; Davies, G. R.; Ismail, S.; Ó hÓgáin, D.; Pine, K. J. *C. R. Acad. Sci. Phys.* **2010**, *11*, 136-148.
235. Koenig, S. H.; Brown, R. D. *Prog. Nucl. Magn. Reson. Spectrosc.* **1990**, *22*, 487-567.
236. Korb, J.-P.; Bryant, R. G. *Magn. Reson. Med.* **2002**, *48*, 21-26.
237. L. Seong-Joo; Jeong H. S., Kim, K., Hwang, S.-M.; Yu, K. K.; Lim, S.; Han, J. H.; Yim, H.; Kim, J.-H.; Y. S., Jung, Kim K. S. *BioMed Res. Int.* **2015**, *2015*, 385428.
238. Baroni, S.; Consonni, R.; Ferrante, G.; Aime, S. *J. Agric. Food Chem.* **2009**, *57*, 3028-3032.
239. Nolte, M.; Privalov, A.; Altmann, J.; Anferov, V.; Fujara, F. *J. Phys. D: Appl. Phys.* **2002**, *35*, 939-942.
240. Fujara, F.; Kruk, D.; Privalov, A. F. *Prog. Nucl. Magn. Reson. Spectrosc.* **2014**, *82*, 39-69.

241. Allgeier, J.; Buntkowsky, G.; Hentrich, S.; Nack, M.; Vieth, H.-M. *Ber. Bunsen-Ges. Phys. Chem.* **1989**, 93, 1281-1285.
242. Wagner, S.; Dinesen, T. R. J.; Rayner, T.; Bryant, R. G. *J. Magn. Reson.* **1999**, 140, 172-178.
243. Stork, H.; Ditter, M.; Plößer, H.; Privalov, A. F.; Fujara, F. *J. Magn. Reson.* **2008**, 192, 173-176.
244. Diakova, G.; Goddard, Y. A.; Korb, J.-P.; Bryant, R. G. *Biophys. J.* **2010**, 98, 138-146.
245. Redfield, A. G. *J. Biomol. NMR* **2012**, 52, 159-177.
246. Kiryutin, A. S.; Pravdivtsev, A. N.; Ivanov, K. L.; Grishin, Y. A.; Vieth, H.-M.; Yurkovskaya, A. V. *J. Magn. Reson.* **2016**, 263, 79-91.
247. Redfield, A. G.; Warner, F.; Bleich, H. E. *Rev. Sci. Instrum.* **1968**, 39, 710-715.
248. Blanz, M.; Rayner, T. J.; Smith, J. A. S. *Meas. Sci. Technol.* **1993**, 4, 48-59.
249. Lips, O.; Privalov, A. F.; Dvinskikh, S. V.; Fujara, F. *J. Magn. Reson.* **2001**, 149, 22-28.
250. Anoardo, E.; Galli, G.; Ferrante, G. *Appl. Magn. Reson.* **2001**, 20, 365-404.
251. Kimmich, R.; Anoardo, E. *Prog. Nucl. Magn. Reson. Spectrosc.* **2004**, 44, 257-320.
252. Ferrante, G.; Sykora, G. *Adv. Inorg. Chem.* **2005**, 57, 405-470.
253. Schauer, G.; Nusser, W.; Blanz, M.; Kimmich, R. *J. Phys. E: Sci. Instrum.* **1987**, 20, 43-46.
254. STELAR s.r.l. ; Mede Italy. (www.stelar.it , June 2016)
255. Kresse, B.; Privalov, A. F.; Fujara, F. *Solid State Nucl. Magn. Reson.* **2011**, 40, 134-137.
256. Kresse, B.; Privalov, A. F.; Herrmann, A.; Hofmann, M.; Rössler, E. A.; Fujara, F. *Solid State Nucl. Magn. Reson.* **2011**, 59-60, 45-47.
257. Roos, M.; Hofmann, M.; Link, S.; Ott, M.; Baalbach, J.; Kuschelnitzky, A.; Rössler, E. A.; Sallwächter, K. *J. Biomol. NMR* **2015**, 63, 403-415.
258. Solomon, I. *Phys. Rev.* **1955**, 99, 559-566.
259. Zimmerman, J. R. ; Brittin, W. E. *J. Phys. Chem.* **1957**, 61, 1328-1333.
260. Brooks, A. A.; Cutnell, J. D.; Stejskal, E. O.; Weiss, V. W. *J. Chem. Phys.* **1968**, 49, 1571-1576.
261. Kalk, A.; Berendsen, H. J. C. *J. Magn. Reson.* **1976**, 24, 343-366.
262. Edzes, H. T.; Samulski, E. T. *J. Magn. Reson.* **1978**, 31, 207-229.
263. Macura, S.; Ernst, R. R. *Mol. Phys.* **1980**, 41, 95-117.
264. Geil, B.; Hinze, G. *Chem. Phys. Lett.* **1993**, 216, 51-55.
265. Fatkullin, Nail: *private communication*.
266. Seyedlar, A. O.; Stapf, S.; Mattea, C. *Phys. Chem. Chem. Phys.* **2015**, 17, 1653-1659.
267. Kariyo, S.; Stapf, S. *Macromolecules* **2002**, 35, 9253-9255.
268. Kimmich, R.; Stapf, S.; Möller, M.; Out, R.; Seitter, R.-O. *Macromolecules* **1994**, 27, 1505-1508.
269. Kariyo, S.; Stapf, S. *Solid State NMR* **2004**, 25, 64-71.
270. Kariyo, S.; Stapf, S.; Blümich, B. *Macromol. Chem. Phys.* **2005**, 206, 1292-1299.

271. Kariyo, S.; Gainaru, C.; Brodin, A.; Novikov, V. N.; Rössler, E. A. *Phys. Rev. Lett.* **2006**, 97, 207803.
272. Hofmann, M.; Herrmann, A.; Abou Elfadl, A.; Kruk, D.; Wohlfahrt, M.; Rössler, E.A. *Macromolecules* **2012**, 45, 2390-2401.
273. Kariyo, S.; Brodin, A.; Gainaru, C.; Herrmann, A.; Schick, H.; Novikov, V. N.; Rössler, E. A. *Macromolecules* **2008**, 41, 5313-5321.
274. Herrmann, A.; Kariyo, S.; Abou Elfadl, A.; Meier, R.; Gmeiner, J.; Novikov, V. N.; Rössler, E. A. *Macromolecules* **2009**, 42, 5236-5243.
275. Herrmann, A.; Rössler, E. A. *ACS Macro Lett.* **2012**, 1, 1339-1342.
276. Luchinat, C.; Parigi, G. *J. Am. Chem. Soc.* **2007**, 129, 1055-1064.
277. Pratner, A. M.; Bretthorst, G. L.; Neil, J. J.; Garbow, J. R.; Ackerman, J. J. H. *Magn. Reson. Med.* **2008**, 60, 555-563.
278. Herrmann, A. Ph.D. Thesis: *Polymer Melts Investigated by Field Cycling NMR Relaxometry: From Simple liquid to Reptation Dynamics*, Universität Bayreuth, **2012**.
279. Cohen-Addad, J. P.; Messa, J. P. *J. Phys. Lett.-Paris* **1976**, 36, 193-196.
280. Filon, L. N. *Proc. Roy. Soc. Edinburgh* **1928**, 49, 38-47.
281. Morita, A.; Ando, I.; Nishioka, A. *J. Polym. Sci.: Polym. Lett. Ed.* **1980**, 18, 109-113.
282. Collignon, J.; Sillescu, H. *J. Polym. Sci.: Polym. Lett. Ed.* **1980**, 18, 669-672.
283. Van der Spoel, D.; Lindahl, E.; Hess, B.; Groenhof, G.; Mark, A. E.; Berendsen, H. J. C. *J. Comput. Chem.* **2005**, 26, 1701-1718.
284. Bormuth, A.; Henritzi, P.; Vogel, M. *Macromolecules* **2010**, 43, 8985-8992.
285. Saalwächter, Kay: *private communication*.
286. Nusser, K.; Schneider, G. J.; Richter, D. *Macromolecules* **2013**, 46, 6263-6272.
287. Courtesy of Thomas Körber (Bayreuth): *private communication/unpublished results*.
288. Courtesy of Anne Lichtigner (Bayreuth): *private communication/unpublished results*.
289. Courtesy of Fathia Mohamed (Bayreuth): *private communication/unpublished results*.
290. Buhleier, E.; Wehner, W.; Vögtle, F. *Synth. Commun.* **1978**, 2, 155-158.
291. Fischer, M.; Vögtle, M. *Angew. Chem. Int. Ed.* **1999**, 38, 884-905.
292. Boas, U.; Heegaard, P. M. H. *Chem. Soc. Rev.* **2004**, 33, 43-63.
293. Davuluri, N.; Punit, S.; Sudha, M.; Lokesh, P. *IJPRBS* **2013**, 2, 346-371.
294. Jain, V.; Maingi, V.; Maiti, P. K.; Bharatam, P. V. *Soft Matter* **2013**, 9, 6482-6496.
295. Murat, M.; Grest, G. S. *Macromolecules* **1996**, 29, 1278-1285.
296. Cai, C.; Chen, Y. *Macromolecules* **1997**, 30, 5104-5117.
297. Biswas, P.; Kant, R.; Blumen, A. *J. Chem. Phys.* **2001**, 114, 2430-2441.

298. Lee, J.; Athey, B. D.; Wetzel, A. W.; Meixner, W.; Baker Jr., J. R. *Macromolecules* **2002**, 35, 4510-4520.
299. Götze, I. O.; Likos, C. N. *Macromolecules* **2003**, 36, 8189-8197.
300. Karasatos, K. *Macromolecules* **2006**, 39, 4619-4626.
301. Dolgushev, M.; Blumen, A. *J. Chem. Phys.* **2009**, 131, 044905.
302. Dolgushev, M.; Blumen, A. *Macromolecules* **2009**, 42, 5378-5387.
303. Fürstenberg, F.; Dolgushev, M.; Blumen, A. *J. Chem. Phys.* **2012**, 136, 154904.
304. Markelov, D. A.; Dolgushev, M.; Gotlib, Y. Y.; Blumen, A. *J. Chem. Phys.* **2014**, 140, 244904.
305. Imae, T.; Funayama, K.; Aoi, K.; Tsutsumiuchi, K.; Okada, M.; Furusaka, M. *Langmuir* **1999**, 15, 4076-4084.
306. Plötschke, D.; Ballauf, M.; Lindner, P.; Fischer, M.; Vögtle, F. *Macromol. Chem. Phys.* **2000**, 201, 330-339.
307. Dingenouts, N.; Rosenfeldt, S.; Werner, N.; Vögtle, F.; Lindner, P.; Roulamo, A.; Rissanen, K.; Ballauf, M. *J. Appl. Cryst.* **2003**, 36, 674-678.
308. Meltzer, A. D.; Irrell, D. A.; Jones, A. A.; Inglefield, P. T.; Hedstrand, D. M.; Tomalia, D. A. *Macromolecules* **1992**, 25, 4541-4548.
309. Meltzer, A. D.; Irrell, D. A.; Jones, A. A.; Inglefield, P. T. *Macromolecules* **1992**, 25, 4549-4552.
310. Scherrenberg, R.; Coussens, B.; van Vliet, P.; Edouard, G.; Brackman, J.; de Brabander, E.; Mortensen, K. *Macromolecules* **1998**, 31, 456-461.
311. Uppuluri, S.; Keinath, S. E.; Tomalia, D. A.; Dvornic, P. R. *Macromolecules* **1998**, 31, 4498-4510.
312. Uppuluri, S.; Morrison, F. A.; Dvornic, P. R. *Macromolecules* **2000**, 33, 2551-2560.
313. Rietveld, I. B.; Bedeaux, D. *Macromolecules* **2000**, 33, 7912-7917.
314. Rietveld, I. B.; Bedeaux, D. *J. Colloid Interface Sci.* **2001**, 235, 89-92.
315. Pavlov, G. M.; Korneeva, E. V.; Meijer, E. W. *Colloid Polym. Sci.* **2002**, 280, 416-423.
316. Rathgeber, S.; Monkenbusch, M.; Kreitschmann, M.; Urban, V.; Brulet, A. *J. Chem. Phys.* **2002**, 117, 4047-4062.
317. Wind, M.; Saalwächter, K.; Wiesler, U.-M.; Müllen, K.; Spiess, H. W. *Macromolecules* **2002**, 35, 10071-10086.
318. Rathgeber, S.; Monkenbusch, M.; Hedrick, J. L.; Trollsås, M.; Gast, A. P. *J. Chem. Phys.* **2006**, 126, 204908.
319. Uppuluri, S.; Keinath, S. E.; Tomalia, D. A.; Dvornic, P. R. *Macromolecules* **1998**, 31, 4498-4510.
320. Uppuluri, S.; Morrison, F. A.; Dvornic, P. R. *Macromolecules* **2000**, 33, 2551-2560.
321. Tande, B. M.; Wagner, N. J.; Kim, Y. H. *Macromolecules* **2003**, 36, 4619-4623.
322. Mijovic, J.; Ristic, S.; Kenny, J. *Macromolecules* **2007**, 40, 512-5221.

323. de Brabander-van der Berg, E. M. M.; Meijer, E. W. *Angew. Chem. Int. Ed. Engl.* **1993**, 21, 1308-1311.
324. Richter, D.; Stühn, B.; Ewen, B.; Nerger, D. *Phys. Rev. Lett.* **1987**, 58, 2462-2465.
325. Richter, D.; Farago, B.; Fetters, L. J.; Huang, J. S.; Ewen, B. *Macromolecules* **1990**, 23, 1845-1856.
326. Meltzer, A. D.; Tirrell, D. A.; Jones, A. A.; Inglefield, P. T.; Hedstrand, D. M.; Tomalia, D. A. *Macromolecules* **1992**, 25, 4541-4548.
327. Meltzer, A. D.; Tirrell, D. A.; Jones, A. A.; Inglefield, P. T. *Macromolecules* **1992**, 25, 4549-4552.
328. Westlund, P.O. *Phys. Chem. Chem. Phys.* **2010**, 12, 3136-3140.
329. Voigt, G.; Kimmich, R. *J. Magn. Reson.* **1976**, 24, 149-154.
330. Anoardo, E.; Pusioli, D. J. *Phys. Rev. Lett.* **1996**, 76, 3983-3986.
331. Onda, S.; Harada, H.; Nakamura, D.; Kubo, M. *J. Magn. Reson.* **1972**, 8, 238-242.
332. Meier, R.; Kruk, D.; Bourdick, A.; Schneider, E.; Rössler, E. A. *Appl. Magn. Reson.* **2013**, 44, 153-168.

Versicherung an Eides statt

Hiermit versichere ich an Eides statt, dass ich die vorliegende Arbeit *“Field-Cycling NMR as a Tool of Molecular Rheology”* selbstständig verfasst und keine anderen als die von mir angegebenen Quellen und Hilfsmittel verwendet habe. Weiterhin erkläre ich, dass ich die Hilfe von gewerblichen Promotionsberatern bzw. –vermittlern oder ähnlichen Dienstleistern weder bisher in Anspruch genommen habe, noch künftig in Anspruch nehmen werde. Zusätzlich erkläre ich hiermit, dass ich keinerlei frühere Promotionsversuche unternommen habe.

Die Informationen zur Bedeutung der eidesstattlichen Versicherung und zu den strafrechtlichen Folgen einer unrichtigen oder unvollständigen eidesstattlichen Versicherung habe ich zur Kenntnis genommen.

..... ,

Ort, Datum Unterschrift